



TOGETHER
for a sustainable future

OCCASION

This publication has been made available to the public on the occasion of the 50th anniversary of the United Nations Industrial Development Organisation.



TOGETHER
for a sustainable future

DISCLAIMER

This document has been produced without formal United Nations editing. The designations employed and the presentation of the material in this document do not imply the expression of any opinion whatsoever on the part of the Secretariat of the United Nations Industrial Development Organization (UNIDO) concerning the legal status of any country, territory, city or area or of its authorities, or concerning the delimitation of its frontiers or boundaries, or its economic system or degree of development. Designations such as “developed”, “industrialized” and “developing” are intended for statistical convenience and do not necessarily express a judgment about the stage reached by a particular country or area in the development process. Mention of firm names or commercial products does not constitute an endorsement by UNIDO.

FAIR USE POLICY

Any part of this publication may be quoted and referenced for educational and research purposes without additional permission from UNIDO. However, those who make use of quoting and referencing this publication are requested to follow the Fair Use Policy of giving due credit to UNIDO.

CONTACT

Please contact publications@unido.org for further information concerning UNIDO publications.

For more information about UNIDO, please visit us at www.unido.org

20709

UNDER THE AUSPICES OF
THE UNITED NATIONS INDUSTRIAL DEVELOPMENT ORGANIZATION

**WORKSHOP ON COMPUTER-BASED
MATHEMATICAL MODELLING
OF
ALUMINIUM PRODUCTION PROCESSES**

**Jawaharlal Nehru Aluminium Research
Development and Design Centre
Nagpur, India
September 1993**

**University of Quebec at Chicoutimi
Quebec, Canada**

UNDER THE AUSPICES OF
THE UNITED NATIONS INDUSTRIAL DEVELOPMENT ORGANIZATION

**WORKSHOP ON COMPUTER-BASED
MATHEMATICAL MODELLING
OF
ALUMINIUM PRODUCTION PROCESSES**

Jawaharlal Nehru Aluminium Research
Development and Design Centre
Nagpur, India
September 1993

University of Quebec at Chicoutimi
Quebec, Canada

UNDER THE AUSPICES OF
THE UNITED NATIONS INDUSTRIAL DEVELOPMENT ORGANIZATION

**WORKSHOP ON COMPUTER-BASED
MATHEMATICAL MODELLING
OF
ALUMINIUM PRODUCTION PROCESSES**

Jawaharlal Nehru Aluminium Research
Development and Design Centre
Nagpur, India
September 1993

Faculty:

Rung T. Bui, Ph.D
Andre Charette, D.Sc.
Selvin Peter, Ph.D
Vinko Potocnik, Ph.D
Laszlo Tikasz, Ph.D

These documents have been prepared for distribution to the course participants. The material is copyrighted by each faculty member and must not be reproduced or referenced without their prior written consent.

FACULTY LISTING

Rung T. Bui

Université du Québec à Chicoutimi
555, boulevard de l'Université
Chicoutimi (Québec) Canada G7H 2B1
Phone: (418) 545-5270
Fax: (418) 545-5012

Rung T. Bui received his Mechanical Engineer's degree from France in 1956 and his Ph.D. in Control Engineering from the Naval Postgraduate School, Monterey, CA in 1964. Professor of engineering at the UQAC since 1975 and former chairman of the University's Unified Engineering Program, he works in the mathematical modelling of industrial thermal processes. Author or co-author of 48 journal papers, 56 conference papers and several industrial reports, he is mostly involved in joint projects with industry mainly the aluminium industry. Dr. Bui is presently the director of UQAC's Groupe de Recherche en Ingénierie des Procédés et Systèmes (GRIPS) to which belong 4 of the Faculty members herein presented. He is the incumbent of an Industrial Research Chair jointly funded by the Natural Sciences and Engineering Research Council (NSERC) of Canada and Alcan for the period 1991-1996.

André Charette

Université du Québec à Chicoutimi
555, boulevard de l'Université
Chicoutimi (Québec) Canada G7H 2B1
Phone: (418) 545-5057
Fax: (418) 545-5012

Dr. André Charette obtained a diploma in chemical engineering at Laval University Québec, Canada in 1966 and a doctorate degree in high temperature chemical kinetics in 1972 from the same University. He joined the Université du Québec à Chicoutimi in 1970 where he is now in charge of the courses in thermodynamics and heat transfer as a full professor. His research activities include the computation of radiative heat transfer in industrial furnaces, general modelling of thermal processes and pyrolysis and calcination of carbonaceous products. He participated actively in numerous research projects conducted jointly with industry, namely Alcan, Comalco, ELF-Atochem. He authored or co-authored more than 60 technical papers, presentations and research reports and supervised 17 graduate students.

Selvin Peter

**Université du Québec à Chicoutimi
555, boulevard de l'Université
Chicoutimi (Québec) Canada G7H 2B1
Phone: (418) 545-5011 ext. 2277
Fax: (418) 545-5012**

Dr. Selvin Peter obtained a B.Sc.E. degree in Chemical Engineering in 1984 and a Ph.D. degree in heat transfer in 1992 at the University of New Brunswick, Fredericton, Canada. Working as a research engineer at the Université du Québec à Chicoutimi since 1989, he has been involved in the electrode baking furnace modelling for Alcan (Canada) and Comalco (Australia). He has been author or co-author of 15 research papers, conferences and industrial reports. He is an active member of the Combustion Institute of Canada and the Order of Engineers of Québec, Canada.

Vinko Potocnik

**Alcan International Limited
P.O. Box 1250
Jonquière (Québec) Canada G7S 4K8
Phone: (418) 699-3332
Fax: (418) 699-3996**

Dr. Vinko Potocnik obtained a diploma in engineering physics at the University of Ljubljana in 1967, and a Ph.D. in plasma physics at the University of British Columbia, Vancouver, Canada in 1973. Since 1973, he has been working at Alcan International Arvida Research and Development Centre, Jonquiere, Canada. There, he is presently senior scientist and consultant. He has been working in the area of mathematical modelling, simulation, process control and expert systems. He also taught a graduate course (master's level) in mathematical modelling and simulation at the Université du Québec à Chicoutimi, Chicoutimi, Canada, for 6 years. He is also one of the lecturers at the bi-annual one-week Aluminium Electrolysis Course at Carnegie Mellon University, Pittsburgh, USA.

Laszlo Tikasz

**Université du Québec à Chicoutimi
555, boulevard de l'Université
Chicoutimi (Québec) Canada G7H 2B1
Phone: (418) 545-5233
Fax: (418) 545-5012**

Dr. Laszlo Tikasz obtained his masters (M.Sc.) degree in electrical engineering in 1978 and his doctorate degree (Dr. Techn.) in 1986, both from the Technical University of Budapest. From 1978 until 1980, he worked at East Hungarian Electricity Board as development engineer. From 1980 until 1989, he worked at Hungalu Engineering and Development Centre, Division of Aluminium Metallurgy in the area of process measurements and process control. In 1989, he joined the Université du Québec à Chicoutimi as invited research professor. There, he has worked in building a computer simulator of an aluminium electrolytic cell and in supervision of expert system applications. In 1984, he lectured as a member of UNIDO expert group at Zheng-Zhou Light Metals Research Institute in China.



Université du Québec à Chicoutimi
555, boulevard de l'Université
Chicoutimi, Québec
G7H 2B1



Groupe de Recherche en Ingénierie des Procédés et Systèmes

THE GROUP

The Research Group on Process and Systems Engineering of the Université du Québec à Chicoutimi, Chicoutimi, Québec, Canada is a well established University research outfit working in the field of mathematical and physical modelling, simulation, analysis and control of industrial processes involving heat, mass, momentum transfer and related phenomena. The acronym GRIPS comes from its french name Groupe de Recherche en Ingénierie des Procédés et Systèmes.

THE DOMAIN: HIGH TEMPERATURE INDUSTRIAL PROCESSES

Canadian processing industries are becoming less and less materials exporters and more and more materials processors. The high temperature industrial processes have become so prominently important that they, far more than the cost of the materials, determine the viability and the success of an industry. The need and the capacity to analyze and optimize the processes constitute the hallmark of future-oriented industries.

Underlying these processes are the basic physical phenomena such as fluid flow, mass transfer, conductive, convective and radiative heat transfer, combustion, chemical reactions, phase change, porous media flow, fluidized bed, volatile matters evolution... Dissecting an industrial process, one always encounters one or the other or more likely a combination of those phenomena. Any one of them, taken separately, is a current research domain. An additional challenge is to combine them into one model that would be representative of the process under study, yet streamlined enough to be usable and useful in an industrial environment.

The purpose of modelling is to better understand the process so that its design on operation can be improved and eventually optimized. The analytic models that give a full physical description of the process are often too complex for control and optimization purpose.

Therefore model identification and reduction are called for, then appropriate control techniques must be applied. These techniques cover a wide range, from PID feedback, knowledge-base control and supervision, to fuzzy logic and neural network applications.

Finally, to facilitate the use of the models by industrial workers, we construct user-friendly, interactive menu-driven interfaces including preprocessors and postprocessors with multi-dimensional graphical representation of outputs.

The Group's interests are therefore not only in the mathematical and physical modelling, but also in model-based control and optimization of these processes, followed by a technology transfer to the user, including friendly interfaces, user's manuals, tutorials, hands-on practice sessions for the model user. Even the best model, if it collects dust on the shelf due to lack of an appropriate transfer, is worse than not having a model at all.

THE METHODOLOGY: STAY CLOSE TO THE REAL THING

We invariably start with an on-site elaborate study of the process that may take several months. We then go to the mathematics, which are to be solved by appropriate numerical methods, resulting in computer models that must then be calibrated and validated, based on the plant test data provided by industry. Other simulations and analyses follow, always in close collaboration with the process operators themselves. A model must faithfully represent the real thing, not the opposite.

Human understanding of many aspects of complex industrial processes is still either incomplete or informal. Mathematical modelling must be complemented, formalized, or validated by physical modelling using small-scale models together with measuring, visualizing, recording, analyzing, processing, filtering techniques that extend the limits of human natural perception to permit the observation and explanation of phenomena otherwise inaccessible. Our Group's efforts are aimed at a complementarity between the two approaches to modelling.

THE RESOURCES: STREAMLINED TO MEET THE NEEDS

GRIPS is composed of 4 Professors, 4 Research Professors, 1 Post-doctoral Fellow and 2 Research Engineers at the M.S. level. Several doctoral and masters students work with the group at all times. Beside the services provided to the Group and the University's CAD-CAM Laboratory, GRIPS has its own network of HP-9000 Apollo 730's, SGI computers and workstations, SUN computers, SPARC workstations, and PC's. We have at our disposal most of the well known commercial general-purpose CFD codes, as well as the computer-aided graphics codes. We also build our own software as the needs arise.

Our heat transfer laboratory is equipped with a 150kW experimental furnace, with data acquisition, fluxmeter, suction pyrometer, five-hole pitot tube, automatic controller, for use in the study of flow, combustion, radiative transfer problems and related phenomena. A laser-doppler velocimetry system by TSI inc. is used in conjunction with an intelligent flow analyzer for flow studies. A MICRO infrared camera with monitor and image processor helps in the analysis of solid surface temperatures. Our thermogravimetry laboratory uses a Lindberg vertical furnace, with programmable controller, Varian chromatograph and data logger. A 5kW induction furnace is also used for faster heating rates up to 150°/minute.

A host of laboratory setups and small-scale models have been built recently and are available for studying various industrial equipments: melting furnace, recycling furnace, rotary kiln, heat transfer in scrap metals..., or for measuring the thermal properties of various materials.

THE INDUSTRIAL INVOLVEMENT: BRIDGING TWO CULTURES.

For more than a decade we have been continuously involved in industrial projects, either as joint research funded by industry and governments, or as contracts funded by industry alone. We recently modelled or are in the course of modelling: the cement clinker, the rotary dryer, the carbon anode baking horizontal flue ring furnace, the carbon electrode baking Riedhammer vertical flue ring furnace, the aluminium casting furnace, the aluminium remelt furnace, the ingot soaking furnace, the petroleum coke rotary calcining kiln, the scrap melter, the dross remelter, the aluminium electrolytic cell, the stirring tank for metallic composites. Several of these activities are undertaken in collaboration with Alcan International Ltd of Jonquière, Québec, Canada, others with Comalco Research of Melbourne, Australia.

Laboratory studies of impregnated carbon electrodes have been carried out for Norsolor, a subsidiary of ORKEM (France). Other projects are undertaken with Alcan for the construction of interactive graphic interfaces and the optimal control of aluminium electrolytic cells using knowledge-base techniques, fuzzy logics, and neural networks. Many of these subjects constitute ideal thesis topics for Ph.D. and M.S. students.

A five-year Industrial Research Chair (IRC) was recently established within the Group with funding from the Natural Science and Engineering Research Council (NSERC) of Canada, ALCAN, the UQAC Foundation Inc., and UQAC. It provides salary support for the chairholder, 3 research professors, in addition to graduate students. Major pieces of computing and laboratory equipment have also been acquired with the Chair's funds. The Chair's research program covers work on phase change, non-newtonian flows and radiative heat transfer, all with a view to industrial applications to high temperature processes.

Through its policies, research strategies, management techniques and business relations, the Group endeavours to bridge the gap between the two cultures, academic and industrial. It offers an environment in which industry can feel that their views and their needs are welcome and differences in expectations are reconciled.

GRIPS operates on a non-profit making basis. The possibilities for funding of the work done at GRIPS are flexible. Funding can take the form of a contract, a project, or in some cases a faculty or graduate student support. The basic criterion lies in the scientific and technological content of the work envisaged, its industrial relevance, and its compatibility with University research.

For more information, or a copy of the Group's annual report, please write or call:

Dr. Rung. T. Bui, Professor
Coordinator of GRIPS
Université du Québec à Chicoutimi
Chicoutimi, Québec, Canada, G7H 2B1
Phone: (418) 545-5270
Fax: (418) (545-5012

(8-93)

TENTATIVE WORKSHOP SCHEDULE

Nagpur, India
September 1993

DATE	TIME	TOPIC	LECTURER
Day 1	9:00 - 9:30	Welcome and introduction.	JNARDDC Director
		Organization of Workshop.	UNIDO Experts Team Leader
	9:30 - 10:00	Mathematical modelling motivation and methodology.	V. Potocnik
	10:00 - 10:30	Process overview.	V. Potocnik
	10:30 - 11:00	Simulation of an Aluminium electrolytic cell: basic mass and energy balance calculations.	L. Tikasz
	11:00 - 11:30	Break	
	11:30 - 13:00	Basic mass and energy balance calculations: approximating selected operation modes.	L. Tikasz
	13:00 - 14:30	Lunch	
	14:30 - 16:00	Developing a control emulator. Using the dynamic cell model; examples.	L. Tikasz
	16:00 - 16:30	Break	
	16:30 - 18:00	Computer demonstration of the dynamic cell simulator and participants' contributions.	L. Tikasz
	18:00 - 19:30	Social time: hosted by UNIDO team.	

Day 2	9:30 - 10:30	3D thermo-electric modelling of the electrolysis cell.	V. Potočník
	10:30 - 11:00	Computer demonstration of the dynamic cell simulator.	L. Tikasz
	11:00 - 11:30	Break	
	11:30 - 12:00	Modelling of potroom activities for cell operation.	L. Tikasz
	12:00 - 13:00	Magnetohydrodynamics (MHD): introduction	V. Potočník
	13:00 - 14:30	Lunch	
	14:30 - 16:00	Electric current calculations. Busbar design. Magnetic field calculations.	V. Potočník
	16:00 - 16:30	Break	
	16:30 - 18:00	Cell hydrodynamics.	V. Potočník
	18:00 - 20:00	Free time	
Day 3	9:30 - 11:00	The anode-baking Riedhammer furnace: Design and operation. Motivation for modelling.	S. Peter
	11:00 - 11:30	Break	
	11:30 - 13:00	Development of the 2D+ model.	S. Peter
	13:00 - 14:30	Lunch	
20:00 - 22:00	Free discussion*: Plant measurements for model validation: MHD, electrical, thermal.	V. Potočník L. Tikasz	

14:30 - 16:00	Simulation results and capabilities of the 2D+ model.	S. Peter
16:00 - 16:30	Break	
16:30 - 18:00	Development of the 3D model. Simulation results and capabilities of the 3D model.	S. Peter
18:00 - 20:00	Free time	
20:00 - 22:00	Free discussion*: A comparison of 1D, 2D, 2D+, 3D models. A comparison of vertical and horizontal furnaces. Plant measurements.	A. Charette S. Peter V. Potočník

Day 4

9:30 - 11:00	Description of some casting furnaces and overview of the related studies carried out at UQAC. Numerical methods in radiative heat transfer.	A. Charette
11:00 - 11:30	Break	
11:30 - 13:00	Numerical methods in radiative heat transfer (continued). Detail of the mathematical modelling of the casting furnaces: 1D analytical model.	A. Charette
13:00 - 14:30	Lunch	
14:30 - 16:00	Details of the mathematical modelling (continued): (a) 1D control model (b) fuel optimization calculations (c) 3D model	A. Charette

	16:00 - 16:30	Break	
	16:30 - 18:00	The remelting furnace	A. Charette
	18:00 - 18:30	Break	
	18:30 - 21:00	Graduation dinner, Dinner speaker	JNARDDC Director
Day 5	9:30 - 11:00	A general presentation on (a) the various research projects undertaken by the faculty members in Canada, and (b) an overview of Canadian aluminium industry.	A. Charette
	11:00 - 11:30	Break	
	11:30 - 13:00	Further elaboration on aspects identified by participants during the week, and / or free discussions.	All staff and participants
	13:00 - 14:30	Lunch	
	14:30 - 16:00	Same topics, continued.	All staff and participants
	16:00 - 18:00	Conclusion - dismissal	JNARDDC Director, UNIDO team leader

Note: * *Discussions may be held on evenings of Day 2 and Day 3 as indicated and / or on Day 5 as part of daytime schedule. Decision will be made on the spot in consultation with the participants.*

UNDER THE AUSPICES OF
THE UNITED NATIONS INDUSTRIAL DEVELOPMENT ORGANIZATION

**WORKSHOP ON COMPUTER-BASED
MATHEMATICAL MODELLING
OF
ALUMINIUM PRODUCTION PROCESSES**

Jawaharlal Nehru Aluminium Research
Development and Design Centre
Nagpur, India
September 1993

MATHEMATICAL MODELLING METHODOLOGY

**OVERVIEW OF PRIMARY ALUMINIUM
PRODUCTION PROCESSES**

**THREE-DIMENSIONAL THERMO-ELECTRIC
MODELLING OF THE CELL**

Vinko Potočnik

Alcan International Limited
Jonquiere, Quebec, Canada

1. Mathematical Modelling Methodology

Mathematical modelling has become one of the most important activities in process analysis and design. It consists of a number of steps that have to be combined in the most appropriate way for a given problem. Process understanding and plant measurements link it to reality. Building the equations, choosing the numerical algorithms and programming used to be the most intensive tasks in the past. The advent of good commercial software packages has shifted the emphasis to process related activities, to setting up the scenarios and to the analysis of the computer runs. Relationships among all these activities are the subject of the mathematical modelling methodology presented in this session.

2. Overview of the Primary Aluminium Production Processes

Primary aluminium production processes comprise alumina production, alumina reduction and casting.

Alumina is produced mostly from bauxite using the Bayer process. Some applications of the mathematical modelling in this area will be mentioned but not analysed in depth, since this part of the process is not a subject of the workshop.

Reduction process includes electrolysis and carbon electrode production. In electrolysis perhaps the most important subject is the thermal and electrical balance, which will be overviewed. Mass balance and process dynamics are closely related to cell operation and control. The electrode production process starts with coke calcination and ends with the cathode and anode baking. Both have been extensively studied by mathematical modelling, but only anode baking will be presented at the workshop.

Casting is preceded by ingot or scrap remelting, impurity elimination and alloying. The remelting as well as casting itself have been the subject of mathematical model development and applications, but only remelting will be presented at the workshop.

3. Three-Dimensional Thermo-Electric Modelling of the Cell

Complex material composition or complex boundary conditions require three-dimensional (3D) models whenever detailed distribution of the temperature or heat loss is required. This is certainly the case when the cathode or the anode is to be designed or redesigned.

In this lecture the issues in 3D modelling will be discussed. Examples of the simulations, obtained with a commercial finite-element software package will be given.

UNDER THE AUSPICES OF
THE UNITED NATIONS INDUSTRIAL DEVELOPMENT ORGANIZATION

**WORKSHOP ON COMPUTER-BASED
MATHEMATICAL MODELLING
OF
ALUMINIUM PRODUCTION PROCESSES**

Jawaharlal Nehru Aluminium Research
Development and Design Centre
Nagpur, India
September 1993

**SIMULATION OF
AN ALUMINIUM ELECTROLYTIC CELL**

Laszlo Tikasz

University of Quebec at Chicoutimi
Quebec, Canada

1. Basic Mass and Energy Balance Calculations

This part is intended to guide the reader through the construction of a simplified dynamic cell model of an aluminium electrolytic cell. The proposed Model itself is an integrated software package for simulating different operational states of aluminium electrolytic cells. The focus is on the theoretical aspects, whereas programming details as well as necessary preparatory steps (e.g. data acquisition problems) are not covered.

A theoretical approach is outlined showing how to derive basic equations to approximate the dynamic and static operation of a cell. The structure of the computation is demonstrated with special emphasis on the user-adjustable subroutines and functions. These user-adjustable parts can serve as starting points toward a more sophisticated description of the process.

The current state of an electrolytic cell is described by lumped parameters averaged over a selected part (lump) of the cell. For educational purposes, considerable simplifications are proposed regarding the granularity of the Model: the geometry is the simplest possible and the upper and lower side-carbon and freeze blocks are put into generalized side-wall and freeze blocks. The selected control volume contains only the bath, freeze and metal lumps, and the boundary conditions are approximated by generalized anode, cathode and side-wall lumps. The environment outside the cell model is represented by temperatures above, below and beside the cell. The material and energy balances are performed on all the selected lumps and during the simulation, the mass and temperature variations are calculated by solving the relevant ordinary differential equations.

Geometrical, chemical and electrical aspects of the aluminium electrolytic cell are considered. Alumina dissolution sub-model is introduced. Algebraic equations for steady-state simulation are also derived.

2. Approximating Selected Operation Modes

The adjustable model components can be used to approximate special operation modes, also. The most important components are:

- line current,
- current efficiency,
- mass densities,
- eutectic temperature,
- heat transfer coefficients,
- specific heat coefficients,
- equivalent thermal resistances,
- bath resistance and conductivity.

In this part, some examples are given showing how to select, tune, verify and validate equations or develop appropriate sub-models.

3. Developing a Control Emulator

In simulating the dynamic behavior of an electrolytic cell, it is a must to provide a unit which approximates the necessary maintenance routines. In real situations, the maintenance is provided partly manually and by an adequate process controller. Here we concentrate on the representation of the automatic control. The main points discussed are the following:

- selection of control variables,
- data exchange between Model and Control Emulator,
- developing a control data base,
- developing a simple alumina feeding routine,
- developing a simple resistance control routine.

4. How to Use the Dynamic Cell Model

An advanced Dynamic Cell Model is presented during the Workshop. The Dynamic Cell Model is a computer program, escorted by a

- User Guide and a
- Set-Up Guide

Based on these Guides, the general structure and the use of the Dynamic Cell Model are discussed. Examples are given where the Dynamic Cell Model is used to simulate different operating conditions.

5. Computer Demonstration

In this part, real computer demonstrations are provided on advanced PC-class computers. Both the basic mass and energy calculations and the Dynamic Cell Model will be presented.

With the basic equations, the participants can carry out static and dynamic computations. This facility helps them understand the process fundamentals as well as the main relations and trends of the process.

Using the Dynamic Cell Model, they will acquire hands-on experience with a complete simulator.

UNDER THE AUSPICES OF
THE UNITED NATIONS INDUSTRIAL DEVELOPMENT ORGANIZATION

**WORKSHOP ON COMPUTER-BASED
MATHEMATICAL MODELLING
OF
ALUMINIUM PRODUCTION PROCESSES**

Jawaharlal Nehru Aluminium Research
Development and Design Centre
Nagpur, India
September 1993

**MAGNETOHYDRODYNAMICS
(MHD)**

Vinko Potočnik

Alcan International Limited
Jonquiere, Quebec, Canada

1. Introduction

Magnetohydrodynamics (MHD) is the study of fluid behaviour under the influence of the electromagnetic forces. This force is a vector product of the electric current density and the magnetic field, therefore, MHD modelling can be divided into: electric current, magnetic field and hydrodynamics calculations.

In this session, we will also explore the consequences of MHD on the cell performance.

2. Electric Current and Magnetic Field Calculations

The objective of the electric current calculations is to determine the current density in the liquid metal and electrolyte (bath). This current density is determined by the cell and busbar design, its thermal state, and its operation. The methods of calculation, software and the influence of the cell design and operation on the current density will be presented. It will be shown how a well balanced current distribution can be obtained.

The magnetic field is generated by the electric current distribution in the cell as well as by cell-to-cell busbar connections. Steel structural elements of the cell redistribute considerably the magnetic field due to currents. This greatly complicates the calculations. Calculation methods and applications to different cell designs will be discussed.

3. Hydrodynamics

Cell hydrodynamics is described by the Navier-Stokes equation that includes the electromagnetic force. The solution of this equation gives the velocity patterns in the metal and in the bath and the metal-bath interface deformation. Steady state and dynamic models will be examined. Criteria for the MHD design will be discussed.

Applications to different cell designs will be shown, including a video presentation of the metal-bath interface waves.

UNDER THE AUSPICES OF
THE UNITED NATIONS INDUSTRIAL DEVELOPMENT ORGANIZATION

**WORKSHOP ON COMPUTER-BASED
MATHEMATICAL MODELLING
OF
ALUMINIUM PRODUCTION PROCESSES**

Jawaharlal Nehru Aluminium Research
Development and Design Centre
Nagpur, India
September 1993

MODELLING OF ANODE BAKING FURNACES

Selvin Peter

University of Quebec at Chicoutimi
Quebec, Canada

1. The Riedhammer Furnace: Design and Operation, Motivation behind Modelling.

This part is intended to give a description of the construction and operation of the Riedhammer furnace. The work it is supposed to do, the general structure of its construction, the main phenomena taking place in the furnace (fuel combustion, air infiltration, release and combustion of volatile matters, combustion of packing coke, heat losses) are described. The role of various furnace sections (preheat sections, firing sections, cooling section) and the configuration of each section ((head wall and fireshaft zone, underlid zone, pit zone, underpit zone) are explained. Comments are made on the operational parameters of the furnace (composition of fire train, fire cycle time, air flowrate, fuel flowrate, baking temperature, finishing temperature) and the effects of changing these parameters on overall furnace behaviour. Therefrom are drawn the motivations leading to the mathematical modelling work.

2. Development of the 2D+ Model

Comments are first given on the reasons for, and the limitations of, approximating the process by a two-dimensional (2D) model, and the need for extending it to a 2D+ model to account for the critical differences between inner and outer pits, due to heat losses through lateral walls.

The model is next presented in its mathematical concept as well as in the way it is solved.

The model extends from the 1st preheat section to the last covered cooling section. This model considers each of the four zones, links them together with common boundary conditions and determines the energy sources and sinks for each zone. This part of the course describes the conceptual approach used in the model by presenting the equations for the control volume of each zone and explaining how the four zones are treated and linked together. In addition, this part will include how the 2D transient conduction is solved and how the volatile matters release and combustion are taken care of by the model.

The solution procedure involves the calculation of mass flow, temperature and composition of the gas and solid temperature for each time step, until the end of the fire cycle period at which time a new preheat section is added and the last cooling section is dropped. A new fire change starts and the program is executed until the total number of the fire changes or a quasi-steady state (5°C temperature difference of the gas temperature between two fire changes) is achieved.

3. Simulation Results and Capabilities of the 2D+ Model

The geometrical parameters and the initial values required to run the model will be presented for a general-purpose base case. The output from the model including draught profile, gas temperature profile, fuel consumption, oxygen profile, gas mass flow, anode temperature profile, anode finishing temperature will be provided and compared with the measured values.

The capabilities of the model include changing operational parameters such as draught, firing scheme, fire cycle time, flow distribution across the furnace as well as changing geometrical parameters such as number of pits, adding or removing a section from the fire train. The effect of firing change on the performance of the furnace will be presented and compared with the base case.

4. Development of a 3D Model

The 3D model is built on the general-purpose code known as PHOENICS™ marketed by CHAM of London, U.K.. A brief introduction to the structure of PHOENICS and how it solves the transport equations will be given. Emphasis will be placed on the Riedhammer Furnace model conception in 3D and how this CFD code suits the needs of the work.

Next, the overall conception of the 3D model is presented. One section of the fire train is considered to be the control volume for the model. Body-fitted coordinates are used to discretize the geometry of a section. How various physical phenomena (air leakage, turbulence, combustion, radiative heat transfer, conduction through the solids and heat losses) are accounted for in the section of interest will be discussed. Further, the initial and boundary conditions along with the solution procedure for the flow and energy simulations will be presented.

5. Simulation Results and Capabilities of the 3D model

A base case considers the simulations for the 4th preheat section. The input parameters for these simulations will be introduced. The resulting flow and energy distribution in this section will be presented and discussed. Wherever general plant observation data are available, a comparison will be made between predicted and observed results on baking temperatures, temperature gradients, baking uniformity or the lack thereof... .

The capabilities of the 3D model include the effect of blocking any fireshafts or any CE5 or AE5 brick holes, non-uniform flow through the fireshafts, changing the geometry of the lid, on flow and energy distribution in the furnace. Examples will be presented to illustrate the flexible use of the model in these parameter studies.

Note: Sponsorship by industries will be duly mentioned.

UNDER THE AUSPICES OF
THE UNITED NATIONS INDUSTRIAL DEVELOPMENT ORGANIZATION

**WORKSHOP ON COMPUTER-BASED
MATHEMATICAL MODELLING
OF
ALUMINIUM PRODUCTION PROCESSES**

Jawaharlal Nehru Aluminium Research
Development and Design Centre
Nagpur, India
September 1993

MODELLING OF CASTING FURNACES

André Charette

University of Quebec at Chicoutimi
Quebec, Canada

1. Description of some melting/holding furnaces and overview of the related studies carried out at UQAC.

Work undertaken on a classical melting-holding furnace and on a top-charged remelting furnace is outlined.

2. Numerical methods in radiative heat transfer

Radiation is the dominant mode of heat transfer in casting furnaces. A number of different numerical techniques are available for its calculation. Some of them are addressed in this presentation. The zone, discrete transfer, imaginary planes, discrete ordinates and Monte Carlo methods are described and compared. Reference is made to assess the accuracy of the methods. Ways by which radiation is introduced into the solution of the conservation equations are discussed. Computer time is also analysed.

3. Details of the mathematical modelling of the furnaces described above.

3.1 The classical melting/holding furnace

3.1.1 1D model (analytical model)

This simplified model is dynamic and it can simulate any sequence of operations such as loading, heating, stirring, skimming, etc... It has been validated on a real furnace. Hottel's real gases formulation has been used for the combustion chamber and the phase change problem has been treated with the enthalpy method. The techniques and the results are explained.

3.1.2 1D reduced model (control model).

A tenth-order non-linear control model has been obtained from the analytical model by least-squares approximation. A detailed description of the methodology is given as well as a comparison of both models.

3.1.3 Fuel optimization calculations.

Such calculations have been performed using the control model in open and closed loop. First the open-loop formulation and

results are presented. More emphasis is laid however on the closed-loop schemes with PID control possibilities. The mathematical formulation is built around the minimization of a cost function.

3.1.4 3D model

This complex model is divided in two parts: the combustion chamber and the metal. The general-purpose code PHOENICS™ is used in both parts. Special algorithms are incorporated in the code: radiation heat transfer in the gas phase is treated by the imaginary planes method, the melting process is modelled with the use of the effective thermal properties concept and an augmented conductivity technique takes care of the convection in the liquid metal. This 3D model can be used to predict for instance the best dimensions of the furnace and the best position of the chimney or of the solid charges. A complete description of the model is presented.

3.2 The remelting furnace

This cylindrical furnace is loaded with pieces of different sizes which form a porous medium. Heat comes from burners imbedded in the walls at specific angles. Predicting the heat transfer in such an arrangement is a very difficult task. Several studies have been undertaken at UQAC to elucidate various aspects of the problem, namely:

- flow visualization studies of the interacting burner jets (in a cold physical model).
- impact convection heat transfer study (also in the cold model).
- experiences on the transmissivity of light through different porous media.
- one - and two-dimensional simplified models of the rate of melting of a typical pile by using an assumed heat penetration depth formulation.

The presentation includes a description of the experimental set-ups and a discussion of the results obtained up to the present time.

UNDER THE AUSPICES OF
THE UNITED NATIONS INDUSTRIAL DEVELOPMENT ORGANIZATION

**WORKSHOP ON COMPUTER-BASED
MATHEMATICAL MODELLING
OF
ALUMINIUM PRODUCTION PROCESSES**

Jawaharlal Nehru Aluminium Research
Development and Design Centre
Nagpur, India
September , 1993.

COURSE MATERIAL

Vinko Potočnik

Alcan International Limited
Jonquiere, Quebec, Canada

P R O C E S S O V E R V I E W

A N D

M O T I V A T I O N F O R

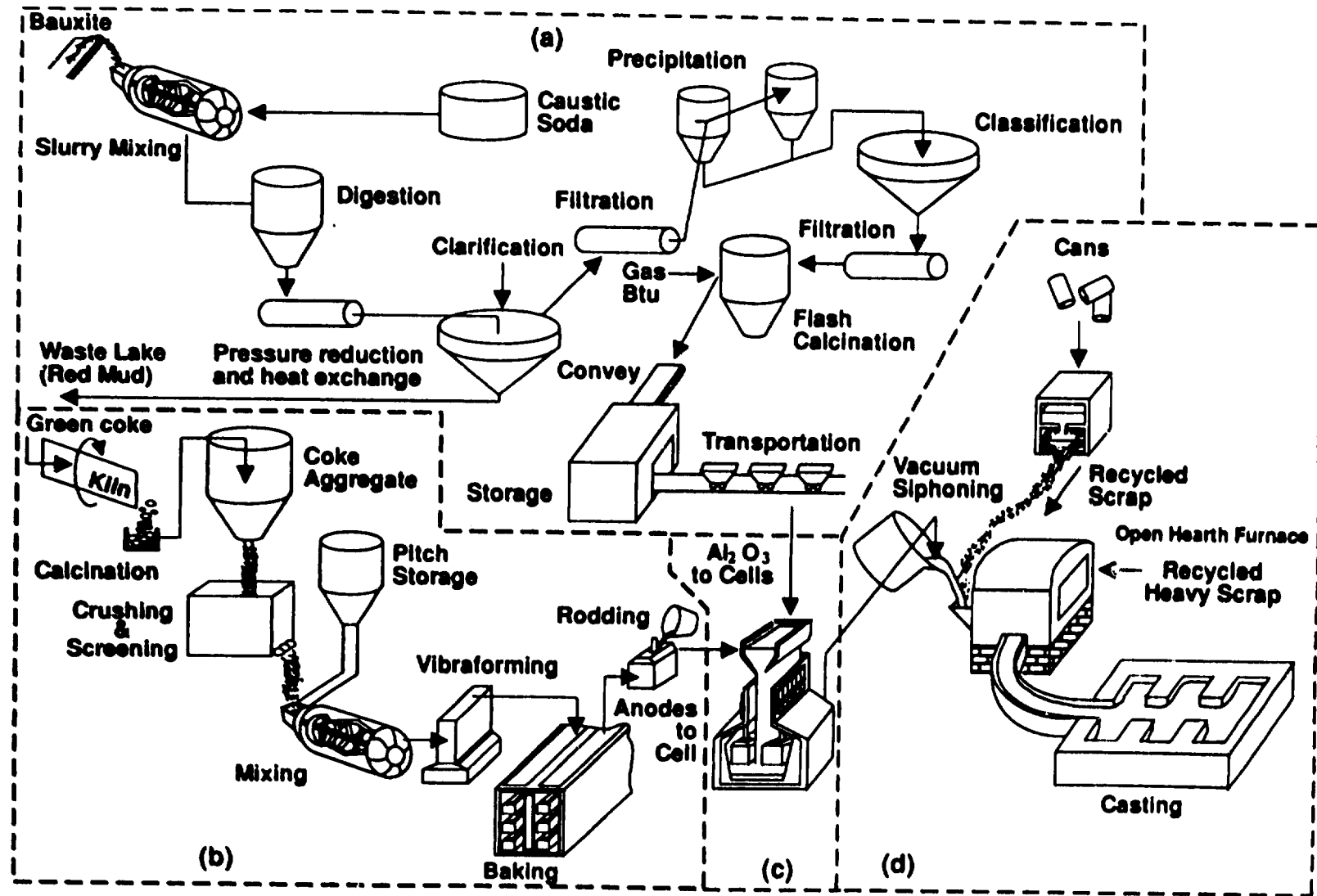
M O D E L L I N G

VINKO POTOČNIK

ALCAN INTERNATIONAL LTD

JONQUIERE, QUÉBEC, CANADA

FLWSHEET OF BAYER-HALL-HÉROULT TRANSFORMATION PROCESS



SOURCE: PRODUCTION OF ALUMINUM & ALUMINA

VP-Models-

RAW MATERIALS

PROCESS

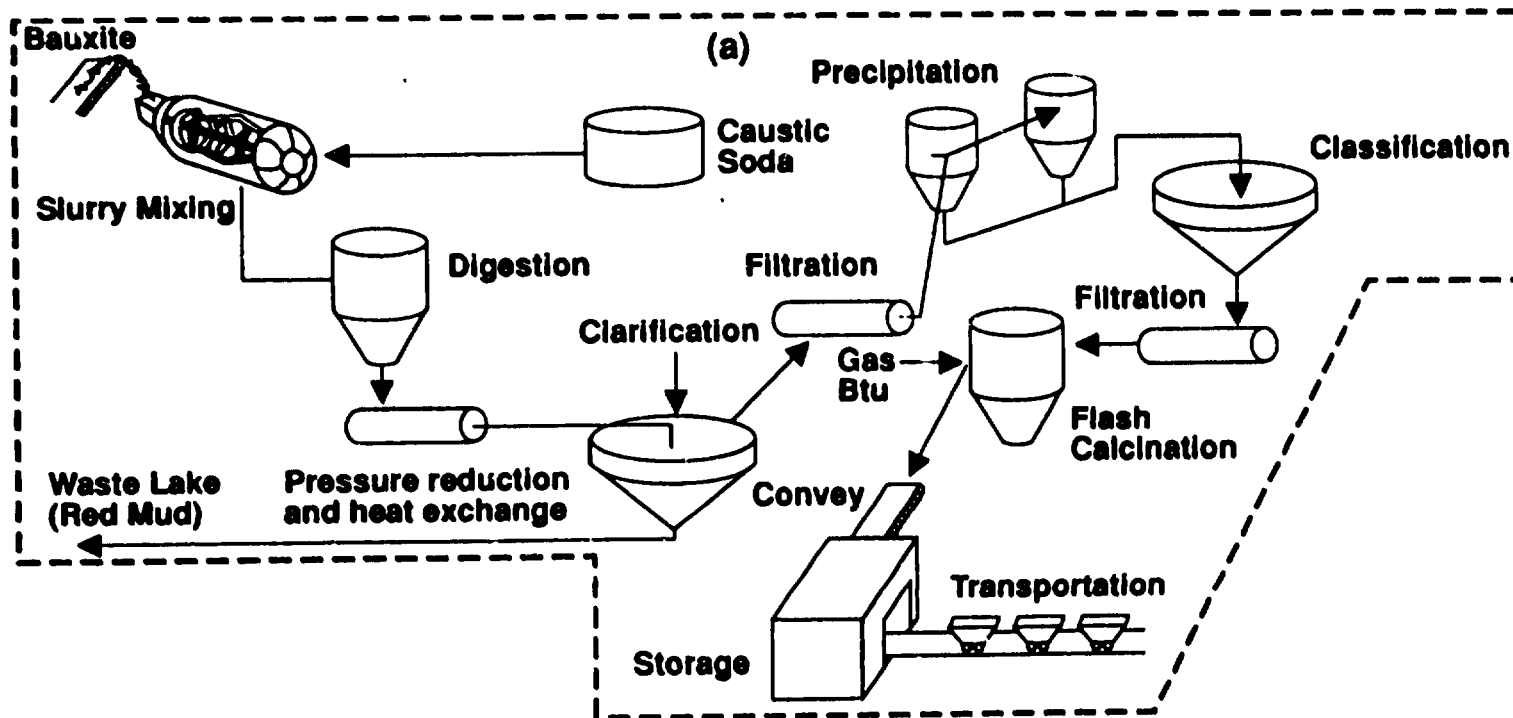
- Neary all alumina produced in the world today is produced by the Bayer process.

Large amounts of energy are used in this process and over a billion dollars is needed to build a one MT capacity alumina plant

Characteristics:

- High energy consumption
- High capital cost

FLWSHEET OF BAYER PROCESS



OBJECTIVES

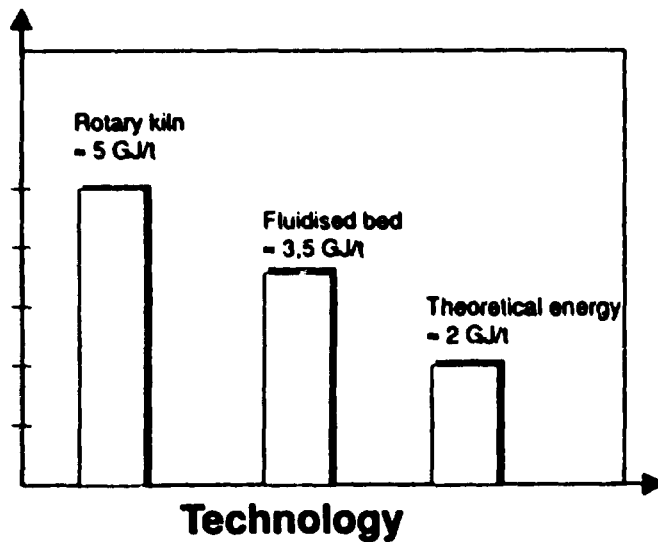
- **Low production cost**
- **Product (alumina) consistency**
- **Process efficiency**
- **Low energy consumption**

CHALLENGES RAW MATERIALS

- **Assure consistency of products**
 - **Size distribution of alumina has direct impact on productivity in electrolysis**
Example: precipitation circuit
- **Adapt to varying quality of bauxites, keeping consistency of products**
 - **Has direct impact on cost.**
Could use cheaper bauxites
Example: silica content, digestion, use of caustic

ALUMINA CALCINATION

Alumina Calcination
Energy GJ/t



PRESENT STATUS

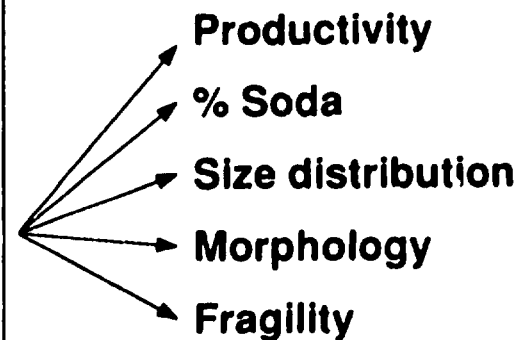
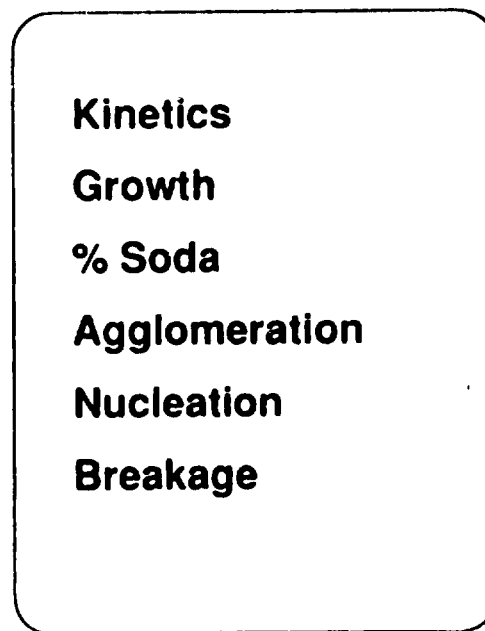
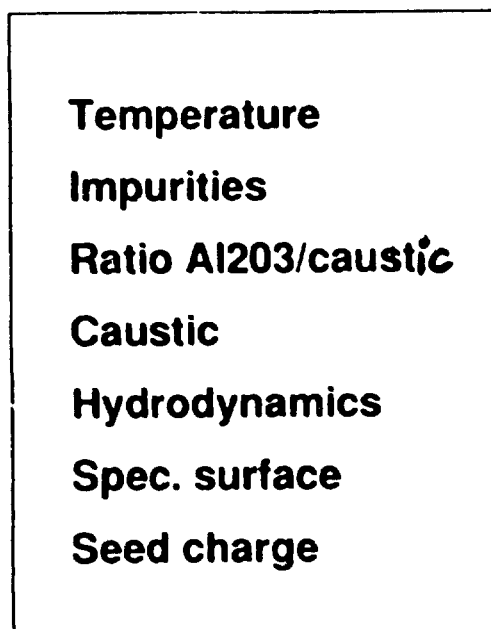
- **Mostly mass and energy balance models for process units**
Example: Bayer plant simulation
- **Some dynamic modelling**
Example: precipitation
- **Starting with multiphase fluid dynamics modelling**
Example: precipitation

PRECIPITATION MODELLING

Have a better knowledge
of the effect of

on

to predict



REDUCTION

Process

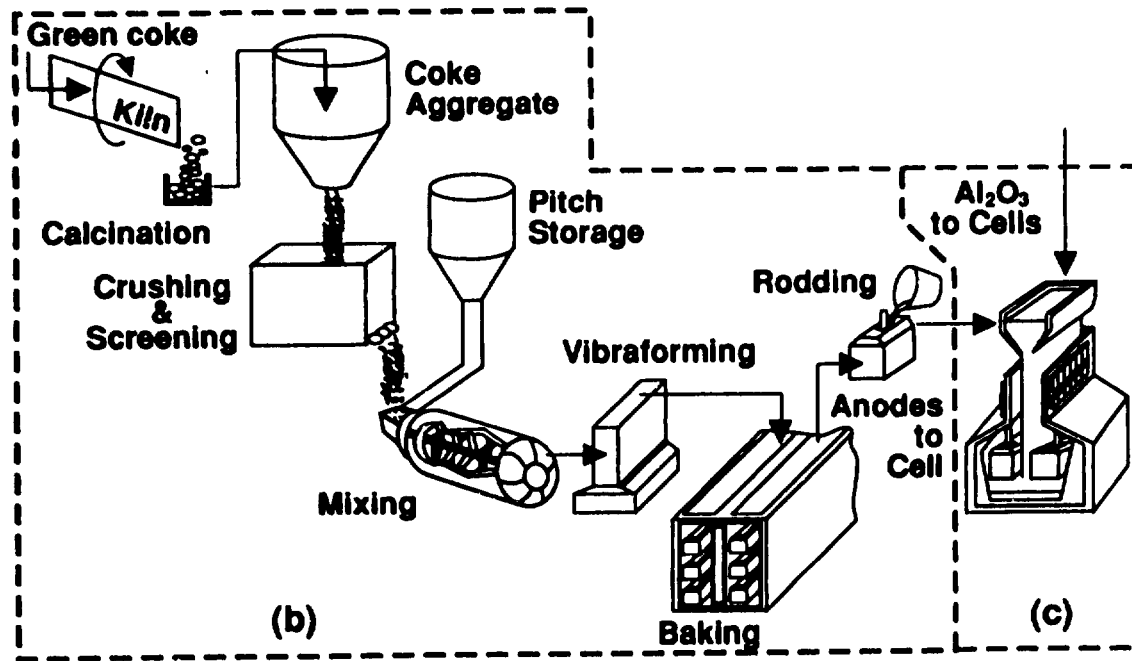
- Neary all aluminum produced in the world today is produced by Hall-Héroult electrolysis process.

Large amounts of electricity are used in this process and over a billion dollars is needed to build a medium capacity smelter (200 kt).

Characteristics:

- High energy consumption
- High capital investment

FLWSHEET OF HALL-HÉROULT PROCESS



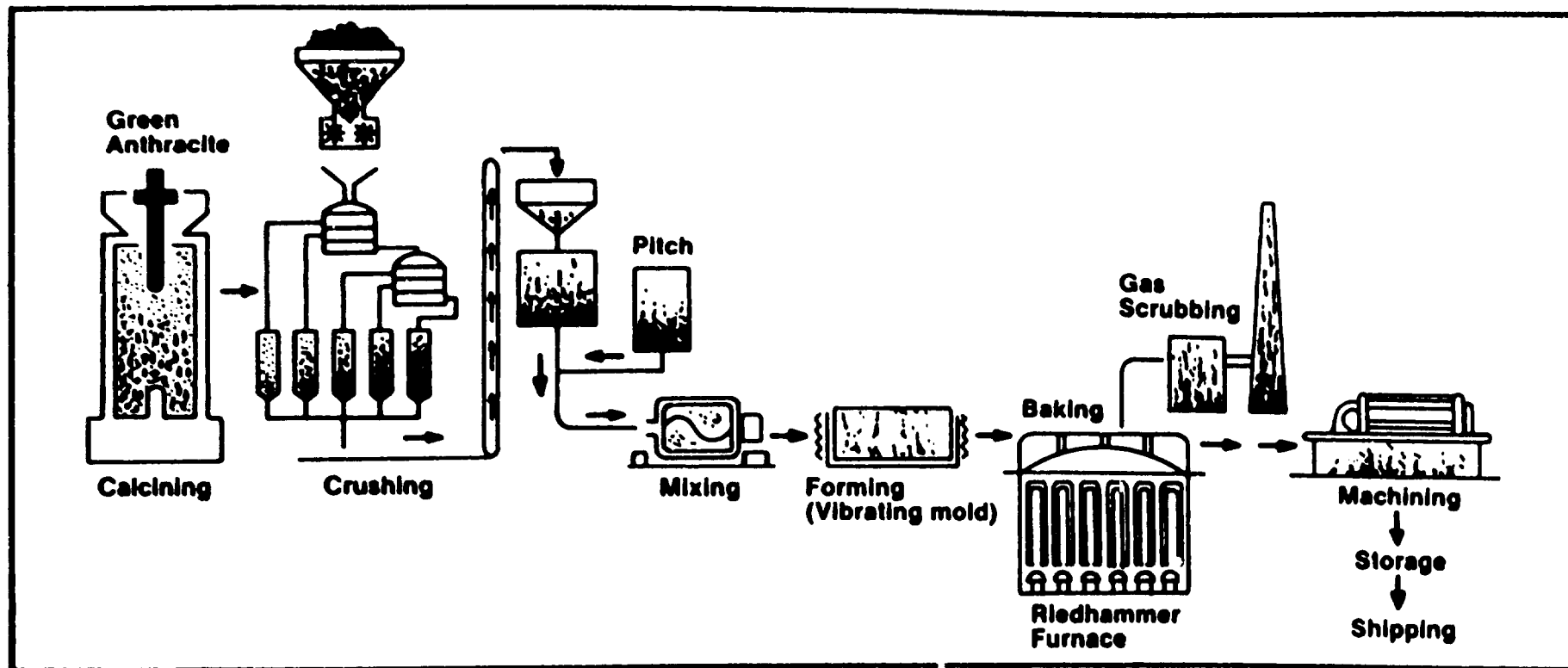


Figure 13. Schematic of the cathode block manufacturing process.

Source : JPMCGEER

BUSINESS CHALLENGES

- **Productivity**
- **Respect for environment**
- **Product quality**
- **Cost reduction**

CHALLENGES REDUCTION

- **Predict current efficiency**
 - **Has direct impact on capital investment and operating cost**
Example: electrolysis cell
- **Predict energy efficiency**
 - **Has direct impact on operating cost**
Example: Electrolysis cells, carbon calcining and baking furnaces

CHALLENGES REDUCTION (CONT)

- **Predict material quality**
 - **Has direct impact on electrolysis performance**
Example: calcined coke, baked carbon blocks

- **Predict working environment**
Example: potroom ventilation

- **Simulate plant operation**
Example: electrolysis cell operation

CHALLENGES REDUCTION (CONT)

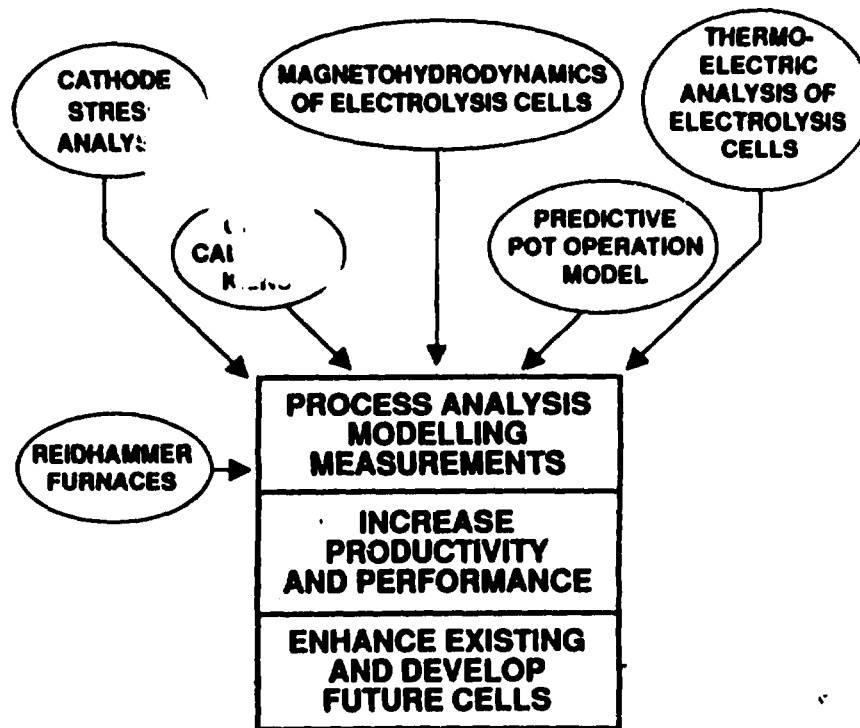
- **Predict life-time of production units**
 - **Has direct impact on operating cost and on environment**
Example: cathode of electrolysis cells

- **Predict generation of reject and toxic materials**
 - **Has direct impact on environment**
Example: cathode of electrolysis cells, coke calcining kiln dust

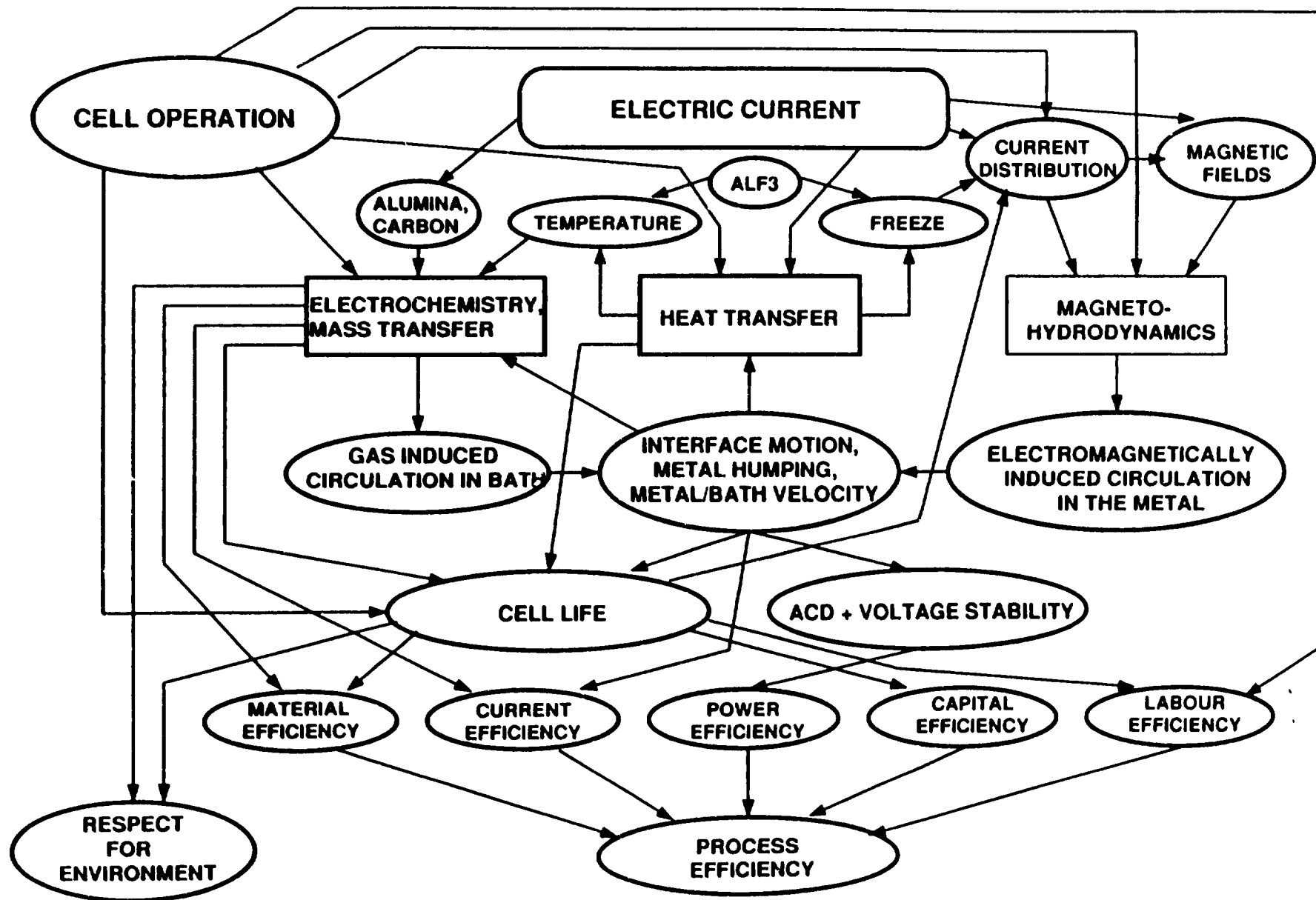
HOW TO GET THERE?

- Increase understanding of processes
- Increase predictive capability
 - for design
 - for plant operation

REDUCTION TECHNOLOGY MODELLING



BASIC INTERACTIONS OF THE ALUMINIUM REDUCTION PROCESS



TRANSFORMATION

Process

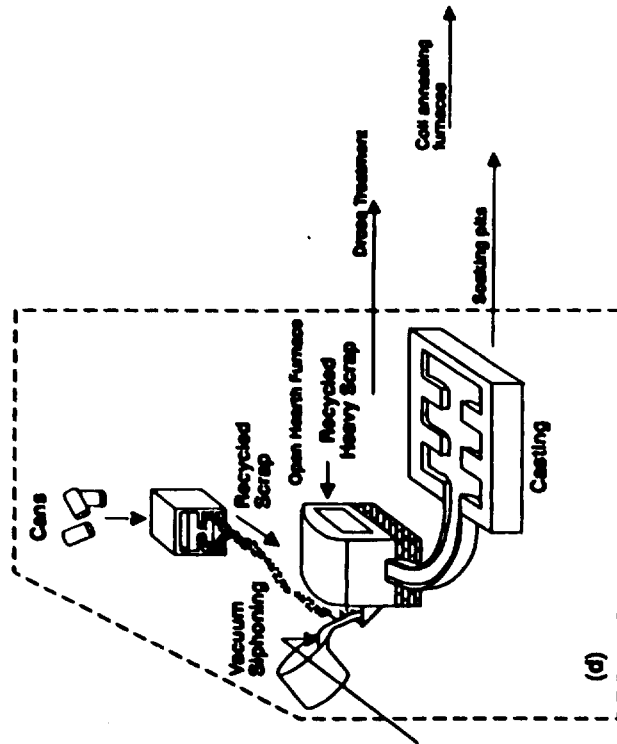
- Neary all aluminum produced in the world today goes through a remelt or casting furnace.

Large amounts of energy are used in the melting process

Characteristics:

- high energy consumption
- low energy efficiency

FLWSHEET OF TRANSFORMATION PROCESS



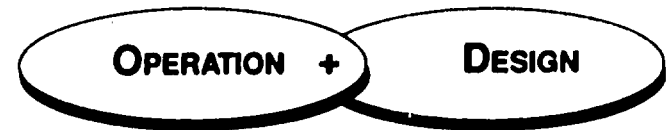
P0-22

VF-Melting

P0-23

MELTING AND HEAT TREATMENT FURNACES

PROCES IMPROVMENT



- Control and
- Optimisation
 - Reduce cycle
 - Reduce thermal gradient

- Optimise design
- New approach
 - Understanding of basic phenomena
 - Radiation
 - Convection
 - Phase change
 - Combustion
 - Model development

CHALLENGES TRANSFORMATION

- **Predict energy efficiency**
 - **Has direct impact on operating cost**
Example: remelt/casting furnaces with jet stirrer

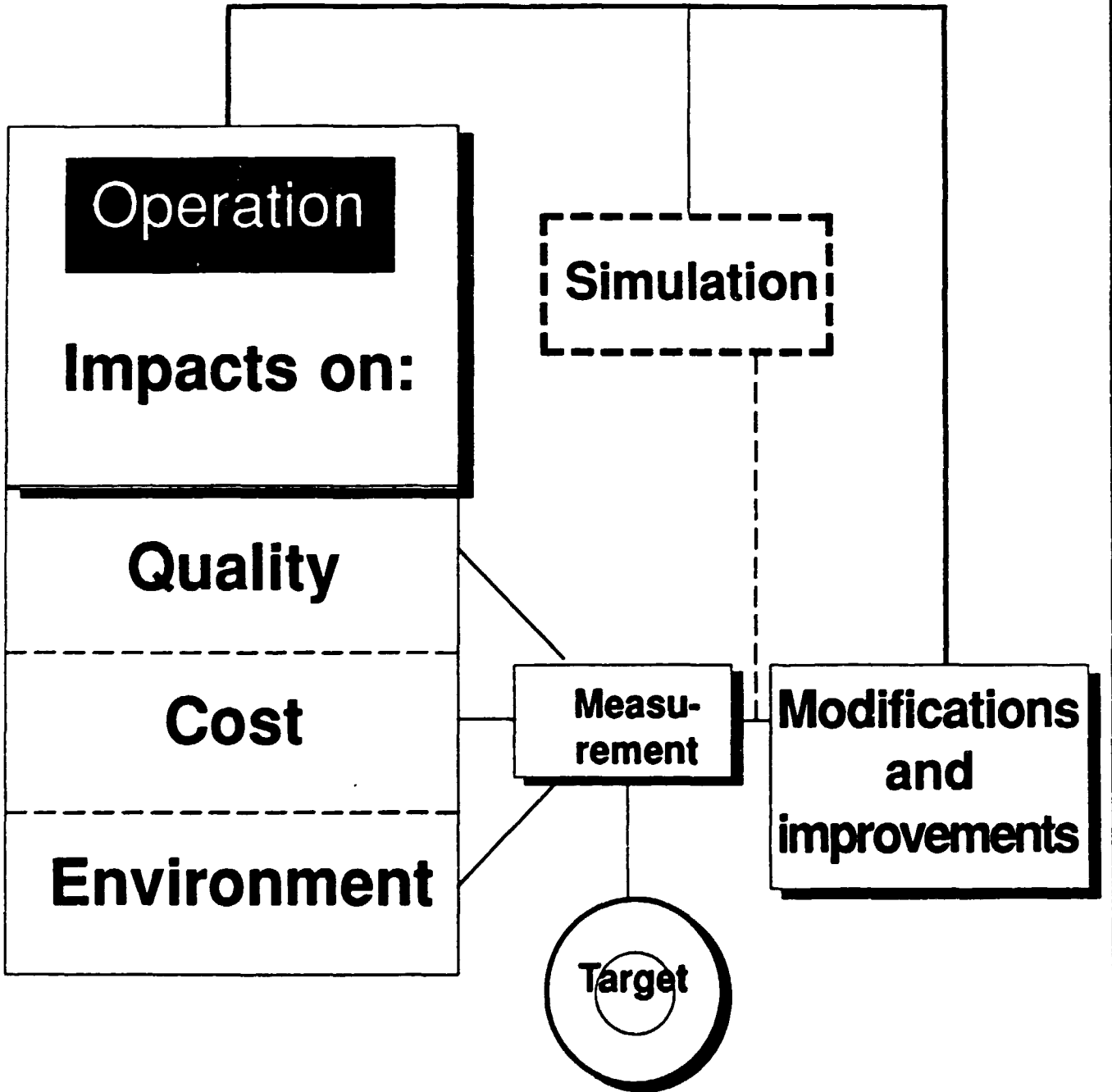
- **Predict productivity**
 - **Has direct impact on capital cost**
Example: remelt/casting furnaces, reheat furnaces

CHALLENGES TRANSFORMATION (CONT)

- **Predict metal cleanliness**
 - **Has direct impact on marketability of ingot**
Example: remelt/casting furnace

- **Create new technologies for recycling of aluminum**
 - **Has direct impact on operating cost and environment**
Example: UBC furnaces

PROCESS OPTIMISATION



EXPERIMENTAL vs. MODELLING APPROACH

Experimental

Shows TRUE behavior of the system.

Gives empirical relationships among variables (limited validity).

Time consuming: few situations can be examined.

Not all important variables are accessible.

Only existing systems can be studied: extrapolation by small steps.

Studying present and past behaviour.

Costly: equipment, production losses, manpower.

Modelling

Is only a representation of reality.

Is based on general laws of nature (general validity).

Time efficient: many situations can be examined.

All important variables can be made accessible (depending on the need).

Radically new designs possible.

Studying present, past and future (predictive capability).

Cost efficient: computers, software, manpower.

Mathematical Modelling Methodology

VINKO POTOČNIK

ALCAN INTERNATIONAL LTD

JONQUIERE, QUÉBEC, CANADA

Definitions:

System: Assembly of elements acting together with a common goal

Model: Representation of a concrete system in a physical or abstract way

Mathematical model: An abstract model composed of a set of predefined rules that determine the behaviour of the system

Simulation: Solution of the mathematical model by non-analytical means

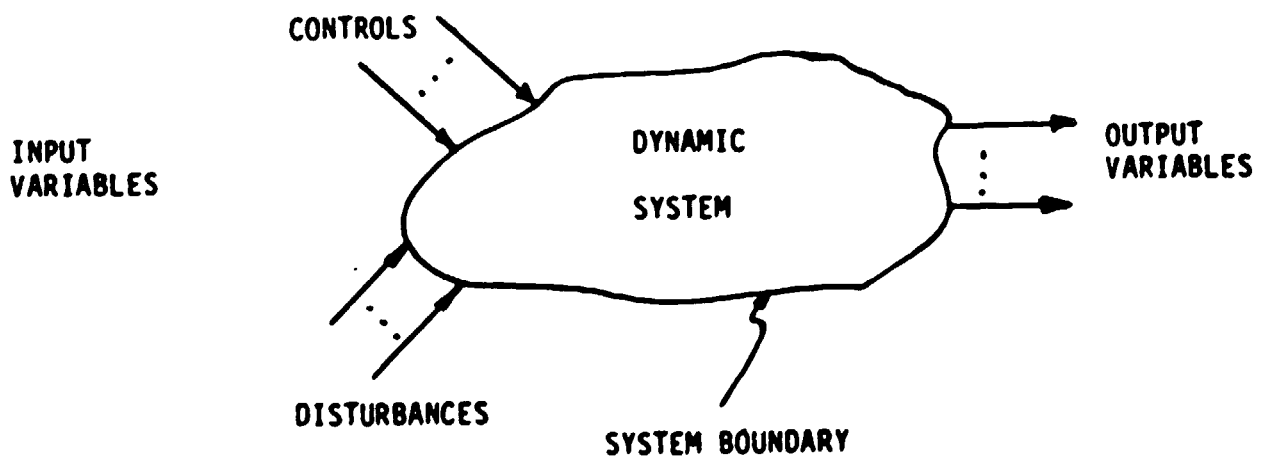


Figure 1.2 Concept of a dynamic system.

Systems concept

A system can be defined as a set or assemblage of entities (elements or components) interrelated to each other and to the whole so as to achieve a common goal.

The emphasis is on the organization of components that act together, and not on the individual elements.

What is a model?

A model is a simplified representation of a system (or process or theory) intended to enhance our ability to understand, predict, and possibly control the behaviour of the system.

Understanding is necessary to change, to preserve, or just to know and explain the behaviour of the system. An understanding of the system may lead to prediction and control while the reverse need not be true. The aim of those involved in fundamental research is to understand the ultimate reality, while others including some modellers are quite satisfied with the prediction and control of the external behaviour of the system even if they cannot explain the underlying principles.

As a minimum, the general set of questions below must be answered before a computer modeling effort is undertaken.

1. **Who** is to use the program?
will develop the model?
will program the model?
will maintain the software?
can authorize resource expenditure for this effort?
2. **What** is the basic objective?
resources will be required?
results can be expected?
range of constraints should it handle?
are the minimum acceptable performance criteria?
language should it be programmed in?
computer should it run on?
3. **Where** is the work to be done?
are the resources needed to complete the job?
4. **When** is the work to commence?
is the work to be completed?
should progress be critically reviewed?
5. **Why** is this simulation model necessary?
isn't it being purchased?
is it being developed in-house?

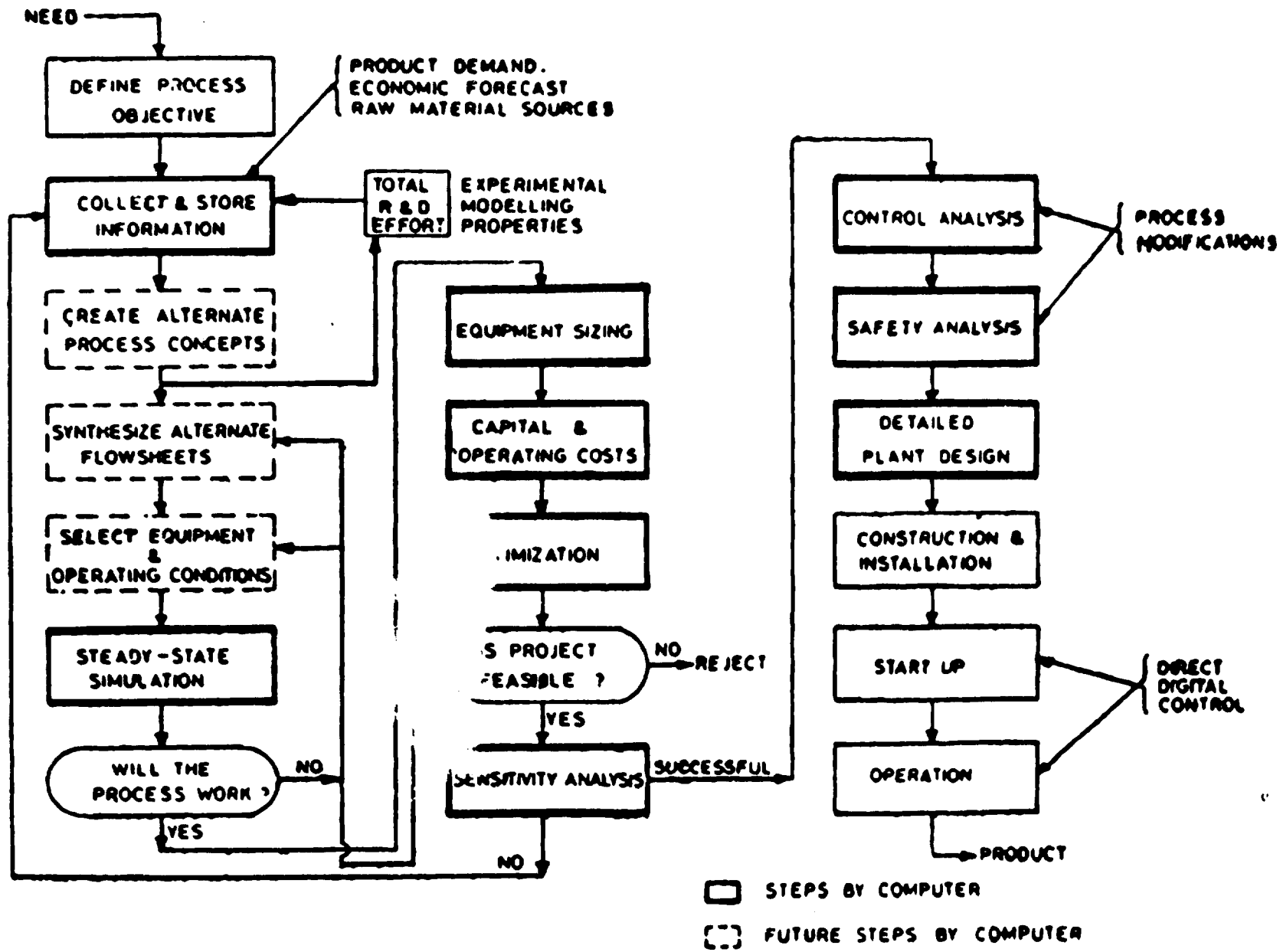
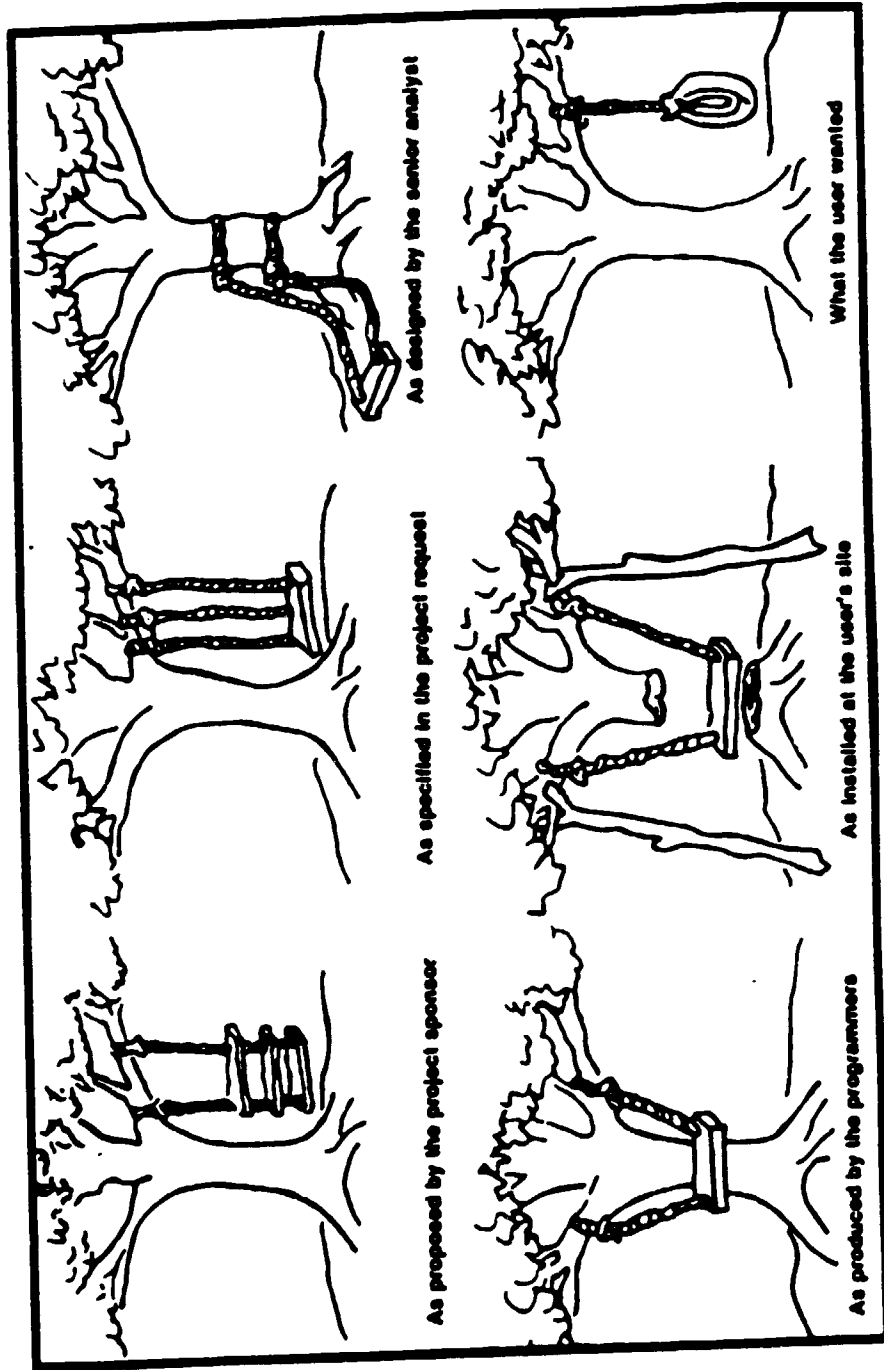


Fig. 1.1. Strategy for Process Engineering.



The systems design procedure

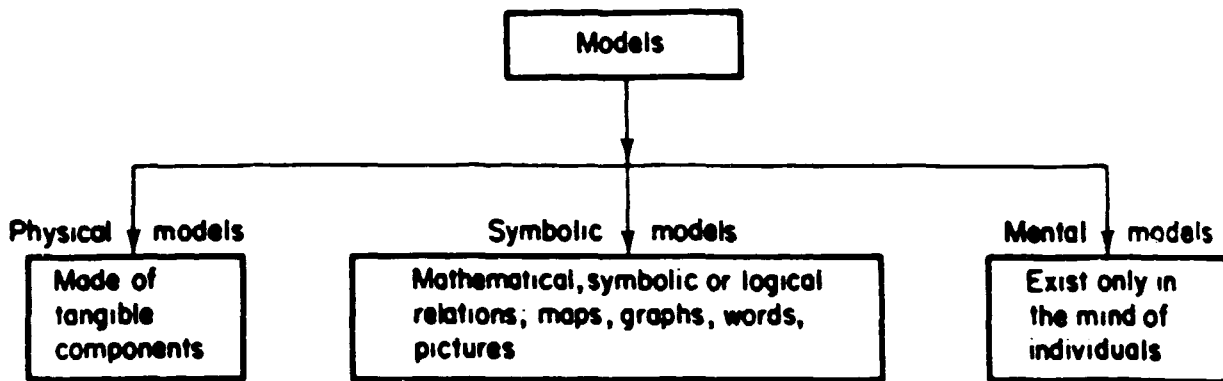


Figure 3.2 Types of models.

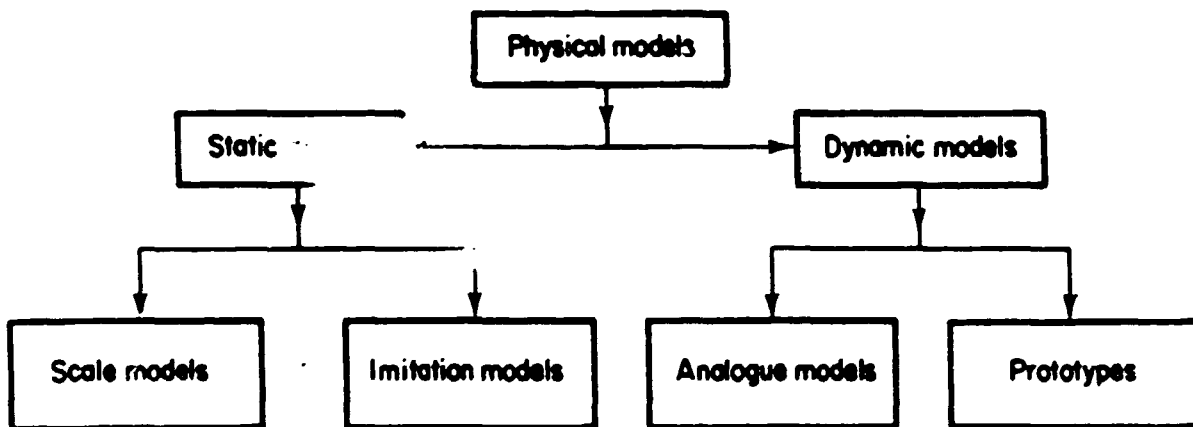


Figure 3.3 Physical models.

MODELS ACCORDING TO PURPOSE

Purpose 1

- Design (new and retrofits)
- Increased understanding

Requires detailed 3D steady-state or dynamic models with all physics

Purpose 2

- Process optimization and control
- Plant personnel training

Requires lumped parameter dynamic models with simplified physics: simulators

MATHEMATICAL MODELING

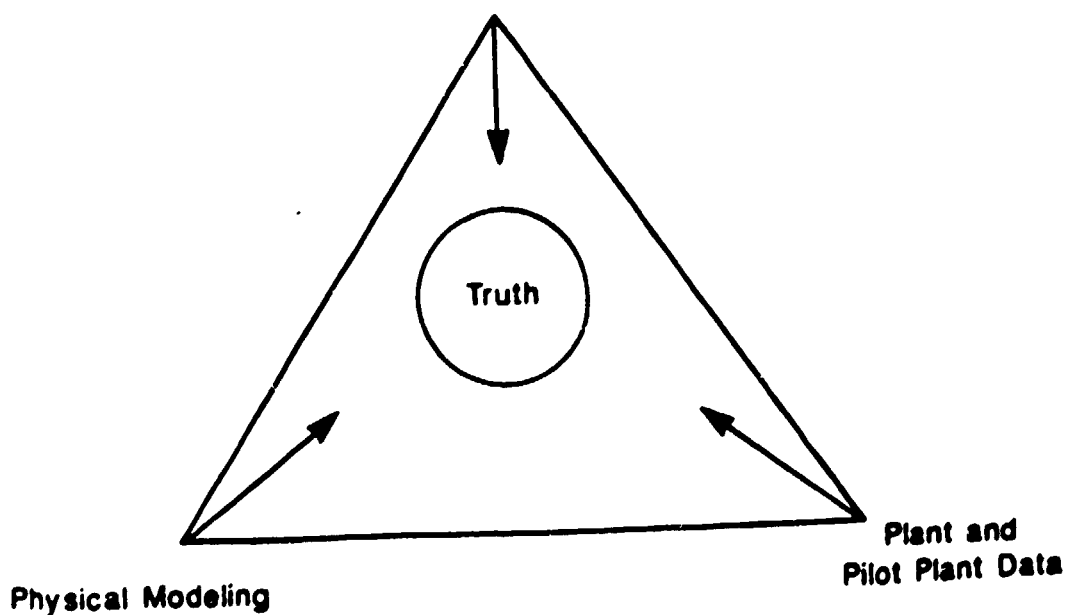
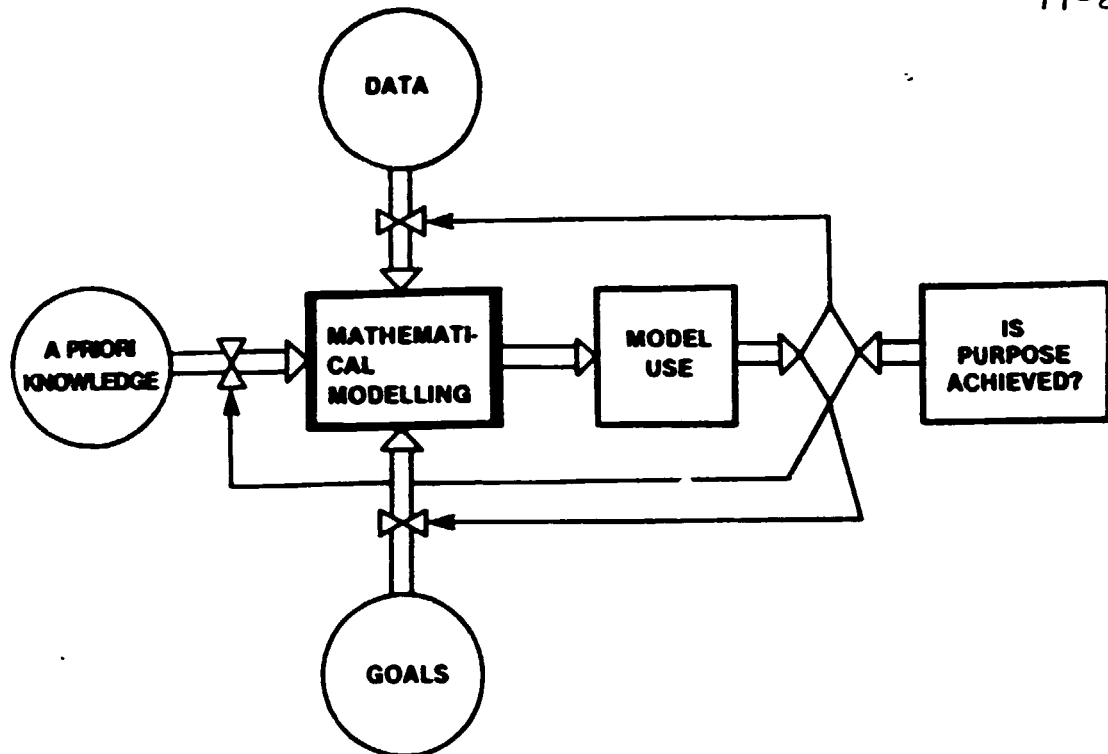
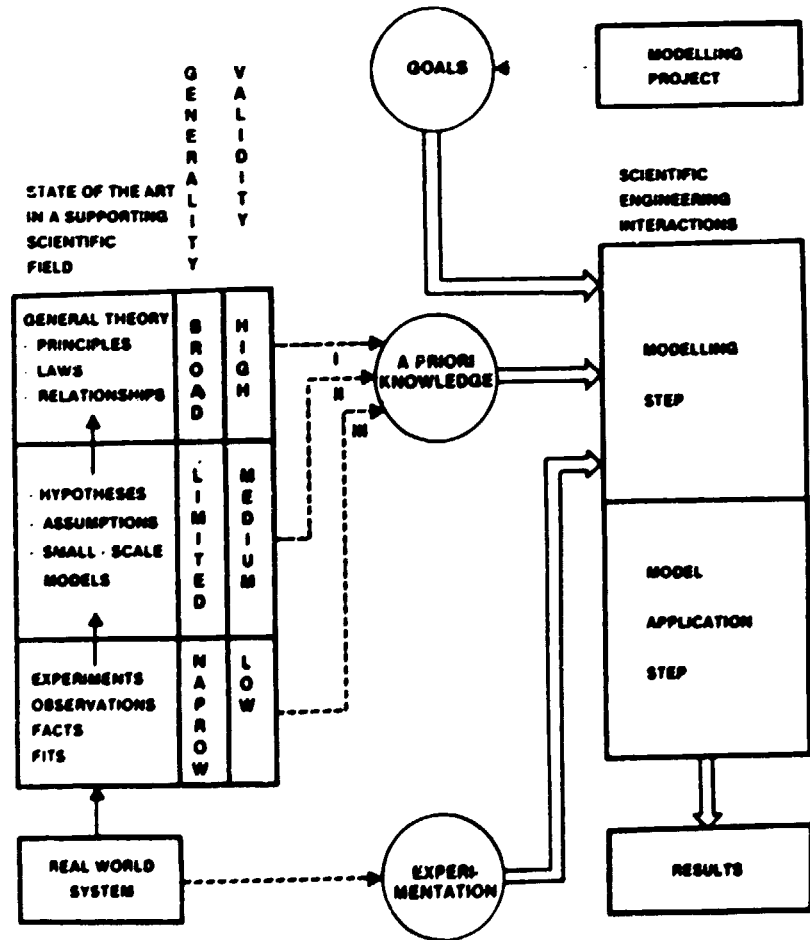


Fig. 3 — The balance between mathematical modeling, physical modeling, and plant-scale experimentation.



Information sources for mathematical modelling



The information environment for scientific-engineering interactions

INDUCTION

GATHER DATA

(EXCITATION/RESPONSE)

- MEASUREMENTS
- OBSERVATIONS
- EXPERIMENTS

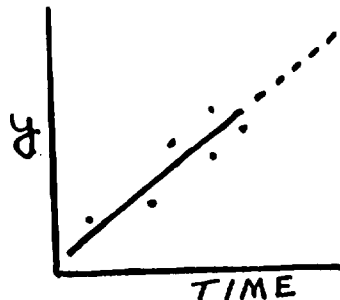
FEATURE EXTRACTION

- CURVE FITTING
- REGRESSION ANALYSIS
- STATISTICS
- PATTERN RECOGNITION

GENERALIZATION

- MODELING

PREDICTION



ANALYSIS MODE.

DEDUCTION

L A W S

- CONSERVATION-CONTINUITY
- (GENERAL TYPE OF EQUATION)

STRUCTURE

- BOUNDARIES
- INTERNAL CAUSAL RELATIONSHIP
- TYPES AND TOPOLOGY OF ELEMENTS
- (SPECIFIC TERMS IN EQUATIONS)

PARAMETERS

- ELEMENT MAGNITUDES
- INITIAL AND BOUNDARY CONDITIONS
- (NUMERICAL VALUES OF COEFFICIENTS)

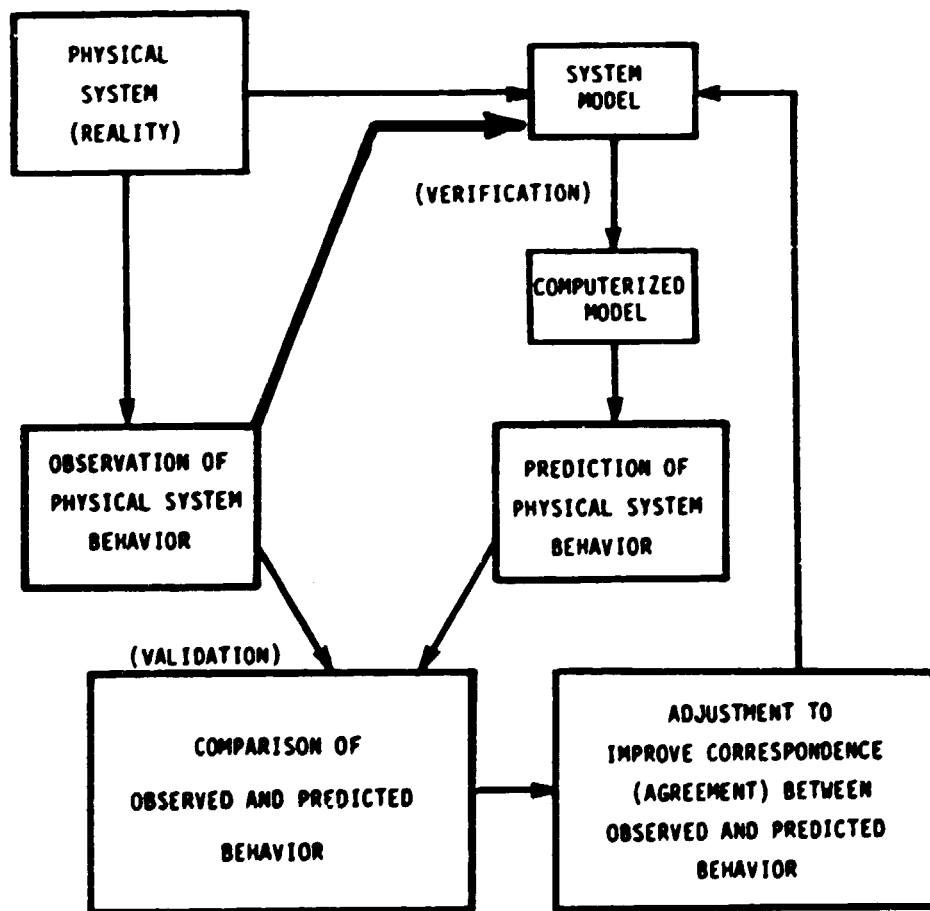
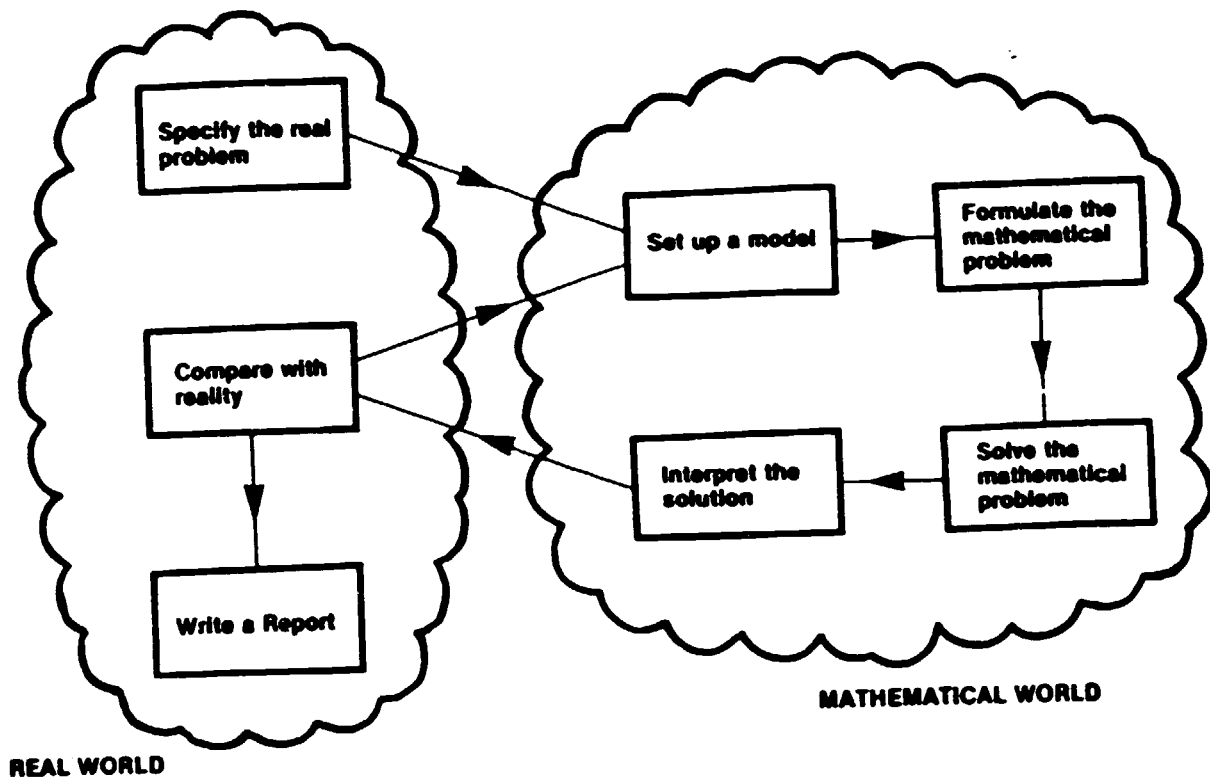
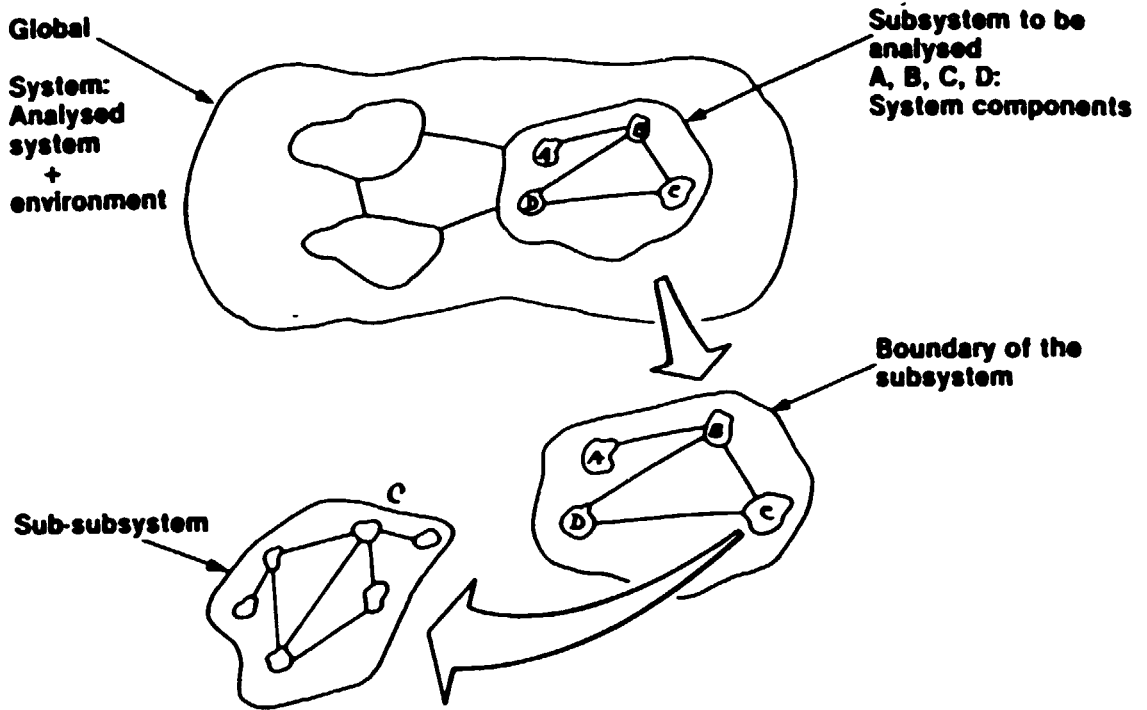


Figure 1.1 Building a credible model.



Hierarchical System Structure: Decomposition of a system into subsystems (Submodelling)

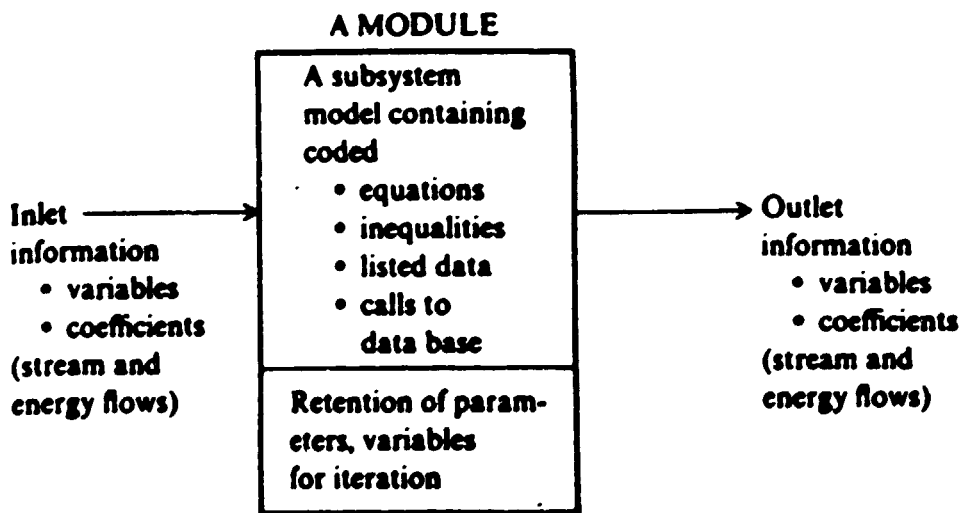
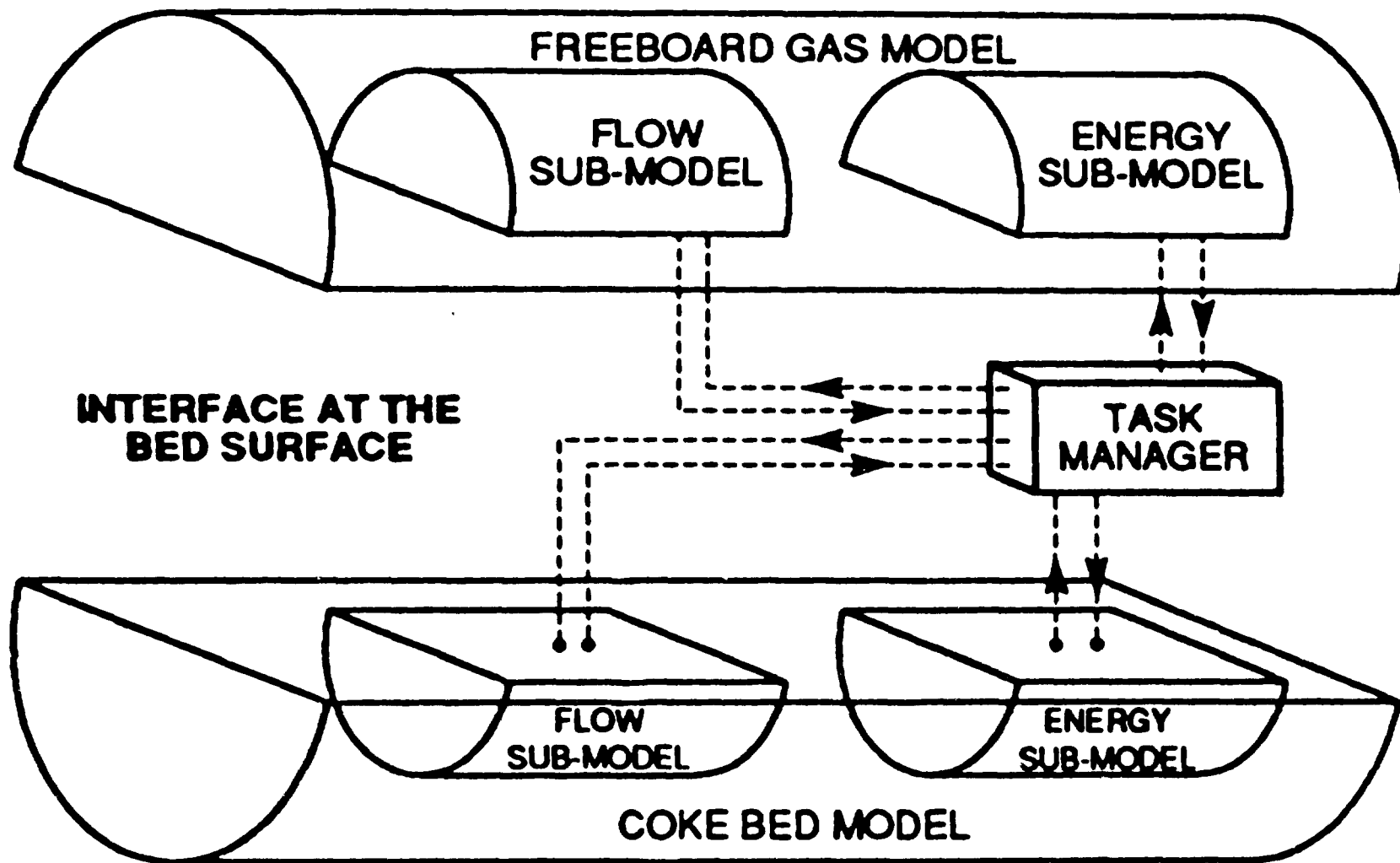


Figure A typical process module showing the necessary interconnections of information.

Model classification

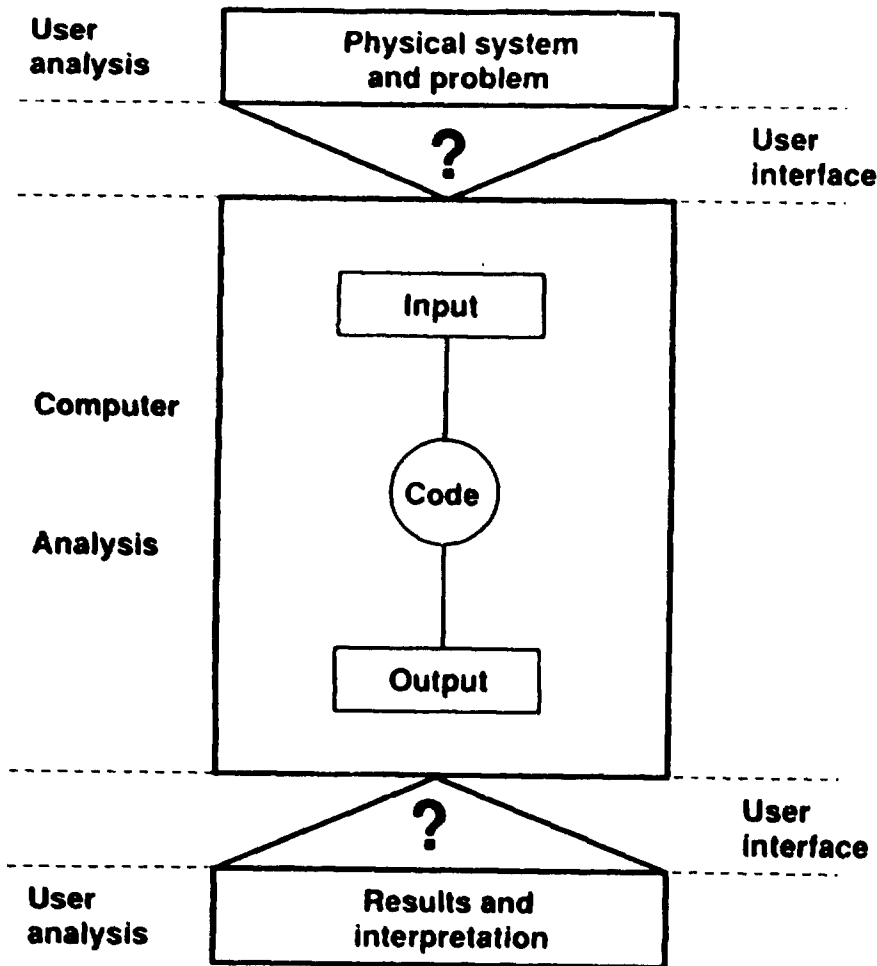
	Model type	Equation type	Examples
Deterministic models	Algebraic or integral	Algebraic	<ul style="list-style-type: none"> • Stationary energy and mass balance • Optimisation
	Lumped parameter	Ordinary differential equations	<ul style="list-style-type: none"> • System dynamics • Control • Optimal control
	Distributed parameter	Partial differential equations	<ul style="list-style-type: none"> • Heat transfer • Diffusion • Fluid flow • Stress analysis
Stochastic or probabilistic models	Continuous time	Probability distributions	<ul style="list-style-type: none"> • Operational research • Job scheduling • Management
	Discrete event	Probability distributions and queuing theory	

M-13



ANALYZING THE HEAT TRANSFER IN A COKE CALCINING KILN

STEPS IN MATHEMATICAL MODELLING



Note: there are two places requiring significant user input. These are labeled by the expression "user interface" in the diagram.

SOFTWARE APPROACH

- Use commercial software
- Enhance it with process specific features
- Validate it on operating units
- Apply it to clients' problems

EXAMPLE

- Remelt/Casting furnace model:
 - PHOENICS is the core
 - Periphery developed by UQAC
- ESTER-PHOENICS:
 - PHOENICS is the core
 - ESTER is a cham addition
 - Electromagnetics added by Alcan

MODEL VISUALISATION

The computer generates a large amount of data, that are very difficult to understand, unless graphics is used to visualize them.

When dynamics of a process is to be represented, static pictures, even if they are in colour do not reveal the dynamic features of the process adequately.

Computer animation solves this problem and can in itself lead to scientific discovery.

Credibility of models

Terminology⁷ for model credibility, developed some years ago, included definitions of reality, conceptual model, domain of intended application of conceptual model, model qualification, computerized model, model verification and model validation, and finally certification and documentation. The distinction between verification and validation is essential. Model verification is the substantiation that a computerized model represents a conceptual model within a specified level of accuracy; model validation is the substantiation that a conceptual model within its domain of applicability possesses a satisfactory range of accuracy consistent with the intended application of the model. Statistical techniques have been suggested and used in the validation of simulation models. Statistical measures of data similarity have been based on correlation coefficient, Theil's Inequality Coefficient, Similarity Coefficient, and other measures.

Some basic questions of concern are:

- (1) Does the simulation model behave as the model builder believes (or expects)?
- (2) Does the simulation model adequately represent the objective(s) of the system developed?
- (3) What is the level of confidence that users have in the model's results?

One should recognize that model validation is not completely separable from model building. Validation techniques should be used during the model building process, which is an iterative process. Thus, confidence in the model is increased from model iteration to model iteration. It is also essential to have system data available if reasonable model confidence is to be obtained. Most recently, the role of model credibility in design of simulators⁷ has been emphasized.

⁷ SCS TECHNICAL COMMITTEE ON MODEL CREDIBILITY
 "Terminology for Model Credibility." *SIMULATION* 32:3 (March 1979),
 103-104.

Simulation Model Verification and Validation

A report prepared by the Futures Research Group of the Congressional Research Service, Library of Congress states: Validation of simulation models have been attempted in at least six ways. These are:

- The degree to which models duplicate past system behavior using historical data,
- The degree to which model behavior conforms to existing and relevant theory,
- The degree to which model accurately forecast future states of the system,
- The degree to which model is found acceptable to other model builders,
- The degree to which model is found acceptable to those who will use it,
- The degree to which model yields opposite results when opposite values are assigned to the variables and opposite relationships are postulated and opposite results are obtained.

The report further states that all these approaches contain flaws and that no one approach can claim it does complete validation. Sargent has reported on several validation techniques that are used to develop confidence in simulation models. These include: face validity, traces, historical method, multi-stage validation, internal validity, parameter variability, comparison to other models, predictive validation, event validity, and sub-model testing. These techniques include both statistical and non-statistical methods [10].

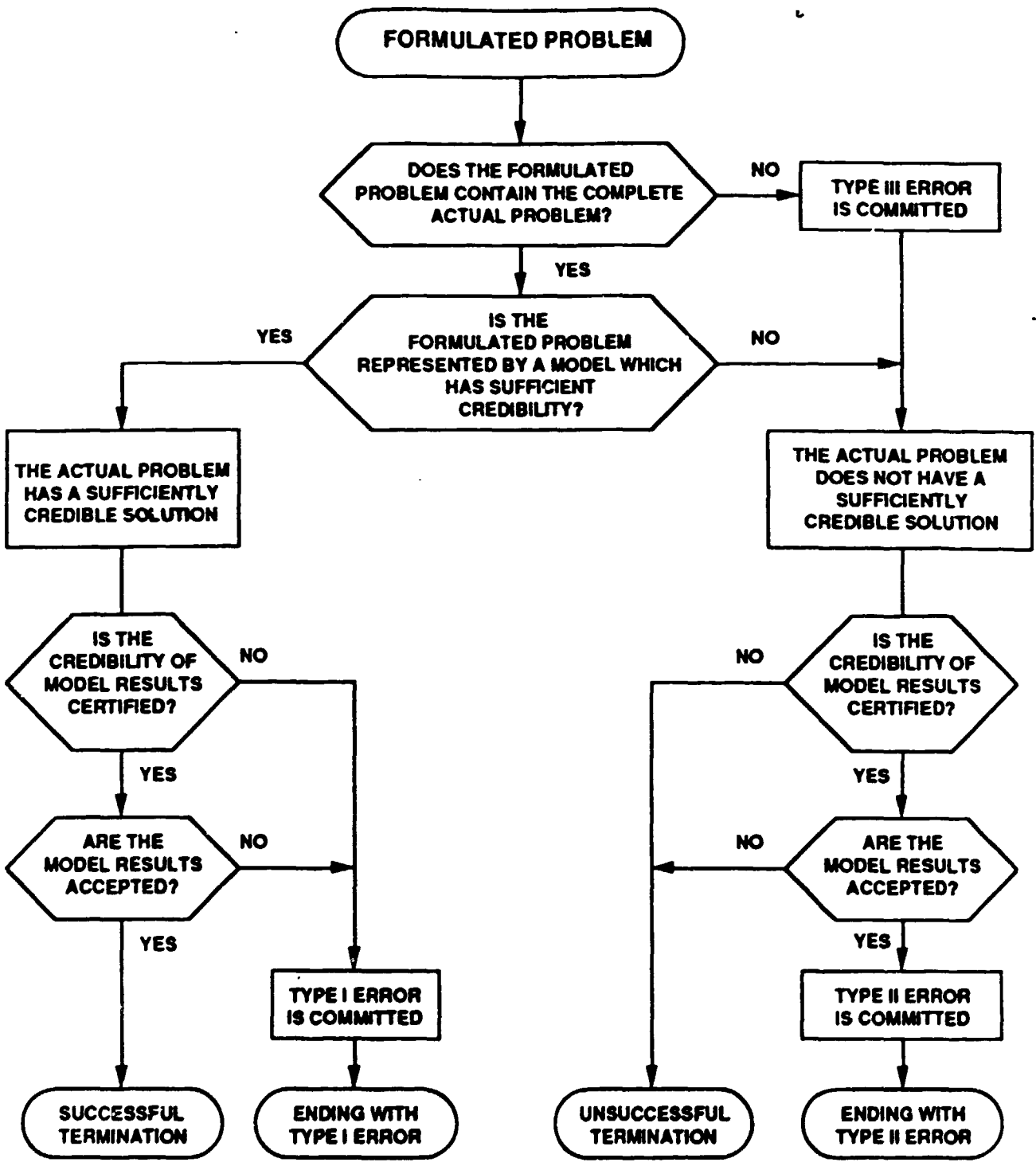
[10] Sargent, Robert G., "Validation of Simulation Models," Proceedings, 1979 Winter Simulation Conference, December 1979, San Diego, CA, Vol. 2, pp. 497-503.

Model Acceptance Problems

- * Misuse of models for purposes of "proving" something or advocating policy rather than for providing insights into cross-disciplinary dependencies.
- * Hidden factors significantly affecting decisions are not communicated to the modeller.
- * Lack of interaction between modeller/user during model development.
- * Focus of modellers on analysis rather than important issues.
- * Failure to integrate model into organizations' information systems.
- * Customers too busy/lazy to understand model.
- * Failure to build model up gradually from mock-up or manual simulation stage.
- * Failure by modeller to prove usefulness of model to client.
- * Inadequate/inappropriate training of modellers.

Conditions for Model Acceptance

- * Model must be very sound.
- * Model must have a good salesperson.
- * Trusted "aides" and decision maker need to participate in model construction process to gain insights necessary to improve decision-making processes.
- * Models must be credible with respect to coherence, correspondence, clarity, and workability.
- * Modellers must be willing to relate findings and methodologies to decision issues and problems as an integral part of an "information system" which includes model, modeller, and uses of model findings.
- * Modeller must effectively communicate results directly to decision maker.



THE OCCURENCE OF ERRORS IN THE MODEL LIFE CYCLE

2-2 FUNDAMENTAL LAWS

2-2.1 Continuity Equations

Total continuity equation (mass balance) The principle of the conservation of mass when applied to a dynamic system says

$$\left(\begin{array}{l} \text{Mass flow} \\ \text{into system} \end{array} \right) - \left(\begin{array}{l} \text{mass flow} \\ \text{out of system} \end{array} \right) = \left(\begin{array}{l} \text{time rate of change} \\ \text{of mass inside system} \end{array} \right) \quad (2-1)$$

The units of this equation are mass per time. Only *one* total continuity equation can be written for one system.

The normal steady-state design equation that we are accustomed to using says "what goes in, comes out." The dynamic version of this says the same thing with the addition of the word "eventually."

The right-hand side of Eq. (2-1) will be either a partial derivative $\partial/\partial t$ or an ordinary derivative d/dt of the mass inside the system with respect to the independent variable, t .

Component continuity equations (component balances) Unlike mass, chemical components are *not* conserved. If a reaction occurs in a system, the number of moles of an individual component will increase if it is a product of the reaction or decrease if it is a reactant. Therefore the component continuity equation for the j th chemical species of the system says

$$\left(\begin{array}{l} \text{Flow of moles of } j\text{th} \\ \text{component into system} \end{array} \right) - \left(\begin{array}{l} \text{flow moles of } j\text{th} \\ \text{component out of system} \end{array} \right) + \left(\begin{array}{l} \text{rate of formation of moles of } j\text{th} \\ \text{component from chemical reaction} \end{array} \right) = \left(\begin{array}{l} \text{time rate of change of moles} \\ \text{of } j\text{th component inside system} \end{array} \right) \quad (2-9)$$

The units of this equation are moles of j per unit time.

The flows in and out can be both convective (due to bulk flow) and molecular (due to diffusion). We can write one component continuity equation for *each* component in the system. If there are J components there are J component continuity equations for any one system. However, the *one* total mass-balance equation and these J component balances are not all independent, since the sum of all the moles times their respective molecular weights equals the total mass. Therefore a given system has only J independent continuity equations. We usually use the total mass-balance and $J - 1$ component balances.

CONSERVATION OF ELECTRIC CHARGE

A fundamental property of the electric charge is the property of *conservation*. Experiments show that no net electric charge can be created or destroyed. Electric charges can be only separated or combined, positive and negative charges always appearing or disappearing in equal quantities.

The conservation of charge is an effect already noted in Section 4-1. It can be expressed mathematically by the *continuity equation*

$$\nabla \cdot \mathbf{J} = -\frac{\partial \rho}{\partial t}. \quad (15-1.1a)$$

This equation represents an experimentally established correlation and constitutes a fundamental law relating a time-variable charge distribution with electric current density.

By means of Gauss's theorem of vector analysis, the continuity equation can be written in an equivalent integral form

$$\oint \mathbf{J} \cdot d\mathbf{S} = -\frac{\partial}{\partial t} \int \rho \, dv. \quad (15-1.1b)$$

This equation shows that whenever the total charge in a given region of space changes, there is a net electric current (conduction, convection, or both) through the surface enclosing the region. Since a conduction or convection current is merely an organized motion of electric charges, the equation also shows that any variation of electric charge within a closed surface is accompanied by an influx or an outflux of electric charges through this surface. The charge contained in the entire universe is thus conserved.

Under steady-state conditions the right-hand parts of Eqs. (15-1.1a) and (15-1.1b) become zero, and these equations reduce to

$$\nabla \cdot \mathbf{J} = 0, \quad \oint \mathbf{J} \cdot d\mathbf{S} = 0.$$

2-2.2 Energy Equation

The first law of thermodynamics puts forward the principle of conservation of energy. Written for a general "open" system (where flow in and out of the system can occur) it is

$$\begin{aligned} & \left(\begin{array}{l} \text{Flow of internal, kinetic, and} \\ \text{potential energy into system} \\ \text{by convection or diffusion} \end{array} \right) - \left(\begin{array}{l} \text{flow of internal, kinetic, and} \\ \text{potential energy out of system} \\ \text{by convection or diffusion} \end{array} \right) \\ & + \left(\begin{array}{l} \text{heat added to system by} \\ \text{conduction, radiation, and} \\ \text{reaction} \end{array} \right) - \left(\begin{array}{l} \text{work done by system on} \\ \text{surroundings (shaft work)} \\ \text{+ } P\bar{V} \text{ work} \end{array} \right) \\ & = \left(\begin{array}{l} \text{time rate of change of internal, kinetic,} \\ \text{and potential energy inside system} \end{array} \right) \end{aligned} \quad (2-18)$$

In most chemical engineering systems the general form reduces, as we will show, to essentially an enthalpy balance.

2-2.3 MOMENTUM EQUATION

Newton's second law of motion is usually expressed for a system as

$$\Sigma F = \frac{d}{dt} (mv)$$

in which it must be remembered that m is the constant mass of the system. ΣF refers to the resultant of all external forces acting on the system, including body forces such as gravity, and v is the velocity of the center of mass of the system.

This says that the time rate of change of momentum in the i direction (mass times velocity in the i direction) is equal to the net sum of the forces pushing in the i direction. It can be thought of as a force balance. Or more eloquently it is called the *conservation of momentum*.

EQUILIBRIUM OF FORCES IN STATICS.

$$\Sigma \vec{F} = 0$$

2-2.5 Equations of State

To write mathematical models we need equations that tell us how the physical properties, primarily density and enthalpy, change with temperature, pressure, and composition.

$$\begin{aligned}
 \text{Liquid density} &= \rho_L = f_{i,p,T,z,i} \\
 \text{Vapor density} &= \rho_v = f_{i,p,T,z,i} \\
 \text{Liquid enthalpy} &= h = f_{i,p,T,z,i} \\
 \text{Vapor enthalpy} &= H = f_{i,p,T,z,i}
 \end{aligned}
 \tag{2-46}$$

Occasionally these relationships have to be fairly complex to describe the system accurately. But in many cases simplification can be made without sacrificing much overall accuracy. We have already used some simple enthalpy equations in the examples of energy balances.

$$\begin{aligned}
 h &= C_p T \\
 H &= C_p T + \lambda_v
 \end{aligned}
 \tag{2-47}$$

The next level of complexity would be to make the C_p 's functions of temperature:

$$h = \int_{T_0}^T C_{p(T)} dT \tag{2-48}$$

A polynomial in T is often used for C_p .

$$C_{p(T)} = A_1 + A_2 T \tag{2-49}$$

Then Eq. (2-48) becomes

$$\begin{aligned}
 h &= A_1 T + A_2 \frac{T^2}{2} \Big|_{T_0}^T = A_1(T - T_0) + \frac{A_2}{2}(T^2 - T_0^2) \\
 &= A_3 + A_4 T + A_5 T^2
 \end{aligned}
 \tag{2-50}$$

Of course, with mixtures of components the total enthalpy is needed. If heat-of-mixing effects are negligible the pure-component enthalpies can be averaged:

$$h = \frac{\sum_{j=1}^J x_j h_j M_j}{\sum_{j=1}^J x_j M_j} \tag{2-51}$$

where x_j = mole fraction of j th component

M_j = molecular weight of j th component, lb_m/mole

h_j = pure-component enthalpy of j th component, Btu/lb_m

The denominator of Eq. (2-51) is the average molecular weight of the mixture.

Liquid densities can be assumed constant in many systems unless large changes in composition and temperature occur.

Vapor densities usually cannot be considered invariant and some sort of PVT relationship is almost always required. The simplest and most often used is the perfect-gas law:

$$PV = nRT \tag{2-52}$$

where P = absolute pressure, lb_f/ft²

V = volume, ft³

n = number of moles

R = constant = 1.545 lb_f-ft/mole-°R

T = absolute temperature, °R

2-2.6 Equilibrium

The second law of thermodynamics is the basis for the equations that tell us the conditions of a system when equilibrium conditions prevail.

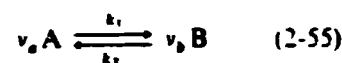
Chemical equilibrium Equilibrium occurs in a reacting system when

$$\sum_{j=1}^J v_j \mu_j = 0 \quad (2-54)$$

where v_j = stoichiometric coefficient of j th component with reactants having a negative sign and products a positive sign

μ_j = chemical potential of j th component

The usual way to work with this equation is in terms of an equilibrium constant for a reaction. For example, consider a reversible gas-phase reaction of A to form B at a specific reaction rate k_1 and B reacting back to A at a specific reaction rate k_2 . The stoichiometry of the reaction is such that v_a moles of A react to form v_b moles of B.



Equation (2-54) says equilibrium will occur when

$$v_b \mu_B - v_a \mu_A = 0 \quad (2-56)$$

The chemical potentials for a perfect-gas mixture can be written¹

$$\mu_j = \mu_j^0 + RT \ln \mathcal{P}_j \quad (2-57)$$

where μ_j^0 = standard chemical potential (or Gibbs free energy per mole) of j th component, which is a function of temperature only

\mathcal{P}_j = partial pressure of j th component

R = perfect-gas constant

T = absolute temperature

Substituting into Eq. (2-56),

$$\begin{aligned} v_b(\mu_B^0 + RT \ln \mathcal{P}_B) - v_a(\mu_A^0 + RT \ln \mathcal{P}_A) &= 0 \\ RT \ln \mathcal{P}_B^{v_b} - RT \ln \mathcal{P}_A^{v_a} &= v_a \mu_A^0 - v_b \mu_B^0 \\ \ln \left(\frac{\mathcal{P}_B^{v_b}}{\mathcal{P}_A^{v_a}} \right) &= \frac{v_a \mu_A^0 - v_b \mu_B^0}{RT} \end{aligned} \quad (2-58)$$

The right-hand side of this equation is a function of temperature only. The term in parentheses on the left-hand side is defined as the equilibrium constant K_p , and it tells us the equilibrium ratios of products and reactants.

$$K_p = \frac{\mathcal{P}_B^{v_b}}{\mathcal{P}_A^{v_a}} \quad (2-59)$$

Phase equilibrium Equilibrium between two phases occurs when the chemical potential of each component is the same in the two phases:

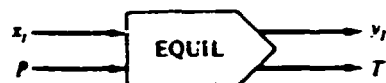
$$\mu_j^I = \mu_j^{II} \quad (2-60)$$

where μ_j^I = chemical potential of j th component in phase I

μ_j^{II} = chemical potential of j th component in phase II

Since the vast majority of chemical engineering systems involve liquid and vapor phases, many vapor-liquid equilibrium relationships are used. They range from the very simple to the very complex. Some of the most commonly used relationships are listed below. More detailed treatments are presented in many thermodynamics texts.

Basically we need a relationship that permits us to calculate the vapor composition if we know the liquid composition, or vice versa. The most common problem is a *bubble-point* calculation: Given the pressure P of a system and the liquid composition x_j , we want to calculate the temperature of the system and the vapor composition y_j . This usually involves a trial-and-error, iterative solution because the equations can be solved explicitly only in the simplest cases.



Sometimes we know x_j and T and want to find P and y_j , or we know y_j and P (or T) and want to find x_j and T (or P).

We will assume ideal vapor-phase behavior in our examples, i.e., the partial pressure of the j th component in the vapor is equal to the total pressure P times the mole fraction of the j th component in the vapor y_j (Dalton's law):

$$P_j = P y_j \quad (2-61)$$

Corrections may be required at high pressures.

1 *Raoult's law*: Liquids that obey Raoult's law are called *ideal*.

$$P = \sum_{j=1}^J x_j P_j^0 \quad (2-62)$$

$$y_j = \frac{x_j P_j^0}{P} \quad (2-63)$$

where P_j^0 is the vapor pressure of the pure j th component. Vapor pressures are functions of temperature only. This dependence is often described by

$$\ln P_j^0 = \frac{A_j}{T} + B_j \quad (2-64)$$

2-2.7 Chemical Kinetics

We will be modeling many chemical reactors, and we must be familiar with the basic relationships and terminology used in describing the kinetics (rate of reaction) of chemical reactions. For more details, consult one of the several excellent texts in this field.¹

Arrhenius temperature dependence The temperature dependence of a specific reaction rate, k , is usually found to be exponential:

$$k = ze^{-E/RT} \quad (2-69)$$

where k = specific reaction rate (units to be defined below)

z = preexponential factor (units same as k), a constant

E = activation energy (Btu/mole): shows the temperature dependence of the reaction rate, i.e., the bigger E , the faster k increases with temperature

T = absolute temperature, °R

R = perfect-gas constant (1.99 Btu/mole-°R)

This exponential temperature dependence represents one of the most severe nonlinearities in chemical engineering systems. Keep in mind that the "apparent" temperature dependence of a reaction may not be exponential if the reaction is mass-transfer limited, not chemical-rate limited. If both zones are encountered in the operation of the reactor, the mathematical model must obviously include both reaction-rate and mass-transfer effects.

Law of mass action Using the conventional notation, we will define an overall reaction rate \mathcal{R} as the rate of change of moles of any component per unit volume due to chemical reaction divided by that component's stoichiometric coefficient.

$$\mathcal{R} = \frac{1}{\nu_j V} \left(\frac{dn_j}{dt} \right)_R \quad \diamond \quad \frac{\text{moles component } j}{\text{sec-ft}^3} \quad (2-70)$$

The stoichiometric coefficients ν_j are positive for products of the reaction and negative for reactants. Note that \mathcal{R} is an intensive property and can be applied to systems of any size. For example, assume we are dealing with an irreversible reaction in which components A and B react to form components C and D.



Then

$$\begin{aligned} \mathcal{R} &= \frac{1}{-\nu_a V} \left(\frac{dn_A}{dt} \right)_R = \frac{1}{-\nu_b V} \left(\frac{dn_B}{dt} \right)_R \\ &= \frac{1}{\nu_c V} \left(\frac{dn_C}{dt} \right)_R = \frac{1}{\nu_d V} \left(\frac{dn_D}{dt} \right)_R \end{aligned} \quad (2-71)$$

The law of mass action says that the overall reaction rate \mathcal{R} will vary with temperature (since k is temperature-dependent) and with the concentration of reactants raised to some powers.

$$\mathcal{R} = k_{(T)} C_A^a C_B^b \quad (2-72)$$

where C_A = concentration of component A, moles of A/ft³

C_B = concentration of component B, moles of B/ft³

The constants a and b are not, in general, equal to the stoichiometric coefficients ν_a and ν_b .

The reaction is said to be first order in A if $a = 1$. It is second order in A if $a = 2$. The constants a and b can be fractions.

Fundamental principles used in engineering design problems

Fundamental Principle	Dependent Variable	Independent Variable	Parameters
Heat balance	Temperature	Time and position	Thermal properties of material and geometry of system
Mass balance	Concentration or quantity of mass	Time and position	Chemical behavior of material, mass transfer coefficients, and geometry of system
Force balance	Magnitude and direction of forces	Time and position	Strength of material, structural properties, and geometry of system
Energy balance	Changes in the kinetic- and potential-energy states of the system	Time and position	Thermal properties, mass of material, and system geometry
Newton's laws of motion	Acceleration, velocity, or location	Time and position	Mass of material, system geometry, and dissipative parameters such as friction or drag
Kirchhoff's laws	Currents and voltages in electric circuits	Time	Electrical properties of systems such as resistance, capacitance, and inductance

M-27

The Building Blocks of Mathematical Models

Component	Application	Remarks
Navier-Stokes equations Fourier's Law	fluid flow heat conduction	complex vector-tensor manipulation relatively simple, more complex if phase change is involved
Fick's Law	diffusion	simple for one component, very complex for multi-component systems
Convective transport Maxwell's equations	heat and mass transfer electrodynamics MHD	combines fluid flow, heat and/or mass transfer very complex problems, <i>i.e.</i> , plasmas, induction furnaces, <i>etc.</i>
Thermodynamics Kinetics Constitutive relationships	equilibria phase diagrams rate predictions deformation processing	often routine calculations needs experimental input very complex, needs realistic input

Examples of fundamental laws that are written in terms of the rate of change of variables (t = time and x = position).

Law	Mathematical Expression	Variables and Parameters
Newton's second law of motion	$\frac{dv}{dt} = \frac{F}{m}$	Velocity (v), force (F), and mass (m)
Fourier's heat law	Heat flux = $-k \frac{dT}{dx}$	Thermal conductivity (k) and temperature (T)
Fick's law of diffusion	Mass flux = $-D \frac{dc}{dx}$	Diffusion coefficient (D) and concentration (c)
Faraday's law (describes voltage drop across an inductor)	Voltage drop = $L \frac{di}{dt}$	Inductance (L) and current (i)

Source : Chapra , Canale , 1988

A FAMILY PORTRAIT OF FIELD PROBLEMS

From the master equation which relates the external influence (E_i) to the primary unknown u_p , through the generic stiffness matrix $[K]$ we solve for the primary unknown:

Start with

$$\{E_i\} = \begin{bmatrix} \text{Generic} \\ K \end{bmatrix} \{u_p\}$$

and solve,

$$\{u_p\} = \begin{bmatrix} \text{Generic} \\ K \end{bmatrix}^{-1} \{E_i\}$$

Then, find the secondary unknowns or SU . They are almost always derived by calculating the

rate of change of u_p , with respect to a geometry variable and multiplied by the material property description

$$SU = (MPD) \frac{\Delta(u_p)}{\Delta(x)}$$

or in calculus terms,

$$SU = (MPD) \frac{d u_p}{d x}$$

In addition, SU may be predictor (a series of values). Thus, MPD will be full equation is

$$\{SU\} = \{MPD\} \left\{ \frac{\Delta u_p}{\Delta x} \right\}$$

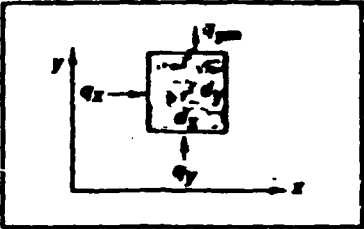
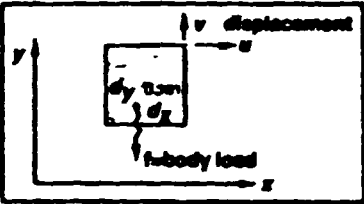
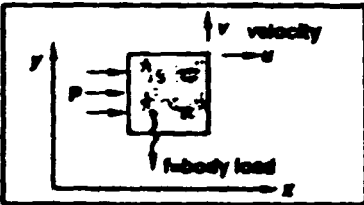
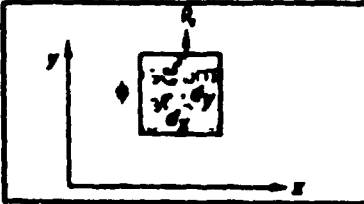
A classic example is where SU is the stress vector and is comprised of $\sigma_x, \sigma_y, \sigma_z, \tau_{xy}, \tau_{yz}, \tau_{zx}$.

The 3D world is similar except that primary unknowns have three components. For instance, in solid mechanics displacements are labeled u, v, w , for three orthogonal directions. Thus, the primary unknown,

$$\{u_p\} = \begin{Bmatrix} u \\ v \\ w \end{Bmatrix}$$

The family portrait

Discipline	Primary unknown, u_p	Material property description, MPD	Derived secondary unknown, u_s
Heat transfer	Temperature, T	Thermal conductivity, k	Heat flux, q'' $q'' = -k \frac{dT}{dx}$
Solid mechanics	Displacement, u	Young's modulus, E	Stress, σ $\sigma = E \frac{du}{dx}$ <i>(du/dx is better known as strain, ϵ)</i>
Fluid mechanics	Velocity, V	Viscosity, μ	Shear stress, τ $\tau = \mu \frac{dV}{dy}$
Pressure, P , is a bit different. Neglect inertia and pressure becomes a primary unknown. Otherwise, pressure is a secondary unknown, $p = -\lambda dV/dx$, where λ is a constant.			
Electrostatics	Electrostatic potential, ϕ (volts)	Permittivity, ϵ Conductivity, σ	Electric displacement, D Current density $D = -\epsilon \frac{d\phi}{dx}$ $j = -\sigma \frac{d\phi}{dx}$

Application	Conservation or balance	Partial differential equations
HEAT TRANSFER Properties: k = conductivity ρ = mass density c = specific heat	CONSERVATION OF ENERGY $Heat_{in} + heat_{generated} = heat_{out} + energy_{stored}$	$\frac{\partial^2 T}{\partial x^2} + \frac{\partial^2 T}{\partial y^2} + \frac{\dot{q}_{gen}}{k} = \frac{\rho c}{k} \frac{\partial T}{\partial t}$
	EQUILIBRIUM (Balance of forces)	$\frac{E}{1-\nu^2} \frac{\partial^2 u}{\partial x^2} + \frac{E}{2(1-\nu)} \frac{\partial^2 v}{\partial x \partial y} + \frac{E}{2(1+\nu)} \frac{\partial^2 u}{\partial y^2} = -f_x$
SOLID MECHANICS Properties: ν = Poisson's ratio E = Young's modulus	Sum of forces in x and y directions = 0	$\frac{E}{1-\nu^2} \frac{\partial^2 v}{\partial y^2} + \frac{E}{2(1-\nu)} \frac{\partial^2 u}{\partial x \partial y} + \frac{E}{2(1+\nu)} \frac{\partial^2 v}{\partial x^2} = -f_y$
	FLUID MECHANICS Properties: μ = viscosity ρ = mass density p = pressure	CONSERVATION OF MOMENTUM (Newton's 2nd law)
	Net force = Rate of change of momentum	$\rho \left[\frac{\partial u}{\partial t} + u \frac{\partial u}{\partial x} + v \frac{\partial u}{\partial y} \right] - \mu \left[\frac{\partial^2 u}{\partial x^2} + \frac{\partial^2 u}{\partial y^2} \right] + \frac{\partial p}{\partial x} = f_x$
Rate of momentum _{in} + Rate of momentum _{gen} = Rate of momentum _{out} + Net forces	$\rho \left[\frac{\partial v}{\partial t} + u \frac{\partial v}{\partial x} + v \frac{\partial v}{\partial y} \right] - \mu \left[\frac{\partial^2 v}{\partial x^2} + \frac{\partial^2 v}{\partial y^2} \right] + \frac{\partial p}{\partial y} = f_y$	
ELECTROSTATIC FIELDS Properties: φ = voltage potential ε = dielectric constant ρ = charge/volume	CONSERVATION OF ELECTRIC CHARGE (Gauss' Law)	$\epsilon \frac{\partial^2 \phi}{\partial x^2} + \epsilon \frac{\partial^2 \phi}{\partial y^2} = \rho$
	Electric flux passing through a surface =	Total charge enclosed by the surface

**THREE DIMENSIONAL ANALYSIS OF
THERMO-ELECTRIC AND
MECHANICAL BEHAVIOUR OF
ALUMINIUM REDUCTION CELLS**

Vinko Potočnik

**Alcan International Limited
Jonquiere, Quebec, Canada**

PURPOSE

To design the cathodes and the anodes so that they provide:

- chosen operating bath temperature,
- freeze on side-walls,
- long cathode life.

MEANS

Choose a commercial finite element program (ANSYS or similar) and adapt it for the purpose.

REQUIREMENTS: TEHRMO-ELECTRIC MODEL

- Every material to be represented.
- Temperature dependent properties.
- Freeze to be calculated (moving boundary).
- Thermal and electrical problems coupled.

$$\rho c_p \frac{\partial T}{\partial t} = \text{div}(k \text{grad} T) + \frac{\vec{j}^2}{\sigma}$$

$$\nabla^2 V = 0$$

$$\vec{j} = -\sigma \nabla V$$

- Fluid-solid boundaries represented with heat transfer coefficients:

- bath/metal to freeze/carbon,
- external surfaces to air.

REQUIREMENTS: MECHANICAL MODEL

- Stress and deformation to be calculated.
- Some criterion of strength needed.
- Thermal and sodium expansion to be considered.
- Predict at least early failures due to carbon cracking (anodes, cathodes).
- Predict plastic (permanent) deformation of the cathode shell. Design enough strength to avoid permanent deformation (for easy relining and minimum repair in the next life cycles).

PROBLEMS ENCOUNTERED: THERMAL/ELECTRICAL

- Heat transfer coefficients (HTC) between bath/metal and freeze/cathode carbon.
 - Use semi empirical coefficients derived from the combination measurements-models.
- Radiation from external boundaries.
 - Represent radiation with heat transfer coefficients, but this makes HTC's highly temperature dependent.
- How to represent cradles (complicated geometry)?
 - Use an increased HTC to avoid too many elements.
- Electrical contact resistances between steel and carbon.
 - Use empirical data.
- Large models.
 - Use submodels.
 - Exploit symmetry.

PROBLEMS ENCOUNTERED: MECHANICAL

- How to represent shell and cradles?
 - Use many small elements.
- How to represent gaps between materials?
 - In anodes: stud-carbon.
 - In cathodes: collector-bar carbon, brick-carbon block, inter-brick.
 - Use gap elements.
- Sodium swelling not well known: difficult to get good data.
 - Use what is best available.
- What strength criterion to use?
 - Energy method with Von Mises stress.
- Model size.
 - Exploit symmetry.

Magnetohydrodynamics (MHD) of Aluminum Electrolytic Cells

VINKO POTOČNIK

**ALCAN INTERNATIONAL LIMITED
Arvida Research and Development Centre
Jonquière, Québec**

Magneto hydrodynamics (MHD) of Aluminum Electrolytic Cells

A. What is MHD?

B. Why to be concerned with it?

C. How to apply it (to electrolytic cells)?

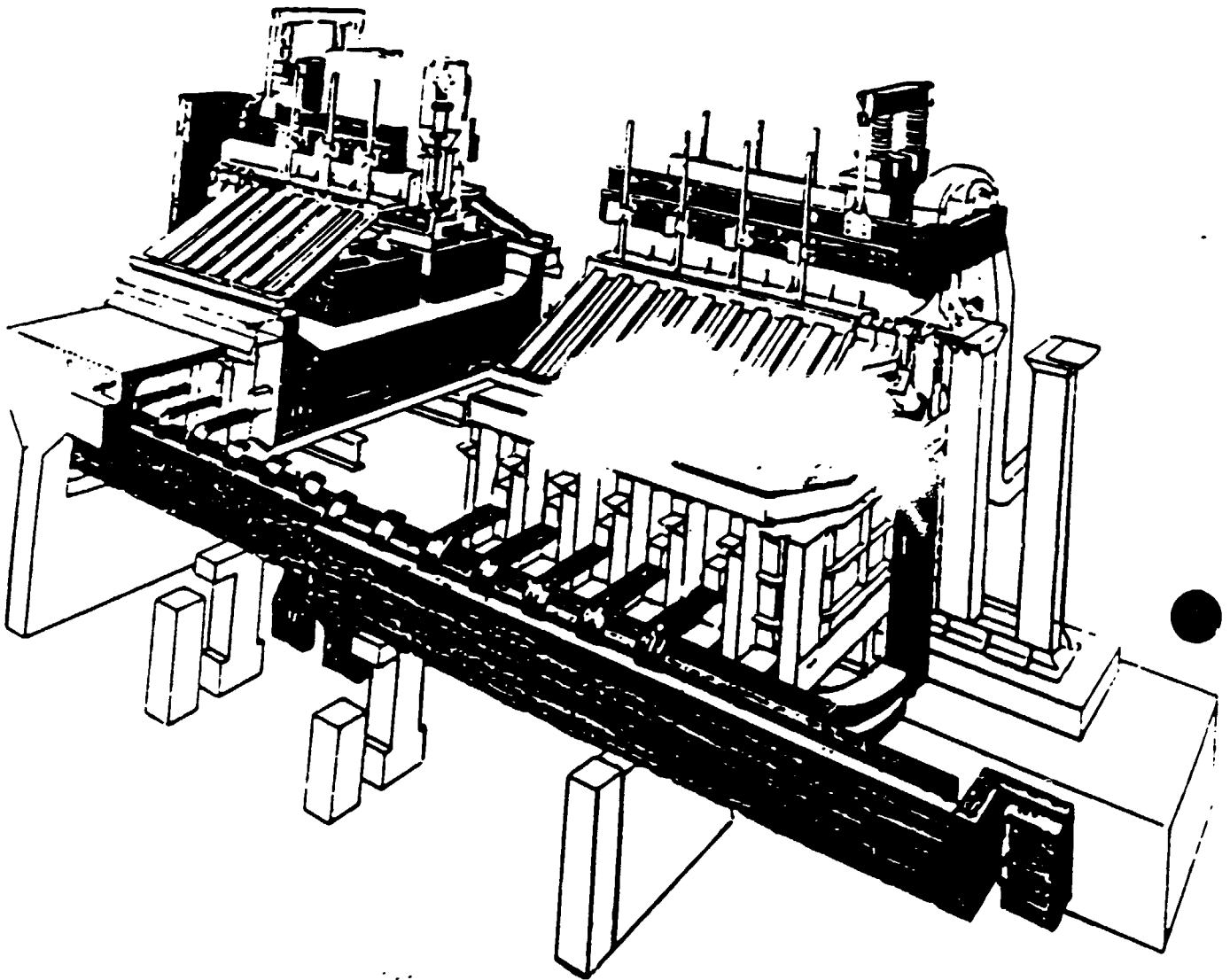


Figure 2: A Modern End-to-End Cell

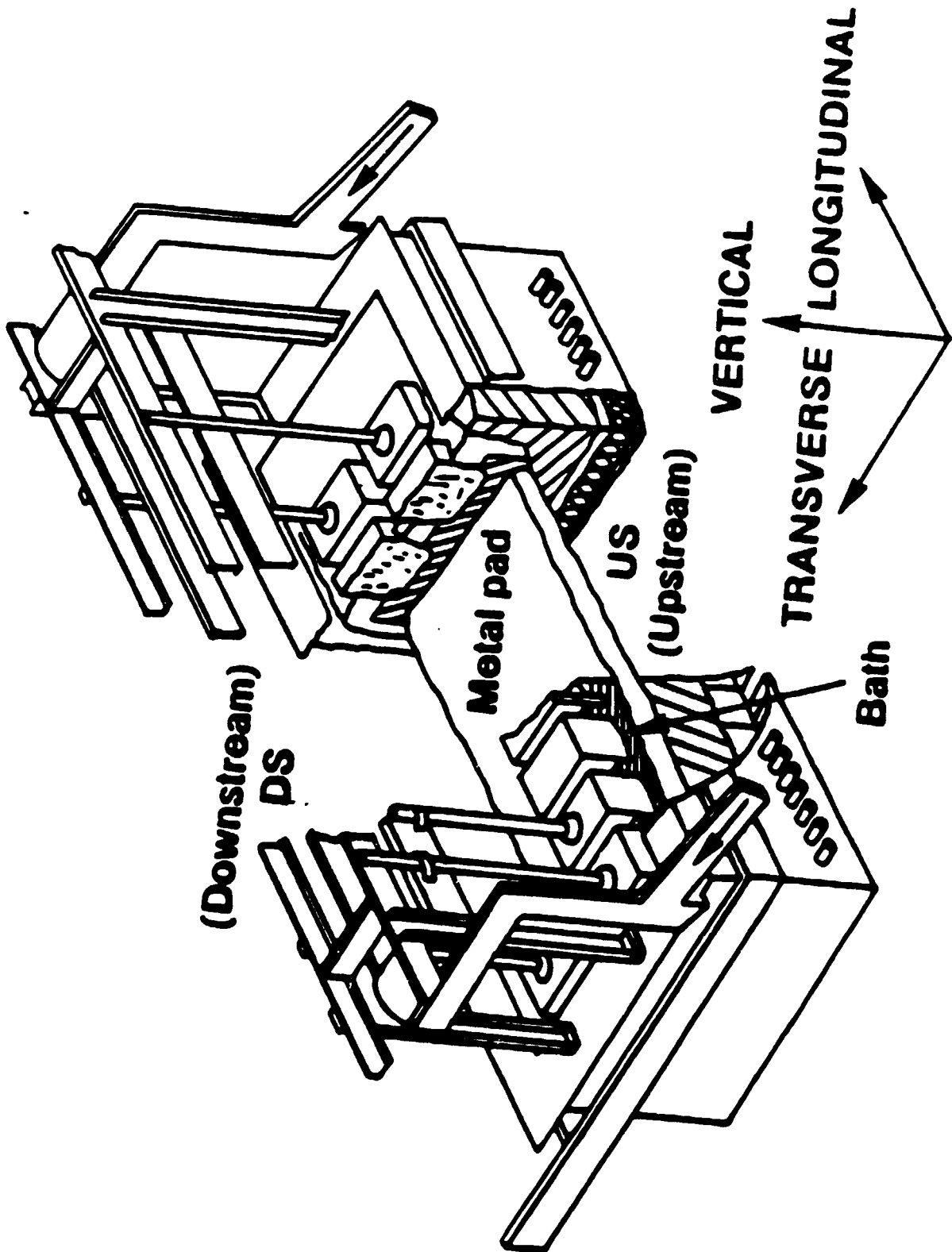


Figure 2 - Sketch of Cell

INTRODUCTION

This lecture will deal with those phenomena of electromagnetics that are encountered in aluminum electrolysis. Examples of these phenomena are: Electric current distribution inside and outside the cells, magnetic forces, metal and bath motion, and interface disturbances. Practical and theoretical efforts to alleviate the undesired effects of electromagnetic nature will be presented and illustrated with experimental results and current and past practice in the magnetics design of the aluminum electrolytic cells.

ELECTROMAGNETIC FORCES

Magnetic fields are a result of electric currents. As the currents in the aluminum electrolysis are very large, the magnetic fields are appreciable in a wide space around the current conductors. We are particularly concerned with the magnetic fields in the metal and bath because there they interact with electric currents to produce a force that disturbs the metal and bath. Since the currents are DC the resulting field is magnetostatic.

The electric current outside the cells is at a large enough distance from the metal pool so that we need not consider its distribution inside a busbar, but only the total current flowing in it, as if it flowed only in a thin conductor at its center. In the cell, however, and for our purposes in the metal and bath, we have to consider a de-

tailed current distribution, expressed as the current density distribution $\vec{j}(x,y,z)$ in A/m^2 .

A unit volume of fluid experiences the following electromagnetic force:

$$\vec{f}_{EM} = \vec{j} \times \vec{B}, \quad (1)$$

where: \vec{f} = force density in N/m^3 ,

\vec{j} = electric current density in A/m^2 ,

\vec{B} = magnetic induction or magnetic flux density in teslas (= T) or gauss (= G).

The direction of the vector \vec{f}_{EM} is determined by the rule of right hand screw (Figure 1a).

It is most convenient to use the cartesian coordinate system shown in Figure 1b.

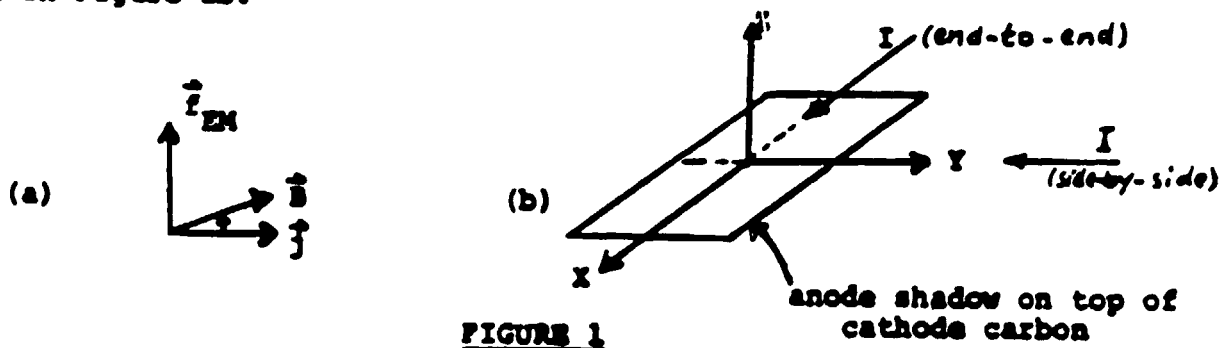


FIGURE 1

In the cartesian coordinate system, the three vectors are:

$$\vec{j} = (j_x, j_y, j_z), \quad \vec{B} = (B_x, B_y, B_z)$$

$$\vec{f}_{EM} = (f_{EMx}, f_{EMy}, f_{EMz}), \text{ where}$$

$$f_{EMx} = j_y B_z - j_z B_y \quad (2)$$

$$f_{EMy} = j_z B_x - j_x B_z$$

$$f_{EMz} = j_x B_y - j_y B_x$$

*1T = $1 \frac{wb}{m^2} = 1 \frac{Vs}{m^2}$. Gauss is a CGS unit still commonly used. 1T = 10^4 G.

In a real pot, all three components of the above three vectors are different from zero. In an ideal pot $j_x = 0$ and $j_y = 0$, i.e., the electric current in the bath and molten metal flows in the vertical direction only (from the anode to the cathode). In this case, the equations (2) are:

$$\begin{aligned} f_{EMx} &= -j_z B_y \\ f_{EMy} &= j_z B_x \end{aligned} \quad (3)$$

The electromagnetic force (1) is responsible for metal flow, metal-bath interface disturbances such as inclination, rippling, and waves, then metal and bath rolling, etc. These processes affect the pot operation: decrease current efficiency (by oxidation), cause voltage instability (by short-circuiting the metal to the anode), and cause a greater energy consumption because the ACD cannot be decreased below a certain value.

EMF

**Force resulting from the Interaction
of Electric Current and Magnetic Field**

$$\vec{F} = \vec{J} \times \vec{B}$$

(Force = Current x Magnetic Field)

$$\frac{N}{m^3} = \frac{A}{m^2} \times \frac{Vs}{m^2}$$

DIRECTION OF ELECTROMAGNETIC FORCES
FROM
INTERACTION OF CURRENT AND FIELD

MAGNETIC FIELD COMPONENT	CURRENT COMPONENT		
	VERTICAL	HORIZONTAL TRANSVERSE	HORIZONTAL LONGITUDINAL
VERTICAL B_z	—	LONGITUDINAL FORCE	TRANSVERSE FORCE
HORIZONTAL TRANSVERSE B_y	LONGITUDINAL FORCE	—	VERTICAL FORCE
HORIZONTAL LONGITUDINAL B_x	TRANSVERSE FORCE	VERTICAL FORCE	—

WORST EFFECTS
NEGLIGIBLE EFFECTS

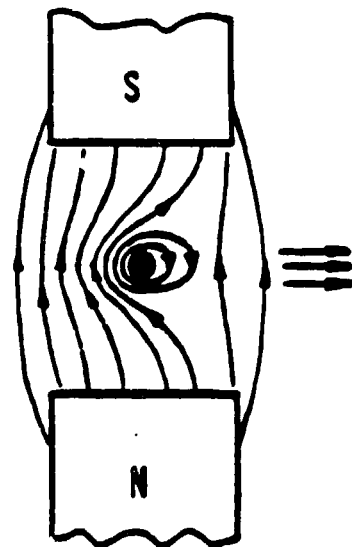
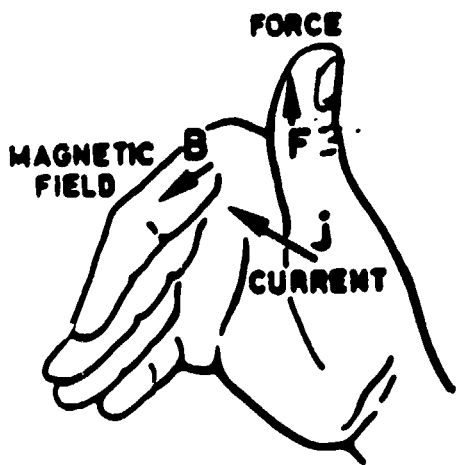
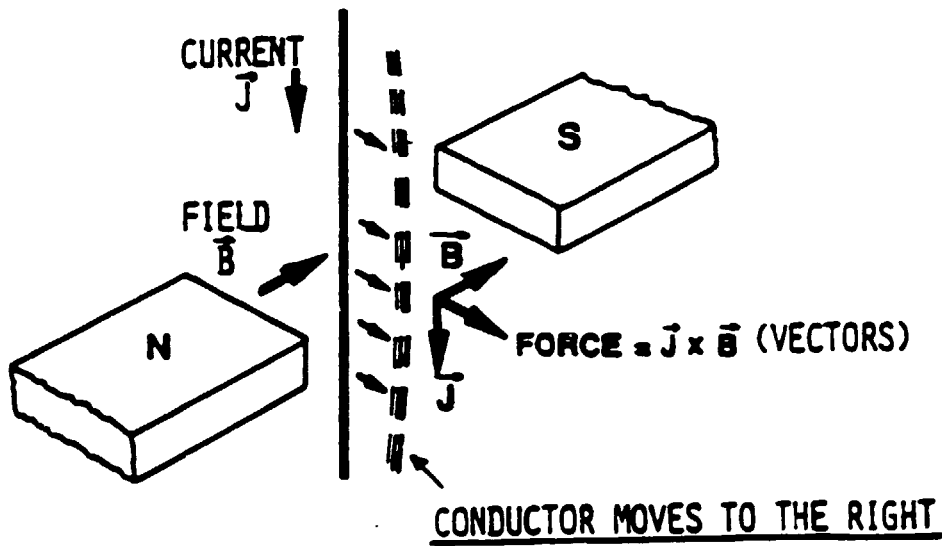
B_z = MAJOR INFLUENCE

$B_z + J_{HORIZ}$ = "PERMANENT" CIRCULATION

FORCES ARE NOT UNIFORM AT ALL LOCATIONS

FORCES ARE NOT SAME IN BATH AS IN METAL

MAGNETIC FORCES : THE INTERACTION OF CURRENT AND FIELD



Motor rule.

Magnetohydrodynamics (MHD) of Aluminum Electrolytic Cells

A. What is MHD?

B. Why to be concerned with it?

C. How to apply it (to electrolytic cells)?

MAGNETOHYDRODYNAMICS IS THE STUDY OF FLUID BEHAVIOUR UNDER THE INFLUENCE OF THE ELECTROMAGNETIC FORCE.

THE ELECTROMAGNETIC FORCE PER UNIT VOLUME IS THE VECTOR PRODUCT OF CURRENT DENSITY AND MAGNETIC INDUCTION.

THE ELECTROMAGNETIC FORCE IS RESPONSIBLE FOR THE CIRCULATION OF THE METAL AND ELECTROLYTE, FOR STATIC DEFORMATION OF METAL-BATH INTERFACE AND FOR WAVES ON THIS INTERFACE.

THE OBJECTIVE OF MHD DESIGN IS TO MAKE THE METAL-BATH INTERFACE DEFORMATION AS SMALL AS POSSIBLE AND THE VELOCITIES OF THE METAL AND ELECTROLYTE AS LOW AS POSSIBLE AND RESTRAINED TO A FEW SYMMETRICAL CIRCULATION POOLS.

ALL THIS HAS TO BE ACHIEVED BY PAYING DUE ATTENTION TO THE BUSBAR AND ENERGY COST.

MAIN STAGES OF A MHD STUDY:

- 1 - CALCULATION OF MAGNETIC FIELD DISTRIBUTION
 - POSITION AND DIVISION OF CURRENT IN EXTERNAL CONDUCTORS
 - EFFECT OF IRON

- 2 - CALCULATION OF CURRENT DISTRIBUTION
 - CALCULATION OF CONDUCTOR SECTIONS
 - CALCULATION OF INTERNAL CURRENT DISTRIBUTIONS

- 3 - CALCULATIONS OF HYDRODYNAMICS
 - CALCULATION OF FORCE (EMF)
 - CALCULATION OF CIRCULATION AND BATH-METAL INTERFACE

- 4 - EXPERIMENTAL VERIFICATION
 - MEASUREMENT OF CURRENTS
 - MEASUREMENT OF MAGNETIC FIELD
 - EVALUATION OF MAGNETIC FIELD
 - EVALUATION OF CATHODE PANEL DEFORMATION
 - EVALUATION OF METAL CIRCULATION
 - STABLE, EFFICIENT CELL

THE FINAL ^{CELL} DESIGN IS ARRIVED AT IN A
PARAMETRIC WAY - A SEVERAL POSSIBLE BUSBAR
ARRANGEMENTS IS STUDIED AND THE BEST ONE IS
CHOSEN ACCORDING TO SPECIFIED MHD CRITERIA.

ELECTRIC CURRENT DISTRIBUTION

THE ELECTRIC CURRENT DENSITY IN THE LIQUID ZONE IS ESSENTIALLY EQUAL TO THE CELL CURRENT DIVIDED BY THE AREA OF THE LIQUID ZONE.

IT IS A VECTOR POINTING VERTICALLY DOWN WARDS IN THE BATH, BUT IT MAY HAVE CONSIDERABLE HORIZONTAL COMPONENTS IN THE METAL.

THE HORIZONTAL CURRENTS ARE DUE TO:

- CATHODE AND BUSBAR DESIGN,
- THERMAL EQUILIBRIUM OF THE CELL, AND
- CELL OPERATION.

BUSBAR DESIGN IS COMPOSED OF TWO PROCESSES:

- SEARCH FOR OPTIMAL BUSBAR LOCATIONS WHICH IS GUIDED BY THE FACT THAT ELECTRICAL CURRENTS GENERATE MAGNETIC FIELDS,
- SEARCH FOR APPROPRIATE BUSBAR SIZES WHICH IS GUIDED BY THE FACT THAT THE BUSBAR CURRENT IS ^{INVERSELY} PROPORTIONAL TO THE BUSBAR RESISTANCE IN A PARALLEL RESISTANCE NETWORK.

THE OVERALL CRITERIA FOR THE BUSBAR DESIGN ARE BASED ON THE PRINCIPLES OF MAGNETO-HYDRODYNAMICS.

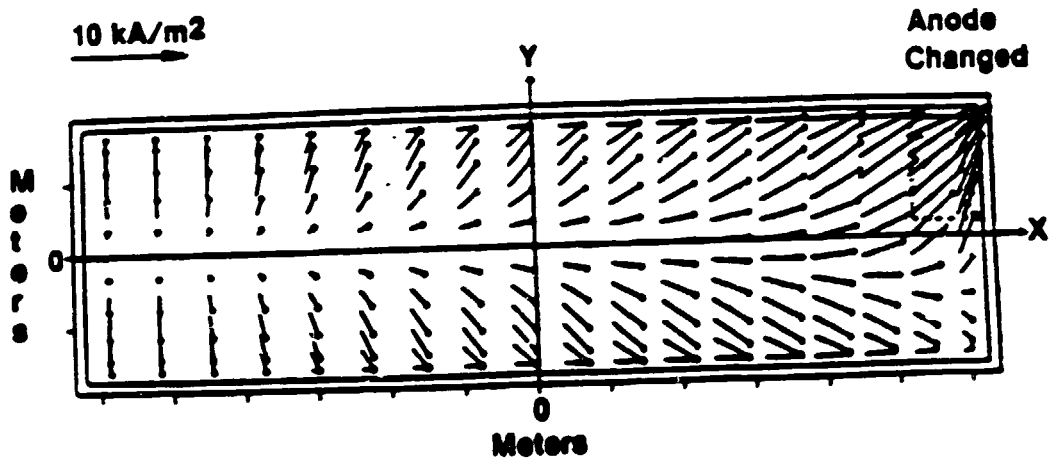
As it is very difficult to control the electric current distribution in the cells since it changes with time, the force on the metal and bath is difficult to control and is also time dependent.

SELECTED PHYSICAL PROPERTIES

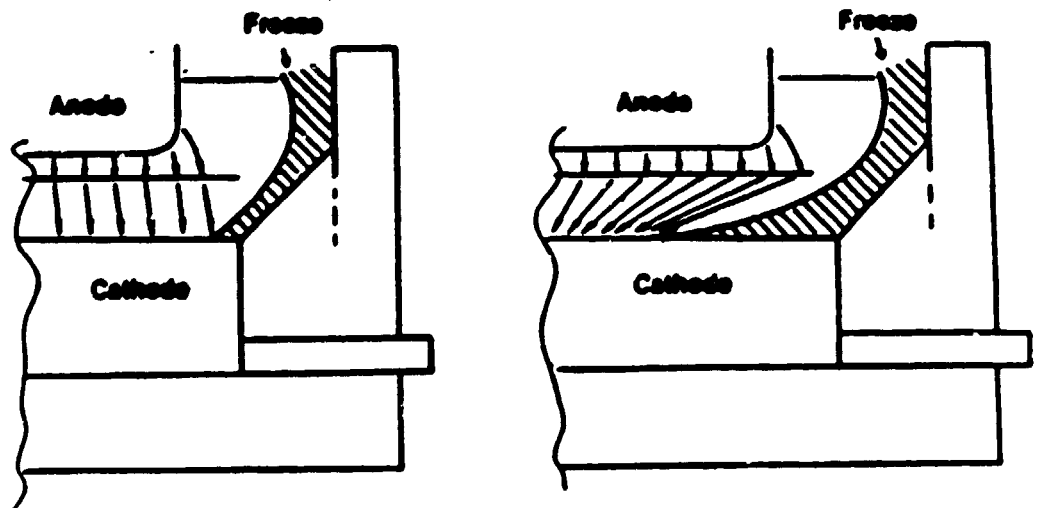
	<u>RELATIVE DENSITY</u>	<u>RELATIVE ELECTRICAL RESISTIVITY</u>	<u>RELATIVE VISCOSITY</u>
MOLTEN BATH	2.1	~ 15 000	3
MOLTEN ALUMINUM	2.3	1	1.5
"SLUDGE"	~ 2.7	(?)	-
CARBON LINING	-	~ 150	-
STEEL AT 800°C	-	~ 4	-
WATER AT 20°C	1.0	-	1

Link between Pot Operation and MHD:

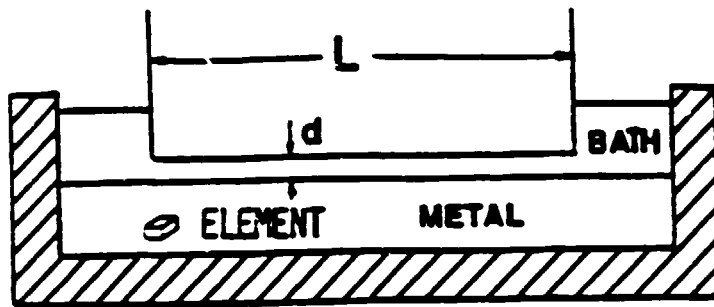
Horizontal current changes with anode change



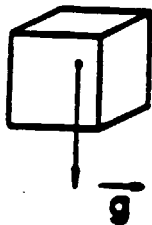
Link between Thermal Equilibrium and MHD



Horizontal Current is influenced by Freeze

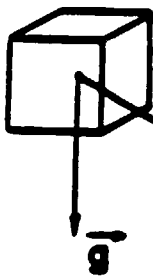


$$80 < \frac{L}{D} < 350$$



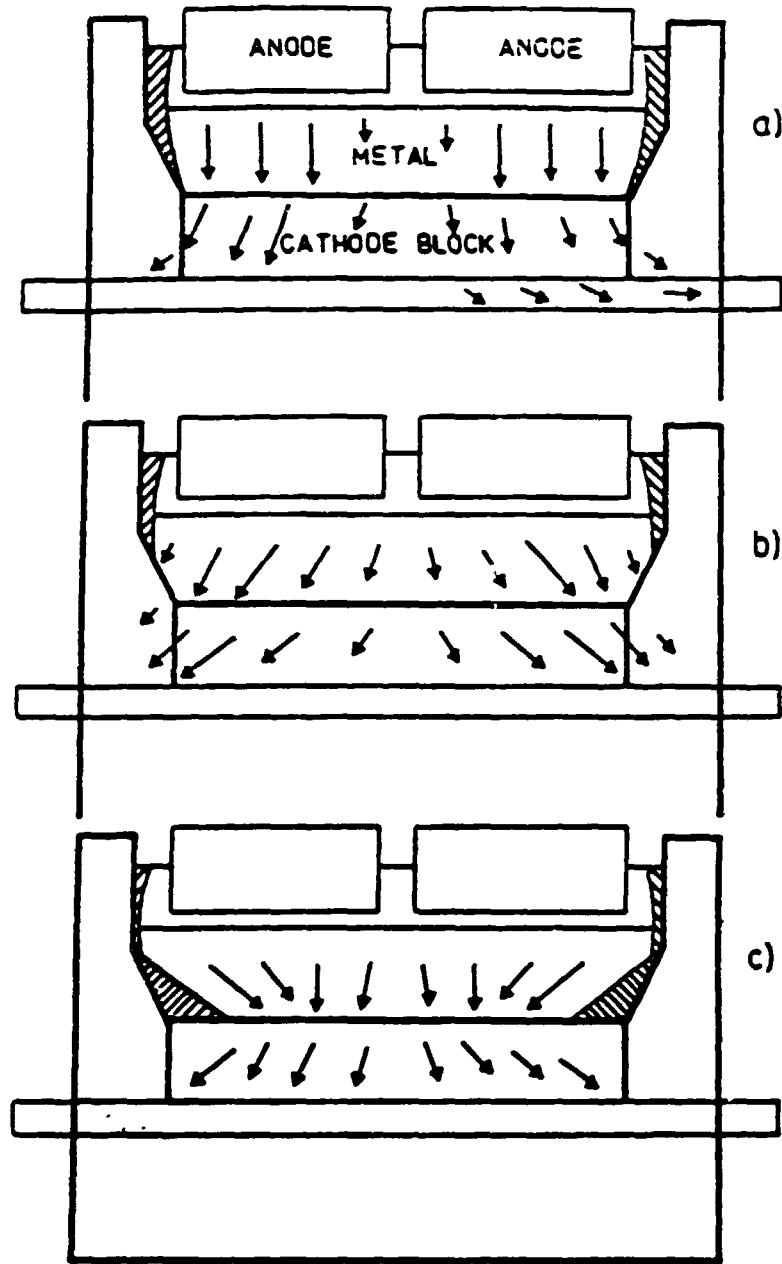
WI:

- NO MOVEMENT OF LIQUIDS
- INTERFACE HORIZONTAL

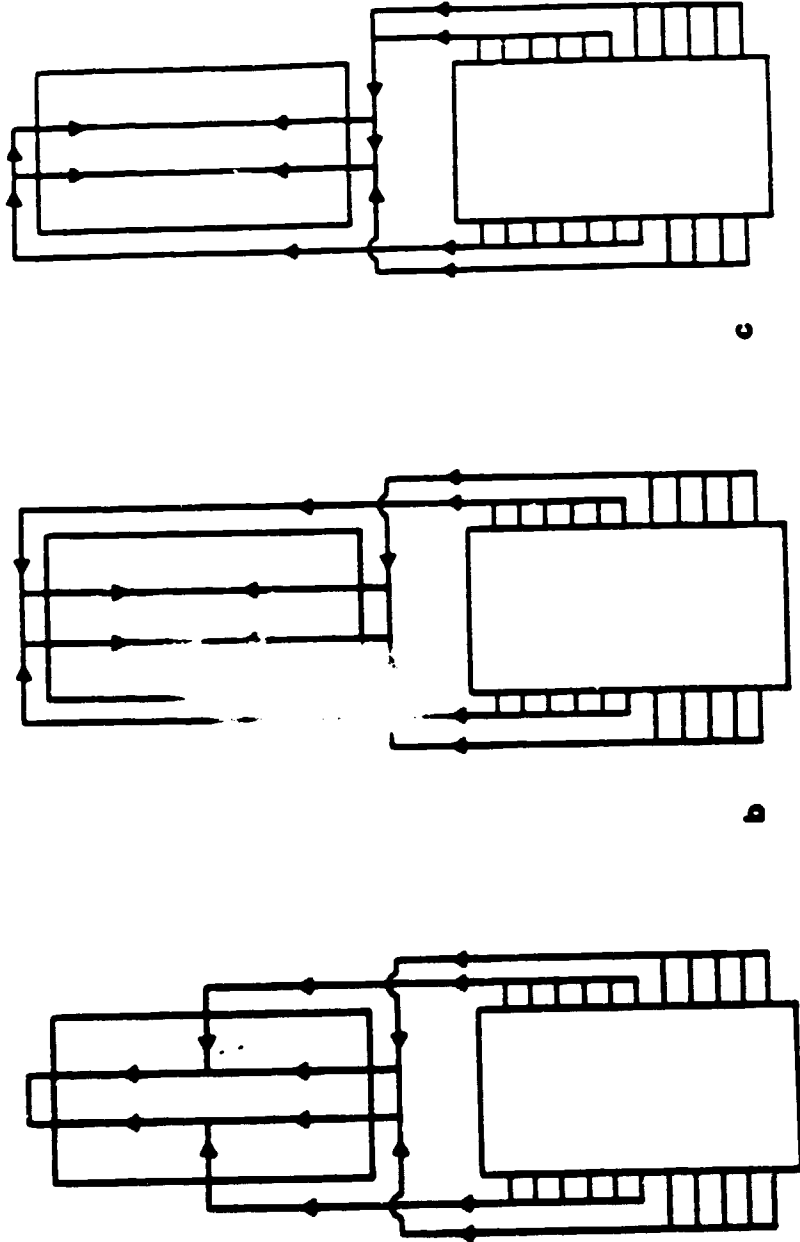


WITH CURRENT :-

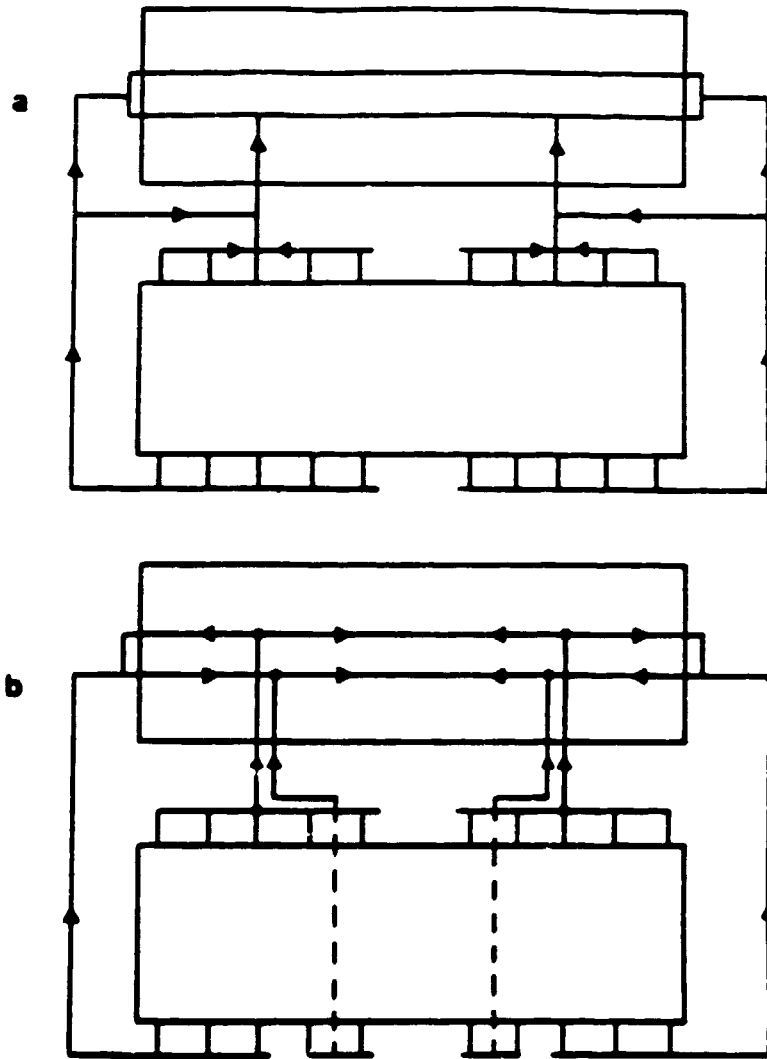
- LIQUIDS MOVE
- INTERFACE DEFORMED



Effect of various side-freeze profiles on the direction of current flow through the metal pad cathode bottom lining of a cell. a) Designed balance. b) Insufficient ledge. c) Too large a ridge.



Busbar configurations for end-to-end cells. a) End and side entry. b) Two-end entry; c) Two-end asymmetric entry.



Busbar configurations for side-by-side cells.
a) End and quarter entry. Riser currents can be varied.
b) End and quarter entry; current passing under the cathode.

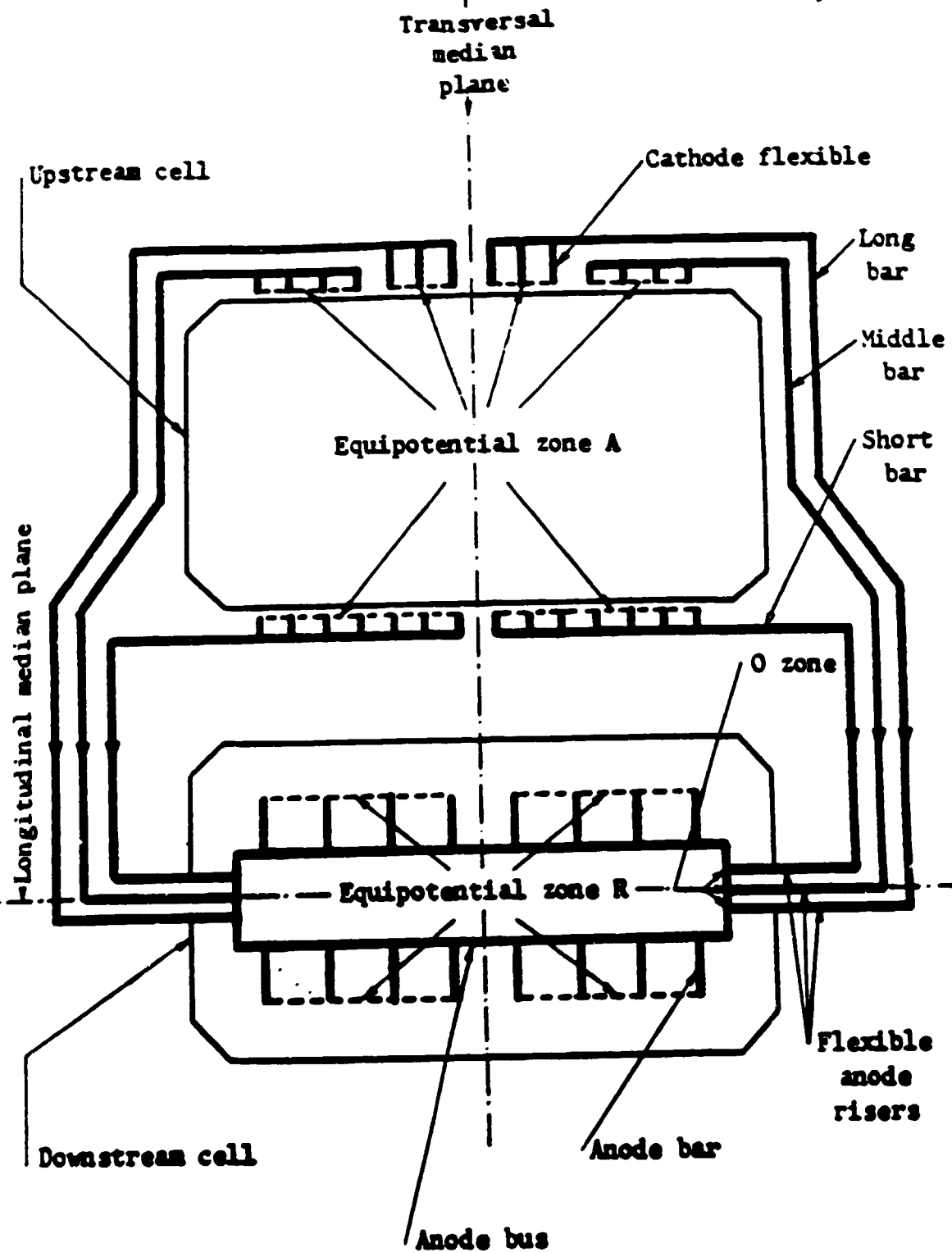


Fig. 1 - Scheme of the aluminum conductor circuit in the reference cell

MAGNETIC FIELD DISTRIBUTION

Magnetic field is produced by the electric currents. It is therefore inevitable in aluminum electrolysis. Fortunately, its distribution in space can be controlled to a certain degree by suitable busbar positions and by the presence of steel (ferromagnetic) components. In order to control the field, we have to be able to calculate it. The magnetic field due to currents only is easy to calculate. The steel enormously complicates the calculations.

1. Magnetic field vectors

For a complete description of the magnetic fields, three vectors are needed: \hat{B} , \hat{H} , and \hat{M} .

\hat{B} = magnetic induction or magnetic flux density, (T),

\hat{H} = magnetic field strength, (A/m),

\hat{M} = magnetization vector, (A/m).

\hat{B} is defined terms of the induced voltage in a moving wire, \hat{H} is defined as the field of a coil or a conductor, and \hat{M} is magnetic moment density in magnetic materials.

The three vectors are related by the equation:

$$\hat{B} = \mu_0 (\hat{H} + \hat{M}) \tag{4}$$

In vacuum, where $\hat{M} = 0$:

$$\hat{B} = \mu_0 \hat{H} \qquad \mu_0 = 4\pi \times 10^{-7} \frac{Vs}{Am}$$

Note that the unit of \hat{H} and \hat{M} is A/m. The unit of \hat{B} is tesla (T):

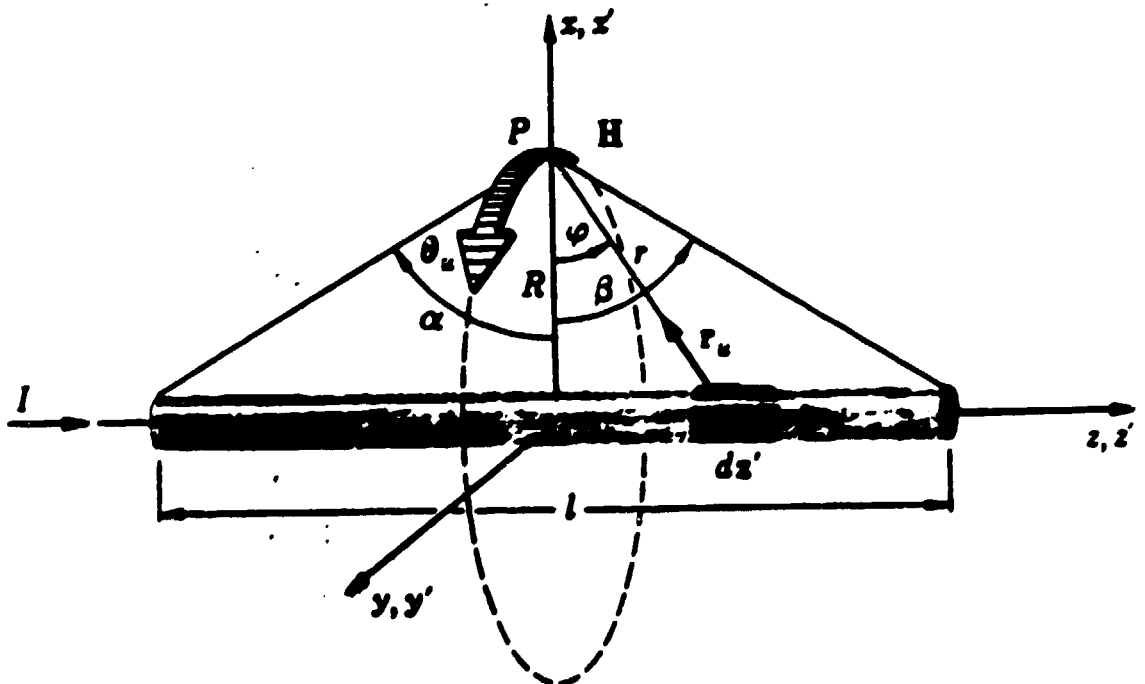
$$1 \text{ tesla} = 1 \text{ weber} \cdot \text{m}^{-2} = \frac{1 \text{ newton}}{\text{coul} \cdot (\text{m} \cdot \text{s}^{-1})} = \frac{1 \text{ newton}}{\text{amp} \cdot \text{m}} = 10^4 \text{ gauss}$$

2. Magnetic field due to currents only

All busbars of the cells are well approximated by straight conductors carrying a current I . Even the continuous currents inside the cell can be approximated by discrete straight line conductors. (This is good if we choose a sufficiently large number of such conductors)

The magnetic field of a finitely long conductor is given by the well known formula of Biot and Savart

$$\mathbf{H} = \frac{I}{4\pi} \int \frac{dz' \times \mathbf{r}_u}{r^2}$$



Calculation of the magnetic field associated with a segment of a current-carrying wire.

The integration of the above formula over the length of the conductor gives:

$$\vec{B} = \frac{\mu_0 I}{4\pi R} (\sin\beta + \sin\alpha) \hat{\theta}_u \quad \text{for } R > a \quad (5)$$

where: I = line current

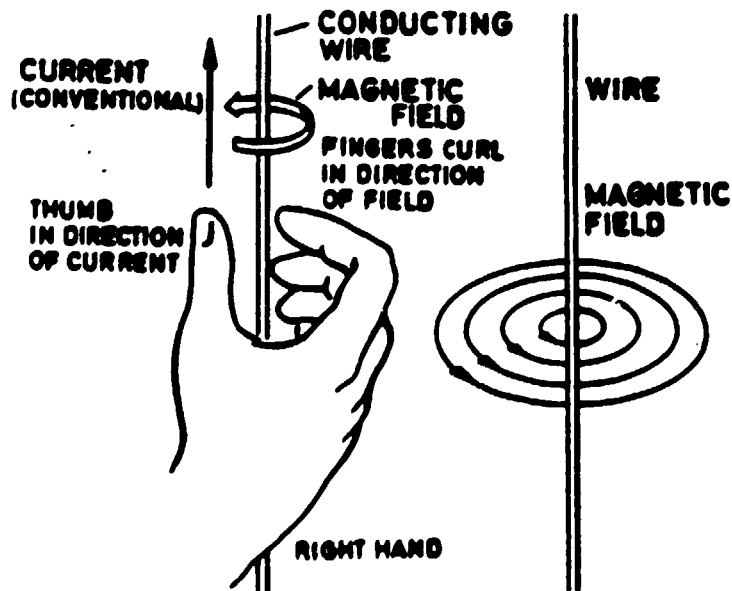
R = distance from the conductor to the observation points

α, β = viewing angles of the conductor ends from the observation point (Figure)

a = conductor radius.

$\hat{\theta}_u$ = unit vector in the circular direction around the conductor.

The magnetic field direction is determined by the rule of the right-hand screw. Its only component is circularly symmetric around the conductor.



The direction of the magnetic field

3. Ampère's law

The magnetic field distribution in space is governed by general laws among which Ampere's law is particularly useful.

This law is written as:

$$\oint_C \vec{H} \cdot d\vec{l} = I, \quad (6)$$

where: the integral is taken along a closed line c in space,

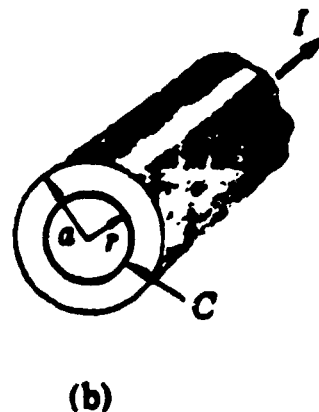
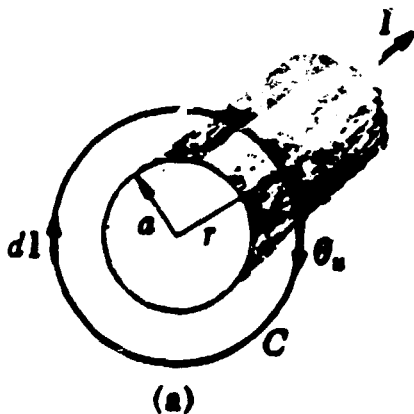
$d\vec{l}$ = a small element of that closed line,

I = total current crossing the surface bounded by the closed line.

This law is valid also in the presence of magnetic materials.

Example No. 1

For an infinitely long conductor, the closed path is a circle. \vec{H} is symmetrical and constant along that circle:



Calculation of the magnetic field of a current-carrying wire.

so that $\oint \mathbf{H} \cdot d\mathbf{l} = \oint H dl = H \oint dl$. Since $\oint dl = 2\pi r$, Ampere's law for this problem reduces to

$$H2\pi r = I_{\text{enclosed}}$$

and hence

$$H = \frac{I_{\text{enclosed}}}{2\pi r}$$

Taking into account the direction of \mathbf{H} and dropping the subscript on I , we finally obtain

$$\mathbf{H} = \frac{I}{2\pi r} \theta_u \quad (r \geq a),$$

where θ_u is a unit vector in the circular direction forming a right-handed system with the direction of the current. To find the field inside the wire, we likewise describe a circular Amperian loop of radius r inside the wire, as shown in Fig. b. Applying Ampere's law to this loop, we obtain, as before,

$$H = \frac{I_{\text{enclosed}}}{2\pi r}$$

However, the enclosed current is now $I_{\text{enclosed}} = (I/\pi a^2)\pi r^2 = I(r^2/a^2)$, where a is the radius of the wire. The field is therefore

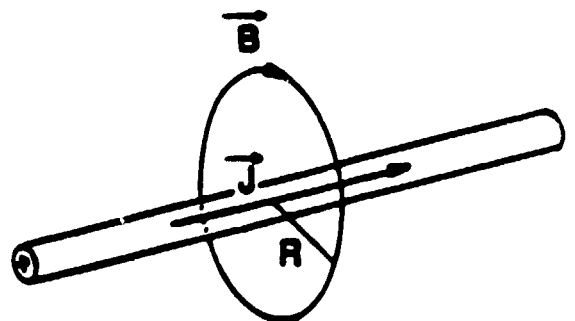
$$\mathbf{H} = \frac{Ir}{2\pi a^2} \theta_u \quad (r \leq a). \quad (10-4.5)$$

A quick evaluation formula for long conductors is:

$$B = \frac{2I}{R}$$

where:

B [gauss]
 I [kiloamperes]
 R [metres].



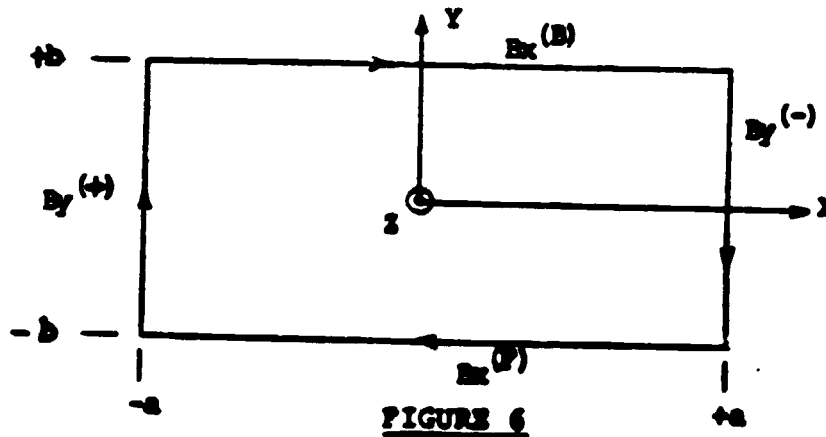
Example No. 2

Take the path as the projection of the anode perimeter in the molten metal. Suppose that for given positions of conductors and steel we calculate the magnetic field \vec{B} everywhere on that

path. Then,

$$\oint_C \vec{B} \cdot d\vec{l} = \int_{-b}^{+b} B_Y^{(+)}(y) dy + \int_{-a}^{+a} B_X^{(B)}(x) dx + \int_{+b}^{-b} B_Y^{(-)}(y) dy + \int_{+a}^{-a} B_X^{(F)}(x) dx \quad (8)$$

I = total current flowing through the cell.



Now suppose that we want to decrease B_Y at the ends of the cell. To do that, we rearrange the busbars and the steel. As the above circulation integral (8) has to be satisfied (we did not change the total current), B_X must increase somewhere along the integration path (anode perimeter). Therefore, the magnetic fields cannot be decreased everywhere in the pot. To avoid trouble, magnetics must be designed so that a good balance of forces is achieved.

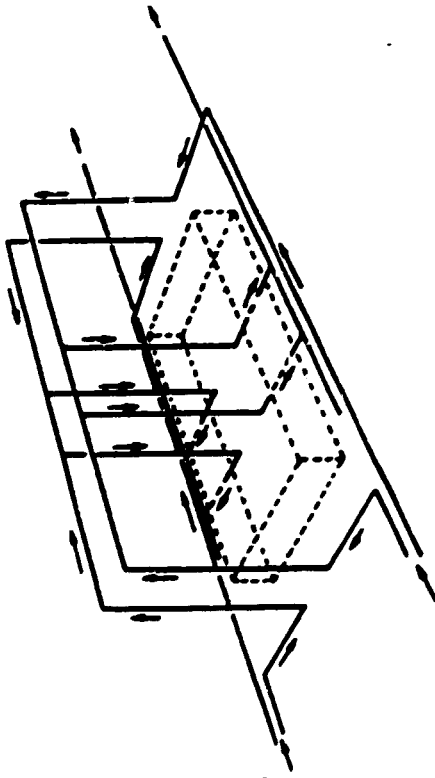
4. Magnetic field distribution in the cells

A big interest in magnetics during the last two decades has been caused by the desire to use high currents. The currents have increased from 60 kA to 200 kA. Magnetics problems are appreciable at currents above 100 kA. Only in the best designs currents above 150 kA can be used.

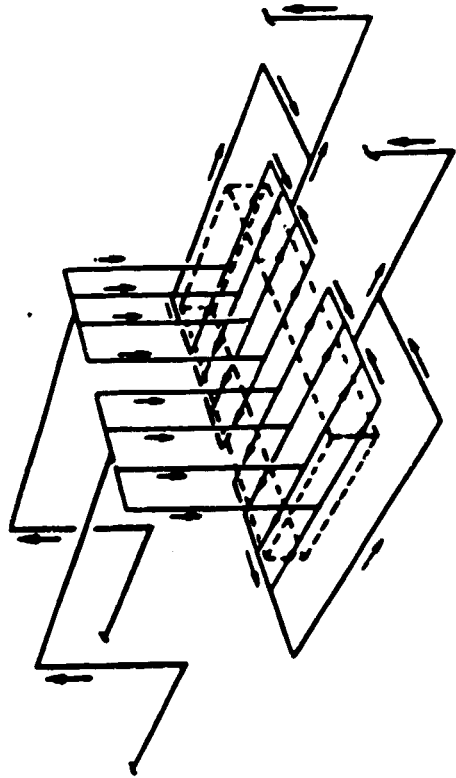
THE MAGNETIC FIELD IS GENERATED BY THE CURRENTS FLOWING IN THE ELECTRICAL CIRCUIT, COMPOSED OF THE CELL-TO-CELL BUSBARS AND THE ELECTRICALLY CONDUCTING CELL INTERIOR.

THE MAGNETIC FIELD IS A VECTOR WITH A COMPLICATED SPATIAL DISTRIBUTION, IT IS USUALLY PRESENTED IN TERMS OF THREE CARTESIAN COMPONENTS:

- LONGITUDINAL COMPONENT B_x
- TRANSVERSE COMPONENT B_y
- VERTICAL COMPONENT B_z



Current Flow in an End-bound Cell



Current Flow in a Slab-by-slab Cell

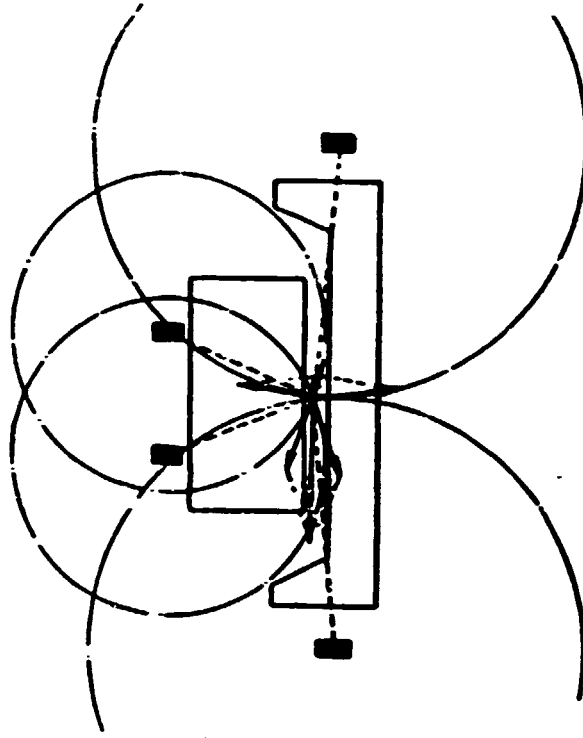
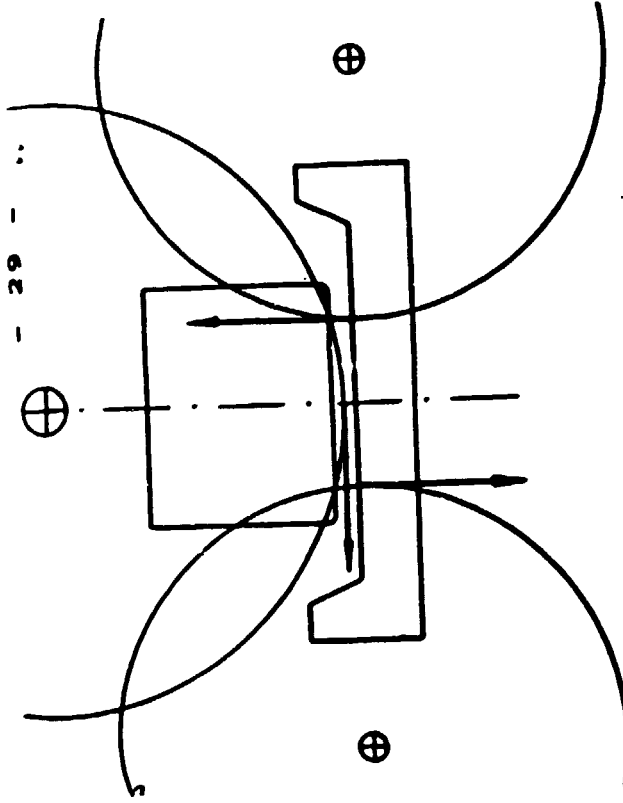


FIGURE 1

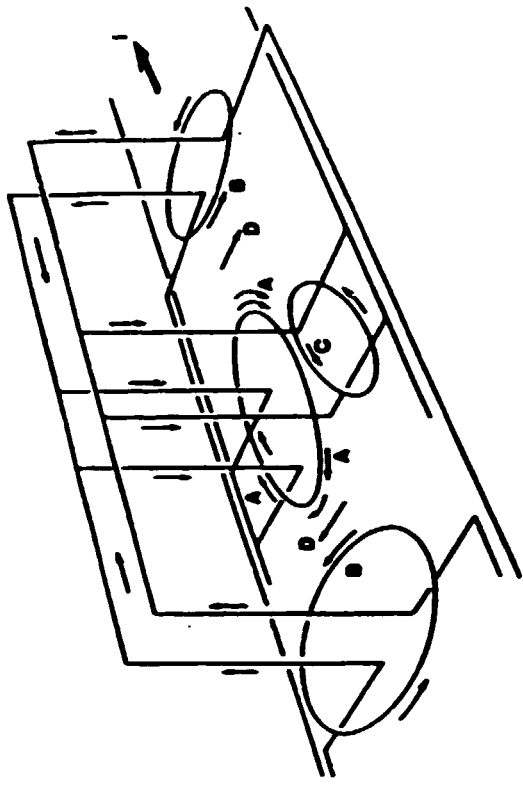
MAGNETIC FIELD AT THE POT CENTER DUE TO ANODE AND CATHODE CURRENTS. THE ZIG-ZAG REPRESENTS THE LOCATION OF ANODES.



- 29 -

HORIZONTAL COMPONENTS OF MAGNETIC FIELD

- 30 -



- A - VERTICAL CURRENT THROUGH ANODE, BATH, METAL
- B - VERTICAL CURRENT IN ANODE RISERS
- C - HORIZONTAL CURRENT THROUGH COLLECTOR BARS
- D - HORIZONTAL CURRENT IN ANODE BUSBAR

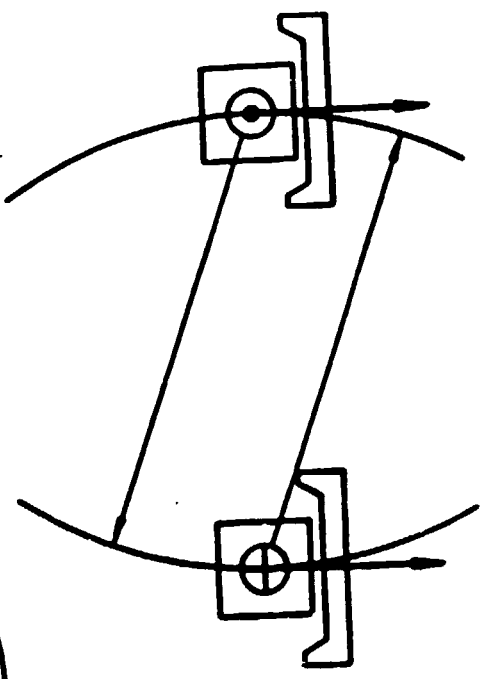
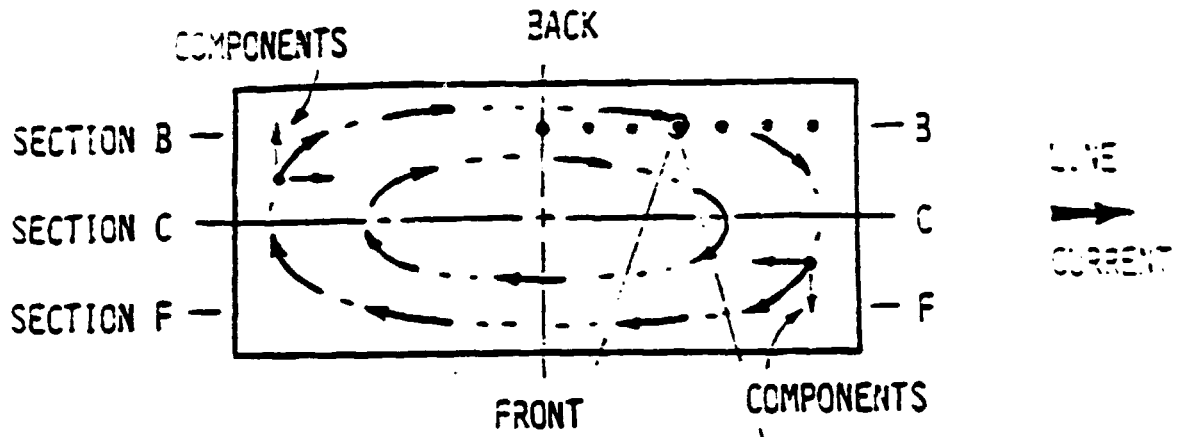


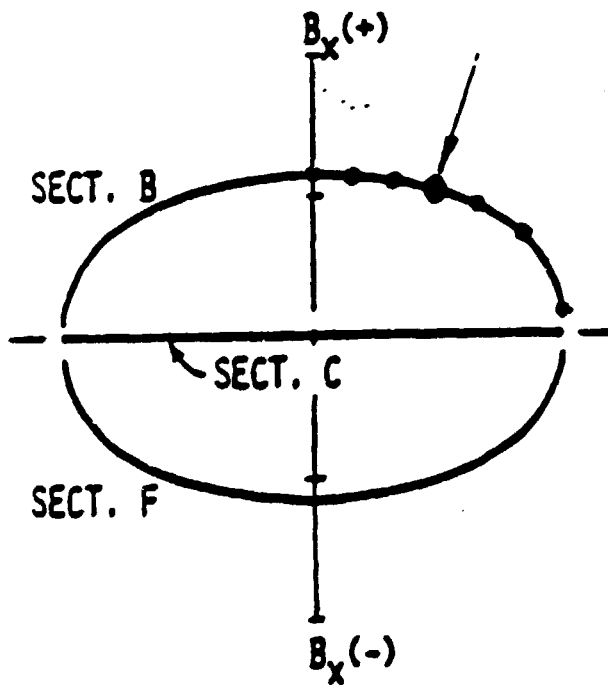
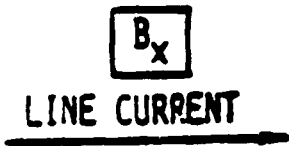
FIGURE 2

ORIGIN OF MAGNETIC FIELDS IN POTB

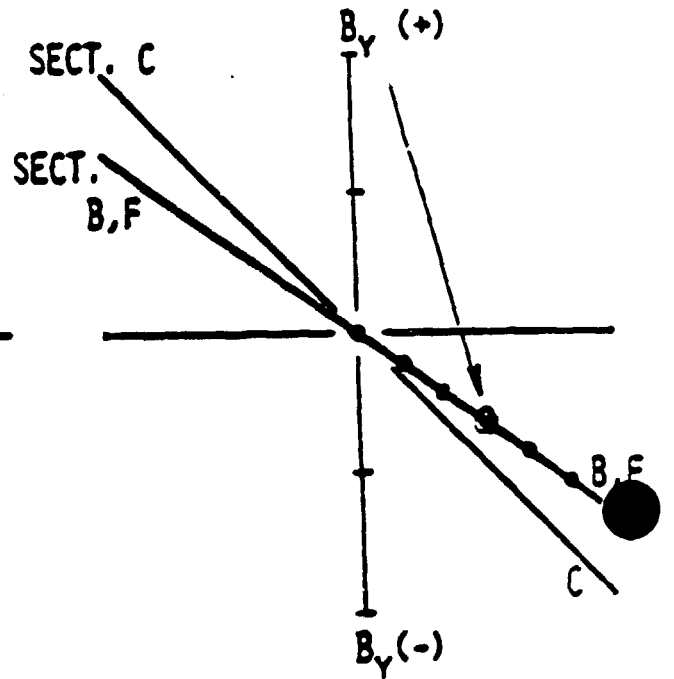
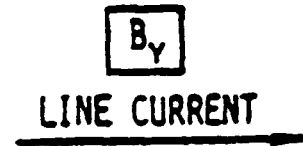
HORIZONTAL FIELDS



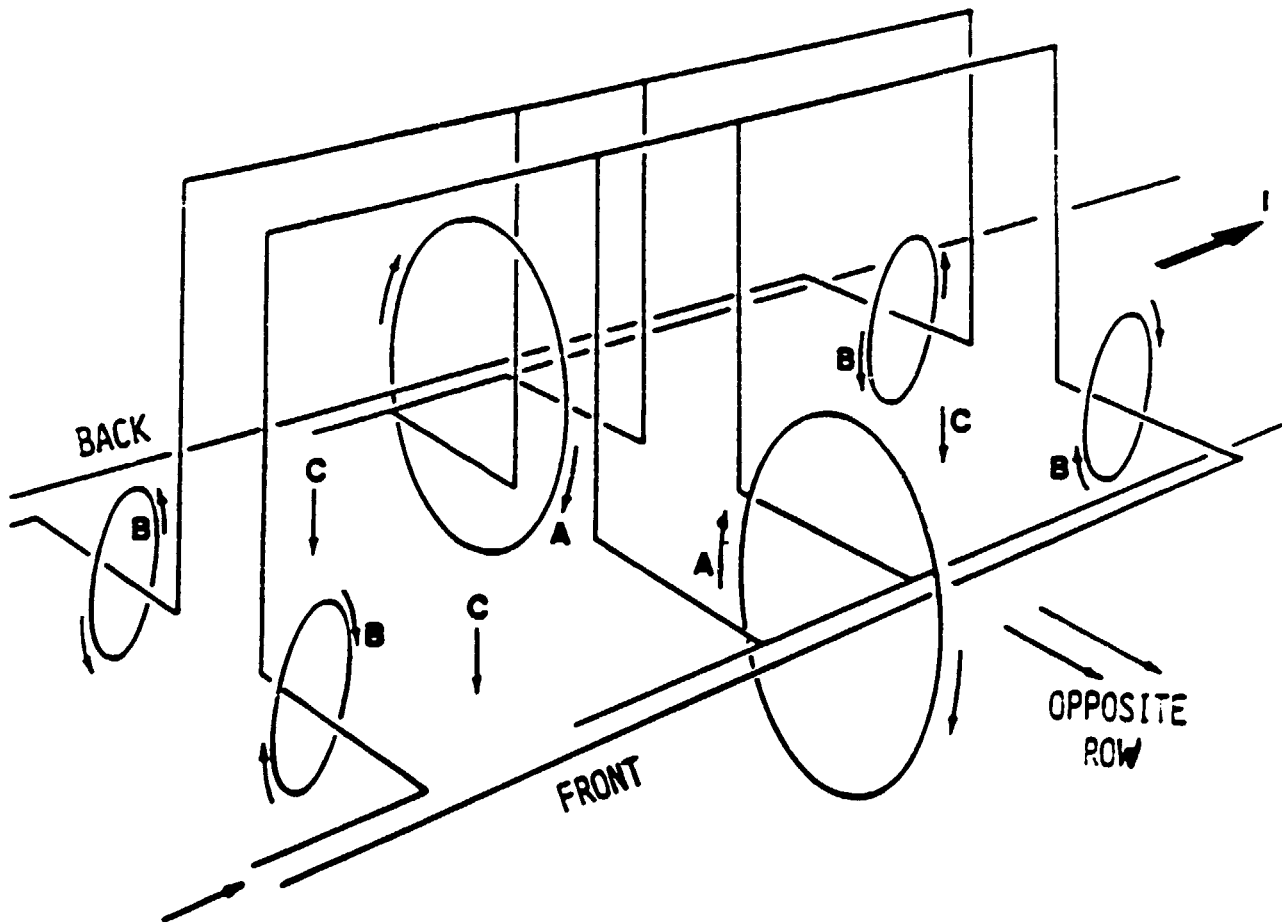
LONGITUDINAL COMPONENT



TRANSVERSE COMPONENT

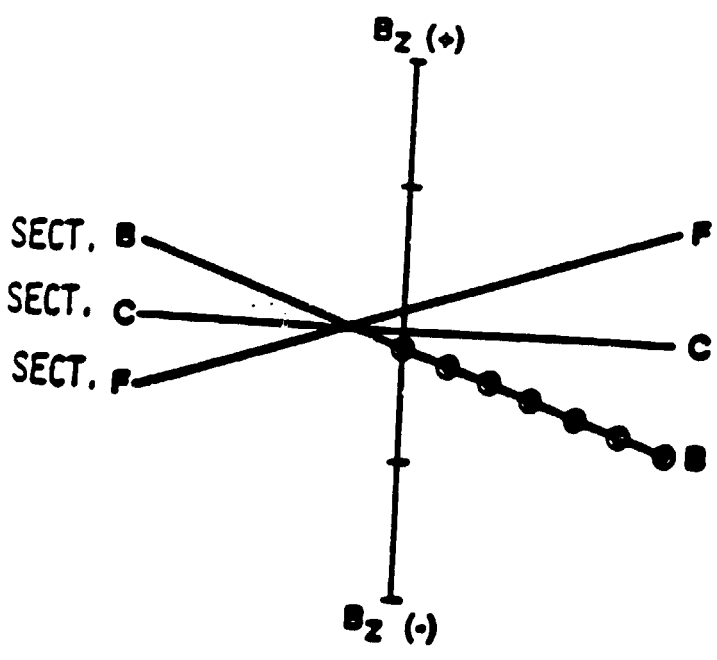
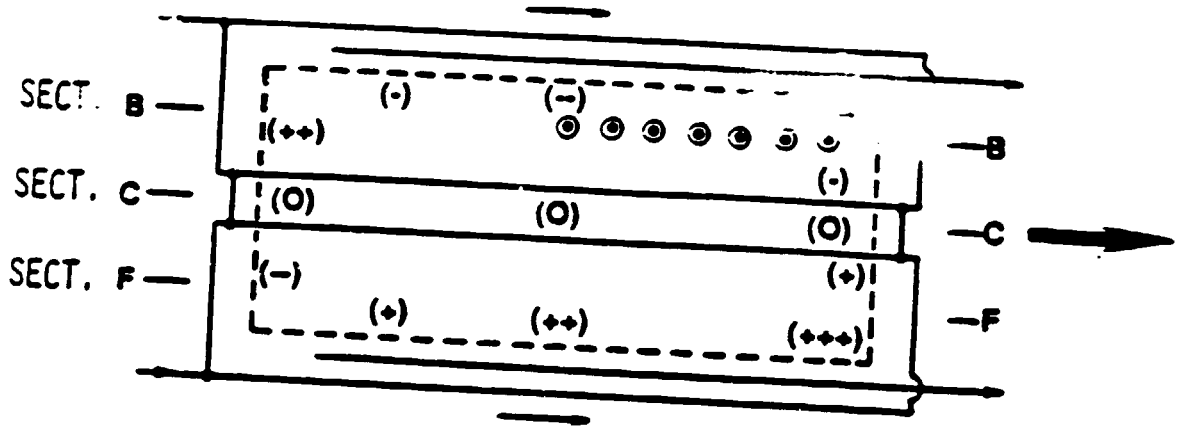


VERTICAL COMPONENTS OF MAGNETIC FIELD

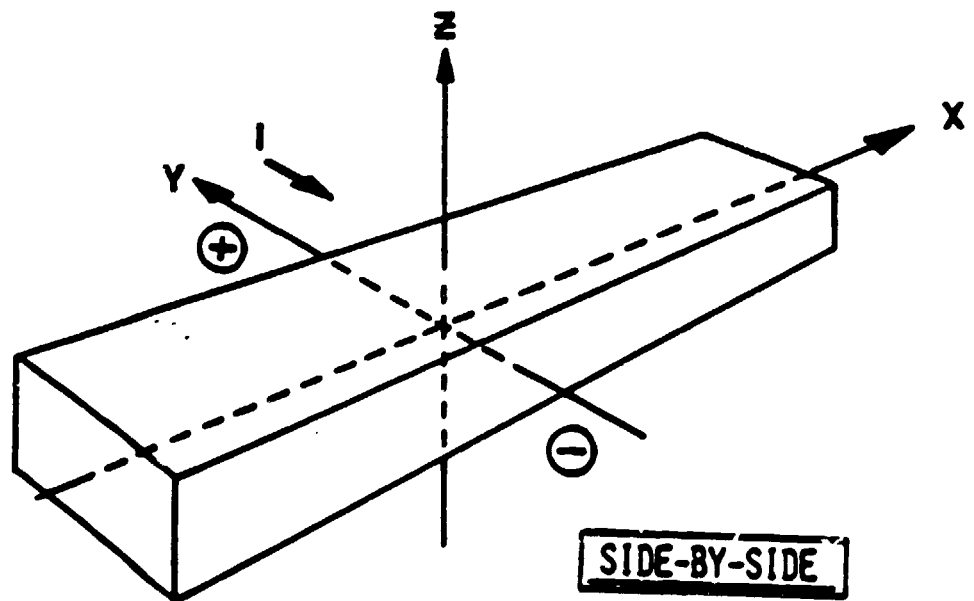
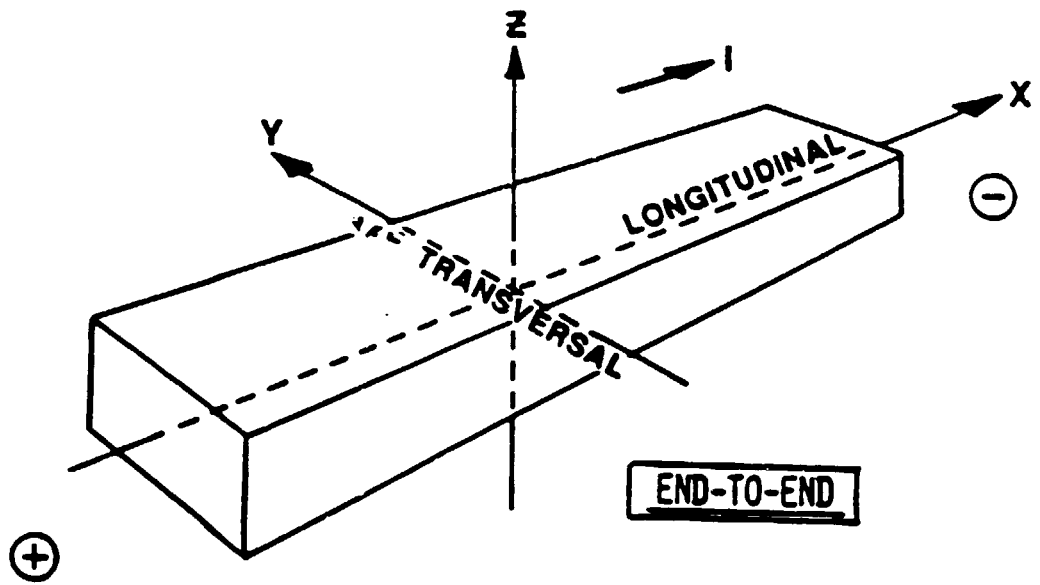


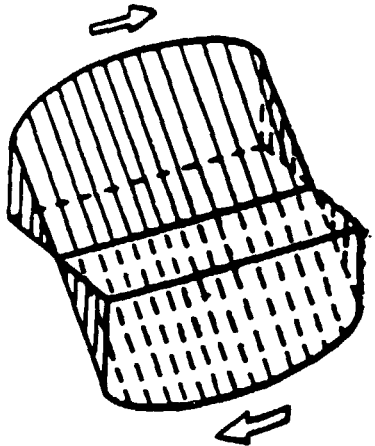
- A - FROM HORIZONTAL CURRENT IN CATHODE BUS**
- B - FROM HORIZONTAL CURRENT IN ANODE RISERS**
- C - FROM OPPOSITE ROW OF POTS (IF PRESENT)**

VERTICAL FIELDS

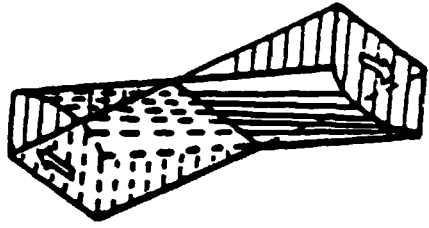


COORDINATES FOR FIELD COMPONENTS

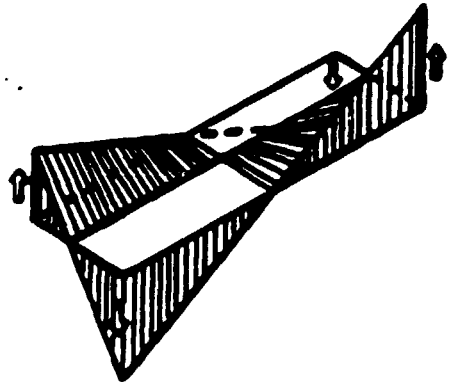




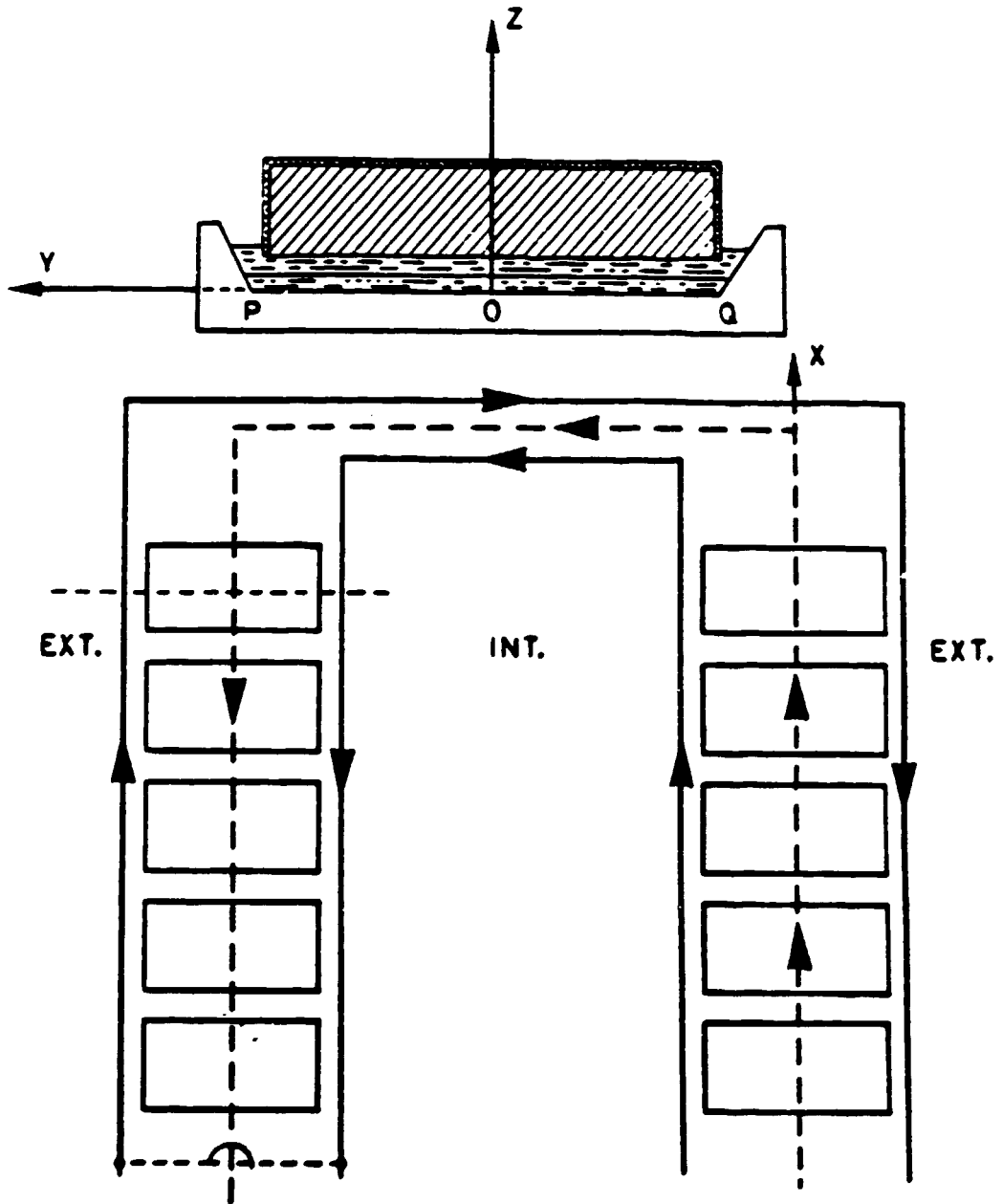
LONGITUDINAL COMP.



TRANSVERSAL COMP.

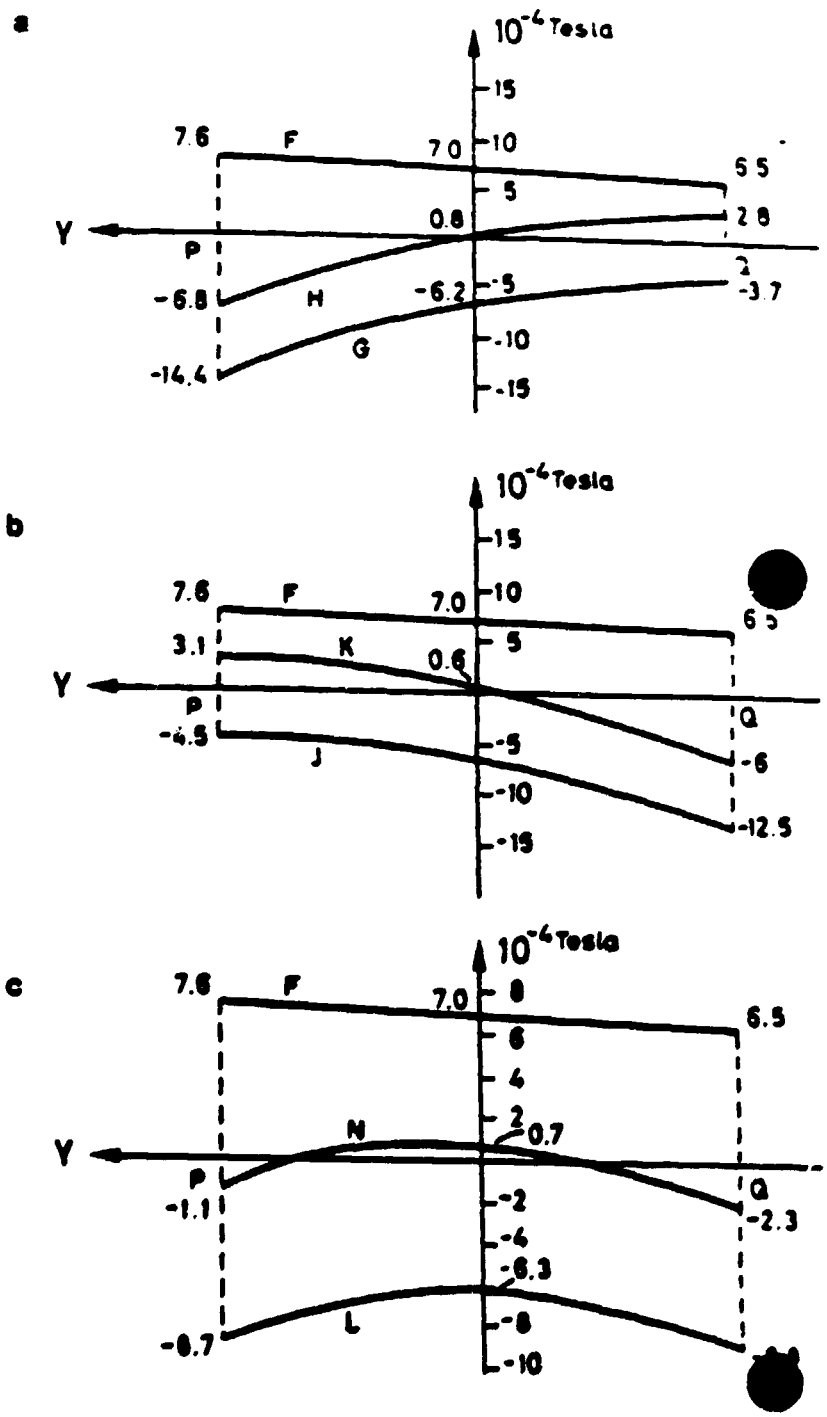


VERTICAL COMP.

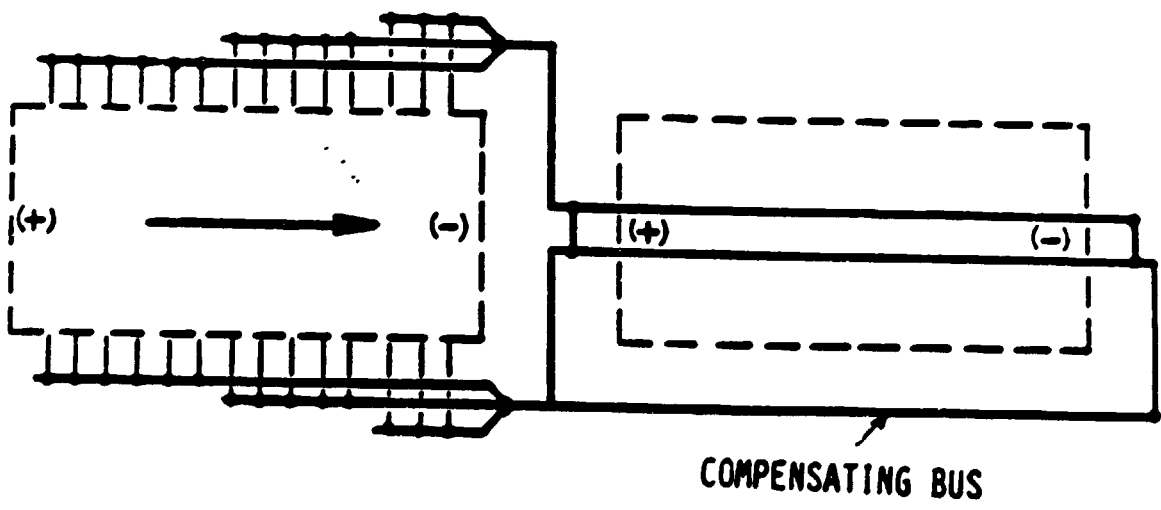
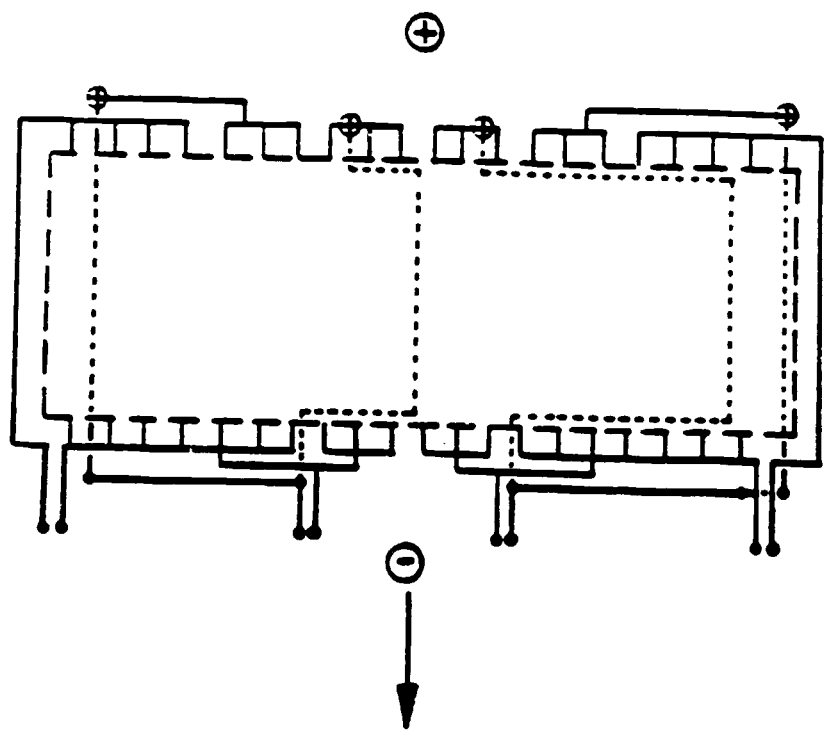


Schematic drawing of external and internal current loops for compensating vertical magnetic fields.

Fig. 2.28:
 Vertical magnetic fields
 from adjacent row and in-
 ternal and external loops.
 Curve F represents the ef-
 fects of the adjacent row.
 a) G: internal loop, 30 kA,
 H: resulting field.
 b) J: external loop, 20 kA,
 K: resulting field.
 c) L: internal and external
 loop in series, 13 kA,
 N: resulting field. Ref. 12).



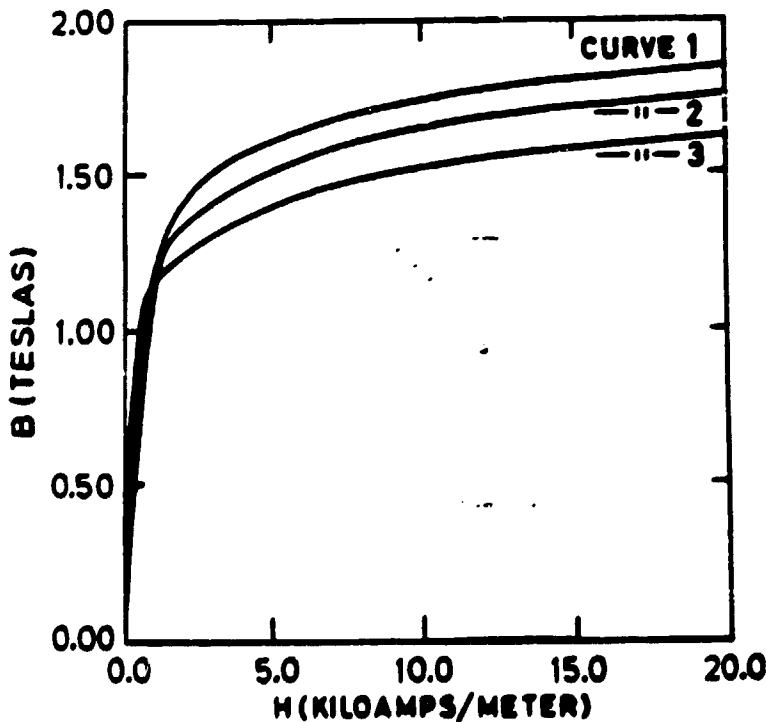
ASYMMETRIC
BUSBAR



5. Magnetic field in the presence of steel

Steel considerably changes the magnetic field distribution caused by the currents. Steel is ferromagnetic material. Put into a magnetic field it gets magnetized and then acts like a permanent magnet giving its contribution to the original magnetic field.

Steel magnetization, expressed by magnetization vector \hat{M} , depends on the magnetizing field \hat{H} . By equation (4), it can be seen that also \hat{B} is a function of \hat{H} . This dependence is determined experimentally and is called B-H or magnetization curve

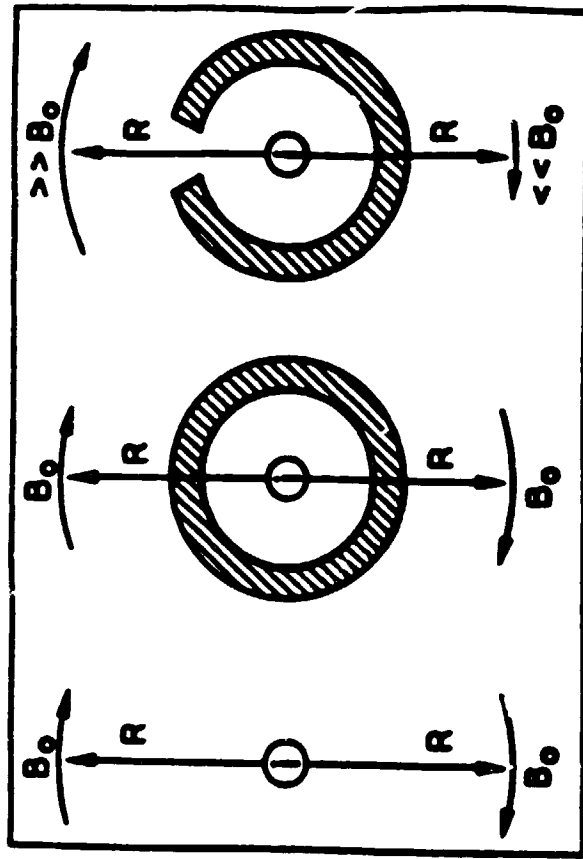


Typical magnetization curves for steel (B-H curves). Ref. ¹).
Curve 1: Cold-rolled steel at 300 °C.
Curve 2: Steel with one per cent more carbon, or 500 °C.
Curve 3: Steel with two per cents more carbon, or 600 °C.

H is the field strength inside the material. Unfortunately, it is very difficult to calculate H inside the steel of a pot, because it depends on the shape and size of steel. Only for a geometrically closed piece of ferromagnetic material \hat{H} inside it is equal to \hat{H} outside it (and example is a torus for which B-H curve is measured). The steel of a pot is not closed (the shell is open at the top, the VS anode casing at the top and at the bottom, the collector bars are not closed into a torus or rectangle, etc.) In a geometrically open piece of steel the field \hat{H} inside steel is in general smaller than the field outside it. However, the field \hat{B} inside steel is much larger than outside because of a large magnetization \hat{M} (see equation (4)).

Figures 12 and 13, pages 19 and 20, show how the magnetic field distribution in space is affected by simple pieces of steel. The illustrations can be easily understood if we use the Ampère's law. As the integration path, we choose a circle through the points of measurement. In case (b) of Figure 12, the field is exactly the same as in case (a). In cases (c) and (d), the field in front of the poles is stronger, because a strong field emerges from steel. By Ampère's law, we find that the field on the other side of the steel has to be smaller.

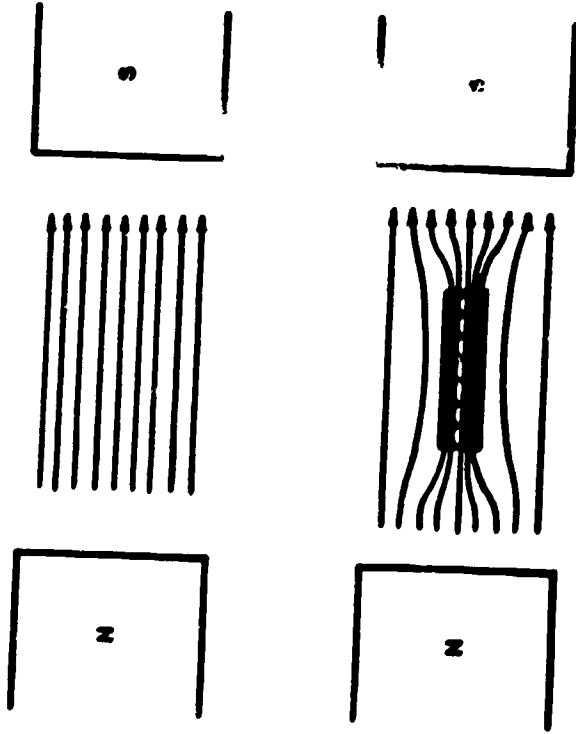
Figure 13 illustrates how we could try to shield the magnetic fields out of the melting zone. The idea is good, but somehow impractical because we would need large pieces of steel to get any effect (the distance between the open faces should be comparable to the distance from the conductor to the melting zone). Also, according to the Ampère's law, we cannot decrease the magnetic field everywhere in the melting zone. Applying this law to the anode perimeter, we see that field components can decrease at some locations, but must increase at others.



a b c

Influence of magnetic material for simple geometry. (Ref. 1).

- a) No magnetic material present.
- b) Iron cylinder present.
- c) Iron cylinder with air gap present.



STEEL MODIFIES THE MAGNETIC FIELDS DISTRIBUTION AS SHOWN

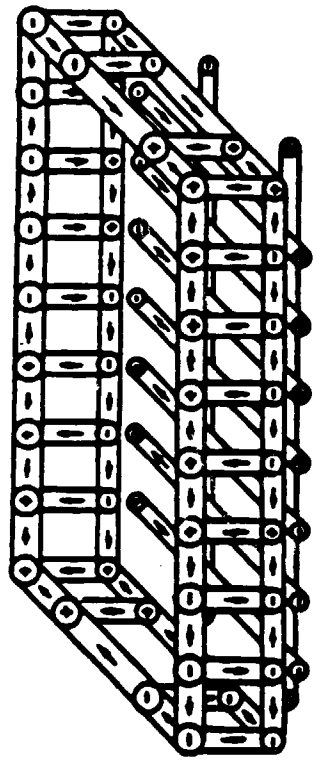
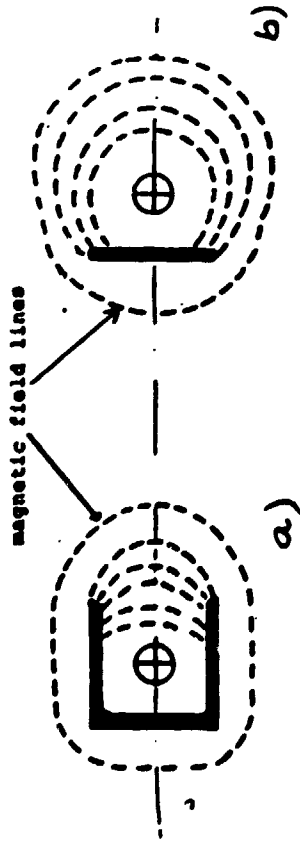


FIGURE 14

DIPOLE MODEL OF BOTTOM SHELL AND SUPPORT BEAMS

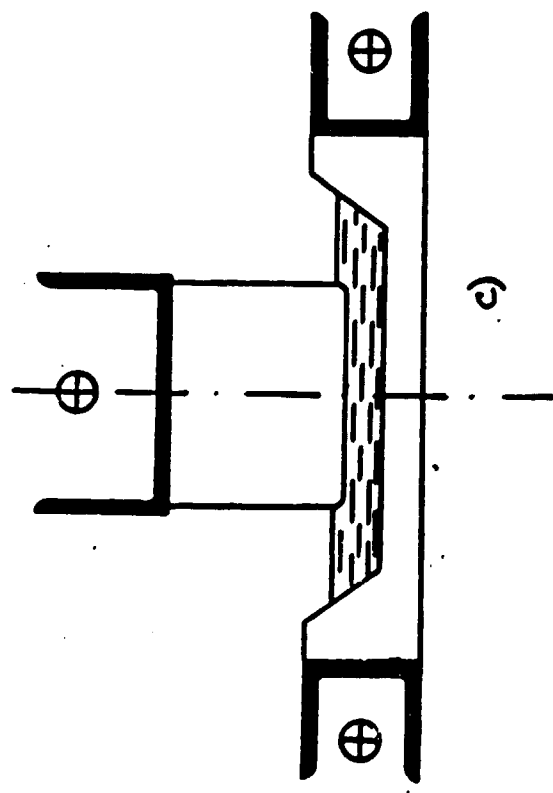


FIGURE 20

AN IDEA FOR SHIELDING MAGNETIC FIELD OUT OF A POT

TO STUDY FHD, THE FOLLOWING MUST BE DETERMINED:

- THE MAGNETIC FIELD DISTRIBUTION, WHICH IS CALCULATED USING BIOT-SAVARD EQUATION.
- THE CURRENT DISTRIBUTION WHICH IS CALCULATED BY OHM'S LAW AND LAPLACE EQUATION.

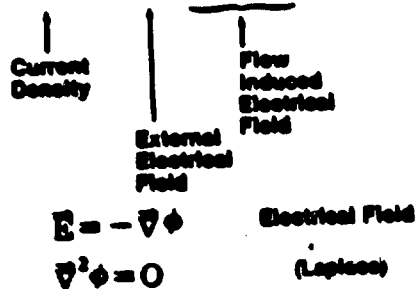
IN OHM'S LAW, FLOW INDUCED ELECTRICAL FIELD MUST BE TAKEN INTO ACCOUNT.

• Magnetic Field Distribution

$$\vec{B} = \frac{\mu_0 I}{4\pi r^2} \int \frac{d\vec{l} \times \vec{r}}{r^3} \quad (\text{Biot - Savart})$$

• Current Distribution

$$\vec{J} = \sigma (\vec{E} + \frac{1}{R} \vec{v} \times \vec{B}) \quad (\text{Ohm})$$



THEN:

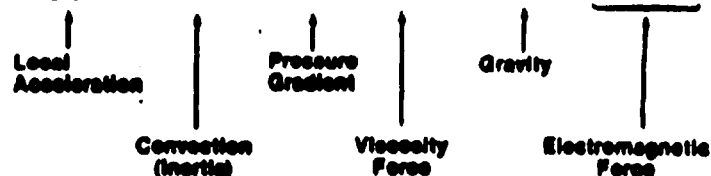
- FLUID DYNAMICS LAWS MUST BE APPLIED, THAT IS, NAVIER-STOKES EQUATION AND CONTINUITY EQUATION. THE FORMER GIVES THE EQUILIBRIUM OF FORCES IN A UNIT VOLUME OF FLUIDS.

THESE EQUATIONS ARE WRITTEN IN DIMENSIONLESS FORM TO SIMPLIFY THE

• A₁ Fluid Dynamics Laws

Navier-Stokes Equation

$$\rho \frac{\partial \vec{v}}{\partial t} + (\vec{v} \cdot \nabla) \vec{v} = -\nabla p + \frac{\mu}{R_e} \nabla^2 \vec{v} + \vec{g} + NK(\vec{J} \times \vec{B})$$



Continuity Equation (Incompressible liquid)

$$\nabla \cdot \vec{v} = 0$$

Dimensionless Analysis Gives the Relative Importance of Phenomena

Table 1. Dimensionless Numbers (for the following typical values)

$V_0 = 0.1 \text{ m/s}$, $B_0 = 10\text{-}2\text{T}$, $L_0 = 0.05 \text{ m}$ (bath),
 0.2 m (metal).

Dimensionless Number	Definition	Bath	Metal
Re	$\frac{\text{Inertial Force}}{\text{Viscosity Force}}$	3 000	77 000
Re_m	$\frac{\text{Induced E}}{\text{Ext. E}}$	1.5×10^{-6}	0.1
Ha	$\frac{\text{Electromag. Force}}{\text{Viscosity Force}}$	0.13	106
K	$\frac{\text{Ext. Elect. Field}}{\text{Induced Elect. Field}}$	3×10^4	1.7
M	$\frac{\text{Electromag. Force}}{\text{Inertial Force}}$	6×10^{-6}	0.4
HK	-	0.18	0.88

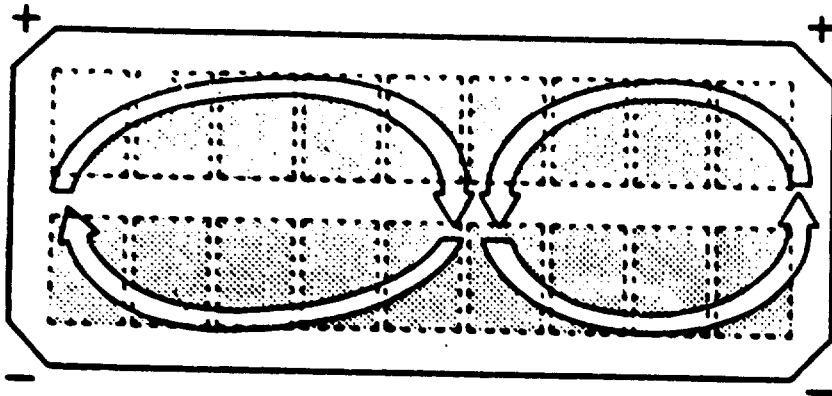
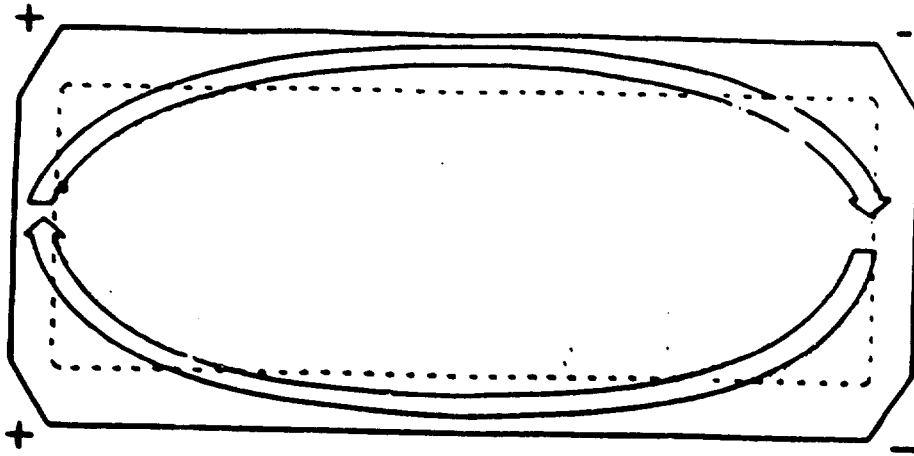
THIS TABLE GIVES THE MOST COMMON DIMENSIONLESS NUMBERS: REYNOLDS, MAGNETIC REYNOLDS, HARTMANN, ELECTRIC LOAD PARAMETER, MAGNETIC INTERACTION PARAMETER, ALSO CALLED THE STEWART NUMBER.

CONCLUSIONS FROM DIMENSIONLESS ANALYSIS.

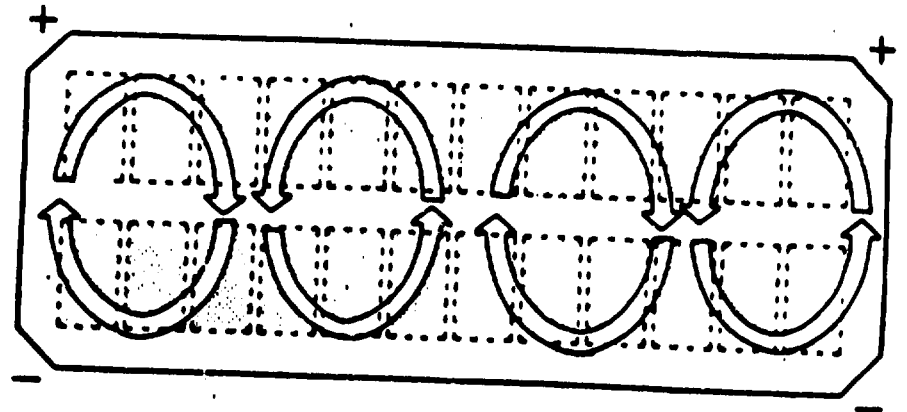
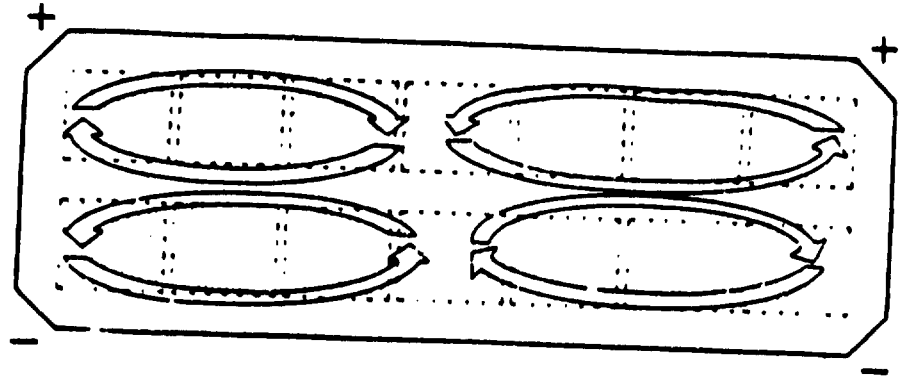
1. THE ELECTROLYTE AND THE METAL ARE VERY DIFFERENT MAGNETOHYDRODYNAMICALLY.
2. THE TWO LIQUIDS ARE TURBULENT.
3. THE ELECTROMAGNETIC FORCE IS IMPORTANT IN BOTH LIQUIDS.
4. THE ELECTRIC CURRENT, INDUCED BY FLUID FLOW, IS NOT NEGLIGIBLE IN THE METAL.
5. THE FLOW INDUCED MAGNETIC FIELD IS NEGLIGIBLE IN BOTH LIQUIDS.
6. THE FLOW IS STATIONARY DURING $\approx 50 \text{ S}$.

I WILL NOW PRESENT SOME TYPICAL DIAGRAMS OF METAL CIRCULATION IN CELLS.

- ONE POOL
- TWO POOLS
- FOUR LONGITUDINAL POOLS
- FOUR TRANSVERSE POOLS



**Metal Circulation in End-to-end Cell
(110 kA, HS) and Side-by-side Cell
(150 kA, prebake, anode risers at cell ends)**



**Metal Circulation in Side-by-side Cell
Top: 76 kA, bottom: 150 kA,
Anode risers at cell sides**

COMPUTER SIMULATION GIVES MORE DETAILS.

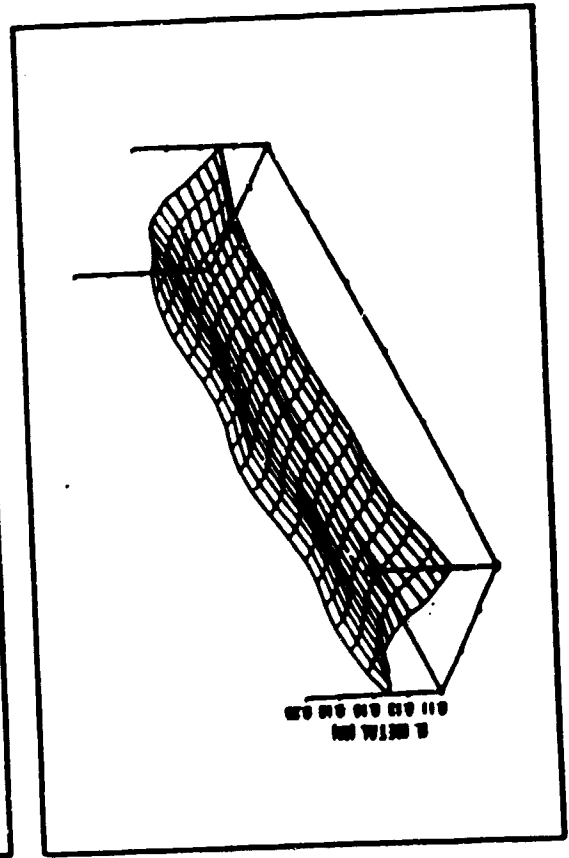
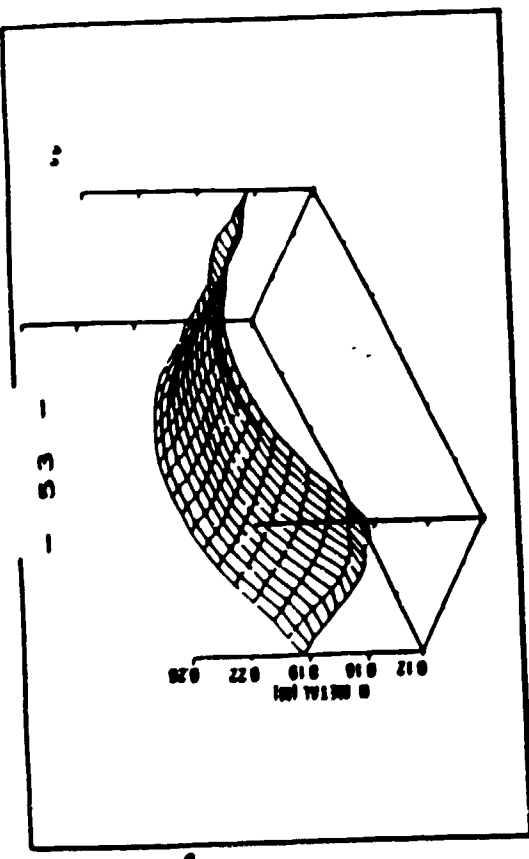
THE DIFFERENCE BETWEEN AN END-TO-END AND A SIDE-BY-SIDE CELL CAN BE SEEN ON THIS SLIDE.

IN THE SIDE-BY-SIDE CELL, THE CIRCULATION IS SYMMETRICAL WITH RESPECT TO THE TRANSVERSE AXIS.

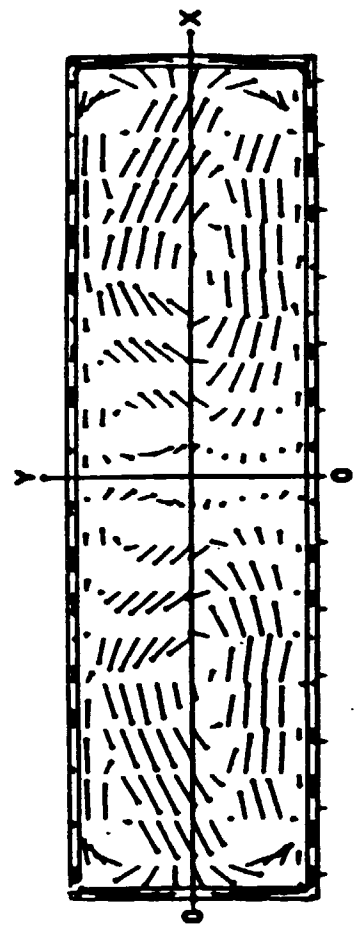
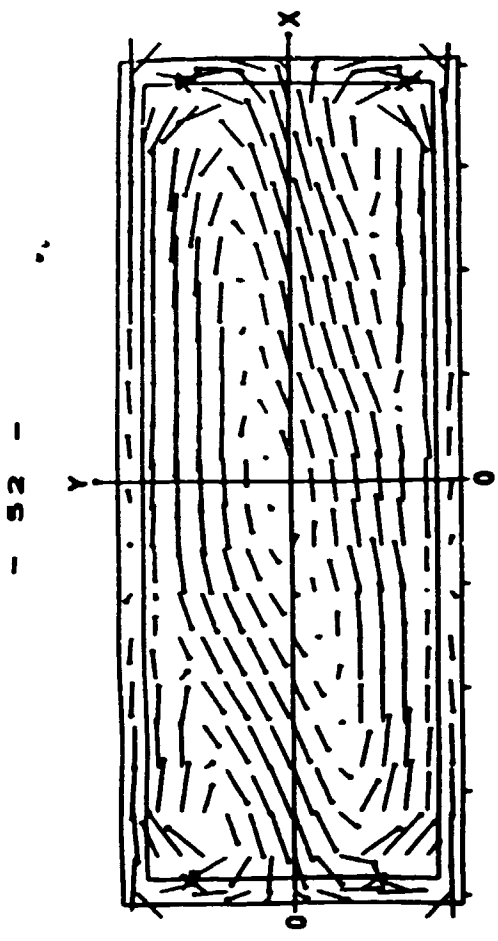
THE METAL-BATH INTERFACE, WHICH IS CALCULATED SIMULTANEOUSLY, IS VERY DIFFERENT IN BOTH TYPES OF CELLS. THERE IS A TRANSVERSE PEAK IN THE END-TO-END CELL AND A LONGITUDINAL PEAK IN THE SIDE-BY-SIDE CELL. IN SIDE-BY-SIDE CELLS THE ABSOLUTE DEFORMATION OF THE INTERFACE IS MUCH SMALLER THAN IN THE END-TO-END CELLS.

Advantages of Side-by-side Cells:

- **The magnetic field is favourable:
Vertical (B_z) and
Transverse (B_y) Components
are Small and Symmetrical.**
- **Metal circulation is divided into
symmetrical pools.**
- **Metal-bath interface deformation is small.**

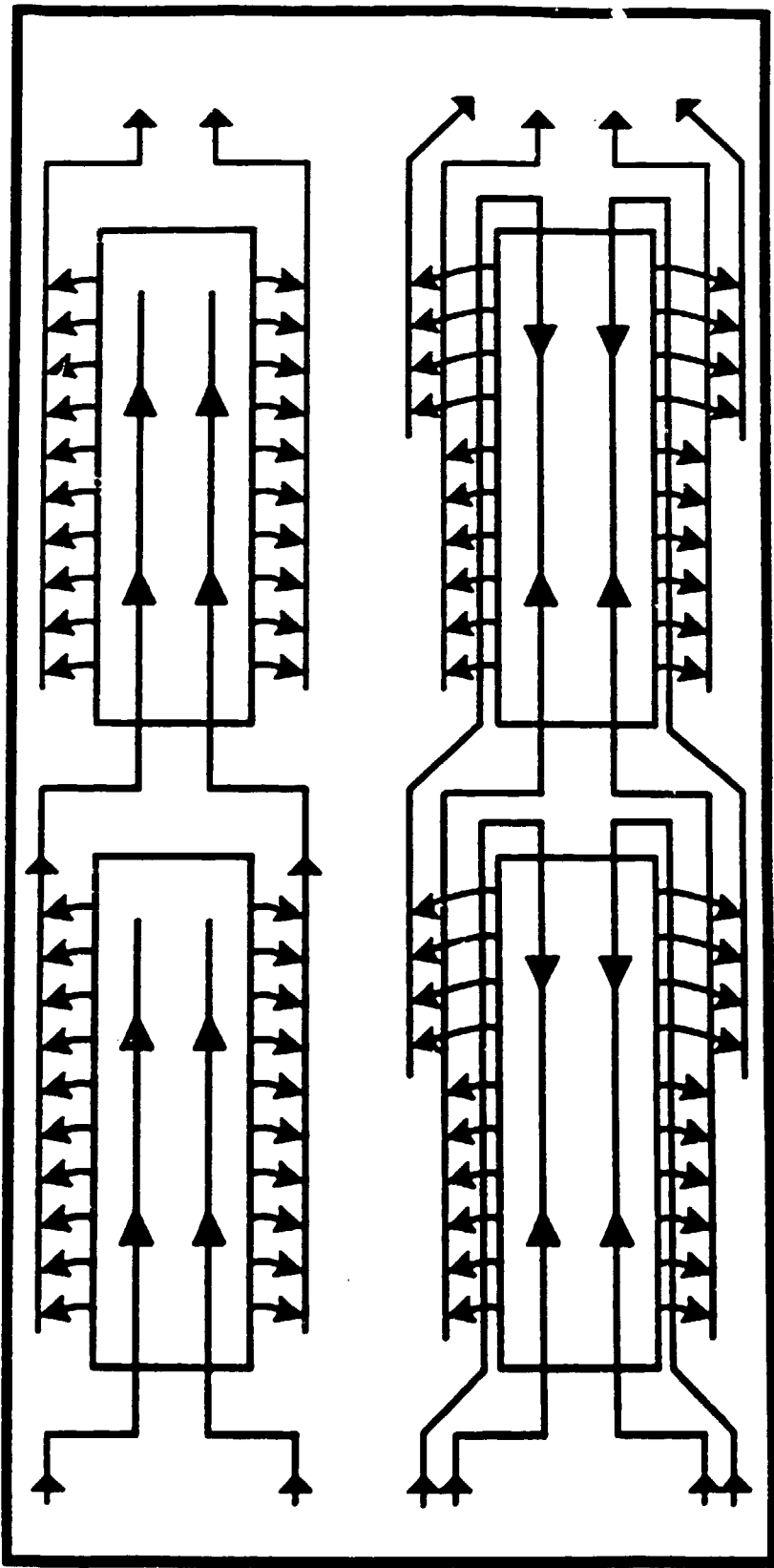


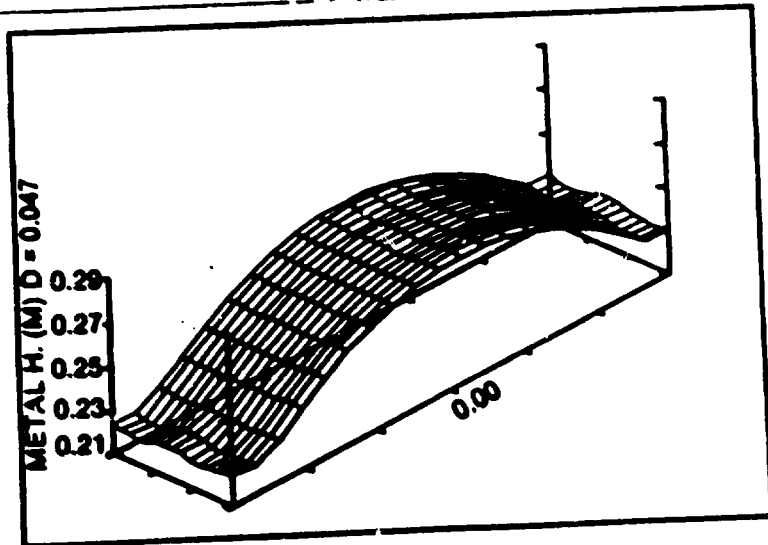
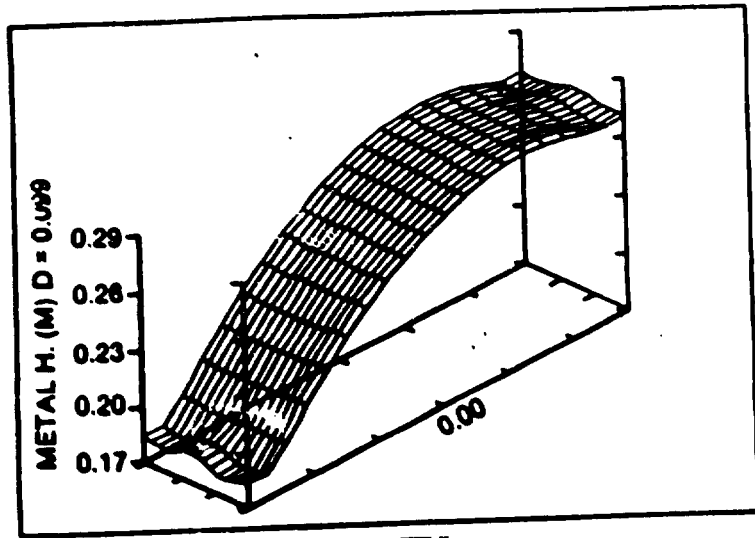
Calculated Deformation of the Metal-Bath Interface
for End-to-end (top)
and Side-by-side (bottom) Cells



Calculated Metal Circulation for
End-to-end (top)
and Side-by-side (bottom) Cells

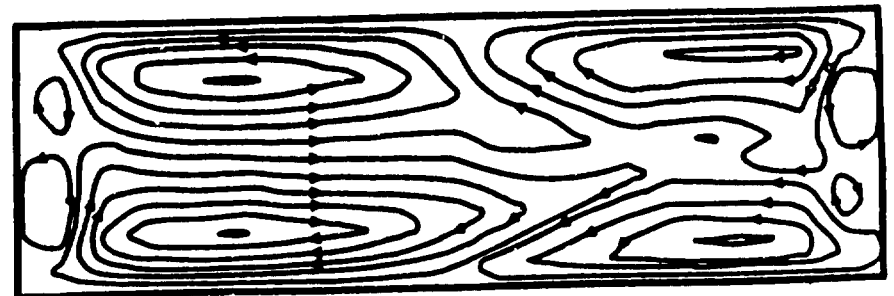
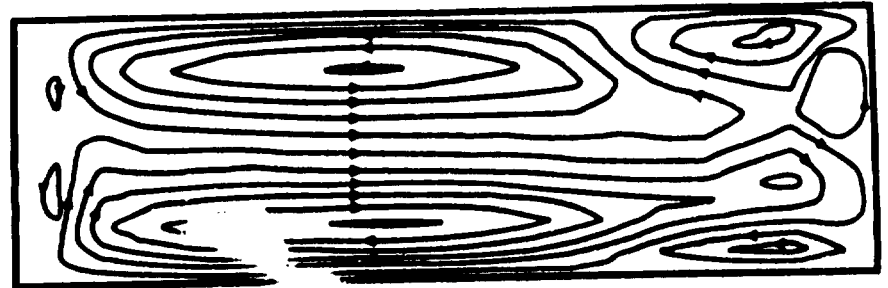
Busbars for end-to-end cells with current feed from one end (top) and both ends (bottom)



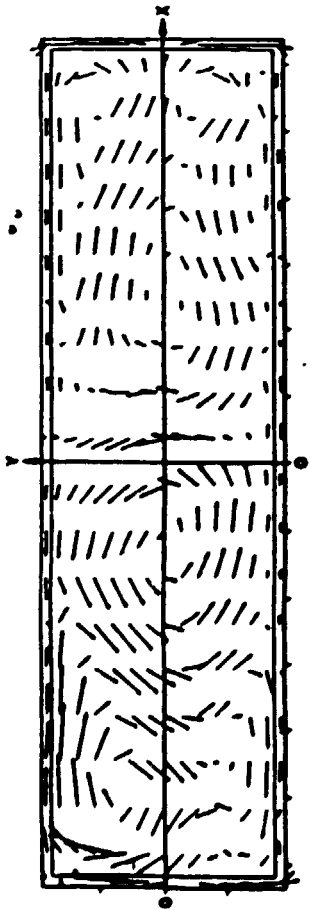


**Calculated Deformation of the Metal-Bath Interface
for End-to-end Cells with Current Feed
at One End (Top) and Both Ends (Bottom)**

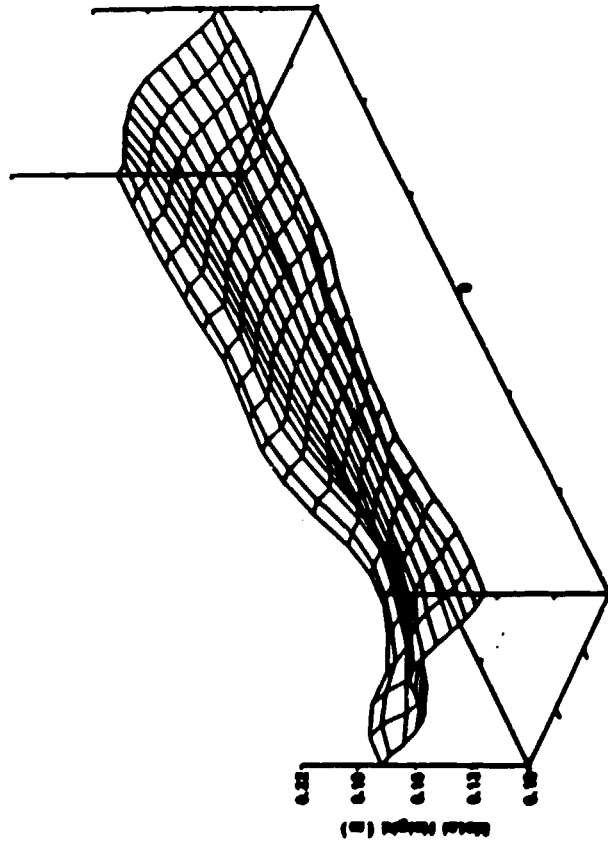
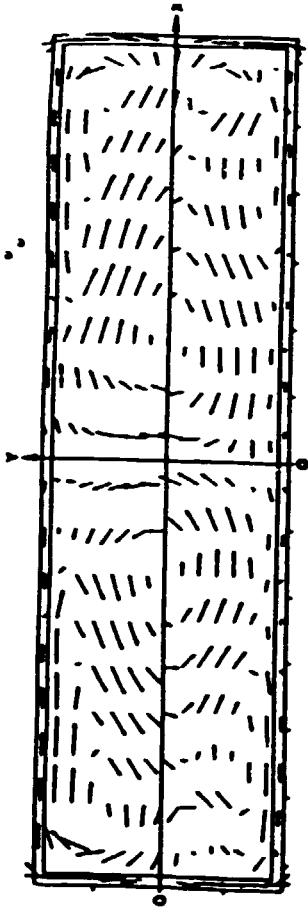
**Circulation patterns
for end-to-end cells with
current feed at one end (top)
and at both ends (bottom)**



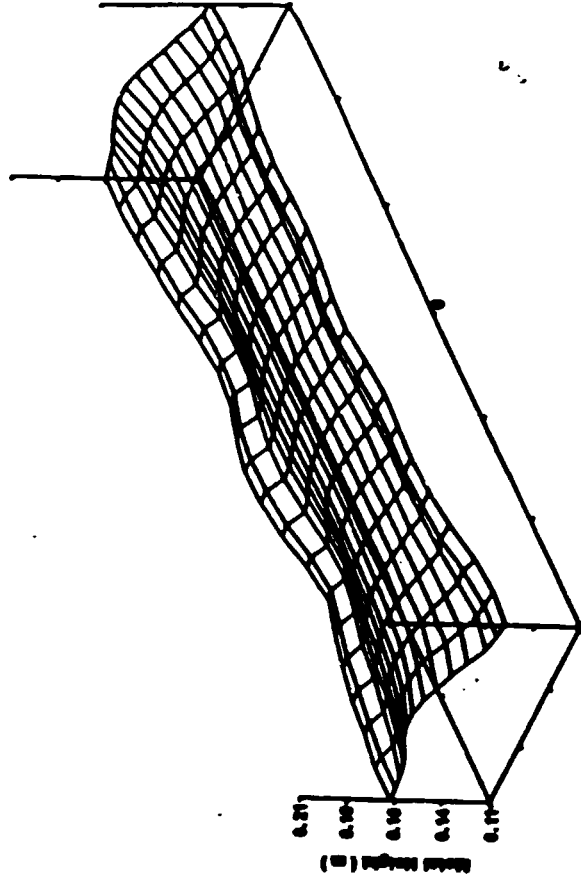
- 58 -



- 57 -



Metal circulation pattern and bath-metal interface height during the changing of an anode in the upstream (left top) corner of the cell.

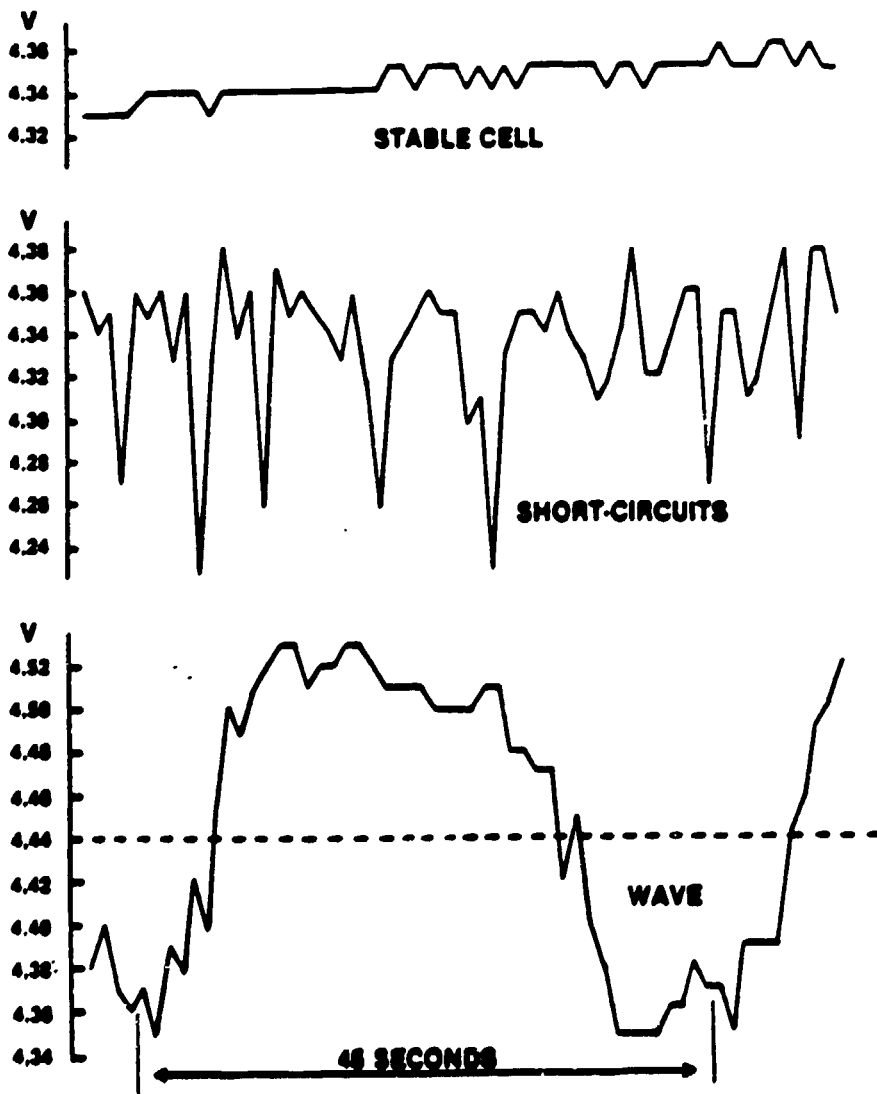


Typical metal circulation pattern and bath-metal interface height.

Stability of Metal-Bath Interface

Most important dynamic phenomena are:

- local short-circuits:
metal surface comes irregularly into contact with the anode
- periodical waves:
metal-bath interface fluctuates regularly (resonant cavity)



170 kA Probake Cells: Traces of Cell Voltage during 60 s.

STABILITY ANALYSIS APPROACH

1. Various analytical perturbation theories have been developed (see LaCamera and al., Light Metals 1992, p. 1179).
2. ESTER/PHOENICS time dependent calculations (see Potocnik, Light Metals 1989, p. 227-235). Growth or damping of interface waves is analyzed.
3. Experimental studies based on :
 - analysis of cell resistance oscillations (noise and kicking index),
 - individual anode current studies which give a picture of metal-bath interface waves (see Laroche, Bui, Boivin, Potocnik, CIM Symposium 1988, p. 169-187).

DESIGN APPROACH

CELL PERFORMANCE



HYDRODYNAMICS



CURRENT DISTRIBUTION

MAGNETIC FIELDS



BUSBAR

DESIGN



TOP DOWN (goal driven) APPROACH in DESIGN



BOTTOM UP (data driven) APPROACH for UNDERSTANDING

MHD

CELL PERFORMANCE

CAPITAL COST

- CURRENT EFFICIENCY
- ENERGY EFFICIENCY
- THERMAL EQUILIBRIUM
- EASE of CELL OPERATION
- CATHODE LIFE
- LINE CURRENT
- CELL SIZE
- CELL SPACING
- BUSBAR WEIGHT
- BUILDINGS

CURRENT EFFICIENCY



- Bath
- Average ACD
- Instabilities (Noise)
- Turbulent kinetic energy
- Relative bath-metal
- Non-uniformity of ACD
- Short circuits (Kicking)
- Turbulent diffusivity
- Patterns

MHD MEASUREMENTS

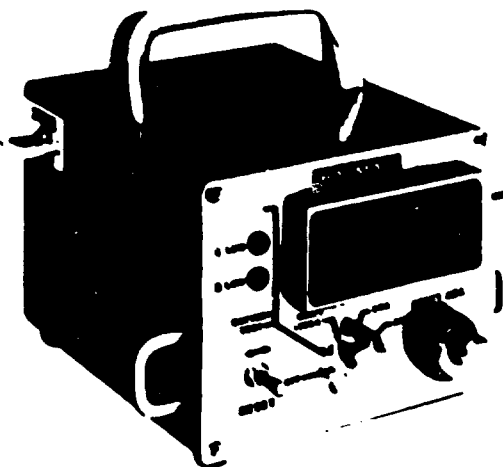
- Electric current distribution is measured by :
 - a) voltage probes or forks (current is deducted from voltage drop),
 - b) Halmar instrument (current is obtained directly).
- Usually measured are :
 - anode currents,
 - collector bar currents,
 - busbar currents.
- Magnetic field distribution is measured by tri-axial Hall probes, cooled when put in liquid metal or bath.
- Liquid metal velocity is measured by :
 - iron rod dissolution technique,
 - radioactive tracers,
 - metallic tracers.
- Metal bath interface shape is measured by iron rod immersion technique (measurement taken from the mark left on the rod at the metal-bath interface).

HALMAR

COP clamp-on portable ammeters

Model COP-D Features

- digital readout — easier, faster
- more accurate
- lighter weight
- battery operated — rechargeable
- non-contacting head



Digital COP

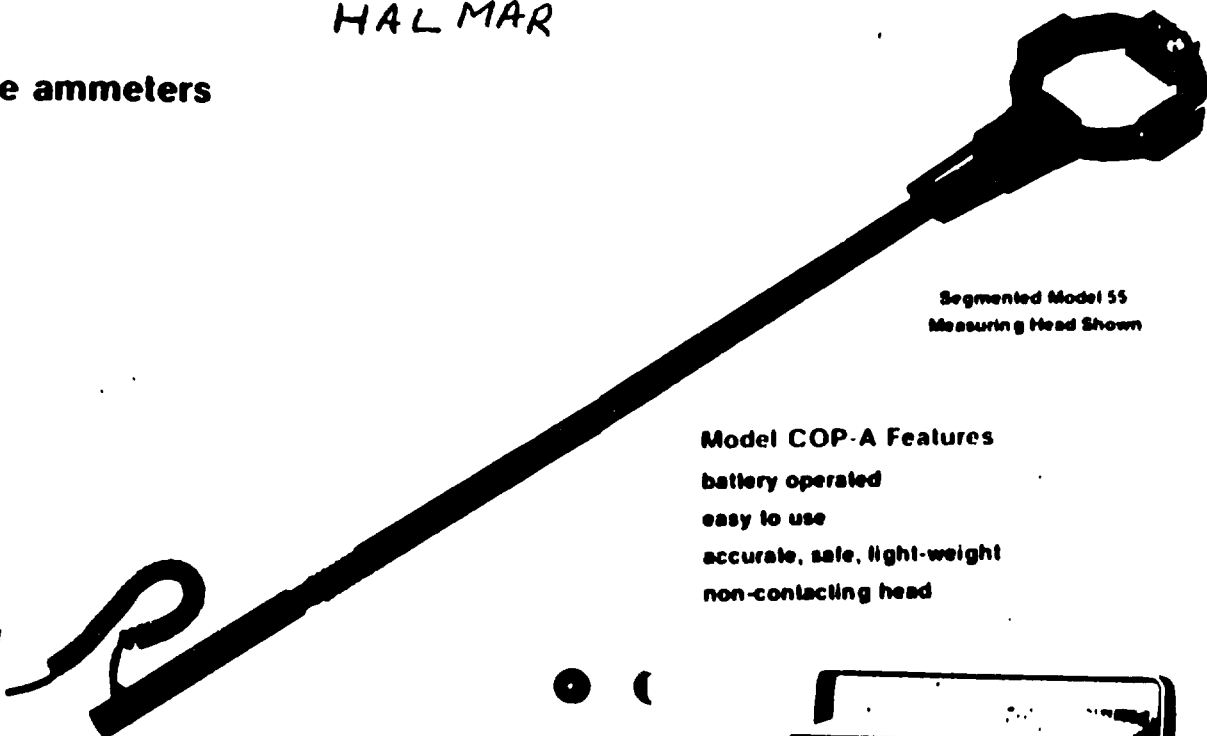
The Digital COP ammeter is a completely new version of the extremely successful analog COP. This new meter retains all of the excellent durability and ruggedness standards established by the analog COP. It goes beyond by making the current measurements easier, faster and more accurate.

Designed for daily use by production people working under the rugged conditions imposed by industry, the Digital COP tolerates corrosive chemical atmospheres, wide temperature variations and high magnetic fields. The solid state unit is powered by a rechargeable battery pack.

The Digital COP reads average dc current. Measurement ranges are 0 to 2 kilowatts and 0 to 20 kilowatts. Overall accuracy is an excellent ± 2.5 percent. The new state-of-the-art design has substantially reduced the metering unit weight. This is important, considering the normal all-day use of the meter.

The rear third of the unit is a modular, rechargeable battery pack which is quickly removable with two snap action fasteners. The meter may be used continuously simply by replacing the battery pack with a freshly charged one. Nominal usage per charge is 20 hours. The removed pack is then placed on the HALMAR battery charger, which is supplied with each COP-D. Recharging time is 8-10 hours; the charger automatically cuts off when the battery pack is fully charged.

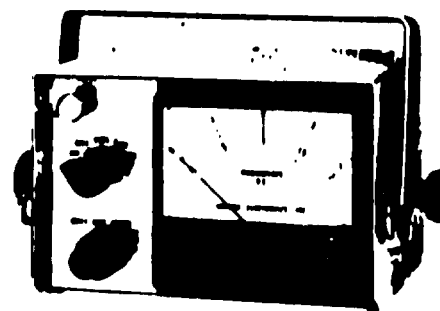
The model COP-D can be supplied with any of the measuring head models described on pages 11



Segmented Model 55
Measuring Head Shown

Model COP-A Features

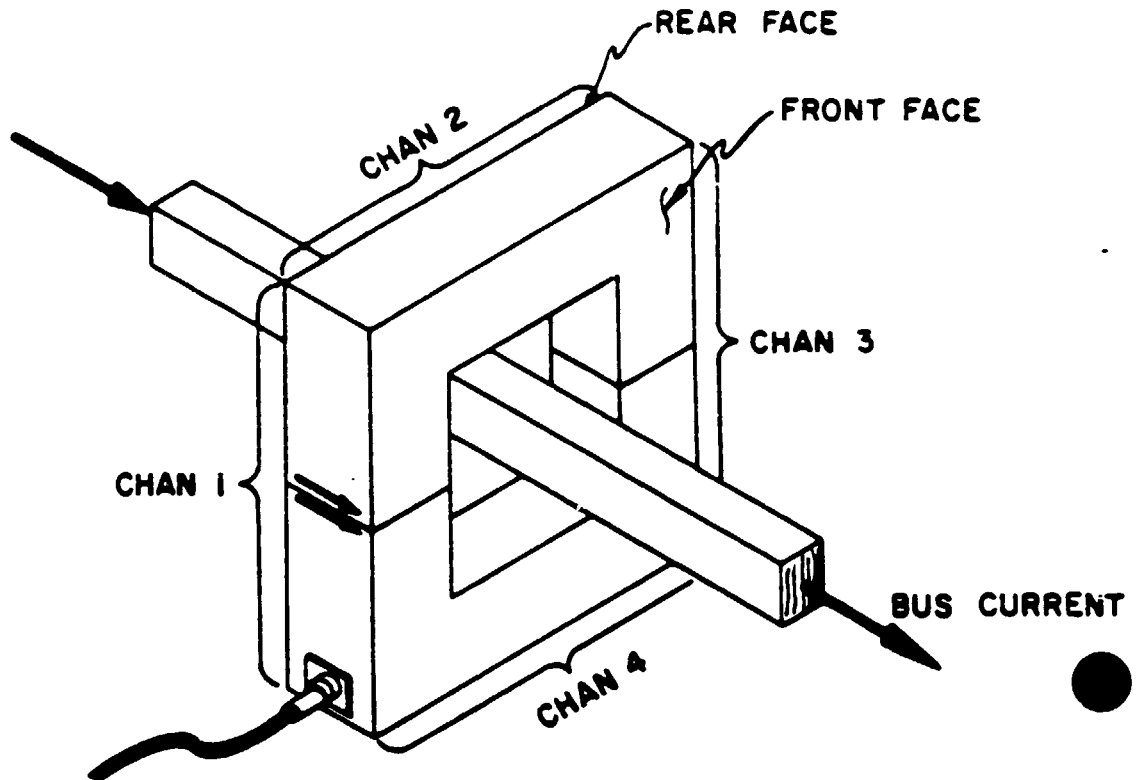
- battery operated
- easy to use
- accurate, safe, light-weight
- non-contacting head



Analog COP

The HALMAR analog COP ammeter is an accurate tool designed for daily use under the toughest conditions imposed by industry. These include corrosive chemical atmospheres, wide temperature variations and high magnetic fields. The solid state circuit is battery powered and ready to go at all times. No warm-up or wait-around!

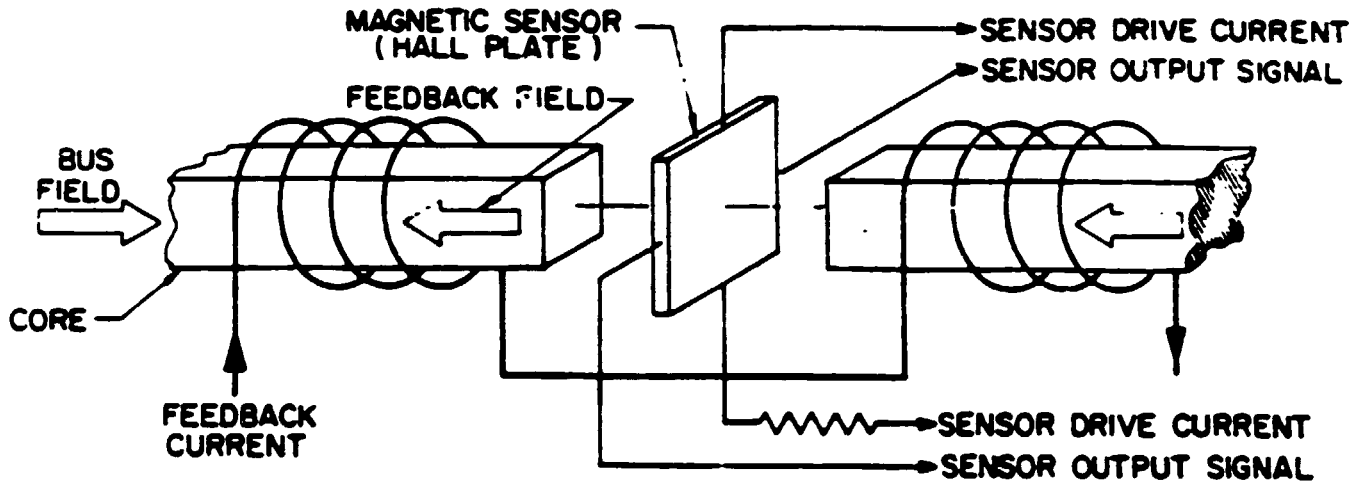
The analog COP measures average dc current. Full measurement ranges are shown in the specifications. The COP-A can be supplied with any of the measuring head models described on pages 11 and 12. (Note: a specification for the COP-A is available from the Group of average current clamp-on ammeters for details.)



1. BUS CURRENT MUST FLOW INTO REAR FACE WHICH IS IDENTIFIED BY RED DOTS ON 4 CXM & 7 CXM HEADS.
2. CURRENT DIRECTION ARROWS ON 12 CXM & 17 CXM HEADS IDENTIFY BUS CURRENT DIRECTION.
3. CHANNEL #1 IS ALWAYS LOCATED ON CABLE EXIT SIDE.
4. CHANNEL NUMBERS PROGRESS CLOCKWISE WHEN VIEWING FRONT FACE.

**HALMAR
MEASURING HEAD
ORIENTATION**

HALMAR



MAGNETIC NULL DETECTOR DIAGRAM
NOT TO SCALE

PRINCIPLE OF OPERATION

All DYN AMP current measuring equipment is based on a magnetic null principle. The magnetic sensor produces a voltage output proportional to the difference between the bus field and the feedback field. The sensor output is amplified and is returned to the magnetic circuit in the form of feedback current. This current is passed through 5000 turns to produce the feedback field.

The DYN AMP measuring head (Series CXM) is divided into (4) null sections which in reality are the four sides of the head. Each side of the head and its associated portion of the signal converter is called a channel. The sum of the four channel currents is the output current which is always in the ratio of 5000:1 to bus current.

HALL-HÉROULT CELL MAGNETICS MEASUREMENTS AND COMPARISON WITH CALCULATIONS

Donald P. Ziegler and Robert L. Kozarek
Alcoa Laboratories

LIGHT METALS 1991, p 381

Magnetic Field Probe

The magnetic field measurements were made by immersing a tri-axial Hall effect probe into the metal pad. The probe was specially constructed by F. W. Bell, Inc., to be used with their Model 811R3 gaussmeter. This probe, shown in figure 1, uses three mutually perpendicular Hall effect crystal plates to simultaneously measure all components of the magnetic field.

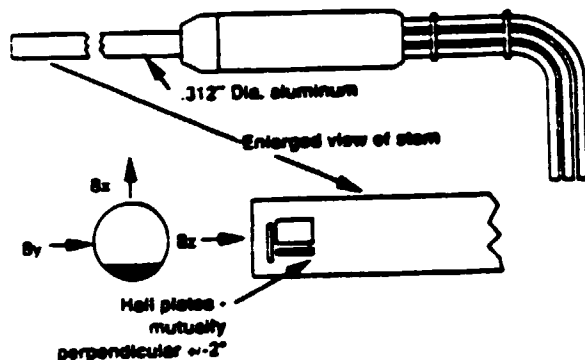


Figure 1: F.W. Bell 3-Axis Probe

An air-cooled sheath, shown in figure 2, was used to protect the probe while making measurements in the bath and metal zones in a Hall-Héroult cell. A thin layer of bath freezes on the surface of the sheath, further protecting the probe during operation. With the present design, the air flow rate is limited by the muffler on the exit. Using 90 psi air, the gaussmeter probe tip is maintained near 50 °C. The useful time the probe may be used inside a Hall cell is limited by air-burning of the carbonaceous jacket on the sheath. This allows the probe to be used for long-term transient measurements.

Current Measurements

Alcoa's Tennessee cells, designated P225, are designed with flexible bus connections to each anode. Anode currents were measured using the voltage drop across a section of this bus. Figure 3 shows a schematic of the flexible bus. Cathode collector bar currents were measured in a similar fashion using the voltage drop across two flexible strap connections as shown in figure 4. Because

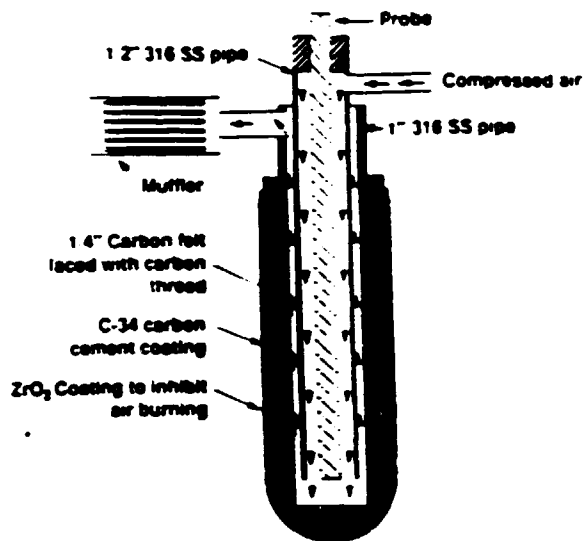


Figure 2: Air Cooled Sheath

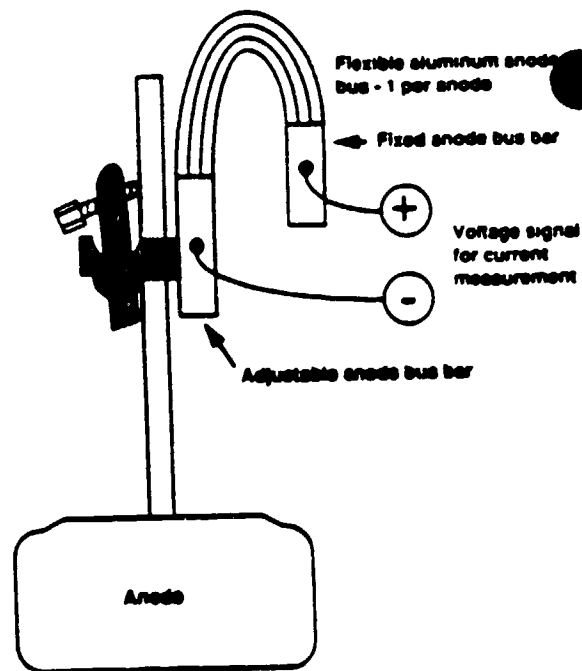


Figure 3: Anode Current Monitoring Rig for Tennessee P225 Cell

there are two straps per bar, a balancing resistor network was used to obtain a single signal per collector bar.

Each of the anode and cathode signals were calibrated independently using a Halmar 1000 portable ammeter. As a check on the calibration, when the anode and cathode currents were summed and compared to the line current, the agreement was always within 7% for the 32 anode currents and 5% for the 40 collector bar currents.

Data Collection and Interfacing

Simultaneous measurements were made of anode and collector bar currents and the three components of the magnetic field at a single point in the cell. Because of our interest in transient as well as steady state data, each of the signals was scanned in a 6 ms. burst 5 times a second. The data for each time step was transmitted to a host computer for storage and processing. Figure 5 is a plan view schematic of the P225 cell showing the anode and cathode locations and average currents at each location.

Electrical measurements are always difficult to perform in a potroom, because of the high voltage of the potline-to-earth ground. Battery powered fiberoptic isolation devices were used to insure signal integrity and minimize safety hazards. Separate units were used for the anode and cathode currents, and the chassis was grounded to the cell at anode or cathode potential to minimize signal noise. The gaussmeter presented special problems since it required 110 VAC power. Two isolation transformers were used in series to provide isolation from a 110 V. source at the wall. One was located at the wall, and the other at the cell where the gaussmeter was located. The three 0-1V DC output signals from the gaussmeter were passed through Burr-Brown isolation amplifiers before connecting to the data acquisition units to provide further isolation.

In a typical magnetic measurement, the probe was placed in the liquid metal region at anode gaps near the periphery and in the center aisle of the cell. Data were collected for 10 - 30 minutes at each probe location. The steady state values were computed by averaging over the data collection period for each probe location.

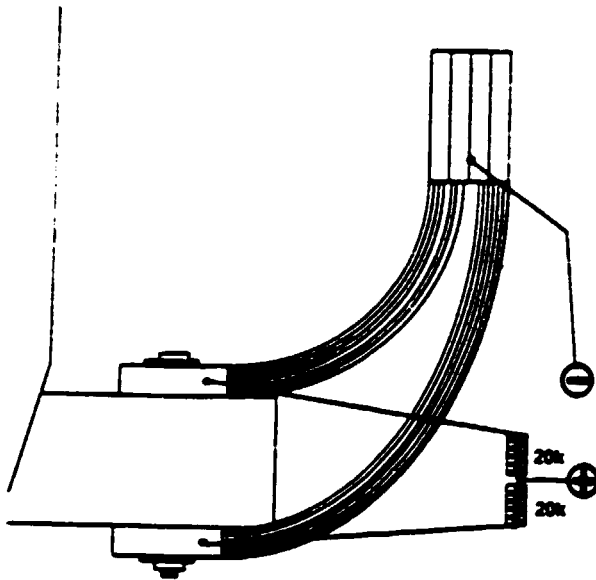
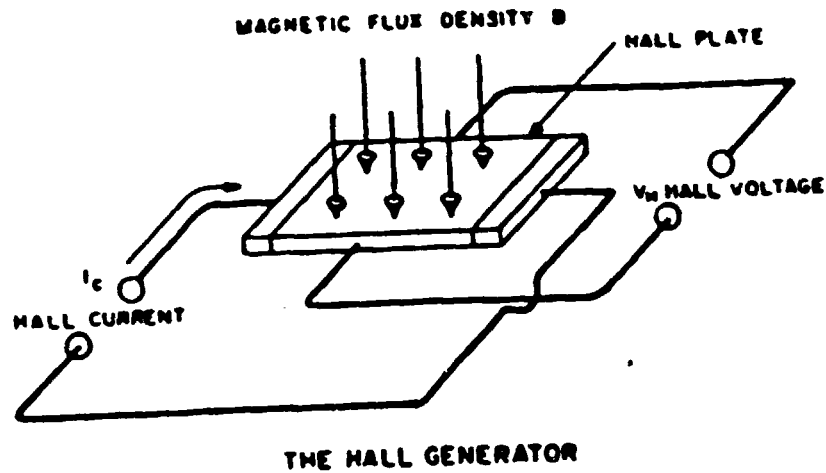


Figure 4: Cathode Current Monitoring Rig for Tennessee P225 Cell

MAGNETIC FIELD PROBE

THE SENSING ELEMENT

The Hall-Pak generator used for magnetic flux sensing is a semiconductor device operating on the Hall-Effect principle. It consists of a thin rectangular wafer of high-purity indium arsenide with 4 leads attached, Fig. 2.



The application of control current I_c to the Hall generator results in a flow of charge carriers through the semiconductor material in the direction of its long dimension. When the Hall generator is placed in a magnetic field, the Lorentz force, acting on the moving charges, deflects them at right angles to the direction of their motion through the Hall plate. This is the same force that deflects the electron beam in a cathode ray tube.

The resulting build-up of charge carriers along the sides of the wafer produces the Hall voltage, and this voltage appears as an output at connections made on each side of the element. Hall voltage V_H is directly proportional to the flux density B and to the magnitude of control current I_c .

$$V_H = K_H (B \times I_c)$$

The three factors V_H , I_c and B are mutually perpendicular. If the magnetic flux vector B is not perpendicular to the face of the Hall generator, the Hall output will be proportional to the component of B that is perpendicular to the element. The constant of proportionality K_H is called the Hall sensitivity constant, and is approximately 0.075 volt per kG-ampere for 1X probes, and 0.0075 volt per kG-ampere for 10X probes.

Brian F. Bradley,

Ernest W. Dewing,

and John N. Rogers

METAL PAD VELOCITY MEASUREMENTS BY THE IRON ROD METHOD

LIGHT METALS 1984

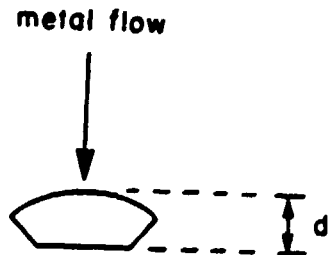
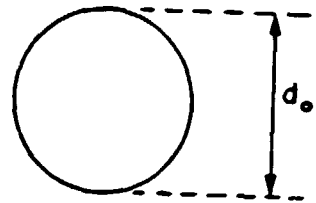
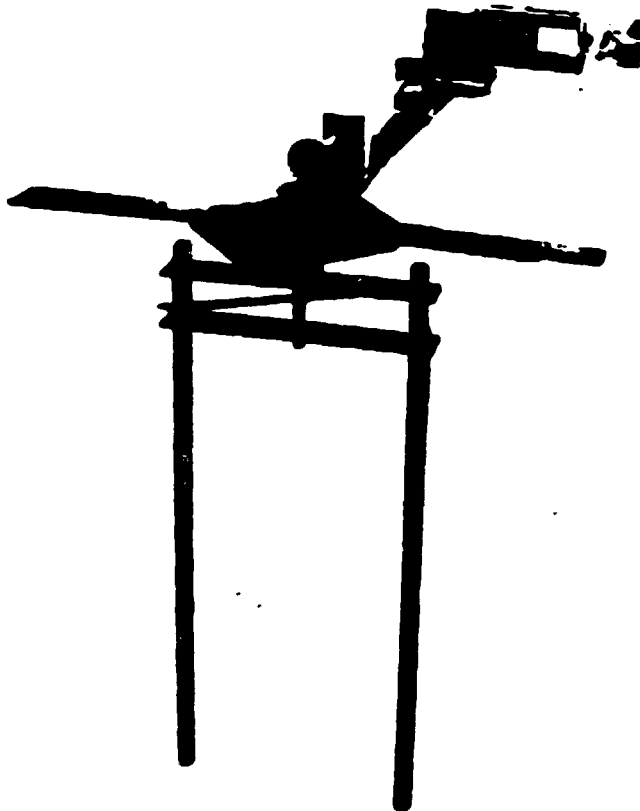


Figure 1 - Rotating rig for calibrating rod dissolution rate.

Figure 2 - Cross section of rod before and after immersion (schematic).

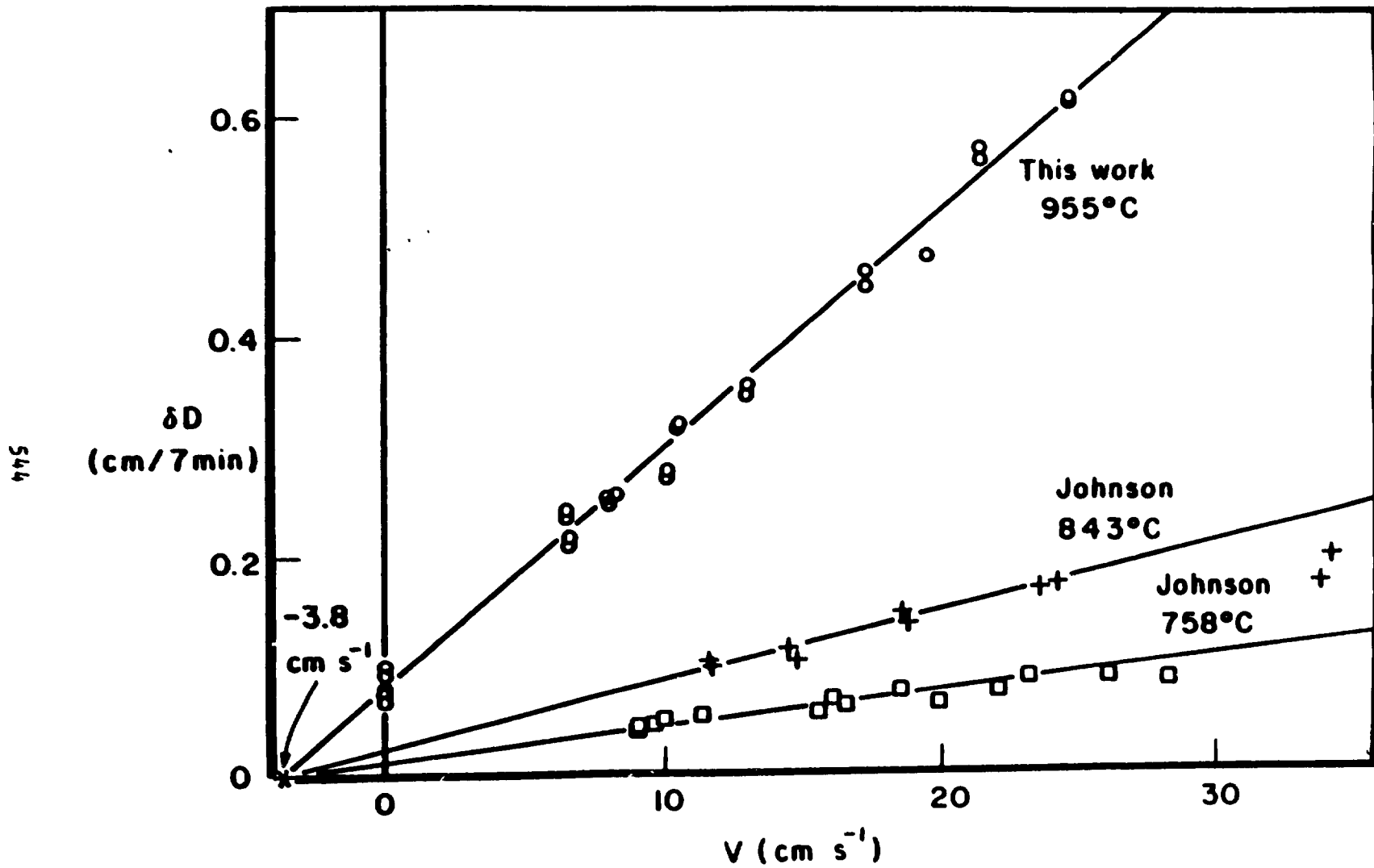


Figure 3 - Reduction of diameter in 7 min vs flowrate.

- 72 -

A. T. Tabereaux and R. B. Hester

METAL PAD VELOCITY MEASUREMENTS IN PREBAKE
AND SODERBERG REDUCTION CELLS

LIGHT METALS 1984

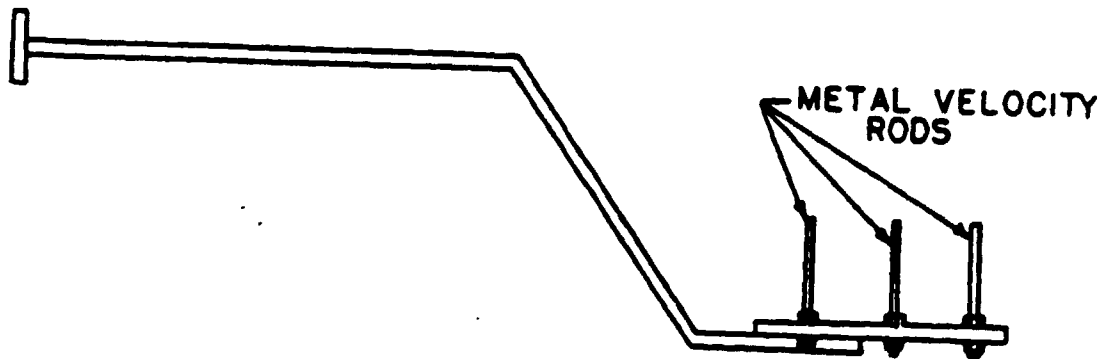


FIGURE 7. SPECIAL METAL ROD HOLDER.

PRINCIPLES OF MHD DESIGN OF ALUMINUM ELECTROLYSIS CELLS

Vinko Potočnik

Alcan International Limited

Arvida Research and Development Centre

1955 Mellon Blvd, P.O. Box 1250

Jonquière, Québec, Canada

Abstract

Magneto-hydrodynamics (MHD) plays an important role in the performance of aluminum electrolysis cells. If MHD is not considered thoroughly enough in the design the current energy efficiency of the cells may be severely decreased and cell operation may be outright impossible. In this paper, principles guiding the cell busbar design process using MHD are reviewed. Special consideration is given to different MHD parameters of the cells, such as electric current and magnetic field distribution, electromagnetic forces, fluid dynamics and their influence on current efficiency.

Introduction

Magneto-hydrodynamic phenomena in aluminum electrolysis have existed ever since the invention of the process over 100 years ago, but their importance was not recognized until much later. In the 1950's when the cells became larger and the line currents reached and surpassed 100 kA, it became evident that the magnetic effects had started to hinder further rapid progression towards higher capacity cells.

Until that time, the design of the cell busbar system was simple: the current from the cathode of a cell was fed directly to the anode of the downstream cell along the shortest (and the cheapest) path as pointed out by Potočnik and Evans [1]. In the 1950's some solutions to the magnetics problem were found on a semi-empirical basis. By the early 1960's a more fundamental but still rather qualitative approach was introduced in this field, most notably by Givry [2]-[4] and Saeger [5]. Originally Givry [2] studied the electromagnetic forces to derive several criteria for the transverse magnetic field of a cell. In a later publication Givry [4] introduced hydrodynamics into these studies and thus introduced magneto-hydrodynamics into the cell design process. Givry [3] and Saeger [5] also laid down the foundations of busbar economics; these allow the determination of the optimum busbar current density which in turn minimizes the total material and operating costs of the busbar.

Later other authors contributed important milestones in cell design practice based on MHD, mostly by including more

complete physics, more geometrical detail and more rigorous mathematical solutions. Of course, all this increased the complexity of the resulting mathematical models, but this was well compensated by the rapidly increasing computing power which became available. Müller and Solberg [6] introduced a two-dimensional MHD model for the calculation of liquid velocities, and metal-bath interface heights. They used a model for magnetic field calculations, developed by Seie [7]. Wahnsiedler [8] presented a three-dimensional time dependent MHD model based on a commercial package, ESTER/PHOENICS. [9] derived a cell stability criterion, based on harmonic analysis of a simplified metal-bath interface wave equation. Potočnik [10] used a three-dimensional, time dependent model, based on ESTER/PHOENICS, for the analysis of metal-bath interface waves.

By mid-1980's many aluminum producers had more or less complete mathematical models of cell MHD; these models were used for new designs and retrofitting. However, the models did not entirely eliminate the need for measurements in the operating cells.

MHD and Current Efficiency

The MHD itself would not be of such importance if it did not have a serious impact on cell performance. Current and energy efficiency are directly affected, but we still do not know how much and by what mechanism. A few hypotheses have been quantified. Lillebuen et al [11] proposed a relationship between the current efficiency and relative metal-bath velocity. Evans et al [12] ascribed the current efficiency loss to the turbulent kinetic energy in the inter-polar space. Robl et al [13] introduced hydrodynamics via turbulent diffusivity. Hauptin [14] combined the models of Lillebuen [11], Evans [12] and Robl [13] and concluded that this combination gives realistic values that track individual practice. However, no publication has confirmed this claim. All these models assume that fluid dynamic conditions in the bath (bath-metal relative velocity, bath turbulence, gas concentration and bubble size) are known from some other model. These conditions are certainly the result of several contributions such as MHD, gas release, anode-to-cathode distance (ACD) and alumina concentration. No model that com-

biner these factors has been proposed except on a qualitative basis: Langon and Peyneau [15] and Rosleth et al [16]. Most studies separate MHD and gas driven flows, which seems to be acceptable for cell design studies based on MHD, if they do not use current efficiency criteria. Gas driven flow of bath, studied by Solheim et al [17] and Dermedde and Cambridge [18], is of the same order of magnitude as MHD flow. The gas driven flow may contribute to the current efficiency loss, because it increases the bath turbulence and adds to the average velocities. It also has some vertical velocity component in the interpolar space and at the anode perimeter, which augments vertical transport of the aluminum dissolved in the bulk of the bath [17].

As shown by Grijotheim et al [19] the reports on the influence of ACD on current efficiency are conflicting. Some laboratory and plant studies show that the current efficiency decreases very rapidly with decreasing ACD below the limit of about 2-3.5 cm [16], [20], [21]. This limit probably depends on the MHD and operating conditions of the cell. Thus, any static or quasi-static metal-bath interface deformation which would decrease the local ACD below this limit may have serious repercussions on the current efficiency. Cell instability, which is associated with metal-bath interface waves (noise) and local short circuits (kicking), may contribute to current efficiency loss in various ways: by the reduction of local ACD [22], by increasing flow velocities and turbulence [15] and by creating metal "streamers" [13], [18]. Particularly detrimental seem to be short circuits between the metal and the anode, as pointed out by Hyland [23] and Tarcy and Sorensen [24]. These may be periodic or random (kicking). No consistent model, relating the current efficiency to the magnitude and type of instability has been published, but some experimental data were analysed in [24]. The influence of anodic current density on current efficiency has not been well established, but in general the data show an increase in current efficiency with increasing current density [19]. This relationship enters the analysis of current efficiency loss due to metal-bath interface waves [22], since these cause large variations of current density locally.

MHD Design Criteria

In an ideal world, the current efficiency models would provide top level criteria for the cell design based on MHD. In the real world, given the state and qualitative nature of these models, they may be used as tendency indicators or to determine what MHD parameters may be important.

The use of MHD criteria on their own has been more clearly established. Mathematical models are now available but some caution must be used in their interpretation. The importance of various MHD parameters has not been well established yet due to the lack of reliable quantitative current efficiency models. Therefore MHD models are best suited for comparative studies of trial proposals, among which should be some that are successful in plant practice. The operating cell data can give comparison standards and can be used for model validation, but we have to bear in mind that the assessment of plant MHD is not easy

because of inherent variability of the parameters from cell to cell as pointed out recently by Ziegler and Kozarek [25].

The evaluation criteria for MHD solutions will also depend on the sophistication of available models and on confidence in their validity. In general, greater weight will be given to hydrodynamic parameters. Criteria related to properties of the electromagnetic force and its constituents - magnetic field and current density distributions - continue to be useful and may help accelerate the design process. It seems that in spite of the increased sophistication of the mathematical models, the MHD-based cell design process is still an art that requires a great deal of experience.

Objectives and Design Approach

The objective of the MHD-based cell design is to find an optimal busbar system which will assure stable cell operation and good cell performance. The elements to be considered are:

- economics:
 - overall busbar cost, including the busbar material and installation cost and the cost of electrical energy released in the busbars during the lifetime of the smelter [3], [5] [26];
 - building cost, influenced by the cell-to-cell spacing [32].
- current and energy efficiency and ease of operation.
- constraints, such as: allowance for equipment access to the cell, cell shutdown and its removal for relining, allowance for busbar construction practices, respect for standard shapes of individual busbar elements, etc. Additional constraints are usually imposed for cell retrofits, for which cell size, busbar supports, potroom structure are often fixed.
- safety:
 - no busbar is allowed to be overloaded by current in regular and cell bypass situations [31];
 - a certain safe distance or insulation is to be kept between the busbars with appreciably different electrical potentials [32].

Designing is usually an iterative process [3]. The MHD is studied first in order to determine acceptable hydrodynamic conditions in the cell. This determines the configuration of the busbars in space and the currents to be carried by each one. Then the busbar cross-sections must be calculated so that busbar currents are provided according to the MHD requirements and that the overall busbar cost is minimized. In the design process regular and exceptional situations have to be considered:

- cells in regular locations in the potline, at the extremities of the line, at the passageways and in the vicinity of the shutdown cells [26];
- cells in regular and exceptional conditions related to free profiles [27] and anode changing [8], [26], [27].

The final design is selected on the basis of a weighted compromise between different situations with respect to MHD and

economics. On the other hand, no compromise can be made on safety issues nor some of the constraints quoted above.

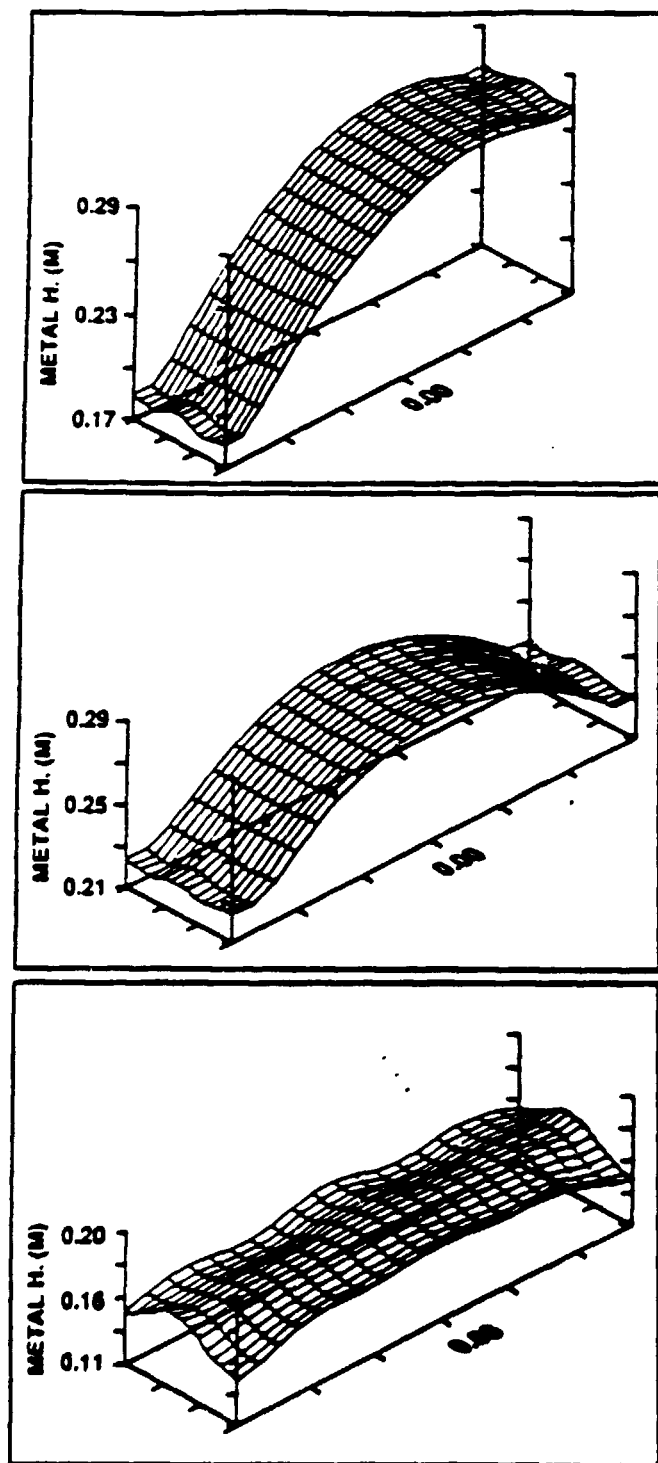


Figure 1: Calculated metal-bath interface shape for an end-to-end cell with current feed at one end (top) and at both ends (center) and a side-by-side cell (bottom).

Hydrodynamics

Due to unreliability of criteria associated with current efficiency, hydrodynamics plays the central role in the cell design. In general, hydrodynamic effects are not wanted, except for accelerating the alumina dispersion in the bath. There are two distinct driving forces for the flow and interface deformation: electromagnetic and gas-induced. For the busbar design, most people consider electromagnetic forces only. This may be rather incomplete, if judgment is made on the basis of current efficiency and/or rather absolute criteria are used for the interface height deformation, both being influenced by the overall hydrodynamics of the metal and the electrolyte.

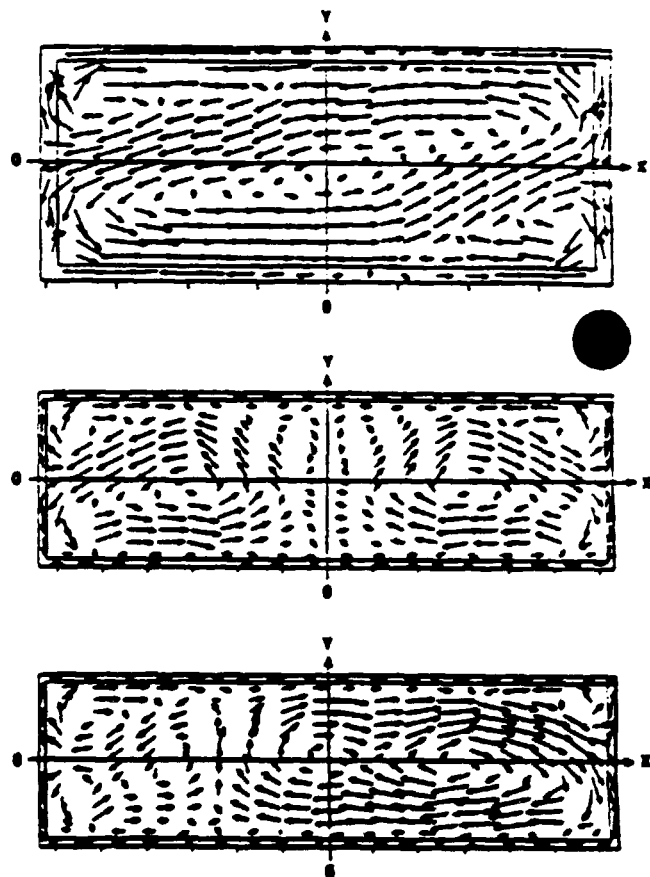


Figure 2: Calculated metal circulation for an end-to-end cell (top) and side-by-side cell with compensated (center) and a non compensated (bottom) vertical magnetic field component.

Considerations about current efficiency show the importance of several MHD parameters such as: relative velocity between metal and electrolyte [11], bath turbulence [12], average and local ACD [11], [16], [21], [22], metal-bath interface in [22], [23], [24]. It is in general agreed that the liquid zone should be made as quiescent as possible, and the metal-bath interface as

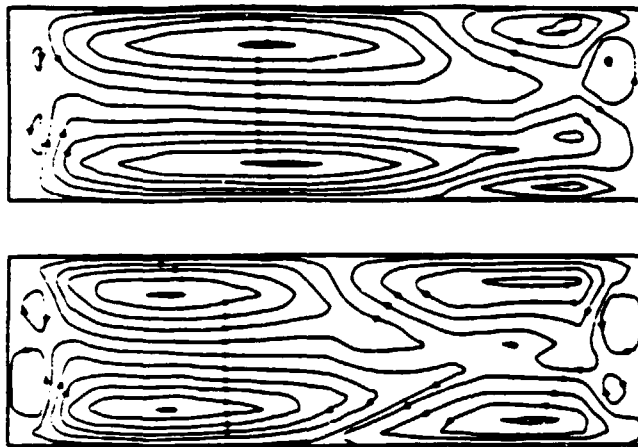


Figure 3: Circulation patterns for the end-to-end cell whose interface deformation is shown in Figure 1 for current feed at one end (top) and both ends (bottom).

flat and stable as possible. The metal circulation pools should be several, equal in size and as symmetrical as possible, at least with respect to the transverse axis of the cell [28]. This requirement is supported also by the fact that uneven circulation may give an uneven freeze profile and possible sidewall erosion. These principles are illustrated in Figures 1 to 3, where cells with greatly different hydrodynamics are shown. The following remarks can be made:

- End-to-end cells are characterized by a large hump on the transverse axis of the cell (this is so also for side-by-side cells with end anode risers). This hump has also an average longitudinal slope in cells whose current feed is not correctly split between positive and negative ends and/or whose magnetic field is not properly compensated for the neighboring row of cells. This feature is the result of the asymmetry of the transverse and vertical magnetic field components [2], [4], [25], [30].
- End-to-end cells usually have poor circulation pool symmetry. One large diagonal pool and two small opposite corner pools are common (Figure 2-top). Likewise, as shown in Figure 3, the pools often lack symmetry with respect to the transverse axis of the cell, even though they are not diagonal. This again is caused by the asymmetry of magnetic field components.
- Side-by-side cells with side risers have a longitudinal hump, with relatively small deformations. Metal circulation is symmetrical, but this symmetry can easily be destroyed by a bias in the vertical magnetic field, generated by the neighboring row of cells [1]. It has been shown that the biased cells are also more unstable [10]. Various ways to compensate this bias have been proposed [1], [26], [32], [34].

It is rather obvious that, given the choice, busbar design giving the MHD of Figure 1 (bottom) and Figure 2 (center) should be

chosen. However, in retrofitting this choice is often not possible, and improvements that can be made economically are limited.

Electromagnetic Force, Magnetic Fields and Electrical Current Distribution

It has already been mentioned that considerable information can be drawn from the distribution of the electromagnetic force, f , magnetic induction, B , and electric current density in the metal pad, j . It can be shown that the solenoidal part of the force, represented by $\text{curl } f$, determines the motion of the liquids. The potential part of the force, represented by $\text{div } f$ (divergence), acts like static pressure and determines the shape of the metal-bath interface, which would be flat if only the force of gravity were present.

The electromagnetic body force is

$$f = j \times B \quad (1)$$

The curl of the force is

$$\text{curl } f = (B \cdot \nabla) j - (j \cdot \nabla) B \quad (2)$$

Where: ∇ = gradient vector with components

$$\left(\frac{\partial}{\partial x}, \frac{\partial}{\partial y}, \frac{\partial}{\partial z} \right)$$

- \times = vector cross product
- \cdot = vector dot product

According to basic hydrodynamic principles there is no liquid motion, wherever $\text{curl } f = 0$. There, the deformation of the metal bath interface can only be static. This would be the case for a round cell with purely radial forces. If $\text{curl } f \neq 0$, there is movement and interface deformation, caused by pressure. It is therefore wise to try to diminish $\text{curl } f$ and reduce the flow and some of the pressure effect at the same time.

From Equation (2) it can be seen that $\text{curl } f$ depends on the field values and their derivatives. It is also well known from Ampere's law that the magnetic field cannot be eliminated from the entire liquid zone, because the electrolysis current passes through it. Moreover this current changes abruptly at the liquid zone perimeter and thus makes it impossible to eliminate $\text{curl } f$ there. The best one can do is to minimize f and $\text{curl } f$ and give them certain symmetry properties near the cell center and on the axes of symmetry. This becomes the objective of the design.

Based on the study of $\text{curl } f$, Givry [2] and others [29] derived magnetic field criteria to minimize the magnetic effects in the cell. Morel and Dugois [30] preferred to study the electromagnetic forces directly and postulated that the average longitudinal

Table I: Required Properties of the Magnetic Field (B) and Current density (j) distributions

Property Components	Symmetry w.r.t. axes		Values on axes		Value at center		Values elsewhere
	Longitudinal	Transverse	Longitudinal	Transverse	Field	Derivative w.r.t. vertical coordinate	
Longitudinal B	Anti	Yes	0	Any	0	0	Any
Transverse B	Yes	Anti*	Small	0*	0	0*	Small
Vertical B	Anti*	Anti*	0*		0	0	Small*
Longitudinal j	Yes	*	Small*	0	0	Any	Small*
Transverse j	Anti*	Yes	0*	Small	0	Any	Small*
Vertical j	Yes		Constant	Constant	Constant	Any	Constant

*Values quoted most often in references

forces should be balanced (equal and opposite) with respect to the transverse axis of the cell and the average transverse forces should be balanced with respect to the longitudinal axis of the cell. Forces and their curl give conditions to be satisfied by the magnetic field and current density components. Curl f gives additional conditions for their first derivatives. As shown in Table I, these conditions relate to symmetry with respect to the coordinate axes and to absolute values of the components. Only the most important derivatives and the ones most difficult to be made zero are listed.

It is required in principle that the horizontal currents be small and this in turn makes the vertical current uniform across the liquid zone. One can do this in four ways that must be maintained simultaneously:

- design the busbar sizes so that each cathode collector bar draws approximately equal currents [3], [30], [31];
- keep the freeze too near or somewhat inside the anode perimeter [27];
- keep the anode currents uniform [33];
- keep sufficient ACD to prevent the occurrence of metal waves [10].

The compliance with the first condition only is the responsibility of the MHD designer, who will see to it by appropriate busbar sizing. It is more difficult to keep the desired operating conditions related to freeze and anode currents at all times (whatever the cell operators may promise!). A way to circumvent this problem is to make the vertical magnetic field component small everywhere. Such a condition is indeed put forward by Chaffy et al [32] who require that, besides the criteria in Table I, the

quadratic average of the vertical magnetic field component over the whole metal area be $< 10^3$ T.

One particularly aggravating circumstance for satisfying the desired criteria for the vertical magnetic field component is the neighbouring row bias. Various compensation schemes have been proposed, such as compensating loops [32], [34], [35] and asymmetrical busbars [1], [26].

The requirements for the symmetry and small magnitude of the transverse component are impossible to satisfy in end anode riser cells because the end anode risers enhance the magnetic field of the anode current. In end-to-end cells even the symmetry of this component with respect to the transverse axis of the cell may be destroyed by efforts to reduce and compensate the vertical magnetic field components [1]. In side-by-side cells both the small magnitude and the antisymmetry with respect to the transverse axis of the cell can be obtained easily.

The longitudinal magnetic field distribution is the least critical, because it contributes to transverse forces that can cause limited interface deformation over the (short) width of the cell [29]. Nevertheless it is desirable to satisfy the symmetry properties of Table I [29], [32].

Busbar Sizing and Optimization

The busbar arrangement and the busbar currents have been chosen so to provide MHD balance in the cell. This busbar system should be provided at minimum cost. The busbar cost is composed of material cost and operating cost incurred by the

power loss in the busbars during the lifetime of the smelter. Kelvin's law states that the cost is minimized when the material cost is equal to the power cost. These two costs vary with the busbar size and can be expressed in terms of current density. The minimum occurs at a current density called optimal or economic current density [2], [5]. The economic current density depends on the busbar properties (resistivity and density); busbar shape, busbar interconnections and economics (fabricating costs, depreciation, scrap value, power cost, interest rate, etc.). The cost curve is quite flat around the minimum. A 10 % departure from the economic current density makes only 0.5 % difference in cost; a 20 % departure makes 1.5 % difference [5]. Moreover, the uncertainties about economic factors projected into the future are great. These facts make life easier, since precise optimization of the busbars with respect to the cross sections (or current densities) may be quite complicated if a lot of busbars are included at once [35]. It is much easier to separate the overall busbar system into sections, optimize these individually and calculate the total cost for a few trials and compare the results. The optimal solution is usually quite easy to find. The busbar current and voltage distribution for each trial are checked with a resistance network program such as NEWBUS [31]. The whole process may start by selecting a trial cross section of the shortest and most loaded busbar. In the end the most loaded busbars have to be verified again as to whether or not they have been overloaded with the current. Care has to be taken also with the cell shutdown bypass loads [31]. The overall busbar voltage drop matters too, since it makes part of the target voltage of the cell.

Conclusions

In spite of the powerful mathematical models available, the cell design process based on MHD still remains somewhat of an art. The link between MHD and current and energy efficiency is still too qualitative to be used for alternative design evaluations. Instead, relative criteria based on hydrodynamics and magnetic field distribution are most often used. The role of plant measurements has shifted from direct design and retrofitting support to model validation.

References

- [1] V. Potočnik, J.W. Evans, Evolution of Busbar Design in Hall-Héroult Cells and its Impact on the Process, Proceedings of a Conversazione on the Production of Liquid Aluminum, 25th Annual Conference of CIM (1986), pp. 23-37.
- [2] J.P. Givry, Magnetics in Aluminum Electrolysis Cells (in French), *Metallurgia Italiana*, n° 8, 1960, pp. 503-509. See also: Improvements in or Relating to Electrolysis Cells, British Patent n° 880 096 (Oct. 18, 1961).
- [3] J.P. Givry, Technical and Economic Aspects of Aluminum Cell Conductors, *Extractive Metallurgy of Aluminum*, Vol. 2 (1963), pp. 115-130.
- [4] J.P. Givry, Computer Calculation of Magnetic Effects in the Bath of Aluminum Cells, *Transactions of the Metallurgical Society of AIME*, Vol. 239 (August 1967), pp. 1161-1166.
- [5] G.C. Seager, The Economic Design of Conduction for Heavy Direct Currents, *Extractive Metallurgy of Aluminum*, Vol. 2 (1963), pp. 107-114.
- [6] T.B. Müller and K.O. Solberg, Numerical Calculation of Mass Convection Patterns in an Aluminum Reduction Cell, *Light Metals* (1973), Vol. 1, pp. 151-158.
- [7] T. Sele, Computer model for magnetic fields in electrolytic cells including the effect of steel parts, *Light Metals* (1973), Vol. 1, pp. 119-132.
- [8] W.E. Wahnsiedler, Hydrodynamic Modelling of Commercial Hall-Héroult Cells, *Light Metals* (1987), pp. 269-287.
- [9] N. Umeta, Magnetics and Metal Pad Instability, *Light Metals* (1985), pp. 581.
- [10] V. Potočnik, Modelling of Metal-Bath Interface Waves in Hall-Héroult Cells Using ESTER/PHOENICS, *Light Metals* (1989), pp. 227-235.
- [11] B. Lillebuen, S.A. Yzerdahl, R. Huglen, K.A. Paulsen, Current Efficiency and Back Reaction in Aluminum Electrolysis, *Electrochimical Acta*, Vol. 25 (1980), pp. 131-137.
- [12] J. Evans, Y. Zundelevich, D. Sharma, A Mathematical Model for Prediction of Currents, Magnetic Fields, Me. Velocities, Melt Topography and Current Efficiency in Hall-Héroult Cells, *Metallurgical Transactions B*, 128 (1981), pp. 353-360.
- [13] R.F. Robl, W.E. Haupin, D. Sharma, Estimation of Current Efficiency by Mathematical Model, Including Hydrodynamics Parameters, *Light Metals* (1977), pp. 185-202.
- [14] W.E. Haupin, "Current Efficiency", *Production of Aluminum and Alumina*, Edited by W.E. Burkin, John Wiley & Sons (1987), pp. 134-149.
- [15] B. Langon and S.M. Peyneau, Current Efficiency in Modern Point Feeding Industrial Potlines, *Light Metals* (1990), pp. 267-274.
- [16] S. Rosleth, T. Müftüoğlu, A. Solheim and J. Thonstad, Current Efficiency at Short Anode-Cathode Distance, *Light Metals* (1986), pp. 517-523.
- [17] A. Solheim, S.T.J. Hansen, S. Rosleth and J. Thonstad, Gas Driven Flow in Hall-Héroult Cells, *Light Metals* (1989), pp. 245-252.
- [18] E. Demedde, E.L. Cambridge, Gas Induced Circulation in an Aluminum Reduction Cell, *Light Metals* (1975), Vol. 1, pp. 111-119.

- [19] K. Grjotheim, C. Krohn, M. Malinovsky, K. Manišovský, J. Thonstad, *Aluminum Electrolysis*, 2nd edition, Aluminium-Verlag (1982), Chapter 9.
- [20] M.J. Leroy, J.M. Jolas, *Continuous Measurement of Current Efficiency by Mass Spectrometry on a 280 kA Prototype Cell*, *Light Metals* (1987), pp. 291-294.
- [21] T.R. Alcorn, C.J. McMinn, A.T. Tabereaux, *Current Efficiency in Aluminum Electrolysis by Anode Gas Analysis*, *Light Metals* (1988), pp. 683-695.
- [22] A.S. Derkach and V.I. Shtern, *Effects of Series Current Instability on the Operating Method of Aluminum Electrolysis Cells*, *Tsvetnye Metally* (1967), Vol. 3, pp. 68-73 (in English).
- [23] W.W. Hyland, *Current Efficiency of a Shorted Anode in Prebake Cells*, *Light Metals* (1984), pp. 711-720.
- [24] G.P. Tarcy, J. Sorensen, *Determination of Factors Affecting Current Efficiency in Commercial Hall-Héroult Cells Using Controlled Potential Coulometry and Statistical Experiments*, *Light Metals* (1991), pp. 453-459.
- [25] D.P. Ziegler, R.L. Kozarek, *Hall-Héroult Cell Magnetics Measurements and Comparison with Calculations*, *Light Metals* (1991), pp. 381-391.
- [26] V. Potočník, *A-275 MHD Design*, *Light Metals* (1987), pp. 203-208.
- [27] R.F. Robl, *Metal Flow Dependence on Leding in Hall-Héroult Cells*, *Light Metals* (1983), pp. 449-456.
- [28] J.M. Blanc and P. Entner, *Applications of Computer Simulation to Improve Electromagnetic Behavior of Pots*, *Light Metals* (1980), pp. 285-295.
- [29] Aluminium Pechiney, *A Method of and Apparatus for the Supply of Electric Current to Transversely Arranged Fused Electrolyte Tanks*, British Patent no. 1 539 765 (1979).
- [30] P. Morel, J.P. Dugois, *Process for Reduction of Magnetic Disturbances in High Amperage Electrolysis Cell Potlines*, Canadian Patent no 1 120 422 (1982) (in French), also British Patent Application GB 2 021 647 (1979).
- [31] T. Tvedt, H.G. Nebell, *NEWBUS, Simulation Program for Calculation of the Current Distribution in the Busbar System of Alumina Reduction Cells*, *Light Metals* (1988), pp. 567-573.
- Thaffy, B. Langon, M. Leroy, *Device for Connection of High Intensity Electrolysis Cells for the Production of Aluminum*, U.S. Patent 4 713 161 (December 1982).
- [33] P. Homma, B. Langon, P. Varin, *Apparatus for Production of Aluminum by Electrolysis Conducted with Very High Density* (in French), French Patent no. 2 505 368 (1982).
- [34] P. Morel, J. P. Dugois, U.S. Patent, 4 169 034 (1979).
- [35] G. A. Solinas, *Current Transportation in Aluminum Conductors, an Approach to Integral Economic Optimization*, *Light Metals* (1979), pp. 432-455.

REFERENCES :

BOOK :

Understanding the Hall-Héroult process for production of aluminium,
Grjotheim, K., and Kvande, H., editors, Aluminium-Verlag, Düsseldorf, 1986,
chap 2, "Influence of magnetic fields", Reidar Huglen.

Articles:

Givry, J.P., 1960,
Les effets magnétiques dans les cuves d'électrolyse,
La Metallurgia Italiana, N° 8, pp. 503-509.

Givry, J.P., 1967,
Computer calculation of magnetic effects in the bath of aluminum cells,
Transactions of the Metallurgical Society of AIME, Vol. 239, pp. 1161-1166.

Selo, T., 1973,
Computer model for magnetic fields in electrolytic cells including the
effect of steel parts,
Light Metals, Vol. 1, pp. 119-132.

Müller, T.B., and Solberg, K.O., 1973,
Numerical calculation of mass convection patterns in an aluminum reduction
cell,
Light Metals, Vol. 1, pp. 151-158.

Selo, T., 1974,
Computer model for magnetic fields in electrolytic cells including the
effect of steel parts,
Metallurgical Transactions, Vol. 5, October 1974, pp. 2145-2150.

Mori, K., Shiota, K., Urata, N., and Ikouchi, H., 1976,
The surface oscillation of liquid metal in aluminum reduction cells,
Light Metals, Vol. 1, pp. 77-96.

Urata, N., Mori, K., and Ikouchi, H., 1976,
Behavior of bath and molten metal in aluminum electrolytic cell,
J. Jpn. Inst. Light Met. (Keikinzoku), Vol. 26, N° 11, pp. 573-583.

Selo, T., 1977,
Instabilities of the metal surface in electrolytic cells,
Light Metals, Vol. 1, pp. 7-24.

Sale, T., 1977,
Instabilities of the metal surface in electrolytic alumina reduction cells,
Metallurgical Transactions B, Vol. 8B, December 1977, pp. 613-618.

Robl, R.F., 1978,
Influence by shell steel on magnetic fields within Hall-Héroult cells,
Light Metals, Vol. 1, pp. 1-13.

Johnson, A.R., 1978,
Metal pad velocity measurements in aluminum reduction cells,
Light Metals, Vol. 1, pp. 45-58.

Blanc, J.M., and Entner, P., 1980,
Application of computer calculations to improve electromagnetic behaviour
of pots,
Light Metals, pp. 285-295.

Arita, Y., and Ikeuchi, H., 1981,
Numerical calculation of bath and metal convection patterns and their
interface profile in Al reduction cells,
Light Metals, pp. 357-371.

Evans, J.W., Zundeleovich, Y., and Sharun, D., 1981,
A mathematical model for prediction of currents, magnetic fields, melt
velocities, melt topography and current efficiency in Hall-Héroult cells,
Metallurgical Transactions B, Vol. 12B, June 1981, pp. 353-360.

Matsui, S., and Era, A., 1982,
Measurement of metal turbulence in aluminum reduction cell,
Light Metals, pp. 373-380.

Lympany, S.D., Evans, J.W., and Moreau, R., 1982,
Magnetohydrodynamic effects in aluminum reduction cells,
Proc. IUTAM Symposium on Metallurgical Applications of Magnetohydrody-
namics, Cambridge, 6-10 Sept. 1982 (publ. by The Metals Society, London),
pp. 15-23.

Cherchi, S., and Degan G., 1983,
Oscillation of liquid aluminium in industrial reduction cells. An experi-
mental study,
Light Metals, pp. 457-467.

Lympany, S.D., Ziegler, D.P., and Evans, J.W., 1983,
The Hall-Héroult cell: some design alternatives examined by a mathematical
model,
Light Metals, pp. 507-517.

Lympany, S.D., and Evans, J.W., 1983,
The Hall-Héroult cell: some design alternatives examined by a mathematical model,
Metallurgical Transactions B, Vol. 14B, pp. 63-70.

Tabereaux, A.T., and Hester, R.B., 1984,
Metal pad velocity measurements in prebake and Soderberg reduction cells,
Light Metals, pp. 519-539.

Bradley, B.F., Dewing, E.W., and Rogers, J.N., 1984,
Metal pad velocity measurements by the iron rod method,
Light Metals, pp. 541-552.

Lee, H.-C., and Evans, J.W., 1985,
A physical model for electromagnetically driven flow in Hall cells,
Light Metals, pp. 569-579.

Urata, N., 1985,
Magnetics and metal pad instability,
Light Metals, pp. 581-591.

Ai, D.K., 1985,
The hydrodynamics of the Hall-Héroult cell. An overview,
Light Metals, pp. 593-607.

Sneyd, A.D., 1985,
Stability of fluid layers carrying a normal electric current,
J. Fluid Mech., Vol. 156, pp. 223-236.

Abramov, A.A., Skvortsov, A.P., and Pryakhin, G.S., 1985,
An analysis of the causes of unstable operation of powerful aluminum electrolyzers,
Sov. J. Non-Ferrous Met., Vol. 26, (6), pp. 47-49.

Moreau, R. J. E., and Ziegler, D., 1986,
Stability of aluminum cells - a new approach,
Light Metals, pp. 358-364.

Evans, J.W., and Banerjee, S.K., 1986,
A physical model for melt flow in Hall cells,
Light Metals, pp. 535-539.

Pant, A., Langille, A., Roy, R., and Wells, M., 1986,
Measurement of liquid metal flow velocities in electrolytic cells: test of the iron rod method,
Light Metals, pp. 541-550.

- Degan, G., 1986,
Use of iron shields for correcting local disturbances of magnetic fields in
the electrolytic pots,
Light Metals, pp. 551-554.
- Potocnik, V., and Evans, J.W., 1986,
Evolution of busbar design in Hall-Héroult cells and its impact on the
process,
Proc. of the 25th Annual CIM Conference, Toronto, 17-20 August 1986, pp.
23-37.
- Banerjee, S.K., and Evans, J.W., 1987,
Further results from a physical model of a Hall cell,
Light Metals, pp. 247-255.
- Wahnsiedler, W.E., 1987,
Hydrodynamic modeling of commercial Hall-Héroult cells,
Light Metals, pp. 269-287.
- Wahnsiedler, W.E., 1987,
Hydrodynamic modeling of the P-155 Hall cell,
Proc. conference on Mathematical Modelling of Materials Processing
Operations, Palm Springs, Calif., USA, 29 Nov.-2 Dec. 1987 (publ. by The
Metallurgical Society of AIME, New York), pp. 643-670.
- Moreau, R.J., 1987,
On the hydrodynamics of aluminum reduction cells,
Paper presented at the 5th International Beer-Sheva Seminar on MHD Flows
and Turbulence, Israel, 2-6 March 1987.
- Abramov, A.A., 1987,
Magneto-hydrodynamic instability of a metal melt in aluminum electrolyzers,
Tsvet. Met., Vol. 9, pp. 36-39.
- Haupt, W.E., 1987,
Fluid dynamics,
in Production of Aluminium and Alumina, Wiley, pp. 159-167.
- Echelini, M., Cobo, O., Lacunza, M., Crespo, N., Romagnoli, J., and
Capisti, N., 1988,
Expansion of a pot line with the aid of mathematical modelling,
Light Metals, pp. 557-566.
- LeBlanc, R., Potocnik, V., Stockman, G.E., and Shannon, D.J., 1988,
Magneto-hydrodynamic analysis of VS Soderberg cells,
Light Metals, pp. 575-582.

Laroche, F., Bui, R.T., Boivin, R., and Potocnik, V., 1988,
Experimental study of the bath-metal interface waves in an electrolytic cell,
Proc. International Symposium on Reduction and Casting of Aluminum,
Montréal, Canada, 28-31 August 1988 (vol. 8 of the Proceedings of the
Metallurgical Society of the Canadian Institute of Mining and Metallurgy,
publ. by Pergamon Press, C. Bickert, ed.), pp. 169-187.

Medina, H., Elarba, N., and Vivas, A.M., 1988,
Modernization of VERTICAL pots,
Proc. International Symposium on Reduction and Casting of Aluminum,
Montréal, Canada, 28-31 August 1988 (vol. 8 of the Proceedings of the
Metallurgical Society of the Canadian Institute of Mining and Metallurgy,
publ. by Pergamon Press, C. Bickert, ed.), pp. 313-320.

Potocnik, V.,
Modelling of Metal-Bath Interface Waves in Hall-Héroult Cells Using
ESTER/PHOENICS, Light Metals 1989, pp. 227-235.

K.J. Fraser, D. Billingham, K.L. Chen and J.T. Keniry,
Some Applications of Mathematical Modelling of Electric Current
Distributions in Hall Heroult Cells, Light Metals 1989, pp. 219-226.

J. Imery Buiza,
Electromagnetic Optimization of the V-350 Cell, Light Metals 1989,
pp. 211-214.

A. Solheim, S.T. Johansen, S. Rolseth and J. Thonstad,
Gas Driven Flow in Hall-Heroult Cells, Light Metals 1989, pp. 245-252.

J.H. Kent,
A Study of Magnetic Screens and the Effect of Pot Room Structure on
Current Efficiency, Light Metals 1989, pp. 215-218.

D.C. Choonis and A.F. LaCamera,
The Influence of Gas-Driven Circulation on Alumina Distribution and
Interface Motion in a Hall-Heroult Cell, Light Metals 1990,
pp. 211-220.

Richard Boivin and Sylvie Martel,
Effect of an Instability of the Metal Surface on the Magnetic Field
Inside a Cell, Light Metals 1990, pp. 233-240.

V.F. Alukhametov, V.A. Krukovsky, V.I. Kolesnichenko,
S.Yu. Khrpchenko,
Magneto-Hydrodynamic Phenomena in Production of Aluminium by
Electrolysis, Light Metals 1990, pp. 249-256.

B. Langon and J.M. Payneau,
Current Efficiency in Modern Point Feeding Industrial Potlines, Light
Metals 1990, pp. 267-274.

D. Vogelsang and M. Segatz, "Simulation Tools for the Development of High-Amperage Reduction Cells", Light Metals 1991, pp. 375-379.

M. Segatz and D. Vogelsang, "Effect of Steel Parts on Magnetic Fields in Aluminum Reduction Cells", Light Metals 1991, p. 393-398.

D.P Ziegler and R.L. Kozarek, "Hall-Héroult Cell Magnetic Measurements and Comparisons with Calculations", Light Metals 1991, pp. 381-391.

A.F. LaCamera, D.P. Ziegler, R.L. Kozarek, "Magnetohydrodynamics in the Hall-Héroult Process, An Overview", Light Metals 1992, pp. 1179-1186.

V.Potocnik, "Principles of MHD Design of Aluminum Electrolysis Cells", Light Metals 1992, pp. 1187-1193.

P.A. Davidson, R.F. Boivin, "Hydrodynamics of Aluminum Reduction Cells", Light Metals 1992, pp. 1195-1204

J. Antille, Y. Krähenbühl, R. Von Kaenel, J.C. Weber, "Fluid Flow Control : A Must for the Aluminum Industry!", Light Metals 1992, pp. 1247-1256.

G. Lossmann, "Utilization of Various Combined Measurements in Reduction Cells", Light Metals 1992, pp. 441-447.

V.V. Ovtchinnikov and al, "MHD-Phenomena and Velocities in Söderberg Cells in USSR", Light Metals 1992, pp. 1205-1211.

M. Segatz, D. Vogelsang, C. Droste and P. Baetler:
Modelling of Trans: Magneto-hydrodynamic
Phenomena in Hall-Heroult Cells. Light
Metals 1993, p. 361-368.

M. F. El-Demerdash et al. : Modelling of Meta
Topography and Flow Regimes in Working
Prebaked Aluminum Pot. Light Metals 1993,
pp. 369 - 374.

UNDER THE AUSPICES OF
THE UNITED NATIONS INDUSTRIAL DEVELOPMENT ORGANIZATION

**WORKSHOP ON COMPUTER-BASED
MATHEMATICAL MODELLING
OF
ALUMINIUM PRODUCTION PROCESSES**

Jawaharlal Nehru Aluminium Research
Development and Design Centre
Nagpur, India
September , 1993.

**SIMULATION OF
AN ALUMINIUM ELECTROLYTIC CELL
(COURSE MATERIAL)**

Laszlo Tikasz

University of Quebec at Chicoutimi
Quebec, Canada

ABSTRACT

1. Basic Mass and Energy Balance Calculations

This part is intended to guide the reader through the construction of a simplified dynamic cell model of an aluminium electrolytic cell. The proposed Model itself is an integrated software package for simulating different operational states of aluminium electrolytic cells. The focus is on the theoretical aspects, whereas programming details as well as necessary preparatory steps (e.g. data acquisition problems) are not covered.

A theoretical approach is outlined showing how to derive basic equations to approximate the dynamic and static operation of a cell. The structure of the computation is demonstrated with special emphasis on the user-adjustable subroutines and functions. These user-adjustable parts can serve as starting points toward a more sophisticated description of the process.

The current state of an electrolytic cell is described by lumped parameters averaged over a selected part (lump) of the cell. For educational purposes, considerable simplifications are proposed regarding the granularity of the Model: the geometry is the simplest possible and the upper and lower side-carbon and freeze blocks are put into generalized side-wall and freeze blocks. The selected control volume contains only the bath, freeze and metal lumps, and the boundary conditions are approximated by generalized anode, cathode and side-wall lumps. The environment outside the cell model is represented by temperatures above, below and beside the cell. The material and energy balances are performed on all the selected lumps and during the simulation, the mass and temperature variations are calculated by solving the relevant ordinary differential equations.

Geometrical, chemical and electrical aspects of the aluminium electrolytic cell are considered. Alumina dissolution sub-model is introduced. Algebraic equations for steady-state simulation are also derived.

2. Approximating Selected Operation Modes

The adjustable model components can be used to approximate special operation modes, also. The most important components are:

- line current,

- current efficiency,
- mass densities,
- eutectic temperature,
- heat transfer coefficients,
- specific heat coefficients,
- equivalent thermal resistances,
- bath resistance and conductivity.

In this part, some examples are given showing how to select, tune, verify and validate equations or develop appropriate sub-models.

3. Developing a Control Emulator

In simulating the dynamic behavior of an electrolytic cell, it is a must to provide a unit which approximates the necessary maintenance routines. In real situations the maintenance is provided partly manually and by an adequate process controller. Here we concentrate on the representation of the automatic control. The main points discussed are the following:

- selection of control variables,
- data exchange between Model and Control Emulator,
- developing a control data base,
- developing a simple alumina feeding routine,
- developing a simple resistance control routine.

4. How to Use the Dynamic Cell Model

An advanced Dynamic Cell Model is presented during the Workshop. The Dynamic Cell Model is a computer program, escorted by three manuals :

- User Guide,
- Set-Up Guide,
- Tutorial.

Based on these Guides, the general structure and the use of the Dynamic Cell Model are discussed. Examples are given where the Dynamic Cell Model is used to simulate different operating conditions.

5. Computer Demonstration

In this part, real computer demonstrations are provided on advanced PC-class computers. Both the basic mass and energy calculations and the Dynamic Cell Model will be presented.

With the basic equations, the participants can carry out static and dynamic computations. This facility helps them understand the process fundamentals as well as the main relations and trends of the process.

Using the Dynamic Cell Model, they will acquire hands-on experience with a complete simulator.

**SIMULATION OF
AN ALUMINIUM ELECTROLYTIC CELL**

Basic Mass and Energy Balance Calculations

Tutorial

**L. TIKASZ,
R.T. BUI,
V. POTOČNIK**

PREFACE

The present Tutorial is intended to guide the users during the construction of a simplified dynamic cell model of an aluminium electrolytic cell.

The Model itself is an integrated software package for simulating different operational states of aluminium electrolytic cells. The Tutorial focuses on the theoretical aspects only. Programming details as well as necessary preparatory steps (e.g. data acquisition problems) are not covered.

The Tutorial proposes an approach to derive basic equations to approximate the dynamic operation of a cell. The structure of the computation is outlined with special emphasis on the user-adjustable subroutines and functions. These user-adjustable parts can serve as starting point toward a more sophisticated description of the process.

In the Literature, the most important sources of data related to the process metallurgy of aluminium are provided. Data extracted from these articles can be used as initial data to start the simulation sessions. Actual data related to a certain realistic situation should be provided by the user.

1. GENERAL CONSIDERATIONS

1.1. Geometrical Aspects

The current state of an electrolytic cell is described by lumped parameters averaged over a selected part (lump) of the cell. The main components (lumps) of the cell are shown in Figure 1.1.1.

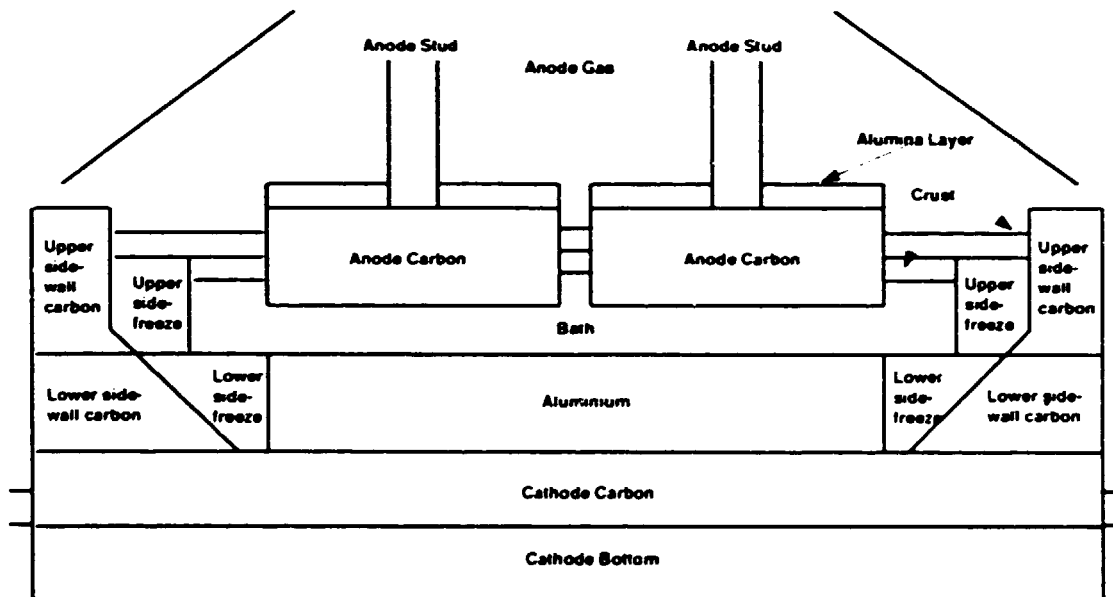


Figure 1.1.1 Components of the Cell

For educational purposes, further simplifications are proposed regarding the geometry. It is proposed/reasonable to join the upper and lower side-carbon and freeze blocks into generalized side-wall and freeze blocks. The result is shown in Figure 1.1.2.

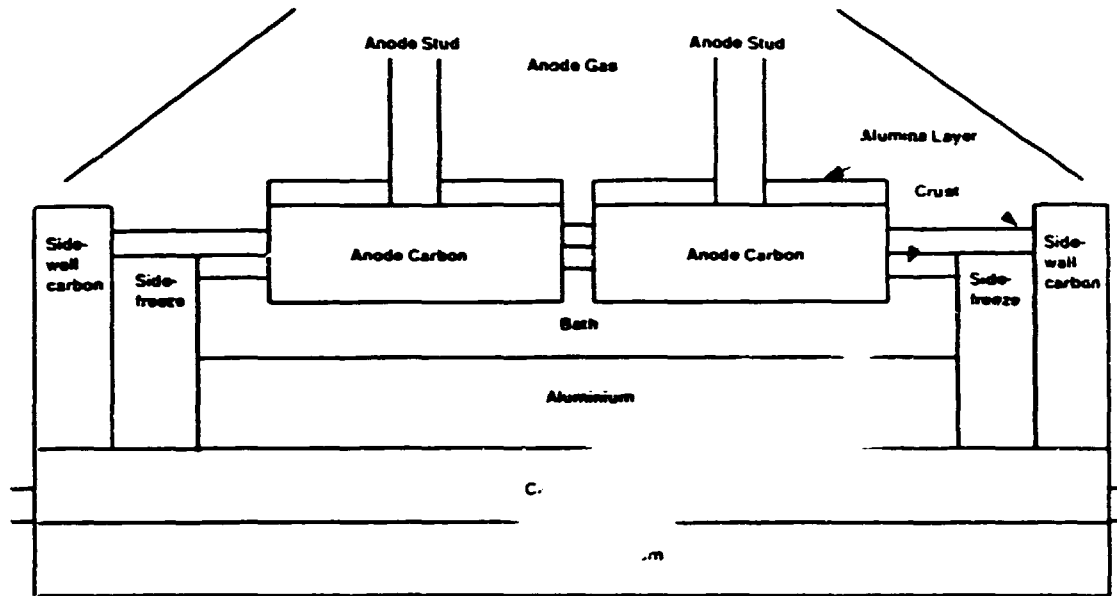


Figure 1.1.2 Simplified Cell Description

Now we focus on the bath-freeze-metal parts of the cell. In other words, the selected control volume contains only the bath, freeze and metal lumps, and the boundary conditions are approximated by generalized anode, cathode and side-wall lumps. The environment outside the cell model is represented by temperatures above, below and beside the cell. The rearrangement is shown in Figure 1.1.3. The applied notation is given below:

m_1	:	mass of electrolyte	[kg]
T_1	:	temperature of electrolyte	[°C]
m_2	:	mass of freeze	[kg]
T_2	:	temperature of freeze	[°C]
m_3	:	mass of aluminium	[kg]
T_3	:	temperature of aluminium	[°C]
Q_A	:	heat flow from electrolyte through anode	[W]
Q_M	:	heat flow from electrolyte to aluminium	[W]
Q_C	:	heat flow from aluminium through cathode	[W]

Q_F	:	heat flow from electrolyte to freeze	[W]
Q_{F2}	:	heat flow from aluminium to freeze	[W]
Q_F	:	heat flow from freezing zone to freeze	[W]
Q_S	:	heat flow from freeze through side wall	[W]
T_A	:	ambient temperature above the cell	[°C]
T_C	:	ambient temperature below the cell	[°C]
T_S	:	ambient temperature beside the cell	[°C]

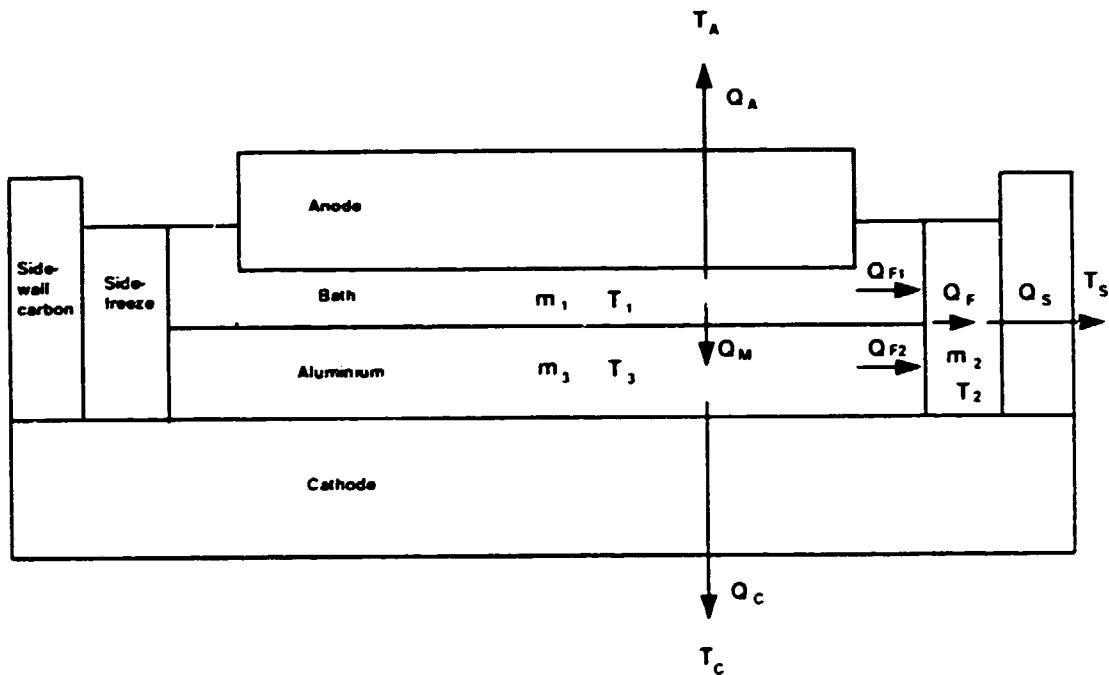


Figure 1.1.3 Components of the Simplified Model

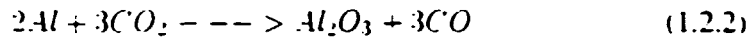
1.2. Chemical Aspects

The following two reactions are considered as a basis of aluminium electrolysis process in the Model.

Primary reaction:



Secondary reaction:



The rate of the primary reaction is proportional to the line current and the rate of the reverse reaction equals the rate of the primary reaction multiplied by the factor $(1-\eta)$ where η is the current efficiency.

1.3. Electrical Aspects

The line current is assumed to be constant. The total cell voltage is the sum of the following terms:

- voltage drop in the anode,
- anode potential,
- voltage drop in part of the bath partially filled with gas bubbles (bubble drop),
- voltage drop in the bath,
- voltage drop in the
- voltage drop in

In the present representation, the voltage drop within the control volume is the sum of the:

- anode potential,
- voltage drop in part of the bath partially filled with gas bubbles (bubble drop),
- voltage drop in the bath.

1.4. Energy and Mass Balance

The balances are performed as per the lumps specified in Figure 1.1.3. All balances, whether material or energy, start with the fundamental balance equation.

$$\text{input} - \text{output} + \text{production} = \text{accumulation} \quad (1.4.1)$$

The energy production term is important in lumps involved in chemical reactions and resistive (ohmic) heating. The mass production term is important in lumps involved in freeze melting or formation and in alumina dissolution. For liquid systems, the energy balance is usually given in terms of enthalpy.¹

If H_i , m_i , c_{pi} are enthalpy, mass and specific heat of lump i , and T_i is the temperature of lump i , T_0 is the reference temperature, h_i^0 is enthalpy of the lump at the reference temperature, then the total enthalpy of the lump can be written as :

$$H_i = m_i \left(h_i^0 + \int_{T_0}^{T_i} c_{pi} dT_i \right) \quad (1.4.2)$$

The time derivative of this equation gives the relationship for the enthalpy (energy) production:

$$\begin{aligned} \frac{dH_i}{dt} &= \frac{dm_i}{dt} \left(h_i^0 + \int_{T_0}^{T_i} c_{pi} dT_i \right) \\ &\quad + m_i c_{pi} \frac{dT_i}{dt} \end{aligned} \quad (1.4.3)$$

We can see that the changes of mass in a given lump participate in the changes of energy of the lump.

1.5. Dissolution of Alumina

When alumina is fed to the cell, it is assumed that a fraction is dispersed and dissolved in the bath almost immediately. The rest forms a reserve of undissolved alumina mass. From the dispersed and the undissolved buffer, the alumina is dissolved at rates proportional to the dispersed or the undissolved mass and which is a linear function of the aluminium temperature. Initial conditions can be set according to a selected situation. The proposed alumina dissolution model is shown in Figure 1.5.1.

¹ This can be done because the work due to the volume changes is negligible

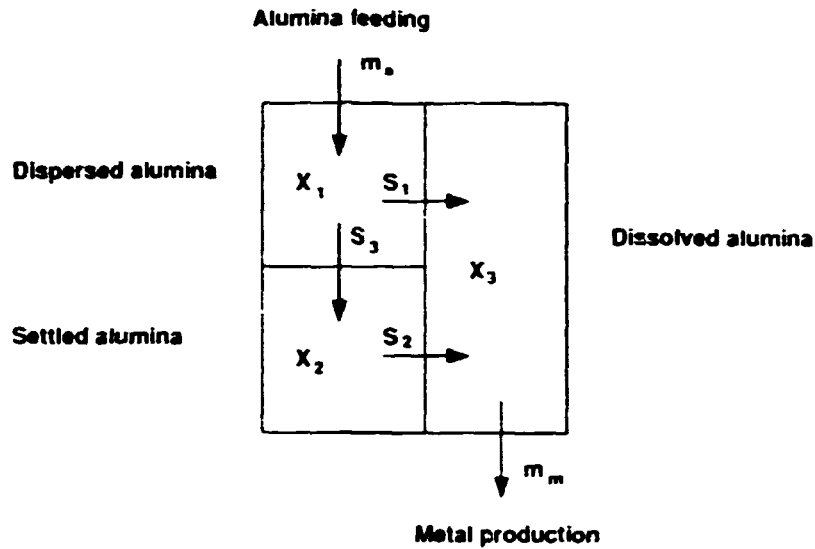


Figure 1.5.1 Components of the Simplified Alumina Balance

Where

m_a	:	mass of added alumina	[kg]
m_m	:	mass of produced metal	[kg]
x_1	:	mass of dispersed alumina	[kg]
x_2	:	mass of settled alumina	[kg]
x_3	:	mass of dissolved alumina	[kg]
S_1	:	dissolution rate from dispersed alumina	[kg/s]
S_2	:	dissolution rate from settled alumina	[kg/s]
S_3	:	settling rate from dispersed alumina	[kg/s]

2. DYNAMIC SIMULATION

2.1. State Equations

During the simulation, the mass and temperature variations are calculated in terms of ordinary differential equations :

$$\frac{dm_i}{dt} = \dots \quad (2.1.1)$$

and

$$\frac{dT_i}{dt} = \dots \quad (2.1.2)$$

These equations are the state equations of the system. Applying the principles mentioned in Section 1.1, first order differential equations with time as independent variable can be derived for each of the following dynamic variables:

1. mass of dispersed alumina,
2. mass of undissolved alumina,
3. mass of dissolved alumina,
4. mass of electrolyte,
5. mass of side-freeze,
6. mass of aluminium.

and

7. temperature of electrolyte,
8. temperature of side-freeze,
9. temperature of aluminium.

To integrate the 9 linked differential equations, subroutine SDRIV2() is proposed from the NMAS (Numerical Methods and Software) library. For detail related to the SDRIV2() routine refer to [1].

2.2. Equations for the Alumina Balance

Mass Balance

The general alumina balance can be written in the form:

$$\frac{dx_1}{dt} + \frac{dx_2}{dt} + \frac{dx_3}{dt} = \Delta m_a - k_6 \Delta m_m \quad (2.2.1)$$

and the components can be expressed as:

$$\frac{dx_1}{dt} = \Delta m_a - S_1 - S_3 \quad (2.2.2)$$

$$\frac{dx_2}{dt} = S_1 - S_2 \quad (2.2.3)$$

$$\frac{dx_3}{dt} = S_1 + S_2 - k_6 \Delta m_m \quad (2.2.4)$$

The settling and dissolution processes as well as alumina feeding and metal production can be written as:

$$S_1 = k_1 x_1 (c_s - c) \quad (2.2.5)$$

$$S_2 = k_2 x_2 (c_s - c) \quad (2.2.6)$$

$$S_3 = k_3 x_1 \quad (2.2.7)$$

$$\Delta m_a = k_4 \delta(t) \quad (2.2.8)$$

$$\Delta m_m = k_5 I_s \quad (2.2.9)$$

where:

c_s	:	saturation concentration of alumina	[weight %]
c	:	actual concentration of alumina	[weight %]
I_s	:	line current	[A]
k_i	:	adequate process constants	

Note, that regarding the process parameters $c = \frac{I}{m_1}$.

2.3. Equations for the Electrolyte

Mass Balance

$$\frac{dm_1}{dt} = \Delta m_a - k_0 \Delta m_m - \frac{dm_2}{dt} \quad (2.3.1)$$

Energy Balance

$$\frac{dT_1}{dt} = \frac{Q - Q_A - Q_M - Q_{F1}}{m_1 c_{p1}} \quad (2.3.2)$$

where:

- c_{p1} : specific heat of electrolyte [J/kg °C]
 Q : total heat loss of the cell [W]

Usually, in steady-state, the total heat loss of the cell is expressed as:

$$Q = (U - U_A)I, \quad (2.3.3)$$

In the dynamic calculation, a modified version of this equation is proposed:

$$Q = UI - (U_{A0}I + Q_H) \quad (2.3.4)$$

where:

- U : cell voltage within the control volume [V]
 U_A : voltage equivalent of enthalpy of metal production [V]
 U_{A0} : voltage equivalent of enthalpy of metal production (isothermal) [V]
 Q_H : energy needed to heat-up and dissolve the alumina added [W]

Heat flows toward the environment (Q_A , and later Q_C and Q_S) can be approximated by equivalent heat resistances in the form of

$$Q_i = \frac{U_i I_i - T_i}{R_{i,j}} \quad (2.3.5)$$

where:

Q_i	:	heat flow from lump (i) to the environment	[W]
A_i	:	adequate surface where the heat flow is considered	[m ²]
T_i	:	temperature of lump (i)	[°C]
T_j	:	temperature of environment (j)	[°C]
$R_{i,j}$:	heat resistance for surface unit between lump (i) and environment (j)	[m ² °C/W]

Heat flows between lumps containing molten materials or between molten and solid phases (Q_M , Q_{F1} and later Q_{F2}) can be approximated by equivalent heat transfer coefficients in the form of

$$Q_i = h_{i,j} \cdot A_i (T_i - T_j) \quad (2.3.6)$$

where:

Q_i	:	heat flow from lump (i) to lump (j)	[W]
A_i	:	area of the surface between the liquid and the solid for lump i	[m ²]
T_i	:	temperature of lump (i)	[°C]
T_j	:	temperature of lump (j)	[°C]
$h_{i,j}$:	heat transfer coefficients between lump (i) and (j)	[W/m ² °C]

Note that for Q_{F1} and Q_{F2} calculation T_j is set to eutectic temperature of the electrolyte.

2.4. Equations for the Freeze

Mass Balance

$$\frac{dm_2}{dt} = \frac{Q_F - Q_{F1} - Q_{F2}}{H_F + \frac{c_{p1}(T_1 - T_F) + c_{p1}(T_2 - T_F)}{2} + c_{p2}(T_F - T_2)} \quad (2.4.1)$$

where:

H_F	:	fusion heat of cryolite	[J/kg]
c_{p2}	:	specific heat of freeze	[J/kg °C]
T_F	:	eutectic temperature of electrolyte	[°C]

Note that in this approximation the freeze change at bath and metal level are considered being equal.

Q_F is calculated according to Equation (2.3.5) with $T_i = T_F$. The equivalent thermal resistance R_F can be expressed as

$$R_F = \frac{1}{k_F} \frac{l_F}{2} \quad (2.4.2)$$

where:

k_F	:	specific thermal conductivity of freeze	[m²C/W]
l_F	:	averaged freeze thickness	[m]

Energy Balance

$$\frac{dT_2}{dt} = \frac{Q_F - Q_2}{m_2 c_{p2}} \quad (2.4.3)$$

2.5. Equations for the Aluminium

Mass Balance

$$\frac{dm_1}{dt} = k_1 I_1 - \Delta m_1 \quad (2.5.1)$$

where:

m_1	:	amount of tapped metal	[kg]
-------	---	------------------------	------

Energy Balance

$$\frac{dT_3}{dt} = \frac{Q_M - Q_C - Q_{F2} + k_7 I_3 c_{p3} (T_1 - T_3)}{m_3 c_{p3}} \quad (2.5.2)$$

where:

c_{p3} : specific heat of aluminium [J/kg °C]

3. STATIC SIMULATION

3.1. Steady-State Balances

In previous sections the state equations were derived for dynamic simulations, as per the lumps specified in Figure 1.1.3. In order to obtain steady-state (static) solution, all balances, whether material or energy, start with the equation

$$\text{input} - \text{output} + \text{production} = 0 \quad (3.1.1)$$

In other words, all the time derivatives of the dynamic variables have to be set to zero:

$$\frac{dm_i}{dt} = 0 \quad (3.1.2)$$

and

$$\frac{dT_i}{dt} = 0 \quad (3.1.3)$$

Moreover, we must assume a continuous addition of raw materials and a continuous tapping of aluminium, as opposed to discrete actions taking place in real operation. From this, it can be seen that the cell in reality, is never in a steady state. The solution obtained will, however, represent the mean state of the cell over a period with constant or periodic operation conditions.

The derived equations have the following forms:

$$0 = \Delta m_a - k_1 x_1 (c_s - c) - k_3 c_1 \quad (3.1.4)$$

$$0 = k_1 x_1 - k_2 x_2 (c_s - c) \quad (3.1.5)$$

$$0 = k_1 x_1 (c_s - c) + k_2 x_2 (c_s - c) - k_3 k_4 I \quad (3.1.6)$$

$$0 = Q - Q_A - Q_M - Q_{T1} \quad (3.1.7)$$

$$0 = Q_F - Q_{F1} - Q_{F2} \quad (3.1.8)$$

$$0 = Q_F - Q_S \quad (3.1.9)$$

$$0 = k_5 I_s - \Delta m_l \quad (3.1.10)$$

$$0 = Q_M - Q_C - Q_{F2} + k_5 I_s c_{p3} (T_1 - T_0) \quad (3.1.11)$$

$$0 = \Delta m_a - k_7 k_0 I_s \quad (3.1.12)$$

Analyzing the formulas, we can see that:

- Equations (3.1.10) and (3.1.12) set the balanced mass flows.
- Substituting Equation (3.1.5) to (3.1.4), the result is Equation (3.1.6).
- Q_F in Equation (3.1.8) can be substituted by Q_S from (3.1.9).

The bath temperature can be considered as a known (measured) parameter. Moreover, Equation (3.1.6) is a closed formula for determining the alumina concentration in bath. In practice, it is better to consider c as known (measured) and try to determine the alumina concentration x_2 . An additional equation is proposed to set the ratio between S_1 and S_2 :

$$n = \frac{S_1}{S_2} = \frac{k_1 x_1 (c_s - c)}{k_2 x_2 (c_s - c)} \quad (3.1.13)$$

3.2. Steady-State Equations

After the proposed modifications, the set of algebraic equations obtained are:

$$0 = k_1 x_1 (c_s - c) - n k_2 x_2 (c_s - c) \quad (3.2.1)$$

$$0 = k_1 x_1 (c_s - c) + k_2 x_2 (c_s - c) - k_7 k_0 I_s \quad (3.2.2)$$

$$0 = Q - Q_A - Q_M - Q_{F1} \quad (3.2.3)$$

$$0 = Q_F - Q_{F1} - Q_{F2} \quad (3.2.4)$$

$$0 = Q_M - Q_c - Q_{F2} - k_5 I_s (p_3) (T_1 - T_3) \quad (3.2.5)$$

The independent variables are:

1. mass of dispersed alumina,
2. mass of dissolved alumina,
3. mass of the freeze,
4. temperature of the freeze,
5. temperature of the aluminium.

Thus, five nonlinear algebraic equations with 5 unknowns are obtained. To solve the set of equations, subroutine SNSQE() from the NMAS library is proposed. For detail related to the SNSQE() routine refer to [1].

4. ADJUSTABLE MODEL COMPONENTS

Starting the computation requires a set of initial data but which remains unchanged during either for finding a steady-state (static) solution or under the dynamic simulation. This set of initial data includes chemical and physical constants, correction factors, certain geometrical quantities and initial values for the chosen independent variables which are to be provided by the user.

The user is proposed to begin the simulation determining a reasonable static solution for the Model. To construct the energy balance equations, further parameters, such as the thermal conductivities, heat transfer constants, specific heat values, densities, bath resistance, voltage balance components and energy production and consumption terms have to be determined. These parameters can be chosen as constants or as functions of other process parameters.

In the dynamic part of the simulation, the time derivatives of the dynamic variables are calculated, which are the right-hand sides of differential equations. During the calculation, the most important parameters (e.g. line current, cell resistance, anode position, bath temperature, alumina concentration) can be printed. On-line graphic representation of calculated process parameters helps the interpretation of the simulation.

During the dynamic simulation, it is essential to maintain the simulated process close to the real one. This means, that the user has to extend the Model with a "maintenance" part. At the early stages, this might be just an embryonic control emulation, but a more realistic representation of scheduled operation interactions and process control system is required.

This Chapter outlines model components, which are proposed to be elaborated by the user. The selected equations can be written in form of subroutines or functions, so the routines are called at every computation step and the programmed calculations are fulfilled.

4.1. Line Current

The line current is the driving force to maintain the electrochemical reaction. For a single cell, the line current is an independent input variable which may be kept constant. However, in order to make the simulation more realistic, it is

proposed construct a line current sub-model which generates a series of data with identical statistical properties as the selected real line current.

By default, the line current is kept constant.

4.2. Current Efficiency

There are several sophisticated formulas for current efficiency calculation in the literature. However, they are hardly suitable for reliable calculation based on available process parameters and related to short-term operation. The user has the freedom to make his best choice.

By default, the current efficiency is kept constant.

4.3. Thermal Resistances

Thermal resistances which are a function of thermal conductivities of the built-in materials can be expressed in form of approximating polynomial as functions of temperature. Equivalent thermal resistances of the lumps can be derived from the size and arrangement of a selected cell using equivalent thermal resistance network approach. The user can involve all the necessary calculations in the provided subroutine or these calculations can be done separately.

By default, the thermal resistance values are kept constant during the simulation.

4.4. Densities

The densities are usually approximated as functions of temperature and / or composition. The user has to choose the proper empirical relations relating to the selected cell.

By default, freeze and liquid aluminium densities are kept constant. Electrolyte density is calculated as a function of composition and temperature.

4.5. Eutectic Temperature

Pure cryolite melts at about 1009°C, but alumina and other additives depress the liquidus temperature. As the alumina content is increased, the liquidus temperature passes through a minimum called eutectic temperature (or, more

correctly, the pseudo-binary eutectic temperature) and then rises again. The two families of curves have been represented by regression equations [7].

The cryolite liquidus for mixtures in the normal range of electrolyte compositions can be given by:

$$\begin{aligned}
 TF = & 1011.7 - 0.1453M_2^2 - 0.000194M_2^4 \\
 & - 7.088c + 0.214c^2 - 2.898M_1 \\
 & - 5.167M_4 - 9.673M_5
 \end{aligned} \quad (4.5.1)$$

A similar equation is generated to represent the alumina liquidus:

$$\begin{aligned}
 TS = & 826.5 - 3.063M_2 + 14.25c \\
 & + 3.404M_3 - 1.930M_5 \\
 & + 0.1811M_2c \\
 & + 0.8143M_4c \\
 & + 0.8559M_5c \\
 & + 0.3301M_3c
 \end{aligned} \quad (4.5.2)$$

The eutectic temperature TE is calculated by solving the following:

$$TE = TF = TS \quad (4.5.3)$$

where

TF	:	cryolite liquidus	[°C]
TS	:	alumina liquidus	[°C]
TE	:	eutectic temperature	[°C]
c	:	alumina concentration	[weight %]
M ₂	:	excess aluminium fluoride	[weight %]
M ₃	:	calcium fluoride	[weight %]
M ₄	:	magnesium fluoride	[weight %]
M ₅	:	lithium fluoride	[weight %]

The user can select other formulas available in the literature.

Eutectic temperature is calculated in function EUT(). The default function solves Equation (4.5.3) and returns the new value of the eutectic temperature.

4.6. Heat Transfer Coefficients

Heat transfer coefficients present the bridge for the heat transfer across the boundary layer between solid surfaces and fluids or between two fluids.

Generally, all heat transfer coefficients are kept constant during a simulation. The bath-to-freeze and metal-to-freeze coefficients can be taken from laboratory experiments, from heat balance calculations or from outputs of more detailed models of the cell. Heat transfer coefficients for external surfaces to air or gas under-the-hood are calculated by standard engineering formulas. The user can insert these calculations into the Model or can keep them separately.

4.7. Bath Resistance and Conductivity

The general formula for bath resistance calculation is:

$$R_B = \frac{l}{A\sigma} \quad (4.7.1)$$

where

R_B	:	bath resistance	[Ω]
l	:	anode-cathode distance	[m]
A	:	area of current path	[m^2]
σ	:	electrical conductivity of the bath	[1/(Ωm)]

This formula is often modified according to the selected gas layer resistance description. In the Model, the gas bubble voltage drop is represented by an equivalent additional anode-cathode distance. This means that the mean thickness of the gas bubbles under the anode is assumed to be about 5 mm, which is the surface tension limited thickness of the gas bubble layer. The modified formula is consequently :

$$R_B = \frac{l + 0.005}{A\sigma} \quad (4.7.2)$$

This method tends to underestimate the bubble resistance when the alumina content of the bath drops and an anode effect approaches.

There are several empirical relations in the literature for the calculation of the electrical conductivity of the bath. The relationship used for the Model is given below [5] :

$$\begin{aligned} \ln \sigma = & 2.0156 - 0.0207c - 0.005.M_2 \\ & - 0.0166.M_4 + 0.0178.M_5 \\ & + 0.0063.M_6 + 0.2175C \cdot B \\ & - \frac{2068.4}{T_1} \end{aligned} \quad (4.7.3)$$

where

T_1	:	bath temperature	[°K]
c	:	alumina concentration	[weight %]
M_2	:	excess aluminium fluoride	[weight %]
M_3	:	calcium fluoride content	[weight %]
M_4	:	magnesium fluoride content	[weight %]
M_5	:	lithium fluoride content	[weight %]

A proposed correction factor (κ) which takes into account the suspended carbon particles in the electrolyte can be written as :

$$\kappa = 0.994 - 0.1191C + 0.0097C^2 \quad (4.7.4)$$

where C is the weight % of suspended particles.

Electrical conductivity of the bath is calculated in function SIG(). The default function calculates Equations (4.7.3) and (4.7.4) and returns the new value of σ .

4.8. Specific Heat Coefficients

Specific heats are used in two ways in the Model :

a) In steady state, to calculate the enthalpy required for heating up reaction materials (anode carbon, alumina and aluminium fluoride) from room temperature to reaction temperature.

b) In transient (dynamic) state, to calculate the enthalpy change due to temperature change in a given lump.

The specific heat coefficients are usually approximated as functions of temperature and / or composition. The user has to choose the proper equations relating to the selected cell.

By default, the specific heat coefficients are kept constant.

4.9. Equilibrium Potential and Overvoltages

Several expressions can be found in the literature either for calculating these components separately or as the sum of them. A standard approximation is taken from [4]. Parameters for the critical current density and the limiting current density formulas can also be taken from [4].

Equilibrium potential:

$$E^0 = \frac{\Delta G^0}{6F} + \frac{RT}{6F} \ln \left(\frac{C_{Ox,init}}{C_{Al}} \right) \quad (4.9.1)$$

Reaction overvoltage at the anode:

$$\eta_{AA} = \frac{RT}{1.08F} \ln \left(\frac{i_a}{i_0} \right) \quad (4.9.2)$$

Concentration overvoltage at the anode:

$$\eta_{AC} = \frac{RT}{2F} \ln \left(\frac{i_{cc}}{i_{cc} - i_a} \right) \quad (4.9.3)$$

Concentration overvoltage at the cathode:

$$\eta_{CC} = \frac{RT}{1.5F} (1.375 - 0.125CB) \ln \left(\frac{i_c}{0.257} \right) \quad (4.9.4)$$

where

E^0	:	equilibrium potential	[U]
η_{AA}	:	reaction overvoltage at the anode	[U]
η_{AC}	:	concentration overvoltage at the anode	[U]

η_{CC}	:	concentration overvoltage at the cathode	[V]
F	:	Faraday's constant	
R	:	universal gas constant	
T	:	bath temperature	[°K]
C_{ox}	:	alumina concentration	[%]
$C_{ox(sat)}$:	saturated alumina concentration	[%]
i_c	:	cathodic current density	[A/cm ²]
i_a	:	anodic current density	[A/cm ²]
i_{cc}	:	critical current density	[A/cm ²]
i_o	:	limiting current density	[A/cm ²]

The equilibrium potential and the overvoltages are calculated in function UANOD(). The default function calculates Equations (4.9.1) to (4.9.3). η_{CC} is kept constant. The function returns the new value of U_{ap} .

5. SYSTEM REQUIREMENTS

The proposed Dynamic Cell Simulator can be run on various popular computational platforms. The hardware and software requirements for a typical PC application are the following:

- any IBM compatible machine with a 386 processor or higher,
- arithmetic co-processor,
- sufficient hard disk (minimum 40MB),
- a floppy drive,
- VGA display,
- sufficient RAM memory (minimum 4 MB),
- DOS version 3.1 or later.

To take the full advantage of this environment, and to develop a good graphic interface, the following or equivalent software packages are proposed:

- DOS Extender (from Phar Lap Software Inc.),
- NDP FORTRAN Compiler (from Microway Inc.),
- HOOPS Graphic Library (from Ithaca Software).

6. LITERATURE

1. D. Kahaner, C. Moler, S. Nash, "Numerical Methods and Software". Prentice Hall, 1989.
2. K. Grjotheim, C. Krohn, M. Malinovsky, K. Matiasovsky, J. Thonstad, "Aluminium Electrolysis, Fundamentals of the Hall-Héroult Process". Aluminium-Verlag, Dusseldorf, 1982.
3. K. Grjotheim, B.J. Welch, "Aluminium Smelter Technology". Aluminium-Verlag, Dusseldorf, 1980.
4. T. Foosnaes, K. Grjotheim, R. Huglen, H. Kvande, B. Lillebuen, T. Mellerud, T. Naterstad, "Understanding the Hall-Héroult Process for Production of Aluminum". Aluminium-Verlag, 1986.
5. Aluminium Electrolysis Seminar, Carnegie Mellon University, Post College Professional Education, Pittsburgh, 1990.
6. International Course on Process Metallurgy of Aluminium, Institute of Inorganic Chemistry, Norwegian Institute of Technology, Trondheim, 1989.
7. E. W. Dewing, "Loss of Current Efficiency in Aluminium Electrolysis Cells", Metallurgical Transaction B. V. 22B, April 1991.

**SIMULATION OF
AN ALUMINIUM ELECTROLYTIC CELL**

Approximating Selected Operation Modes

Tutorial

**L. TIKASZ,
V. POTOČNIK**

PREFACE

The present Tutorial is intended to guide the users how to approximate selected operation modes with the simplified dynamic cell model proposed in the Basic Mass and Energy Balance Calculation chapter.

First, two items from the user-adjustable model components are treated:

- line current generation and
- equivalent thermal conductivities for major Model parts.

Then, the Tutorial proposes an approach to approximate basic operation states and events such as:

- balanced dynamic operation,
- changing alumina feeding rate,
- changing anode position,
- tapping the aluminium.

These user-adjustable parts can serve as starting point for a more sophisticated description of the process.

1. ADJUSTABLE MODEL COMPONENTS

The Basic Mass and Energy Balance Calculation chapter proposes a simplified model of an aluminium electrolytic cell. Some of the model components are proposed to be worked out by the user. The most important adjustable components are:

1. equivalent thermal resistances.
2. equivalent heat transfer coefficients,
3. specific heat coefficients,
4. various mass densities.
5. current efficiency,
6. line current.
7. eutectic temperature.
8. bath resistance and conductivity,
9. equilibrium potential and overvoltages.

In this chapter two of the above listed items: line current generation and equivalent thermal resistances, are treated only.

1.1. Line Current Generation

Electrolytic cells are connected in series in a cell line. The line current is determined by :

- the status of the cells in the line and
- the properties of the line current control system.

The line current is an independent input variable which is attempted to be kept constant. This often is not obtained in practice because of poor line current controller or because of anode effects. In order to make the simulation realistic and flexible, it is a good idea to construct a line current sub-model which provides a new line current data at every computational step. The data for such a sub-model are obtained from the line current monitoring which is usually recorded on the computer. However, this is only possible for existing lines.

During the simulation, there are several possibilities to treat the simulated line current variable. The line current can be:

1. kept constant,
2. taken from pre-recorded real data,
3. taken directly from the process if the simulator is on-line,

4. generated mathematically.

The simplest solution is to keep the simulated line current constant during the whole simulation. The selected value can be the average or the target line current. This approach is perfect for steady-state calculations and acceptable for operation periods where the line current is smooth.

Use of pre-recorded real data is relatively simple and gives very good results. Data can be recorded directly from the plant information system. Stand-alone data acquisition systems can be applied, also. By selecting the operation periods, a good line current data bank can be set up. A major drawback is the memory requirement from the huge data files.

Direct application of on-line current data requires to synchronize the time-base of the simulation to the real time. Moreover, an appropriate interface has to be developed between the simulator and the plant information system. This method is advised for control system design and verification only.

Mathematical generation of an auxiliary signal is quite common in the simulation. It gives a relatively simple solution with adjustable properties. This approach fits well into the whole simulation approach. There are standard signal processing methods for analyzing data as well as for construction of data series with pre-

Without going into much detail, two examples for line current construction are introduced below. The signal construction is based on a group of selected real data. Figure 1.1.1 shows a real recording for a day-long period.

A possible method is to analyze the recorded data using standard statistical tools: start to calculate histograms, determine characteristic values (mean value, standard deviation, higher order momentums, etc.). Based on these, random number generators can be selected and tuned. The final signal can be mixed from several random signals. Figure 1.1.2 shows both the original line current (top) and the simulated signal (bottom). With some further adjustment of the components, much better approximation can be reached.

Another method is to keep the original, real data as base and construct the new signal from the fragments of the original. First, the original data set should be cut into parts. Next a (random) logic is needed to guide the selection from these parts. Finally, the reconstruction can be done repeating selected parts each after other. Figure 1.1.3. shows the result, in the same way as the previous Figure.

Note: Both these mathematical approaches give excellent results for a period much longer than the typical rate of line current variation.

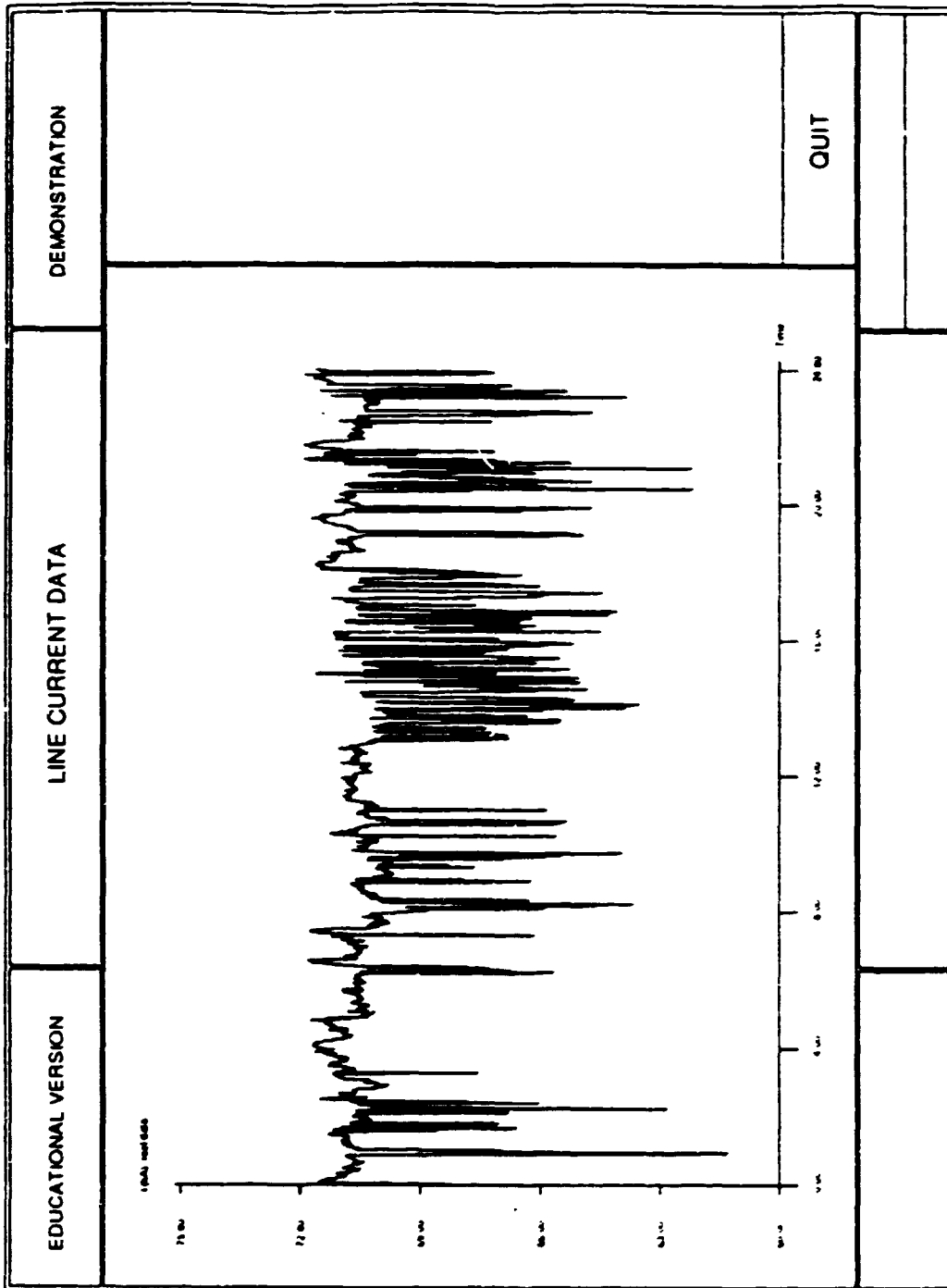


Figure 1.1.1 Real Line Current

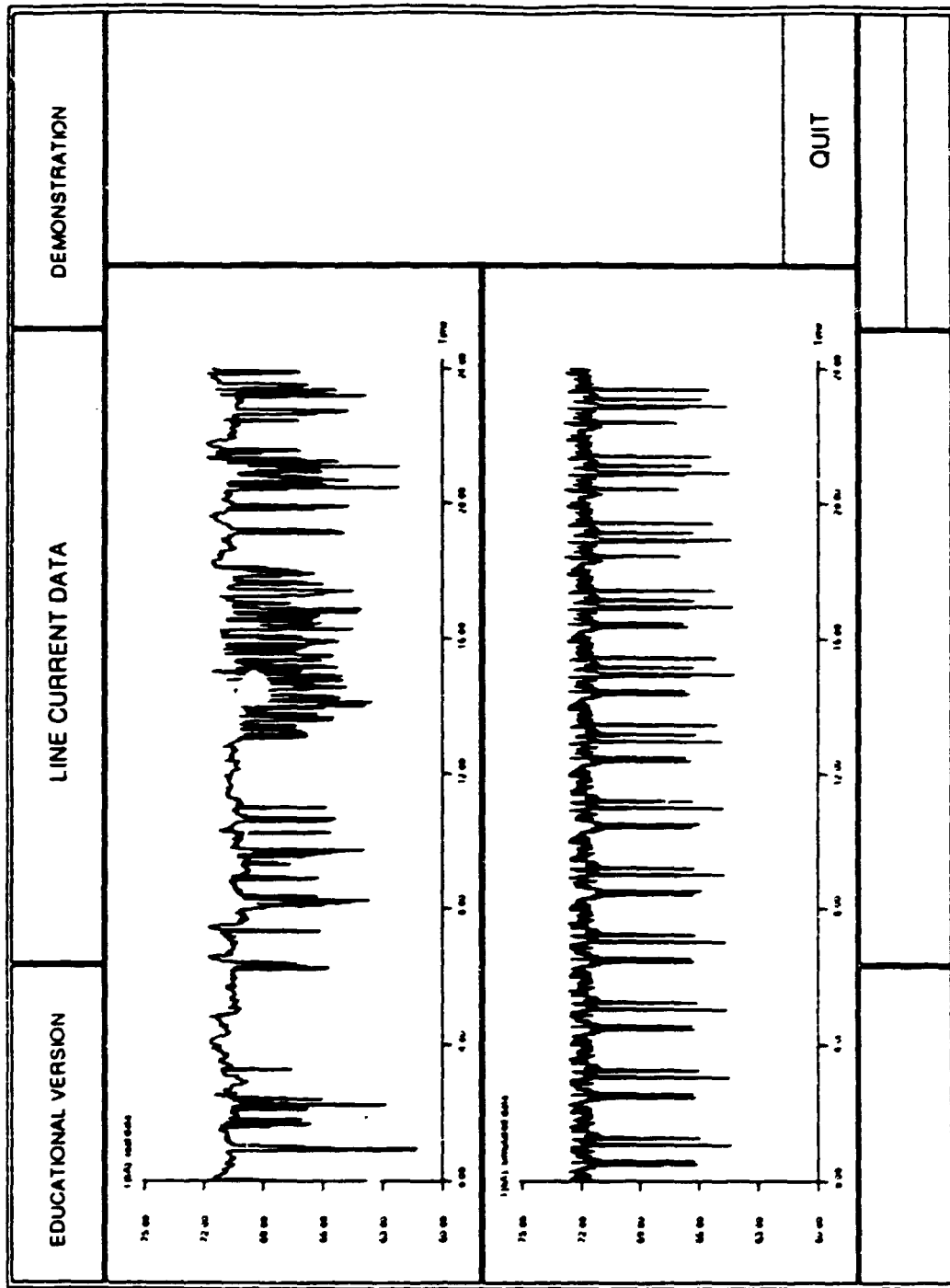


Figure 1.1.2 Simulated Line Current, Statistical Approach

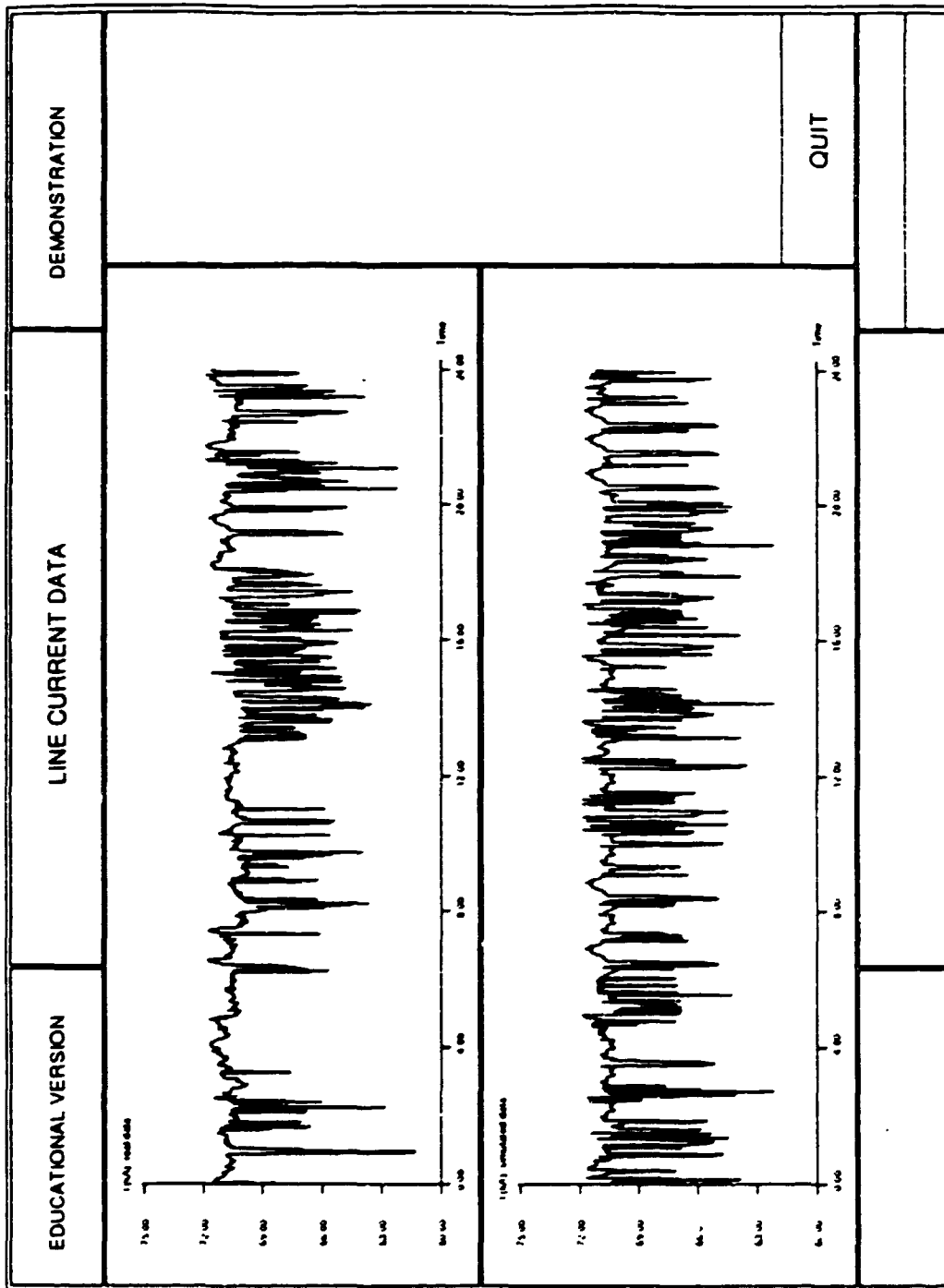


Figure 1.1.3 Simulated Line Current, Repetition Approach

1.2. Equivalent Thermal Resistances

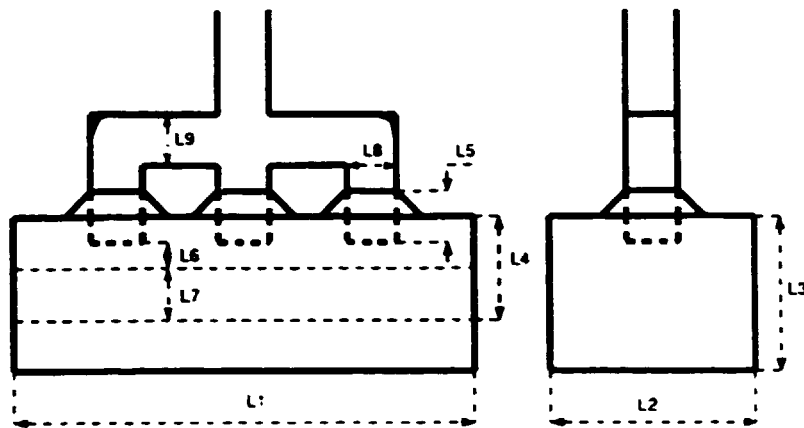
Equivalent thermal resistances of the lumps can be derived from the size and arrangement of a selected cell using equivalent thermal resistance network approach from which we deduce the equivalent thermal resistance for each lump of the model. In the cell model, the parts where the equivalent thermal resistances can be introduced are the following:

1. anode block (including carbon and steel parts).
2. cathode block (including carbon and steel parts).
3. cathode pier region (including carbonaceous, steel and isolating parts).

Figures 1.2.1 and 1.2.2 show the characteristic size of an anode carbon block and the proposed equivalent heat resistance network. Figures 1.2.3 and 1.2.4 show the characteristic size of a cathode carbon block and the equivalent heat resistance network. These lumps are relatively simple and the equivalent resistances calculated with the applied simplifications give good results.

The pier region (outer cathode side) has a more complex structure with different built-in materials. The user should respect the differences between the side-wall and the end-wall parts. Moreover, when both horizontal and vertical heat flows are calculated between the lumps, the user should pay attention to the anisotropic properties of the pier region. For demonstration purposes, examples are given for a typical side-wall and end-wall arrangement of the pier. Figures 1.2.5 to 1.2.7 relate to a side-wall while Figures 1.2.8 to 1.2.10 relate to an end-wall part. The differences in the computation of an equivalent thermal resistance in horizontal or vertical directions are evident.

The resistance networks shown in these figures may change for a different cell design. The user has to decide how to take into account the different materials, using the examples shown here as the basis



- L_1 : length of an anode block
- L_2 : width of an anode block
- L_3 : height of an anode block
- L_4 : estimated half-height of an anode block
- L_5 : length of steel parts inside anode block
- L_6 : length of butt
- L_7 : estimated height of carbon bar
- L_8 : diameter of nipples
- L_9 : diameter of stubs

Figure 1.2.1 Characteristic Size of an Anode Carbon Block

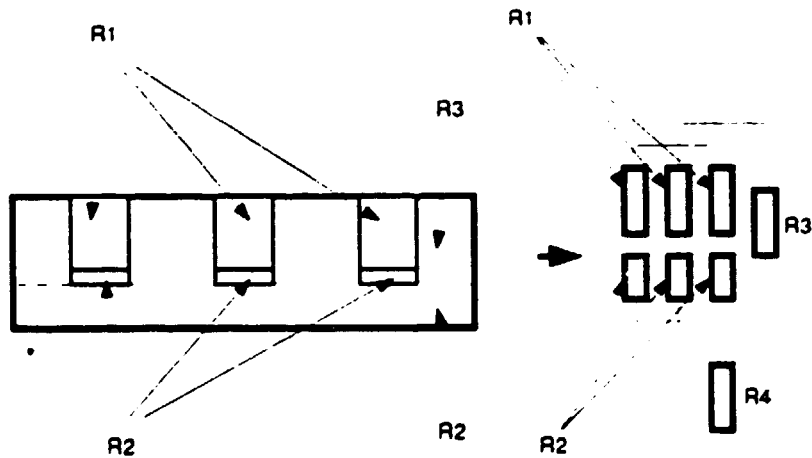
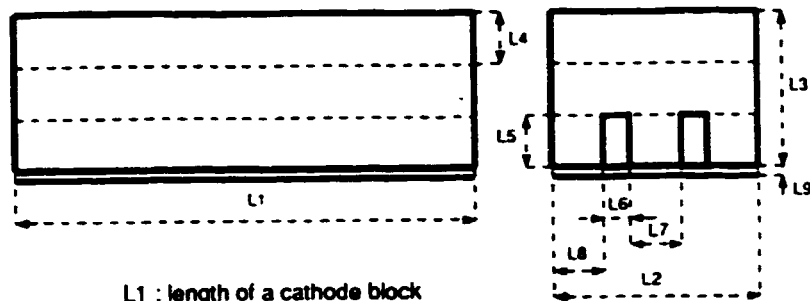


Figure 1.2.2 Equivalent Heat Resistance Network of an Anode Carbon Block



- L1 : length of a cathode block
- L2 : width of a cathode block
- L3 : height of a cathode block
- L4 : estimated height of penetrated layer
- L5 : height of a cathode bar
- L6 : width of a cathode bar
- L7 : carbon between steel bars
- L8 : distance between bar-side and block-side
- L9 : estimated height of alumina layer

Figure 1.2.3 Characteristic Sizes of a Cathode Carbon Block

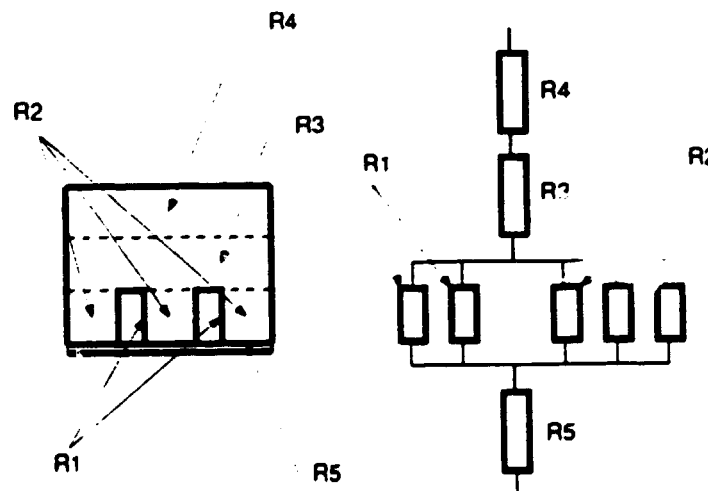
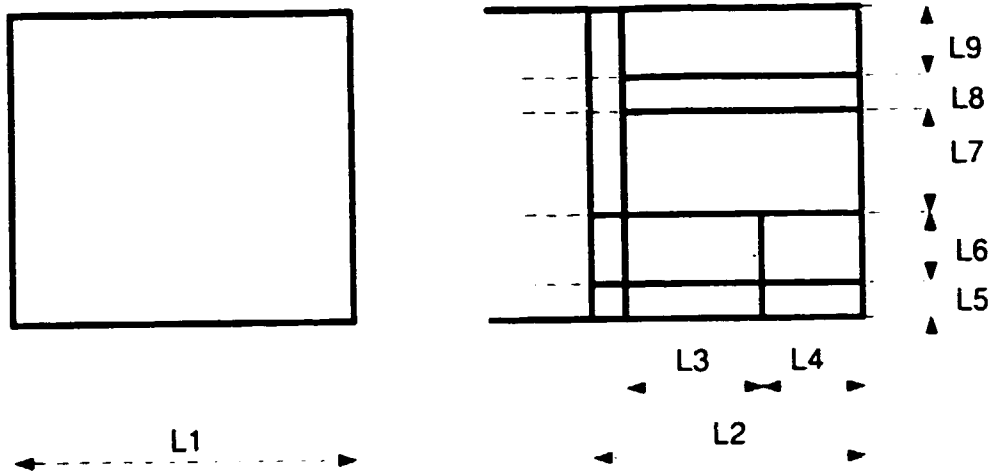


Figure 1.2.4 Equivalent Heat Resistance Network of a Cathode Carbon Block



- L1 : width of one cathode block + one ramming mix layer
- L2 : length of outer cathode (pier) region
- L3 : length of inner brick layer
- L4 : length of outer brick layer
- L5 : height of layer 1.
- L6 : height of layer 2.
- L7 : height of layer 3.
- L8 : height of layer 4.
- L9 : height of layer 5.

Figure 1.2.5 Characteristic Sizes of a Cathode Pier Region (Side-Wall)

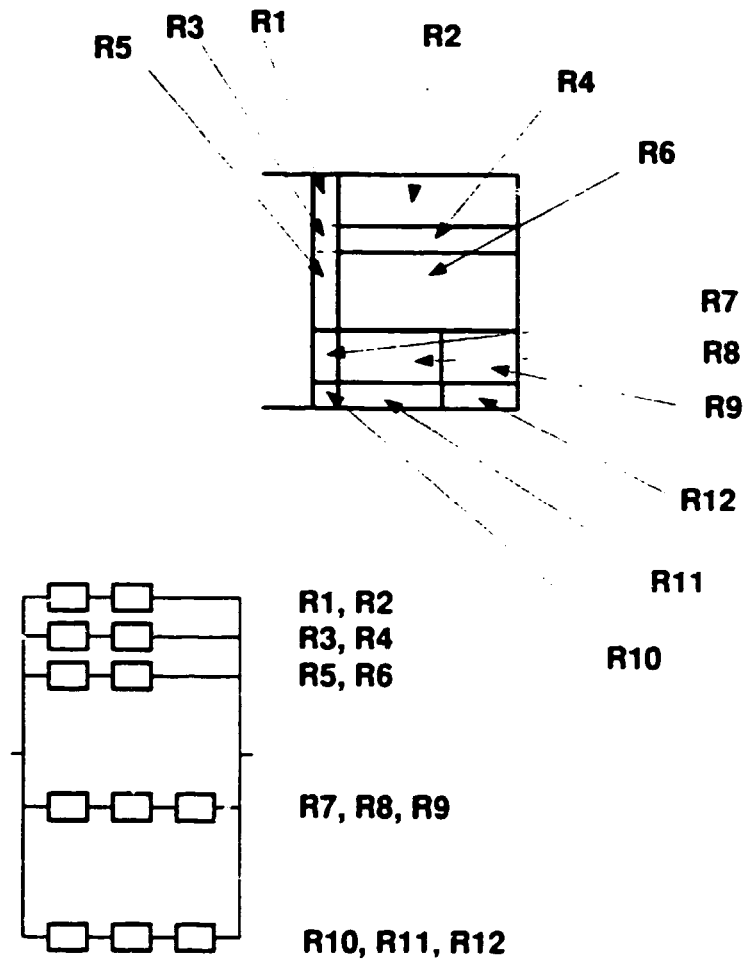


Figure 1.2.6 Equivalent Heat Resistance Network of a Cathode Pier Region (Horizontal Direction, Side-Wall)

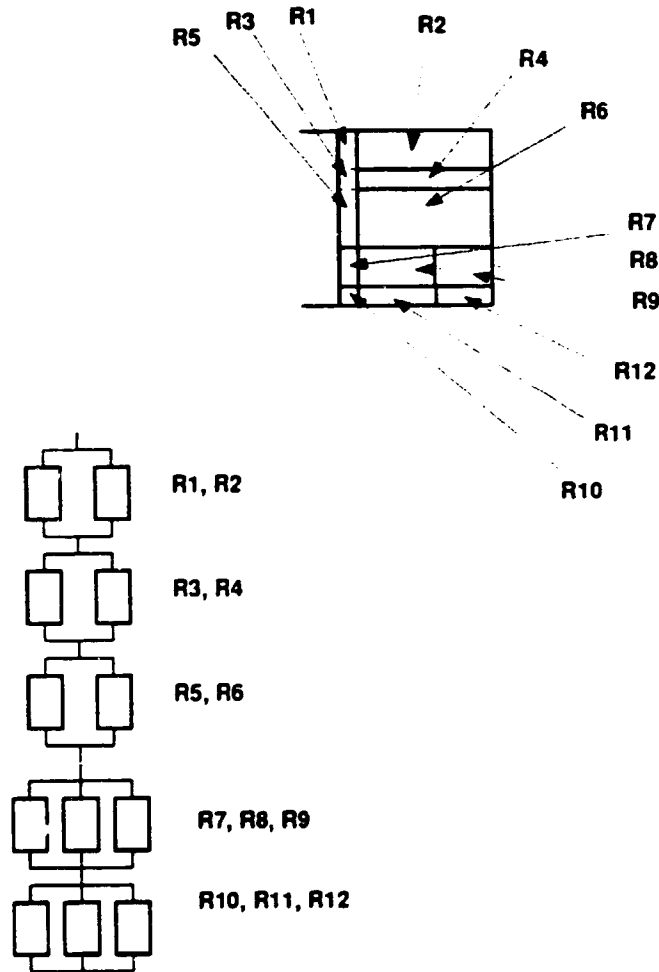
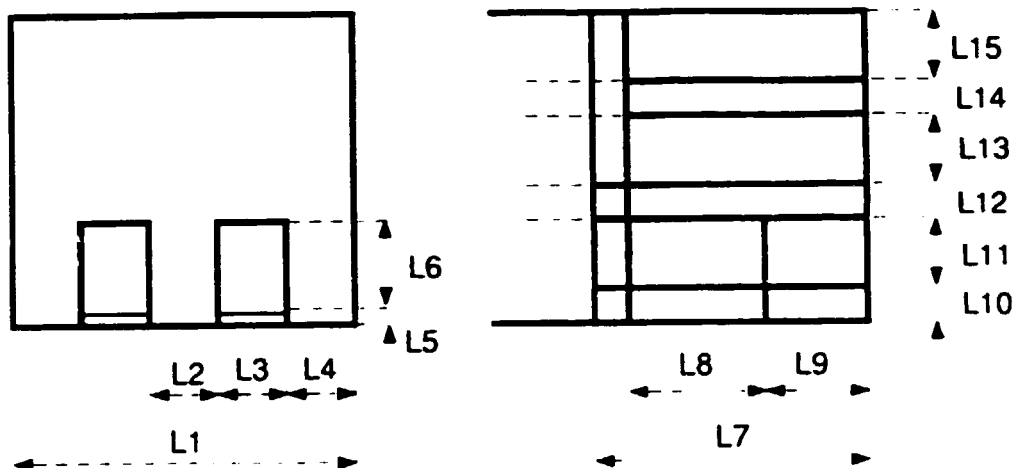
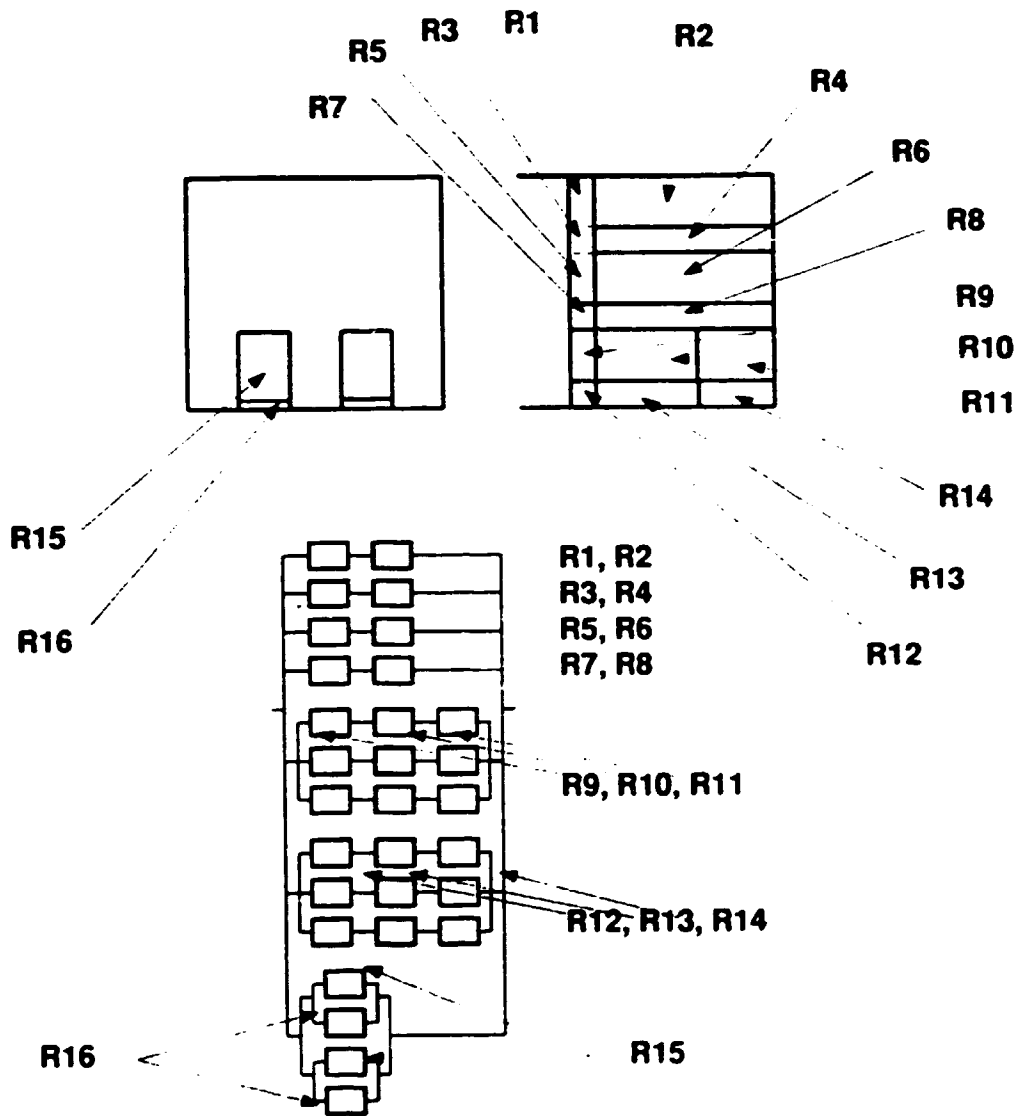


Figure 1.2.7 Equivalent Heat Resistance Network of a Cathode Pier Region (Vertical Direction, Side-Wall)



- L1 : width of one cathode block + one ramming mix layer
- L2 : width of one carbon wing
- L3 : width of one cathode steel bar
- L4 : width of one carbon wing + a half ramming mix layer
- L5 : height of alumina layer below cathode bar
- L6 : height of cathode steel bar
- L7 : length of outer cathode (pier) region
- L8 : length of inner brick layer
- L9 : length of outer brick layer
- L10 : height of layer 1.
- L11 : height of layer 2.
- L12 : height of layer 3.
- L13 : height of layer 4.
- L14 : height of layer 5.
- L15 : height of layer 6.

Figure 1.2.8 Characteristic Sizes of a Cathode Pier Region (End-Wall)



**Figure 1.2.9 Equivalent Resistance Network of a
Cathode Pier Region (Horizontal Direction, End-Wall)**

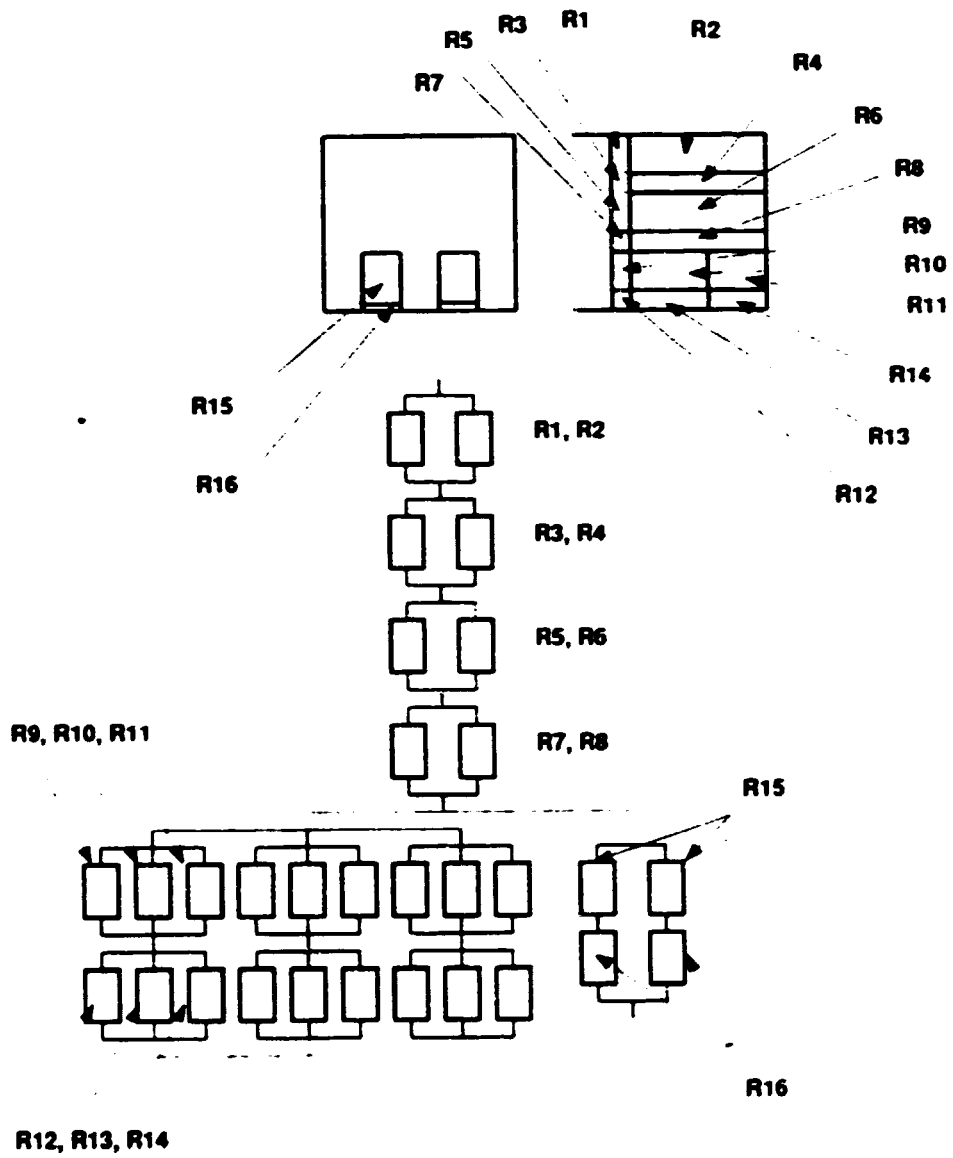


Figure 1.2.10 Equivalent Resistance Network of a Cathode Pier Region (Vertical Direction, End-Wall)

2. Selected Operation Modes

When the user adjustable components of the proposed model are completed, the next stage is to approximate some selected operation modes with the model. To do this, the user has to provide the initial values of the state variables and the time functions of control variables.

The initial values of the state variables can be based on the steady-state solution of the state equations. These values have to be compared to plant measurements or to results from more detailed static model for validation.

The selection of control variables depends on the user also, but regarding the reality, the fundamental control actions are alumina feeding, metal tapping and anode position adjustment.

The alumina feeding is essential to supply raw material to the chemical process, that is to make aluminium. The alumina feeding can be realized in various manners. Usually, batch and point feeding modes are distinguished as standard feeding procedures. The details about the possible batch or point feeding operations are beyond the scope of this Tutorial.

The metal tapping is intended to remove the produced aluminium. Comparing to the alumina feeding, it is a relatively simple action and its implementation is quite similar even on different cells.

The anode position is regularly adjusted on the cells to keep the cell resistance between desired limits, thus limiting the electrical energy input to the cell. The theory of cell resistance evaluation and anode position control is not treated here.

For the model the essential is that at every computation step current values have to be provided for the control variables which represent the amount of added alumina, the amount of tapped metal and the size of anode adjustment at that certain computation step. In a more elaborated stage of the model, a control module might take care of the alumina feeding and anode adjustment logic. The metal tapping can be added to the list of the scheduled operation events.

With the above mentioned extensions, the simple cell model is ready for dynamic simulation. In the remaining part of this chapter, a balanced dynamic operation as well as the effects of adjusting control variables are demonstrated.

2.1. Balanced Dynamic Operation

As a consequence of the operational practice, the cell is never in a static state. The target is to keep the cell close to a selected operation point. This can be reached with sophisticated adjustments of the control variables. For test purposes, it is very advantageous to approximate an almost perfectly balanced dynamic operation mode. Although this mode can never be realized in the plant practice, it is an essential stage in the model verification and validation process.

To reach this artificially balanced state, the control variables should be set to the following values at every computation step:

- the amount of added alumina is equal with the alumina consumed,
- the amount of tapped metal is equal with the metal produced,
- the anode position is kept constant.

Figure 2.1.1 shows an one hour period of this balanced operation mode. The diagrams are the following from top down: alumina concentration in the electrolyte, electrolyte mass, electrolyte temperature, freeze mass and freeze temperature. For demonstration purposes, the initial value of electrolyte temperature was slightly different than in the static equilibrium. It can be seen that after a few steps, the solution (the electrolyte temperature) converges to a value and this value is kept in the remaining part of the simulation.

It is a good practice to produce this balanced state. The calculated alumina balance, metal production rate, several mass and temperature values can be compared to plant data. Starting from this state, the results of individual control actions can be evaluated more reliably.

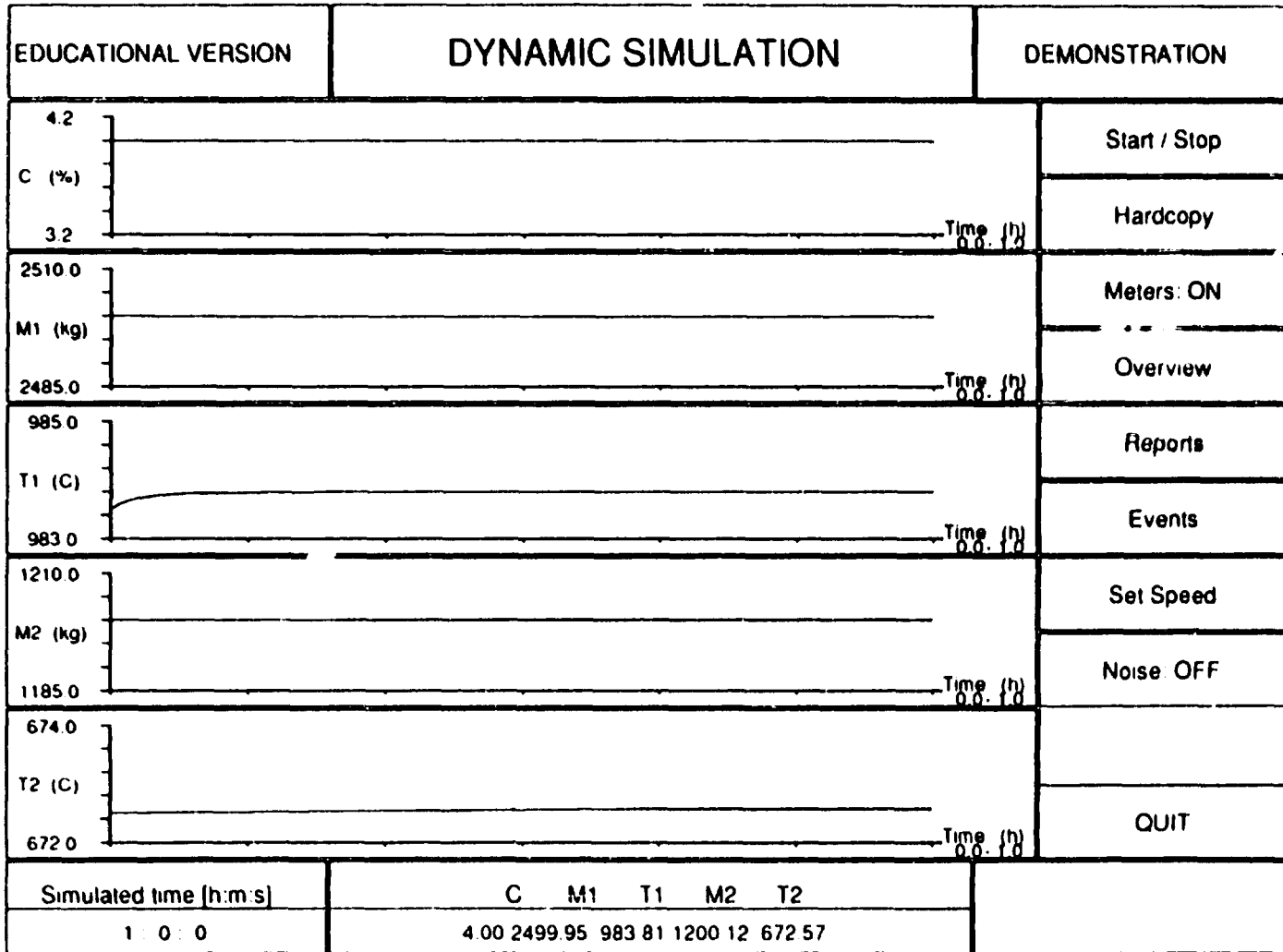


Figure 2.1.1 Balanced Dynamic Operation

2.2. Changing Alumina Feeding

Considering a longer period of time, and the relevant averages, the amount of added alumina equals to the amount consumed. However, as far as second or minute-long time slices of the process, or the individual time steps of the simulation are concerned, this balance does not exist.

This is evident in batch feeding mode. With point feeders, theoretically this balance can fairly well be approximated, but usually another approach is used in practice: overfed and underfed periods are used in the cell operation. This means, that the effect of changing the amount of added alumina should be studied with a great care.

Figure 2.2.1 demonstrates a special simulated test period. The simulation was started from the same initial values as given in Figure 2.1.1. The cell reached the balanced state shortly after the beginning. The control variables were set according to the balanced state. This state is maintained until simulated time 2:00 hours. At 2:00 hours, the amount of added alumina was reduced by 15%. This action can be interpreted as start the of underfeeding, or with other words, the beginning of an underfed period. The displayed functions are the same as in Figure 2.1.1. The results can be explained as follows.

The alumina concentration is decreasing. This is natural, because the alumina supply is less than the consumption.

The mass of the electrolyte starts to decrease. This is understandable, because the amount of fed alumina contributes to the mass of the electrolyte and again, the supply is less than the consumption. However, as seen in the following diagrams, the freeze mass gradually decreases and in this way it contributes to the electrolyte mass. Finally, the change in the electrolyte mass depends on these two factors and the result is determined by the ratio between the change in the supply and freeze volume.

The temperature of the electrolyte started to increase. The reason is that less alumina should be warmed up. The main result of this "extra" energy is seen in the temperature. Of course, the warming effect propagates and influences all the temperature dependent components of the model: freeze volume, internal heat flows, bath resistance, etc. The user is advised to check and analyze all the changes carefully.

The mass of the freeze is slowly decreasing and the freeze temperature is slowly increasing as the result of the warming period. See explanations above.

Note, that this is just a test period. After a while, the alumina feeding should be balanced again otherwise the simulated cell would not be realistic anymore.

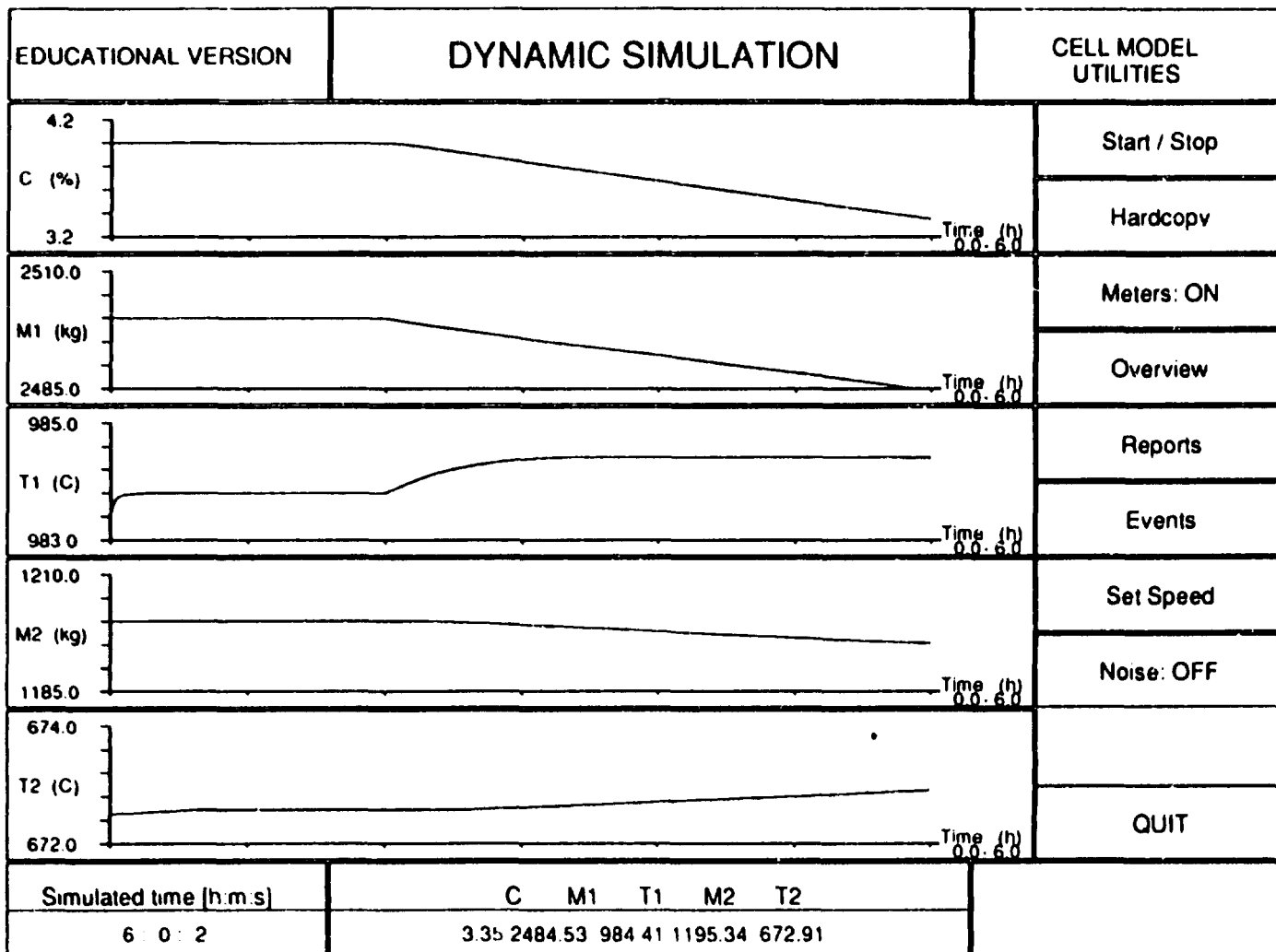


Figure 2.2.1 Changing Alumina feeding

2.3. Changing Anode Position

Changing the anode position is the simplest way to change the cell resistance and control the energy input to the cell. To demonstrate the effect of a single anode position adjustment, we follow the way introduced in the previous examples: the cell is in the balanced dynamic mode until the simulated time 2:00 hours when the anode position is adjusted. At this moment, a single up movement was done. The results can be seen in Figure 2.3.1. The diagrams are the same as in the previous examples. The results are explained as follows:

The alumina concentration is unchanged, because the perfectly balanced feeding is maintained during the whole simulation period.

The mass of electrolyte increases because the freeze melts and contributes to the electrolyte mass.

The electrolyte temperature increases as a result of increased anode-cathode gap which causes an increase of the electrolyte voltage drop. Note, the line current is considered constant.

The mass of the freeze decreases and the temperature of the freeze increases as the secondary result of this warming period. Of course, the effect of the warming period propagates and influences all the temperature dependent parameters of the model.

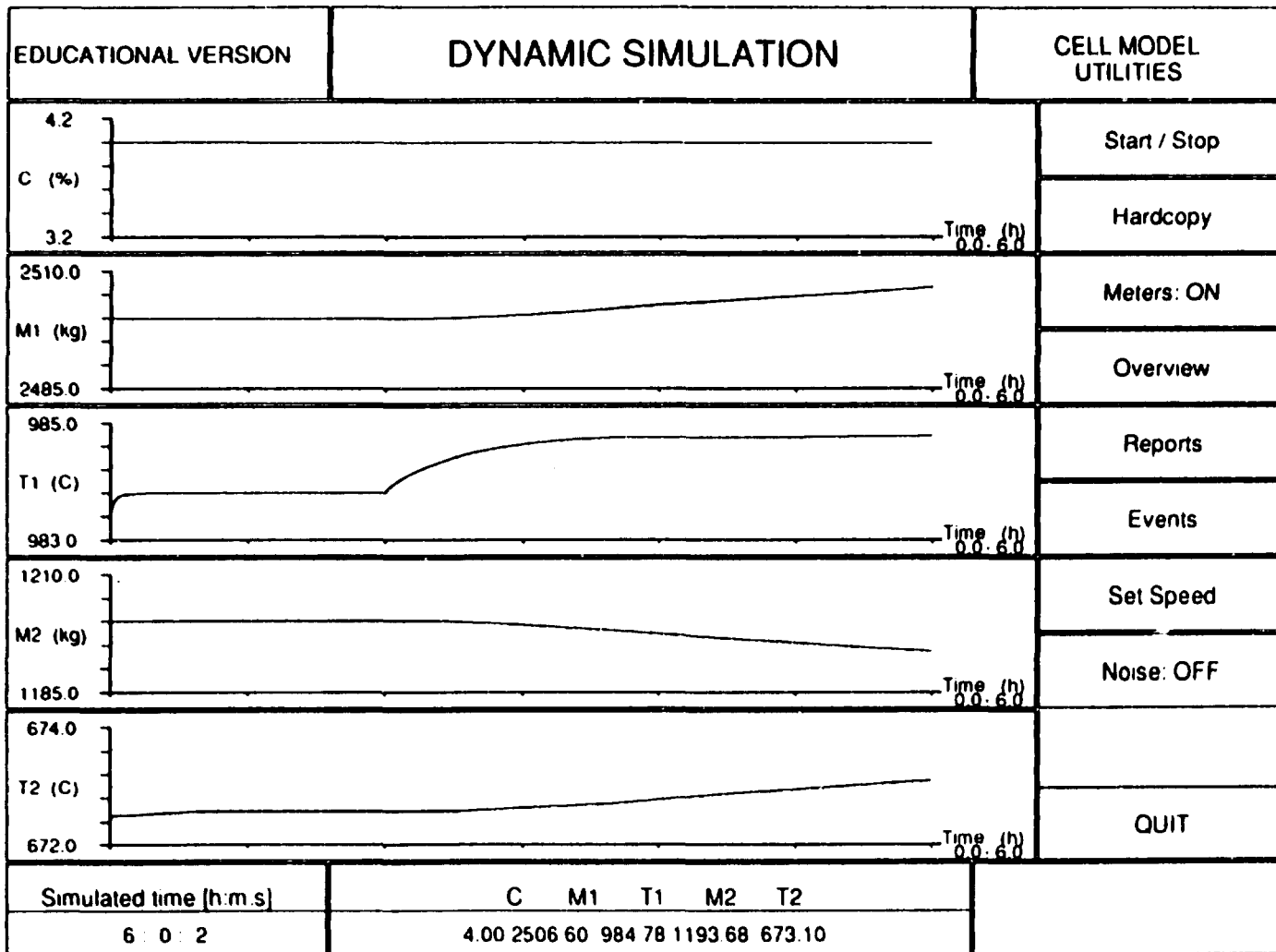


Figure 2.3.1 Changing Anode Position

2.4. Introducing Metal Tapping

Metal tapping is a well separated operation event scheduled in advance. Its result can easily be traced and explained. The simulation was done according to the previous examples. To aid the explanation, two figures were generated: Figure 2.4.1 contains the previously used variables, while Figure 2.4.2. shows the alumina concentration, electrolyte mass, electrolyte temperature, metal mass and metal temperature (from top down).

Figure 2.4.1 is not adequate to study the effect of metal tapping: here only the warming can be recognized. The main effect is hidden from the user.

Figure 2.4.2. shows the tapping more clearly. The mass of metal gradually increases due to the metal production. At simulated time 2:00 hours the metal tapping started and at 2:10 hours it finished. The decrease in the mass of the metal can be seen. After the tapping, the mass of the metal slowly increases, as it did before, according to the continuous production.

All the rest is just a warming process, caused by the increased anode-cathode gap. Note, there was no anode adjustment connected to the metal tapping. Of course, in the plant practice, the anode position is carefully adjusted during and after the tapping to avoid unwanted warming periods. This situation can easily be approximated with the model combining the metal tapping and anode position adjustment accordingly. The users are advised to put this simple case into practice.

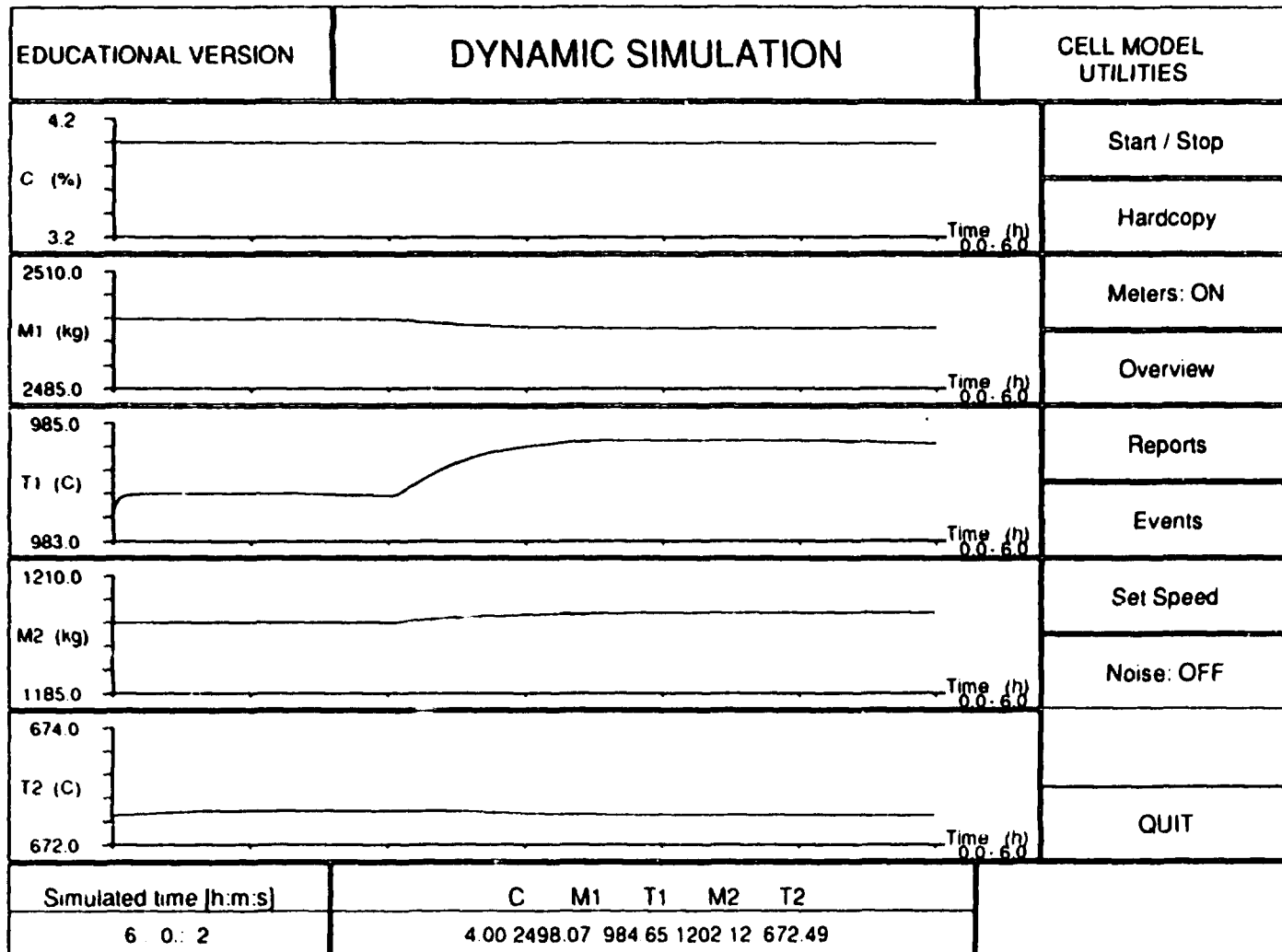


Figure 2.4.1 Metal Tapping (1.)

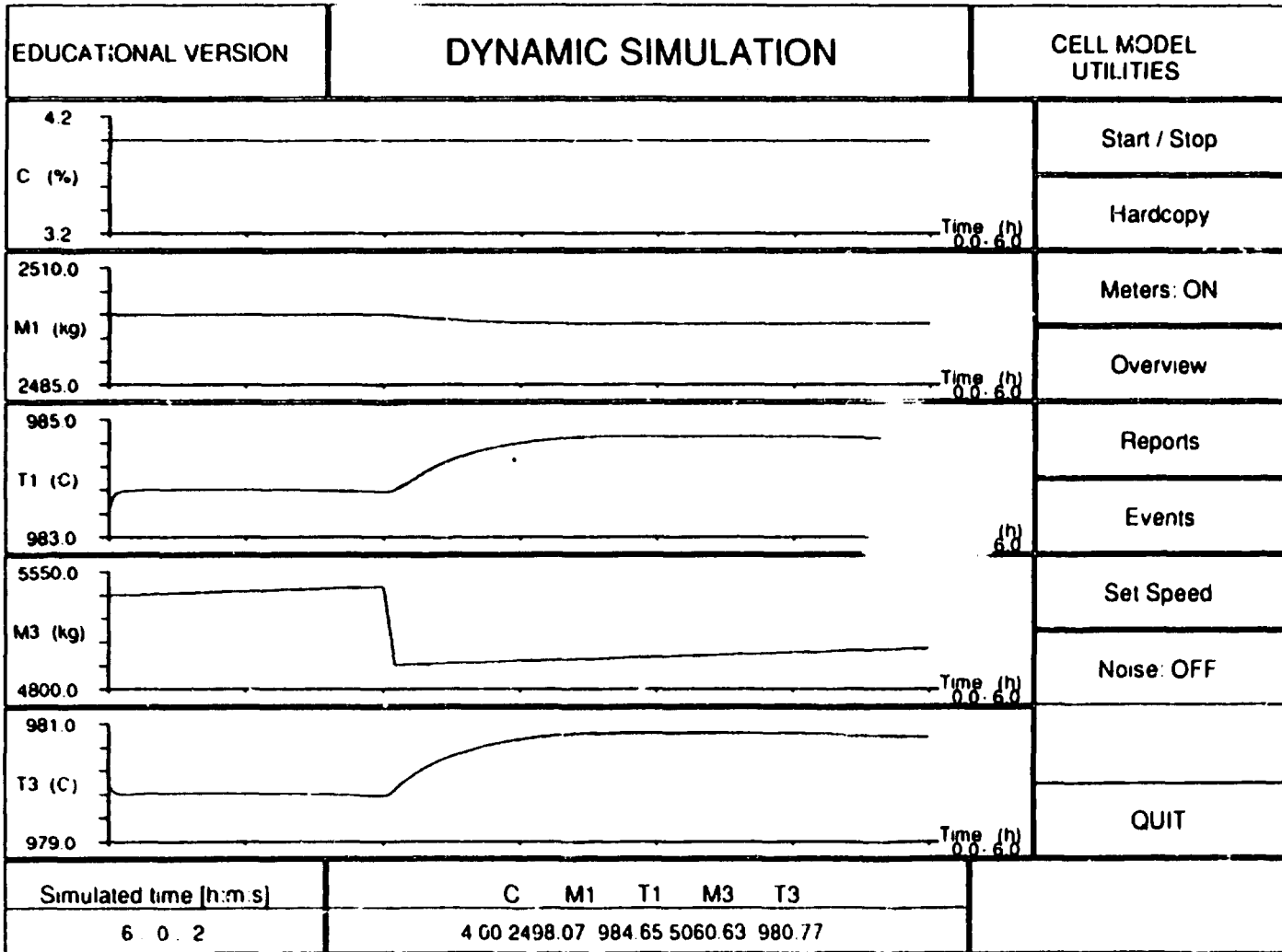


Figure 2.4.2 Metal Tapping (II.)

**SIMULATION OF
AN ALUMINIUM ELECTROLYTIC CELL**

Developing a Control Emulator

Tutorial

**L. TIKASZ,
V. POTOCNIK**

PREFACE

The present Tutorial is intended to guide the users how to develop a simplified control emulation which cooperates with the simplified dynamic cell model proposed in the Basic Mass and Energy Balance Calculation Chapter. The Model and the Controller form the main parts of the Simulator.

The items discussed are the following:

- basic control scheme,
- data exchange between Model and Control Emulator,
- anode position control,
- alumina feeding by point feeders.

Some parts of the Simulator and some internal elements of the Control Emulator (control data base, control interface, control logic, etc.) are user-adjustable. The proposed user-adjustable control parts can serve as starting point toward a more sophisticated description of the control system.

Note: the proposed anode position and alumina feeding control logic is for demonstration purpose only. Much more sophisticated algorithms are needed for real applications.

1. CONTROL SCHEME

From control point of view, the operation of an electrolytic cell can be interpreted as follows.

There are several input signals and operation actions done either manually or by the automated control system, which are essential to keep the process close to the target. In the operating cell, several measurements can be made in order to gain information about the state of the process.

In the plant practice, the inputs are: line current, alumina feeding, anode adjustment, metal tapping, anode removal, anode supply and aluminium fluoride feeding. As far as the measurements are concerned, only the line current and the cell voltage are measured and logged continuously. All the other measurements (e.g. bath temperature, metal and bath height, freeze thickness, bath ratio, alumina concentration, etc.) are done occasionally.

In connection with the presented simplified cell model, a simplified control scheme is proposed. Figure 1.1 shows the arrangement.

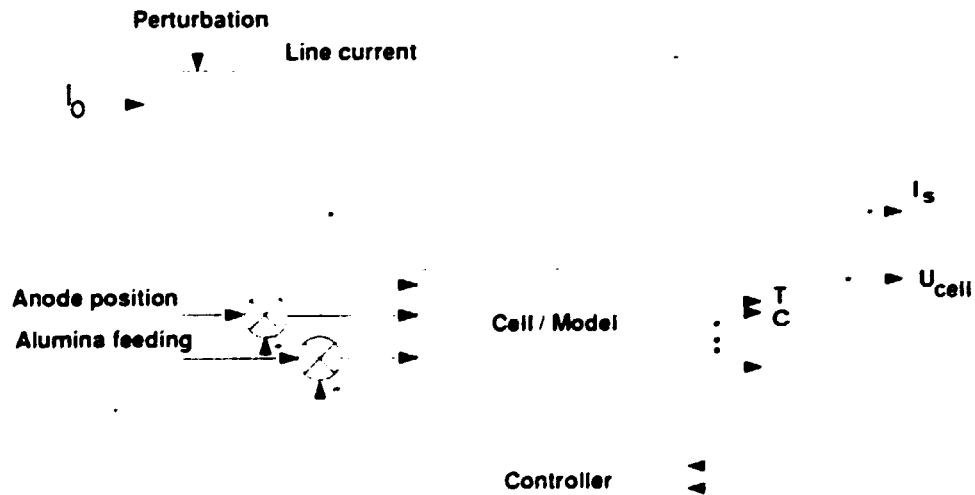


Figure 1.1 Control Scheme

The line current is independent of the cell, it is an input variable and available as a measurement for the controller, also. As input signals (or actions), two

control variables are kept as essential: the alumina feeding and the anode position adjustment. At the output of the model, only the simulated cell voltage is available for the controller as source of information about the process.

Based on the line current and cell voltage measurements, the cell controller calculates the cell resistance. The internal control logic is based on the trend analysis of this cell resistance.

The controller can generate two control actions at a time: feeding a fixed amount of alumina and adjusting the anode position up or down. Combining these control actions, the cell can be held in the vicinity of the target values (target concentration and target cell resistance).

Developing a Control Emulator usually means to reproduce or approximate some existing or planned control logic. A reasonable approach is to determine the really important part of the control logic and emulate that one only. Too many details might hide important relationships. It is a good practice to develop a separate control data base, independent of the internal Model data. All the data used by the control logic (raw and computed data, temporary and averaged values, trends, results of statistical analysis, etc.) should be stored in this database.

A control interface has to be provided where the user can access and set those data which are available in the real control system. This interface should be similar to the real one. It is a good practice to provide a training environment similar to the real one. It facilitates the familiarization with the Simulator for users who are already familiar with the practical cell operation.

2. DATA EXCHANGE

The cell Model and the emulated Controller are put to a shell which is named Simulator. Inside the Simulator these main components are supported by other modules to provide the necessary operation environment. Figure 2.1 shows a possible arrangement of such a system with their typical interactions.

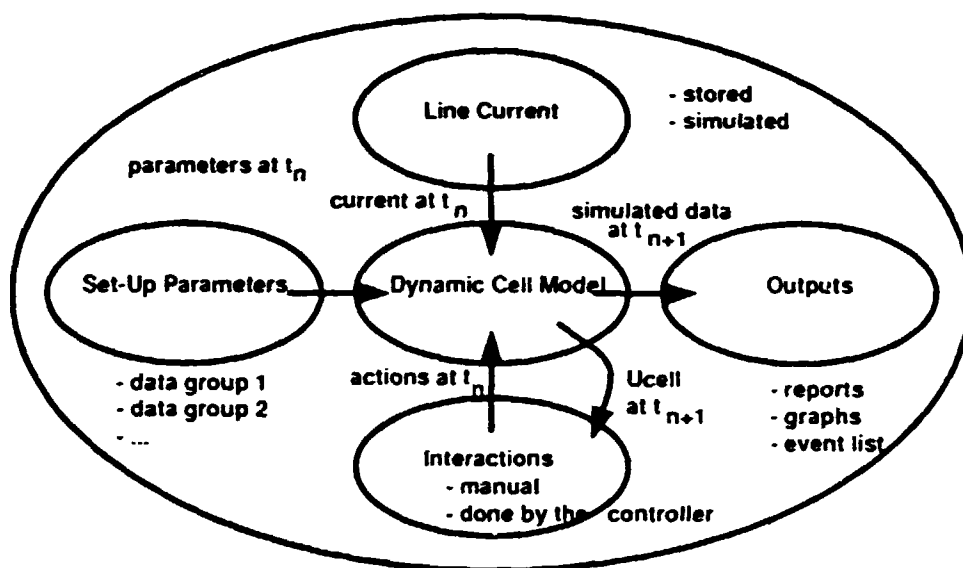


Figure 2.1 Data Exchange Scheme

The dynamic cell Model is in the heart of the Simulator. At the beginning of a simulation session, set-up parameters are transferred to the Model determining the initial conditions of the applied equations. These initial parameters are usually grouped in advance to describe certain selected plant situations (overfed or underfed cell state, cell before or after metal tapping, etc.).

During the simulation, line current data and all the actual interactions are sent to the Model at every computation step. The algebraic equations inside the Model are solved and the differential equations are integrated one step ahead. The results of every new computation steps are sent to the output module where reports, graphs, event lists can be generated on demand.

3. ANODE POSITION CONTROL

The fundamental idea behind the resistance control is to keep the cell resistance between limits by adjusting the interelectrode gap. The interelectrode gap might change for several other reasons (anode consumption, metal production, freezing-warming trends, etc.), so it is more precise to name it anode position control.

The anode position control is usually based on cell resistance observation. The cell resistance is obtained from line current and cell voltage measurements.

A real anode position control logic is a quite sophisticated collection of advanced data acquisition and data processing tasks. To establish a reliable anode position control, the main steps to be done are the following.

Preparatory phase:

- select proper sampling rate.
- select proper measuring method.
- select proper data logging structure.

Analysis phase:

- verify measured data.
- provide data conditioning (averaging, pre-filtering, etc.).
- compute resistance values.
- process these resistance (filtering, statistical analysis, etc.).
- recognize trends in the resistance data.
- respect possible restrictions and limitations (signal values, timing, coincidences, etc.).

Command phase:

- generate a control command.
- verify this control command.
- activate the control command.

It is almost impossible to provide a general purpose anode position control logic. However, a possible (default) control algorithm might work in the following manner:

- at every computation step (e.g. one second), take a cell voltage and a line current value,
- calculate resistance from individual readings,
- average resistances for about 30–60 seconds,
- compare this resistance value to the prescribed resistance limits (dead band limits, acceptable minimum and maximum values, etc.),
- generate a proper up or down control command if the resistance value is out of the dead band but within the acceptable limits,
- pass the control command (usually a control flag and the size of the action) to the Model according to a pre-defined format so the Model be able to handle the command.

Note, that in this list there are no preliminary data verification, trend analysis or any timing limitations. The generated control signal can be proportional to the resistance deviation but a fixed-size up or down movement command also possible. There are no functions which might take care of any special situation (anode position control during metal tapping, anode change, etc.). It is a major job to elaborate all of the details and provide a reliable, realistic anode position control logic.

4. ALUMINA FEEDING CONTROL

This chapter applies to a cell with automatic breaking/feeding. The fundamental task of the alumina feeding control in a modern breaker/feeder cell is to keep the alumina content in the electrolyte continuously at a low level, in spite of the continuous metal production process in action.

The cells are equipped with remote control crust breakers and alumina feeders. The alumina feeding control logic should generate control orders to trigger the breaking — feeding actions at proper times. Unfortunately, direct measurements related to the alumina concentration of the electrolyte are not available. The control logic should rely on the measured data (cell voltage and line current) and some additional (manually, occasionally measured) data.

Usually, the alumina feeding logic is a simple, rule-based, almost open-loop controller. The control base is the theoretical alumina consumption (metal production) of a cell at an average current efficiency. The amount of alumina in one-shot is fixed by the geometry of the feeder, so the feeding rate is the only adjustable parameter. It is common to define some fixed feeding rates (nominal, normal, fast, very fast) which are further determined by the solubility of the applied alumina, mechanical strength of the breaker, etc.

Lack of direct measurements makes the control task difficult, so it is a must to introduce planned perturbations such as tracking to the feeding in order to gain extra information about the process.

Preparatory phase:

- define applicable basic feeding rates (nominal, normal, low, high, etc.),
- set time limits (durations) for these feeding rates.

Analysis phase:

- at every step, make a decision whether to change the feeding rate or keep the current one,
- at every step, make a decision whether to feed alumina or not.

Command phase:

- generate a control command if alumina feeding has to be done.
- activate the control command.

A real alumina feeding control logic contains several restrictions for special situations. The proposed (default) alumina feeding logic works in the following very simple manner:

- based on the nominal feeding rate, define a low (80%) and at least one high (150%) feeding rate: usually an extra fast feeding is also necessary (300–400%).
- set time limits (durations) of these feeding rates according to the plant situation (alumina solubility, restrictions by the breaker-feeder mechanism, etc.).
- analyze the cell resistance (based on 60–300 second averages) and judge the state of the process (based on 1–10 minute averages) with special emphasis on the alumina balance.
- at every step, make a decision whether to change the feeding rate.
- at every step, make a decision whether to feed alumina or not.
- synchronize the feeding and the anode adjustment logic.
- respect all the restrictions (timing, event coincidences, etc.).
- generate a control command if alumina feeding has to be ordered.
- pass the control command (usually a control flag and the size of the action) to the Model according to a pre-defined format so, that the Model will be able to handle the command.

Note, that there are no preliminary data verification, resistance trend analysis and any limitations listed above. No tracking routine is ready made and there are no functions which might take care of any special situation (feeding control before and during metal tapping, anode change, etc.). These important details should be elaborated by the user. It is a major task to develop a good quality alumina feeding control logic.

**SIMULATION OF
AN ALUMINIUM ELECTROLYTIC CELL**

How to Use the Dynamic Cell Model

Tutorial

L. TIKASZ

PREFACE

The Dynamic Cell Model (Simulator) is an integrated software package containing a cell Model, an emulated Controller and several other modules which complete the operation environment and make the Simulator work.

There are three manuals accompanying the Simulator: User Guide, Set Up Guide and a Tutorial. The User Guide outlines the theoretical background of the Model, the Set Up Guide gives all the information needed to prepare a simulation session. The Tutorial contains complete examples demonstrating the basic operation as well as the basic usage of the Simulator.

The user is advised to study carefully these manuals. On that base, he can construct his own input data files and can do the necessary modifications of the adjustable model parts. When these preparatory phases are completed, the Dynamic Cell Model can be started and several simulation sessions have to be done to be fully familiarized with the Simulator.

This Chapter does not attempt to replace the three Manuals mentioned above. Here, we point to a few important items, instead. A quick overview is given for:

- user-adjustable data files,
- user-adjustable model parts,
- user-adjustable control parts,
- user interface.

It is supposed that the user has access to the properly installed Dynamic Cell Model and can do all the preparations, modifications and test runs at his own pace.

1. USER-ADJUSTABLE DATA FILES

Considering the Dynamic Cell Simulator, the whole cell is divided into elements or lumps as shown in Figure 1.1.

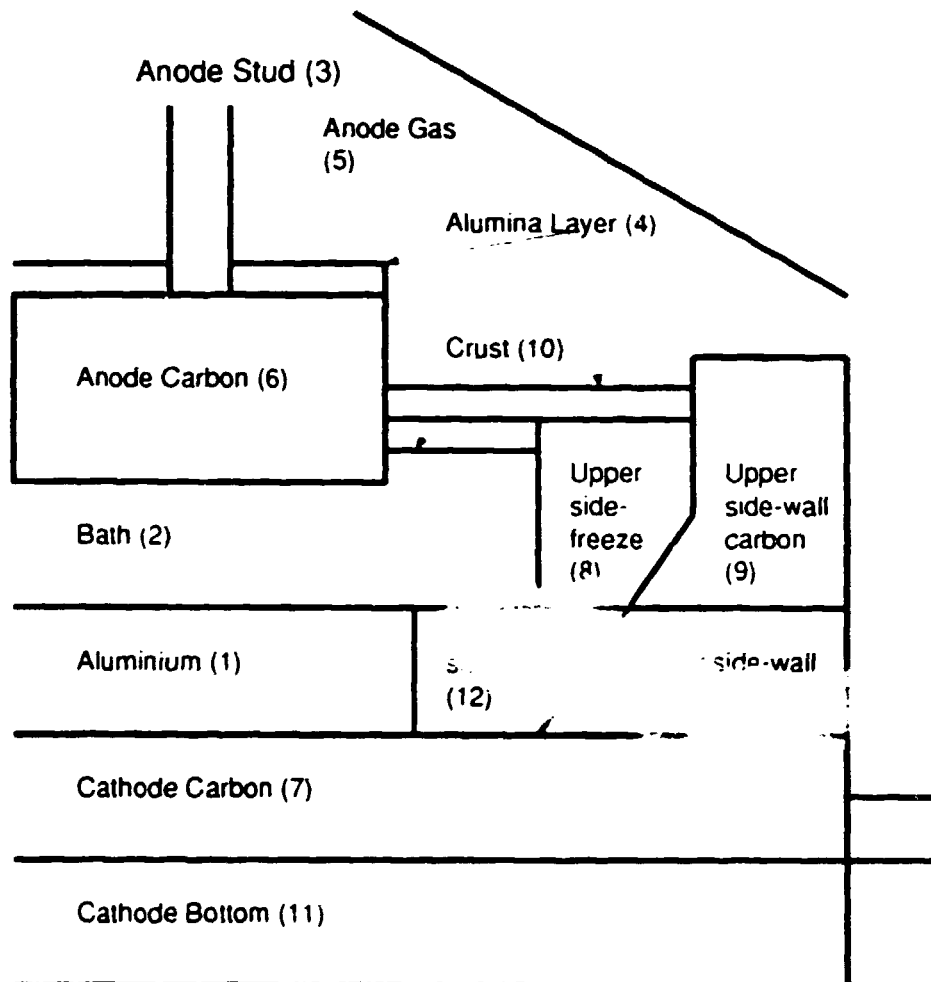


Figure 1.1 Components of the Model

The user-adjustable data files are designed to contain the information needed to describe a selected cell under selected operation mode. The user-adjustable data files are the following:

input.dat	:	for input data
dynam.dat	:	for dynamic data
event.dat	:	for events data
plots.dat	:	for plots data
workpl.dat	:	for workplace data

1.1. Basic Input Data

The most important data file is the basic input data file. Its content (the data relating to a certain cell) is grouped to facilitate the setup and the maintenance of the Simulator. These data groups have names such as Thermal Conductivities, Heat Transfer Coefficients, etc. They are listed below.

Title	Name of Data Groups	No. of Items
COND	Thermal Conductivities	14
HTCO	Heat Transfer Coefficients	13
SPEC	Specific Heat Coefficients	10
DENS	Densities	6
REAC	Reaction Parameters	3
RESI	Resistances Parameters	3
VOLT	Voltage Parameters	2
CURR	Line Current Parameters	2
LENG	Length	18
AREA	Areas	11
MASS	Masses	8
REFE	Reference Values	11
INIT	Initial Values	16

The user has to provide all these data unless he specifies some equations using the adjustable model components to obtain the required values. For details, refer to the Dynamic Cell Model Set-Up Guide and see a sample input.dat file..

1.2. Dynamic Data

The Dynamic Data file consists four parts starting with the following control words:

- STRT, for START parameters.
- SAMP, for SAMPLING parameters.
- SOLU, for SOLUTION parameters.

In STRT data part, the start and the end time of the simulation have to be given. The SAMP data part contains the time step (sampling rate) of the simulation. In SOLU data part, the following parameters have to be specified:

Fraction of alumina added which dissolves immediately concerning one feeding action

Fraction of undissolved alumina and sludge which is assumed to lie under the aluminium pad

Volume of crust which is knocked into the pot on the routine side-type crust breaking (m³)

Initial value of the time constant for the dissolution of alumina (s)

Reference temperature for alumina dissolution (°C)

Initial quantity of undissolved alumina in the cell (kg)

Initial volume of sludge in the cell (m³)

For programming details, refer to a sample dynam.dat file and the Set-Up Guide.

1.3. Scheduled Events

For batch feeding operation, this file lists all the scheduled feeding-breaking actions besides the planned manual interactions like metal tapping, anode block removal, anode block supply.

For automated alumina feeding, this file is somewhat less important because the alumina feeding is controlled by the control emulation routine. Of course, the scheduled manual interactions have to be enlisted, too.

The scheduled time of actions has to be given in day-hour-minute-second format. At metal tapping, another time parameter, the duration of the tapping has to be given, also. The relevant amount or size of an action has to be given in proper units: breaking in % of the total crust area, supplied alumina, tapped metal, removed and supplied anode carbon in kg. The possible commands and the units are the following:

BRK	:	part of the total crust area broken in	%
A2O3	:	supplied alumina	kg
REMC	:	removed anode carbon	kg
SUPC	:	supplied new anode carbon	kg
AL	:	tapped metal	kg

For programming details refer to a sample events.dat file.

1.4. Plots Data

The Simulator is programmed to display simultaneously up to 5 variables as functions of time. The variables can be selected from predefined variables such as:

- line current,
- cell voltage,
- cell resistance,
- anode position,
- anode-cathode distance,
- metal height,
- bath height,
- thickness of upper freeze block,
- thickness of lower freeze block,
- bath temperature,
- anode temperature,
- cathode temperature,
- cathode bottom temperature.

- eutectic temperature.
- bath ratio.
- alumina concentration.
- mass of anode.
- mass of bath.
- mass of metal.
- mass of freeze.

Plots Data files control the graphical representation of the simulated results. The line numbers from the above list serve as codes for parameter selection. For programming details refer to a sample plots.dat file.

1.5. Workplace Data

The Simulator is designed to fulfil the needs of different users. In general, potential users are classified as STUDENT, MASTER and EXPERT level users selected by confidential passwords. With a valid password, the user has access to different, pre-arranged sets of input files. These pre-arranged input files are listed in the Workplace Data file.

A Workplace Data file contains three groups of data inside, each containing names of available basic input data, scheduled event, plot parameter, current data and dynamic data files. For programming details refer to a sample workpl.dat file.

2. USER-ADJUSTABLE MODEL PARTS

Advanced users can modify certain parts of the Simulator to tailor it to their particular needs. These model parts are FORTRAN subroutines or functions. For programming details refer to the available source code files.

User-adjustable Model parts are:

a_ceff	:	current efficiency calculation
a_cond	:	equivalent thermal conductivity calculation
a_curr	:	line current generation
a_dens	:	mass density calculation
a_eut	:	eutectic temperature calculation
a_htc	:	heat transfer coefficient calculation
a_rgas	:	additional gas layer resistance calculation
a_sig	:	bath conductivity calculation
a_spec	:	specific heat value calculation
a_uanod	:	equilibrium potential and overvoltages calculation

Subroutine where passwords can be set is:

a_pass	:	password definition
--------	---	---------------------

Subroutines where data save options can be set are:

a_dsave	:	data save option
a_esave	:	event save option

3. USER-ADJUSTABLE CONTROL PARTS

Subroutines for adjusting the interface of the emulated control system are the following:

a_cell	:	Cell Controller definition
a_cent	:	Central Computer level definition
a_group	:	Group Controller level definition

Subroutines where the control frame and the selected control logic can be implemented are:

CONTROL1	:	for CTRSTART(), CTREND() and CTRMESS() definition
CONTROL2	:	for CONTROL(), RCONTROL() and FCONTROL() definition

The design of the frame program and the arrangement of the special tasks should be done by the user of the Simulator.

Data from the Model are sent as command line parameters to both CTRSTART() and CONTROL(). Inside, there is a control data base where parameters related to the control logic are stored. The CTRSTART() subroutine suggests a possible arrangement for this data base. For details, refer to the available source files.

At every computation step CONTROL() gets new values from the Model. It calls RCONTROL() and FCONTROL() control routines which realize the anode position and the alumina feeding control. These control routines are not treated here. For details, refer to the Set-Up Guide and the available source code files.

4. USER INTERFACE

When all the necessary data files are ready made the user can start the simulation. At first, the Simulator asks for a password and when the given password is accepted, the user can continue and fulfill the simulation session.

During the simulation session, the user communicates with the Simulator via the user interface. A typical screen arrangement is shown in Figure 4.1.

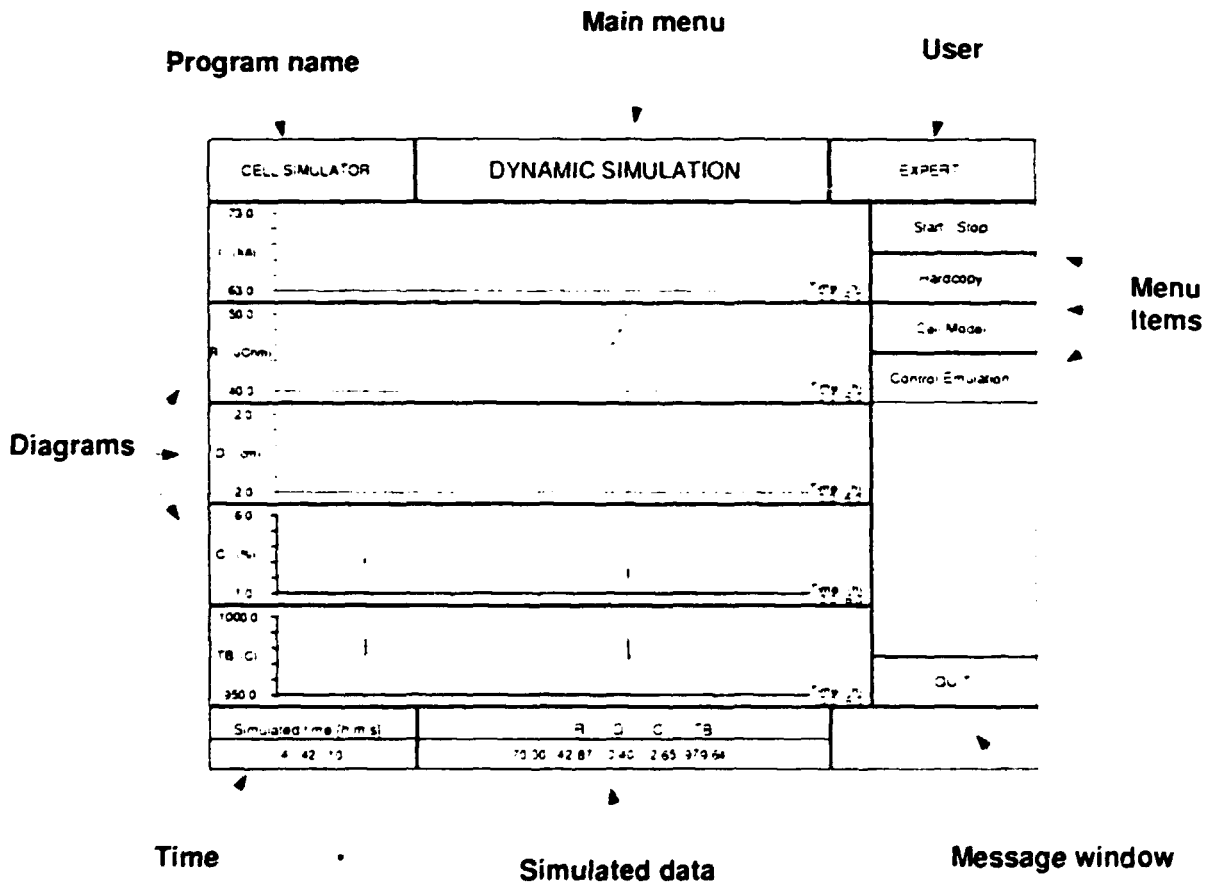


Figure 4.1 Typical Screen Arrangement

The interface is screen oriented, menu driven. For details and examples refer to the Dynamic Cell Model Tutorial.

**SIMULATION OF
AN ALUMINIUM ELECTROLYTIC CELL**

Computer Demonstration

L. TIKASZ

PREFACE

The computer demonstration is an important part of the Workshop: the Dynamic Cell Model (Simulator) will be introduced using several examples.

The computer demonstration is intended to be held under expert guidance. The course participants can ask questions, follow the demonstrated examples even realize their own simulation sessions.

This Chapter contains only two examples taken from the Dynamic Cell Model Tutorial. For further details refer to this Tutorial and follow the demonstration.

1. DYNAMIC SIMULATION EXAMPLES

Simulate the dynamic behaviour of a cell with target values given below.

Line current	:	70.0	(kA)
Cell voltage	:	4.95	(V)
Bath temperature	:	965.0	(°C)
Ratio	:	1.17	(weight ratio)
CaF ₂	:	5.8	(%)
Anode effect frequency	:	1.1 - 1.3	(day ⁻¹)
Anode current density	:	0.942	(A/cm ²)
ACD	:	5.0	(cm)
Current efficiency	:	90.4	(%)
Anode cover thickness	:	9.0	(cm)
Metal height	:	22.0	(cm)
Bath height	:	23.0	(cm)

The other parameters needed to describe the cell's state are collected in linput.dat file. For details refer to the Dynamic Cell Model Tutorial and study the sample linput.dat file.

1.1. Example 1. Batch Feeding Operation Mode

This Example shows a very simple dynamic simulation session. The steady-state calculation with linput.dat parameters has been completed before. The dynamic simulation is started from the steady-state.

Dynamic parameters for the simulated period were in ldynam.dat file. The content of the dynamic data file is given in Table 1.1.1

During the simulation period, some of the regular pot operations were skipped: no anode change and metal tapping were involved. Table 1.1.2 shows the scheduled events (crust breaking and alumina feeding actions).

For plot parameters, 2plots.dat file was selected with the content shown in Table 1.1.3.

The diagrams shown in Figures 1.1.1 contain a six hour long slice of the simulation. The line current is simulated, and the alterations in the Resistance, Anode Position, Alumina Concentration and Electrolyte Temperature diagrams are recognizable. Usually, a 24 hour long diagram is the best to see process tendencies. To cover the gap between these kinds of diagrams, an Overview item has been added to the Model Utilities. With its aid, working in a short time slice, the user can ask for a 0 to 24 h overview to evaluate the trends then he can return his time slice immediately.

Report lists from the dynamic simulation — generated at six hour — are given in Figures 1.1.2 to 1.1.4 where operational parameters, calculated masses and temperatures are shown.

We propose that you replay this dynamic simulation and become familiar with the facilities provided. You can modify the simulation changing the State Selector or introducing operational events. In the subsequent Examples, there are several suggestions which will help you develop your simulation skills.

Table 1.1.1 Dynamic Data

STRT		start and end time definition	
1	:	start day	
0	:	start hour	
0	:	start minute	
0	:	start second	
1	:	end day	
24	:	end hour	
0	:	end minute	
0	:	end second	
SAMP	:	sampling rate	
0	:	day	
0	:	minute	
10	:	second	
SOLL		alumina dissolution parameters	
0.2		fraction of added alumina which dissolves immediately	
0.6		fraction of undissolved alumina	
0.13		volume of crust broken by side-type breaking	(m ³)
7200.0		initial value of alumina dissolution time constant	(s)
925.0		reference temperature for alumina dissolution calculation	(°C)
100.0		initial amount of alumina	(kg)
0.0		initial volume of electrolyte	(m ³)
END		end of data file	

Table 1.1.2 Scheduled Events

BRK	1	01	00	00	10.0
Al2O3	1	01	30	00	100.0
BRK	1	04	00	00	15.0
Al2O3	1	04	30	00	150.0
BRK	1	07	00	00	15.0
Al2O3	1	07	30	00	150.0
BRK	1	10	00	00	15.0
Al2O3	1	10	30	00	100.0
BRK	1	13	00	00	10.0
Al2O3	1	13	30	00	150.0
BRK	1	16	00	00	15.0
Al2O3	1	16	30	00	100.0
BRK	1	19	00	00	15.0
Al2O3	1	19	30	00	150.0
BRK	1	22	00	00	15.0
Al2O3	1	22	30	00	150.0
END					

Table 1.1.3 Plot Data

5		number of X-Y axes	
	0.0	Time lower limit	(hour)
	6.0	time upper limit	(hour)
1		Y1 (line current)	
	55.0	l. limit	(kA)
	75.0	u. limit	(kA)
3		Y2 (resistance)	
	40.0	l. limit	(Ω)
	50.0	u. limit	(Ω)
4		Y3 (anode position)	
	-2.0	l. limit	(mm)
	2.0	u. limit	(mm)
16		Y4 (alumina concentration)	
	1.0	l. limit	(%)
	6.0	u. limit	(%)
10		Y5 (bath temperature)	
	950.0	l. limit	($^{\circ}$ C)
	1000.0	u. limit	($^{\circ}$ C)

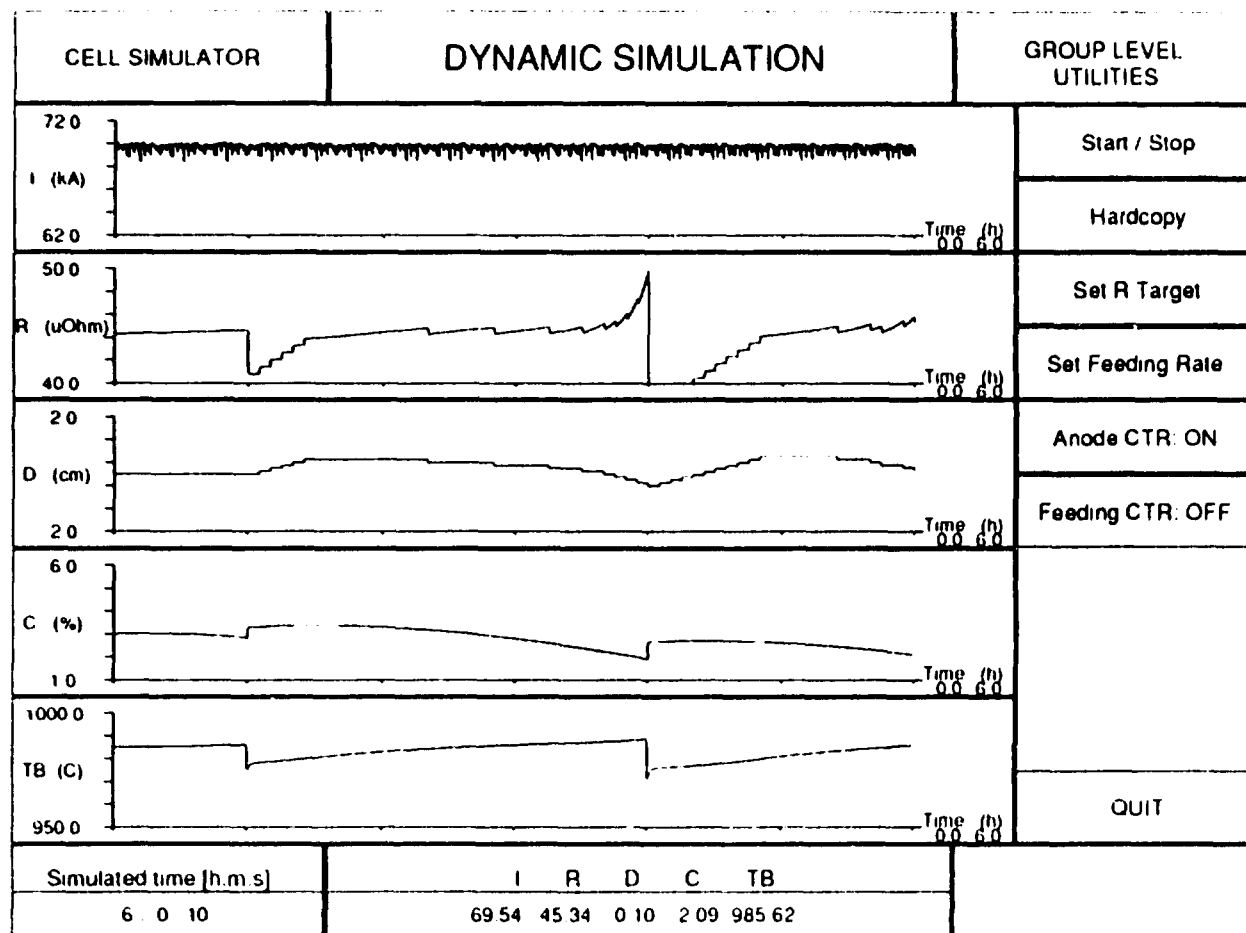


Figure 1.1.1

CELL SIMULATOR	DYNAMIC SIMULATION	EXPERT
<p>*** Report from the dynamic simulation ***</p> <p>OPERATIONAL PARAMETERS</p> <p>Cell voltage (V) 6.00</p> <p>Current (Amps) 4000</p> <p>Current efficiency (%) 90.60</p> <p>Current utilization (%) 7.7</p> <p>Volts x amp (W) 24.00</p> <p>Amperes x volt (VA) 16000</p> <p>Efficiency (%) 7.7</p> <p>Current (A) 4000</p> <p>Volts (V) 6.00</p>	<p>Turn Page ...</p> <p>Hardcopy</p>	<p>QUIT</p>

Figure 1.1.2

CELL SIMULATOR	DYNAMIC SIMULATION	EXPERT
<p>... Select from the dynamic simulation ...</p> <p>5. 2000.0 1000.0 500.0 250.0 125.0 62.5 31.25 15.625 7.8125 3.90625 1.953125 0.9765625</p>	<p>... Select from the dynamic simulation ...</p> <p>5000.0 (Kg) 2500.0 1250.0 625.0 312.5 156.25 78.125 39.0625 19.53125 9.765625 4.8828125</p>	<p>Turn Page ...</p> <p>Hardcopy</p> <p>QUIT</p>

Figure 1.1.3

CELL SIMULATOR	DYNAMIC SIMULATION	EXPERT
<pre> *** Report from the dynamic simulation *** CELL PARAMETERS ----- Anode surface area (cm²) 80.0 Anode surface temperature (K) 300.0 Anode surface area fraction (cm²) 0.175 Cathode surface area (cm²) 879.0 Cathode surface temperature (K) 980.0 Cathode surface area fraction 0.825 Electrolyte temperature (K) 600.0 Anode surface area (cm²) 80.0 Anode surface temperature (K) 300.0 Cathode surface area (cm²) 879.0 Cathode surface temperature (K) 980.0 Electrolyte temperature (K) 600.0 Anode surface area (cm²) 80.0 Anode surface temperature (K) 300.0 Cathode surface area (cm²) 879.0 Cathode surface temperature (K) 980.0 Electrolyte temperature (K) 600.0 </pre>	<pre> CELL PARAMETERS ----- Anode surface area (cm²) 80.0 Anode surface temperature (K) 300.0 Anode surface area fraction (cm²) 0.175 Cathode surface area (cm²) 879.0 Cathode surface temperature (K) 980.0 Cathode surface area fraction 0.825 Electrolyte temperature (K) 600.0 Anode surface area (cm²) 80.0 Anode surface temperature (K) 300.0 Cathode surface area (cm²) 879.0 Cathode surface temperature (K) 980.0 Electrolyte temperature (K) 600.0 </pre>	<p>Turn Page ...</p> <p>Hardcopy</p> <p>QUIT</p>

Figure 1.1.4

1.2. Example 2. Point Feeding Operation Mode

This Example demonstrates a cell's behavior under point feeding operation. The dynamic data and the plot data are the same as in Example 1. No scheduled events were defined for this simulation period.

The diagrams of the simulation are given in Figures 1.2.1.

Figures 1.2.2 to 1.2.4 are report pages taken at the end of the simulation.

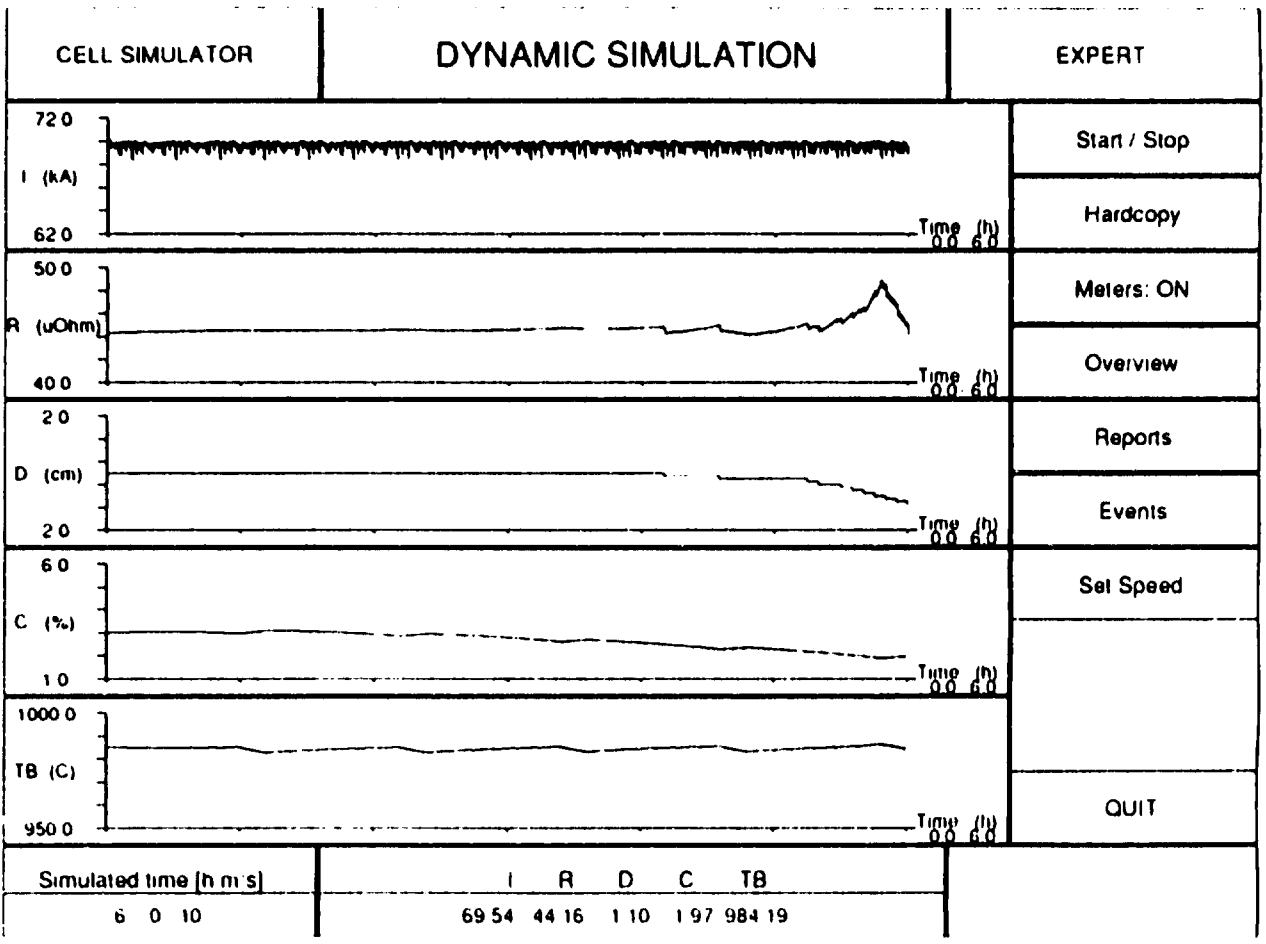


Figure 1.2.1

**SIMULATION OF
AN ALUMINIUM ELECTROLYTIC CELL**

Additional Readings

L. TIKASZ

PREFACE

Two articles recently published are annexed for additional readings.

The *Resistance Fluctuations in an Aluminium Electrolytic Cell* was prepared for the CIM 32nd Annual Conference of Metallurgists, Quebec City, Quebec, Canada, 1993.

This article can be considered as an example how to add new facilities to the Dynamic Simulator. The Simulator has been extended to simulate various instability types and to emulate control routines for eliminating them. Resistance fluctuations included arise from waves in the metal, gas bubbles and local short circuits. Different cells under different operating conditions can be simulated, and the main characteristics of a noisy state can be studied.

The *Discrete Event Simulation Approach for an Aluminium Electrolysis Potroom* was prepared for the VII. Aluminium Symposium, Banska Bystrica, Slovakia, 1993.

In this article, servicing of a small group of cells in a potroom is simulated by a simple discrete event model, which includes manual operator actions, regular alumina feeding, anode changing and metal tapping. The model demonstrates the feasibility and usefulness of discrete event simulation for testing, planning and optimizing the potroom operation.

RESISTANCE FLUCTUATIONS IN AN ALUMINIUM ELECTROLYSIS CELL SIMULATOR

L. Tikasz, V. Potocnik*, R. Ouellet and R.T. Bui

Université du Québec à Chicoutimi
Chicoutimi, Québec, Canada G7H 2B1

*Alcan International Ltd
Jonquière, Québec, Canada G7S 4K8

ABSTRACT

Resistance fluctuations in an aluminium electrolytic cell, often referred to as noise or instability, are closely related to its operational state. Analysis of these fluctuations yields information about the process. Modern cell control and supervision systems have built-in routines to analyze and treat these fluctuations.

A computer simulator for the cell, recently published, has been extended to simulate various instability types and to emulate control routines for eliminating them. Resistance fluctuations included arise from waves in the metal, gas bubbles and local short circuits. Different cells under different operating conditions can be simulated, and the main characteristics of a noisy state can be studied. The control emulator detects instabilities and provides automatic treatment.

In this paper, it is shown that the model can serve as a research tool for analysis of process fluctuations and for testing and developing control routines for instability treatment. An educational version can be used for demonstration and training.

INTRODUCTION

Aluminium electrolysis cells are designed on the basis of the thermal equilibrium between the heat generated in the cell, the heat absorbed by the reaction and the heat lost to the environment. The generated heat comes predominantly from the ohmic dissipation, which is determined by the cell resistance and the electric current. Thus in order to control the thermal state of the cell it is necessary to control the resistance. In normal operation the resistance is controlled to a fixed, pre-selected target within a control interval by raising or lowering the anode panel.

Deviations from the target larger than the control interval are allowed or even deliberately set in special circumstances, such as during resistance tracking, anode effect waiting, anode changing or instability treatment. In such circumstances, the resistance is regulated by different control actions.

The resistance variations are caused by a variety of phenomena such as

- anode consumption and metal production, the difference between the two resulting in a change in the anode-cathode distance.
- anode movement.
- bath resistivity changes due to bath temperature, chemical composition and alumina concentration changes.
- local changes of the interpolar distance (ACD) due to bath-metal interface movement.
- gas bubbling.

The cell control logic must recognize the source of the resistance variations in order to choose appropriate action to keep the resistance close to the target or to monitor its evolution when a fixed target is not followed, such as in tracking. The central element in this control is the average resistance and some measure of variance such as standard deviation over a given time interval, composed of a fair number of sampled values. In resistance tracking, the average rate of resistance increase or decrease is also often used.

Short term resistance variations, often within a time interval from a fraction of a second to several minutes, are either random or periodic. Random variations, due to the gas bubble release from the bath, are always present. Occasionally, large amplitude random oscillations are also present [1], [2]. These are thought to be due to local short circuits between the metal surface and one or more anodes. These are often superposed on periodic oscillations appearing at each trough of the resistance vs. time curve.

The periodic resistance variations are due to the presence of waves on the metal-bath interface [2], [3], [4]. The periodicity can vary from perfectly sinusoidal to quite complex. In the latter case it is obviously composed of a number of harmonics of different amplitudes. Sometimes it is even impossible to say, whether these are truly periodic or not, or what their frequencies are. Fourier analysis may help in this sense.

In the pursuit of obtaining a good average resistance and a good measure of deviation, the above mentioned short term resistance variation appears as an obstacle. The more variations there are, the more difficult it is to obtain a good average, unless one resorts to longer averaging interval and smoothing. This, however, increases the reaction time of the control system and is often unacceptable. A typical example is an approaching anode effect which causes very rapid resistance changes just before it occurs. The control system action must be very rapid if we want to avoid the anode effect, but this would be impossible if the resistance had been overly smoothed. Good control logic is therefore a compromise between these contradicting factors. Such logic is often developed on a trial-and-error basis and on operating cells.

The purpose of our development was to provide a model of cell resistance variations and to incorporate it into the cell simulation reported earlier [5], [6], [7]. The simulation would then be able to generate cell resistance having all kinds of regular or irregular variations. This would enhance its realism, be it for training or for control system development and testing.

THE MODEL

As described earlier, the evolution of the average resistance is the result of physico-chemical changes in the cell and of manual or automatic actions carried out on the cell. This resistance is calculated by the process model in the cell simulator.

The resistance fluctuation model is phenomenological. The variations are not the result of fundamental changes in metal waviness or gas release or some short circuit mechanism. They can only be represented by a mathematical construct, built on a set of user-adjustable parameters. In the present form of the model, these parameters are assigned default values or a range of values, on the basis of experimental data taken from operating cells. However, the user can freely change them in order to test his perception or test a given control logic or its computer implementation.

The total resistance of the cell is split into three parts:

$$res_{total}(t) = res_{sim}(t) + res_{bubbles}(t) + res_{waves}(t) \quad (1)$$

where

- res_{sim} = average resistance calculated by the process model of the simulator,
- $res_{bubbles}$ = base random resistance, caused by gas bubble action,
- res_{waves} = resistance due to the waves, in general of a periodic nature.

The bubble resistance, $res_{bubbles}$ is defined in terms of res_{sim} and minimum amplitude as a percentage of the average resistance res_{sim} . It is also a function of ACD . The randomness is created by a uniform random number generator:

$$res_{bubbles}(t) = f_b(ACD) * res_{sim}(t) * UNI_1 \quad (2)$$

where

- f_b = weighting factor for bubble generation,
- UNI_1 = uniform random number generator between -1 and +1

The resistance variation due to waves, res_{waves} , is much more complex. Its basic variation is expressed with sinusoidal functions, presently with one single, user-specified frequency:

$$res_{waves}(t) = f_w(ACD) * res_{sim}(t) * (1 - e^{-t/\tau}) \sin \omega t + f_w(ACD) * res_{sim}(t) * UNI_2 \quad (3)$$

where

- f_w = weighting factor for wave generation,
- α = amplification or damping factor for waves,
- τ = time of wave formation,

- ω = frequency of basic sinus function,
- f_s = weighting factor for short circuit generation,
- UNI_2 = uniform random number generator between -1 and +1

The first term in Equation (3) describes the regular oscillations and the second the random oscillations that appear at the trough of the resistance when the amplitudes get larger. The derivations and detailed explanations of weighting factors f_b , f_w and f_c are beyond the scope of this paper. Instead, a brief description of the real operational states and some possible approximations are given below.

Various phenomena, appearing either alone or superposed, have been observed in practice:

1. It has been observed in operating cells and in an MHD wave model [4], that, when a wave appears or disappears, the average resistance decreases or increases. This variation was approximated with exponential functions, with the rate of decrease or increase as a parameter. The default values of these parameters were derived from the signals measured in operating cells. They also depend on ACD.
2. The amplitude of the oscillations depends on ACD. The model defines this by ranges of ACD changes with respect to a given value, typically chosen as the operating value for a given cell. The relationship between the wave amplitude and a given ACD range is determined according to observed values or according to common sense. Of course, in the model the required variation is then followed whether the ACD is changed manually or automatically by the control system.
3. In some cases, particularly at low ACD's or when the cell is in bad condition, it has been observed in practice that, superposed on a regular oscillation, a random resistance decrease occurs, usually at the trough of the resistance. This is associated with local short circuits, when the wave crest approaches the anode. The randomness may be due to spurs of metal, released from the crest. This is modelled by superposition of a random component at the resistance trough (see last term in Equation (3)). The amplitude of this component is a function of the wave amplitude itself and of some user-specified parameters.
4. A special condition in the cell is short circuiting. In this case, the average resistance drops to very low values within a few oscillations, typically corresponding to a voltage of 2.5 to 3.5 V, if by control action the anodes are not raised rapidly. It was also noticed that the recovery from a short circuit is often not symmetric with respect to ACD. In order to get rid of the oscillations at the end of an experiment, the anode panel had to be raised 1-2 mm above its base level. This can also be simulated by the model by choosing different sets of ACD-dependent parameters for the recovery and destabilizing stages.

To conclude the model description, a simulation using a stand-alone noise model is shown in Figure 1. There was no automatic anode adjustment by a control system. The simulated resistance fluctuations are the result of four 1 mm down movements of the anode taken manually after 5, 10, 15 and 20 minutes. All types of fluctuations described are present:

- In the first part of the simulation (0-5 minutes), the basic noise was set to almost zero showing an "undisturbed" period as reference.
- Next, the second part (5-10 minutes) is "slightly noisy", some random noise of moderate amplitude are present.
- Then in the third part (10-15 minutes), a small "wavy" component is added to the increased random noise.

- Later, in the fourth period (15–20 minutes), a significant increase of fluctuations can be detected. Even a "short circuit" type resistance drop is present.
- Finally, in part five (20 minutes until the end), a heavy short circuit state is simulated with all the noise types present.

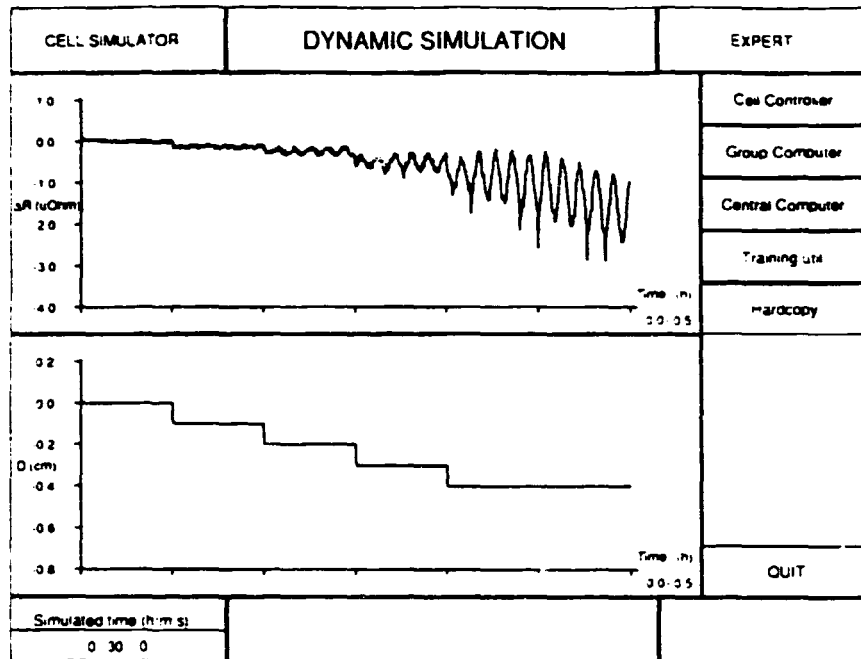


Figure 1 - Simulation of resistance fluctuations.

The recovery part is not shown here. At this stage, it should form a symmetric shape, according to the anode upward adjustments. A more realistic recovery and further dynamic characteristics of the simulated fluctuations are discussed below.

COMPARISON OF REAL AND SIMULATED FLUCTUATIONS

When the noise model was integrated into the dynamic simulator, some real plant data were selected for cells in which noisy states were present spontaneously or were induced by experiments. The plant data shown in Figures 2 to 4, top two diagrams, are the line current (I) and the real cell voltage (U_r). To help the comparison, the generated resistance fluctuations have been converted to voltages. The simulated cell voltage (U_s) as well as the real anode position (D) are shown in the third and fourth diagrams of the same figures, respectively. Note that the real anode adjustments on operating cells were used as inputs to the simulator.

Figure 2 shows the results, generally from a single set of model parameters. As seen in Figure 2, the simulated cell voltage is quite far from the measured one. The main problem is that the real recovery is usually not symmetrical, it does not follow the anode adjustments strictly. In this particular case, the experimental recovery from the noisy state occurs only after the anodes were raised 2mm above the starting position.

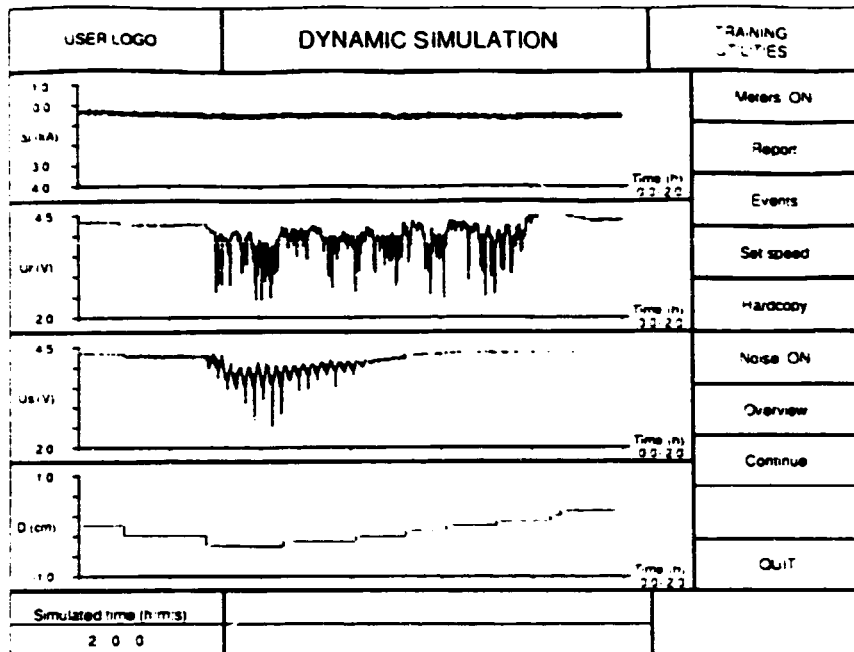


Figure 2 - Simulated fluctuations with symmetrical recovery.

A possible approximation to the real recovery can be described as a modification of res_{waves} :

$$res_{waves}(t) = s_r(ACD_r) * res_{waves}(t) \quad (4)$$

and

$$s_r(ACD_r) = f_r(ACD_r) * res_{sim}(t) \quad (5)$$

where

- s_r = shape factor for recovery phase.
- f_r = weighting factor for recovery phase.
- ACD_r = adjusted ACD for recovery.

By introducing such a shape factor, a better simulation can be achieved. Figure 3 shows the results. Note that the noisy state is eliminated also in the model by raising the anode panel 2 mm above the initial position.

Another example is shown in Figure 4, where a noisy state with gradual recovery was studied. Adjusting the above introduced s_r factor, good results can be obtained, especially at the starting and finishing periods. Further refinements can be made by the user according to the current requirements.

The comparison of the measured and simulated resistance traces shown in Figures 3 and 4 indicates a reasonable fit, except for much more regularity in the simulated signal; this is understandable, considering that the base frequency in the model is constant. This could be improved by combining several functions of different frequency.

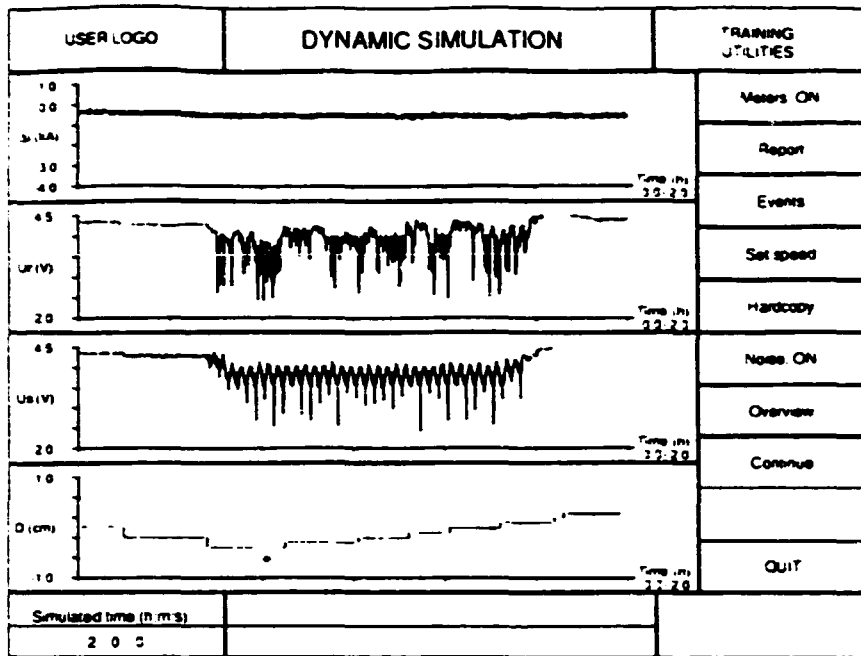


Figure 3 - Simulated fluctuations with retarded recovery.

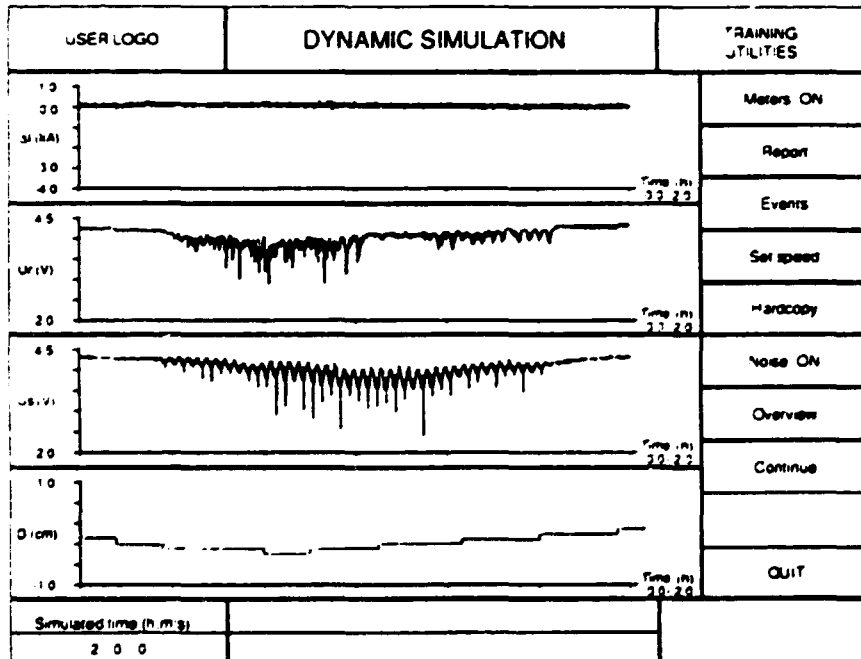


Figure 4 - Simulation with gradual recovery.

EXAMPLES

In Figures 5 and 6 another example is shown in which several successive down movements of the anode produced more moderate instability than the one shown in previous figures. Here the heavy short circuits are not present, but the random noise still is. Of course, the amplitude of this noise can be freely adjusted.

The unstable state was induced by the following steps (Figure 5):

1. The simulation starts from the operational anode position (0 level).
2. The anode panel is moved down by 2 mm; the cell is still stable, only the noise component due to gas bubbles is stronger.
3. Another 2mm down movement pushes the cell to the stability limit.
4. The third 2 mm down movement causes a well developed wavy state.

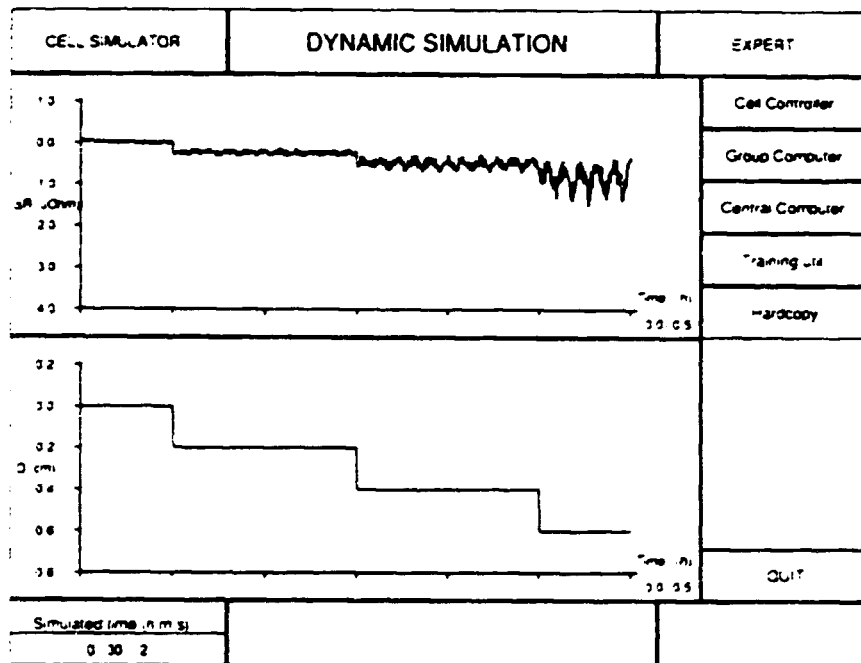


Figure 5 - Inducing an unstable state.

The recovery from an unstable state is shown in Figure 6:

1. The cell is in an unstable state. Strong waves and random noise are present.
2. The recovery process is started with a significant (4 mm) anode panel raising. A decrease of the wave amplitude as well as a significant bubble noise reduction can be clearly seen.
3. The second anode raising (3 mm) fully restabilizes the cell; only small random noise is present.

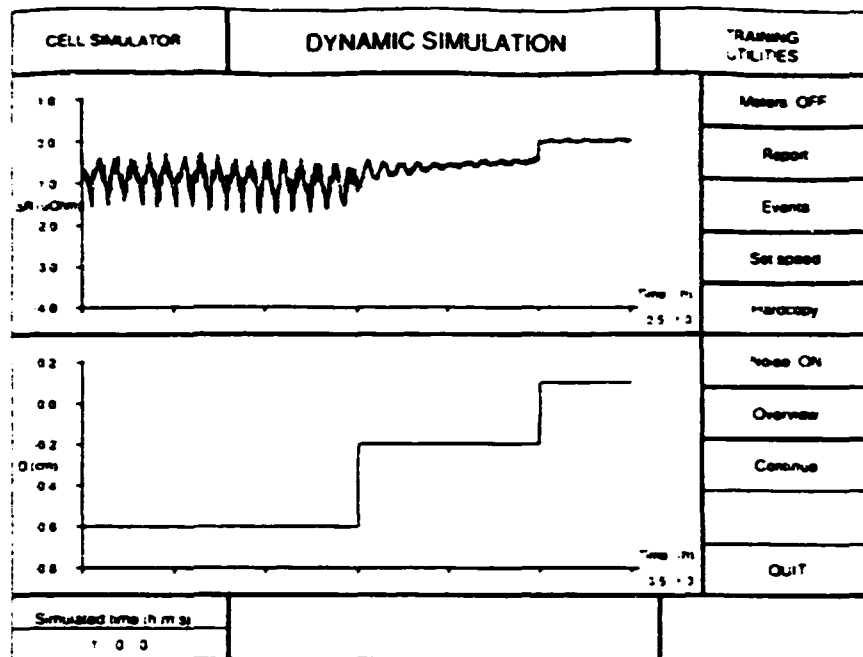


Figure 6 - Recovery from an unstable state.

CONCLUSION

The purpose of the model was not to simulate the short circuits precisely. It was to provide the simulator with a reasonable variety of resistance variations for the purpose defined at the outset. A user's freedom to vary the parameters was an important element in this development. All this, we believe, has been achieved.

ACKNOWLEDGMENT

This study is part of a joint project funded by Alcan International Limited of Jonquière, Québec, and Natural Sciences and Engineering Research Council of Canada. The interest and support of engineers from Alcan Smelter and Chemicals, Jonquière, are gratefully acknowledged. The authors thank Alcan International Limited for the authorization to publish this paper.

REFERENCES

1. J.P.R. Hurni, "A-275 - Individual Anode Control". Light Metals. The Metallurgical Society of AIME. Warrandale, PA, USA, 1987. 199-202.
2. S. Matsui, A. Era, "Measurement of Metal Turbulence in Aluminium Reduction Cell". Light Metals. The Metallurgical Society of AIME, Warrandale, PA, USA, 1982. 373-389.
3. F. Laroche, R.T. Bui, R. Boivin, V. Potocnik, "Experimental Study of the Bath-Metal Interface Waves in an Electrolytic Cell". International Symposium on Reduction and Casting of Aluminium CIM, 1988, Vol. 8. 169-187.
4. V. Potocnik, "Modelling of Metal-Bath Interface Waves in Hall-Heroult Cells Using ESTER/PHOENICS". Light Metals. The Metallurgical Society of AIME, Warrandale, PA, 1989, 227-235.
5. L. Tikasz, R.T. Bui, V. Potocnik, M. Barber, "Simulation of Different Alumina Feeding Strategies on a Training Workstation". International Symposium on Reduction and Casting of Aluminium CIM, 1991, Vol. 24. 329-338.
6. L. Tikasz, R.T. Bui, V. Potocnik, "A Process Simulator of Aluminium Electrolytic Cells for Expert System-Based Supervision". IFAC Conference on Identification and System Parameter Estimation, Budapest, Hungary, 1991, 298-303.
7. L. Tikasz, R.T. Bui, V. Potocnik, "Aluminium Electrolytic Cells: A Computer Simulator for Training and Supervision". Engineering with Computers, in press.

DISCRETE EVENT SIMULATION APPROACH FOR AN ALUMINIUM ELECTROLYSIS POTROOM

L. Tikasz, R.T Bui
Université du Québec à Chicoutimi,
Chicoutimi, Québec, G7H 2B1, Canada

V. Potocnik
Alcan International Ltd,
Jonquière, Québec, G7S 4K8, Canada

ABSTRACT

The operation of aluminium electrolytic cells is essentially based on mass and energy balances, which are sensitive to perturbations in raw materials and cell control. This stresses the importance of correct cell operation and, as a consequence, the importance of the availability of service equipment and operating personnel when needed.

In this article, servicing of a small group of cells in a potroom is simulated by a simple discrete event model, which includes manual operator actions, regular alumina feeding, anode changing and metal tapping. The model demonstrates the feasibility and usefulness of discrete event simulation for testing, planning and optimizing the potroom operation.

The model is based on SIMAN/CINEMA simulation language from Systems Modeling Corporation.

INTRODUCTION

Aluminium electrolysis is a continuous process at high temperature, in the presence of aggressive melts and gases. The driving force for the reactions is the electric current passing through the cells, which are electrically connected in series and located in potrooms.

Scheduled and unscheduled interactions with the process — either automatic or manual — are essential to keep the process close to the steady-state targets. The cells are regularly fed with alumina, and the produced metal is tapped out. The consumed anode carbon, aluminium fluoride and other additives have to be supplied on a regular basis. The cell operation practice is different in each smelter, depending on cell type and potroom arrangement as well as available service and control equipment.

Considering the costs and risks involved, the very hostile environment in which the cells operate, plant tests and learning by trial-and-error are not always recommended or even possible. An alternative is to develop computer-based simulators, built on the basis of mathematical models of the cell and of the cell operation.

PROCESS MODELS

Simulation may be considered as an experimental and applied methodology. A selected model describes the characteristic behavior of the system. Model parameters tune the model to a special state and calculations can be done to predict system behavior. Experiments can be performed with different sets of parameters in order to explore the reaction of the system to parameter variations and in order to find an optimum set.

Models can be classified in various ways, such as deterministic, stochastic, static, dynamic, continuous, discrete, distributed-parameter and lumped-parameter. In the context of aluminium electrolysis, the models serve different purposes:

— Detailed, distributed-parameter models simulate thermal, electrical and magnetic fields and hydrodynamics of the cells [1], [2]. These models are used mainly for cell design and optimization.

— Lumped-parameter models simulate mass and energy balance of cells as functions of previous operational states and current interactions. Such models are used to investigate static and dynamic behavior [3], [4]. They can also be

used for developing and testing process control and supervision algorithms and for personnel training.

— Discrete event models deal with utilization of personnel and objects to carry out certain activities. They are based on probability and queueing theory. In the context of this article, they are used for studying the activities of service equipment and cell operators in an aluminium electrolysis potroom.

In this article, a simple discrete event model of a potroom section is described. An integrated simulation tool named SIMAN/CINEMA was used. The model described here is limited to three cells, because the educational version of the software was used, which is limited to 100 modelling blocks only. Despite this, the principles and the feasibility of such an approach have been demonstrated. The extension to a full potroom is relatively easy if the full version of the software is available.

SIMULATION WITH SIMAN/CINEMA

In the SIMAN environment, there is a distinction between Model and Experiment [5]. A Model is a functional description of the system's components and their interaction. An Experiment defines the Model parameters. Animation of the system's activities is done by CINEMA. The animation helps the interpretation of the simulated results. An integrated Siman Environment (SE) is provided for fast Model and Experiment development and output processing. Although SIMAN targets models with discrete-change state variables, it can equally well represent continuous processes and can handle a combination of discrete and continuous processes.

SIMAN Model Frame

The SIMAN language uses entities, attributes and processes as generic terms. Entities (objects, persons) move in the system between stations and they cause changes in the state of the system. Characteristics of entities are referred to as attributes. A sequence of operations or activities through which the entities move is called process. The Model Frame integrates entities and processes forming a model of the real system. Individual statements in the process description are called blocks. The whole process can be modelled by block diagrams. Basic block types with their symbols, operands and adjustable parameters are pre-defined. Typical blocks are shown in Figure 1 and these are explained below.

CREATE blocks generate physical or logical (control) entities which progress through the model. QUEUES are places where the entities can stay and even accumulate according to current situation. WAIT blocks stop the entity flow until some defined conditions are fulfilled. DELAY blocks hold entities until the defined delay times elapse. ALLOCATE blocks are used to change the logical state of machines and operators. MOVE blocks define the position change of machines and operators. BRANCHes are general purpose control blocks for inserting conditional jumps into the entity flow.

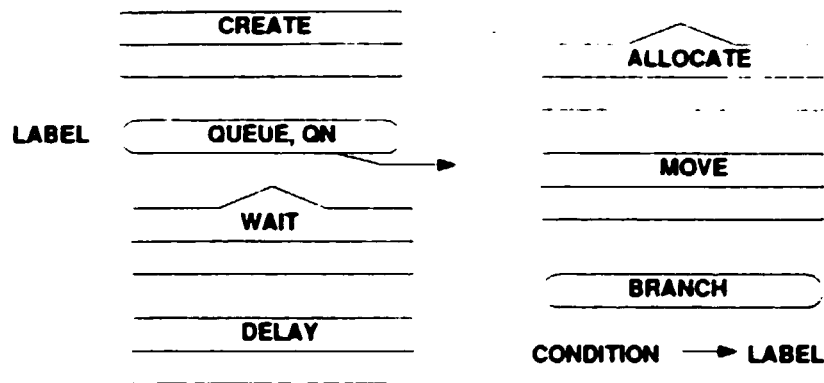


Figure 1. Basic Block Types

SIMAN Experiment Frame

The experimental conditions for the model are defined in this Frame. Statements are called elements. Generic format of an Experiment file is shown in Table 1.

The PROJECT item contains a project title and any comments about the simulation inside its element list. The items following define — according to their names — attributes and variables with initial values, stations, applicable layouts, queue names and queue capacities, available resources, storage places, applicable transporters, distances between stations as well as counters to collect statistical information.

Table 1. Generic Format of an Experiment File

	BEGIN	
1.	PROJECT	(element list)
2.	ATTRIBUTES	(element list)
3.	VARIABLES	(element list)
4.	STATIONS	(element list)
5.	LAYOUTS	(element list)
6.	QUEUES	(element list)
7.	RESOURCES	(element list)
8.	STORAGE	(element list)
9.	TRANSPORTERS	(element list)
10.	DISTANCES	
11.	COUNTERS	
	END	

CINEMA Animation

Animation building is a two-step process. The first step consists in building a model to represent the system. This is followed by the construction of an animation layout, a graphical representation of the model.

A layout contains static and dynamic objects, representing the fixed and changing parts of the model, respectively. Static objects are background elements, routes, walls, aisles, etc. Dynamic objects might change their position, shape, color and are used for representing work tasks, mobile equipment, transport elements and workers. In CINEMA, a graphic editor is provided. Assignment of model components and graphic symbols must be done inside CINEMA.

SIMAN Environment (SE)

SE integrates all SIMAN/CINEMA tools into a window-based, menu-driven environment. Block-oriented Model and Experiment editors and interactive debugger are provided. From Model and Experiment source files, Model and Experiment object files can be compiled. Linking these files with other SIMAN library routines, a ready-to-run Program file can be generated. If Animation is to be done, the necessary tools are integrated to the Program file and the CINEMA interface is activated.

SETTING UP A POTROOM SIMULATION

The aluminium production within a cell is essentially a continuous process, supported and controlled by events from the environment on a discrete time basis. This means that a combination of continuous and discrete approaches is needed for an acceptable representation. In this article, we focus on the discrete aspects of the process. Continuous aspects of the process are modelled by a simple submodel built with SIMAN mathematical functions.

As metal is produced in every cell, individual cell models are assigned to the simulated cells accordingly. The models have common structure but are individually tuned to specific operational states.

Control and regular maintenance of these individual cells need a potroom-wide cooperation of operators and machines. A full potroom model would incorporate all operating cells, machines, operators as well as a description of the operator activities and of scheduled use of dedicated machines. In the present model of three cells only, the same elements are present, but the model is much smaller than for a full potroom. The generic tools provided by SIMAN/CINEMA can be relatively easily adapted to potroom simulation.

The core of a meaningful simulation is the experimental data. Geometrical data, basic potroom arrangement and typical machine parameters are easy to get. The problems arise with service times, waiting times, routes, personnel availability and event coincidence. Reliable statistical descriptions of these need good historical records and some theoretical considerations. For example, a realistic identification of anode effect duration, anode effect handling, metal tapping and anode changing, etc. determines the quality of the model and of the simulation. For model verification and validation several simulations need to be done with regular and exceptional input conditions. The validation must be based on plant data.

In the simulation, presented here, the data were fictitious and no plant validation was done. The purpose of the work is to demonstrate the principles and the methodology involved.

Model components

SIMAN was intended to simulate fabrication, assembly and client-server type processes. In such cases, location of the machinery is usually fixed and

entities are passed from station to station, from machine to machine, from one worker to another. In the aluminium production, the machines as well as the potroom operators move among fixed cells. The model components are selected accordingly.

One part of the model is shown in Figure 2 in order to illustrate the SIMAN modeling approach.

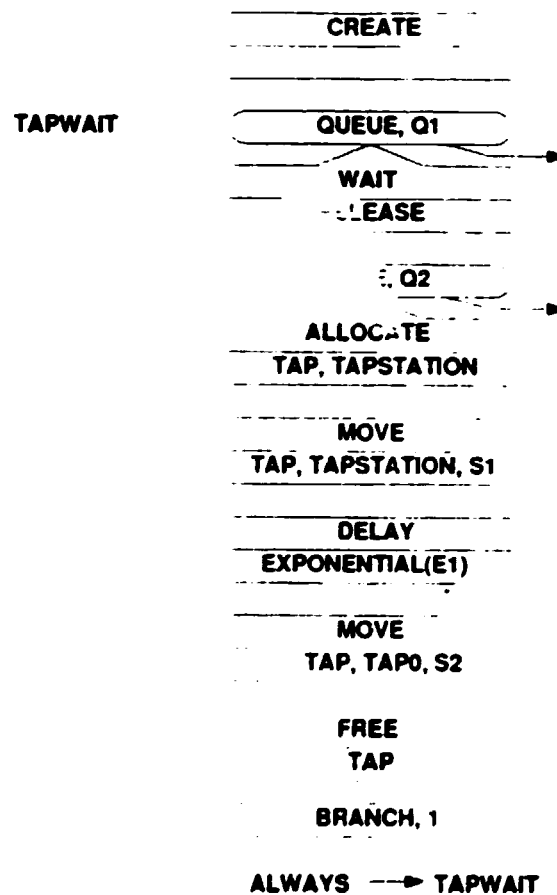


Figure 2. SIMAN Model of a Tapping Cycle

This part describes the metal tapping of a cell. The anode effect quenching by crust breaking and anode changing submodels are very similar and will not be presented here. Altogether, close to 100 blocks were used for describing these three processes for the three cells.

The tapping cycle is approximated in the following way.

1. A logical (control) entity is created (CREATE) and put to a queue (QUEUE Q1) waiting for a release signal (RELEASE). The queue has a label (TAP-WAIT).
2. Signal (RELEASE) triggers a tapping action while the logical entity passes through a temporary queue (QUEUE Q2).
3. A tapping action is started with the logical allocation of the tapping machine (TAP) to a current cell (TAPSTATION).
4. The machine (TAP) is moved (MOVE) to the cell (TAPSTATION) with the speed of S1, via previously specified length of the route. Route specifications are done in the Experiment frame.
5. The metal tapping duration is approximated by a delay block (DELAY), containing the exponential distribution with a mean value of E1. This distribution is quite commonly used for representing service times.
6. When tapping is completed, the machine is guided (MOVE) to the unloading station (TAP0) with a speed of S2. Now, the machine (TAP) is declared to be free (FREE).
7. Finally, the control entity is sent back to label (TAPWAIT), that is, to the main waiting queue (QUEUE 13). The model-part is waiting for a new release signal again.

Experiment components

In general, these parameters define the cell operation conditions, but in our case they provide possibilities to adapt a model to different potroom situations that we wish to simulate. Modifying the parameters of STATIONS, STORAGES and QUEUES, new temporary stations, storages and queues can be defined and new situations can be tested keeping the original cell arrangement and machinery. Modifying the parameters of STATIONS and DISTANCES, new service routes can be generated. With new TRANSPORTERS, some machines can be introduced or replaced (e.g. truck and fork lift service can be replaced by multipurpose overhead crane).

Animation components

It seems reasonable to model a small part of a potroom first. This helps understanding the concept. A simple outlay of a potroom section is shown in Figure 3.

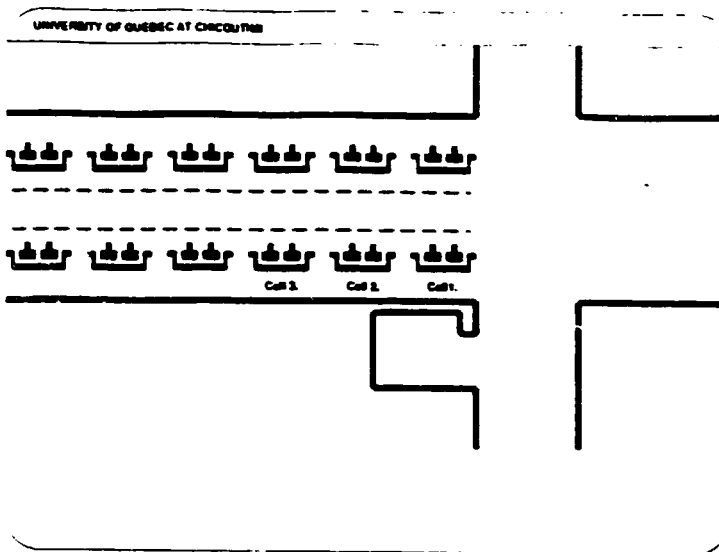


Figure 3. Outlay of a Potroom Section

Into this outlay, we have to draw pictograms for the personnel and the machinery representing busy and idle states. There is a possibility to define different pictograms for different busy states (e.g. moving trucks with full or empty containers). A simple set is given in Figure 4.

	Busy 1.	Busy 2.	Idle
Wheel-type crust breaker			
Tapping Truck			
Anode Carrier			
Operator			

Figure 4. Machines and Operators

Finally, there are different possibilities to display calculated variables during the simulation. Typical examples for simulated time, alumina concentration level, status vs. time graphs and numerical value display are shown in Figure 5. On the screen, these displays change dynamically. The machine and the operator movements as well as alarm signals when they occur are also animated.

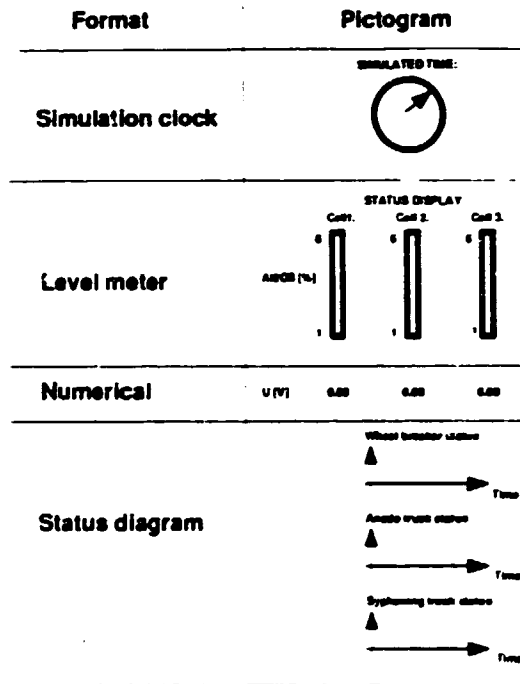


Figure 5. Examples of Variables Displays

A CASE STUDY

In the remainder of the article, details of a simulation session are described. The whole simulation time was 12 hours. Figure 6 shows a snapshot taken at about 11 hours.

The simulation is done for a section of a prebake potline with end-to-end cell arrangement and floor-rolling service equipment. The initial feeding (crust breaking) is done by a wheel crust breaker. New anodes are transported by a truck. Metal is tapped into a crucible, transported by another truck. Each

vehicle is operated by a person not shown. In idle mode, these vehicles stay at the end of the potroom.

The two operators stay in a dedicated waiting area when they are idle. They go to a certain cell when an adequate signal is sent to the waiting room. When they finish a task, they return to the operator room. This is done so, because of the 100-block limitation in the model. Normally, they would check if there is another cell in need of service nearby before they would return.

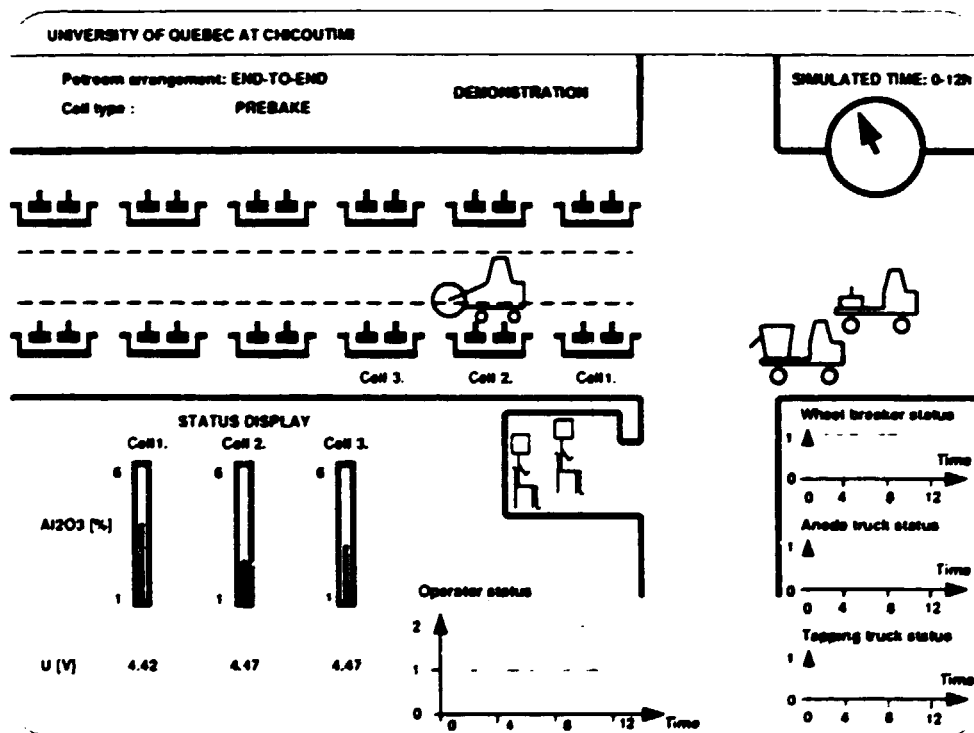


Figure 6. Snapshot of a Simulation

The anode effects occur when the alumina concentration is below a specified limit, here 1.8 %. The alumina concentration as well as the voltage are generated by a simple model using SIMAN mathematical functions. In a more serious simulation, SIMAN continuous blocks would be used for such rate dependent processes.

Status display for the three simulated cells is shown on the screen. Level meters display alumina concentrations, cell voltages are displayed in a digital form.

Other diagrams show busy and idle periods of the operators and of the three service machines considered. The status shows how many entities are busy at a given time.

Further information about the simulation session is available in the SIMAN Summary Report. Detailed statistics for every variable and event (presence of anode effects, anode effect start and stop times, services done by the operators, percentage of busy time for machines and operators, etc.) are listed if requested. Some signals are not displayed on the screen continuously (e.g. a flashing light appears on a cell when it is on anode effect).

The selected snapshot shows a quiet situation: operators rest in the waiting room, anode carrier and tapping trucks are idle, only the regular crust breaking is in progress. The crust breaker is at Cell 2 now.

The status display indicates a low alumina concentration for Cell 2. This means that Cell 2 is approaching an anode effect. But, considering that the breaker is just working Cell 2, this effect will very likely be avoided. This will depend on the crust breaking action done at Cell 2 (size of crust broken, amount of alumina fed into the cell, dissolution rate of the alumina, etc.) Note, that the higher (and increasing) alumina concentration of Cell 1 reflects the crust breaking done a few minutes earlier.

The status diagrams for the machines show a well-balanced operation. The crust breaker works almost continuously: after returning to the end of the potroom, it starts a new cycle shortly thereafter. The anode truck did a short service at about 3 hours, otherwise it was idle. The tapping truck was active at 1:30, 5:30 and 6:30 hours. During this simulation, there was only one occasion when both operators were busy.

With a full version of SIMAN, this simulation could be easily extended to a longer time and to the whole potroom. In this case, more realistic parameters on resources and operational events would need to be provided. With such a model, the whole representation could be studied and optimized. Simulations like this would help the potroom management to localize potential bottlenecks or overabundance of resources (equipment and personnel).

CONCLUSION

A discrete event simulator of a section of the aluminium electrolysis potroom has been built. It has been shown that the simulator can be used efficiently for testing and optimization of the potroom operation in terms of cell events and resources (machines, operators) to be assigned. The authors believe that the use of such simulators can help optimize potroom operation in terms of potroom machinery and personnel.

ACKNOWLEDGMENT

The authors acknowledge the financial support of the National Science and Engineering Research Council of Canada under an Industry Oriented Research (IOR) grant, together with a counterpart funding from Alcan International Limited, Jonquière, Québec, Canada.

REFERENCES

1. V. Potocnik, "Modelling of Metal-Bath Interface Waves in Hall-Heroult Cells Using ESTER/PHOENICS", Light Metals, The Metallurgical Society of AIME, Warrendale, PA, 1989, pp. 227-235.
2. M. Dupuis, I. Tabsh, "Thermo-Electric Analysis of Aluminium Reduction Cells", Advances in Production and Fabrication of Light Metals and Metal Matrix Composites, Proceedings of International Symposium of The Metallurgical Society of CIM, 1992, pp. 55-62.
3. A. Ek, G.E. Fladmark, "Simulation of Thermal, Electric and Chemical Behaviour of an Aluminium Cell on a Digital Computer", Light Metals, The Metallurgical Society of AIME, Warrandale, PA, 1973, pp. 85-104.
4. L. Tikasz, R.T. Bui, V. Potocnik, "A Process Simulator of Aluminium Cells for Expert System-Based Supervision", Preprints of the IFAC Conference on Identification and System Parameter Estimation, Budapest, Hungary, 1991, pp. 298-303.
5. C. D. Pedgen, R. E. Shannon, R.P. Sadowski, "Introduction to Simulation Using SIMAN", McGraw-Hill, Inc. 1990.

UNDER THE AUSPICES OF
THE UNITED NATIONS INDUSTRIAL DEVELOPMENT ORGANIZATION

**WORKSHOP ON COMPUTER-BASED
MATHEMATICAL MODELLING
OF
ALUMINIUM PRODUCTION PROCESSES**

Jawaharlal Nehru Aluminium Research
Development and Design Centre
Nagpur, India
September 1993

MODELLING OF ANODE BAKING FURNACES

Course Material

Selvin Peter

University of Quebec at Chicoutimi
Quebec, Canada

1. INTRODUCTION

1.1 - DESIGN AND OPERATION

1.2 - MOTIVATION FOR MODELLING

1.1 Design and Operation

Fire train

Gas flow direction

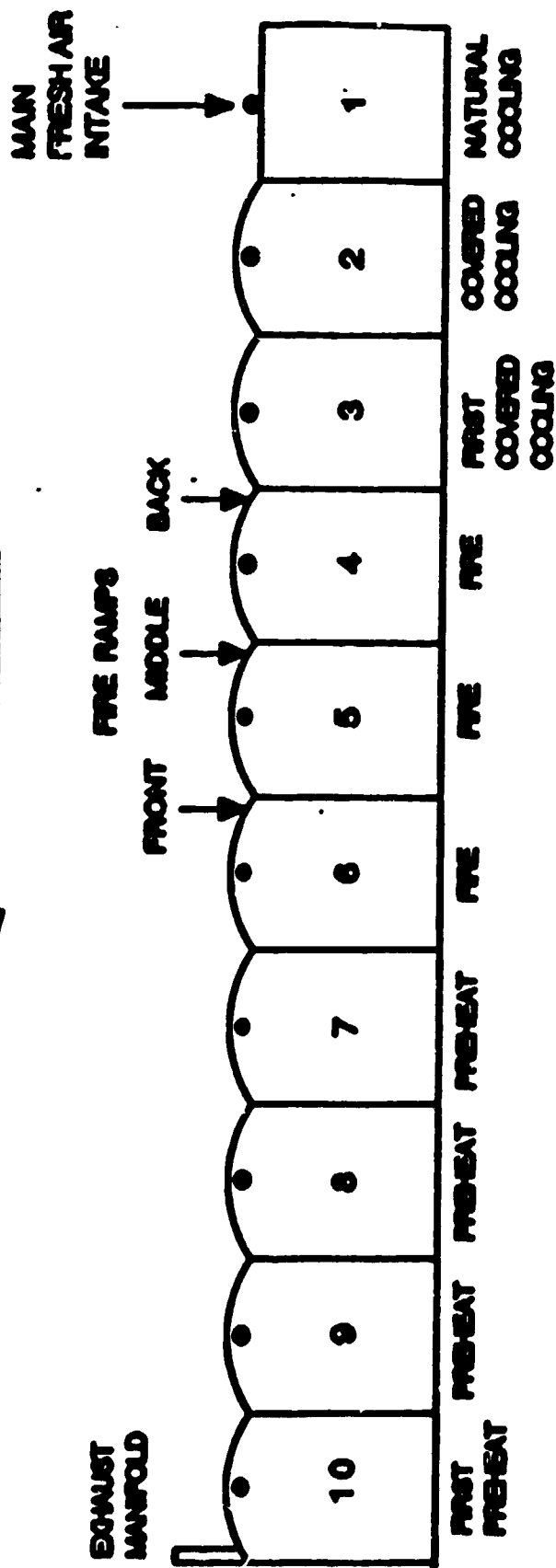
Various sections

Preheating

Firing

Cooling

GAS FLOW DIRECTION
←



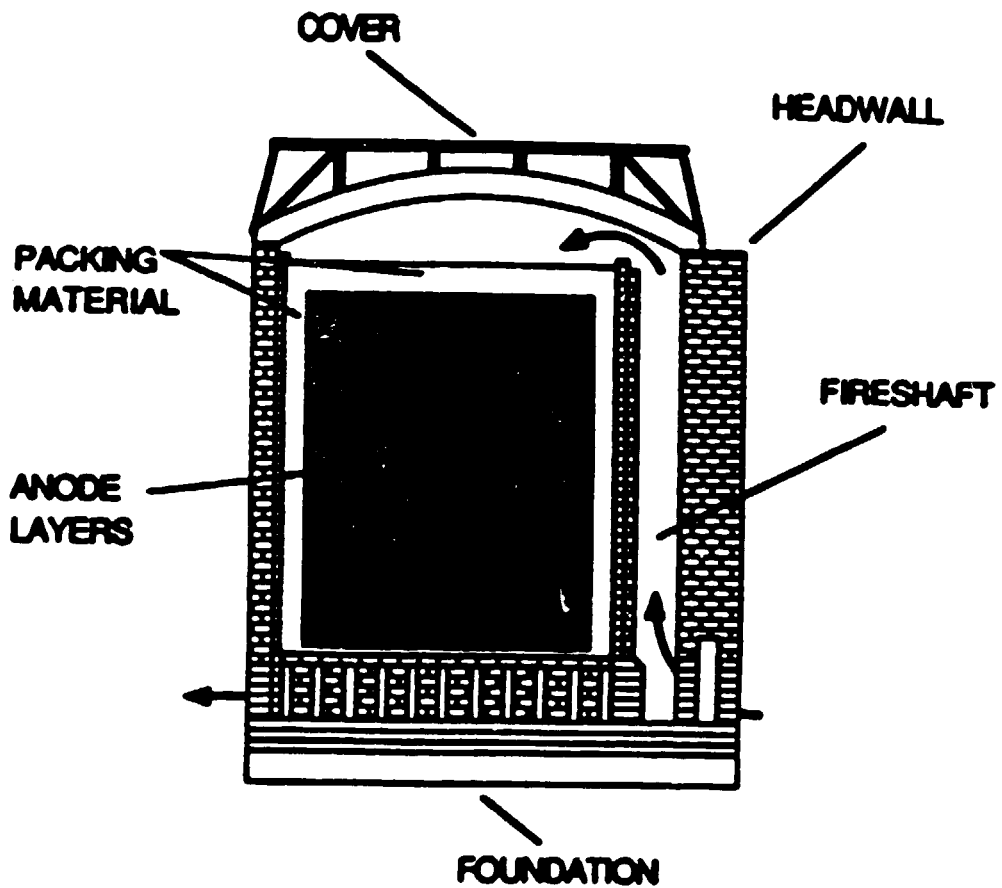
Four zones

Underlid

Pit

Underpit

Headwall and fireshaft



Side view of a vertical ring furnace section.
Arrows indicate gas flow path.

Physical Phenomena

Air infiltration

Volatile release

Volatile combustion

Packing coke combustion

Fuel combustion

Heat losses

**OPERATIONAL CHARACTERISTICS OF
RIEDHAMMER FURNACE**

Fire cycle	36 hours
Liquid fuel consumption	599 kcal/(kg b.a.)
Packing coke consumption (16.5% ash content on average)	40 kg/t.b.a.
Baking loss	≈ 6.3 %
% tar recovered	≈ 10 %
Average anode finishing temperature (\bar{L}_C)	1255 deg. equiv.
Target gas temperatures	≈ 820 to 1250° C
Ramp (12 hours)	1250° C
Soaking (84 hours)	

1.2 Motivation for Modelling

Operational Modification

Fire ramp

Air infiltration

Packing coke

Fire cycle time

Anodes

Design Modifications

Number of pits

Number of sections

Cover design

Blocking fireshaft

Blocking brick holes

2. DEVELOPMENT OF THE 2D+ MODEL

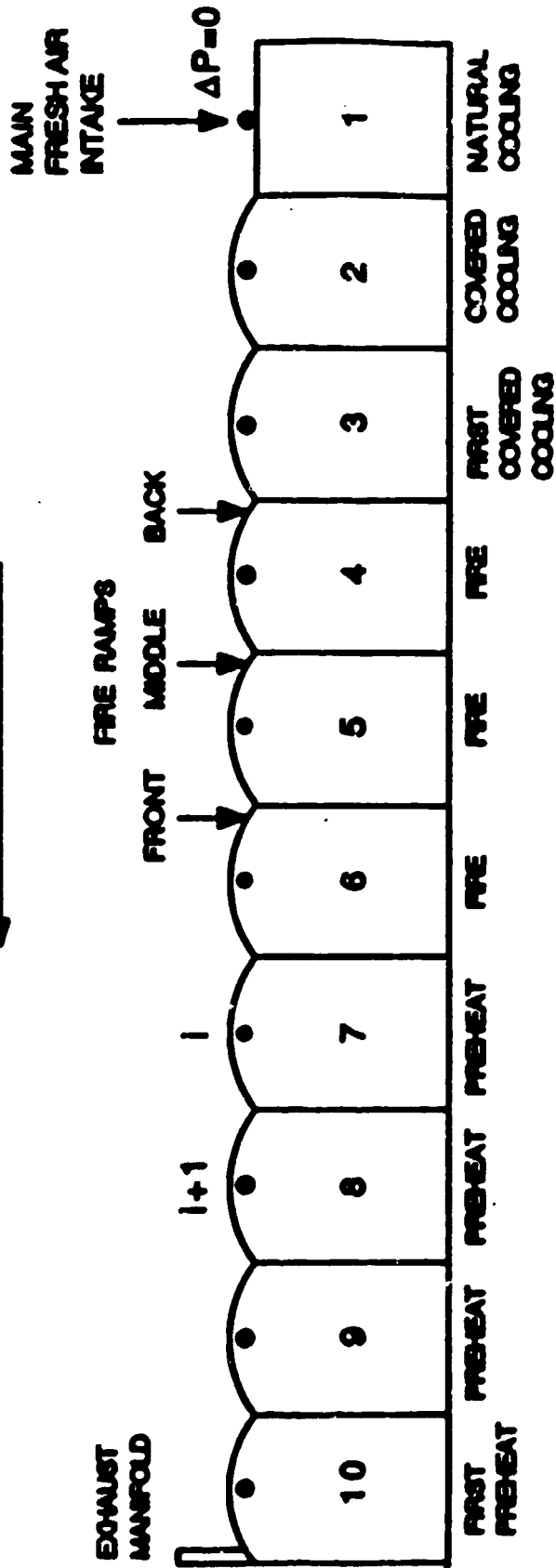
S. Peter, A. Charette, R.T. Bui, A. Tomsett[†], V. Potocnik^{††}

Université du Québec à Chicoutimi
Chicoutimi, Québec
Canada, G7H 2B1

† Comalco Research Center
15, Edgars Road, Thomastown
Melbourne, Victoria 3074
Australia

†† Alcan International Ltd
Jonquière, Québec
Canada, G7S 4K8

GAS FLOW DIRECTION

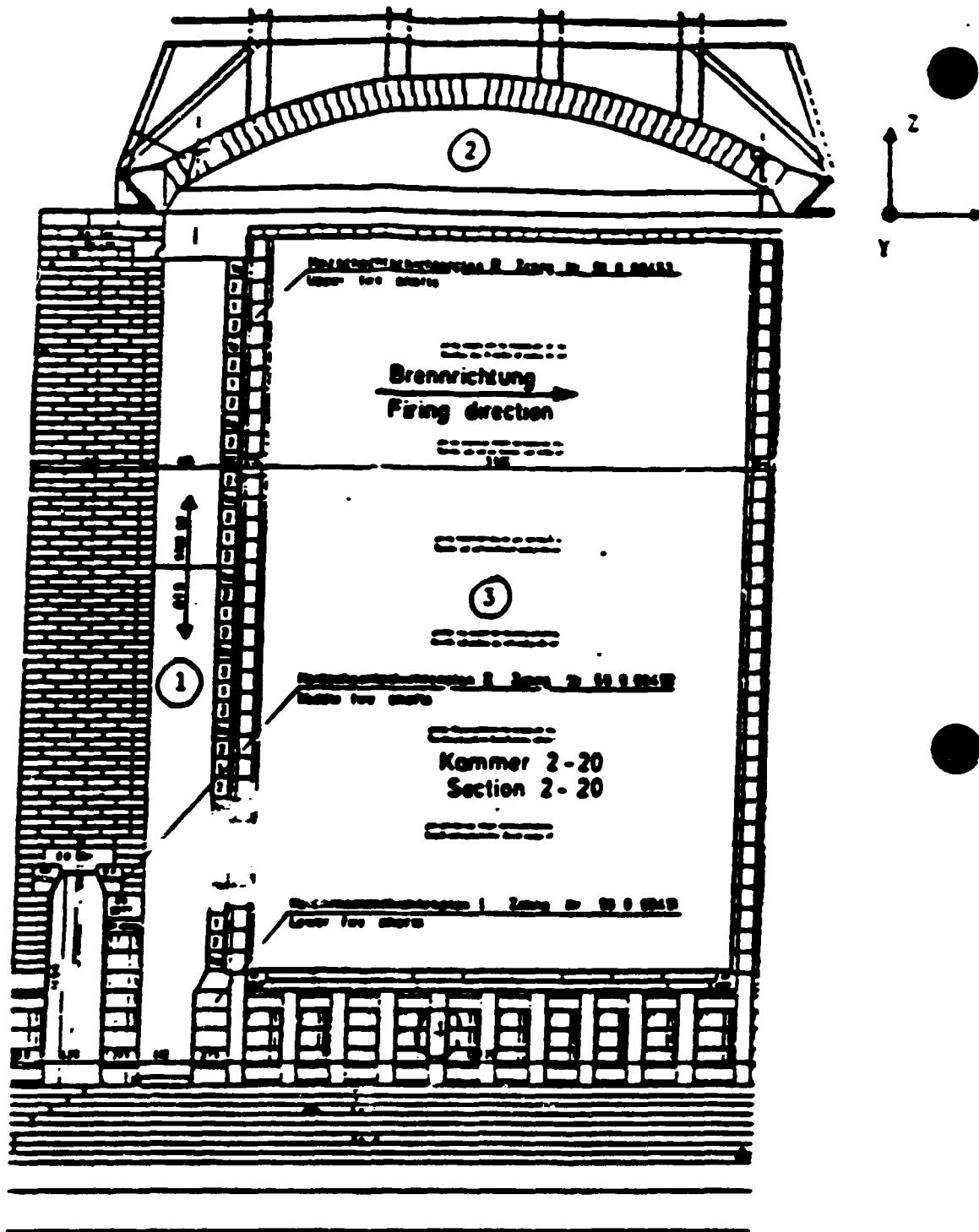


$$\begin{aligned}
 P_{i+1} = P_i & - \frac{b \dot{m}_R}{\rho A_e} (p_{i+1} - p_i) - \frac{2b \dot{m}_R}{A_e} \left(\frac{\dot{m}_{Ri+1}}{\rho_{i+1}} - \frac{\dot{m}_{Ri}}{\rho_i} \right) \\
 & - \frac{\dot{m}_R^2 f_D L_{eq}}{2 \rho D_e A_e^2} - \bar{p} g (z_{i+1} - z_i)
 \end{aligned}$$

$$\dot{m}_{s_{i+1}} = \dot{m}_{s_1} + \dot{m}_{inf}$$

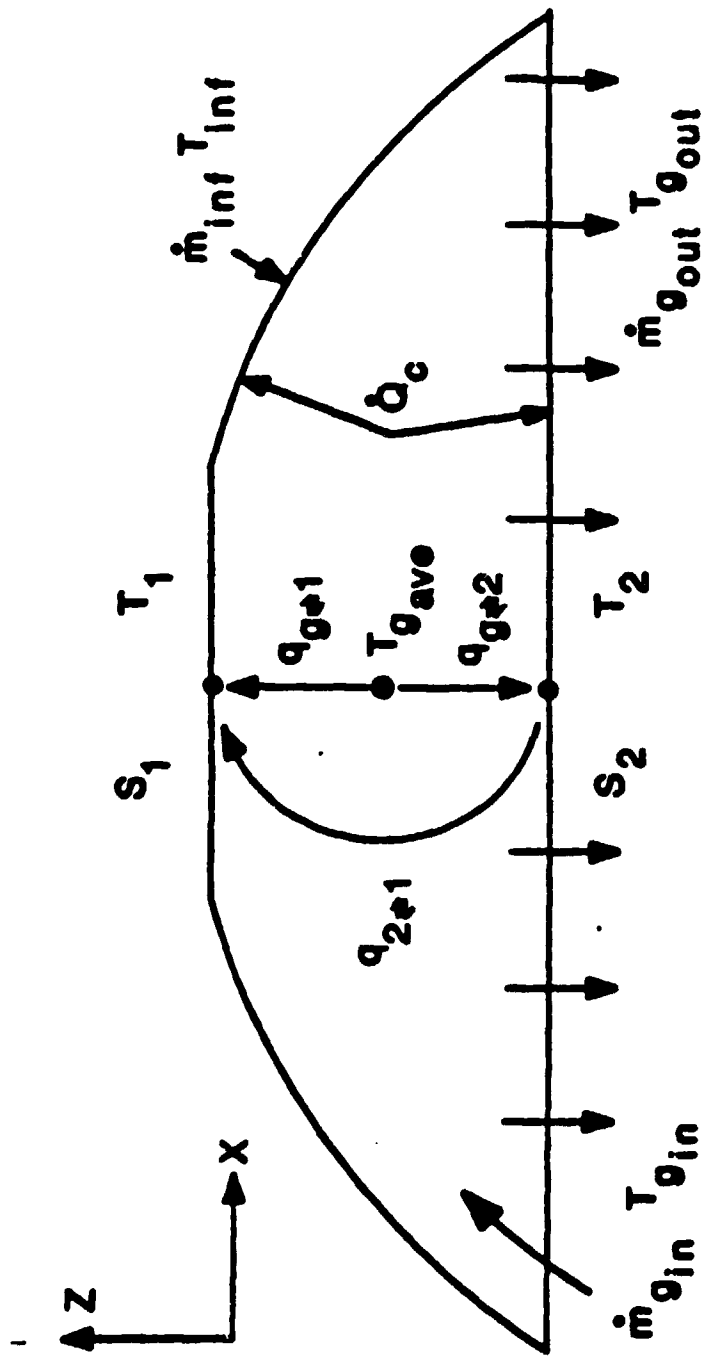
$$\dot{m}_{inf} = C A_0 \sqrt{2 \rho \Delta P}$$

$$C = \sqrt{\frac{D_e}{f_D L_{eq}}}$$



Description of Control Volume with Flow Regions.

1. Head wall and Fireshaft
2. Underlid
3. Pits
4. Underpits



$$\dot{Q}_c = \sum_{i=1}^2 h_i A_i (T_{s_{ave}} - T_i)$$

$$\dot{Q}_T = \dot{q}_{s+1} + \dot{q}_{s+2}$$

$$\dot{Q}_{COKE} = \dot{m}_{COKE} H_{COKE}$$

$$h_C = 0.023 \frac{k}{D} Re_D^{0.8} Pr^{\frac{1}{4}}$$

$$q_{s \rightarrow 1} = \sigma \overline{GS}_1 (T_s^4 - T_1^4)$$

$$q_{s \rightarrow 2} = \sigma \overline{GS}_2 (T_s^4 - T_2^4)$$

$$q_{2 \rightarrow 1} = \sigma \overline{S_1 S_2} (T_2^4 - T_1^4)$$

$$\overline{GS}_1 = \frac{C_g e_g e_1 S_T}{e_g + [C_g e_1 + (1-C_g) e_2] (1 - e_g)}$$

$$\overline{GS}_2 = \frac{(1-C_g) e_g e_2 S_T}{e_g + [C_g e_1 + (1-C_g) e_2] (1 - e_g)}$$

$$\overline{S}_1 S_2 = \frac{C_g (1-C_g) (1 - e_g) e_2 e_1 S_T}{e_g + [C_g e_1 + (1-C_g) e_2] (1 - e_g)}$$

where $C_g = \frac{S_1}{S_T} = \frac{S_1}{S_1 + S_2}$

$$\epsilon_B = C \cdot (\epsilon_{H_2O} + \epsilon_{CO_2})$$

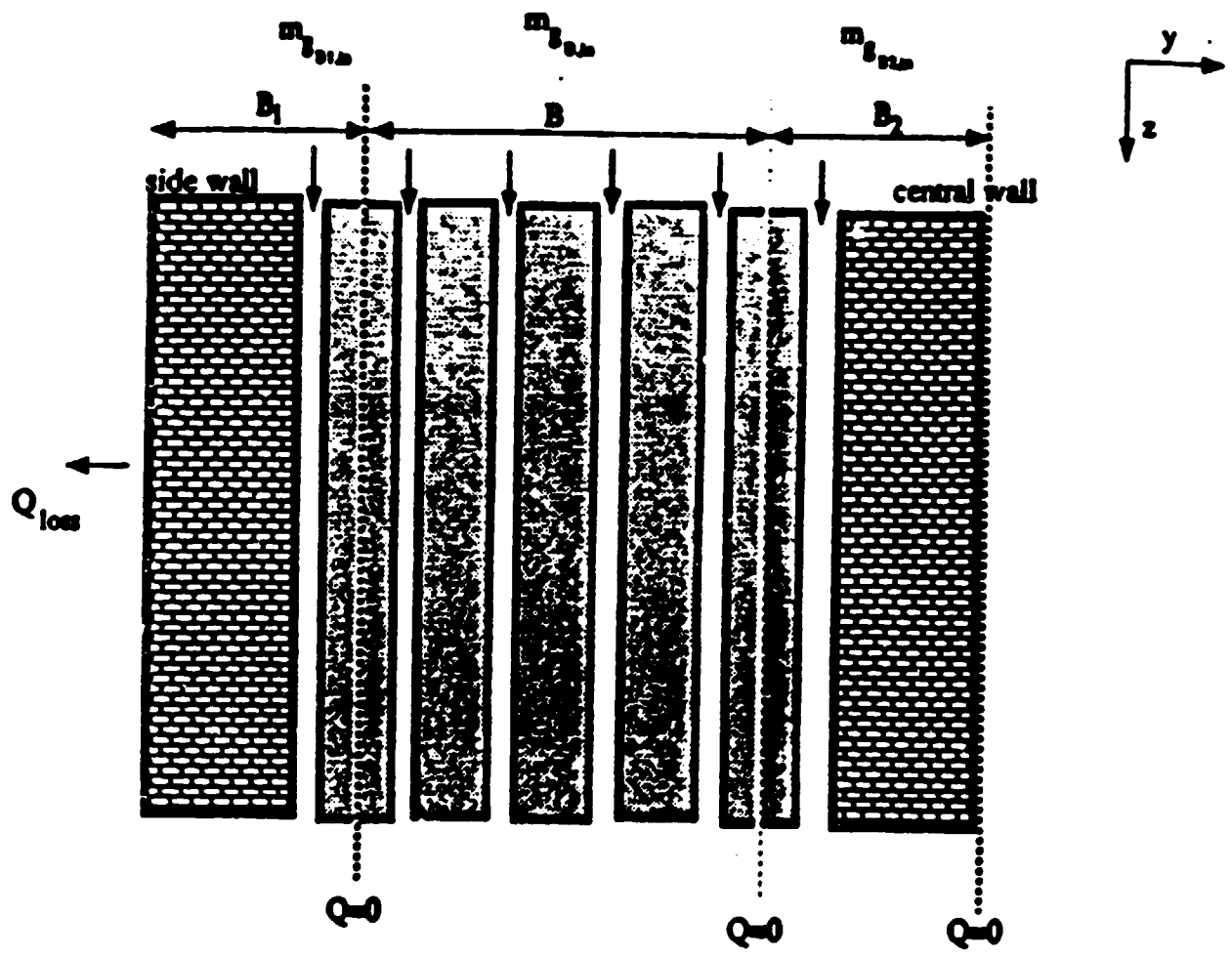
$$\epsilon_{H_2O} = 10 (A + 0.001 BT)$$

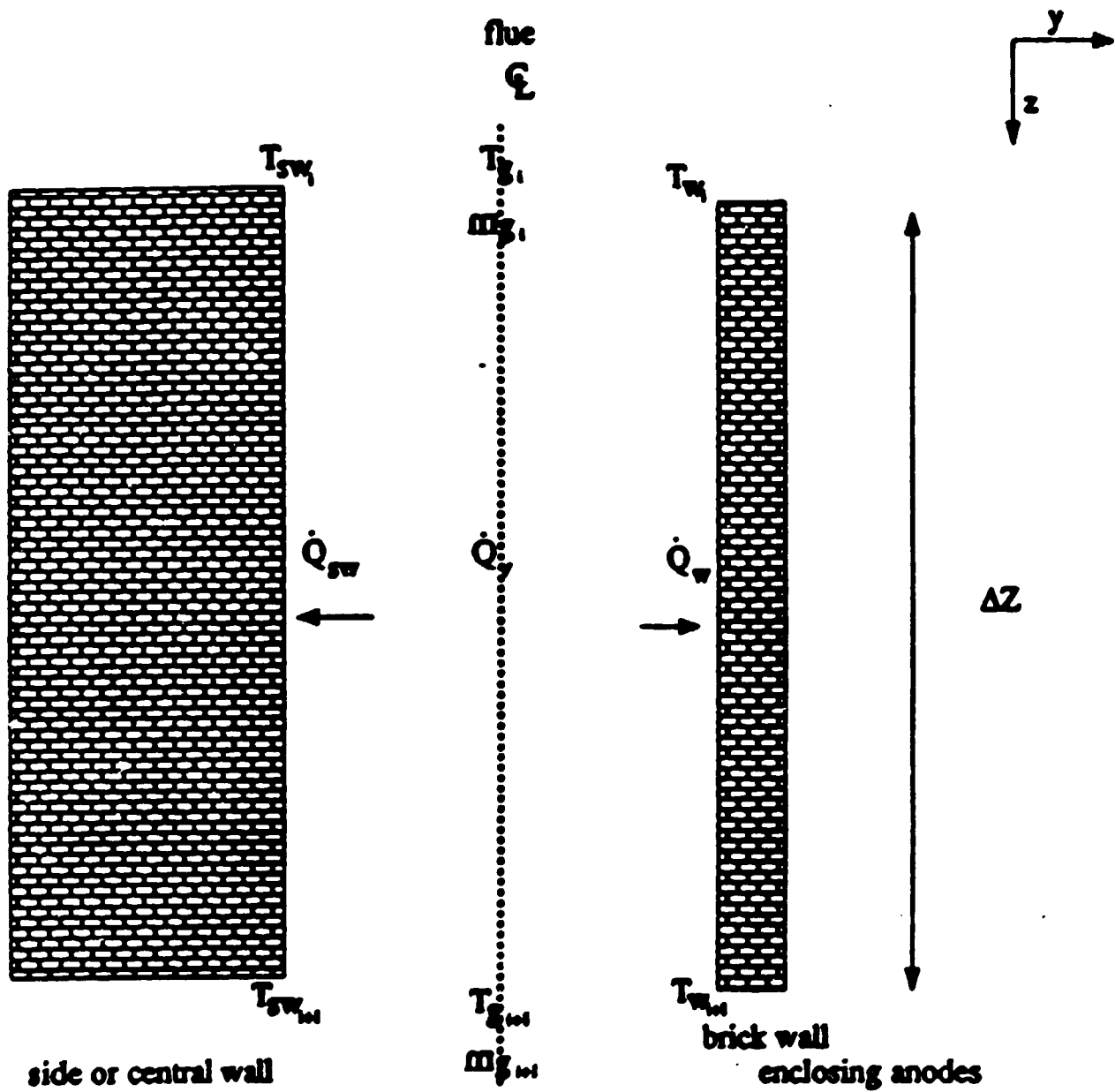
$$A = -0.3429 + 0.5763 \log_{10} (P_H L)$$

$$B = -0.2663 + 0.2090 \log_{10} (P_H L)$$

T = gas temperature ($^{\circ}C$)

$P_H L$ = partial pressure of H_2O multiplied by mean beam length
(atm. ft)

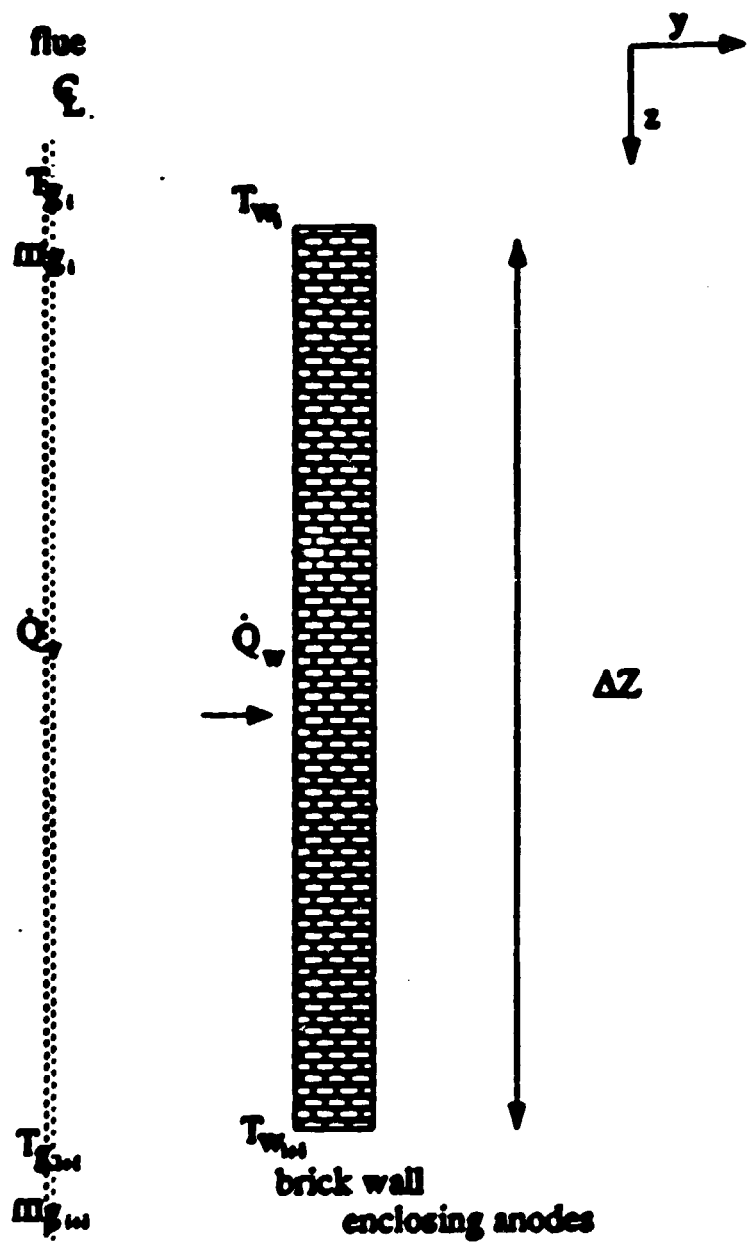


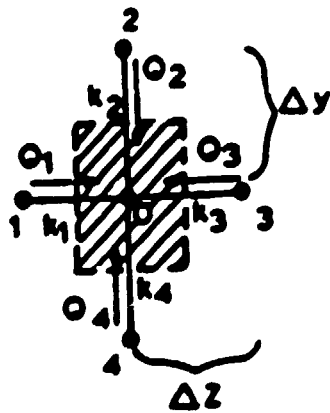
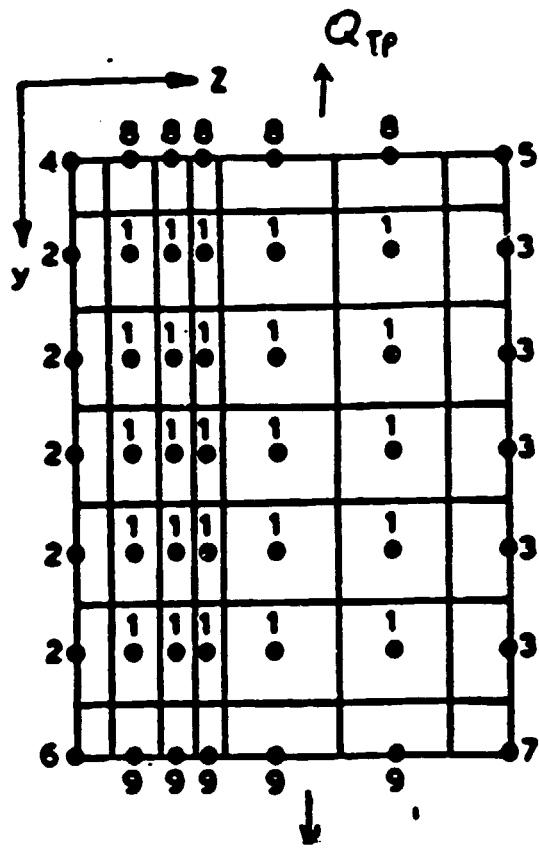


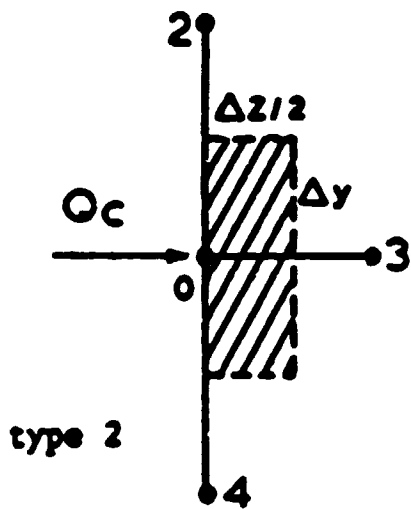
side or central wall

flue

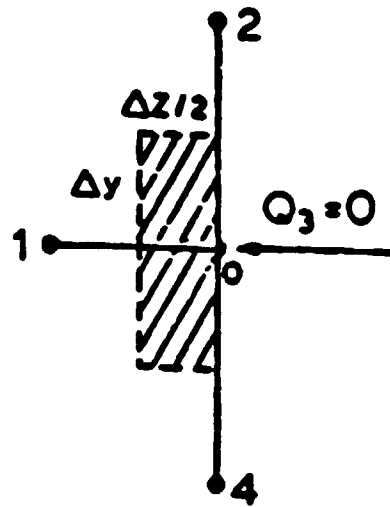
brick wall enclosing anodes



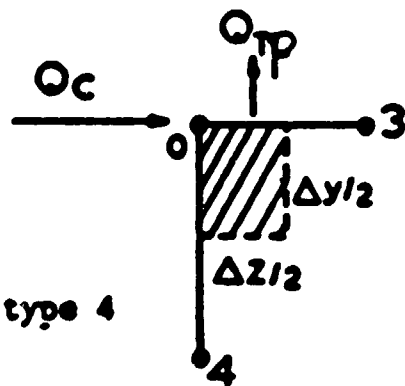




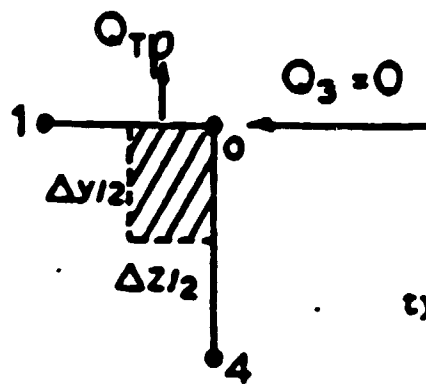
type 2



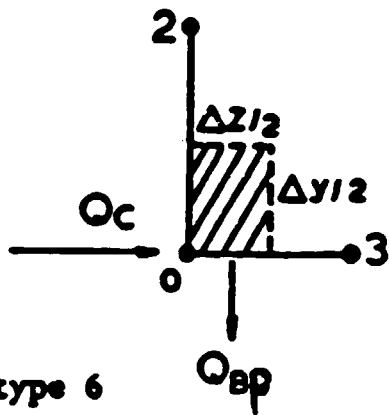
type 3



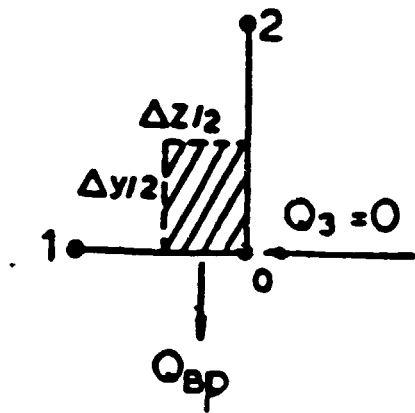
type 4



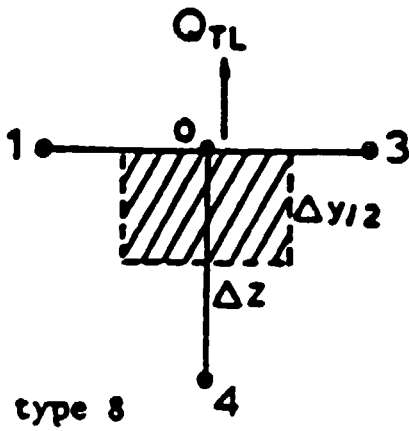
type 5



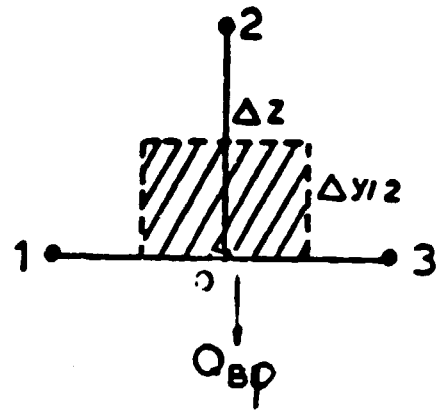
type 6



type 7



type 8



type 9

$$T_0^{v+1} = T_0^v + \frac{\Delta t}{\rho c_p} \left[\frac{k_1}{\Delta z^2} (T_1^v - T_0^v) + \frac{k_3}{\Delta z^2} (T_3^v - T_0^v) + \frac{k_2}{\Delta y^2} (T_2^v - T_0^v) + \frac{k_4}{\Delta y^2} (T_4^v - T_0^v) \right]$$

Type 1

$$T_0^{v+1} = T_0^v + \frac{\Delta t}{\rho c_p} \left[\frac{2k_3}{\Delta z^2} (T_3^v - T_0^v) + \frac{k_2}{\Delta y^2} (T_2^v - T_0^v) + \frac{k_4}{\Delta y^2} (T_4^v - T_0^v) + \frac{2h_T}{\Delta z} (T_g^v - T_0^v) \right]$$

Type 2

$$T_0^{v+1} = T_0^v + \frac{\Delta t}{\rho c_p} \left[\frac{2k_1}{\Delta z^2} (T_1^v - T_0^v) + \frac{k_2}{\Delta y^2} (T_2^v - T_0^v) + \frac{k_4}{\Delta y^2} (T_4^v - T_0^v) \right]$$

Type 3

$$T_0^{v+1} = T_0^v + \frac{2\Delta\tau}{\rho c_p} \left[k_1 \frac{T_1^v - T_0^v}{\Delta z^2} + k_2 \frac{T_2^v - T_0^v}{\Delta y^2} - \frac{q_{BP}}{\Delta y} \right]$$

type 7

$$T_0^{v+1} = T_0^v + \frac{2\Delta\tau}{\rho c_p} \left[\frac{k_1}{2} \frac{T_1^v - T_0^v}{\Delta z^2} + \frac{k_3}{2} \frac{T_3^v - T_0^v}{\Delta z^2} + k_4 \frac{T_4^v - T_0^v}{\Delta y^2} - \frac{q_{TL}}{\Delta y} \right]$$

type 8

$$T_0^{v+1} = T_0^v + \frac{2\Delta\tau}{\rho c_p} \left[\frac{k_1}{2} \frac{T_1^v - T_0^v}{\Delta z^2} + k_2 \frac{T_2^v - T_0^v}{\Delta y^2} + \frac{k_3}{2} \frac{T_3^v - T_0^v}{\Delta z^2} - \frac{q_{BL}}{\Delta y} \right]$$

type 9

$$\dot{m}_1 = \frac{(X^1(T_2) - X^1(T_1))}{\Delta t} \cdot PC \cdot PCVR \cdot ANMAS$$

where \dot{m}_1 = mass flow of volatile 1
in temperature interval considered [kg/s]

$X^1(T)$ = converted fraction of volatile 1 at
temperature T

Δt = time to raise temperature T_1 to T_2 [s]

PC^1 = fraction of volatile 1 over all volatile released
(mass basis, taken at the end of the pyrolysis)

$$\frac{dx^i}{dT} = \frac{K_o^i}{a} [\exp(-E_o^i/RT)] (1 - x^i)^{n^i}$$

where i is the volatile constituent considered

x^i is the converted (evolved) mass fraction of i

T is the sample temperature [K]

K_o^i is the pre-exponential factor [h^{-1}]

a is the heating rate of the sample [K/h]

E_o^i is the activation energy of species i [KJ/mol]

R is the gas constant : 8.3143×10^{-3} [KJ/mol K]

n^i is the reaction order for species i

KINETIC PARAMETERS n , E_0 AND K_0

CONSTITUENT	n	E_0 (KJ/mol)	K_0 (h ⁻¹)
TAR	0.7	4.167 ln(a) + 35.0	exp[0.273E ₀ - 6.417]
H ₂	1.1	5.882 ln(a) + 57.65	exp[0.233E ₀ - 10.39]
CH ₄	0.8	10.0 ln(a) + 76.0	exp[0.225E ₀ - 11.325]

Tar : 425° C ± 50° C

H₂ : 575° C

CH₄ : 630° C

$$h_R = \sigma \cdot C (T_g^3 + T_g T_w^2 + T_w T_g^2 + T_w^3)$$

where σ = Stefan-Boltzmann constant 5.67×10^{-8}

c_w = wall emissivity

$$C = \frac{1}{\frac{1}{c_w} + \frac{1}{c_g} - 1}$$

c_g = gas emissivity

T_g = gas temperature (K)

T_w = brick wall temperature (K)

$$m_{gB.in} = (\text{fraction})m_{g.in}$$

$$m_{gB1.in} = (\text{fraction1})m_{g.in}$$

$$m_{gB2.in} = (\text{fraction2})m_{g.in}$$

$$\dot{Q}_g - \dot{Q}_{g,i+1} + \dot{Q}_v - \dot{Q}_w - \dot{Q}_{sw} = \dot{Q}_{acc}$$

$$\dot{Q}_g = \dot{m}_g h_g$$

$$\dot{Q}_{g,i+1} = \dot{m}_{g,i+1} h_{g,i+1}$$

$$\dot{Q}_v = \dot{m}_v H_v$$

$$\dot{Q}_w = h_w \Delta z (T_{g,avg} - T_{w,avg})$$

$$\dot{Q}_{sw} = h_{sw} \Delta z (T_{g,avg} - T_{sw,avg})$$

$$T_{g,avg} = (T_{g_i} + T_{g,i+1})/2$$

$$T_{w,avg} = (T_{w_i} + T_{w,i+1})/2$$

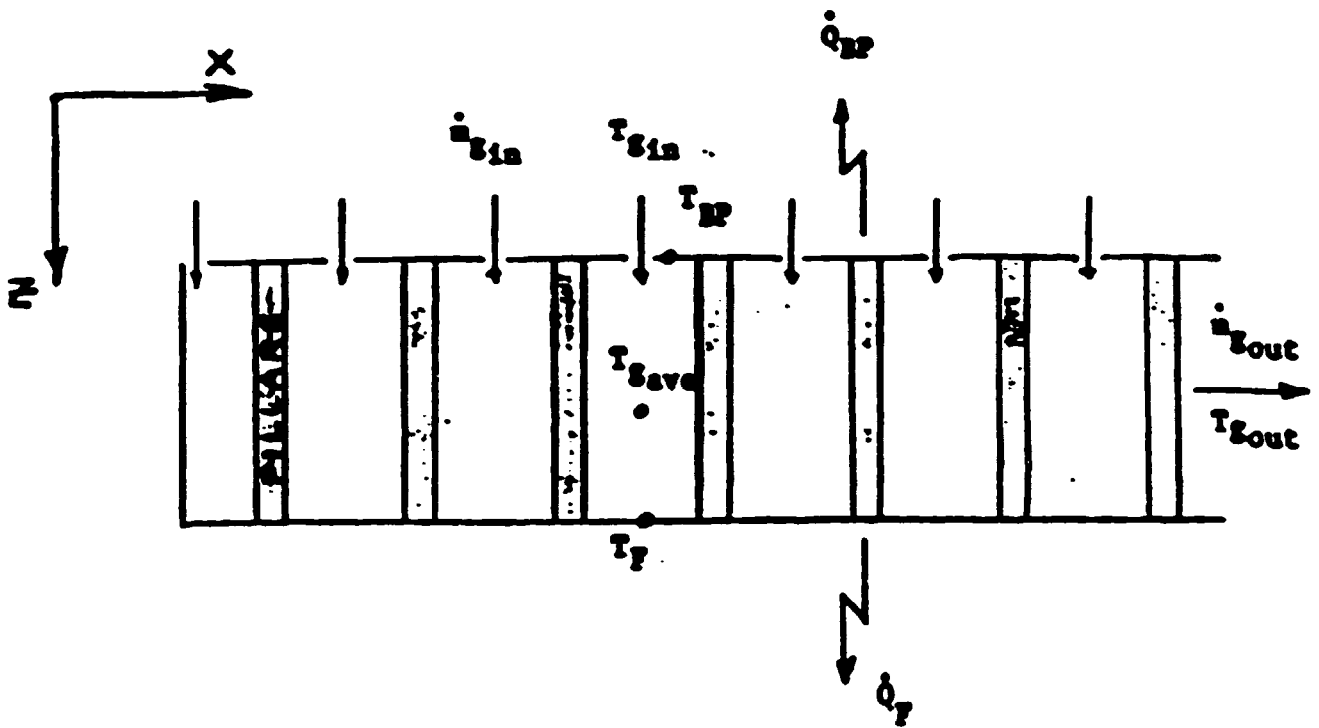
$$T_{sw,avg} = (T_{sw_i} + T_{sw,i+1})/2$$

$$\dot{Q}_g - \dot{Q}_{g,i+1} + \dot{Q}_v - \dot{Q}_w = \dot{Q}_{acc}$$

$$h_{loss} = 1.31(T_E - T_{amb})^{0.333} + \sigma\epsilon(T_E^3 + T_E T_{amb}^2 + T_{amb} T_E^2 + T_{amb}^3)$$

where

- T_E = temperature of the outside surface of sidewall, °K
- T_{amb} = ambient temperature, °K
- σ = Stefan-Boltzmann Constant, $5.67 \times 10^{-8} \text{ W/m}^2 \text{ K}^4$
- ϵ = Sidewall emissivity, 0.95
- h_{loss} = Total (Convective + Radiative) heat transfer coefficient used in the heat loss calculations.

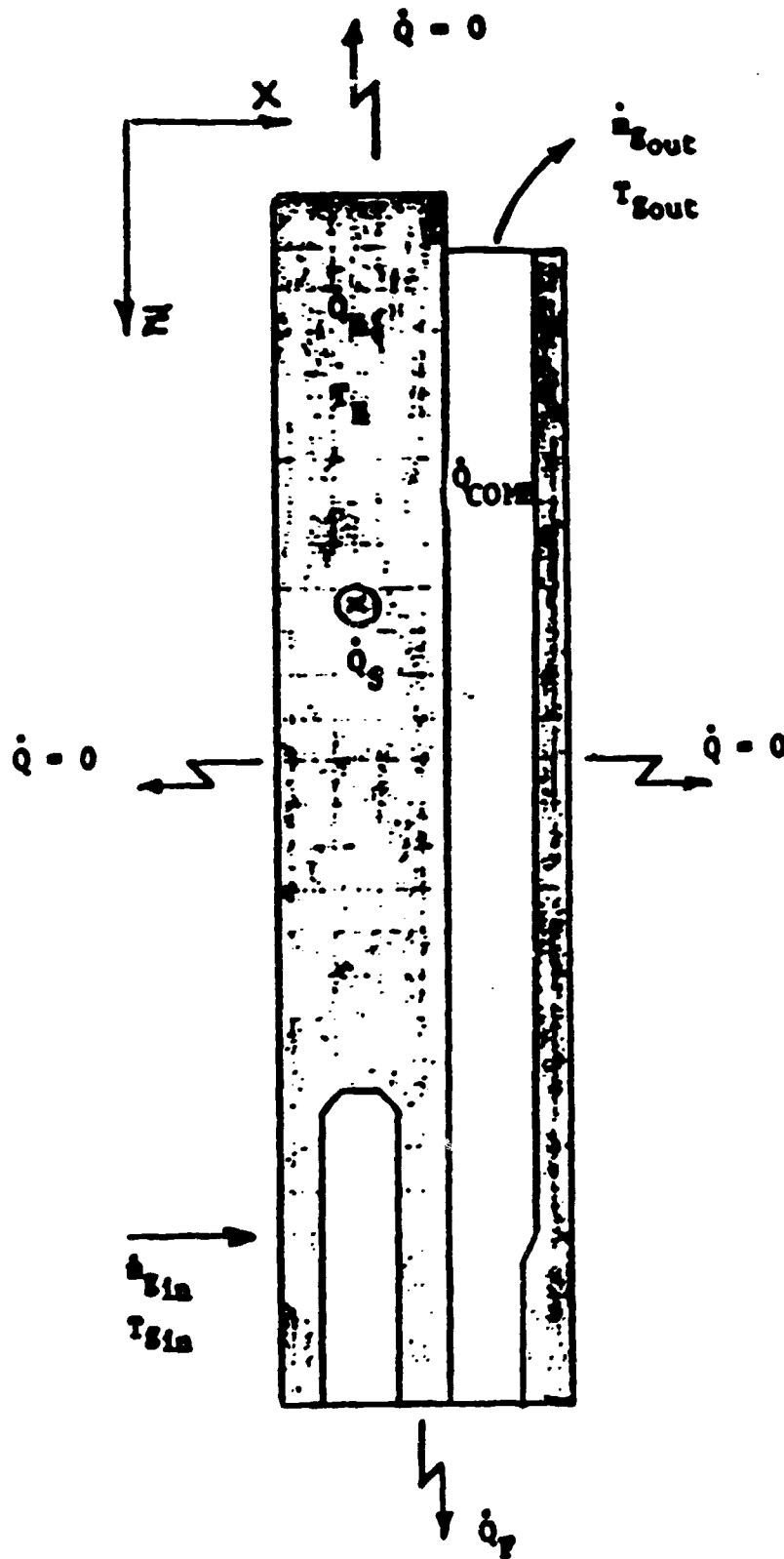


THE UNDER-PIT ZONE

$$\dot{Q}_{S_{in}} - \dot{Q}_{S_{out}} - \dot{Q}_F - \dot{Q}_{BP} - \dot{Q}_{PIL} - \dot{Q}_{acc}$$

$$\dot{Q}_{S_{in}} - \dot{Q}_{S_{out}} = \dot{m}_{S_{in}} h_{S_{in}} - \dot{m}_{S_{out}} h_{S_{out}}$$

$$\dot{Q}_F = h_F A_F (T_{S_{ave}} - T_F)$$



ASSUMED CONTROL VOLUME FOR HEADWALL
AND FIRESHAFT ZONE

$$\dot{Q}_{S_{in}} - \dot{Q}_{S_{out}} - \dot{Q}_F - \dot{Q}_S - \dot{Q}_H + \dot{Q}_{COMB} = \dot{Q}_{acc}$$

$$\dot{Q}_{S_{in}} - \dot{Q}_{S_{out}} = \dot{m}_{S_{in}} h_{S_{in}} - \dot{m}_{S_{out}} h_{S_{out}}$$

$$\dot{Q}_{COMB} = \dot{m}_F H_F$$

where \dot{m}_F : mass flowrate of fuel

H_F : fuel heating value

$$H_2O_{INF} = (X_{H_2O} \times \dot{m}_{inf}) / 18.0$$

$$O_2_{INF} = (X_{O_2} \times \dot{m}_{inf}) / 32.0$$

$$N_2_{INF} = (X_{N_2} \times \dot{m}_{inf}) / 28.0$$

$$X_{H_2O} = \frac{w}{1 + w}$$

$$X_{O_2} = \frac{0.232}{1 + w}$$

$$\left[\frac{\text{kg } O_2}{\text{kg moist air}} \right]$$

$$X_{N_2} = \frac{0.768}{1 + w}$$

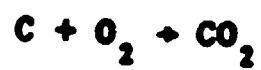
$$\left[\frac{\text{kg } N_2}{\text{kg moist air}} \right]$$

$$w = 0.622 \left(\frac{P_v}{P_a} \right)$$

$$P_v = \phi \cdot P_g$$

$$P_a = P_{atm} - P_v$$

$$C = \frac{(1 - X_{ash}) \dot{m}_{P.C.}}{12.0}$$



$$O_2 = \frac{(1 - X_{ash}) \dot{m}_{P.C.}}{12.0}$$

$$CO_2 = \frac{(1 - X_{ash}) \dot{m}_{P.C.}}{12.0}$$

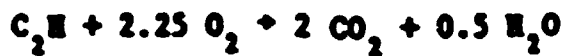
$$O_2REM(2) = O_2REM(1) + O_2INF - \frac{(1-X_{ash}) \dot{m}_{P.C.}}{12.0}$$

$$N_2REM(2) = N_2REM(1) + N_2INF$$

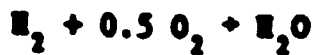
$$H_2OREM(2) = H_2OREM(1) + H_2OINF$$

$$CO_2REM(2) = CO_2REM(1) + \frac{(1-X_{ash}) \dot{m}_{P.C.}}{12.0}$$

Zone B



(combustion of tar)



(combustion of hydrogen)



(combustion of methane)

$$\text{O2REM}(3) = \text{O2REM}(2) - \text{ALPHA} * \left[\frac{2.25 \dot{m}_{\text{tar}}}{25.0} + \frac{0.5 \dot{m}_{\text{H}_2}}{2.0} + \frac{2.0 \dot{m}_{\text{CH}_4}}{16.0} \right]$$

$$\text{N2REM}(3) = \text{N2REM}(2)$$

$$\text{H2OREM}(3) = \text{H2OREM}(2) + \text{ALPHA} * \left[\frac{2.0 \dot{m}_{\text{tar}}}{25.0} + \frac{\dot{m}_{\text{H}_2}}{2.0} + \frac{2.0 \dot{m}_{\text{CH}_4}}{16.0} \right]$$

$$\text{CO2REM}(3) = \text{CO2REM}(2) + \text{ALPHA} * \left[\frac{0.5 \dot{m}_{\text{tar}}}{25.0} + \frac{\dot{m}_{\text{CH}_4}}{16.0} \right]$$

Zone C

$$O2REM(4) = O2REM(3) - BETA * \left[\frac{2.25 \dot{m}_{tar}}{25.0} + \frac{0.5 \dot{m}_{H_2}}{2.0} + \frac{2.0 \dot{m}_{CH_4}}{16.0} \right]$$

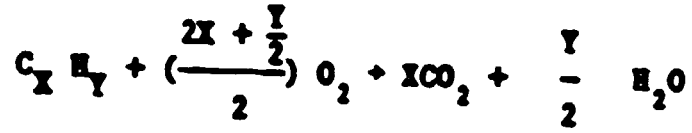
$$N2REM(4) = N2REM(3)$$

$$H2OREM(4) = H2OREM(3) + BETA * \left[\frac{2.0 \dot{m}_{tar}}{25.0} + \frac{\dot{m}_{H_2}}{2.0} + \frac{2.0 \dot{m}_{CH_4}}{16.0} \right]$$

$$CO2REM(4) = CO2REM(3) + BETA * \left[\frac{0.5 \dot{m}_{tar}}{25.0} + \frac{\dot{m}_{CH_4}}{16.0} \right]$$

Zone D

FUEL COMBUSTION



$$C_X H_Y = \frac{\dot{m}_f}{W_f}$$

$$O_2 = \left(\frac{2X + \frac{Y}{2}}{2}\right) \cdot \frac{\dot{m}_f}{W_f}$$

$$CO_2 = X \cdot \frac{\dot{m}_f}{W_f}$$

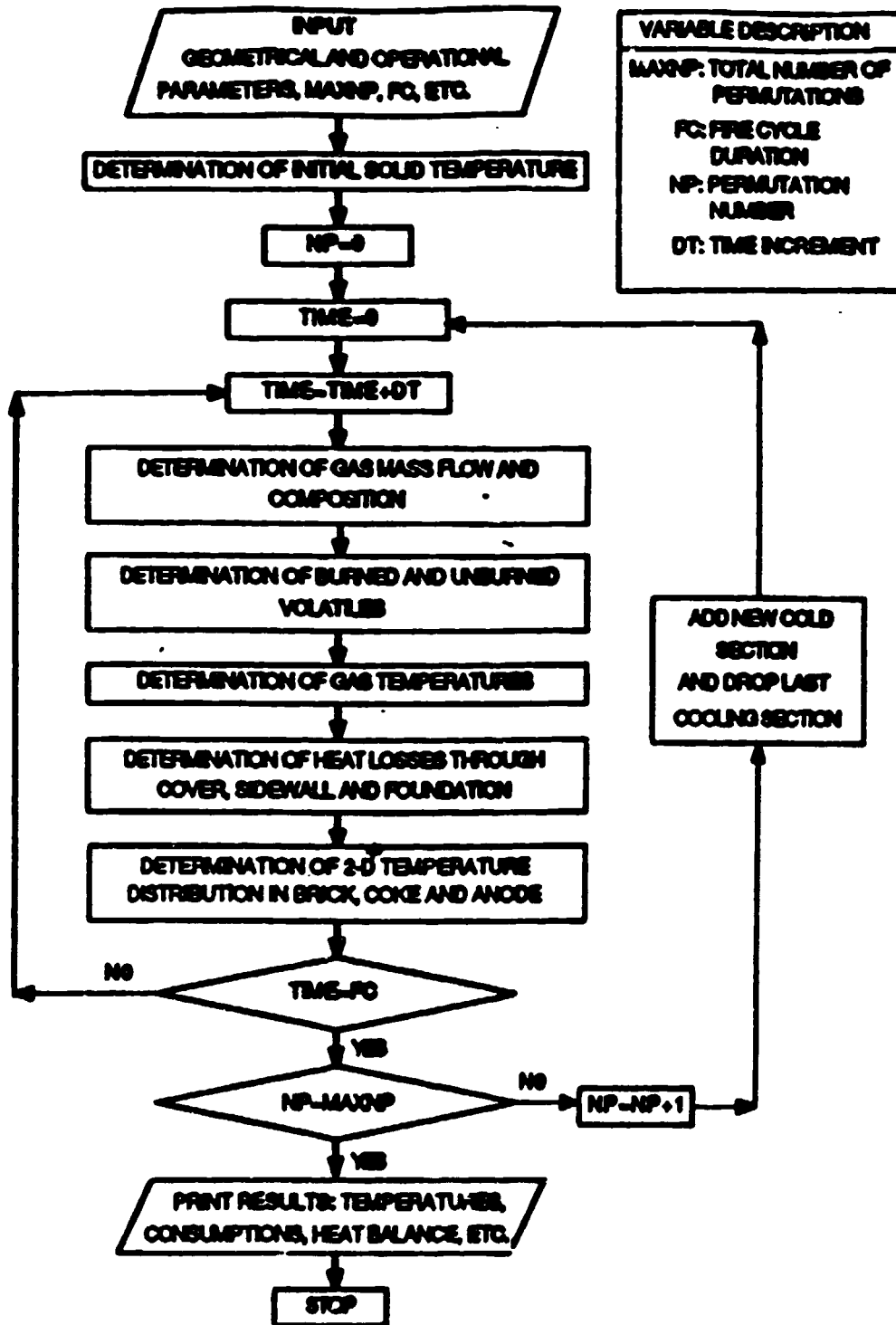
$$H_2O = \frac{Y}{2} \cdot \frac{\dot{m}_f}{W_f}$$

$$O2REM(1) = O2REM(4) - \left(\frac{2X + \frac{Y}{2}}{2} \right) \cdot \frac{\dot{m}_f}{W_f}$$

$$N2REM(1) = N2REM(4)$$

$$H2O(1) = H2O(4) + X \cdot \frac{\dot{m}_f}{W_f}$$

$$CO2(1) = CO2(4) + \frac{Y}{2} \cdot \frac{\dot{m}_f}{W_f}$$



VARIABLE DESCRIPTION

MAJNP: TOTAL NUMBER OF PERMUTATIONS

FC: FIRE CYCLE DURATION

NP: PERMUTATION NUMBER

DT: TIME INCREMENT

SOLUTION PROCEDURE

**3. SIMULATION RESULTS AND CAPABILITIES OF THE 2D+
MODEL**

```

.....
.
. VERTICAL RING FURNACE                                MATHEMATICAL MODEL
.
. UNAR RIECHHAMMER FURNACE                             .
. TEST RUN                                             .
.
.                                     DATE OF RUN:     .
.
.....

```

PART I: FIRE TRAIN ARRANGEMENT

MAXIMUM NUMBER OF PERMUTATIONS: 15

FIRE CYCLE DURATION: 30.00 HOURS

```

          0                1        1        1
                V        V        V
-----
000-000000-----
-----
00      000      TYPE      PRE      PRE      PRE      PRE      FIR      FIR      FIR      000      0
3       2      POSITION    11      10      9       8       7       6       5       4
-----

```

fire direction
<-----

CONVERGENCE CRITERION ON GAS TEMPERATURE (°C): 5.00

PART II: SOLID (BRICK, COKE, ANODE) RELATED PARAMETERS

A) HORIZONTAL DIMENSIONS

BRICK THICKNESS (M): 0.35000
 COKE LAYER THICKNESS (M): 0.39500
 HALF ANODE THICKNESS (M): 0.35500

B) VERTICAL DIMENSIONS

COKE LAYER HEIGHT (M) ON TOP OF ANODE: 0.35000
 TOTAL ANODE HEIGHT (M): 4.98000
 BOTTOM BRICK HEIGHT (M): 0.16400

C) TIME INCREMENTS

GAS TEMPERATURE TIME INCREMENT (S): 180.000
 SOLID TEMPERATURE TIME INCREMENT (S): 180.000
 FIRST FIRE SECTION POSITION: 5

MATERIAL PROPERTIES

	TEMP.	ROA	ROB	ROC	CPA	CPB	CPD	COA	COB	CD
	°C	KG/C.M.	KG/C.M.	KG/C.M.	J/KGK	J/KGK	J/KGK	W/MK	W/MK	W/M
	COOLING PERIOD									
0	100.	1530.00	2150.00	670.00	894.40	1254.00	1177.70	3.64	1.80	0.5
3	300.	1530.00	2150.00	670.00	1380.00	1254.00	1600.32	4.90	1.80	0.8
1	500.	1530.00	2150.00	670.00	1613.17	1254.00	1887.34	5.58	1.80	1.2
5	700.	1530.00	2150.00	670.00	1731.19	1254.00	2137.41	5.86	1.80	1.8
3	900.	1530.00	2150.00	670.00	1820.00	1254.00	2373.38	5.90	1.80	2.7
4	1100.	1530.00	2150.00	670.00	1914.16	1254.00	2602.83	5.88	1.80	3.7
3	1300.	1530.00	2150.00	670.00	1996.87	1254.00	2828.85	5.90	1.80	5.0
6										
	HEATING PERIOD									
0	100.	1600.00	2150.00	670.00	993.09	1254.00	1177.70	2.49	1.80	0.5
3	300.	1600.00	2150.00	670.00	1452.11	1254.00	1600.32	2.75	1.80	0.8
1	500.	1600.00	2150.00	670.00	1645.27	1254.00	1887.34	3.26	1.80	1.2
5	700.	1600.00	2150.00	670.00	1747.43	1254.00	2137.41	4.15	1.80	1.8
3	900.	1600.00	2150.00	670.00	1850.10	1254.00	2373.38	5.55	1.80	2.7
4	1100.	1600.00	2150.00	670.00	1961.47	1254.00	2602.83	5.90	1.80	3.7
3	1300.	1600.00	2150.00	670.00	2000.00	1254.00	2828.85	5.90	1.80	5.0
6										

E) MATERIAL DISTRIBUTION PER NODE

DES

TEMPERATURE MATRIX DIMENSIONS ARE: 10

* 9 : 30 NC

A=ANODE
B=BRICK
C=COKE

	1	2	3	4	5	6	7	8
1	B	B	C	C	C	C	C	C
2	B	B	C	C	C	C	C	C
3	B	B	C	C	A	A	A	A
4	B	B	C	C	A	A	A	A
5	B	B	C	C	A	A	A	A
6	B	B	C	C	A	A	A	A
7	B	B	C	C	A	A	A	A
8	B	B	C	C	A	A	A	A
9	B	B	B	B	B	B	B	B
10	B	B	B	B	B	B	B	B

F) ASSUMED INITIAL SOLID TEMPERATURE (°C)

SECT. POS.	TEMPERATURE
1	700.0
2	850.0
3	1000.0
4	1050.0
5	1050.0
6	600.0
7	400.0
8	270.0
9	180.0
10	90.0
11	30.0

PART III: HEAT LOSSES RELATED PARAME

TERS

A) COVER LOSSES:

EXTERNAL COVER EMISSIVITY: 0.950
TIME INCREMENT (S): 180.000

NUMBER OF MATERIAL LAYERS: 2

MATERIAL THICKNESS DIVISIONS	DENSITY	SP. HEAT	CONDUCT
(M)	(KG M ⁻³)	(J/KG*K)	(W/M*K)
1 0.125000	1.500	950.000	921.000
2 0.125000	1.500	950.000	921.000

B) SIDEWALL LOSSES:

EXTERNAL SIDEWALL EMISSIVITY: 0.950
 TIME INCREMENT (S): 180.000

NUMBER OF MATERIAL LAYERS: 5

	MATERIAL THICKNESS DIVISIONS (M)	DENSITY (KG/M**3)	SP.HEAT (J/KG*K)	CONDUCT (W/M*K)
1	0.312500	3.500	2000.000	1250.000
2	0.250000	1.000	1050.000	1047.000
3	0.432500	1.000	1600.000	840.000
4	0.030000	1.000	50.000	670.000
5	0.200000	2.500	2200.000	1047.000

D) FOUNDATION LOSSES:

BOTTOM FOUNDATION TEMPERATURE (°C): 90.0
 TIME INCREMENT (S): 180.000

NUMBER OF MATERIAL LAYERS: 6

	MATERIAL THICKNESS DIVISIONS (M)	DENSITY (KG/M**3)	SP.HEAT (J/KG*K)	CONDUCT (W/M*K)
1	0.068000	2.500	2000.000	1250.000
2	0.068000	1.000	2000.000	1250.000
3	0.204000	1.000	1000.000	1047.000
4	0.204000	1.000	700.000	1047.000
5	0.200000	1.000	1200.000	1170.000
6	0.300000	2.500	2200.000	1047.000

D) ASSUMED INITIAL INNER SURFACE TEMPERATURE (°C):

SECT.POS.	COVER	SIDEWALL	FOUNDATION
1	700.0	700.0	700.0
2	950.0	950.0	950.0
3	1000.0	1000.0	1000.0
4	1050.0	1050.0	1050.0
5	1050.0	1050.0	1050.0
6	600.0	600.0	600.0
7	400.0	400.0	400.0
8	270.0	270.0	270.0
9	180.0	180.0	180.0
10	90.0	90.0	90.0
11	30.0	30.0	30.0

SIDEWALL TEMP. (°C) PROFILE IN FIRST PREHEAT AT TIME 0:

NODE:	1	2	3	4	5	6	7	8
TEMP.:	50.0	62.0	75.0	90.0	130.0	180.0	120.0	60.0

FOUNDATION TEMP. (°C) PROFILE IN FIRST PREHEAT AT TIME 0:

```

9      10      NCDE:      1      2      3      4      5      6      7      8
10     90.0     TEMP.: 100.0 100.0 100.0 100.0 100.0 100.0 100.0 100.0 100

```

PART IV: GAS MASS FLOW RELATED PARA METERS

A) GEOMETRICAL AND OPERATIONAL PARAMETERS

```

      POSITION OF FIRST UNCOVERED SECTION:
      POSITION OF PRESSURE CONTROL SECTION: 1
      PRESSURE CONTROL TARGET (PASCALS): -44.00
      ASSUMED INLET GAS MASS FLOW (KG/S): 1.30
      AVERAGE SECTION PERPENDICULAR TO FLOW (M**2):
3.4569
      AVERAGE EQUIVALENT DIAMETER (M): 0.650
      EQUIVALENT LENGTH OF ONE SECTION (M): 165.5
      PRESSURE CONVERGENCE CRITERION (PASCALS):
0.01000
      CORRECTION COEFFICIENT ON PRESSURE EQUATION :
0.70
      INFILTRATION EQUATION COEFFICIENT: 1.0
      AMBIENT TEMPERATURE (°C): 20.
      PIT HEIGHT (M): 5.39
      RELATIVE HUMIDITY (FRACTION): 0.70
      AMBIENT ATMOSPHERIC PRESSURE (PASCALS): 101325.
      PERCENT ASH IN PACKING COKE: 7.5
      FUEL MOLECULAR WEIGHT (KG/KMOLE): 16.00
      STOE. O2 REQUIRED (KMOLES) PER KMOLE OF FU
EL: 2.000
      STOE. CO2 PRODUCED (KMOLES) PER KMOLE OF FU
EL: 1.000
      STOE. H2O PRODUCED (KMOLES) PER KMOLE OF FU
EL: 2.000

```

B) COMBUSTION IN FURNACE SECTIONS, INFILTRATION AREAS
AND ASSUMED UNDER COVER GAS TEMPERATURE:
PACKING COKE IS KNOWN, FUEL IS ASSUMED.

PERCENT COKE COMB. ENERGY RELEASED IN GAS: 88.00

12.00 PERCENT COKE COMB. ENERGY RELEASED IN TOP COKE HALF LAYER

SECT. POS.	FUEL (KG/S)	P. COKE (KG/S)	INF. AREA (SQ.M)	GAS TEMP. (°C)
1	0.00000	0.00000	0.03330	100.0
2	0.00000	0.00417	0.03330	700.0
3	0.00000	0.00277	0.03330	950.0
4	0.00000	0.00171	0.03330	950.0
5	0.01530	0.00496	0.03330	1000.0
6	0.01020	0.00355	0.03330	1050.0
7	0.00800	0.00349	0.03330	1050.0
8	0.00000	0.00000	0.03330	750.0
9	0.00000	0.00000	0.03330	600.0
10	0.00000	0.00000	0.03330	300.0
11	0.00000	0.00000	0.03330	100.0

3) TARGET DRAUGHT PROFILE AT SECTION 10:

TIME (H)	PRESSURE (PA)
0.00	-44.00
4.00	-44.00
16.00	-44.00
20.00	-44.00
30.00	-44.00

PART V: VOLATILE RELATED PARAMETERS

3.50 PERCENT VOLATILE RELEASED (BAKING LOSS):

PERCENT TAR IN VOLATILES (MASS BASIS):	92.00
PERCENT H2 IN VOLATILES (MASS BASIS):	6.00
PERCENT CH4 IN VOLATILES (MASS BASIS):	2.00
TAR LOWER HEATING VALUE (J. KG):	0.348700E+09
TAR ACTIVATION ENERGY (CAL/MOLE):	33000.0
TOTAL ANODE MASS (KG) PER SECTION:	99993.0
AVERAGE ANODE HEATING RATE (°C/H):	25.00

PART VI: ZONE "A" GAS RELATED PARAMETERS

INFILTRATED AIR TEMPERATURE (°C):	20.0
BRICK COVER AREA (M**2):	42.000
PIT TOP AREA (M**2):	18.900
ZONE "A" LENGHT (M) ALONG X AXIS:	5.200
ZONE "A" WIDTH (M) ALONG Y AXIS:	6.400
ZONE "A" HEIGHT (M) ALONG Z AXIS:	0.800
INTERNAL COVER SURFACE EMISSIVITY:	0.750
PIT TOP EMISSIVITY:	0.750
PERCENT INFILTRATION IN ZONE "A":	95.00

PART VII: FIRED SECTIONS RELATED

PARAMETERS

TOTAL NUMBER OF FIRED SECTIONS: 3
SECTION POSITIONS IN FIRE TRAIN: 5 6 7

5 TARGET GAS TEMPERATURE PROFILE FOR SECTION No:
TIME (H) TEMP. (°C)
0.00 1250.0
30.00 1250.0

5 TARGET GAS TEMPERATURE PROFILE FOR SECTION No:
TIME (H) TEMP. (°C)
0.00 1250.0
30.00 1250.0

- TARGET GAS TEMPERATURE PROFILE FOR SECTION No:
TIME (H) TEMP. (°C)
0.00 760.0
26.00 1250.0
30.00 1250.0

PART VIII: ZONE "B" GAS RELATED PARAMETERS

NUMBER OF PITS PER SECTION: 6
NUMBER OF TYPE 1 BRICK HOLES: 126
AREA (M**2) OF ONE TYPE 1 BRICK HOLE: 0.02575
NUMBER OF TYPE 2 BRICK HOLES: 35
AREA (M**2) OF ONE TYPE 2 BRICK HOLE: 0.01683
LENGTH (M) OF ZONE "B" ALONG X AXIS: 3.500
BRICK WALL EMISSIVITY: 0.960
FRACTION OF VOLATILES BURNING IN ZONE "B": 0.800
EXTRA BRICK MASS (KG) IN ZONE "B": 55000.00
EXTRA COKE MASS (KG) IN ZONE "B": 10000.00
ANODE TEMP. (°C) IN FIRST PREHEAT: 40.0
BRICK TEMP. (°C) IN FIRST PREHEAT: 50.0
COKE TEMP. (°C) IN FIRST PREHEAT: 200.0

PART IX: ZONE "C" GAS RELATED PARA

METERS

FOUNDATION AREA (M**2) PER SECTION:	35.604
BOTTOM PIT AREA (M**2) PER SECTION:	19.900
TOTAL PILLAR MASS (KG) PER SECTION:	4040.000
PILLAR HEAT CAPACITY (J KG*K):	1254.0
TOTAL PILLAR SURFACE PER SECTION (M**2):	63.730
TOTAL PILLAR VOLUME PER SECTION (M**3):	4.000
ZONE "C" LENGHT (M) ALONG X AXIS:	4.600
ZONE "C" WIDTH (M) ALONG Y AXIS:	6.400
ZONE "C" HEIGHT (M) ALONG Z AXIS:	0.670
FOUNDATION FLOOR EMISSIVITY:	0.750
BOTTOM PIT EMISSIVITY:	0.750
FRACTION OF VOLATILES BURNING IN ZONE "C":	0.000

PART X: ZONE "C" GAS RELATED PARAMETERS

FOUNDATION AREA UNDER HEADWALL (M**2):	10.016
SIDEWALL AREA ALONG HEADWALL (M**2):	20.079
FIRESHAFT WIDTH ALONG X AXIS (M):	0.495
HEADWALL BRICK MASS (KG):	93000.0
HEADWALL HEAT CAPACITY (J KG*K):	1254.000
FUEL HEATING VALUE (J KG):	0.500000E+08
FUEL DENSITY (KG LITER):	0.00069
PERCENT INFILTRATION IN ZONE "C":	15.00

GAS TEMP. PROFILE AFTER PERM. NO: 1

172.4 371.7 703.9 971.6 1250.0 1250.0 1250.0 706.3 431.0 267.0

FUEL CONSUMPTION AT END OF PERM.: 0.01303 0.01309 0.02591

GAS TEMP. PROFILE AFTER PERM. NO: 2

173.0 416.1 776.0 900.9 1250.0 1250.0 1250.0 724.3 431.7 266.4

FUEL CONSUMPTION AT END OF PERM.: 0.01192 0.01901 0.02419

GAS TEMP. PROFILE AFTER PERM. NO: 3

175.2 457.7 910.0 927.4 1250.0 1250.0 1250.0 732.6 479.5 269.2

FUEL CONSUMPTION AT END OF PERM.: 0.01479 0.01729 0.02401

GAS TEMP. PROFILE AFTER PERM. NO: 4

175.3 475.2 936.5 971.0 1250.0 1250.0 1250.0 744.5 507.7 270.4

FUEL CONSUMPTION AT END OF PERM.: 0.01492 0.01714 0.02374

GAS TEMP. PROFILE AFTER PERM. NO: 5

178.4 488.9 789.2 857.3 1250.0 1250.0 1250.0 743.8 527.3 277.3

FUEL CONSUMPTION AT END OF PERM.: 0.01500 0.01704 0.02376

GAS TEMP. PROFILE AFTER PERM. NO: 6

181.1 459.7 770.6 851.8 1250.0 1250.0 1250.0 738.0 521.0 282.2

FUEL CONSUMPTION AT END OF PERM.: 0.01501 0.01703 0.02333

GAS TEMP. PROFILE AFTER PERM. NO: 7

182.9 450.1 763.0 850.3 1250.0 1250.0 1250.0 735.2 523.6 285.0

FUEL CONSUMPTION AT END OF PERM.: 0.01501 0.01662 0.02331

GAS TEMP. PROFILE AFTER PERM. NO: 8

184.1 446.2 760.9 850.5 1250.0 1250.0 1250.0 733.6 525.2 286.9

FUEL CONSUMPTION AT END OF PERM.: 0.01471 0.01658 0.02328

PERMUTATION NUMBER: 9

TIME (HRS) = 1.000

SECT.	POSITION	GAS TEMP. (C)	EMISSIVITY	CO2 (% vol.)	OXYGEN (% vol.)
1	2	20.0	0.005	0.00	20.66
1	3	521.0	0.007	0.00	20.66
1	4	560.1	0.006	0.00	20.66
1	1	646.9	0.032	0.00	20.66
1	2	724.2	0.012	0.81	19.85
2	3	880.2	0.017	0.81	19.85
2	4	977.7	0.027	0.81	19.85
3	1	885.1	0.027	0.80	19.86
3	2	863.5	0.011	1.25	19.41
3	3	925.0	0.016	1.25	19.41
3	4	917.7	0.019	1.25	19.41
4	1	921.4	0.026	1.23	19.43
4	2	960.4	0.011	1.42	19.24
4	3	1077.9	0.016	1.42	19.24
4	4	1062.1	0.021	1.42	19.24
5	1	1286.8	0.043	3.26	15.12
5	2	1213.2	0.020	3.69	14.88
5	3	983.4	0.035	3.69	14.85
5	4	964.9	0.035	3.69	14.84

6	1	1310.2	0.0000	5.43	11.91
6	2	1199.9	0.0000	5.35	11.71
6	3	916.3	0.0000	5.44	11.71
6	4	709.1	0.0000	5.44	11.71
6	5	704.1	0.0000	5.44	11.71
6	6	680.2	0.0058	5.06	11.22
6	7	674.9	0.0344	5.08	11.91
6	8	592.9	0.0114	5.93	11.79
6	9	514.9	0.0477	6.23	11.55
6	9	388.0	0.0719	7.14	11.51
6	9	368.0	0.062	7.37	11.25
6	9	316.9	0.041	7.22	11.51
6	9	279.6	0.064	6.50	11.82
6	9	233.0	0.035	6.60	11.91
6	9	224.6	0.0178	6.60	11.82
10	1	138.2	0.0174	7.38	11.74
10	2	117.5	0.0377	6.77	11.91
10	3	155.7	0.0119	6.77	11.91
10	4	151.9	0.0103	6.77	11.91
10	1	159.7	0.0186	6.66	11.85
10	1	146.2	0.0383	5.14	11.81
10	3	126.3	0.0124	6.14	11.81
10	4	97.2	0.0197	6.14	11.81

SECTION POSITION: 1

SIDEWALL TEMPERATURES (°C):

788.9 739.2 696.4 660.3 540.2 300.0 140.5 57.2 47.6 38.3

CENTRAL WALL TEMPERATURES (°C):

786.5 733.3 697.1 662.6 550.0 333.6 236.1 185.3 181.6 180.4

FOUNDATION TEMPERATURES (°C):

743.6 746.2 746.3 742.6 686.2 508.6 289.9 164.2 127.2 90.0

SECTION POSITION: 2

COVER TEMPERATURES (°C):

717.2 522.2 310.9 94.7

SIDEWALL TEMPERATURES (°C):

734.9 685.4 642.9 607.3 490.6 262.2 124.1 52.1 43.9 36.0

CENTRAL WALL TEMPERATURES (°C):

728.3 680.2 639.1 604.9 493.8 282.5 190.6 142.7 139.3 138.2

FOUNDATION TEMPERATURES (°C):

851.0 844.5 837.9 825.5 739.5 531.6 294.1 164.7 127.2 90.0

SECTION POSITION: 3

COVER TEMPERATURES (°C):

816.9 579.3 341.5 100.8

SIDEWALL TEMPERATURES (°C):

767.5 719.0 675.5 639.7 522.1 389.6 236.0 55.9 46.7 37.9

CENTRAL WALL TEMPERATURES (°C):

766.1 719.0 677.1 643.1 533.2 325.6 234.7 187.4 194.0 182.9

FOUNDATION TEMPERATURES (°C):

996.4 989.9 983.0 969.4 773.9 544.5 291.1 161.7 125.5 91.1

SECTION POSITION: 4

COVER TEMPERATURES (°C):

1066.7 834.9 489.1 129.1

SIDEWALL TEMPERATURES (°C):

712.5 663.1 621.1 596.2 473.5 256.9 120.0 51.6 43.5 35.9

CENTRAL WALL TEMPERATURES (°C):

708.3 660.4 619.9 586.7 480.8 285.9 205.2 163.2 160.1 159.2

FOUNDATION TEMPERATURES (°C):

979.4 960.6 944.2 916.7 776.3 519.6 267.1 151.0 119.8 90.0

SECTION POSITION: 5

COVER TEMPERATURES (°C):

1212.9 853.1 490.8 128.3

SIDEWALL TEMPERATURES (°C):

655.5 606.4 565.0 531.2 424.1 225.9 108.7 47.6 40.6 33.9

CENTRAL WALL TEMPERATURES (°C):

649.3 601.6 561.6 529.3 428.4 249.1 178.9 142.3 139.7 138.9

FOUNDATION TEMPERATURES (°C):

922.5 906.9 890.6 863.0 714.1 458.3 226.1 133.6 111.8 90.0

SECTION POSITION: 6

COVER TEMPERATURES (°C):

1208.6 832.3 470.1 124.4

SIDEWALL TEMPERATURES (°C):

594.2 545.3 504.7 472.2 372.4 196.8 96.3 43.9 37.9 32.1

CENTRAL WALL TEMPERATURES (°C):

586.6 539.1 499.8 469.7 374.3 214.9 155.4 104.3 100.1 101.4

FOUNDATION TEMPERATURES (°C):

566.1 450.5 434.9 405.8 412.9 341.5 263.5 111.2 99.8 91.0

SECTION POSITION: 7

COVER TEMPERATURES (°C):

701.6 511.9 308.6 94.4

SIDEWALL TEMPERATURES (°C):

527.1 478.6 439.0 408.3 317.9 171.2 95.5 40.8 35.7 30.7

CENTRAL WALL TEMPERATURES (°C):

518.9 471.8 433.5 403.9 318.1 184.9 135.1 109.0 107.3 106.7

FOUNDATION TEMPERATURES (°C):

538.2 510.4 496.0 447.8 303.8 190.3 120.0 98.9 94.1 90.0

SECTION POSITION: 8

COVER TEMPERATURES (°C):

486.7 316.2 190.4 65.3

SIDEWALL TEMPERATURES (°C):

452.6 404.6 366.8 338.0 260.4 150.0 77.8 39.0 34.4 29.9

CENTRAL WALL TEMPERATURES (°C):

444.7 398.0 361.0 333.6 259.7 161.6 118.7 96.4 94.8 94.3

FOUNDATION TEMPERATURES (°C):

471.4 259.7 249.6 233.9 180.6 133.3 103.6 94.1 91.9 90.0

SECTION POSITION: 9

COVER TEMPERATURES (°C):

242.4 164.6 101.1 45.3

SIDEWALL TEMPERATURES (°C):

367.8 320.5 284.5 259.5 200.3 143.6 75.0 39.2 34.8 30.2

CENTRAL WALL TEMPERATURES (°C):

361.0 315.0 280.1 255.9 199.9 149.1 106.9 84.9 83.9 82.7

FOUNDATION TEMPERATURES (°C):

169.6 164.6 160.1 153.4 130.2 109.8 97.0 92.5 91.2 90.0

SECTION POSITION: 10

COVER TEMPERATURES (°C):

151.5 118.5 71.0 36.9

SIDEWALL TEMPERATURES (°C):

266.2 220.2 199.2 169.5 142.0 151.8 90.5 43.2 38.0 30.4

CENTRAL WALL TEMPERATURES (°C):

261.5 216.7 185.7 167.6 141.5 153.7 100.2 72.3 70.3 69.6

FOUNDATION TEMPERATURES (°C):

121.9 119.7 117.9 114.9 106.1 100.5 96.7 93.0 91.7 90.0

SECTION POSITION: 11

COVER TEMPERATURES (°C):

125.4 99.0 69.9 36.8

SIDEWALL TEMPERATURES (°C):

78.2 65.6 75.6 88.8 128.8 179.0 99.9 58.5 49.8 39.9

CENTRAL WALL TEMPERATURES (°C):

77.6 65.5 75.6 88.8 128.8 179.0 100.0 58.6 50.6 45.4

FOUNDATION TEMPERATURES (°C):

95.4 96.6 97.9 99.5 100.0 100.0 100.0 99.9 98.8 90.0

SECTION POSITION: 1

AVER. GAS TEMP. (°C) IN ZONE "B-INSIDE": 163.3

20.0	329.5	326.1	287.1	268.1	263.7	266.1	268.1	268.7
30.8	612.8	620.9	629.2	638.6	651.3	662.1	668.2	670.2
59.1	750.7	762.8	774.6	786.5	796.6	803.4	807.4	808.7
104.0	774.4	786.9	799.1	811.0	821.1	827.9	831.9	833.2
148.3	766.4	778.1	789.4	800.4	809.8	815.9	819.6	820.9
191.5	756.0	766.7	777.0	786.9	795.2	800.7	803.9	805.0
233.5	751.2	761.1	770.5	779.5	786.9	791.8	794.6	795.6
274.4	746.6	755.8	764.1	772.1	778.8	783.1	785.6	786.5
297.2	703.0	710.6	718.2	725.5	735.2	742.7	746.9	748.2
302.9	675.0	681.8	688.6	695.0	703.0	710.2	714.5	715.9

AVER. GAS TEMP. (°C) IN ZONE "B-MIDDLE": 358.4

20.0	301.5	306.0	273.9	259.6	256.1	259.6	262.2	263.1
44.2	539.2	543.3	594.3	603.3	623.8	639.9	648.8	651.7
115.1	660.1	691.7	719.8	745.6	765.6	777.8	764.9	767.3
226.4	713.3	744.7	772.0	796.5	816.0	828.0	835.1	837.4
332.4	748.9	778.0	802.8	824.8	842.4	853.4	859.9	862.0
430.9	780.1	806.4	828.3	847.3	862.9	872.7	878.4	880.3
521.7	809.1	832.2	851.1	867.4	880.7	889.3	894.3	896.0
604.0	831.9	851.3	866.7	879.8	890.8	897.9	902.2	903.6
647.4	810.6	824.1	836.2	847.0	860.0	870.5	876.3	878.2
655.8	787.9	799.9	809.9	818.2	829.4	839.5	845.5	847.4
AVER. GAS TEMP. (°C) IN ZONE "B-OUTSIDE": 152.8								

20.0	334.5	330.5	290.6	271.2	266.5	269.7	270.5	270.1
30.2	626.5	633.1	640.3	648.6	660.3	670.2	675.8	677.6
56.3	768.8	778.9	798.7	798.6	807.2	812.9	816.4	817.5
97.8	791.4	801.8	812.1	822.0	830.6	836.3	839.8	840.9
138.7	780.1	789.9	799.4	808.7	816.6	821.9	825.0	826.1
178.7	767.4	776.3	785.0	793.4	800.6	805.3	809.1	809.0
217.7	762.1	771.5	781.5	786.2	792.7	797.0	799.5	801.4
256.0	757.7	765.5	772.7	779.7	785.6	789.6	792.9	792.7
277.4	711.7	718.2	725.1	732.1	741.5	749.8	752.8	754.0
282.6	683.2	689.1	695.2	701.3	709.1	716.1	720.2	721.6

SECTION POSITION: 2

AVER. GAS TEMP. (°C) IN ZONE "B-INSIDE": 759.0

704.0	719.0	724.5	722.3	725.7	730.1	734.3	736.8	737.7
726.7	799.7	803.8	806.6	809.8	814.7	819.1	821.7	822.5
734.9	869.4	878.5	885.3	891.2	896.3	899.7	901.7	902.4
747.6	867.9	876.2	882.8	888.4	893.1	896.3	899.0	898.8
758.5	845.4	851.3	856.0	860.1	863.6	865.9	867.3	867.7
767.2	825.3	829.1	832.2	834.9	837.2	838.7	839.5	839.9

774.4	815.1	817.8	820.0	821.9	823.5	824.6	825.2	825.4
790.5	815.1	817.4	819.3	821.1	822.6	823.6	824.2	824.3
783.8	803.5	804.8	806.2	807.8	810.0	811.7	812.5	812.8
798.0	797.2	797.9	798.8	799.9	801.6	803.1	804.0	804.2
AVER. GAS TEMP. (°C) IN ZONE "B-MIDDLE": 844.5								

724.2	736.3	738.2	741.4	745.3	750.9	756.8	760.6	761.9
730.7	798.9	808.2	814.7	820.9	829.3	836.9	841.3	842.8
757.8	859.0	875.8	889.1	900.6	910.4	917.1	921.1	922.4
801.8	890.7	907.1	920.5	931.9	941.8	948.4	952.5	953.8
841.3	909.4	923.1	934.5	944.3	952.9	958.8	962.3	963.5
874.2	923.6	934.3	943.5	951.5	958.6	963.5	966.4	967.4
901.0	935.8	943.9	951.2	957.7	963.4	967.4	969.8	970.6
922.8	946.6	952.6	958.4	963.5	968.2	971.5	973.4	974.1
933.4	941.9	944.6	948.8	953.6	959.5	964.3	967.0	967.8
935.0	937.4	938.8	942.0	946.2	951.6	956.4	959.1	960.0
AVER. GAS TEMP. (°C) IN ZONE "B-OUTSIDE": 758.0								

724.2	716.1	716.6	719.6	723.2	727.8	731.9	734.4	735.2
726.6	800.9	804.2	806.6	809.4	813.9	817.9	820.3	821.0
734.4	875.3	882.9	888.5	893.3	897.5	900.3	902.0	902.5
746.4	871.6	878.5	883.8	888.3	892.2	894.7	896.3	896.8
756.9	945.9	950.6	954.3	957.6	960.4	962.2	963.3	963.6
765.6	924.9	927.9	930.3	932.4	934.1	935.3	936.0	936.2
773.1	816.3	818.5	820.2	821.8	823.1	823.9	824.4	824.6
779.8	819.5	821.6	823.2	824.7	826.0	826.9	827.4	827.5
783.5	807.7	809.0	810.4	811.8	813.9	815.4	816.1	816.4
787.0	801.1	801.9	802.8	803.9	805.5	806.9	807.6	807.9

SECTION POSITION: 3

AVER. GAS TEMP. (°C) IN ZONE "B-INSIDE": 955.8

863.5	808.0	806.6	810.4	813.9	818.1	822.2	824.7	825.6
862.0	877.5	879.2	881.6	884.7	889.8	894.4	897.2	898.1

861.4	849.1	856.7	863.5	869.5	875.1	879.1	881.6	882.4
860.5	823.5	829.9	834.1	838.8	843.1	845.0	847.8	848.3
858.3	808.0	830.5	833.4	836.1	838.5	839.2	841.2	841.5
855.0	860.0	862.7	863.8	864.9	866.0	866.7	867.1	867.3
851.2	842.3	849.3	849.6	850.1	850.5	850.7	850.9	850.9
847.6	855.1	855.3	856.5	857.3	858.0	858.4	858.7	858.8
845.7	854.3	855.0	855.8	856.6	857.6	858.1	858.4	858.5
849.8	850.4	850.7	851.3	852.0	852.8	853.4	853.7	853.7
AVER. GAS TEMP. (°C) IN ZONE "B-MIDDLE": 825.7								
863.5	835.5	833.7	838.3	843.5	850.7	858.2	863.0	864.7
863.5	887.7	893.3	899.9	906.9	915.9	925.2	931.8	933.5
879.0	853.6	869.7	884.4	897.1	909.1	919.1	923.7	925.5
884.3	872.1	887.1	900.4	911.7	922.3	933.3	935.1	936.7
826.7	877.5	889.0	899.1	907.6	915.7	923.6	925.2	926.4
843.4	879.3	887.4	894.6	900.6	906.2	911.3	912.7	913.5
855.3	880.3	885.9	890.8	894.8	898.5	901.2	902.7	903.2
864.3	884.4	888.9	892.6	895.6	898.4	900.3	901.4	901.8
868.7	882.6	885.7	888.9	891.9	895.3	897.9	899.1	899.5
869.4	879.3	881.6	884.2	886.9	890.0	892.5	893.8	894.2
AVER. GAS TEMP. (°C) IN ZONE "B-OUTSIDE": 857.0								
863.5	839.5	839.0	842.0	845.5	849.4	853.0	855.0	855.9
862.0	873.3	874.4	876.1	878.5	882.9	886.8	889.1	889.8
861.8	848.5	854.4	859.6	864.3	868.6	871.7	873.6	874.2
861.1	817.9	821.7	825.5	829.0	832.1	834.3	835.6	836.0
859.1	879.3	880.8	882.5	884.2	885.8	886.9	887.6	887.8
856.2	853.2	853.2	853.6	854.0	854.5	854.8	855.0	855.1
852.9	843.2	842.8	842.7	842.7	842.7	842.7	842.7	842.7
849.9	854.3	854.7	855.1	855.6	856.0	856.3	856.4	856.5
848.3	855.0	855.4	856.0	856.5	856.9	857.1	857.2	857.2
850.8	851.0	851.2	851.5	852.0	852.4	852.6	852.6	852.6

SECTION POSITION: 4

AVER. GAS TEMP. (°C) IN ZONE "B-INSIDE": 979.9

960.4	1071.9	1079.1	1075.8	1073.2	1070.3	1068.1	1066.9	1066.5
963.9	1135.2	1149.4	1152.7	1152.9	1150.9	1147.8	1145.7	1145.0
970.5	1070.9	1077.4	1077.3	1074.4	1069.7	1064.6	1061.2	1060.0
977.5	995.3	993.7	987.5	979.8	971.2	964.1	959.5	958.0
981.2	942.8	936.6	927.0	916.4	905.7	897.5	890.3	890.6
982.9	905.3	896.3	885.0	872.9	861.4	852.8	847.4	845.6
983.5	881.8	871.6	860.0	848.0	836.9	828.9	824.0	822.3
983.7	885.6	876.2	866.9	857.9	849.7	844.0	840.5	839.3
983.9	931.9	926.5	920.0	913.2	903.7	895.8	891.2	899.6
988.7	960.1	956.5	951.8	946.7	939.7	932.5	927.9	926.4

AVER. GAS TEMP. (°C) IN ZONE "B-MIDDLE": 1098.1

960.4	1077.2	1102.7	1113.1	1119.9	1124.4	1129.2	1139.2	1139.8
984.3	1147.2	1193.3	1199.3	1206.3	1211.6	1213.7	1214.4	1214.6
1032.6	1135.3	1157.3	1165.9	1168.0	1167.6	1164.5	1162.2	1161.3
1088.2	1123.6	1129.9	1126.9	1122.5	1116.3	1109.7	1105.5	1104.0
1119.3	1107.9	1101.2	1092.0	1083.2	1073.5	1065.3	1060.2	1058.5
1132.7	1097.3	1072.4	1058.2	1046.4	1034.5	1025.5	1020.0	1019.1
1133.8	1065.4	1045.3	1029.5	1014.9	1002.2	993.2	987.8	986.1
1129.5	1051.7	1030.7	1014.4	1001.9	990.7	983.2	979.7	977.1
1125.3	1070.9	1058.7	1045.4	1035.5	1024.9	1016.3	1011.3	1009.6
1126.2	1093.1	1083.2	1073.4	1066.0	1059.0	1050.2	1045.3	1043.6

AVER. GAS TEMP. (°C) IN ZONE "B-OUTSIDE": 986.1

960.4	1067.1	1071.4	1065.7	1061.7	1057.9	1054.0	1052.2	1051.6
964.3	1131.1	1141.3	1142.1	1140.9	1137.4	1133.1	1130.4	1129.5
971.3	1060.0	1063.6	1061.4	1057.0	1051.0	1045.1	1041.2	1039.9
980.9	979.3	976.5	968.7	959.3	949.5	941.5	936.5	934.7
987.0	928.3	921.3	910.6	898.6	886.6	877.3	871.5	869.5
991.4	990.6	984.5	972.6	959.4	946.7	937.2	931.3	929.0

994.8	974.8	964.8	952.8	939.8	927.8	919.1	913.6	911.9
997.8	985.7	976.9	967.2	957.6	948.6	942.2	939.2	936.9
999.6	989.6	984.3	976.9	973.5	966.4	966.4	960.6	958.7
1003.9	969.0	965.2	959.6	952.7	943.1	933.6	927.7	925.7

SECTION POSITION: 5

AVER. GAS TEMP. (°C) IN ZONE "B-INSIDE": 1044.6

1213.2	1208.1	1207.0	1207.0	1206.2	1204.6	1202.3	1200.5	1199.9
1199.1	1186.8	1147.9	1142.5	1136.2	1128.3	1121.2	1116.9	1115.6
1182.2	1044.7	1021.7	1002.3	995.7	970.1	958.7	951.7	949.4
1095.4	949.0	922.1	897.0	873.3	851.2	835.3	825.3	821.9
1043.1	891.4	865.6	840.2	814.8	791.4	774.6	764.1	760.6
1008.2	850.0	826.2	802.0	776.9	753.8	737.6	727.4	723.9
974.2	822.0	800.8	778.7	755.3	734.2	719.3	710.1	707.0
948.3	826.6	810.6	794.4	777.8	762.7	751.0	745.4	743.1
930.6	892.2	886.3	878.6	869.1	858.9	840.8	832.9	831.3
933.9	923.5	921.0	916.6	909.9	899.1	887.2	879.5	876.9

AVER. GAS TEMP. (°C) IN ZONE "B-MIDDLE": 1111.5

1213.2	1223.1	1236.8	1244.3	1248.2	1252.4	1255.4	1256.8	1257.2
1214.8	1205.1	1200.4	1197.7	1195.9	1193.3	1191.2	1189.9	1189.5
1199.1	1185.6	1130.7	1116.0	1101.7	1088.0	1077.3	1070.7	1068.5
1165.8	1104.1	1073.9	1049.0	1024.7	1004.8	989.9	984.7	981.6
1126.6	1059.2	1027.0	1000.1	976.9	955.1	934.2	929.3	926.1
1097.5	1015.8	985.4	959.3	933.9	911.1	894.5	884.1	880.6
1050.2	979.8	950.1	924.1	900.0	877.5	861.2	851.0	847.6
1017.8	957.3	934.6	913.8	894.3	876.3	863.2	855.1	852.3
1002.8	983.1	975.3	965.4	953.9	937.5	923.0	914.3	911.4
1002.4	1003.9	1002.6	998.3	992.3	979.9	965.7	957.3	954.5

AVER. GAS TEMP. (°C) IN ZONE "B-OUTSIDE": 1069.6

1213.2	1201.1	1199.8	1197.6	1196.1	1194.4	1193.9	1197.5	1196.7
1197.8	1146.4	1136.6	1129.1	1123.0	1117.8	1113.7	1110.9	1109.7

1163.7	1021.3	997.4	976.7	958.4	941.3	928.9	921.1	919.5
1115.8	925.2	897.4	870.8	844.7	820.4	810.9	791.9	788.1
1074.5	870.6	846.0	819.1	791.4	765.8	747.5	736.0	732.1
1038.7	836.2	811.5	785.8	758.6	733.6	715.9	704.9	701.1
1007.5	813.1	790.9	767.4	742.2	719.2	703.2	693.1	689.7
980.5	826.1	808.9	791.3	772.9	756.2	744.3	736.9	734.4
966.6	803.7	835.7	885.5	873.1	854.1	837.8	828.2	825.0
968.9	836.8	831.9	824.7	814.9	807.0	794.9	875.8	870.1

SECTION POSITION: 6

AVER. GAS TEMP. (°C) IN ZONE "B-INSIDE": 1015.4

1189.8	1208.7	1212.1	1210.8	1208.4	1203.8	1197.6	1193.1	1191.5
1168.6	1108.5	1091.2	1078.1	1066.1	1047.3	1029.5	1018.6	1014.8
1125.2	925.2	878.0	830.3	779.8	730.8	694.5	671.3	663.3
1065.7	844.3	799.3	749.7	699.1	639.9	600.4	575.6	567.0
1017.5	797.9	757.8	711.7	657.4	606.5	570.2	546.8	538.7
977.6	763.1	727.0	684.6	633.3	585.4	552.0	530.2	522.6
944.1	737.6	705.4	666.4	619.8	575.1	544.0	523.8	516.7
915.7	742.6	716.6	685.9	649.2	615.4	590.6	574.1	568.3
901.5	865.2	858.4	848.7	834.1	807.5	791.3	764.2	758.3
904.9	901.0	898.7	893.2	881.1	864.8	840.8	824.2	818.3

AVER. GAS TEMP. (°C) IN ZONE "B-MIDDLE": 1040.2

1199.8	1215.6	1230.0	1236.4	1239.1	1239.7	1235.2	121	731.4
1191.7	1164.1	1146.0	1132.4	1121.2	1104.2	1088.7		1.5
1161.0	1063.4	1005.7	953.4	904.5	844.6			79.9
1103.8	995.8	938.8	884.1	829.3	775.4	731.9	709.0	699.8
1050.0	942.3	891.1	839.8	786.4	734.9	696.0	670.6	661.8
1002.2	896.4	850.5	802.9	751.6	702.4	665.6	641.4	633.0
960.1	857.7	816.8	772.9	724.4	679.2	643.6	620.8	612.7
925.3	838.8	806.1	771.0	732.4	695.8	667.7	648.9	642.3
910.4	896.9	890.9	882.1	869.0	848.2	819.3	801.4	794.9

910.3 901.7 923.4 921.3 914.0 898.2 875.1 857.7 851.3
 AVER. GAS TEMP. (°C) IN ZONE "B-OUTSIDE": 1043.6

1169.8	1074.1	1015.1	1002.0	1198.6	1192.7	1165.5	1160.5	1178.7
1173.4	1093.7	1075.9	1062.3	1049.7	1029.9	1011.2	999.6	995.7
1139.3	898.7	843.3	795.6	743.3	693.0	656.3	632.9	624.9
1088.9	813.3	769.2	718.8	659.3	603.2	563.4	538.1	529.4
1047.4	774.1	734.2	686.7	629.2	575.6	537.9	513.8	505.8
1010.1	744.9	709.7	664.8	609.9	559.5	524.2	501.4	493.8
981.7	724.2	691.4	650.5	599.7	553.1	520.9	499.1	491.6
955.4	736.4	709.1	676.3	636.6	599.9	573.1	555.3	549.1
942.0	878.2	868.4	854.9	836.0	803.5	772.4	752.7	745.9
944.7	916.2	910.5	900.8	886.1	861.6	832.7	813.2	806.3

SECTION POSITION: "

AVER. GAS TEMP. (°C) IN ZONE "B-INSIDE": 714.3

717.2	713.1	709.8	711.7	711.0	707.0	699.8	694.0	691.9
719.0	667.8	661.2	652.8	641.8	623.7	605.6	593.7	589.5
707.8	546.1	526.7	496.7	451.1	410.7	397.9	371.6	366.0
716.6	515.9	494.3	458.4	405.8	361.6	335.0	318.1	312.3
715.0	501.8	479.5	442.4	398.0	342.9	316.8	300.5	295.0
713.5	490.5	467.9	430.1	374.9	329.8	304.5	288.9	283.6
711.8	481.7	458.9	421.0	365.9	321.4	297.1	282.3	277.3
710.3	484.9	462.7	427.2	376.5	336.0	313.6	300.2	295.7
709.6	562.9	546.7	527.7	505.1	472.4	444.6	428.8	423.7
712.6	620.6	608.4	592.5	573.1	546.1	519.9	504.9	499.2

AVER. GAS TEMP. (°C) IN ZONE "B-MIDDLE": 693.2

717.2	719.5	721.3	726.5	729.5	732.9	728.7	725.9	724.7
721.6	697.7	690.7	683.3	674.9	662.0	648.8	633.8	636.6
719.8	633.4	608.2	574.5	530.5	492.4	464.5	446.7	440.5
711.1	608.4	579.6	539.1	494.4	436.7	405.8	386.1	379.1
699.9	589.0	559.1	516.1	456.9	406.2	374.9	355.4	348.7

687.6	569.3	539.4	494.6	432.6	392.3	349.4	332.6	324.2
674.7	552.2	522.6	474.3	422.3	359.6	328.3	312.1	305.1
662.1	539.3	503.3	465.3	426.0	357.3	332.4	314.6	303.4
655.3	527.6	559.1	535.9	511.0	477.3	449.7	434.4	423.6
656.5	622.5	611.3	595.5	576.0	549.1	523.7	509.1	504.3

AVER. GAS TEMP. (°C) IN ZONE "B-OUTSIDE": 722.6

707.2	703.3	703.2	704.2	722.5	697.2	689.7	682.3	682.2
719.7	655.4	648.3	642.2	629.3	609.9	589.4	576.3	572.2
720.2	515.0	497.2	467.1	422.9	385.1	362.5	346.2	342.9
721.6	493.2	463.5	429.3	376.3	333.3	308.9	293.0	287.6
722.7	470.2	449.3	414.1	362.5	316.3	292.2	277.0	271.3
723.5	460.3	439.6	403.3	349.1	325.5	281.6	267.1	262.1
724.1	453.1	432.2	395.9	341.9	329.0	276.0	262.1	257.5
724.9	459.6	439.2	405.1	355.7	316.6	295.5	282.3	279.6
725.2	546.4	530.8	512.3	489.8	457.2	429.9	414.3	409.3
727.3	606.6	594.1	578.1	559.4	531.4	505.4	492.0	485.0

SECTION POSITION: 3

AVER. GAS TEMP. (°C) IN ZONE "B-INSIDE": 477.3

514.3	492.2	477.3	492.3	482.3	473.6	476.3	474.3	474.1
502.2	392.3	372.6	358.2	339.6	315.4	297.1	287.7	284.9
504.2	323.6	294.2	267.3	229.2	202.6	189.4	181.4	179.1
492.2	292.6	277.4	252.5	211.2	193.4	177.4	164.5	162.3
492.6	292.3	268.3	242.9	204.9	179.3	166.7	162.1	159.2
469.7	274.3	262.1	237.2	211.3	175.5	164.6	159.3	156.2
459.1	264.2	257.1	232.5	194.2	175.2	164.3	159.7	156.3
449.2	270.3	259.6	238.4	207.6	192.4	177.1	171.7	170.2
443.7	294.6	284.6	270.3	260.8	244.1	231.2	224.3	222.1
443.5	320.2	311.1	302.6	289.2	274.3	262.5	255.6	253.4

AVER. GAS TEMP. (°C) IN ZONE "B-MIDDLE": 430.5

514.3	507.2	515.3	508.1	509.2	505.4	500.7	497.3	496.1
-------	-------	-------	-------	-------	-------	-------	-------	-------

510.2	445.1	430.6	411.7	399.2	359.1	334.2	321.5	317.6
492.4	393.6	370.5	337.2	287.2	257.2	232.6	222.6	219.4
464.2	365.8	346.2	312.4	264.2	228.9	212.9	203.7	200.9
437.6	342.3	324.6	293.4	249.7	216.7	202.3	194.1	191.5
412.6	320.2	305.1	276.5	235.6	206.7	193.8	186.5	184.1
389.2	301.9	287.6	261.7	224.6	198.8	187.4	180.9	178.8
367.4	287.9	275.6	253.4	222.3	200.9	191.5	186.2	184.4
355.7	286.5	287.2	276.7	265.8	251.7	240.9	235.2	233.2
353.6	316.9	312.2	302.1	293.1	291.7	271.7	266.2	264.2
AVER. GAS TEMP. (°C) IN ZONE "B-OUTSIDE": 480.4								

514.9	469.4	467.4	470.4	471.8	471.6	469.9	468.6	468.2
512.2	363.4	354.3	341.5	324.7	302.9	286.7	279.4	275.9
505.2	281.8	269.4	245.5	212.8	186.6	176.1	170.1	168.2
494.3	264.4	252.1	228.1	193.2	168.7	158.3	152.4	150.5
483.7	256.2	244.3	221.1	187.2	163.6	153.6	147.9	146.2
473.6	249.7	238.5	216.3	183.6	161.3	151.7	146.2	144.4
463.8	245.3	234.7	213.6	182.6	161.8	152.4	147.2	145.5
454.4	249.5	239.7	220.6	193.2	174.1	166.2	161.3	159.8
449.2	278.8	269.9	259.9	246.6	233.4	221.6	215.3	213.4
448.9	325.2	297.2	287.5	277.3	264.3	253.1	246.9	244.9

SECTION POSITION: 9

AVER. GAS TEMP. (°C) IN ZONE "B-INSIDE": 271.2

279.6	240.3	233.2	240.7	241.7	241.5	240.1	238.8	239.3
279.2	221.1	197.5	191.3	183.1	172.9	165.3	161.4	160.2
277.4	166.4	161.4	151.2	135.8	125.4	121.6	119.1	118.9
274.6	158.4	153.2	142.3	126.4	115.9	111.5	108.9	108.1
271.9	155.9	150.7	139.9	123.9	113.4	109.2	106.4	105.5
269.3	154.6	149.5	138.8	123.1	112.6	108.3	105.7	104.9
266.7	154.1	149.1	138.7	123.4	113.1	109.2	106.5	105.7
264.2	158.3	153.7	144.1	132.2	121.2	117.2	114.8	114.1

262.8	175.0	170.8	166.1	160.7	153.1	147.1	143.8	142.7
263.1	197.8	184.0	179.6	174.7	168.0	162.5	159.0	158.0
AVER. GAS TEMP. (°C) IN ZONE "B-MIDDLE": 246.3								

279.6	264.2	262.4	262.8	262.0	259.8	256.7	254.4	253.7
277.5	239.0	232.2	222.8	210.9	196.8	186.4	180.9	179.3
270.7	215.6	207.4	191.6	168.9	153.7	147.2	143.4	142.2
259.9	205.1	197.0	181.5	158.8	143.6	137.2	133.5	132.3
249.4	196.8	189.4	174.5	152.9	138.4	132.3	128.8	127.6
239.4	189.3	182.4	168.4	148.1	134.5	129.7	125.4	124.3
229.9	182.5	176.1	163.1	144.2	131.5	126.2	123.1	122.1
220.9	178.4	172.8	161.5	145.3	134.5	130.0	127.3	126.4
216.1	184.3	179.9	175.0	169.7	162.4	156.5	153.3	152.1
215.2	194.6	191.4	187.5	183.0	177.0	171.6	168.4	167.4
AVER. GAS TEMP. (°C) IN ZONE "B-OUTSIDE": 271.0								

279.6	233.7	232.6	234.8	236.5	237.0	236.2	235.3	234.9
279.0	192.1	189.0	183.6	176.4	167.3	160.6	157.1	156.0
277.3	154.5	150.2	142.2	129.1	119.5	115.9	113.7	113.0
274.7	145.5	141.1	131.7	117.9	109.9	105.1	102.9	102.0
272.0	142.9	139.5	129.1	115.3	106.2	102.5	100.3	99.5
269.9	141.7	137.4	128.1	114.5	105.5	101.8	99.6	98.9
266.7	141.4	137.2	128.2	115.0	106.2	102.6	100.5	99.4
264.2	146.7	142.7	134.5	122.5	114.7	111.4	109.4	108.9
262.8	166.8	163.2	159.3	154.5	147.7	142.4	139.4	138.5
263.0	190.0	176.7	172.9	168.6	163.0	157.9	155.0	154.1

SECTION POSITION: 10

AVER. GAS TEMP. (°C) IN ZONE "B-INSIDE":

177.5	154.9	154.0	155.1	155.5	155.2	154.4	153.8	153.6
177.3	137.4	135.8	132.9	129.7	123.3	119.4	117.4	116.7
176.9	112.3	109.8	104.4	96.5	91.2	99.0	95.7	97.3
176.0	105.5	102.8	97.0	98.2	82.5	80.1	79.7	79.2

175.1	104.3	102.6	95.7	96.8	92.0	78.5	77.1	76.6
174.3	103.4	101.1	95.0	96.4	90.6	79.2	76.9	76.3
173.4	103.5	100.8	95.0	96.3	90.6	79.2	76.9	76.4
172.6	105.2	102.7	97.3	89.3	94.1	81.9	80.5	80.1
172.1	109.1	106.0	113.5	110.4	106.0	102.4	100.4	99.7
172.4	106.8	104.8	102.5	119.7	116.0	112.6	110.6	110.0

AVER. GAS TEMP. (°C) IN ZONE "B-MIDDLE": 161.4

177.5	168.1	167.1	166.9	165.9	164.0	161.8	160.3	159.8
176.5	156.3	153.7	148.9	142.4	134.5	128.6	125.5	124.5
173.4	141.8	137.5	129.3	114.7	105.6	101.8	99.6	98.8
168.2	135.3	130.9	121.2	106.8	97.2	93.2	91.9	90.1
163.1	131.2	127.0	117.6	103.7	94.4	90.5	89.0	87.4
159.1	127.6	123.5	114.7	101.3	92.5	88.8	86.6	85.9
153.4	124.2	120.4	112.0	99.4	91.0	87.5	85.4	84.7
148.8	122.1	118.6	111.1	100.1	92.6	89.5	87.7	87.0
146.4	126.8	124.1	121.0	117.3	112.2	107.9	105.4	104.6
145.9	133.6	131.8	129.2	125.2	122.0	117.9	115.5	114.7

AVER. GAS TEMP. (°C) IN ZONE "B-OUTSIDE": 174.6

177.5	152.1	151.6	152.6	153.4	153.5	153.1	152.7	152.8
177.3	133.6	132.3	129.7	126.1	121.3	117.7	116.0	115.4
176.9	106.6	104.5	99.9	93.1	88.7	86.8	85.7	85.3
175.9	99.2	96.9	91.9	84.5	79.6	77.6	76.4	76.0
175.0	97.9	95.6	90.6	83.1	78.1	76.1	74.8	74.4
174.0	97.5	95.2	90.2	82.7	77.8	75.8	74.5	74.1
173.1	97.2	95.0	90.1	82.7	77.9	75.8	74.7	74.3
172.3	99.3	97.1	92.6	85.8	81.5	79.6	78.0	78.1
171.8	114.4	112.6	110.5	107.9	103.9	100.7	99.0	98.4
171.9	123.3	121.6	119.6	117.2	114.0	111.0	109.3	108.7

SECTION POSITION: 11

AVER. GAS TEMP. (°C) IN ZONE "B-INSIDE": 132.9

146.2	99.3	102.1	129.1	172.9	202.1	207.2	207.7	207.7
145.0	92.6	95.4	125.1	166.2	190.0	193.5	193.6	193.6
142.3	87.2	87.6	97.0	91.4	67.7	52.0	44.6	42.8
138.3	86.4	97.0	96.5	90.6	66.5	50.6	43.1	41.2
134.3	95.3	96.5	96.3	90.6	66.5	50.6	43.1	41.2
130.4	85.1	86.0	96.0	90.5	66.5	50.6	43.1	41.2
126.5	84.5	85.6	95.9	90.4	66.5	50.6	43.1	41.2
122.9	93.9	84.9	95.2	90.1	66.3	50.6	43.2	41.4
120.6	55.3	53.4	52.2	51.6	51.1	50.3	50.0	50.0
120.3	59.4	57.6	56.5	56.0	55.9	55.6	55.6	55.6
AVER. GAS TEMP. (°C) IN ZONE "B-MIDDLE": 120.7								

146.2	113.1	112.7	134.8	174.4	202.2	207.2	207.7	207.7
143.9	105.9	105.0	130.1	167.5	190.1	193.5	193.6	193.6
139.5	98.6	95.7	101.1	92.4	67.9	52.0	44.6	42.8
130.4	94.9	92.7	99.3	91.3	66.6	50.6	43.1	41.2
122.7	91.4	90.2	99.0	91.0	66.6	50.6	43.1	41.2
115.5	98.5	97.9	96.9		66.6	50.6	43.1	41.2
109.3	86.0	86.1	95		66.5	50.6	43.1	41.2
102.4	93.7	84.3		90.0	66.3	50.6	43.2	41.4
99.3	57.0	53.6		51.6	51.1	50.3	50.0	50.0
97.7	60.9	57.6	56.3	56.0	55.9	55.6	55.6	55.6
AVER. GAS TEMP. (°C) IN ZONE "B-OUTSIDE": 103.6								

146.2	97.7	100.9	128.6	172.6	202.0	207.2	207.7	207.7
145.0	91.0	94.5	124.8	166.0	190.0	193.5	193.6	193.6
142.6	85.9	86.7	96.6	91.3	67.7	52.0	44.6	42.8
139.7	85.4	86.0	96.2	90.5	66.5	50.6	43.1	41.2
134.9	84.8	85.8	96.0	90.5	66.5	50.6	43.1	41.2
131.2	84.0	95.0	95.8	90.4	66.5	50.6	43.1	41.2
127.6	93.9	95.1	95.6	90.4	66.5	50.6	43.1	41.2
124.0	93.0	94.6	95.1	90.0	66.3	50.6	43.2	41.4
121.9	54.6	53.1	52.1	51.6	51.1	50.3	50.0	50.0

121.6 58.7 57.3 56.4 56.0 55.8 55.6 55.6 55.6

BURNED VOLATILE MASS FLOW (KG S):

SECT.POS.	TAR	H2	CH4
1	0.00000	0.00000	0.00000
2	0.00000	0.00000	0.00000
3	0.00000	0.00000	0.00000
4	0.00000	0.00000	0.00000
5	0.00000	0.00000	0.00000
6	0.00000	0.00107	0.00109
7	0.01249	0.00000	0.00000
8	0.00000	0.00000	0.00000
9	0.00000	0.00000	0.00000
10	0.00000	0.00000	0.00000
11	0.00000	0.00000	0.00000

LOST VOLATILE MASS FLOW (KG S):

SECT.POS.	TAR	H2	CH4
1	0.00000	0.00000	0.00000
2	0.00000	0.00000	0.00000
3	0.00000	0.00000	0.00000
4	0.00000	0.00000	0.00000
5	0.00000	0.00000	0.00000
6	0.00000	0.00000	0.00000
7	0.00000	0.00000	0.00000
8	0.00026	0.00000	0.00000
9	0.00002	0.00000	0.00000
10	0.00000	0.00000	0.00000
11	0.00000	0.00000	0.00000

FUEL CONSUMPTION (KG S):

FUEL CONSUMPTION (KG S):

SECT.POS.	FUEL	G.M.F.	PRESS.
1	0.00000	1.09454	0.00000
2	0.00000	1.14539	-0.93874
3	0.00000	1.23142	-2.92449
4	0.00000	1.35127	-5.48695
5	0.01032	1.50876	-9.47362
6	0.01946	1.70791	-15.13502
7	0.00000	1.95041	-22.47284
8	0.00000	2.23003	-29.95730
9	0.00000	2.54207	-37.19185
10	0.00000	2.88156	-44.00944
11	0.00000	3.24598	-50.71024

GAS TEMP. PROFILE

152.9 685.6 874.3 940.9 1250.0 1290.0 740.7 553.9 298.2 187.9

FUEL CONSUMPTION 0.01032 0.01946 0.00000

PERMUTATION NUMBER: 9

TIME (HRS) = 2.000

SECT.	POSITION	GAS TEMP. (C)	EMISSIVITY	CO2 (% vol.)	OXYGEN (% vol.)
1	2	20.0	0.004	0.00	20.66
1	3	450.3	0.005	0.00	20.66
1	4	485.6	0.006	0.00	20.66
2	1	559.9	0.024	0.00	20.66
2	2	643.4	0.010	0.76	19.90
2	3	856.9	0.013	0.76	19.90
2	4	863.2	0.020	0.76	19.90
3	1	878.2	0.023	0.75	19.91
3	2	857.6	0.010	1.17	19.49
3	3	924.4	0.015	1.17	19.49
3	4	919.4	0.015	1.17	19.49
4	1	921.2	0.023	1.15	19.51
4	2	919.9	0.008	1.32	19.34
4	3	1058.3	0.013	1.32	19.34
4	4	1050.6	0.018	1.32	19.34
5	1	1289.3	0.038	2.56	16.56
5	2	1210.7	0.018	3.00	16.26
5	3	991.2	0.034	2.99	15.95
5	4	970.4	0.031	2.99	15.97
5	1	1310.9	0.054	4.90	11.97
5	2	1129.1	0.025	4.93	12.03
5	3	916.2	0.048	4.90	11.91
5	4	907.2	0.036	4.91	11.97
6	1	790.8	0.095	4.82	11.55
7	2	729.2	0.040	4.69	12.11
7	3	662.0	0.066	5.77	10.87
7	4	653.4	0.055	6.04	10.56
8	1	576.3	0.120	5.92	10.76
8	2	506.4	0.056	5.33	11.74
8	3	385.5	0.092	5.33	11.74
8	4	365.6	0.066	5.33	11.74
9	1	317.0	0.152	5.23	11.91
9	2	280.9	0.069	4.73	12.76
9	3	234.7	0.105	4.73	12.76
9	4	225.8	0.091	4.73	12.76
10	1	199.9	0.165	4.64	12.90
10	2	179.8	0.075	4.21	13.62
10	3	157.6	0.111	4.21	13.62
10	4	153.7	0.103	4.21	13.62
11	1	142.5	0.168	4.14	13.74

SECTION	HRS	CASE 2	CASE 3
		TEMPERATURE °C	
F1	2	760	760
	26	1350	1250
	30	1350	1250
F2	0	1350	1250
	30	1350	1250
F3	0	1350	1250
	24	1350	1250
	30	-	1250

ANODE FINISHING TEMPERATURES-INSIDE(°C):

1191.6	1186.9	1184.8	1184.4
1099.5	1094.8	1093.7	1093.7
1036.7	1033.6	1033.3	1033.3
993.5	992.1	992.0	992.1
969.8	969.6	969.8	969.8
969.1	969.1	969.2	969.2

ANODE FINISHING TEMPERATURES-MIDDLE(°C):

1248.6	1244.3	1242.3	1241.9
1193.7	1177.4	1175.7	1175.6
1133.0	1127.6	1126.7	1126.6
1090.9	1087.6	1087.1	1087.1
1059.8	1059.0	1059.1	1059.2
1053.1	1053.1	1053.3	1053.3

ANODE FINISHING TEMPERATURES-OUTSIDE(°C):

1193.2	1178.3	1176.1	1175.7
1090.5	1086.1	1085.4	1085.4
1029.7	1027.3	1027.0	1027.1
990.5	989.1	988.9	989.0
968.6	968.4	968.5	968.6
970.2	970.2	970.2	970.2

AVERAGE FINISHING TEMPERATURE:INSIDE	1041.5
AVERAGE FINISHING TEMPERATURE:MIDDLE	1126.4
AVERAGE FINISHING TEMPERATURE:OUTSIDE	1037.0

ANODE FINISHING TEMPERATURES-INSIDE (°C):

1113.0	1115.1	1113.6	1113.2
1044.1	1045.4	1039.7	1039.7
991.2	998.6	996.2	999.2
953.4	952.1	952.1	952.1
932.1	932.1	932.1	932.2
934.5	934.3	934.4	934.4

ANODE FINISHING TEMPERATURES-MIDDLE (°C):

1168.0	1164.7	1163.2	1162.9
1116.3	1111.5	1110.1	1110.1
1074.7	1070.1	1069.1	1069.1
1033.6	1035.5	1035.2	1035.2
1012.2	1011.6	1011.7	1011.7
1007.7	1007.5	1007.6	1007.6

ANODE FINISHING TEMPERATURES-OUTSIDE (°C):

1109.5	1105.7	1104.1	1103.7
1033.3	1030.3	1029.7	1029.8
982.2	980.2	979.9	979.9
947.7	946.2	946.1	946.1
929.7	929.6	929.8	929.9
933.6	933.4	933.4	933.4

AVERAGE FINISHING TEMPERATURE:INSIDE 994.1

AVERAGE FINISHING TEMPERATURE:MIDDLE 1067.3

AVERAGE FINISHING TEMPERATURE:OUTSIDE 987.7

FUEL CONSUMPTION SUMMARY:

TOTAL FUEL CONS. PER SECTION:

SECT.POS.	FUEL (L)
5	2166477.25
6	3441170.20
7	2541691.75

TOTAL FUEL ENERGY (30 T.B.A.): 2.97

FUEL CONSUMPTION SUMMARY:

TOTAL FUEL CONS. PER SECTION:

SECT. POS.	FUEL (L)
5	2206960.50
6	2392121.50
7	2158241.25

TOTAL FUEL ENERGY (30 T.B.B.): 2.62

VOLATILE SUMMARY:

VOLATILE EVOLUTION PER SECTION (KG):

SECT.POS.	BTAP	BH2	BCH4	LTAP	LH2	LCH4
5	0.00	17.79	0.00	0.00	0.00	0.00
6	0.00	154.49	39.77	0.00	0.00	0.00
7	2925.85	36.51	31.24	0.00	0.00	0.00
8	265.79	0.00	0.00	120.48	0.00	0.00
9	0.00	0.00	0.00	7.73	0.00	0.00
10	0.00	0.00	0.00	0.69	0.00	0.00
11	0.00	0.00	0.00	0.16	0.00	0.00

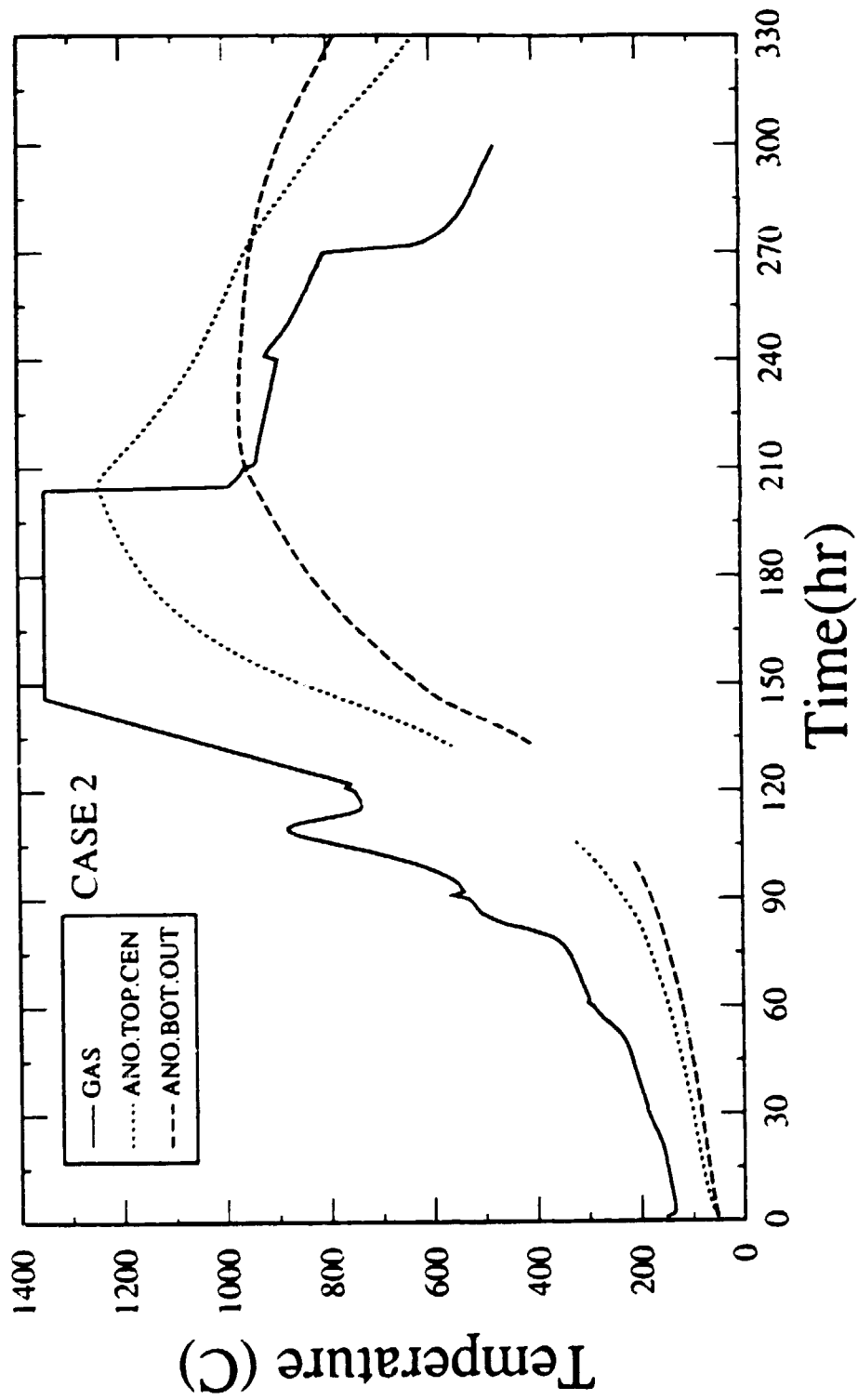
TOTAL VOLATILE LOST (KG): 129.47
 PERCENT VOLATILE LOST (%): 3.70

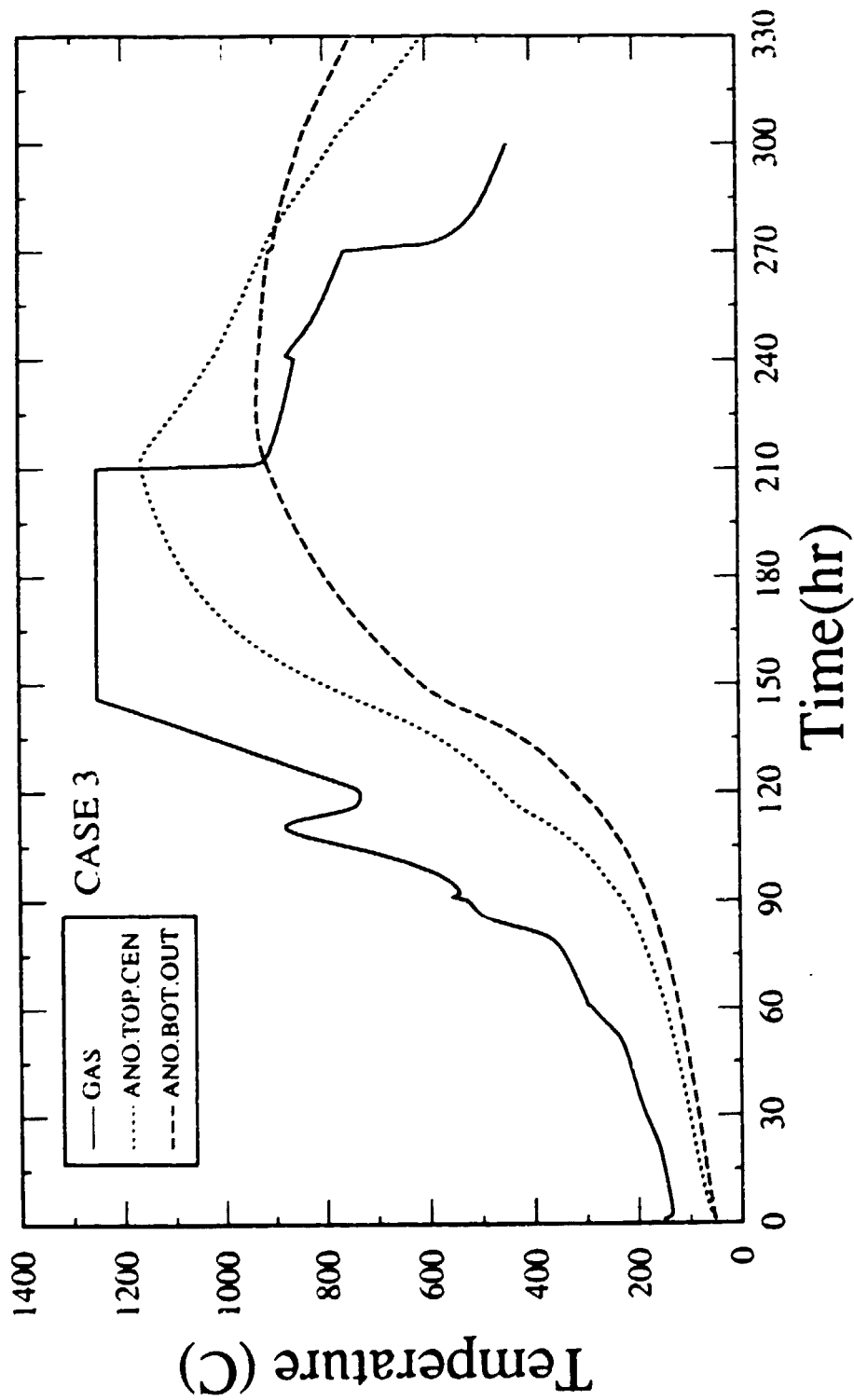
VOLATILE SUMMARY:

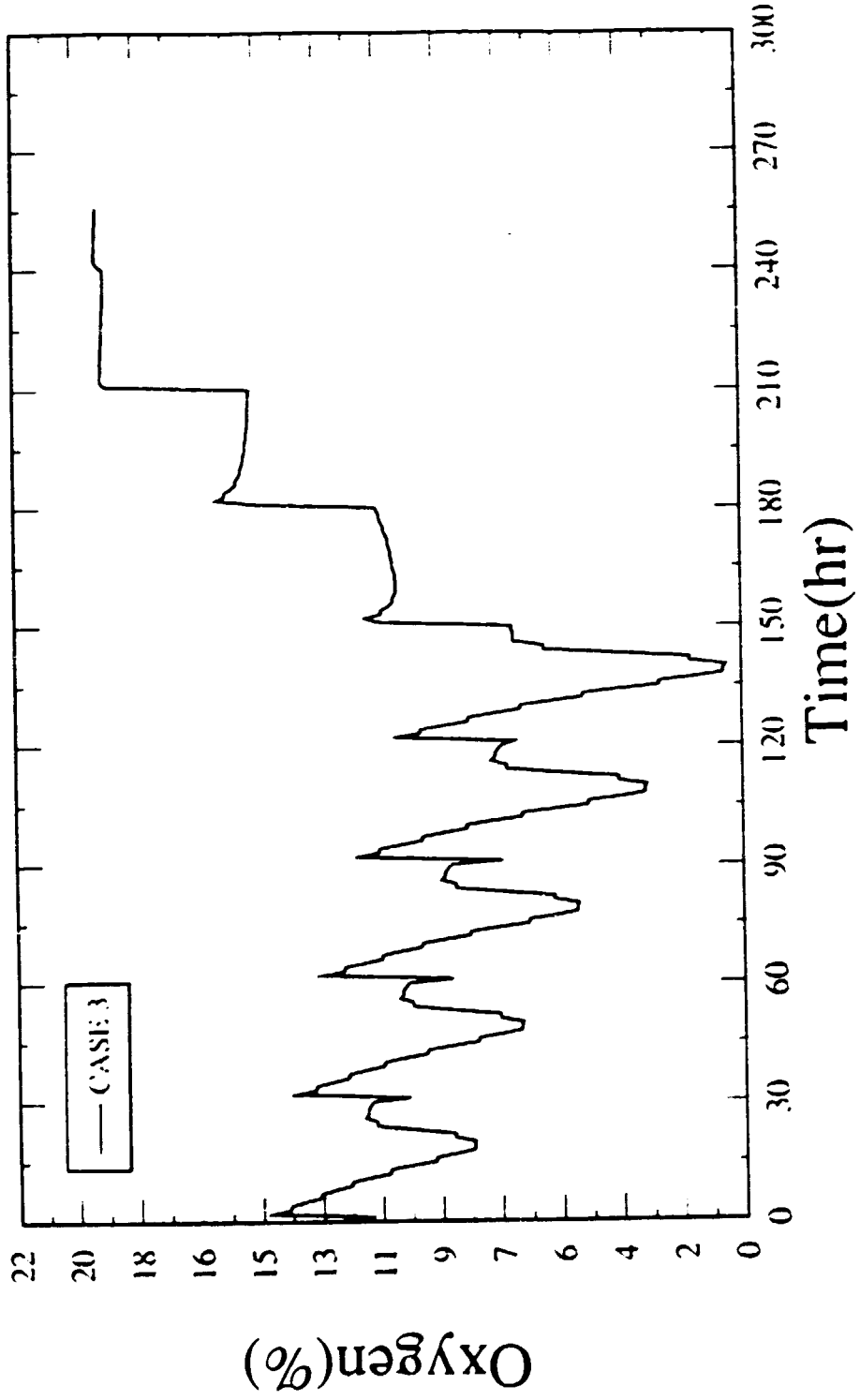
VOLATILE EVOLUTION PER SECTION (KG):

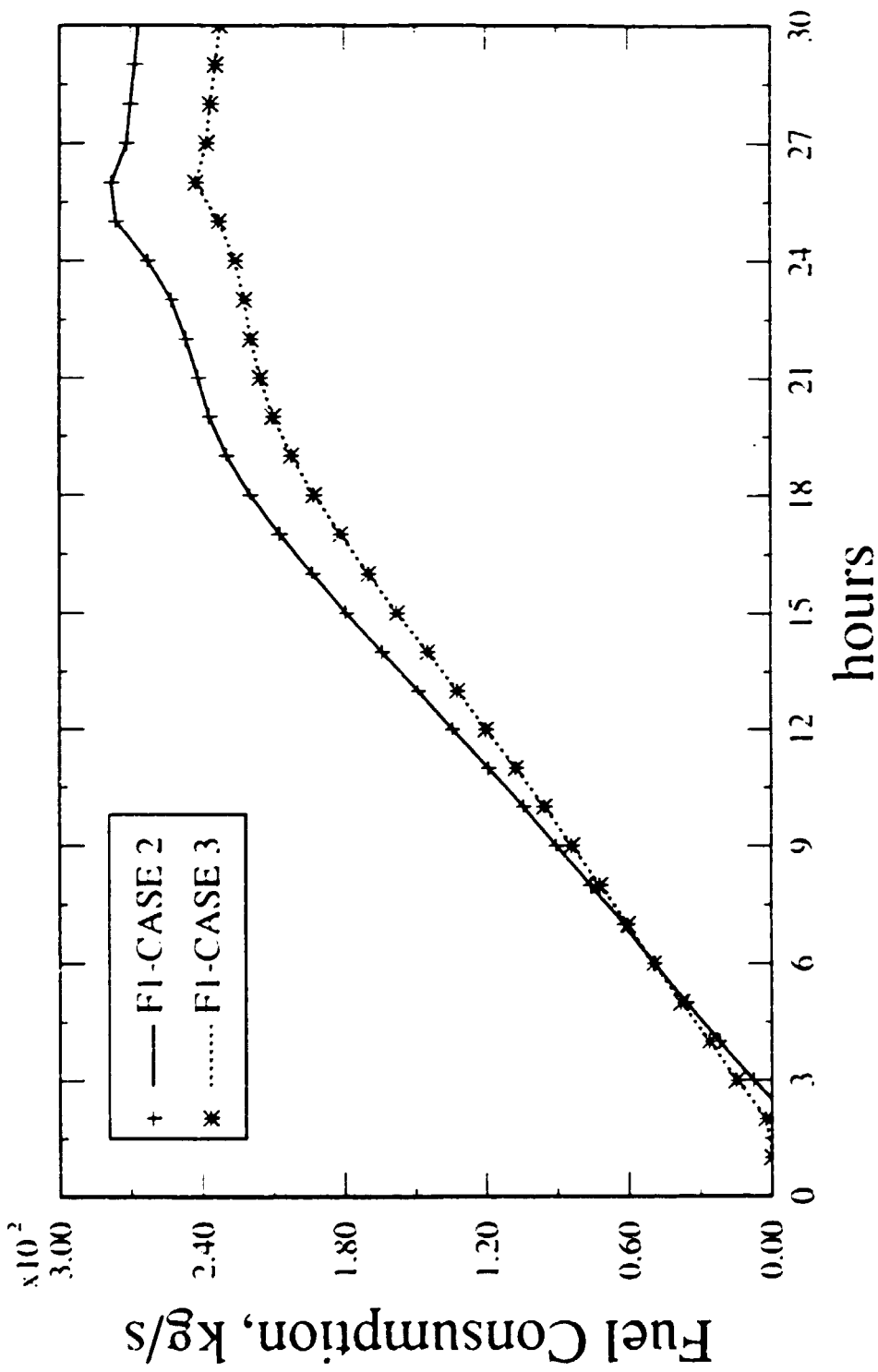
SECT.POS.	BTAP	BH2	BCH4	LTAR	LH2	LCH4
5	0.00	37.06	0.00	0.00	0.00	0.00
6	0.00	142.34	47.64	0.00	0.00	0.00
7	2860.07	27.83	22.51	0.00	0.00	0.00
8	142.22	0.00	0.00	116.54	0.00	0.00
9	0.00	0.00	0.00	7.39	0.00	0.00
10	0.00	0.00	0.00	0.69	0.00	0.00
11	0.00	0.00	0.00	0.16	0.00	0.00

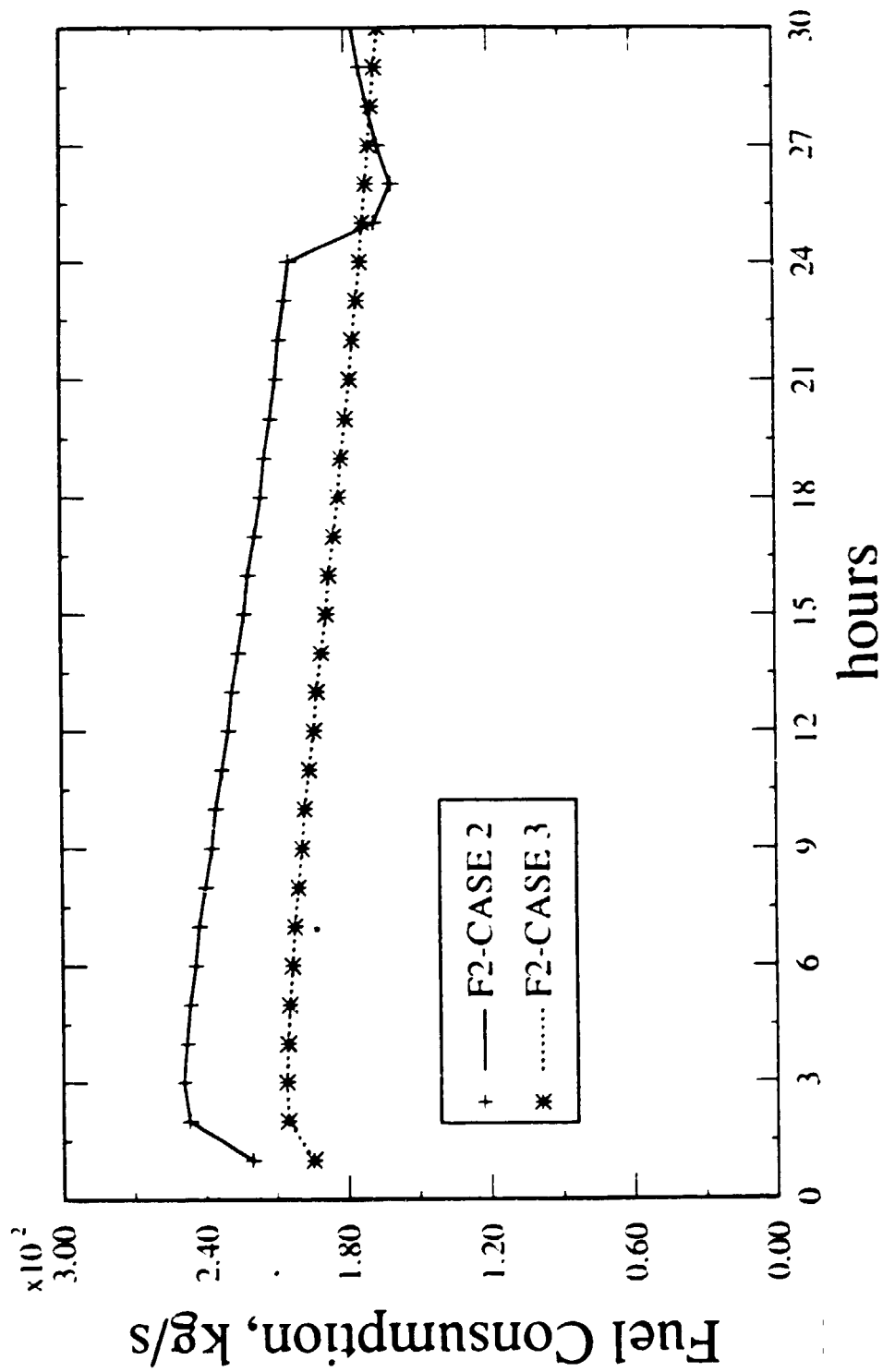
TOTAL VOLATILE LOST (KG): 129.23
 PERCENT VOLATILE LOST (%): 3.57

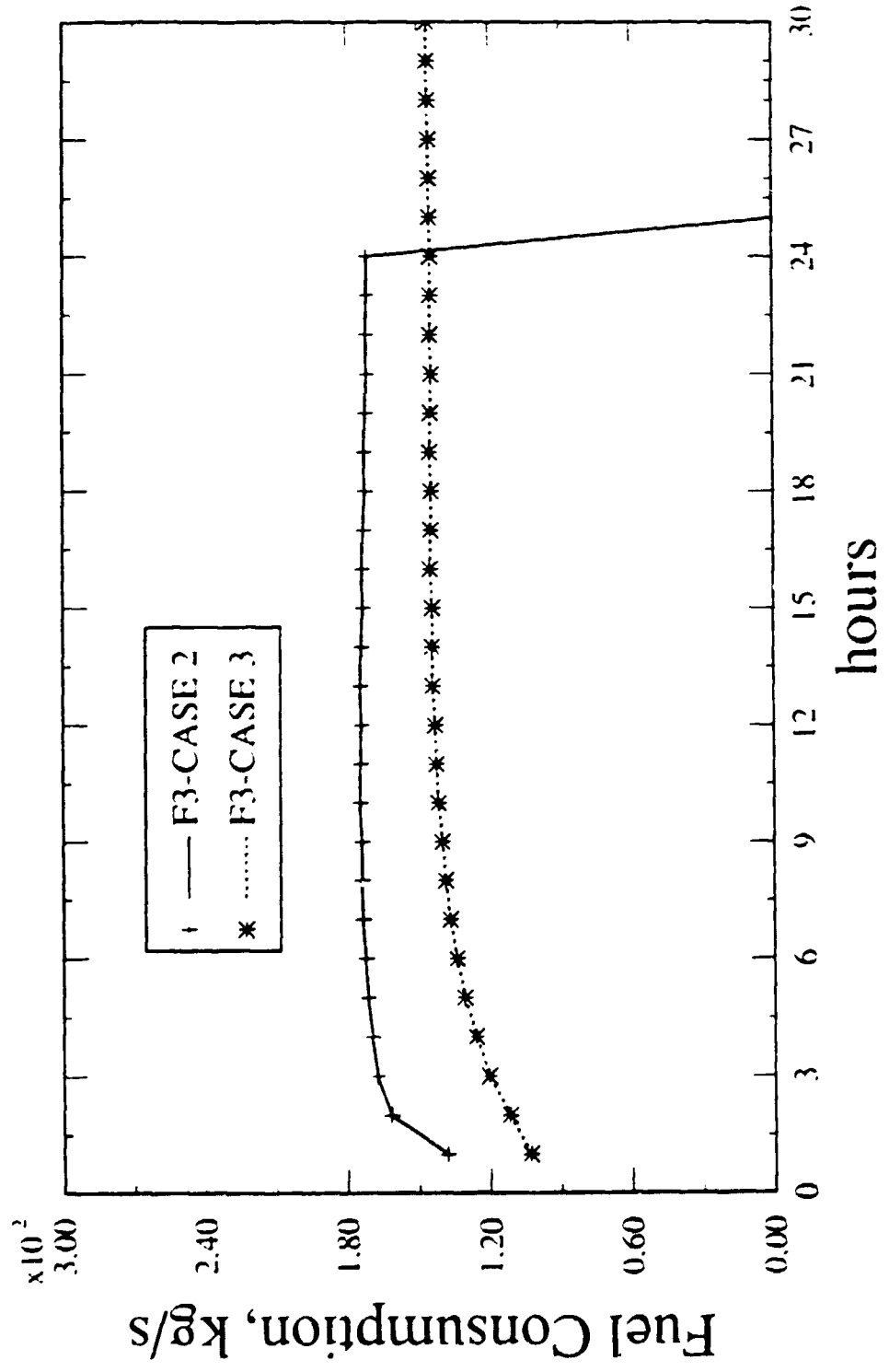












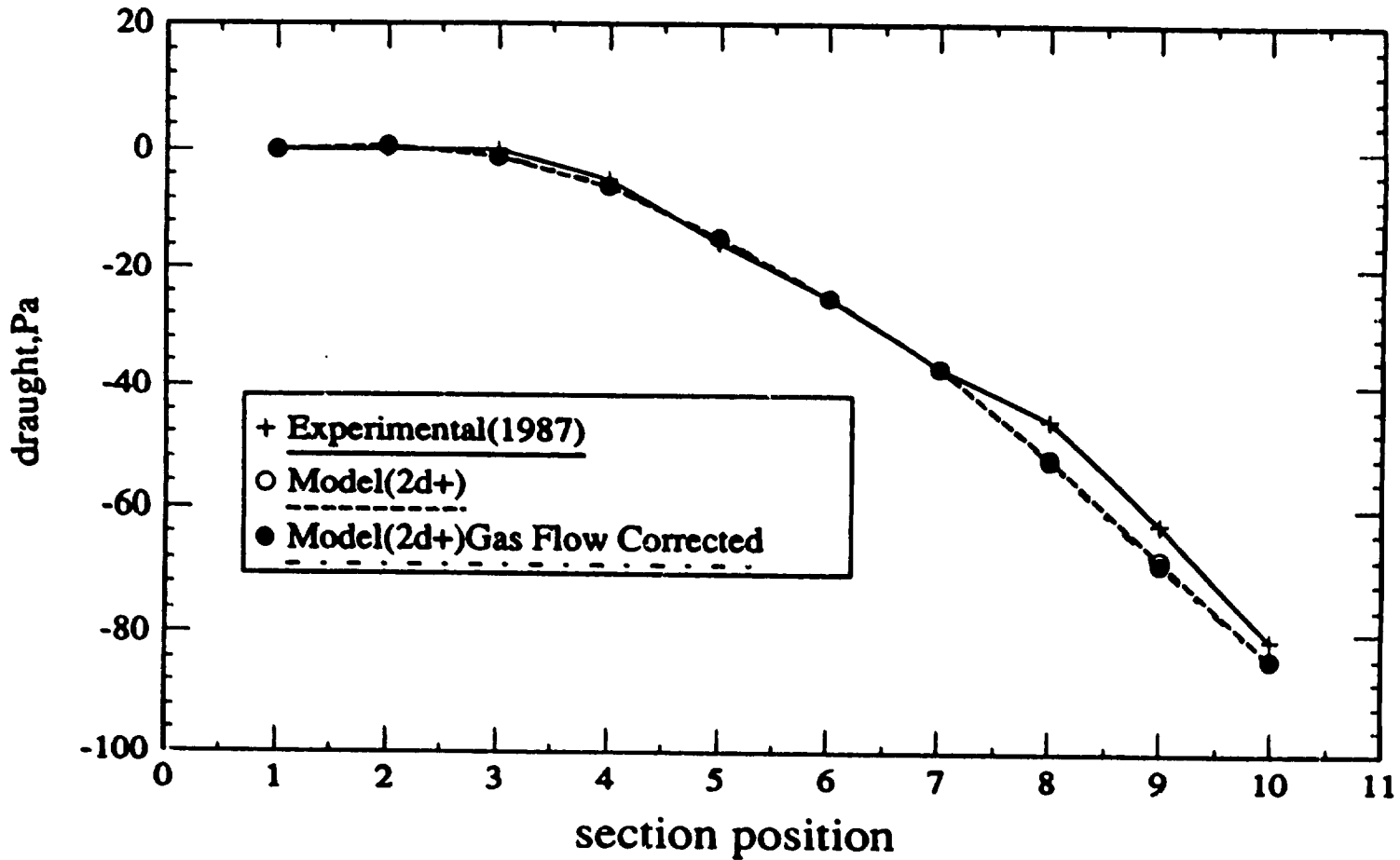
**EFFECT OF FLOW VARIATIONS THROUGH CONTROL VOLUMES
ON AVERAGE ANODE FINISHING TEMPERATURE**

1 - GAS MASS FLOW

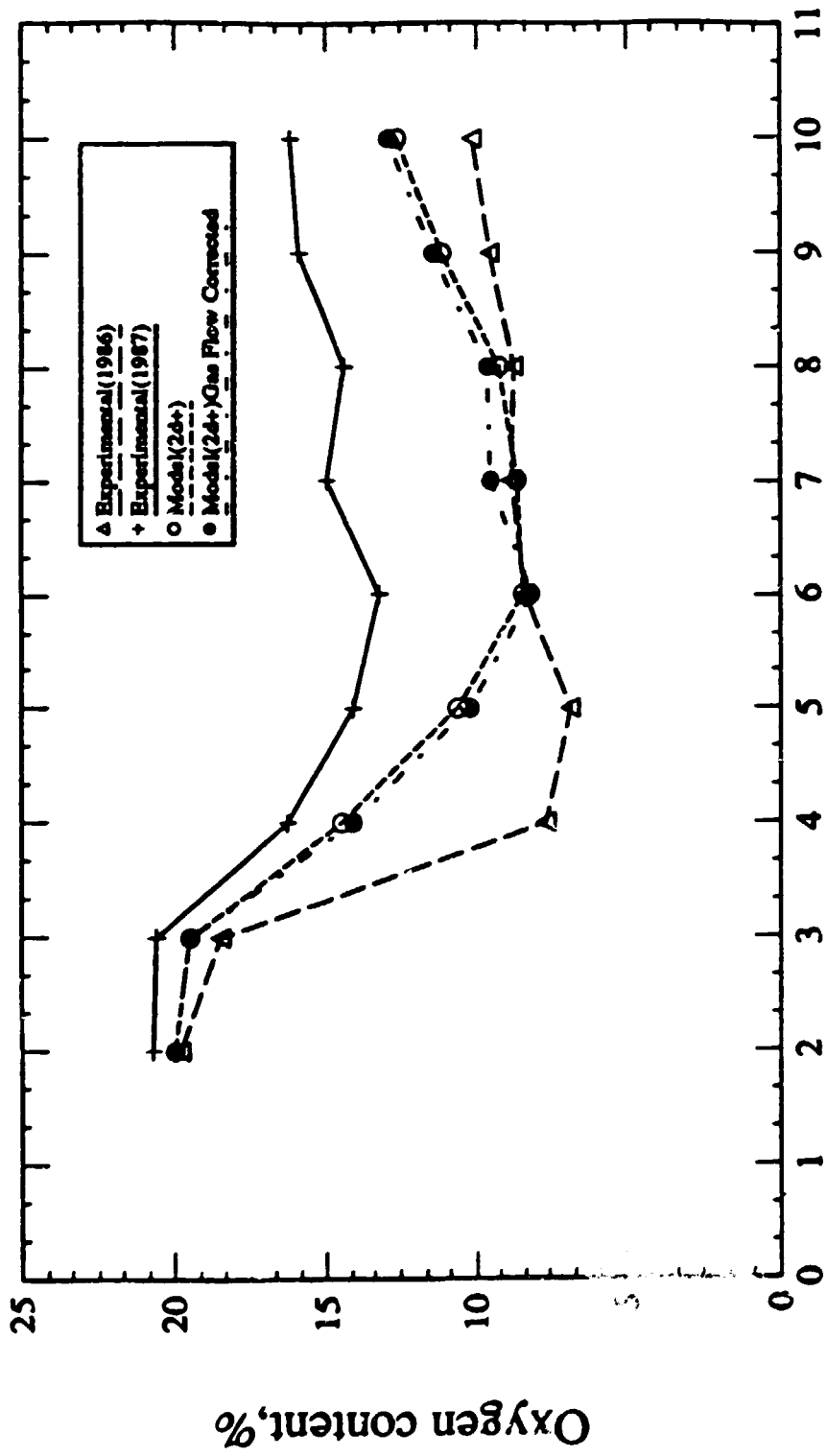
POSITION	PREVIOUS MASS FRACTION OF FLOW (Uniformly distributed)	NEW MASS FRACTION OF FLOW (Non-uniformly distributed)
Inside	1/6	1.5/6
Middle	4/6	2.6/6
Outside	1/6	1.9/6

2 - ANODE TEMPERATURES

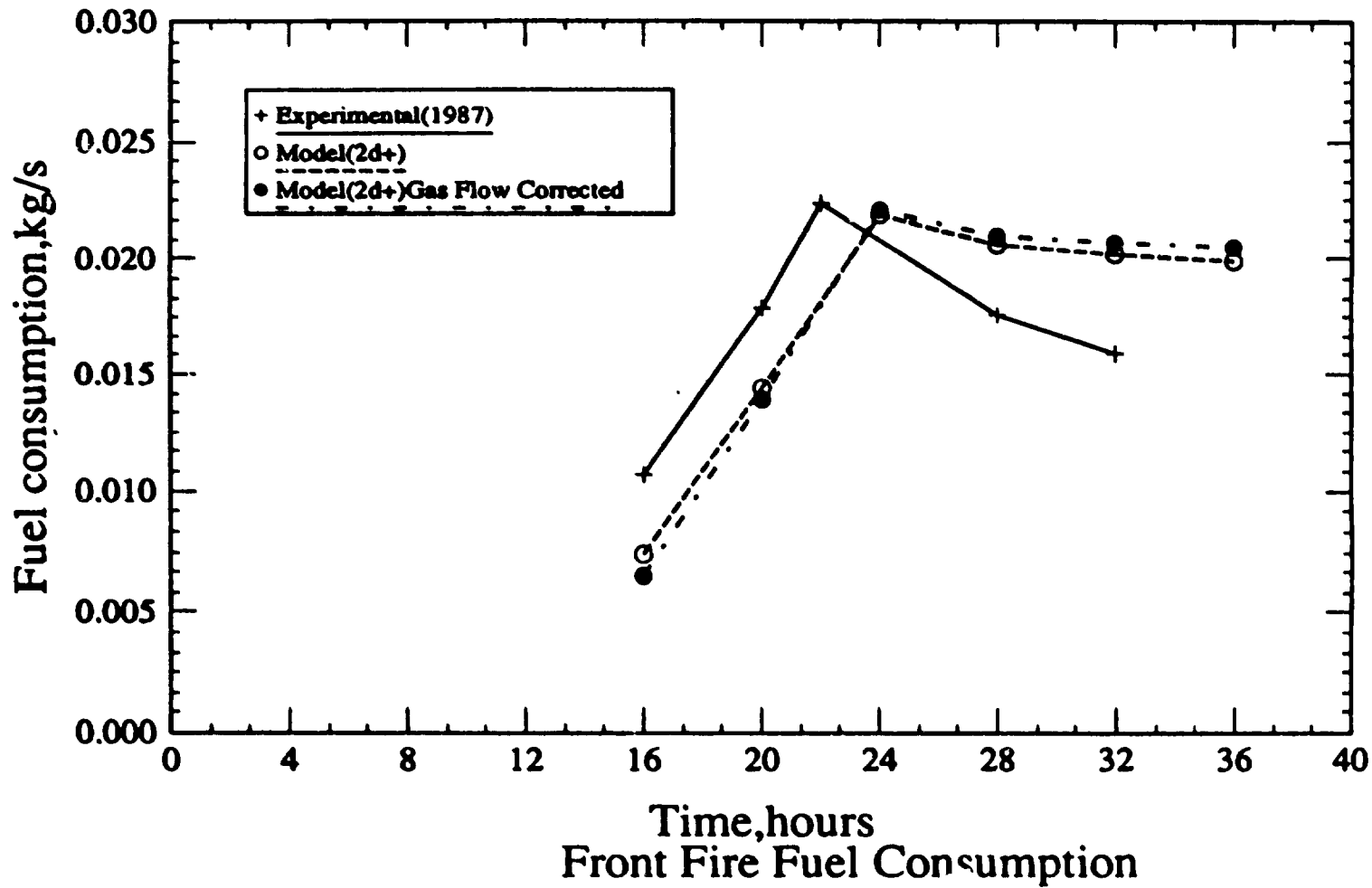
POSITION	LAYER	AVERAGE, ANODE FINISHING TEMPERATURE, °C		
		PREVIOUSLY CALCULATED (2D*)	NEWLY CALCULATED (2D*)	MEASURED
INSIDE	1	1094	1156	1160
	2	966	1033	1086
	3	899	999	1019
	AVERAGE	986	1063	1088
MIDDLE	1	1207	1185	1171
	2	1100	1054	1101
	3	1085	1026	1031
	AVERAGE	1130	1088	1101
OUTSIDE	1	993	1108	1132
	2	851	986	10432
	3	828	962	985
	AVERAGE	891	1019	1053

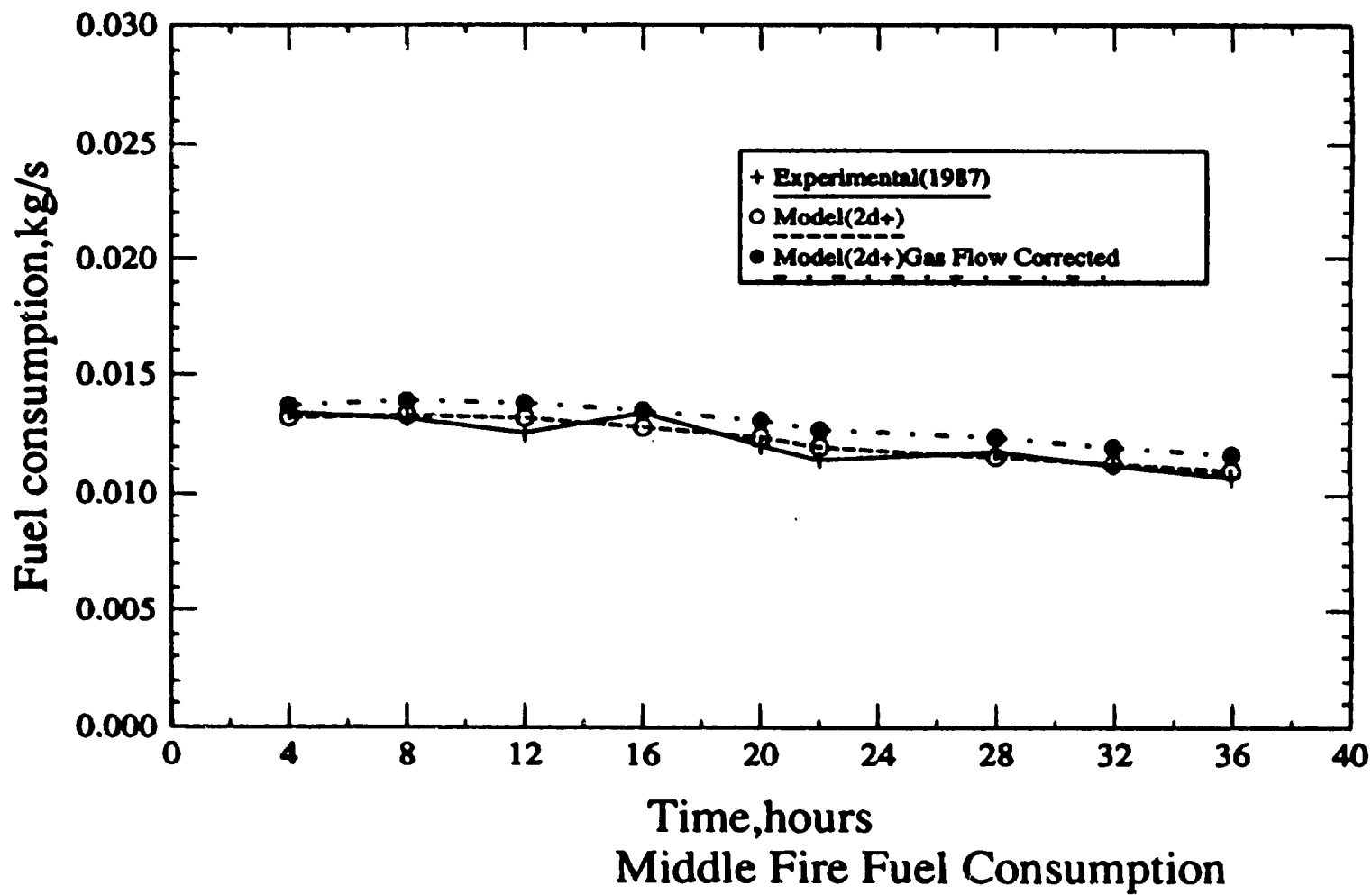


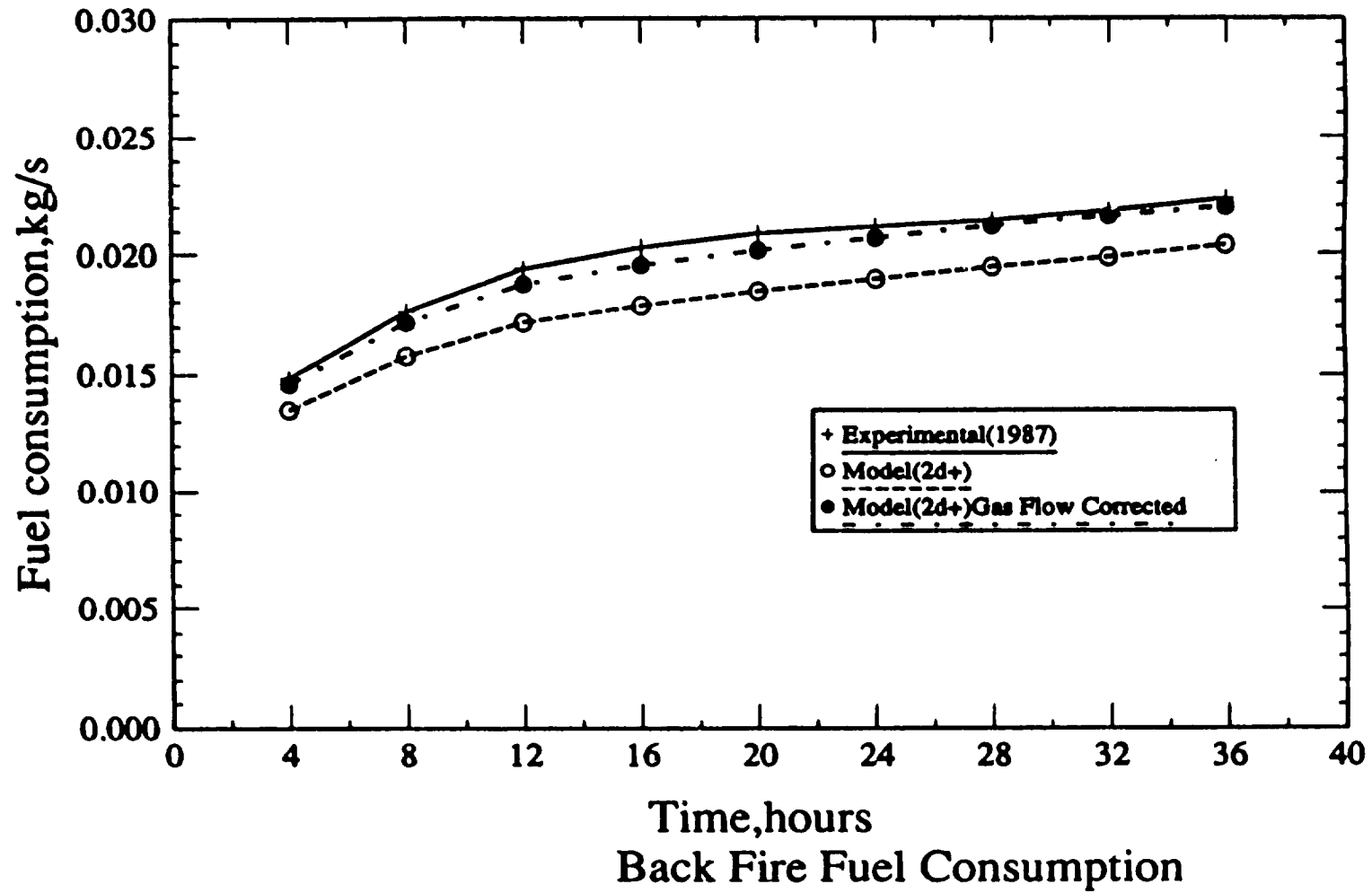
Measured and Calculated Draught Profiles

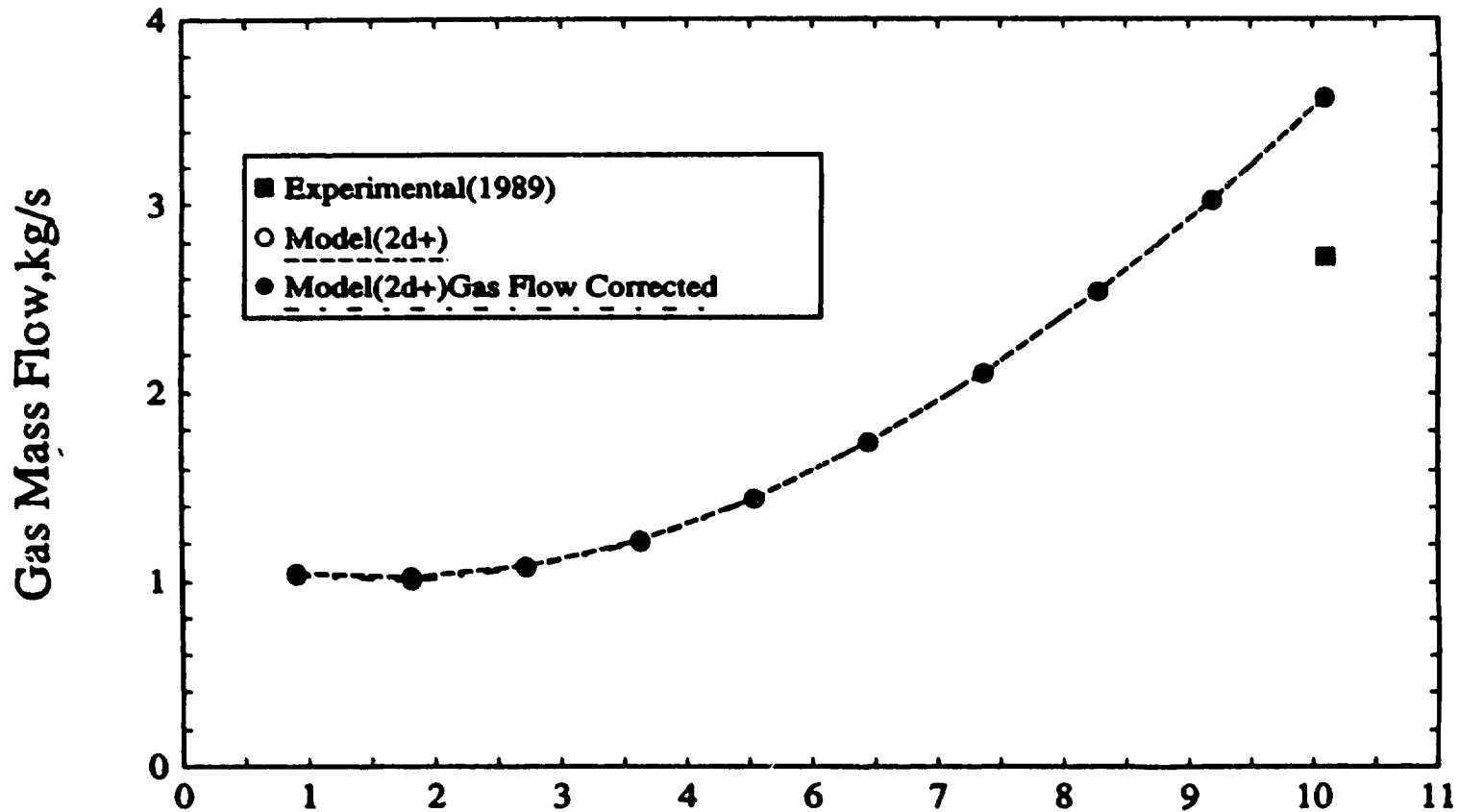


Section position
Oxygen Content Along Fire Train

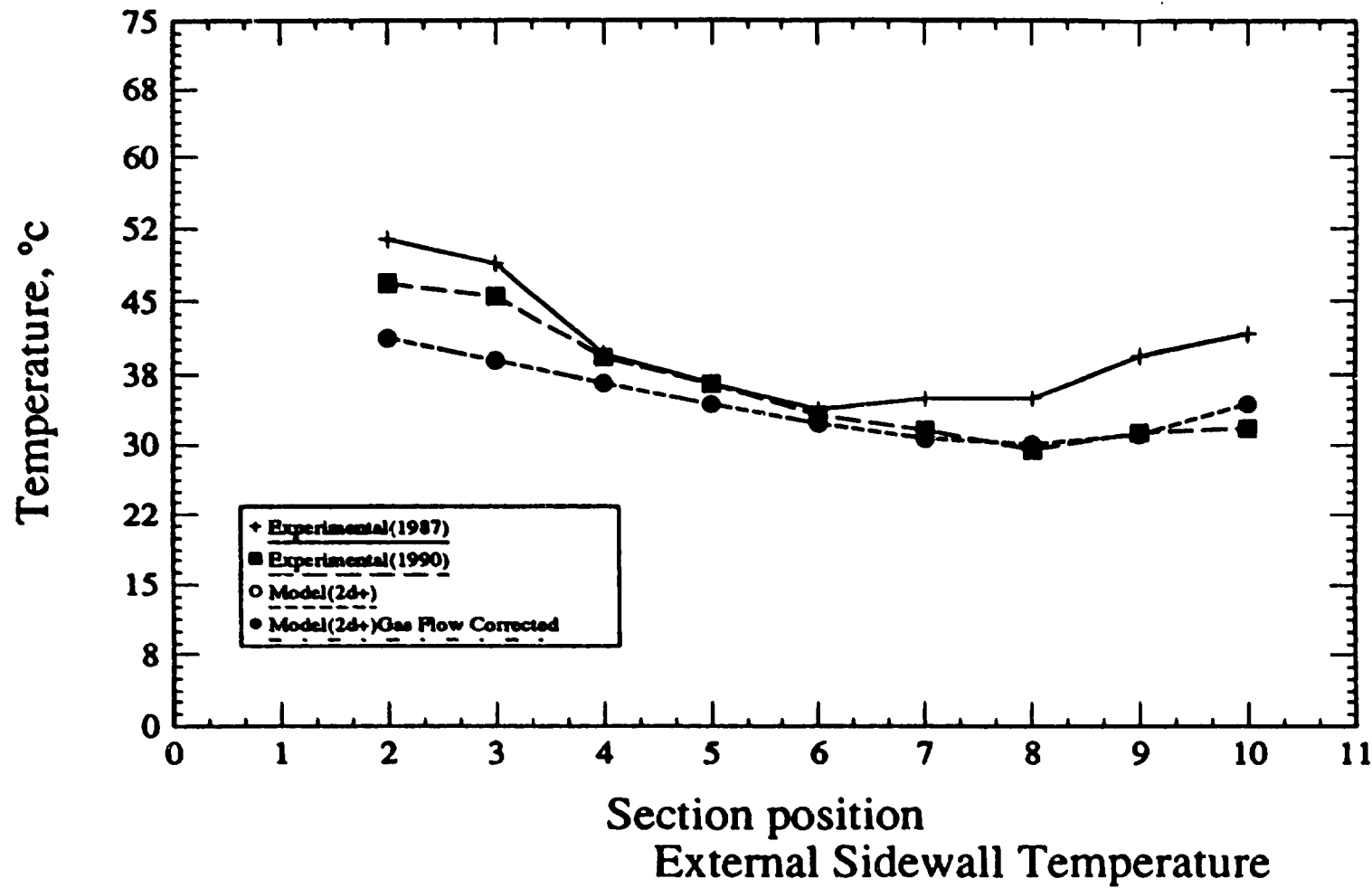


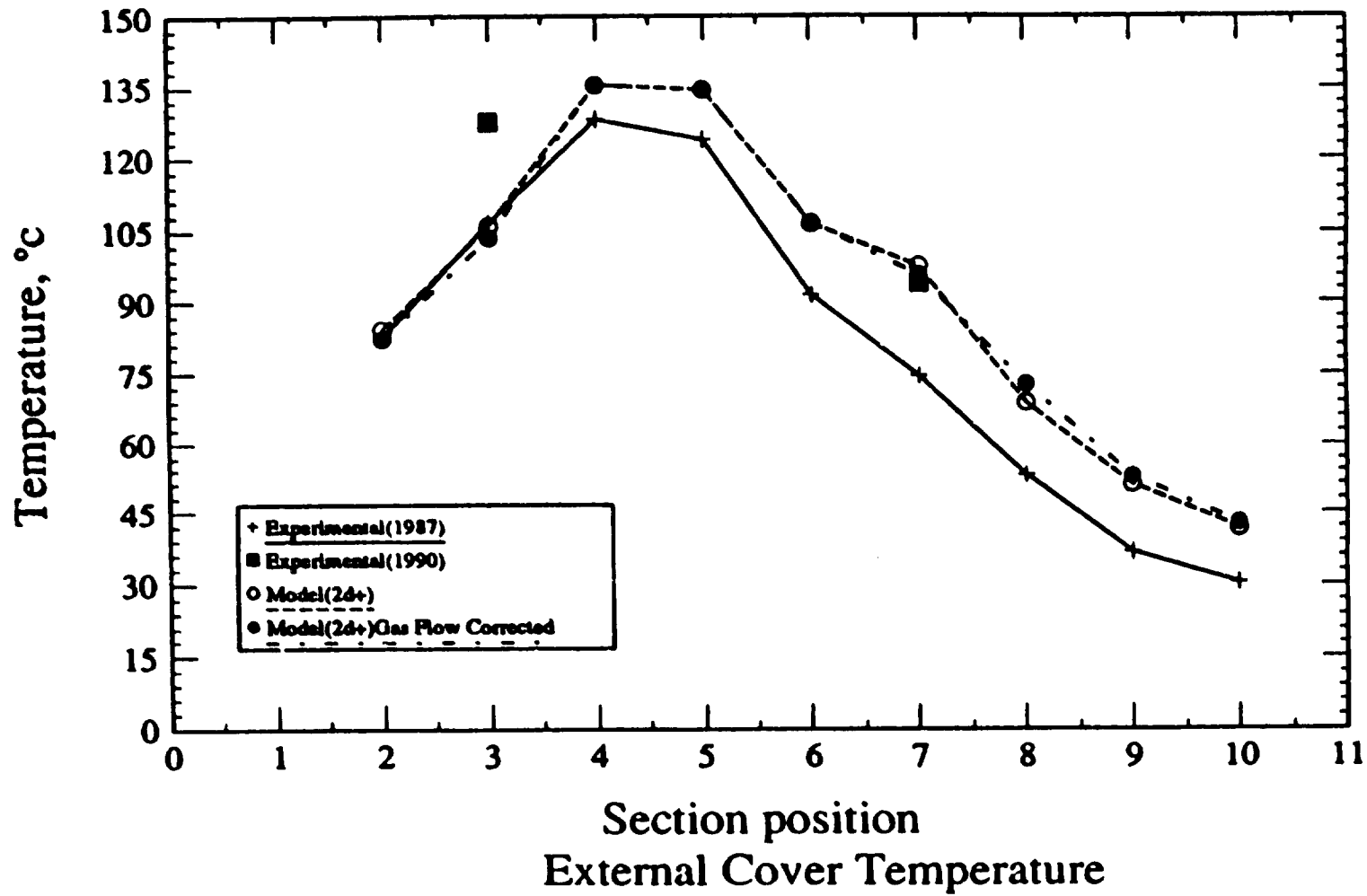


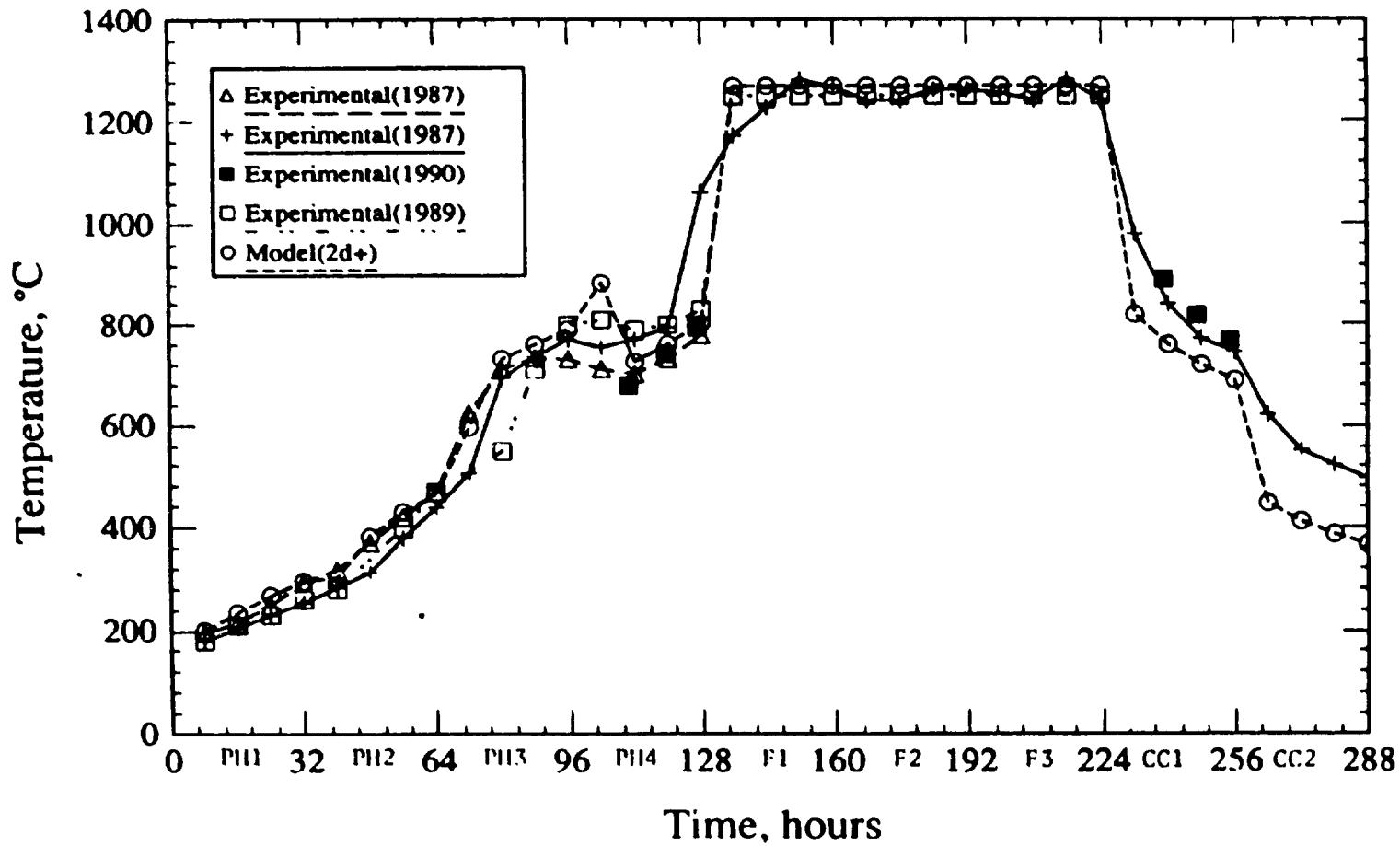




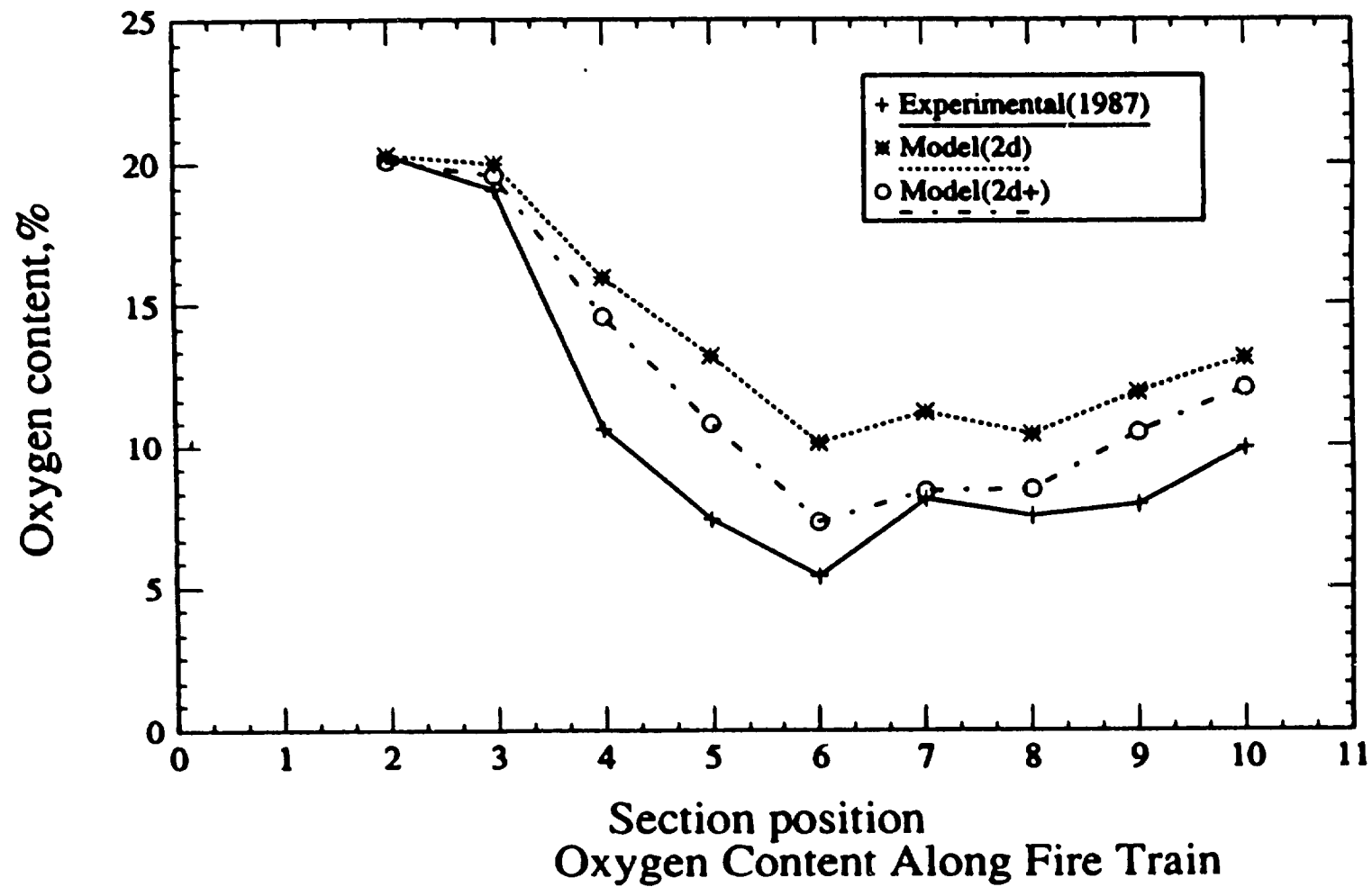
Section Position
Gas Mass Flow Profile

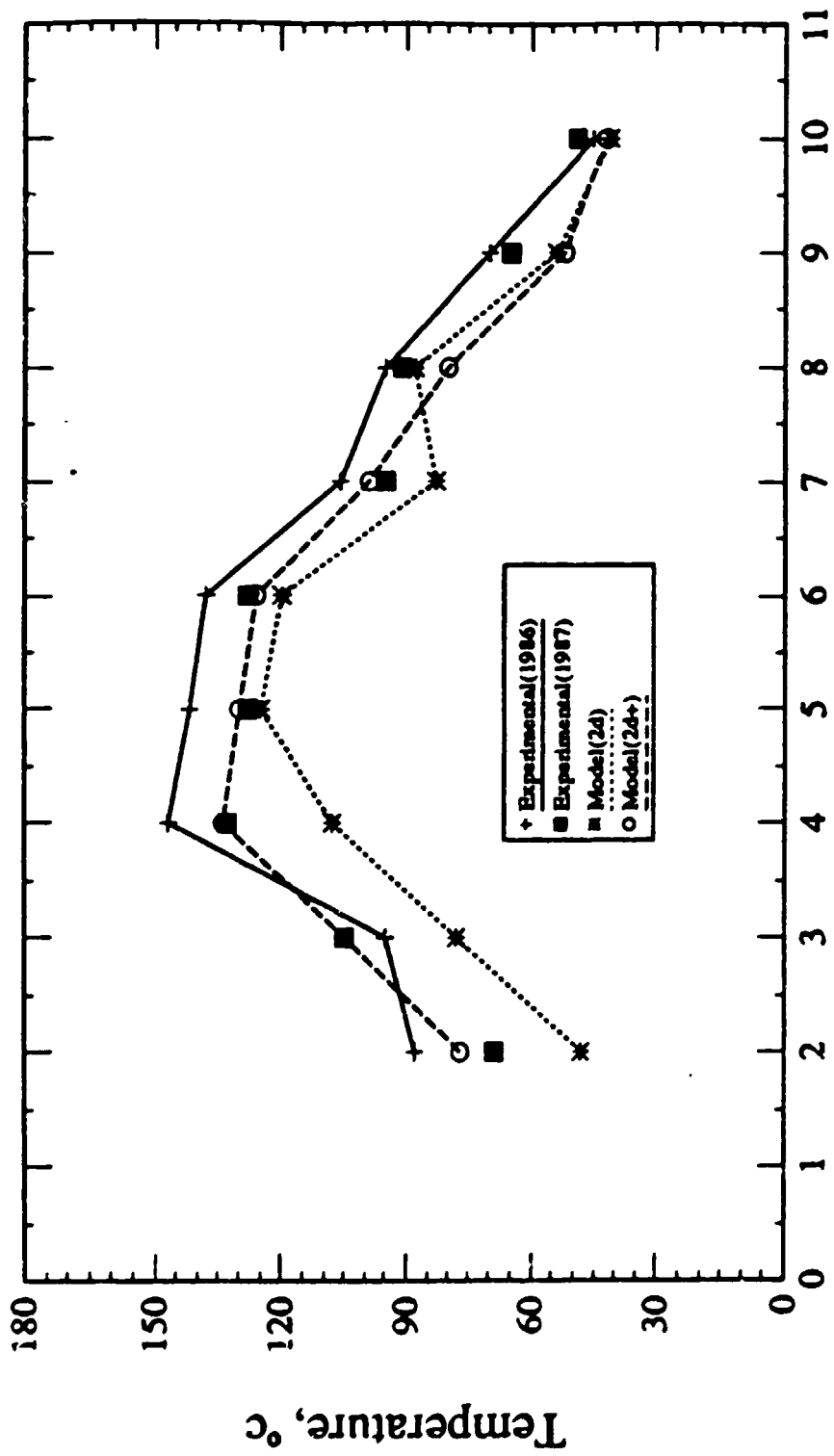






Comparison of Gas Temperature Profiles Along the Furnace.





Section position
External Cover Temperature

4. 3D MODEL

R.T. BUI, S. PETER, A. CHARETTE
Université du Québec à Chicoutimi
Chicoutimi, Québec
Canada, G7H 2B1

A.D. TOMSETT
Comalco Research Center
Thomastown, Victoria
Australia, 3074

V. POTOČNIK
Alcan International Ltd.
Jonquière, Québec
Canada, G7S 4K8

4.1 - DEVELOPMENT OF THE 3D MODEL

4.2 - SIMULATION RESULTS AND CAPABILITIES OF THE 3D MODEL

Conservation of Phase Mass

$$\frac{\partial}{\partial t} (r_i \rho_i) + \text{div} (r_i \rho_i \vec{v}_i) = \dot{m}$$

$\frac{\partial}{\partial t}$ \equiv differential coefficient with respect to time.

div \equiv divergence operator, ie limit as volume $\rightarrow 0$ of outflow \div volume.

r_i \equiv volume fraction
 ρ_i \equiv density
 \vec{v}_i \equiv velocity vector

} of phase i .

\dot{m} \equiv mass per unit volume entering phase, from all sources per unit time.

General Form of Conservation Equation

The laws of 'conservation' of mass, chemical species, momentum, energy and other fluid properties for which PHOENICS solves can all be expressed in the form:

$$\frac{\partial}{\partial t} (r_i \rho_i \phi_i) + \text{div} (r_i \rho_i v_i \phi_i - r_i \Gamma_{\phi_i} \text{grad} \phi_i) = r_i S_{\phi_i}$$

ϕ_i = general conserved property for phase i

Γ_{ϕ_i} = exchange coefficient for ϕ_i .

S_{ϕ_i} = source of ϕ per unit phase volume.

The Momentum Equations

- There are 3 equations for each phase. Their ϕ 's are: u , the velocity in the x -direction; v , the velocity in the y -direction; w , the velocity in the z -direction.
- In the polar-coordinate mode of operating PHOENICS, x is an angular coordinate. Then u represents the tangential velocity component, v the radial one and w the axial one.
- Γ_{ϕ} for velocities is μ_{eff} , the effective viscosity.

Conservation of Energy

- $\phi \approx h$, the specific enthalpy of the phase. Then $\Gamma_\phi \approx \lambda_{\text{eff}}/C_p$, the effective thermal conductivity divided by the constant-pressure specific heat.
- S_ϕ may contain contributions representing:
 - pressure variation with time;
 - interphase heat transfer;
 - phase-to-environment heat transfer;
 - radiation absorption and emission;
 - aerodynamic heating;
 - other heat sources.

Turbulence Quantities

- $\phi = k$. the turbulence energy:
 ϵ . the rate of dissipation of turbulence energy per unit volume:
 W . the mean-square vorticity fluctuations:
 kL . the product of energy and length:
 m' . RMS concentration fluctuations:
 u' . RMS velocity fluctuations:
 $u'v'$. Reynolds stress
etc.

For the (k- ϵ) model:

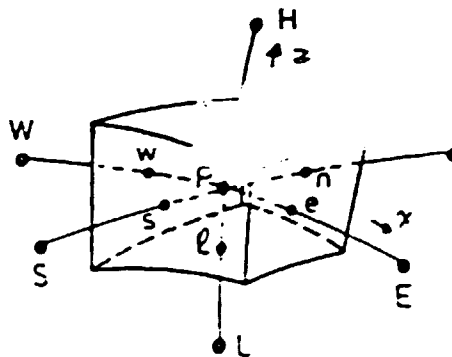
- $\Gamma_{\phi} =$ exchange coefficient for k or ϵ . as appropriate. usually taken as μ_{eff}/σ_{ϕ} . with:

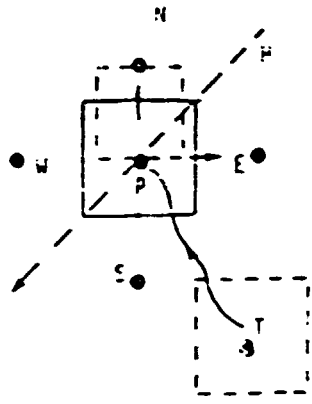
$$\sigma_k = 1.0. \quad \sigma_{\epsilon} = 1.3$$

- When the k- ϵ model is used the 'turbulence' kinematic viscosity, ν_t . is given by:

$$\nu_t = \text{const. } k^2/\epsilon$$

- PHOENICS embodies a 'finite-volume' (also called 'finite-domain') formulation of the differential equations for conservation.
- Finite-volume equations are derived by integration of the differential equations over control volumes of finite size (called 'cells' or 'sub-domains') which, taken together, wholly fill the domain under study.
- The cells are 'topologically Cartesian', having six sides and eight corners (in the general 3D case).
- Within each cell is a 'typical point' (called a 'grid node'), for which the fluid-property values, ϕ 's, are regarded as representative of the whole cell.





- Integration leads to 'finite-domain equations' (FDE's), having the form

$$a_p \phi_p = a_N \phi_N + a_S \phi_S + a_E \phi_E + a_W \phi_W + a_H \phi_H + a_L \phi_L + a_T \phi_T + b$$

where:

a_p, a_N etc are coefficients;

b is a representation of the source appropriate to ϕ for the cell

- Subscripts have the meanings (see diagram on previous page):

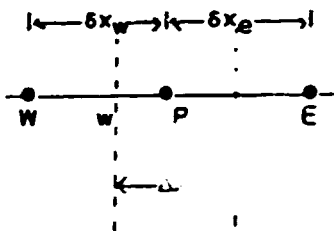
- P typical point (i.e. node) within cell.
- N north-neighbour node, in positive-y direction;
- S south-neighbour node, in negative-y direction;
- E east-neighbour node, in positive-x direction;
- W west-neighbour node, in negative-x direction;
- H high-neighbour node, in positive-z direction;
- L low-neighbour node, in negative-z direction; and
- T grid node at earlier time.

A Simple Example

Consider 1D heat conduction with source described by the equation:

$$\frac{d}{dx} \left[k \frac{dT}{dx} \right] + S = 0$$

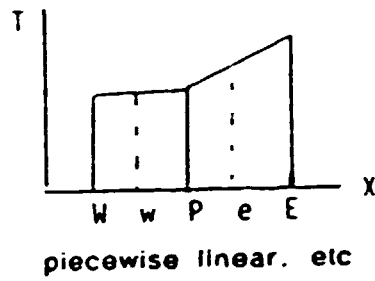
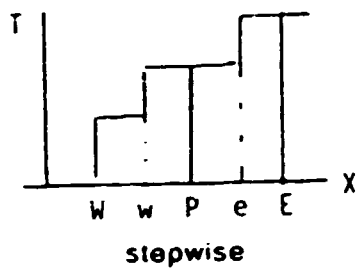
(a) Discretise space:



(b) Integrate over control cell w-e:

$$\int_w^e \frac{d}{dx} \left[k \frac{dT}{dx} \right] + S = \left[k \frac{dT}{dx} \right]_e - \left[k \frac{dT}{dx} \right]_w + \int_w^e S dx = 0$$

(c) Using interpolation assumption. eg:



we get:

$$k_e(T_E - T_p)/(\delta x)_e - k_w(T_p - T_W)/(\delta x)_w + \bar{S}\Delta x$$

(d) Collecting terms:

$$\left[\frac{k_e}{(\delta x)_e} + \frac{k_w}{(\delta x)_w} \right] T_p = \frac{k_e}{(\delta x)_e} T_E + \frac{k_w}{(\delta x)_w} T_W + \bar{S} \Delta x; \text{ or}$$

$$a_p T_p = a_E T_E + a_W T_W + b$$

where:

$$a_E = \frac{k_e}{(\delta x)_e} ; a_W = \frac{k_w}{(\delta x)_w} ; b = \bar{S} \Delta x$$

- The PHOENICS FDE's differ from 'finite-difference equations' in:
 - origin (no Taylor-series expansion is used);
 - values of coefficients (as a consequence).
- The PHOENICS FDE's differ from 'finite-element' equations in:
 - origin (neither variational principle nor Galerkin weighting is used);
 - number of nodes referred to (8 in PHOENICS, for 3D transient problems; usually more in finite-element methods).
- PHOENICS solves the set of FDE's for the cells and ϕ 's in question in an iterative manner.
- Iteration (as distinct from direct matrix inversion) is essential because the FDE'S are non-linear, by reason of the a's and b's being themselves dependent on the ϕ 's.

Boundary and Internal Conditions in PHOENICS

- These points, lines, etc need not actually be at boundaries: they can be within the domain of flow.
- PHOENICS expresses conditions by integration over the cells containing the points, lines etc: the boundary and internal conditions therefore make contributions to source terms, ie to the b and ap of the FDE's.
- PHOENICS expresses the contributions in linear form, so that the total source is expressed as:

$$S = c.(\phi_{BC} - \phi_p).$$

where:

ϕ_{BC} is a prescribed quantity having the dimensions of ϕ ;

ϕ_p is the unknown value ϕ for the cell; and

c is a prescribed coefficient, always positive.

- Splitting as described above gives:

$$S_1 = c. \phi_{BC} .$$

$$S_2 = -c$$

The Correction Form of the Equations

- Before being supplied to the equation solvers, the PHOENICS FDEs are expressed in 'correction' form, thus:

$$ap\phi^i = a_N\phi_N^i + a_S\phi_S^i + a_E\phi_E^i + a_W\phi_W^i + a_H\phi_H^i + a_L\phi_L^i$$

$$+ (a_N\phi_N^* + a_S\phi_S^* + a_E\phi_E^* + a_W\phi_W^* + a_H\phi_H^* + a_L\phi_L^* + a_T\phi_T^* + b - ap\phi^*).$$

where the ϕ^* 's are the in-store values of the ϕ 's and the ϕ^i 's are the corrections which must be supplied to these values in order to make all the equations balance.

- In PHOENICS, this kind of solution control is effected through proper selection of values of the quantities VARMIN and VARMAX, which can differ from variable to variable

Thermodynamic-Property Relations

- PHOENICS contains several ρ and $\partial\rho/\partial p$ functions; and access points are provided enabling users to supply new ones.
- PHOENICS solves for enthalpy, not temperature; but the latter can be calculated.

Transport-Property Relations

- The transport properties required, for each phase, are:

μ the viscosity;

Γ_h the exchange coefficient for heat, ie λ/c where λ = thermal conductivity and c = constant-pressure specific heat;

- For turbulent flows, the μ employed in the momentum equations, and in those for Γ if the built-in formulae are used, is μ_{eff} , related to turbulence quantities k and ϵ by:

$$\mu_{eff} = \text{const. } \rho k^2 / \epsilon$$

PHYSICAL PHENOMENA

- 1. AIR INLEAKAGE**
- 2. TURBULENCE**
- 3. PACKING COKE COMBUSTION**
- 4. VOLATILE COMBUSTION**
- 5. RADIATIVE HEAT TRANSFER**
- 6. CONDUCTION THROUGH THE SOLIDS**
- 7. HEAT LOSSES**

MODEL DESCRIPTION

EQUATIONS SOLVED:

CONTINUITY

MOMENTUM

k- ϵ EQUATIONS FOR TURBULENCE

ENERGY INCLUDING RADIATIVE HEAT TRANSFER

VARIABLES SOLVED: TOTAL NO OF VARIABLE = 10

PRESSURE

x, y AND z DIRECTION VELOCITIES

TEMPERATURE

RADIATIVE FLUXES IN THE x, y AND z DIRECTION

BOUNDARY CONDITIONS

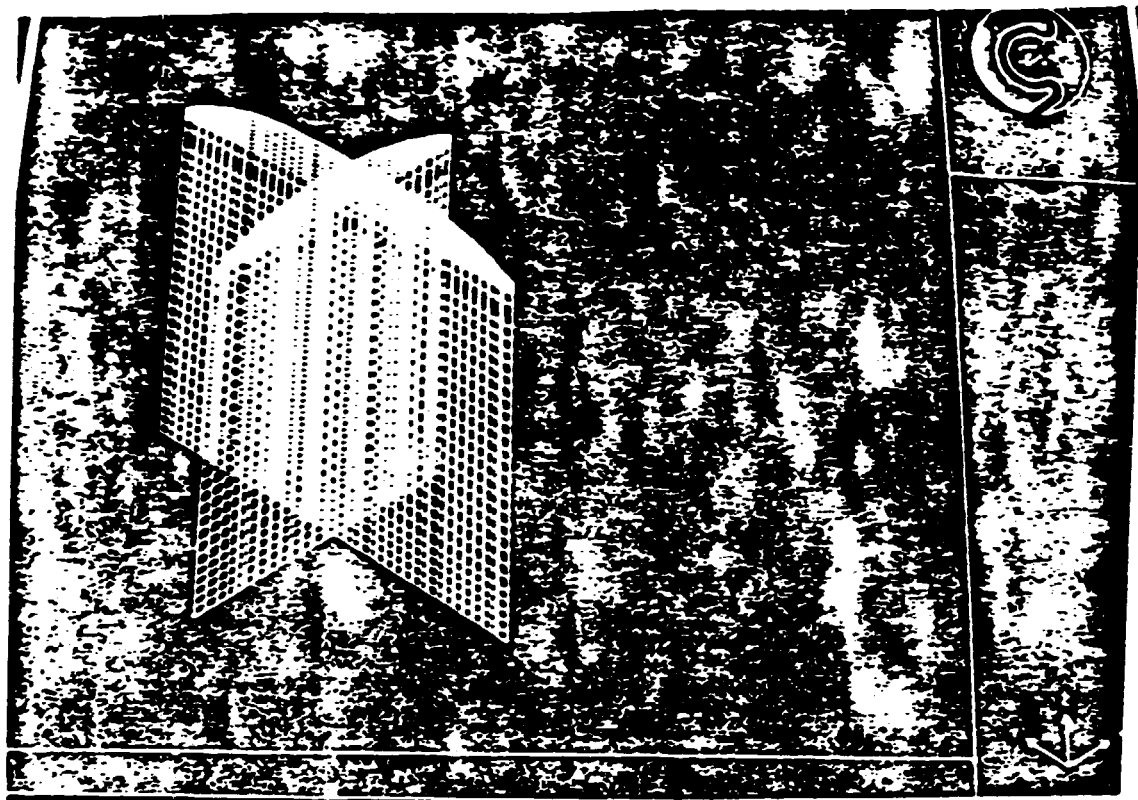
- **INLET MASS FLOW AND TEMPERATURE**
- **WALL SHEAR STRESS (TURBULENT)**
- **WALL HEAT TRANSFER (TURBULENT)**
- **HEAT LOSSES THROUGH THE LID, SIDEWALL,
CENTRAL WALL AND HEADWALL**
- **AIR INLEAKAGE**
- **OUTGOING GAS (GAS LEAVING PIT ZONE)
HAS THE SAME VELOCITY AND TEMPERA-
TURE AS THE LOCAL CELLS**

SOLUTION PROCEDURE USING PHOENICS

STEPS

- 1. SOLVE FLOW AND ENERGY (INCLUDING CONVECTION, VOLATILE COMBUSTION AND AIR INLEAKAGE) EXCLUDING RADIATION FOR THE GAS SIDE AND STORE THE RESULTING FLOW**
- 2. INCLUDE RADIATION FOR THE SYSTEM CONSIDERED AND STORE THE ENERGY FLUX ON THE SOLIDS BY THE GAS IN THE PIT**
- 3. SOLVE THE 3D-TRANSIENT CONDUCTION INTO THE SOLIDS FOR PART OF THE FIRE CYCLE (6HRS) USING THE ENERGY FLUX FROM (2) AS THE BOUNDARY CONDITION**

4. STORE THE RESULTING ANODE TEMPERATURE DISTRIBUTION AND USE THIS AS THE INITIAL CONDITION FOR THE NEXT PART OF THE FIRE CYCLE
5. REPEAT FROM (1) FOR THE NEXT PART OF THE FIRE CYCLE



(42 x 71 x 36) at $x = 21$ and $y = 36$.

**Model Parameters and Input Data Used in the Simulations
of the 4th Preheat Section**

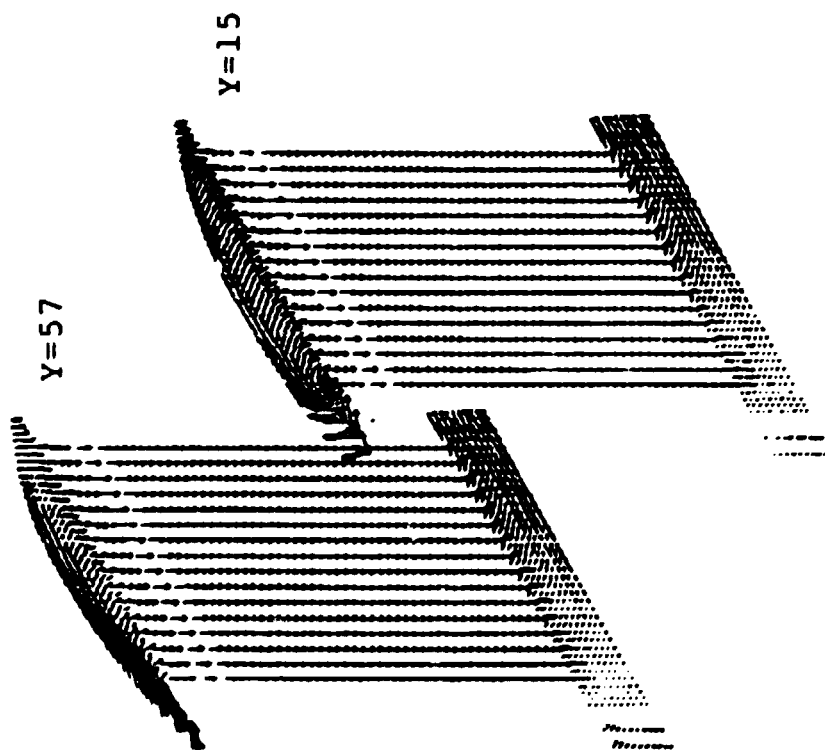
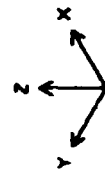
Gas mass flow rates:	
Total flow rate through all fireshafts	: 2.01 kg/s
Flow distribution in each fireshaft	: see Table 2
Total air leakage	: 0.4 kg/s
Gas temperatures:	
Inlet gas temperature through fireshafts	: 760 °C
Inlet temperature of air leakage	: 25 °C
Initial wall temperatures:	
Initial temperature of West Wall (near fire shaft)	: 450 °C
Initial temperature of East Wall (opposite end)	: 425 °C
Initial temperature North Wall (outside, i.e. sidewall)	: 425 °C
Initial temperature South Wall (inside, i.e. central wall)	: 450 °C
Initial temperature High Wall (inner lid surface)	: 425 °C
Initial temperature Low Wall (coke surface on top of pits)	: 450 °C
Initial temperature of Cassette Walls	: 360 °C
Volatile combustion:	
Mass of volatiles consumed in section	: 3.3×10^{-2} kg/s
Heat of combustion of volatiles	: 3.487×10^7 J/kg

Lid:		
Thickness of lid	:	0.25 m
Effective thermal conductivity	:	0.410 W/m.K
Outer surface temperature	:	96 °C
Sidewall:		
Thickness	:	1.3 m
Effective thermal conductivity	:	0.410 W/m.K
Outer surface temperature	:	31.5 °C
Headwall:		
Mass	:	87000 kg
Heat capacity	:	1254 J/kg.K
Central wall:		
Mass	:	55000 kg
Heat capacity	:	1254 J/kg.K
Pillars in underpit zone:		
Mass	:	10050
Heat capacity	:	1254 J/kg.K
Foundation:		
Depth	:	1 m
Effective thermal conductivity	:	0.778 W/m.K
Radiative properties:		
Emissivity of Low Wall (coke surface)	:	0.75
Emissivity of other walls including lid top and cassette walls	:	0.9
Absorption coefficient of gray gas	:	0.3 m ⁻¹

Flow Distribution through Fireshafts for all Three Cases (kg/s)

Fireshaft no	Case 1	Case 2	Case 3
1	0.42	0.5250	0.4976
2	0.42	0.5250	0.3676
3	0.42	0.0	0.0
4	0.42	0.5250	0.5628
5	0.42	0.5250	0.6720
Total	2.1	2.1	2.1

- 1. Fireshaft no. 1 is innermost, no. 5 is outermost, no. 3 is middle.**
- 2. Non-uniform flow distribution is taken identical to a non-uniform flow that has been previously measured experimentally. Such measurement will not be needed if a complete simulation of a whole fire train is made starting from a section where the flow distribution is known.**



→ : 10.55 m/s.

DSL : 4 cm PRESENT SECTION (Grid: 42x71x64)

PHOENICS



Z=15

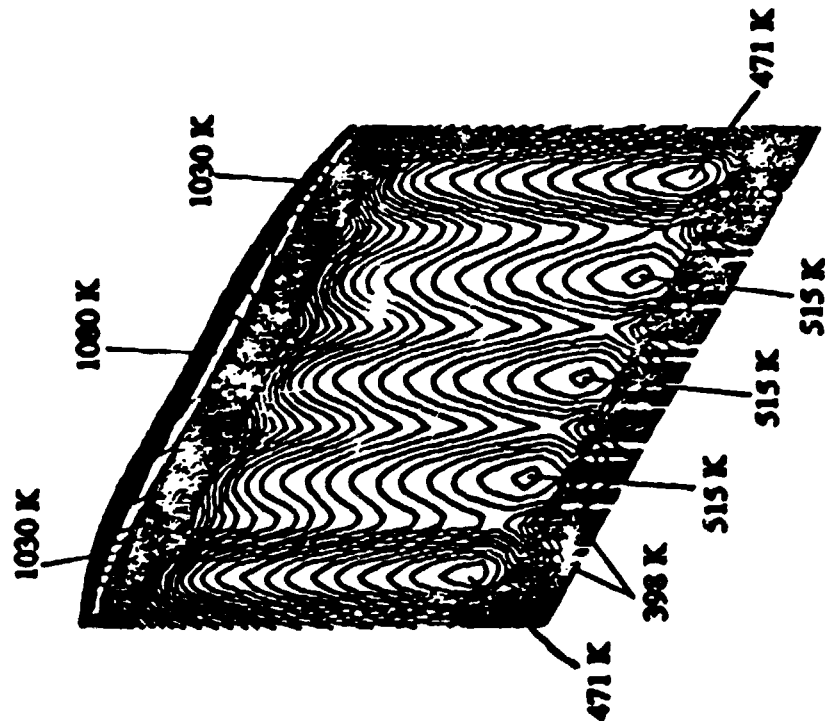
→ : 14.77 m/s.

BSL : 3 rd FIRING SECTION

PHOENICS



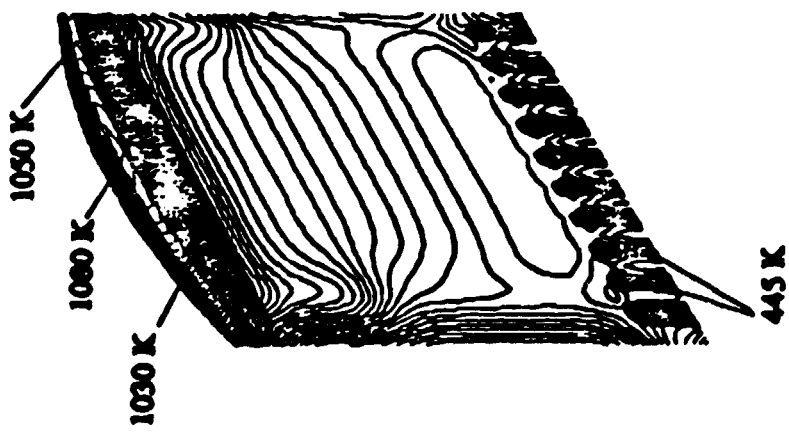
Temperature Interval = 10 K



4th Preheat Section

PROBES

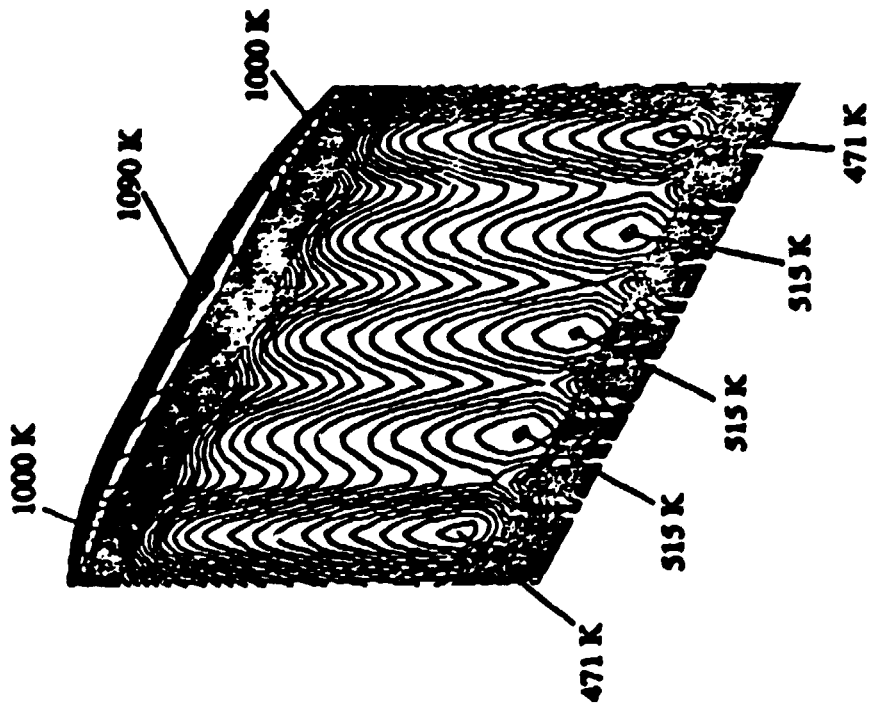
Temperature Interval = 10 K



4 th Preheat Section

PHOENIX

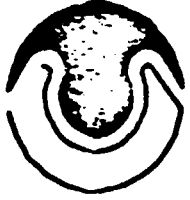
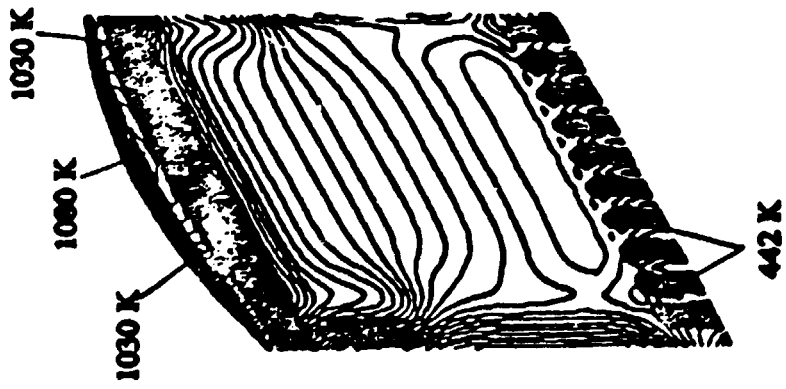
Temperature Interval = 10 K



4th Probes Section

PROBES

Temperature Interval = 10 K

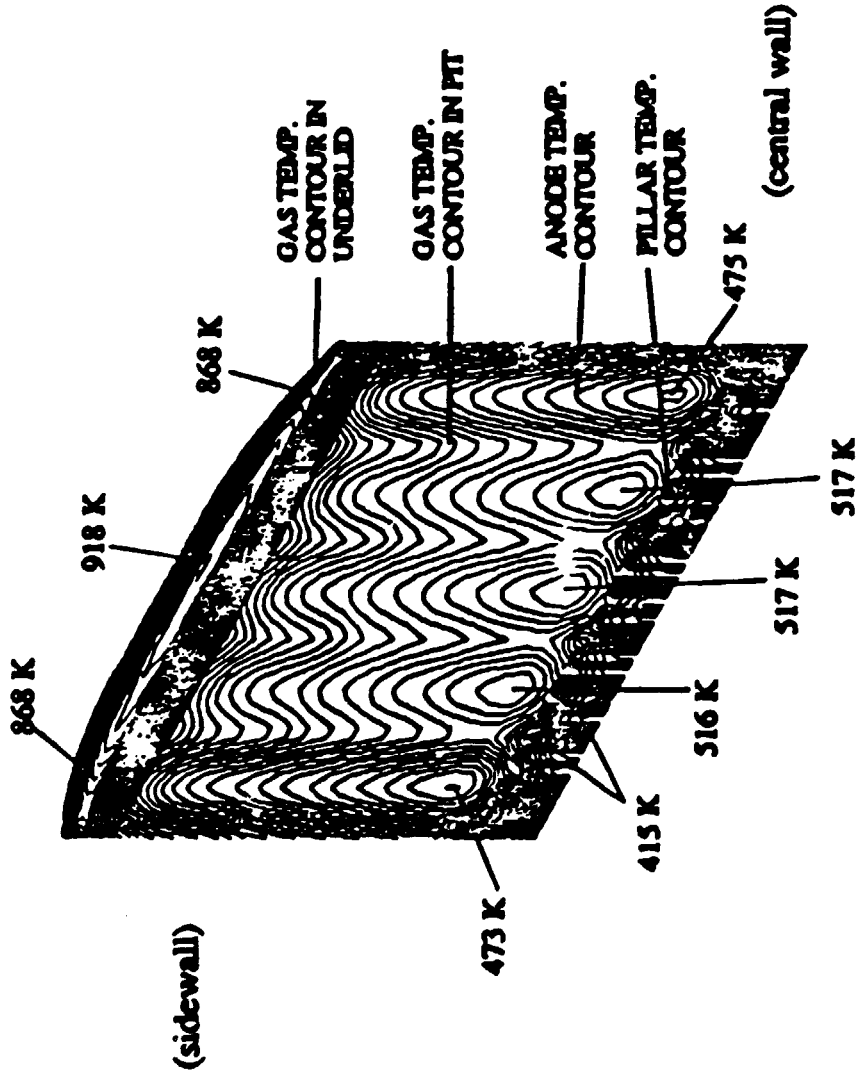


PROBES

4th Probe Section

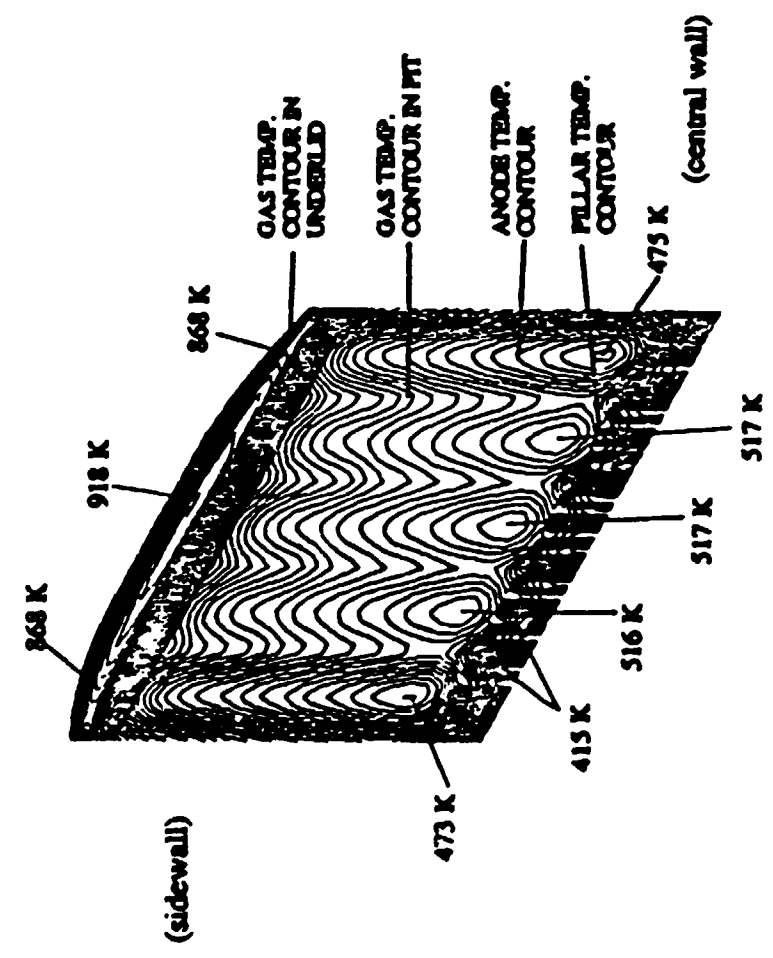


Temperature Interval = 10 K





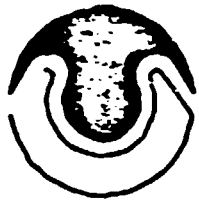
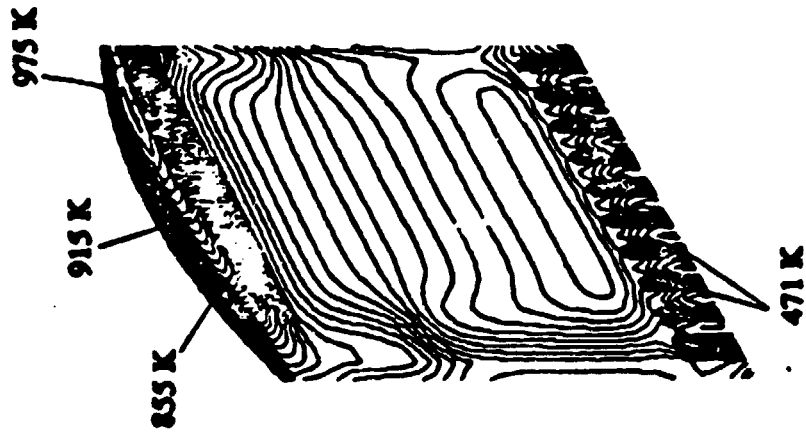
Temperature Interval = 10 K



4th Preheat Section

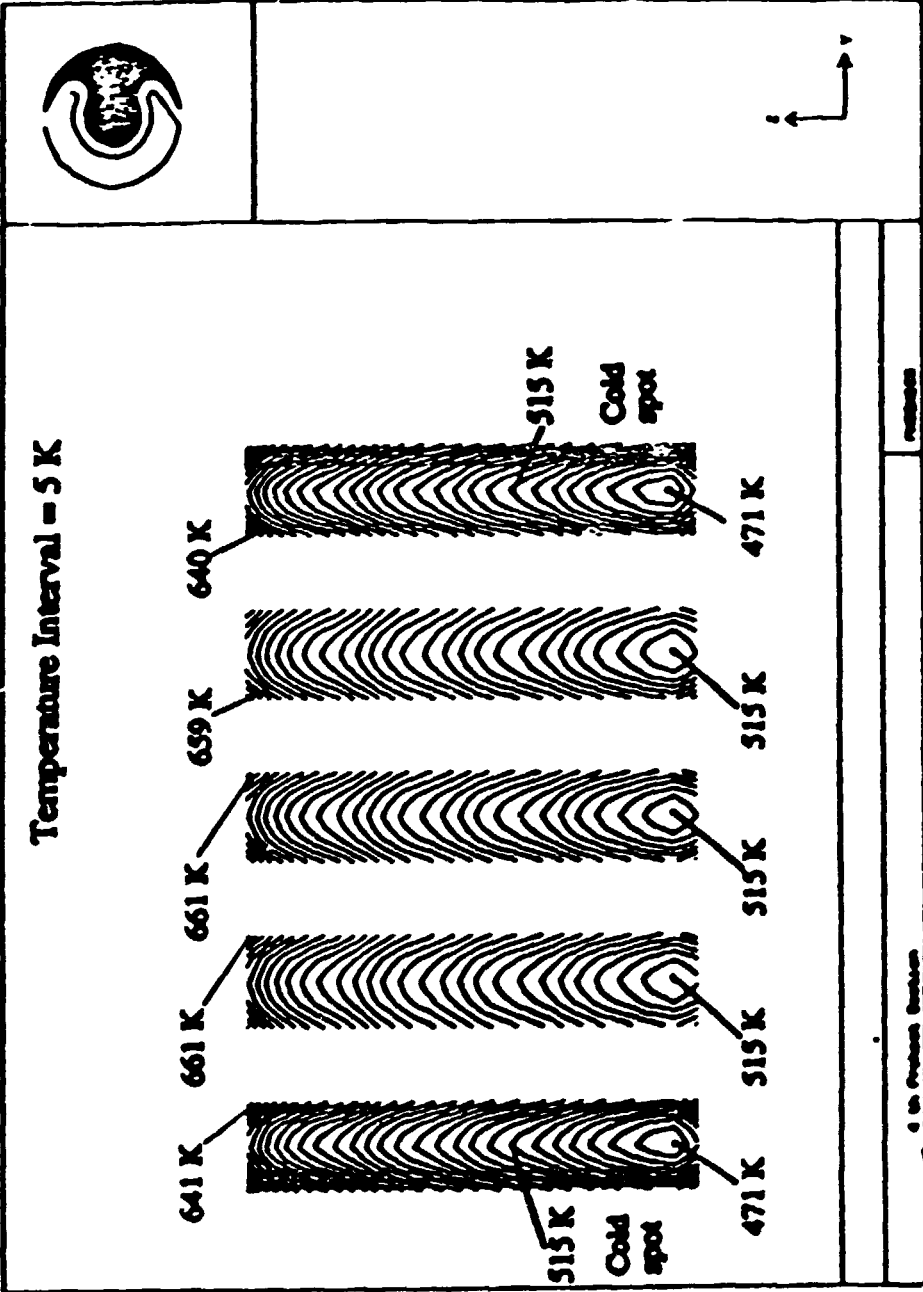
PHENICS

Temperature Interval = 10 K



PROBES

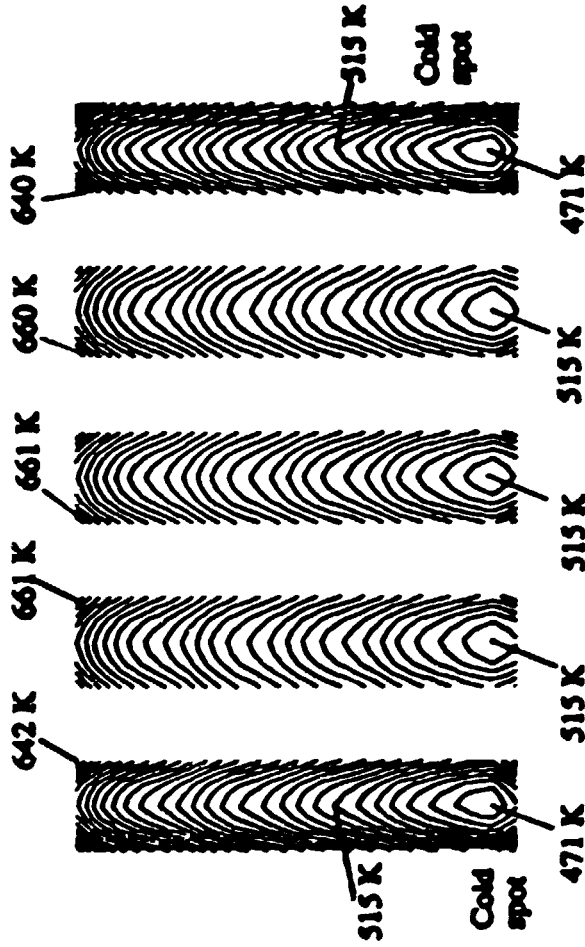
4th Probed Section



U. S. GOVERNMENT PRINTING OFFICE

1968 O-348-800

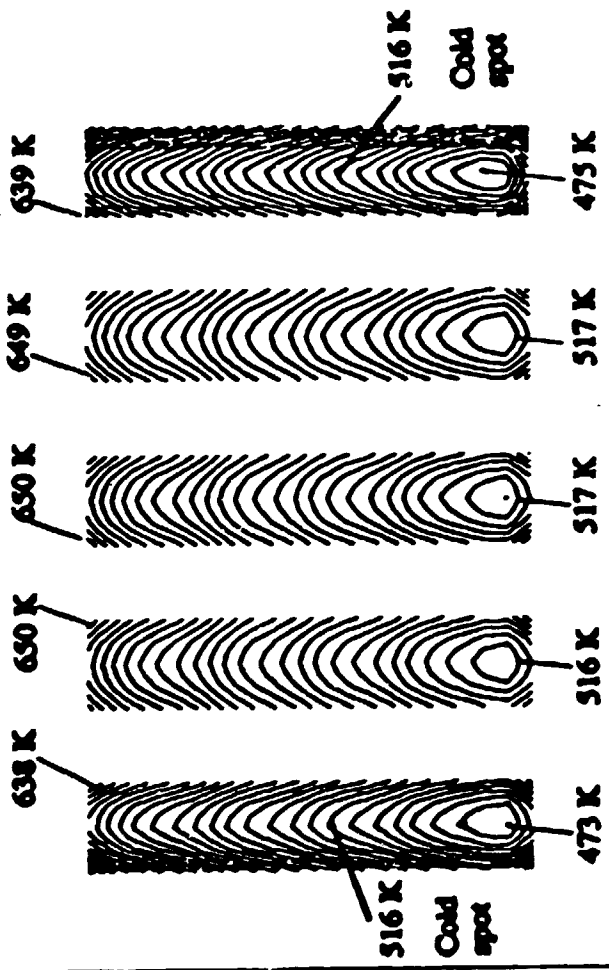
Temperature Interval = 5 K



Dr. Professor Stephen

Page 10

Temperature Interval = 5 K



PRODUCTS

© 1997 Proton Services

Temperature Range of Anodes (K) for case 1

		x = 8	x = 16	x=23	x=31	x = 38
		Near end				Far end
		Fireshaft				Fireshaft
(Near Inner wall) Pit	1	496-626	471-628	473-638	474-646	502-665
	2	526-643	516-645	516-650	517-657	529-671
	3	526-643	517-645	517-650	517-657	530-671
	4	526-643	516-644	517-649	518-655	530-671
(Near outer wall)	5	498-626	474-629	475-639	476-648	500-660

Temperature Range of Anodes (K) for case 2

		x = 8	x = 16	x=23	x=31	x = 38
		Near end				Far end
		Fireshaft				Fireshaft
(Near Inner wall) Pit	1	498-635	471-638	471-642	471-643	500-659
	2	525-653	515-656	515-661	515-662	528-669
	3	523-657	515-660	515-661	515-662	528-671
	4	526-656	515-659	515-660	515-662	527-671
(Near outer wall)	5	498-637	471-637	471-640	471-641	500-658

Comparison of Temperature Range of Anodes (K) for all 3 cases at $x = 16$

		Case 1	Case 2	Case 3
(Near Inner wall) Pit	1	471-628	471-638	471-639
	2	516-645	515-656	515-662
	3	517-645	515-660	515-662
	4	516-644	515-659	515-658
(Near Outer wall)	5	474-629	471-637	471-635

Comparison of Temperature Range of Anodes (K) for all 3 cases at $x = 23$

		Case 1	Case 2	Case 3
(Near Inner wall) Pit	1	473-638	471-642	471-641
	2	516-650	515-661	515-661
	3	517-650	515-661	515-661
	4	517-649	515-660	515-659
(Near Outer wall)	5	475-639	471-640	471-640

Maximum Simulated Anode Temperatures (K) for the Three Cases

$x =$	8	16	23	31	38
Case 1	643	645	650	657	671
Case 2	657	660	661	662	671
Case 3	660	661	661	663	671

Computation time

	Number of variables	Number of sweeps	Number of cells	Computation time (min)
1 Gas flow and energy excluding radiation	7	200	28224	360
2 Energy of gas including radiation	4	1400	28224	330
3 Transient conduction into solids	1	2 Time step = 6 min.	83496	30
Total				720

4th PREHEAT SECTION - GRID SENSITIVITY STUDY

**COMPARISON OF TEMPERATURE RANGE OF ANODES (K) FOR THE ORIGINAL GRID
(42X71X36) AND THE NEW GRID (42X71X64)**

			x=8	x=16	x=23	x=31	x=38
Near Inner wall	Pit 1	Original	496-626	471-628	473-638	474-648	502-655
		New	510-634	477-635	477-641	478-648	510-658
	Pit 2	Original	526-643	516-645	516-650	517-657	529-671
		New	538-657	538-657	523-663	523-666	538-674
	Pit 3	Original	526-643	517-645	517-650	517-657	530-671
		New	538-656	538-656	523-663	523-666	538-674
	Pit 4	Original	526-643	516-644	517-649	518-655	530-671
		New	538-655	538-655	523-663	523-666	538-673
Near Outer wall	Pit 5	Original	498-626	474-629	475-639	476-648	500-660
		New	510-635	478-635	478-643	478-647	510-659

CAPABILITIES OF THE MODEL

- **UNEVEN FLOW THROUGH THE FIRESHAFTS**
- **BLOCKING ANY FIRESHAFT**
- **BLOCKING ANY CE5 OR AE5 HOLES IF NECESSARY**
- **THE EFFECT OF VARIATION DUE TO VARIOUS HEAT SINKS AND SOURCES SUCH AS FUEL PACKING COKE, VOLATILE, AIR INFILTRATION AND HEAT LOSS**
- **DIFFERENT GEOMETRY OF THE LID (THE POSITION OF AE5 AND CE5 HOLES REMAIN THE SAME)**

2.1 INTRODUCTION

Vertical ring furnaces are widely used in the aluminium industry for the baking of carbon electrodes. The furnace is operated in such a way to bring the electrodes to a target temperature following a given temperature profile as function of baking time.

In a vertical ring furnace the fuel combustion takes place in the fire shafts. The hot gases leave the fire shafts, mix with infiltrated air, and exchange heat with the upper part of the furnace (lid) before it flows down in more than a hundred separate vertical ducts along the AE5 and CE5 brick walls, which are uniformly distributed among the pits. In the pits, the gases exchange heat with the brick walls enclosing the coke covered anodes before reuniting in the underpit region. As they pass the pillars in the underpit region, they exchange heat with the solids before entering the next shaft downstream.

This paper presents the work involved in the development of the extended two-dimensional (2D⁺) mathematical model and the simulations of BSL and NZAS furnaces.

The reason for developing a 2D⁺ model subsequent to the building of the 2D model [1] is to enable the new model to account for the variations in anode baking temperature across the furnace, and as a consequence, achieve a better prediction of furnace performance.

2.2 MODEL DESCRIPTION

2.2.1 General Arrangement :

The model consists of several sub-models. The primary ones are the Gas Mass Flow sub-model, the Gas Composition sub-model which is linked to the packing coke combustion and volatile combustion sub-models: the Solid Conduction sub-model which gives the temperature distribution in anodes is linked to the volatile evolution sub-model.

Other secondary sub-models are also available to calculate the heat transfer coefficients and emissivities. Each section is divided in to four zones and the zones are connected by common boundary conditions. The zones are identified in Figure 1.

The gas mass flow sub-model gives the gas mass flow and draught profiles along the fire train. Figure 2 shows the general fire train arrangement considered in the gas mass flow sub-model.

For two adjacent sections $i + 1$ and i , the relation between pressure loss and gas velocity is obtained by a momentum balance which leads to [2]:

$$P_{i+1} = P_i - \frac{b \dot{m}_g^2}{\rho^2 A_0^2} (\rho_{i+1} - \rho_i) - \frac{2b \dot{m}_g}{A_0} \left(\frac{\dot{m}_{g,i+1}}{\rho_{i+1}} - \frac{\dot{m}_{g,i}}{\rho_i} \right) - \frac{\dot{m}_g^2 f_D L_{eq}}{2 \rho D_0 A_0^2} - \bar{\rho} g (z_{i+1} - z_i)$$

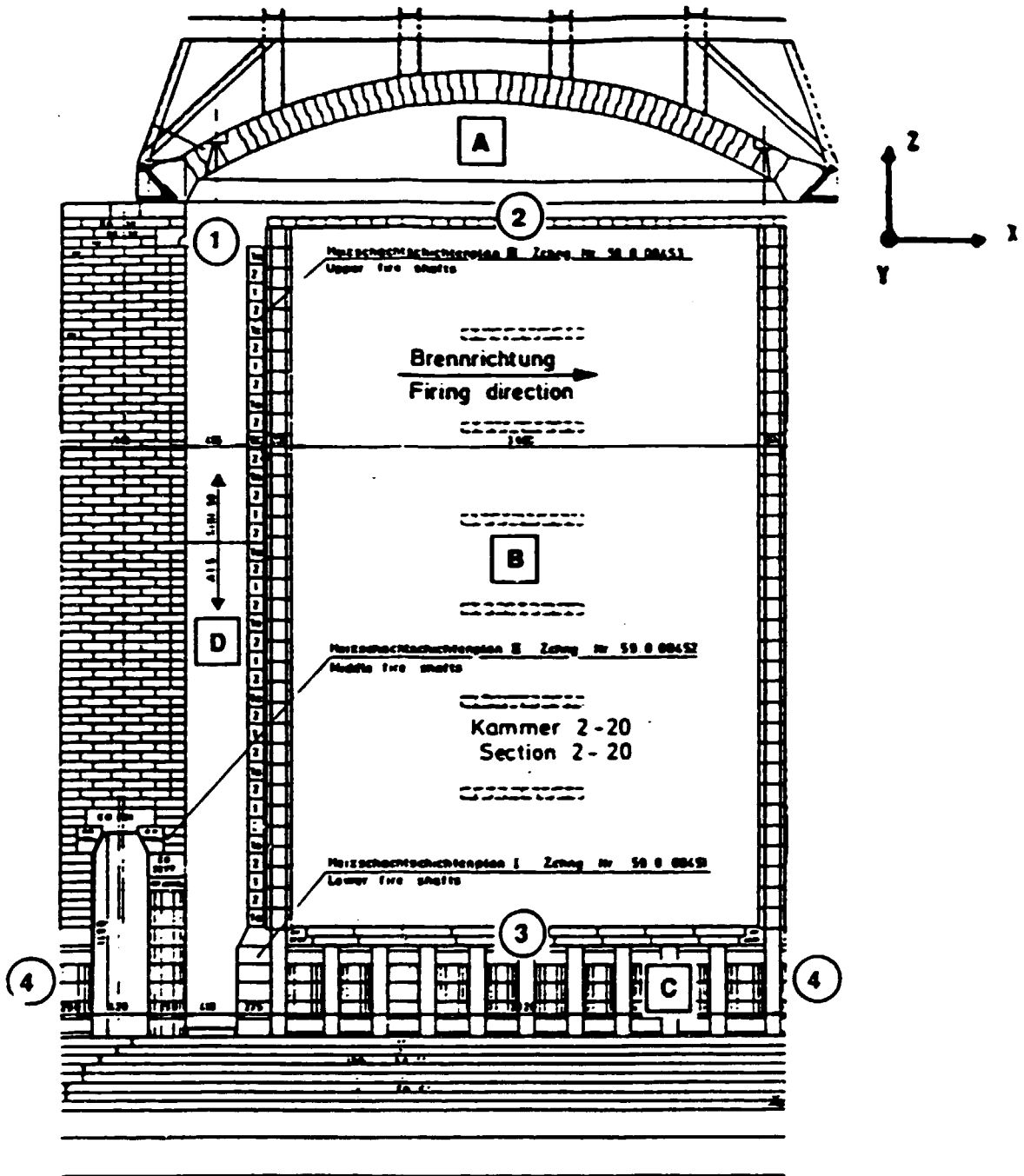


Figure 1. Description of control volume flow regions.

1. Head wall and fireshaft
2. Underlid
3. Pits
4. Underpits

(1, 2, 3 and 4 indicate locations of calculated gas composition)

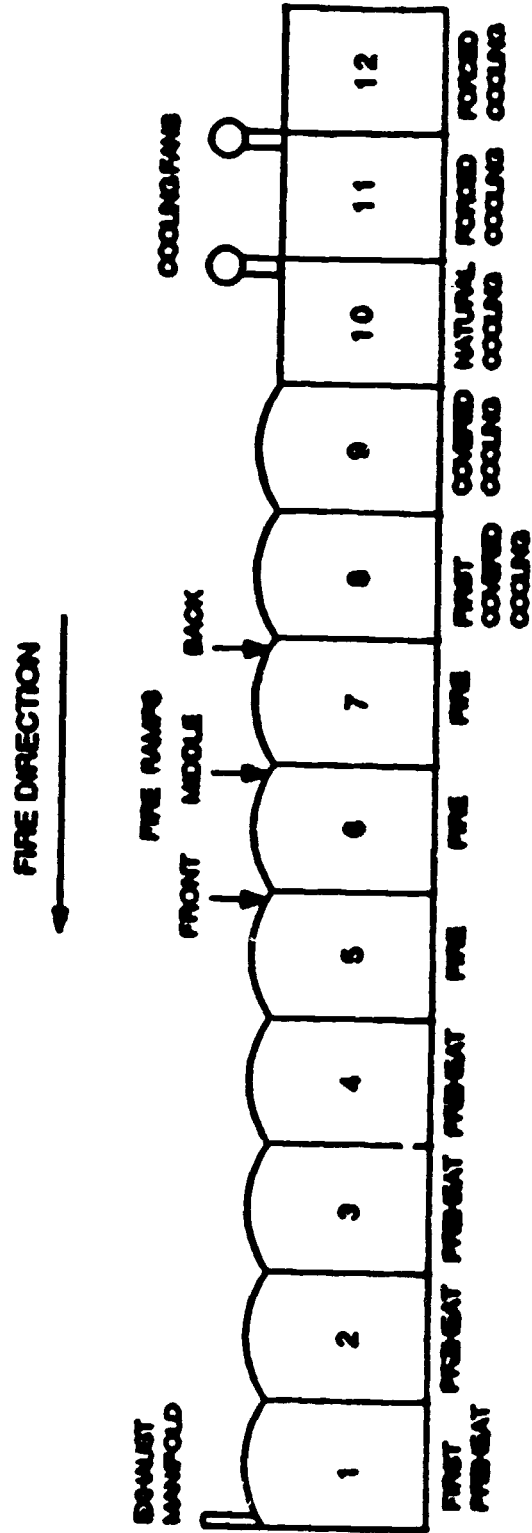


Figure 2. General fire train arrangement.

where

- b : a constant equal to 0.7 (according to ref. 2)
- \dot{m}_g : gas mass flow [kg/s]
- $\bar{\dot{m}}_g$: average gas mass flow = $\frac{\dot{m}_{i+1} + \dot{m}_i}{2}$ [kg/s]
- A_c : average section perpendicular to flow [m²]
- ρ : gas density [kg/m³]
- $\bar{\rho}$: average gas density = $\frac{\rho_{i+1} + \rho_i}{2}$ [kg/s]
- P : pressure [Pa]
- f_D : darcy friction factor
- L_{eq} : equivalent length of a section
- D_c : equivalent duct diameter [m]
- $Z_{i+1} - Z_i$: vertical distance between points $i + 1$ and i [m]

Note that $\dot{m}_i = \rho_i V_i A_i$, where V_i is the gas velocity

Due to the infiltration, \dot{m} is not a constant:

$$\dot{m}_{g,i+1} = \dot{m}_{g,i} + \dot{m}_{inf}$$

where \dot{m}_{inf} is the total air infiltration between positions i and $i+1$.

Infiltration through openings or cracks can be modeled by considering flow through an orifice of given section A_0

$$\text{This gives } \dot{m}_{inf} = C A_0 \sqrt{2\rho\Delta P}$$

where

$$\Delta P = P_{in} - P_{out}$$

$$C = \sqrt{\frac{D_c}{f_D L_{eq}}}$$

The underlid zone

The heat balance on gas elements of the underlid zone (Figure 3) gives :

$$\dot{Q}_{gin} - \dot{Q}_{gout} + \dot{Q}_{inf} - \dot{Q}_c - \dot{Q}_r + \dot{Q}_{COKE} = \dot{Q}_{acc}$$

where

$$\dot{Q}_{gin} - \dot{Q}_{gout} = \dot{m}_{gin} h_{gin} - \dot{m}_{gout} h_{gout}$$

$$\dot{Q}_{inf} = \dot{m}_{inf} h_{inf}$$

h_g and h_{inf} are the enthalpies of the gas and infiltrated air respectively. where

\dot{m}_{gin} : total gas mass flow rate at inlet [kg/s]

\dot{m}_{inf} : total infiltrated air flow rate [kg/s]

\dot{m}_{gout} : total gas mass flow rate at outlet [kg/s]

$$\dot{m}_{gout} = \dot{m}_{gin} + \dot{m}_{inf}$$

$q_{g=1}$: radiative heat transfer exchange between gas and lid [W]

$q_{g=2}$: radiative heat exchange between gas and pit top [W]

$q_{2=1}$: radiative heat exchange between gas and combined pit top [W]

\dot{Q}_c : convective exchange between gas and combined pit top and lid [W]

$$\dot{Q}_c = \sum_{i=1}^2 h_i A_i (T_{g,ave} - T_i)$$

where h_i is the convective heat transfer coefficient between gas and surface i .

$$\dot{Q}_r = q_{g=1} + q_{g=2}$$

$$\dot{Q}_{COKE} = \dot{m}_{COKE} H_{COKE}$$

where \dot{m}_{COKE} is the assumed combustion rate ofm coke and H_{COKE} is the heating value of packing coke.

$$\dot{Q}_{acc} = m_g c_{p_g} \left(\frac{T_{g,ave}^{t+\Delta t} - T_{g,ave}^t}{\Delta t} \right)$$

where \dot{Q}_{acc} is the heat accumulation term. It is small and is neglected.

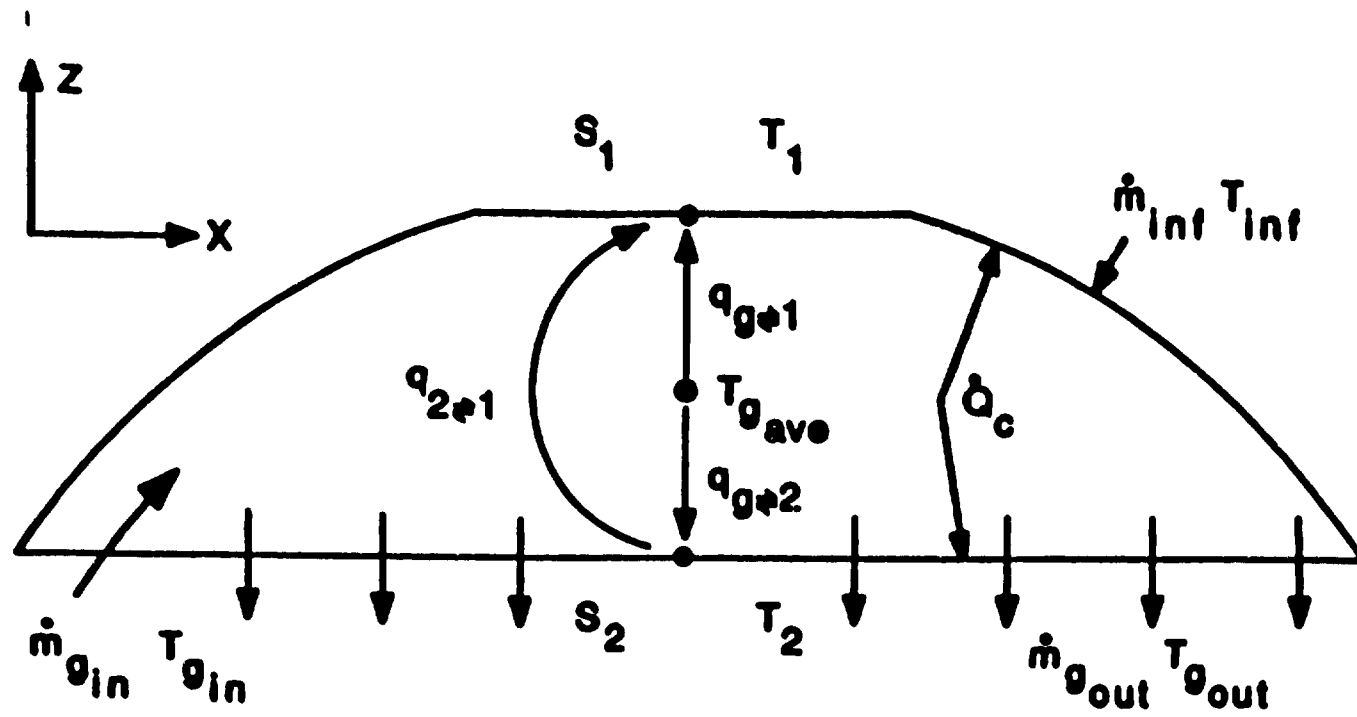


Figure 3. Radiative heat transfer in the under-lid zone.

The convective heat transfer coefficient is given by the Dittus-Boelter correlation :

$$h_c = 0.023 \frac{k}{D} Re_D^{0.8} Pr^n$$

where

$n = 0.4$ in cooling sections

$n = 0.3$ in preheat and fire sections

Pr = Prandtl number

D = equivalent diameter, $D = \frac{4A}{P}$ where A = cross-sectional area of flow.

P = wetted perimeter

k = gas conductivity taken equal to air conductivity $k = 5.45 \times 10^{-5} T + 0.00882$ (T in K)

Re_D = Reynolds number

The radiative heat transfer is calculated from the following relations :

$$q_{j=1} = \sigma \overline{GS}_1 (T_j^4 - T_1^4)$$

$$q_{j=2} = \sigma \overline{GS}_2 (T_j^4 - T_2^4)$$

$$q_{2=1} = \sigma \overline{S}_1 S_2 (T_2^4 - T_1^4)$$

where

S_1 is the cover surface at temperature T_1

S_2 is the pit surface at temperature T_2

Under the assumption that surfaces S_1 and S_2 form a speckled surface of total area S_T , the total interchange areas are given by (gray gas) :

$$\overline{GS}_1 = \frac{C_1 \epsilon_1 S_T}{\epsilon_1 + (C_1 \epsilon_1 + (1 - C_1) \epsilon_2)(1 - \epsilon_1)}$$

$$\overline{GS_2} = \frac{(1-C_s)\epsilon_g\epsilon_2S_T}{\epsilon_g + [C_s\epsilon_1 + (1-C_s)\epsilon_2](1-\epsilon_g)}$$

$$\overline{S_1S_2} = \frac{C_s(1-C_s)(1-\epsilon_g)\epsilon_2\epsilon_1S_T}{\epsilon_g + [C_s\epsilon_1 + (1-C_s)\epsilon_2](1-\epsilon_g)}$$

where

$$C_s = \frac{S_1}{S_T} = \frac{S_1}{S_1 + S_2}$$

ϵ_g = overall gas emissivity

ϵ_1 = emissivity of S_1

ϵ_2 = emissivity of S_2

The overall gas emissivity is given by the following expression :

$$\epsilon_g = C (\epsilon_{H_2O} + \epsilon_{CO_2})$$

where C is a correction factor used to consider solid particles.

Calculations made on average liquid fuel flame showed that C can be as high as 1.7 - 1.8. For natural gas flames, the value of C is lower ($\approx 1.1 - 1.3$). For a gas stream without solid particles, the value of C should be 1.0.

The following equation [3] (Lavoie, 1982) can be adapted to either water vapor or carbon-di-oxide:

$$\epsilon_{H_2O} = 10^{(A+0.001BT)}$$

where for water vapor :

$$A = -0.3429 + 0.5763 \log_{10} (P_H L)$$

$$B = -0.2663 + 0.2090 \log_{10} (P_H L)$$

T = gas temperature [$^{\circ}C$]

$P_H L$ = partial pressure of H_2O multiplied by mean length [atm.ft]

and for CO₂ :

$$A = -0.5494 + 0.3023 \log_{10} (P_C L)$$

$$B = -0.2586 + 0.09913 \log_{10} (P_C L)$$

T = gas temperature [°C]

P_HL = partial pressure of CO₂ multiplied by mean length [atm.ft]

A one-dimensional sub-model of transient heat conduction through the cover bricks has been linked to the under-lid zone model to determine the atmospheric losses and the external cover temperature.

2.2.2 THE PIT ZONE

The pit zone has three sub-control volumes, namely control volume B - middle pit, B1 - external pit near the sidewall and B2 - external pit near central wall, as shown in Figure 4. There is no temperature or flow variation along the x-axis from one CE5 brickwall to the next. The flow variation is accounted for in the transversal direction.

The need to distinguish the external pits from the internal ones became apparent when it was noticed that the temperature of anodes in the external pits, especially near the outside wall, was significantly lower. With the present 2D⁺ model, the temperature variation is accounted for along the y-axis, from gas to anode centre line, and along the z-axis, from pit top to bottom for each control volume; and for the external sub-control volumes the temperature variation is accounted for along the y-axis from gas to sidewall and from gas to sidewall and from gas to middle of central wall as the case may be.

With the present model, the total mass flow along the one-meter thick (z-axis) control volume, $m_{g,m}$ can be divided in to three fractions.

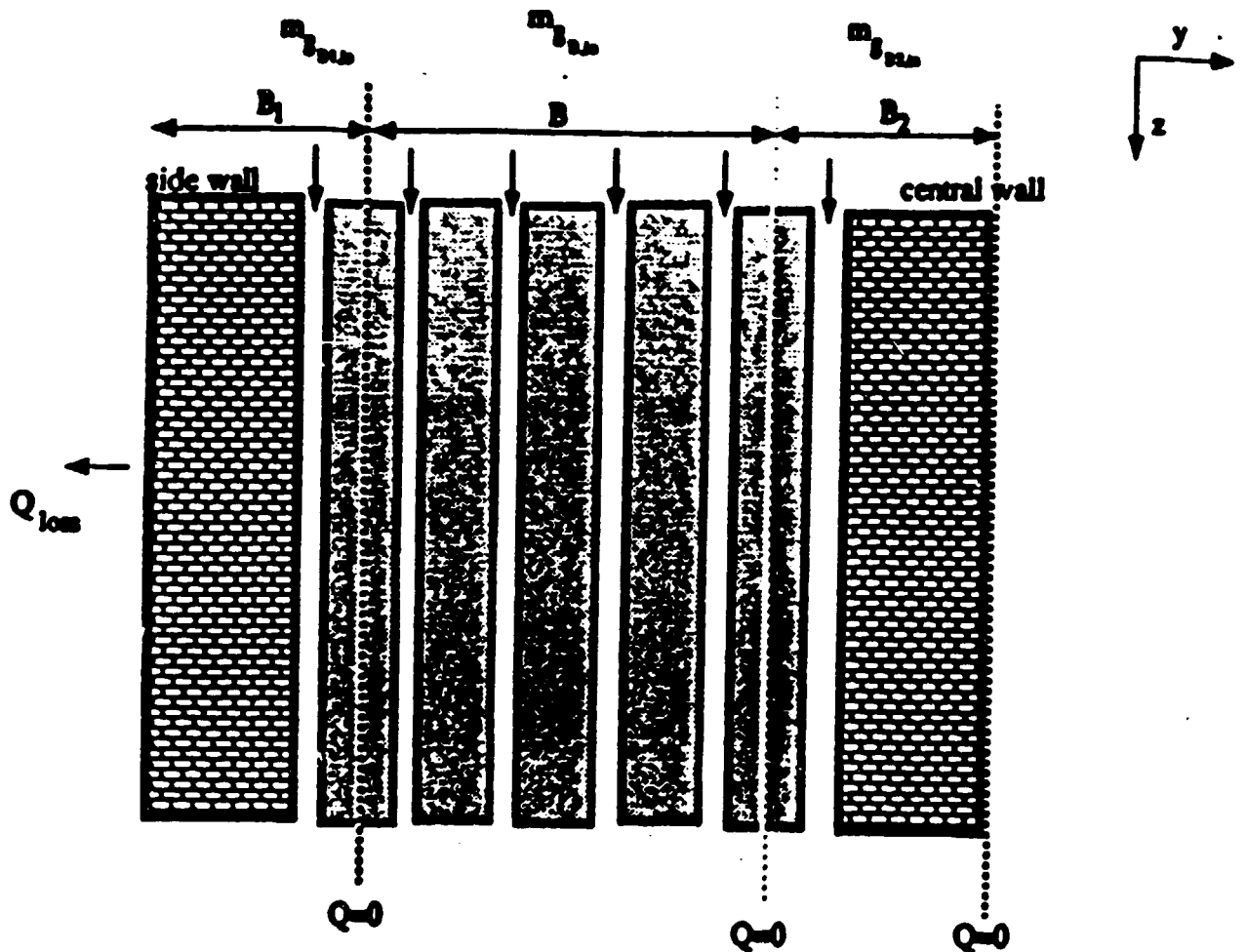


Figure 4. Three sub control volume for the pit zone

For control volume B (middle pit)

$$m_{gB,in} = (\text{fraction}) m_{g,in}$$

For control volume B1 (pit near outside wall)

$$m_{gB1,in} = (\text{fraction 1}) m_{g,in}$$

For control volume B2 (pit near inside wall)

$$m_{gB2,in} = (\text{fraction 2}) m_{g,in}$$

where fraction + fraction 1 + fraction 2 = 1. These fractions can be calculated from the experimental measurements of flow rates through the fire shaft(s) located near each control volume. This is part of the calibration work required for the model.

The energy balance done on the gas element in these sub-control volume is shown in Figure 5 and discussed below.

This discussion applies to the gas element in either of the external control volumes. It should be noted that a full flue is considered as the control volume for gas element in external pits.

The energy balance on the control volume given in Figure 5 gives

$$\dot{Q}_{g_i} - \dot{Q}_{g_{i+1}} + \dot{Q}_v - \dot{Q}_w - \dot{Q}_{sw} = \dot{Q}_{acc}$$

where

$$\dot{Q}_{g_i} = \dot{m}_{g_i} h_{g_i}$$

$$\dot{Q}_{g_{i+1}} = \dot{m}_{g_{i+1}} h_{g_{i+1}}$$

$$\dot{Q}_v = \dot{m}_v H_v$$

$$\dot{Q}_w = h_w \Delta z (T_{g,avg} - T_{w,avg})$$

$$\dot{Q}_{sw} = h_{sw} \Delta z (T_{g,avg} - T_{sw,avg})$$

with

$$T_{g,avg} = (T_{g_i} + T_{g_{i+1}})/2$$

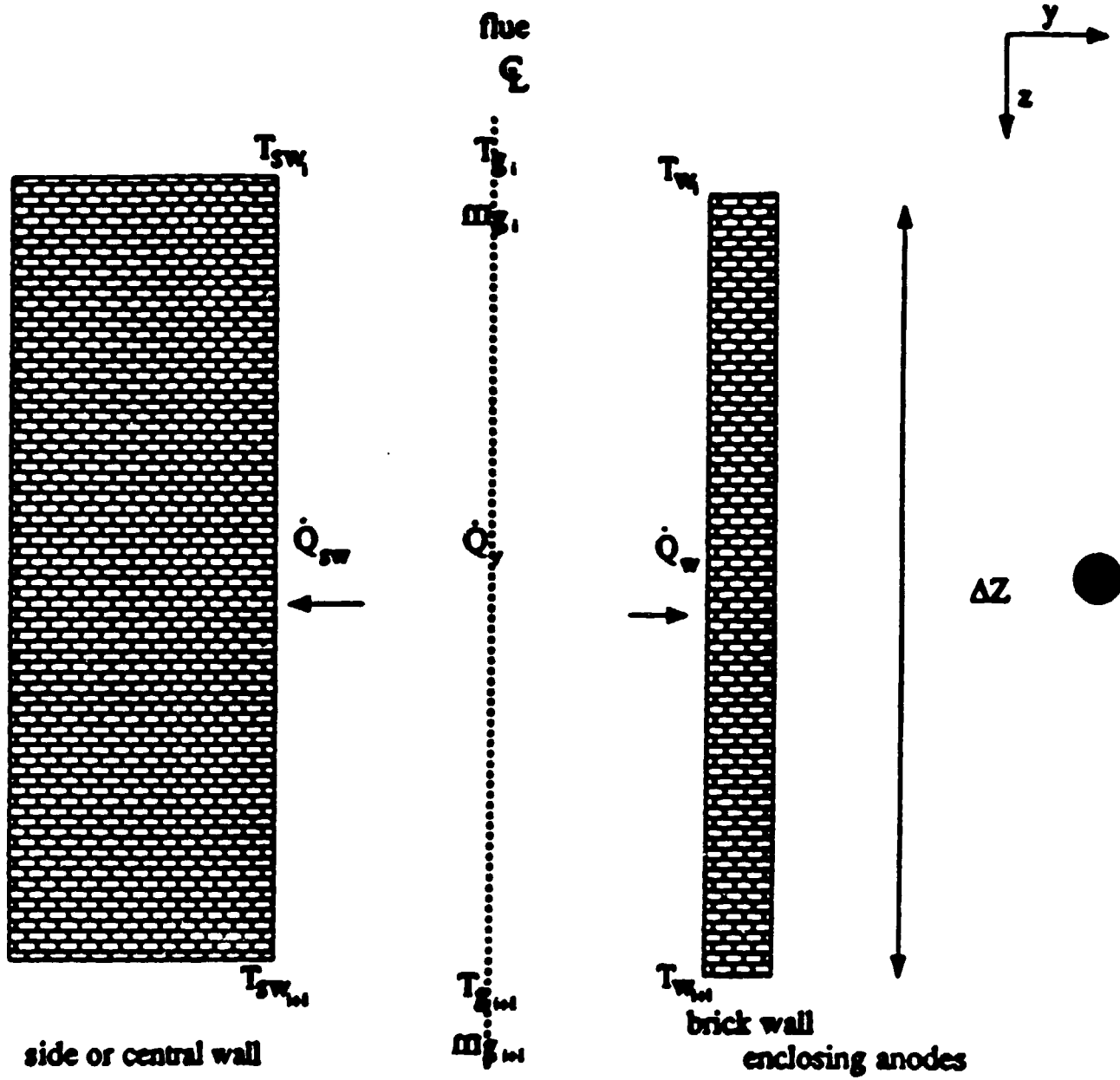


Figure 5. Control volume for one gas element in external pits (B_1 or B_2)

$$T_{v,avg} = (T_{w_i} + T_{w_{i+1}})/2$$

$$T_{sw,avg} = (T_{sw_i} + T_{sw_{i+1}})/2$$

and the symbols are defined below:

- \dot{Q}_g = Heat content of gas at position i
- $\dot{Q}_{g,i+1}$ = Heat content of gas at position i + 1
- \dot{m}_g = Gas mass flow at position i for a unit distance (1 meter) along x-axis
- $\dot{m}_{g,i+1}$ = Gas mass flow at position i + 1 for a unit distance (1 meter) along x-axis
- \dot{Q}_v = Rate of heat release from volatile combustion
- T_g = Gas temperature at position i
- $T_{g,i+1}$ = Gas temperature at position i + 1
- T_{sw_i} = Inside temperature of external wall at position i
- $T_{sw_{i+1}}$ = Inside temperature of external wall at position i+1
- \dot{Q}_{sw} = Heat flux on the inside of external wall
- \dot{Q}_w = Heat flux on the brick wall enclosing the coke covered anode
- Δz = Length of vertical division
- \dot{Q}_{acc} = Energy accumulation
- T_w = Temperature of brick wall enclosing anodes at position i
- $T_{w,i+1}$ = Temperature of brick wall enclosing anodes at position i+1
- \dot{m}_v = Mass flow of volatiles burned in control volume
- H_v = Heating value of volatiles
- h_w = Total (convective + radiative) heat transfer coefficient between gas and brick wall surface which encloses anodes
- h_{sw} = Total (convective + radiative) heat transfer coefficient between gas and inside of external wall.

\dot{Q}_{acc} , the energy accumulation is considered small and therefore omitted. It should be noted that the heat transfer coefficients h_{gw} and h_w are assumed to be equal. Although heat transfer coefficients are the same, the heat flux varies since the temperature of the inside of an external wall is different from the temperature of the brick wall enclosing the anodes.

This heat transfer coefficient, h_w varies for each control volume based on the temperature of the gas, flow rate and the geometry.

As shown in Figure 6, the control volume for the gas element in the middle pits covers only half a flue. The energy balance in the control volume for the gas element gives

$$\dot{Q}_B - \dot{Q}_{B_{out}} - \dot{Q}_c - \dot{Q}_w = \dot{Q}_{acc}$$

and the symbols have the same meanings as before.

It should be noted that there is no heat loss term here since we are dealing with the middle pits. Also an average temperature of the gas leaving zones B, B1 and B2 is calculated, to be used in energy balance calculations in zone C, the underpit zone.

For the central wall and sidewall in zone B2 and B1 respectively, the number of material layers, the material properties and the initial temperature distribution are taken as the same in both walls.

But it should be noted that the boundary conditions imposed on the two walls are different. Hence the heat fluxes would vary based on their internal wall temperatures exposed to the flowing gas.

For the central wall, an adiabatic condition ($Q=0$) is imposed on the vertical centerline of the wall. For the sidewall, the heat loss by convection

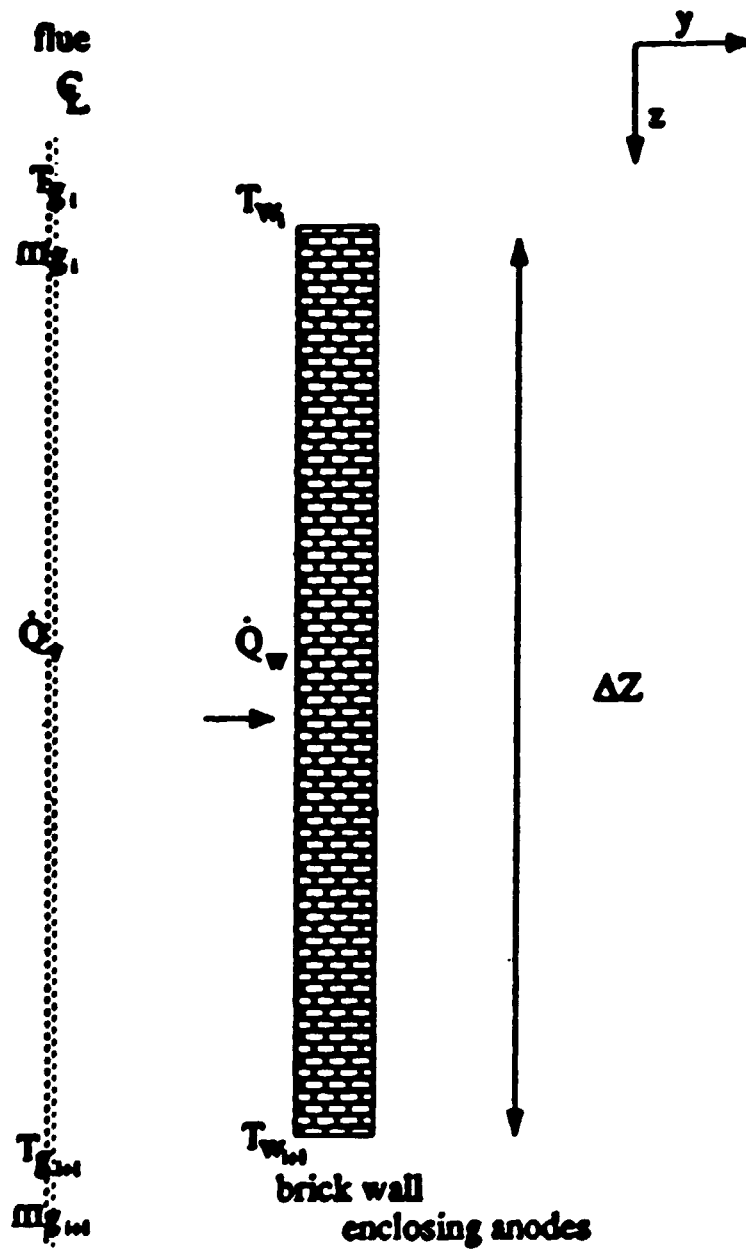


Figure 6. Control volume for one gas element in middle pits (B)

plus radiation is imposed on the external part of the sidewall which is exposed to the ambient air. Therefore,

$$h_{loss} == 1.31 (T_E - T_{amb})^{0.33} + \sigma \epsilon (T_E^3 + T_E T_{amb}^2 + T_{amb} T_E^2 + T_{amb}^3)$$

where

T_E = temperature of the outside surface of sidewall, [°K]

T_{amb} = ambient temperature, [°K]

σ = Stefan-Boltzman Constant. $5.67 \times 10^{-8} \frac{W}{m^2 K^4}$

ϵ = sidewall emissivity, 0.95

h_{loss} = Total (Convective+Radiative) heat transfer coefficient used in the heat loss calculations.

One dimensional transient conduction is applied for both walls.

The convective heat transfer coefficient, h_C is calculated as done before and the radiative heat transfer coefficient h_R in the pit zone is given by

$$h_R = \sigma C (T_j^3 + T_j T_W^2 + T_W T_j^2 + T_W^3)$$

where

$$C = \frac{1}{\frac{1}{\epsilon_w} + \frac{1}{\epsilon_g} - 1}$$

ϵ_w = wall emissivity

ϵ_g = gas emissivity

T_j = gas temperature [k]

T_w = brick wall temperature

The energy contribution to volatiles is calculated from the mass flow of

volatiles undergoing combustion. The release of volatiles is determined by the volatile evolution sub-model which is explained below.

As determined by Tremblay [4]

$$\frac{dX^i}{dT} = \frac{K_o^i}{a} [\exp(-E_o^i/RT)] (1 - X^i)^{n^i}$$

where i is the volatile constituent considered

X^i is the converted (evolved) mass fraction of i

T is the sample temperature [K]

K_o^i is the pre-exponential factor [h^{-1}]

a is the heating rate of the sample [K/h]

E_o^i is the activation energy of species i [KJ/mol]

R is the gas constant : 8.3143×10^{-3} [KJ/mol K]

n^i is the reaction order for species i

For each constituent i , the value E_0 and K_0 depend upon the heating and are listed in table 1; the reaction order n is also given in Table 1.

KINETIC PARAMETERS n , E_0 AND K_0

CONSTITUENT	n	E_0 (KJ/mol)	K_0 (h ⁻¹)
TAR	0.7	4.167 ln(a) + 35.0	exp[0.273E ₀ - 6.417]
H ₂	1.1	5.882 ln(a) + 57.65	exp[0.233E ₀ - 10.39]
CH ₄	0.8	10.0 ln(a) + 76.0	exp[0.225E ₀ - 11.325]

As X^i , the converted fraction of volatile i , can be determined for any anne temperature T , it is now possible to find the average volatile mass flow for one furnace section during a temperature raise from T_1 to T_2 :

$$\dot{m}_i = \frac{(X^i(T_2) - X^i(T_1))}{\Delta t} \cdot PC \cdot PCVR \cdot ANMAS$$

where \dot{m}_i = mass flow of volatile i
in temperature interval considered [kg/s]

$X^i(T)$ = converted fraction of volatile i at
temperature T

Δt = time to raise temperature T_1 to T_2 [s]

PC^i = fraction of volatile i over all volatile released
(mass basis, taken at the end of the pyrolysis)

In view of the difficulties of handling correctly the behaviour of tar in the present mathematical model, its combustion was assumed instantaneous as for hydrogen and methane, the reaction takes place in the pit or underpit zone at the release location.

Any volatile that evolves when the adjacent gas temperature is below the ignition temperature is considered lost. Below are the ignition temperatures, as reported by Dervedde (1986):

Tar : 425 ± 50 °C

H₂ : 575 °C

CH₄ : 630 °C.

Solid Elements

As presented in [6] there are nine types of nodes in the solid element. The mesh is shown in Figure 7. The nine types of nodes are shown in Figure 7a and 7b. Note that 0 stands for a node, surrounded by four others numbered 1, 2, 3 and 4 (this numbering has nothing to do with the node types just mentioned). Each node receives heat Q_1 , Q_2 , Q_3 and Q_4 . This results in the following equations depending on the node. Note that an explicit scheme as shown in References 7 and 8 has been used. The number of grids can be changed if desired. Normally for our simulation a 10×8 grid (80 nodes) is used with a time increment of 160 seconds.

The 2D* model allows the variation of thermal properties, density, heat capacity and conductivity with temperature for the solids: brick, coke and anode in the pit zone.

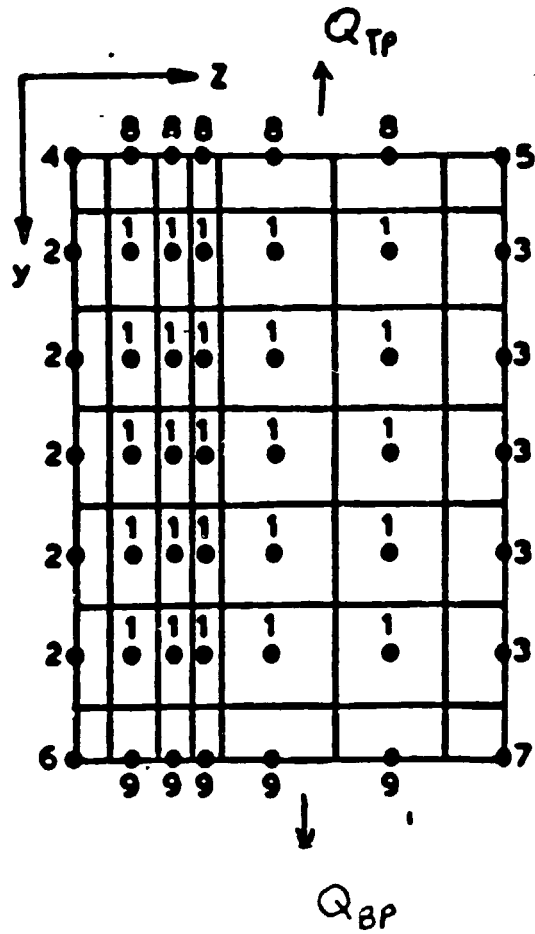


Figure 7. Mesh with 9 types of nodes.

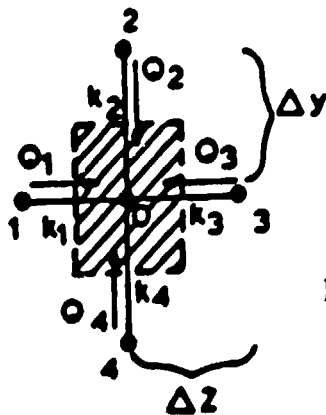
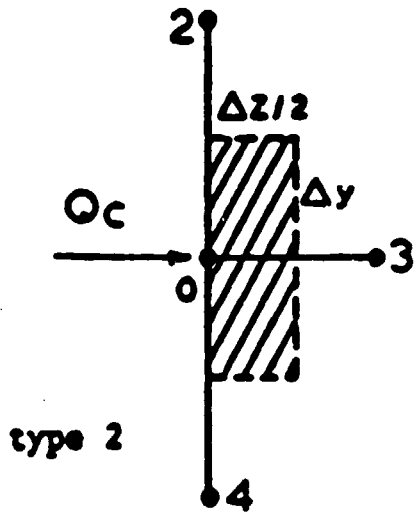
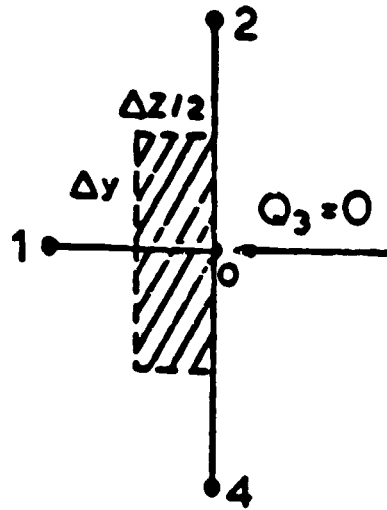


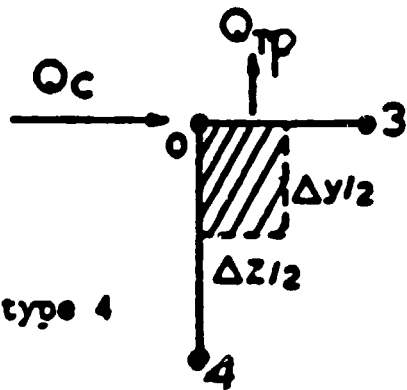
Figure 7a. Node o of Type 1.



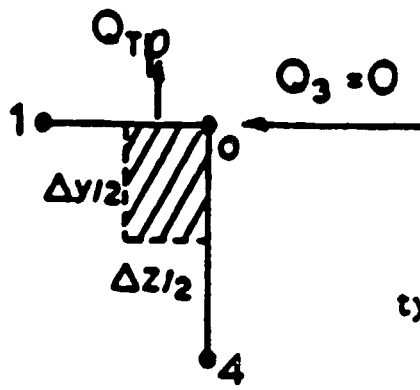
type 2



type 3



type 4



type 5

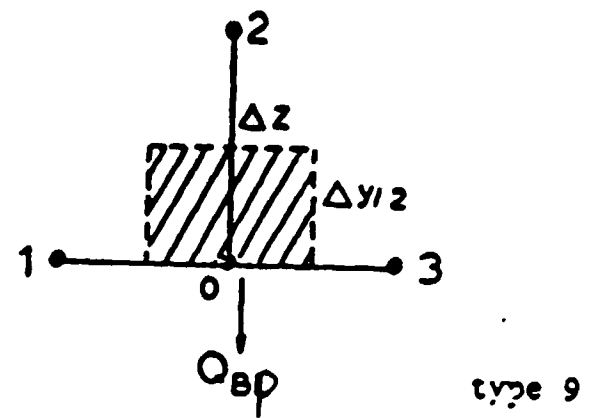
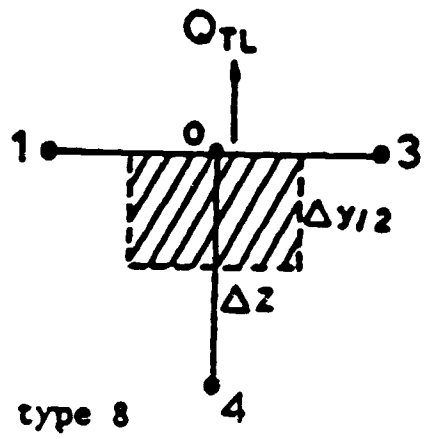
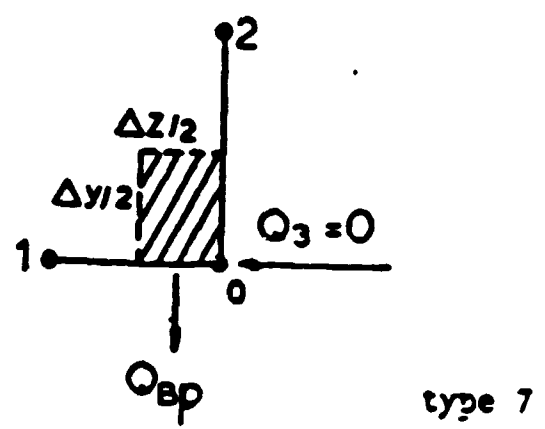
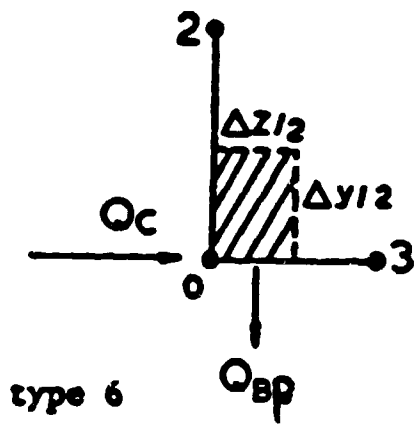


Figure 7b. The type of nodes 2 to 9.

The equations are

$$T_0^{v+1} = T_0^v + \frac{\Delta t}{\rho c_p} \left[\frac{k_1}{\Delta z^2} (T_1^v - T_0^v) + \frac{k_3}{\Delta z^2} (T_1^v - T_0^v) + \frac{k_2}{\Delta y^2} (T_2^v - T_0^v) + \frac{k_6}{\Delta y^2} (T_6^v - T_0^v) \right]$$

Type 1

$$T_0^{v+1} = T_0^v + \frac{\Delta t}{\rho c_p} \left[\frac{2k_3}{\Delta z^2} (T_1^v - T_0^v) + \frac{k_2}{\Delta y^2} (T_2^v - T_0^v) + \frac{k_6}{\Delta y^2} (T_6^v - T_0^v) + \frac{2h_T}{\Delta z} (T_8^v - T_0^v) \right]$$

Type 2

$$T_0^{v+1} = T_0^v + \frac{\Delta t}{\rho c_p} \left[\frac{2k_1}{\Delta z^2} (T_1^v - T_0^v) + \frac{k_2}{\Delta y^2} (T_2^v - T_0^v) + \frac{k_6}{\Delta y^2} (T_6^v - T_0^v) \right]$$

Type 3

$$T_0^{v+1} = T_0^v + \frac{2\Delta t}{\rho c_p} \left[k_3 \frac{T_3^v - T_0^v}{\Delta z^2} + k_4 \frac{T_4^v - T_0^v}{\Delta y^2} + h_T \frac{T_g^v - T_0^v}{\Delta z} - \frac{q_{TP}}{\Delta y} \right]$$

type 4.

$$T_0^{v+1} = T_0^v + \frac{2\Delta t}{\rho c_p} \left[k_1 \frac{T_1^v - T_0^v}{\Delta z^2} + k_5 \frac{T_5^v - T_0^v}{\Delta y^2} - \frac{q_{TP}}{\Delta y} \right] \quad \text{type 5}$$

$$T_0^{v+1} = T_0^v + \frac{2\Delta t}{\rho c_p} \left[k_2 \frac{T_2^v - T_0^v}{\Delta y^2} + k_3 \frac{T_3^v - T_0^v}{\Delta z^2} + h_T \frac{T_g^v - T_0^v}{\Delta z} - \frac{q_{BP}}{\Delta y} \right] \quad \text{type 6}$$

$$T_0^{v+1} = T_0^v + \frac{2\Delta t}{\rho c_p} \left[k_1 \frac{T_1^v - T_0^v}{\Delta z^2} + k_2 \frac{T_2^v - T_0^v}{\Delta y^2} - \frac{q_{BP}}{\Delta y} \right]$$

type 7

$$T_0^{v+1} = T_0^v + \frac{2\Delta t}{\rho c_p} \left[\frac{k_1}{2} \frac{T_1^v - T_0^v}{\Delta z^2} + \frac{k_3}{2} \frac{T_3^v - T_0^v}{\Delta z^2} + k_4 \frac{T_4^v - T_0^v}{\Delta y^2} - \frac{q_{TL}}{\Delta y} \right]$$

type 8

$$T_0^{v+1} = T_0^v + \frac{2\Delta t}{\rho c_p} \left[\frac{k_1}{2} \frac{T_1^v - T_0^v}{\Delta z^2} + k_2 \frac{T_2^v - T_0^v}{\Delta y^2} + \frac{k_3}{2} \frac{T_3^v - T_0^v}{\Delta z^2} - \frac{q_{BL}}{\Delta y} \right]$$

type 9

Solving these equations give the temperature distribution at all the nodes as a function of time.

2.2.3 The Underpit Zone

The underpit zone is shown in Figure 8.

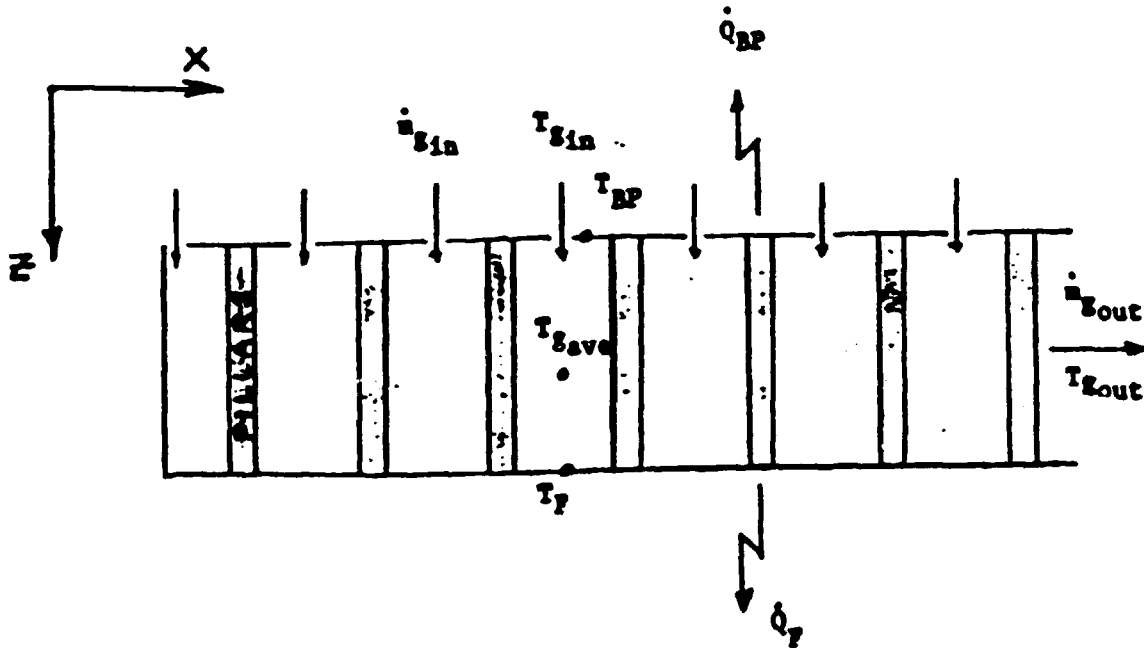


Figure 8. The underpit zone.

- T_{BP} : Average bottom pit temperature (K)
- T_F : Average foundation floor temperature (K)
- $T_{S_{ave}}$: Average gas temperature in the under-pit zone (K)
- \dot{m}_{Sin} : Total inlet gas mass flow (kg/s)
- \dot{m}_{Sout} : Total outlet gas mass flow (kg/s)

It is treated exactly as the under-lid zone. The following equation applies :

$$\dot{Q}_{gin} - \dot{Q}_{gout} - \dot{Q}_F - \dot{Q}_{BP} - \dot{Q}_{PIL} = \dot{Q}_{acc}$$

where

$$\dot{Q}_{gin} - \dot{Q}_{gout} = \dot{m}_{gin} h_{gin} - \dot{m}_{gout} h_{gout}$$

$$\dot{Q}_F = h_F A_F (T_{gacc} - T_F)$$

h_F is the total (convective and radiative) heat transfer coefficient between gas and foundation floor area A_F .

$$\dot{Q}_{BP} = h_{BP} A_{BP} (T_{gacc} - T_{BP})$$

h_{BP} is the total (convective and radiative) heat transfer coefficient between gas and pit bottom A_{BP} .

$$\dot{Q}_{PIL} = m_{PIL} c_p \frac{T_{PIL}^{t+\Delta t} - T_{PIL}^t}{\Delta t}$$

\dot{Q}_{PIL} is the energy accumulated in the brick pillars sustaining the pits. The average pillar temperature T_{PIL} is assumed to be equal to $\frac{T_{BP} + T_F}{2}$.

\dot{Q}_{acc} is the energy accumulated in the gas control volume. It is neglected.

The underpit zone model is linked to a one dimensional transient heat conduction sub-model to determine the heat losses to the foundations.

The radiative heat fluxes in the underpit zone are given by the same expressions as the under-lid zone. S_1 is in this case the under pit surface at temperature T_1 and S_2 is the foundation floor at temperature T_2 .

2.2.4 The Headwall and Fireshaft Zone

Since the temperature distribution in the head wall is not of critical importance, it was decided to consider its global influence on the furnace behaviour. Therefore a unique average temperature is assigned to the headwall and fireshaft and this temperature is taken to be the average solid temperature of the two adjacent sections.

Figure 9 gives a sketch of the assumed control volume.

The variables are :

$T_{g,in}$: Average inlet gas temperature (K)

$T_{g,out}$: Average outlet gas temperature (K)

T_H : Average headwall and fireshaft brick temperature (K)

$\dot{m}_{g,in}$: Total gas mass flow at inlet (kg/s)

$\dot{m}_{g,out}$: Total gas mass flow at outlet (kg/s)

We then have the following equation:

$$\dot{Q}_{g,in} - \dot{Q}_{g,out} - \dot{Q}_F - \dot{Q}_S - \dot{Q}_H + \dot{Q}_{COMB} = \dot{Q}_{acc}$$

where

$$\dot{Q}_{g,in} - \dot{Q}_{g,out} = \dot{m}_{g,in} h_{g,in} - \dot{m}_{g,out} h_{g,out}$$

$$\dot{Q}_F = h_F A_F (T_{g,acc} - T_F)$$

\dot{Q}_F is the heat loss through a foundation area corresponding to the headwall and fireshaft foundation area. It is considered equal in W/m^2 to the foundation losses calculated in the underpit zone.

\dot{Q}_S is the heat loss through a sidewall area corresponding to the headwall and fireshaft sidewall area. It is considered as the average of heat losses per unit area through the sidewall and through the central wall calculated in the pit zone.

$$\dot{Q}_{COMB} = \dot{m}_F H_F$$

where \dot{m}_F is the mass flow rate of fuel

H_F is the fuel heating value

\dot{Q}_H is the energy accumulated in the headwall during Δt seconds.

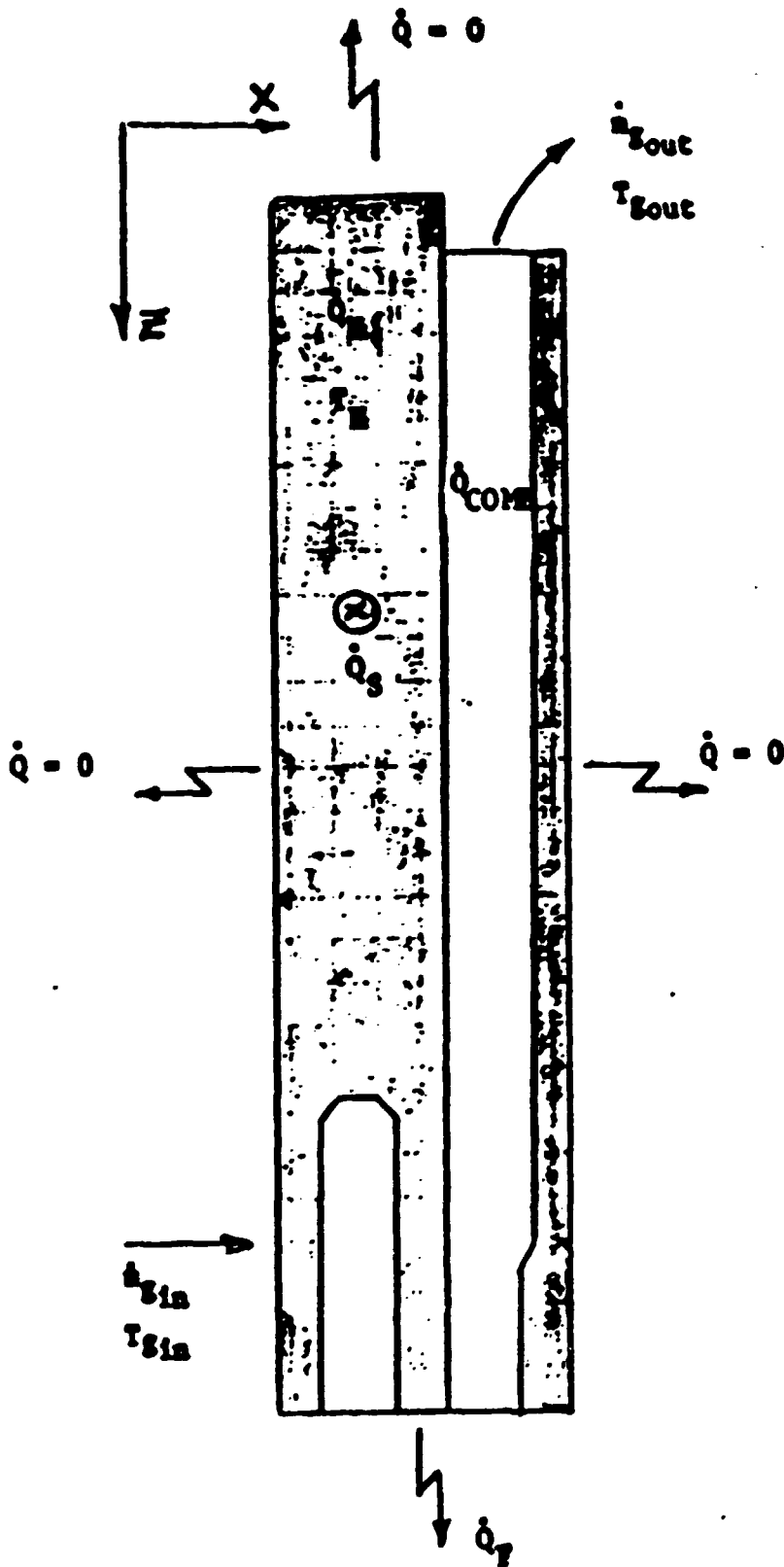


Figure 9. Control volume for headwall and fireshaft zone.

$$\dot{Q}_H = m_H c_{pH} \frac{T_H^{t+\Delta t} - T_H^t}{\Delta t}$$

where m_H is the total mass of headwall and fresh shaft.

c_{pH} is the average brick heat capacity and T_H is taken equal to the average solid temperature determined in the two adjacent sections. \dot{Q}_{acc} , is the energy accumulation term in the gas, is neglected.

2.2.5 GAS COMPOSITION SUB-MODEL

The gas composition sub-model is applied at four locations inside each furnace section corresponding to the points of entry flow regions (or zones) A, B, C, D (Figure 1).

2.2.5.1 Zone A :

Gas composition is known at location 1 (Figure. 1); it has to be determined at location 2.

Let O2REM(1), N2REM(1), H2OREM(1), CO2REM(1) be the known gas composition (kmoles/s) at location 1. Air infiltration and packing coke combustion occur in Zone A.

The molar flow of constituents for a given mass flow \dot{m}_{inf} of infiltrated air will be :

$$H_2OINF = (X_{H_2O} \dot{m}_{inf})/18.0$$

$$O_2INF = (X_{O_2} \dot{m}_{inf})/32.0$$

$$N_2INF = (X_{N_2} \dot{m}_{inf})/28.0$$

where H2OINF, O2INF and N2INF are expressed in terms of kmoles/s and \dot{m}_{inf} in kg/s.

The proportion of water in moist air on a mass basis is :

$$X_{H_2O} = w/1 + w$$

The proportion of oxygen and nitrogen in moist air on a mass basis is :

$$X_{O_2} = \frac{0.232}{1+w} \left[\frac{\text{kg } O_2}{\text{moist air}} \right]$$

$$X_{N_2} = \frac{0.768}{1+w} \left[\frac{\text{kg } N_2}{\text{moist air}} \right]$$

where w has the units of Kg H₂O/kg dry air and can be expressed by :

$$w = 0.622 (P_v/P_a)$$

P_v = partial pressure of H₂O [Pa]

P_a = partial pressure of dry air [Pa]

$$P_v = \phi \cdot P_g$$

where ϕ is the relative humidity and P_g is the saturation pressure of water vapor at ambient temperature.

$$P_a = P_{atm} - P_v$$

where p_{atm} is the atmospheric pressure.

PACKING COKE COMBUSTION

Packing coke is assumed to be pure carbon associated with certain amount of non-reacting ash.

The molar flow of carbon burned is given by :

$$C = \frac{(1 - X_{ash}) \dot{m}_{PC}}{12.0}$$

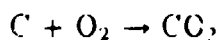
where C is expressed in kmoles/s

X_{ash} : proportion of ash in packing coke on a mass basis

\dot{m}_{PC} : mass flow of packing coke consumption [kg/s]

12.0 is the molecular weight of carbon C [kg/kmole]

Assuming ideal combustion, the reaction is :



The molar flow of O₂ required for carbon combustion is equal to that of

carbon burned :

$$O_2 = \frac{(1-X_{ash})\dot{m}_{PC}}{12.0}$$

The molar flow of CO₂ produced by packing coke combustion is also :

$$CO_2 = \frac{(1-X_{ash})\dot{m}_{PC}}{12.0}$$

where O₂ and CO₂ are expressed in kmoles/s.

The following equations apply :

$$O_2REM(2) = O_2REM(1) + O_2INF - \frac{(1-X_{ash})\dot{m}_{PC}}{12.0}$$

$$N_2REM(2) = N_2REM(1) + N_2INF$$

$$H_2OREM(2) = H_2OREM(1) + H_2OINF$$

$$CO_2REM(2) = CO_2REM(1) + \frac{(1-X_{ash})\dot{m}_{PC}}{12.0}$$

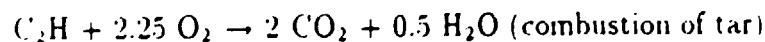
where suffices REM and INF stand for remaining and infiltrated respectively.

2.2.5.2 Zone B

Gas composition is known at location 2; it is now being determined at location 3.

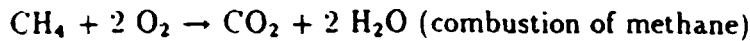
In zone B, only volatile combustion is assumed to take place. Let ALPHA be the fraction of volatiles burning in zone B and BETA, the fraction burning in zone C such that ALPHA + BETA = 1.

The exact chemical composition of tar is difficult to define but it is generally accepted that C and H are in the ratio of 2 : 1. Assuming tar to be (C₂H)_n, the governing reaction for complete combustion comes :



The complete combustion reaction for hydrogen and methane are more standard :





According to these reactions.

In zone B, the following equations apply:

$$\text{O2REM}(3) = \text{O2REM}(2) - \text{ALPHA} * \left[\frac{2.25 \dot{m}_{\text{tar}}}{25.0} + \frac{0.5 \dot{m}_{\text{H}_2}}{2.0} + \frac{2.0 \dot{m}_{\text{CH}_4}}{16.0} \right]$$

$$\text{N2REM}(3) = \text{N2REM}(2)$$

$$\text{H2OREM}(3) = \text{H2OREM}(2) + \text{ALPHA} * \left[\frac{2.0 \dot{m}_{\text{tar}}}{25.0} + \frac{\dot{m}_{\text{H}_2}}{2.0} + \frac{2.0 \dot{m}_{\text{CH}_4}}{16.0} \right]$$

$$\text{CO2REM}(3) = \text{CO2REM}(2) + \text{ALPHA} * \left[\frac{0.5 \dot{m}_{\text{tar}}}{25.0} + \frac{\dot{m}_{\text{CH}_4}}{16.0} \right]$$

2.2.5.3 Zone C

Gas composition being known at location 3, the computation is extended to location 4. In zone C, it is assumed that only volatiles (the BETA fraction) is burning. Therefore :

$$\text{O2REM}(4) = \text{O2REM}(3) - \text{BETA} * \left[\frac{2.25 \dot{m}_{\text{tar}}}{25.0} + \frac{0.5 \dot{m}_{\text{H}_2}}{2.0} + \frac{2.0 \dot{m}_{\text{CH}_4}}{16.0} \right]$$

$$\text{N2REM}(4) = \text{N2REM}(3)$$

$$\text{H2OREM}(4) = \text{H2OREM}(3) + \text{BETA} * \left[\frac{2.0 \dot{m}_{\text{tar}}}{25.0} + \frac{\dot{m}_{\text{H}_2}}{2.0} + \frac{2.0 \dot{m}_{\text{CH}_4}}{16.0} \right]$$

$$\text{CO2REM}(4) = \text{CO2REM}(3) + \text{BETA} * \left[\frac{0.5 \dot{m}_{\text{tar}}}{25.0} + \frac{\dot{m}_{\text{CH}_4}}{16.0} \right]$$

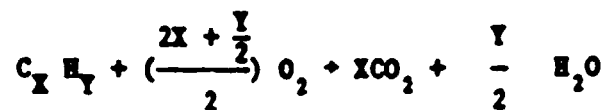
2.2.5.4 Zone D

One step is left now : proceed from location 4 to location 1. leading to next section. It is assumed that fuel combustion takes place in Zone D.

FUEL COMBUSTION

Fuel composition is assumed to be of the type: C_xH_y which covers a wide range of liquid and gaseous fuels.

The governing reaction is :



Let \dot{m}_f be the mass flow rate of fuel burned. the molar flow is then:

$$C_x H_y = \frac{\dot{m}_f}{W_f}$$

where \dot{m}_f is in kg/s. C_xH_y in kmoles/s and W_f , the molecular weight of fuel, in kg/kmole.

The molar flow of oxygen required for combustion of fuel becomes :

$$O_2 = \left(\frac{2x + \frac{y}{2}}{2}\right) \cdot \frac{\dot{m}_f}{W_f}$$

The molar flow of CO₂ and H₂O produced is :

$$\text{CO}_2 = X \cdot \frac{\dot{m}_f}{W_f}$$

$$\text{H}_2\text{O} = \frac{Y}{2} \cdot \frac{\dot{m}_f}{W_f}$$

Therefore, the following equations can apply :

$$\text{O}_2\text{REM} = \text{O}_2\text{REM}(4) - (2X+Y/2)/2 \cdot \dot{m}_f/W_f$$

$$\text{N}_2\text{REM} = \text{N}_2\text{REM}(4)$$

$$\text{H}_2\text{O}\text{REM} = \text{H}_2\text{O}\text{REM}(4) + X \cdot \dot{m}_f/W_f$$

$$\text{CO}_2\text{REM} = \text{CO}_2\text{REM}(4) + (Y/2) \dot{m}_f/W_f$$

The procedure is repeated for the next section and so on until the end of the furnace is reached.

2.3 THE OVERALL SOLUTION PROCEDURE

The model thus proposed is dynamic and extends from the first preheat section to the last covered cooling section. The user has to define all relevant operational and geometrical parameters and the total simulation time, the latter being equal to the duration of the number of permutations (fire changes) he wants to calculate.

Since the model is dynamic, the user has to define initial conditions (mass flow, gas and solid temperature at time $t = 0$ for each section in the fire train).

The overall solution procedure is shown on Figure 10. At time $t = 0$ the initial solid temperature distribution is known. Assuming these temperatures to be constant over time increment Δt the program calculates the corresponding gas temperatures which are applied during Δt seconds to the solids to reach new temperatures. The procedure iterates over time until it reaches the fire cycle time. A new (cold) section is then added to the fire train and the last cooling section is dropped. A new permutation starts and the program runs until the total number of permutations is covered or steady state (5 °C temperature difference of the gas temperature between two fire changes) is reached.

The total number of permutations necessary to achieve steady state depends on the assumed initial temperature distribution. If the initial distributions are adequately approximated, the total number of permutations will be small.

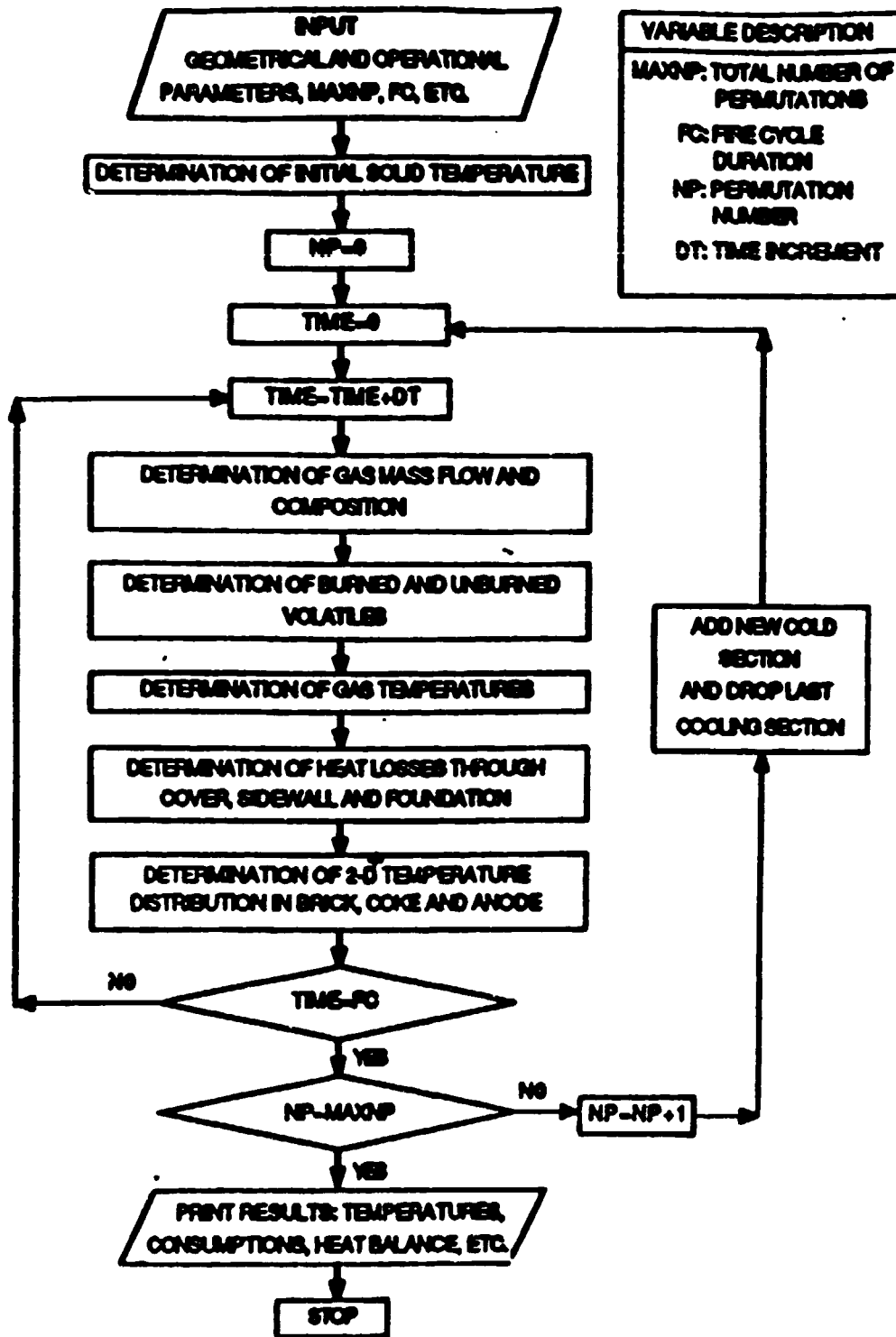


Figure 10. Solution procedure.

REFERENCES

1. Bourgeois, T., Bui, R.T., Charette, A., Salder, B.A. and Tomsett, A.D., *Computer Simulation of a Vertical Ring Furnace*, Light Metals, AIME, 1989.
2. Thibault, M.A., *Modele dynamique du four de cuisson d'anodes*, Master's Thesis, UQAC, 1985.
3. Lavoie, S., *Equation des courbes d'emissivite du CO₂ et H₂O d'apres les graphiques de Hottel et al*, Letter from Alcan to UQAC dated June, 1982.
4. Tremblay, F. *Cinetique de degagement des matieres volatiles lors de pyrolyse d'electrodes de carbone industrielles*, Master's Thesis, UQAC, 1987.
5. E. Dervedde, A. Charette, T. Bourgeois and L. Castonguay, *Kinetic Phenomenon of the Volatiles in Ring Furnaces*, Light Metals, AIME, 1986.
6. Bui, R.T., Charette, A. and T. Bourgeois, *Simulating the Process of Carbon Anode Baking Used in the Aluminium Industry*, Metallurgical Transactions, Vol. 15B, 1984.
7. Schenk, A., *Fortran Methods in Heat Flow*, Ronalds Press, 1963.
8. Bui, R.T., Charette, A. and T. Bourgeois, *Modelling the Ring Furnace*, Report no 1, UQAC, 1982.

9. Kovacs, D., *Preliminary Investigations into Heat Transfer Conditions in the Riedhammer Ovens*, Boyne Smelters Limited, Carbon Products Department, July, 1986.

**UNDER THE AUSPICES OF
THE UNITED NATIONS INDUSTRIAL DEVELOPMENT ORGANIZATION**

**WORKSHOP ON COMPUTER-BASED
MATHEMATICAL MODELLING
OF
ALUMINIUM PRODUCTION PROCESSES**

**Jawaharlal Nehru Aluminium Research
Development and Design Centre
Nagpur, India
September 1993**

**MODELLING OF CASTING FURNACES
(COURSE MATERIAL)**

André Charette

**University of Quebec at Saguenay
Quebec, Canada**

OUTLINE OF THE PRESENTATIONS

PART 1- Description of some typical casting furnaces.

PART 2- Numerical methods in radiative heat transfer

PART 3- Mathematical modelling

- **The melter/holder furnace**
 - **Analytic model (1D)**
 - **Simplified model**
 - **Fuel optimization calculations**
 - **3D model**
- **The circular remelting furnace**

PART 1

***FURNACE DESIGN,
EQUIPMENT AND
PERFORMANCE***

FURNACE DESIGN AND EQUIPMENT

- DEFINITIONS

**- TYPICAL FURNACES: ENVIRONMENT
CONFIGURATION
EQUIPMENT**

WITHIN THE ALUMINIUM INDUSTRY, FURNACES, MAINLY GAS OR FUEL FIRED, ARE SIMPLE ENCLOSURES WHERE HEAT IS TRANSFERRED TO THE CHARGE BROUGHT OR HELD AT A TARGET TEMPERATURE AND PREPARED FOR CASTING

DEFINITIONS:

HOLDER:

A FURNACE IN WHICH LIQUID ALUMINIUM IS HELD AND PREPARED FOR CASTING

EX: TILTING CASTING FURNACE IN A REMELT PLANT

HOLDER/MELTER:

AS ABOVE BUT ABLE TO MELT UP TO 20% OF ITS CHARGE WEIGHT AS SOLID (COLD) METAL

EX: TILTING CASTING FURNACE IN A SMELTER TO MELT RUN-AROUND SCRAP

MELTER:

MOST OF ITS CHARGE IS MADE OF SOLID ALUMINIUM TO BE MELTED

EX: CIRCULAR TOP-CHARGED MELTER IN REMELT PLANT OR STATIONARY SIDEWELL FURNACE IN RECYCLING PLANT

THE HOLDER AND HOLDER/MELTER ARE VERY SIMILAR IN DESIGN.

THE FOLLOWING CONFIGURATIONS WILL BE PRESENTED:

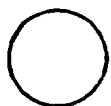
- 1) TILTING HOLDER/MELTER IN A SMELTER**
- 2) SIDEWELL FURNACE IN A RECYCLING PLANT**
- 3) ROUND, TOP CHARGED MELTER IN A REMELT PLANT**

HOLDER/MELTER IN A SMELTER

- ENVIRONMENT**
- TYPICAL CHARGE**
- FURNACE OPERATIONS**
- CONFIGURATION AND EQUIPMENT**

HOLDER/MELTER IN A SMELTER ENVIRONMENT

HOLDER/MELTER TYPICAL CHARGE:

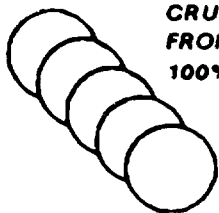


HOT METAL FROM
HOLDER OR
CRUCIBLES
85%

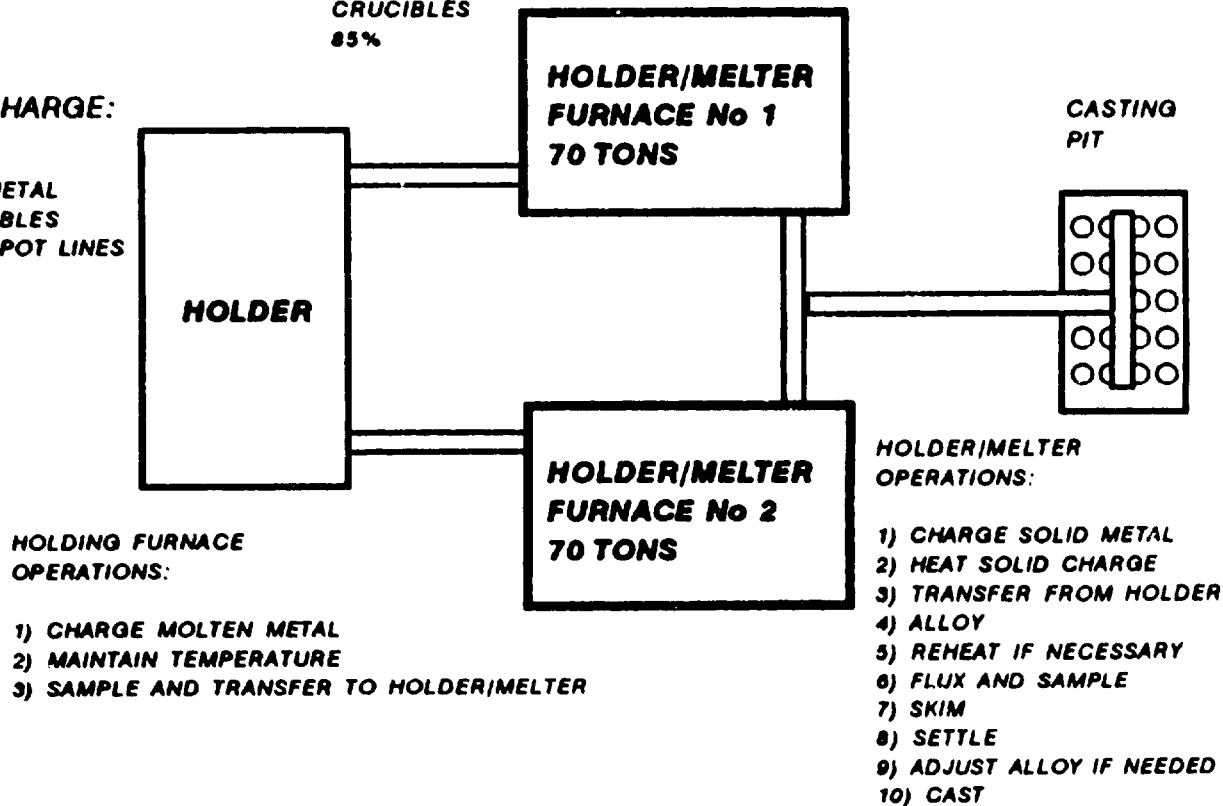


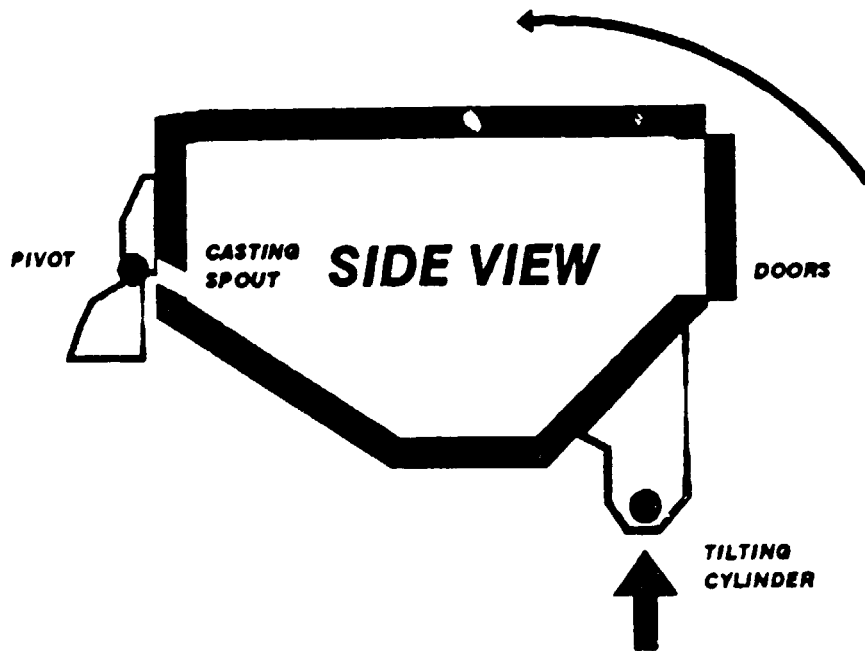
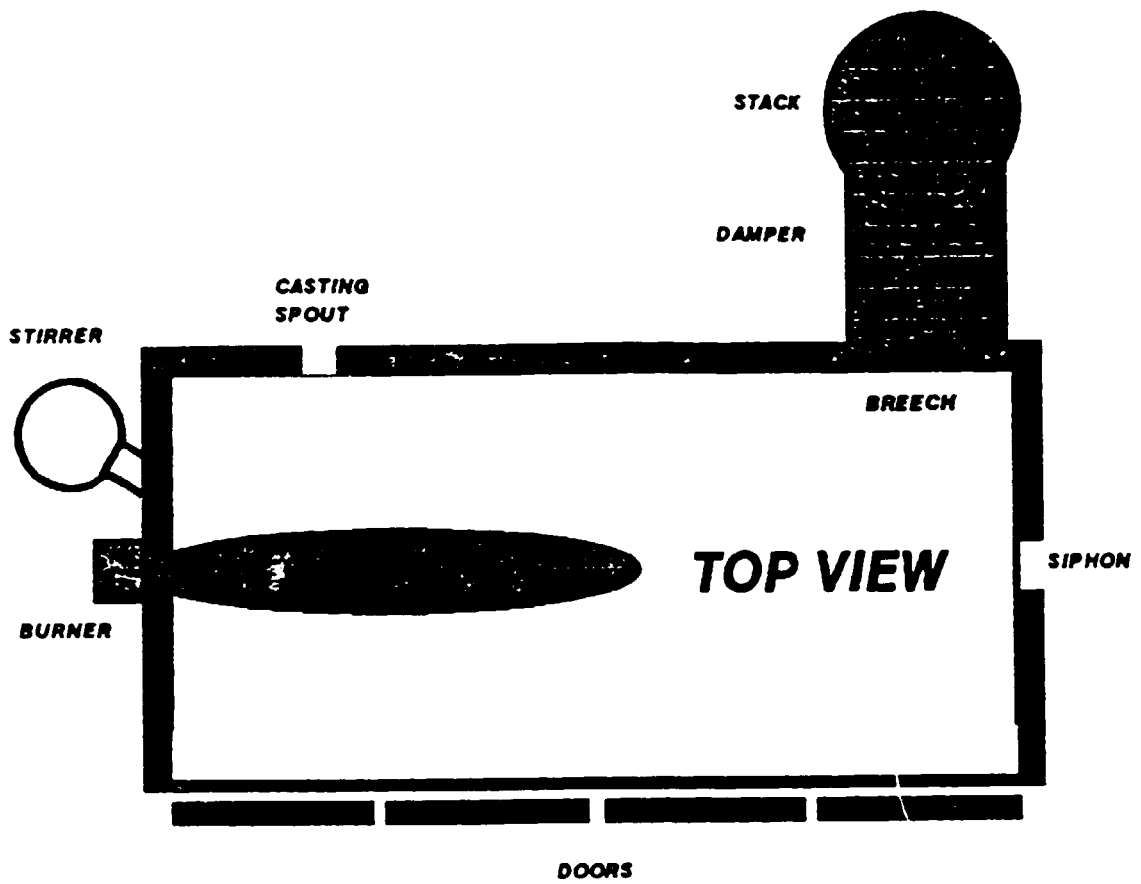
SOLID REJECTS
SCRAP INGOTS,
DRAINING PANS
ETC.
15%

HOLDER TYPICAL CHARGE:



HOT METAL
CRUCIBLES
FROM POT LINES
100%



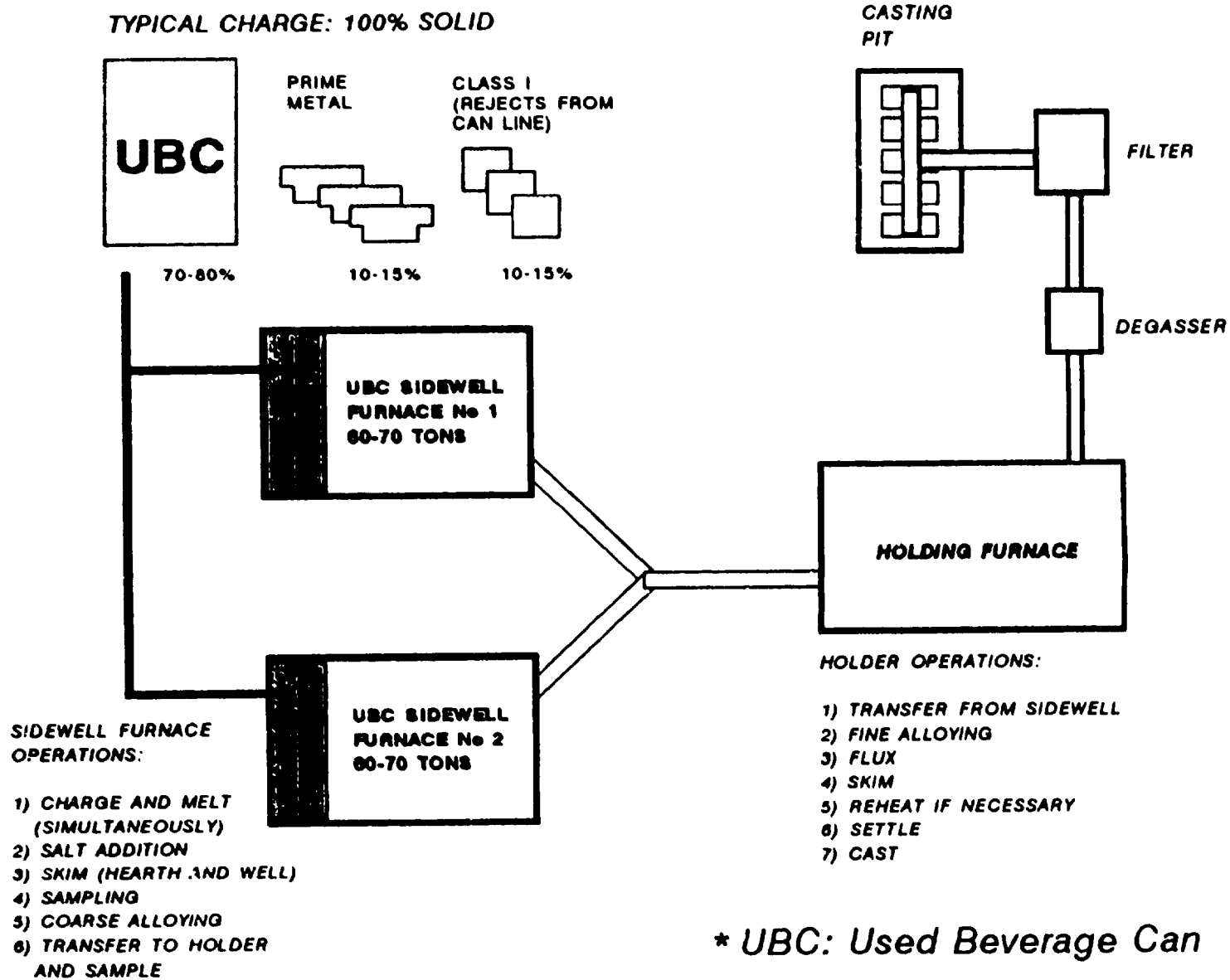


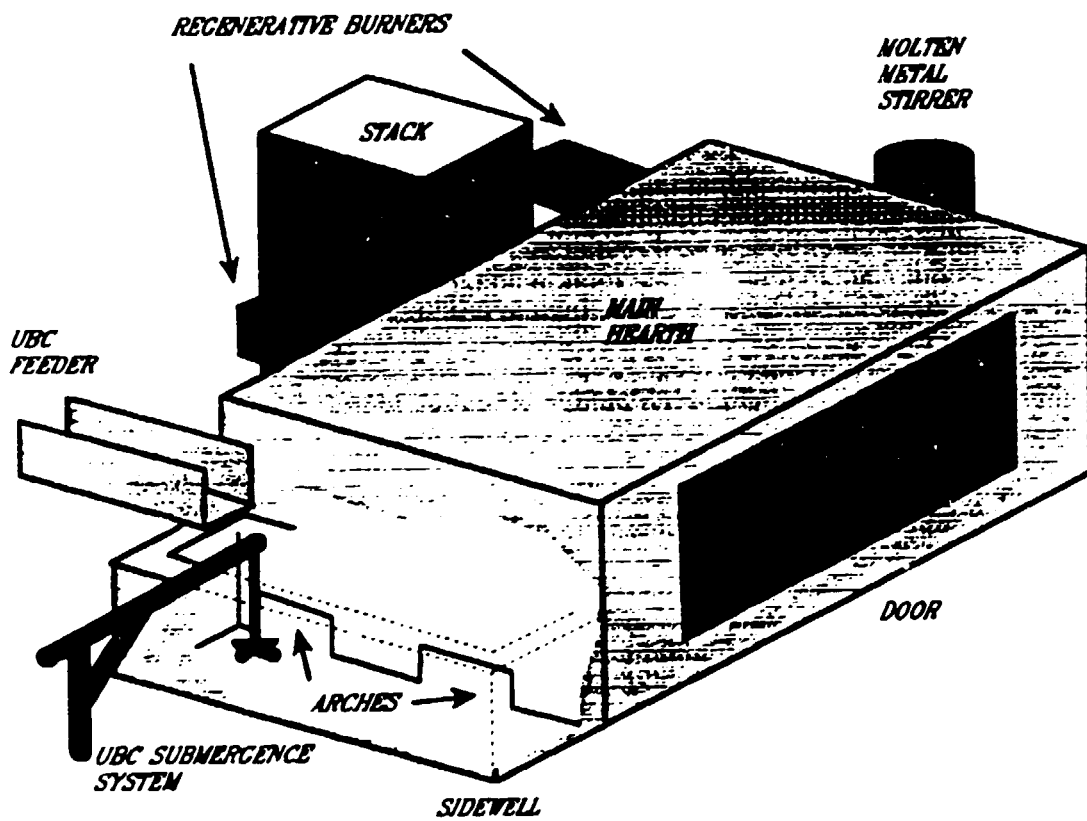
SCHEMATIC REPRESENTATION OF HOLDER/MELTER

SIDEWELL FURNACE IN A RECYCLING PLANT

- ENVIRONMENT**
- TYPICAL CHARGE**
- FURNACE OPERATIONS**
- CONFIGURATION AND EQUIPMENT**

UBC* SIDEWELL FURNACE IN A RECYCLING PLANT



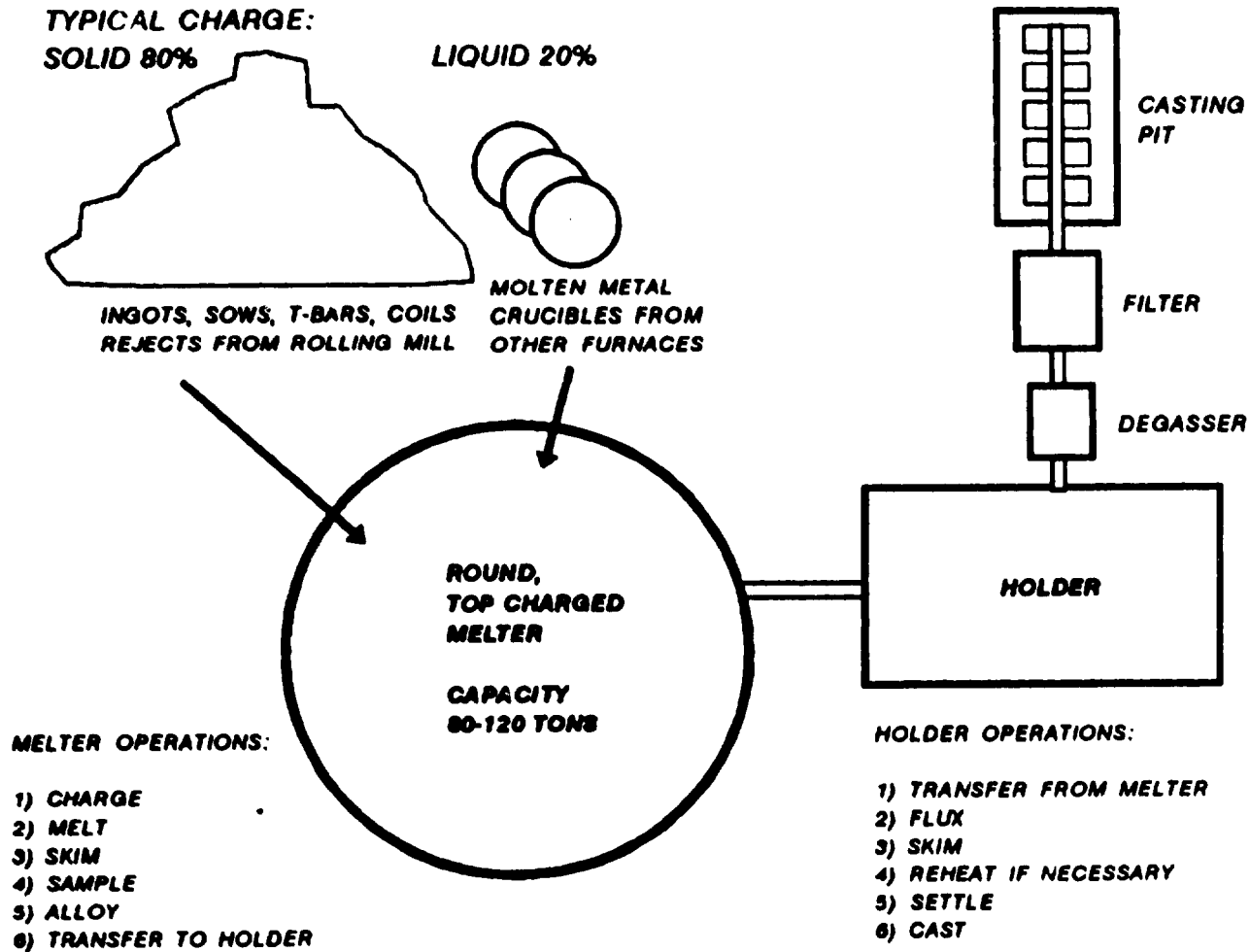


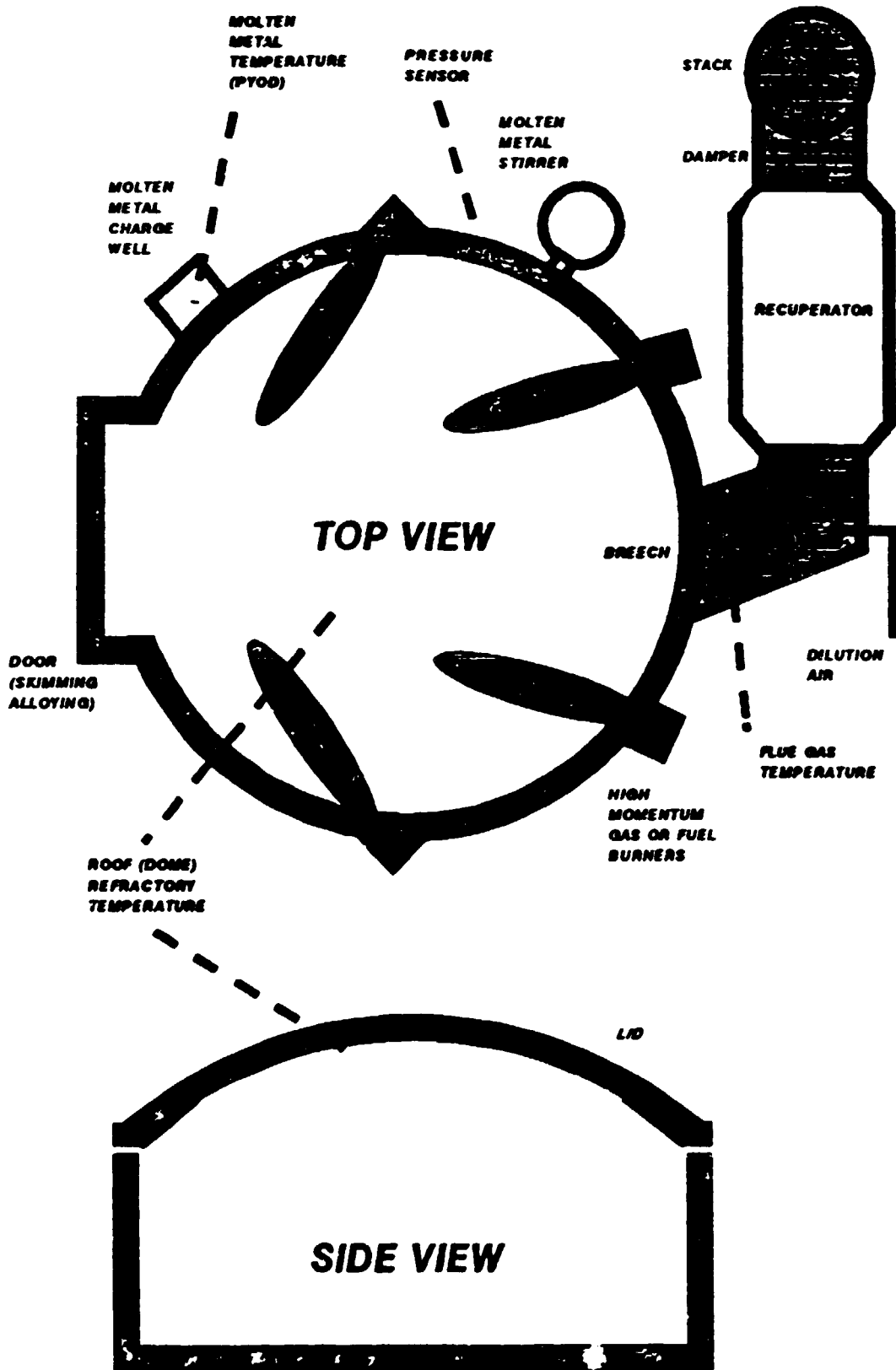
SCHEMATIC REPRESENTATION OF UBC RECYCLING FURNACE

CIRCULAR MELTER IN A REMELT PLANT

- ENVIRONMENT**
- TYPICAL CHARGE**
- FURNACE OPERATIONS**
- CONFIGURATION AND EQUIPMENT**
- CONTROLS**

MELTING FURNACE IN A REMELT CASTING CENTRE

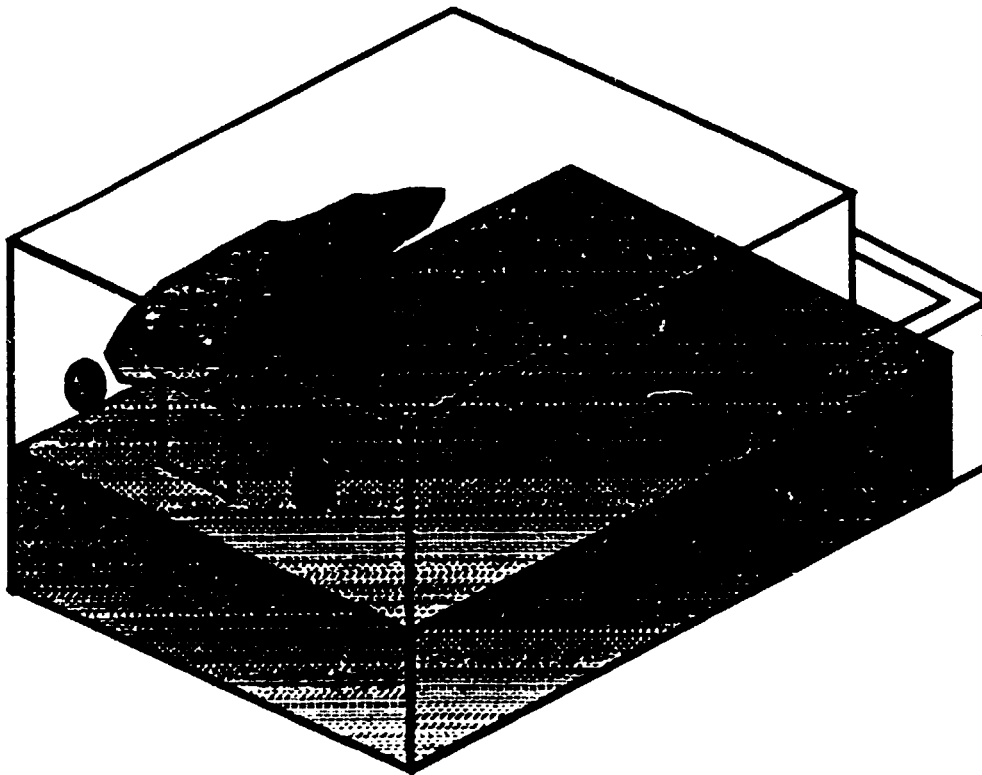




SCHEMATIC REPRESENTATION OF ROUND, TOP CHARGED MELTER

FURNACE PERFORMANCE

- MAJOR PHYSICAL PHENOMENA OCCURRING IN FURNACE**
- A TYPICAL FURNACE HEAT BALANCE**
- PERFORMANCE EVALUATION**
- PARAMETERS AFFECTING FURNACE PERFORMANCE**



MAJOR PHYSICAL PHENOMENA OCCURRING IN FURNACE

IN THE COMBUSTION CHAMBER:

- **RADIATIVE AND CONVECTIVE HEAT TRANSFER**
- **COMBUSTION REACTION**
- **HEAT CONDUCTION IN WALLS**
- **HEAT LOSSES TO THE ENVIRONMENT**

IN THE METAL CHARGE:

- **HEAT CONDUCTION**
- **PHASE CHANGE (SOLID TO LIQUID)**
- **NATURAL AND FORCED CONVECTION**
- **HEAT CONDUCTION THROUGH FLOOR**
- **HEAT LOSSES TO ENVIRONMENT**

A TYPICAL FURNACE HEAT BALANCE MAY CONTAIN THE FOLLOWING ELEMENTS:

A) HEAT SOURCES:

- 1) HEAT FROM THE FUEL**
- 2) HEAT FROM THE PREHEATED COMBUSTION AIR**
- 3) HEAT FROM THE PREHEATED SOLID CHARGE**

B) HEAT SINKS:

- 1- HEAT ACCUMULATED IN THE CHARGE**
- 2- HEAT ACCUMULATED IN REFRACTORIES**
- 3- HEAT LOSS THROUGH THE STACK**
- 4- HEAT LOSS TO THE ENVIRONMENT**

PERFORMANCE EVALUATION INDICES:

A) HOW FAST ?

1- MELT RATE:

defined as solid charge mass divided by duration of melting period

2- PRODUCTION RATE:

defined as solid charge mass divided by total batch duration

B) HOW MUCH ?

1- SPECIFIC FUEL CONSUMPTION

defined as total fuel energy input divided by solid charge mass

2- FUEL EFFICIENCY:

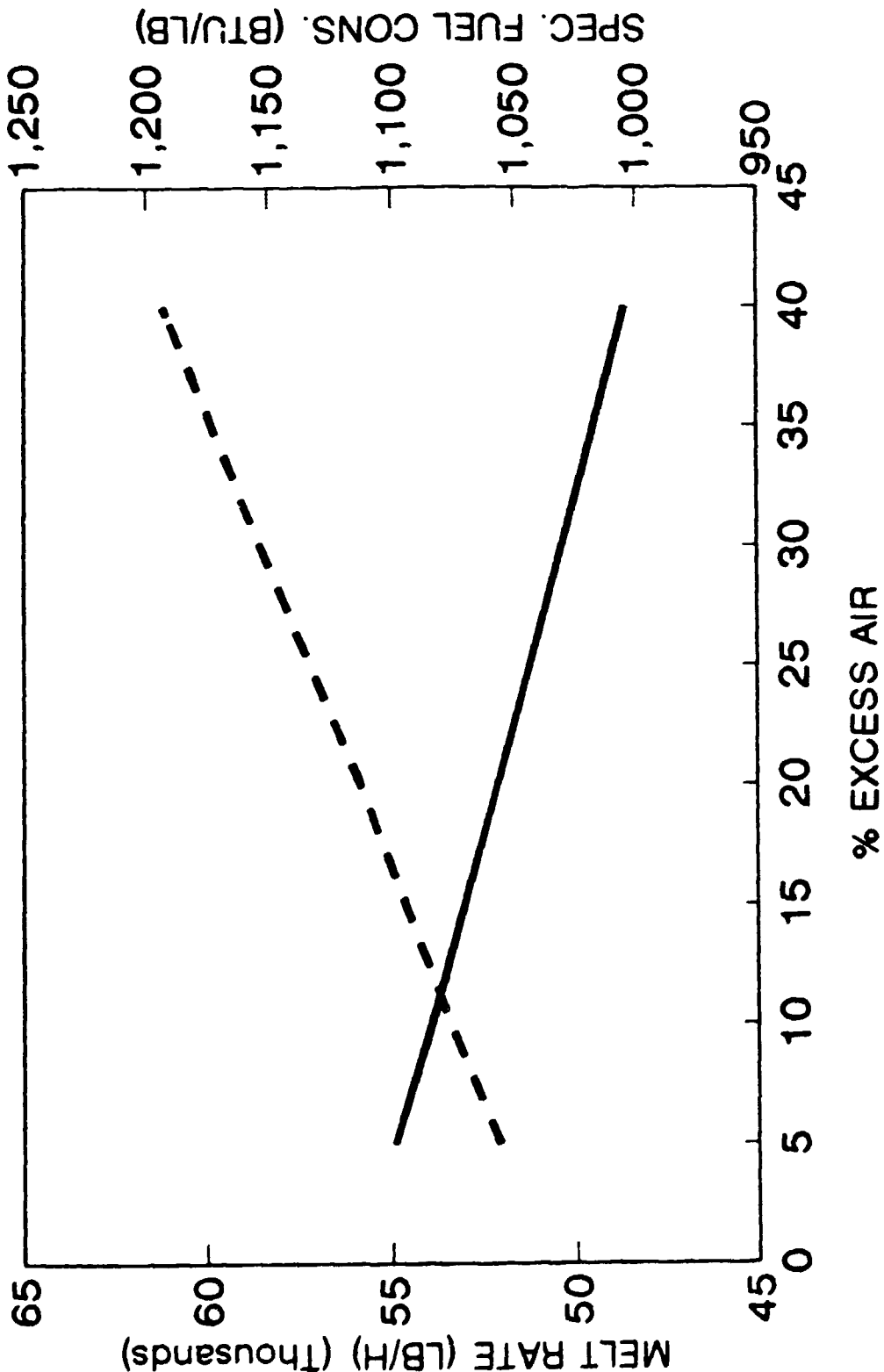
defined as energy transferred to charge divided by total fuel energy input

PARAMETERS AFFECTING FURNACE PERFORMANCE:

- 1- EXCESS AIR**
- 2- COMB. AIR TEMPERATURE (RECUPERATORS)**
- 3- OXYGEN ENRICHMENT**
- 4- SCRAP CHARGE TEMPERATURE (PREHEATERS)**
- 5- CHARGING TIME (REFRACTORY INITIAL TEMPERATURE)**
- 6- DOOR OPENING**
- 7- FLUE GAS TEMPERATURE**
- 8- FIRING RATE**
- 9- AMOUNT OF SOLID CHARGE**
- 10- DROSS THICKNESS**
- 11- AIR INLEAKAGE (DRAUGHT CONTROL)**
- 12- STIRRING THE MELT (JET PUMP)**
- 13- FURNACE DESIGN AND CAPACITY**

EFFECT OF EXCESS AIR ON FURNACE PERFORMANCE FOR A TYPICAL ROUND, TOP-CHARGED MELTER

— MELT RATE - - - SPEC. FUEL CONS.



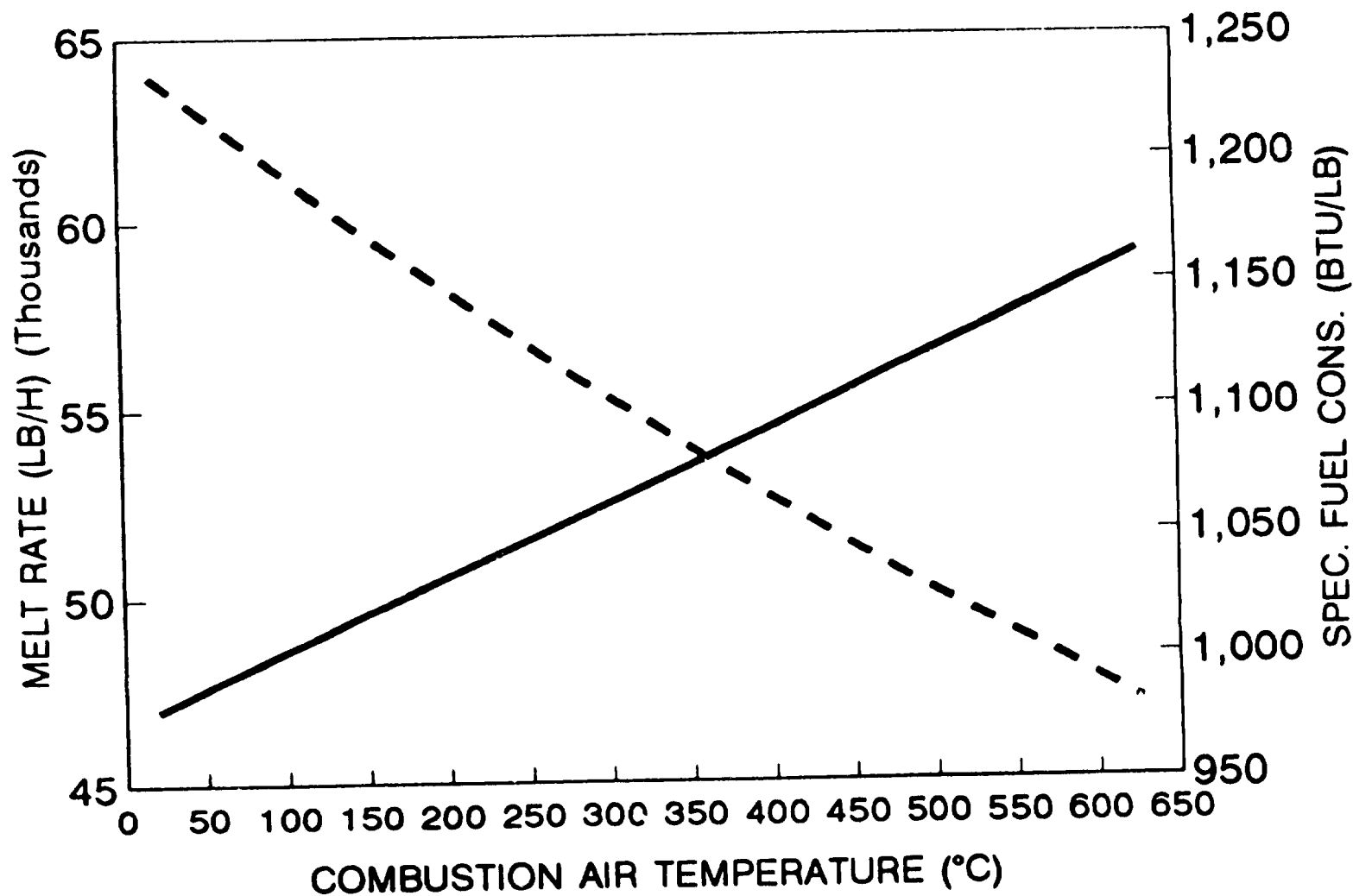
PART 2

METHODS IN

RADIATIVE TRANSFER

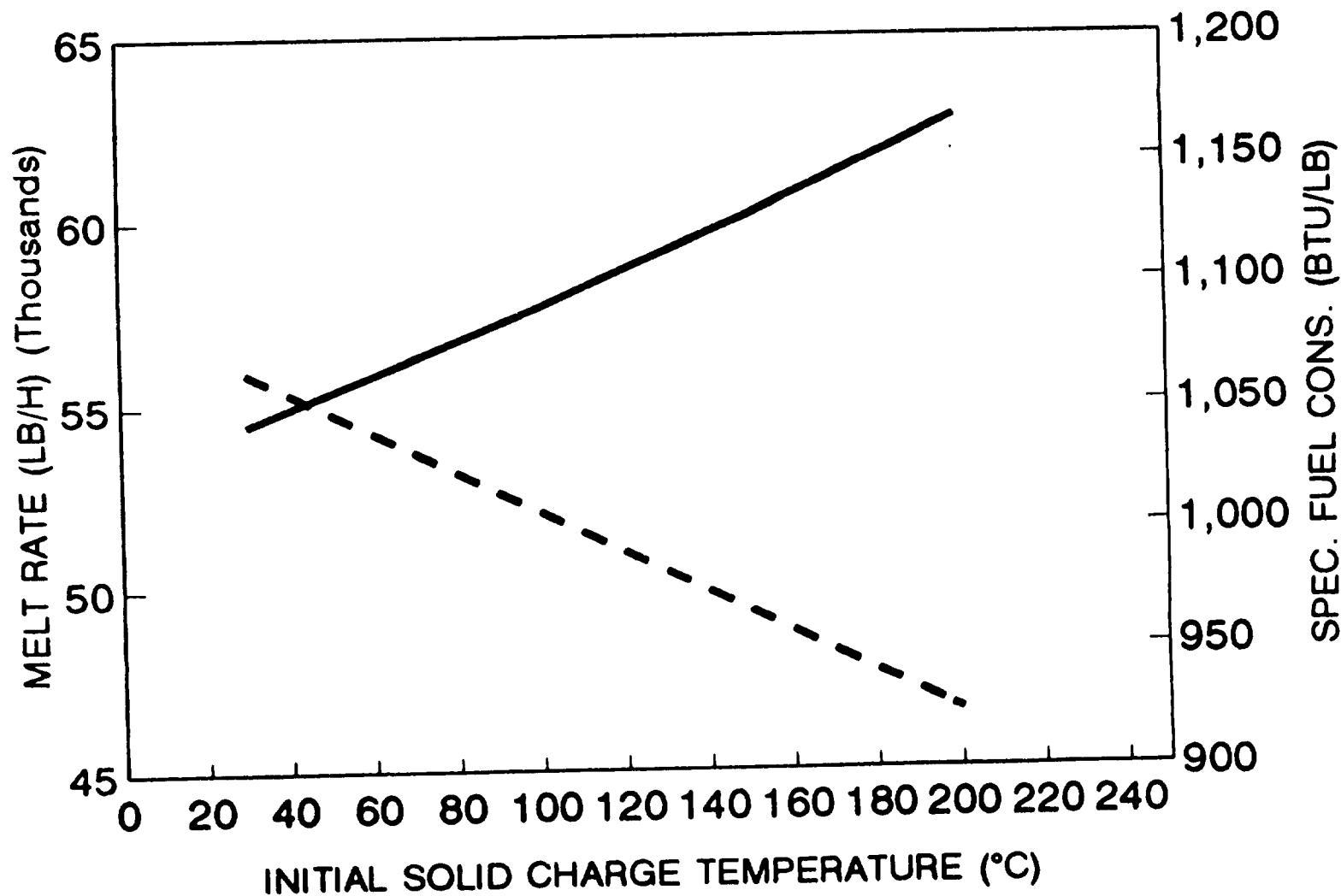
EFFECT OF COMBUSTION AIR TEMPERATURE ON FURNACE PERFORMANCE FOR A TYPICAL ROUND, TOP-CHARGED MELTER

-- MELT RATE -- SPEC. FUEL CONS.



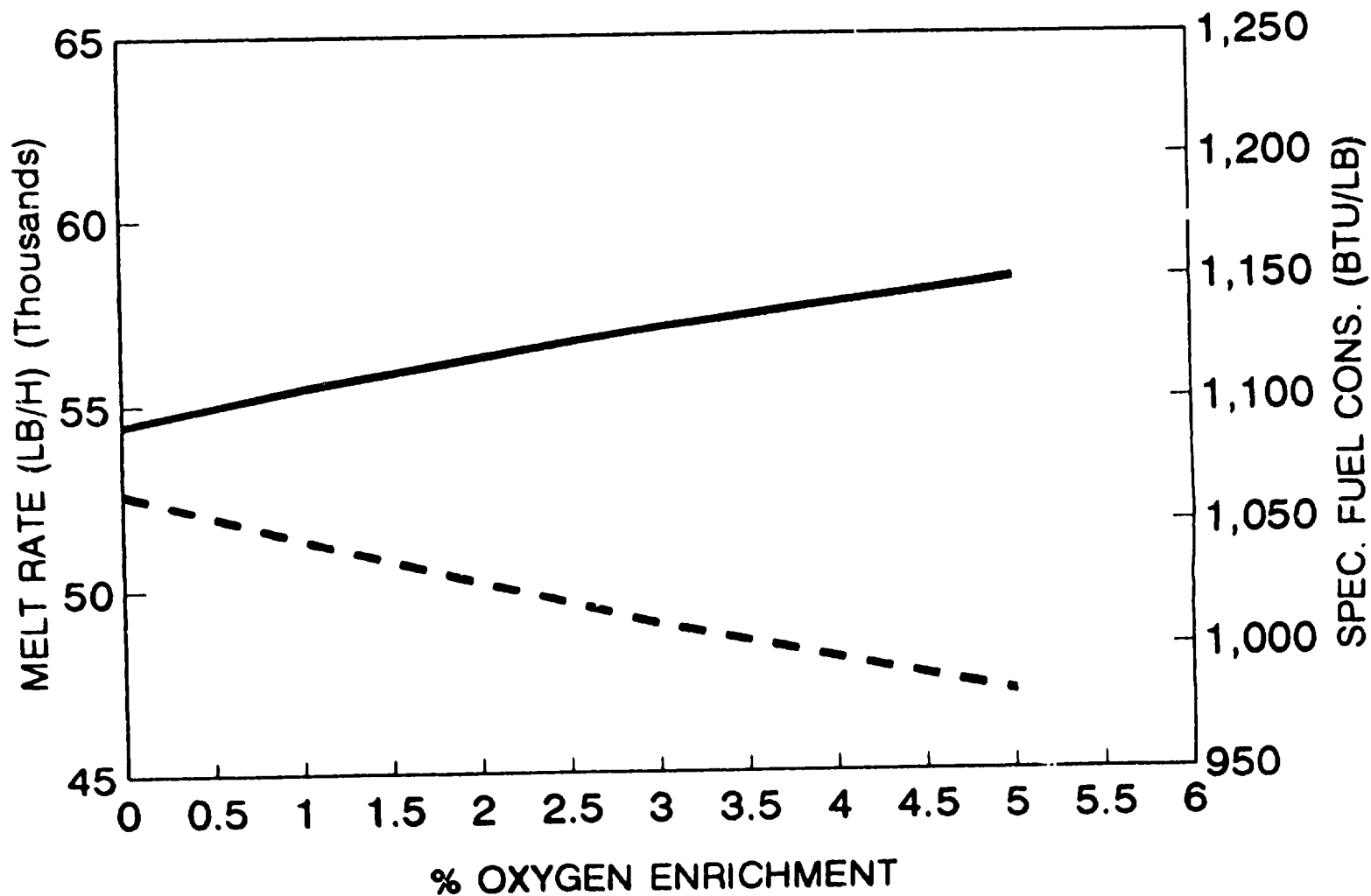
EFFECT OF INITIAL SOLID CHARGE TEMP. ON FURNACE PERFORMANCE FOR A TYPICAL ROUND, TOP-CHARGED MELTER

— MELT RATE - - SPEC. FUEL CONS.



EFFECT OF OXYGEN ENRICHMENT ON FURNACE PERFORMANCE FOR A TYPICAL ROUND, TOP-CHARGED MELTER

— MELT RATE - - SPEC. FUEL CONS.



RADIATIVE HEAT TRANSFER

Some numerical methods:

- 1- Zone method**
- 2- Monte Carlo method**
- 3- Imaginary planes method**
- 4- Discrete transfer method**
- 5- Discrete ordinates method**
- 6- 6 flux method**

FUNDAMENTAL EQUATIONS

$$\mu \frac{\partial I}{\partial x} + \eta \frac{\partial I}{\partial y} + \xi \frac{\partial I}{\partial z} = \kappa I_{b, gas} - \kappa I$$

$$\nabla \cdot (\vec{\Omega} I) = \kappa I_{b, gas} - \kappa I$$

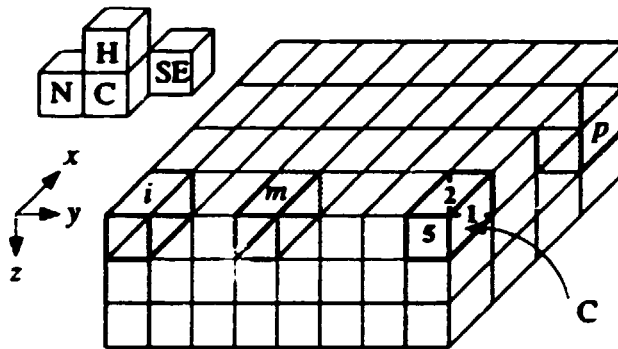
$$\mu^2 + \eta^2 + \xi^2 = 1$$

$$I_{leaving}(\vec{\Omega}) = \epsilon I_{b, surface} + \frac{\rho}{\pi} \int_{\vec{n} \cdot \vec{\Omega} < 0} |\vec{n} \cdot \vec{\Omega}| I_{incident}(\vec{\Omega}) d\Omega \quad \vec{n} \cdot \vec{\Omega} > 0,$$

$$\nabla \cdot \vec{q} = 4\pi\kappa I_{b, gas} - \kappa \int_{4\pi} I(\vec{\Omega}) d\Omega$$

$$\begin{aligned} q_{surface} &= \vec{q} \cdot \vec{n} \\ &= \pi I_{surface}(\vec{\Omega}) - \int_{\vec{n} \cdot \vec{\Omega} < 0} |\vec{n} \cdot \vec{\Omega}| I(\vec{\Omega}) d\Omega \end{aligned}$$

ZONE METHOD (HOTTEL AND COHEN)



$$Q_{i \rightleftharpoons j} = \overline{S_i S_j} (E_{s,i} - E_{s,j})$$

$$Q_{i \rightleftharpoons j} = \overline{G_i S_j} (E_{g,i} - E_{s,j})$$

$$Q_{i \rightleftharpoons j} = \overline{G_i G_j} (E_{g,i} - E_{g,j})$$

ZONE method

$$Q_{i.net} = \sum_j \overline{S_j S_i} E_{s,j} + \sum_j \overline{G_j S_i} E_{g,j} - \epsilon_i A_i E_{s,i}$$

$$Q_{i.net} = \sum_j \overline{S_j G_i} E_{s,j} + \sum_j \overline{G_j G_i} E_{g,j} - 4K_i V_i E_{g,i}$$

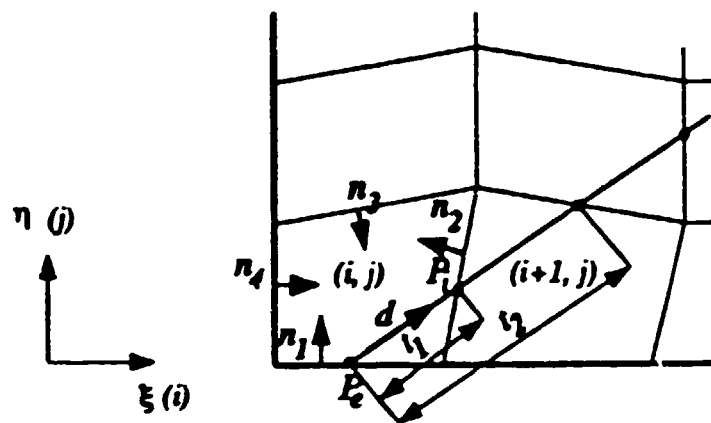
Determination of the total exchange areas

-by the HotteI method

(via \overline{ss} , \overline{sg} , \overline{gg})

-by the Monte Carlo method

THE MONTE CARLO TECHNIQUE



$$R(\epsilon) = \frac{\int_{l_1}^{\epsilon} f(\xi^*) d\xi^*}{\int_{l_1}^{l_2} f(\xi) d\xi}$$

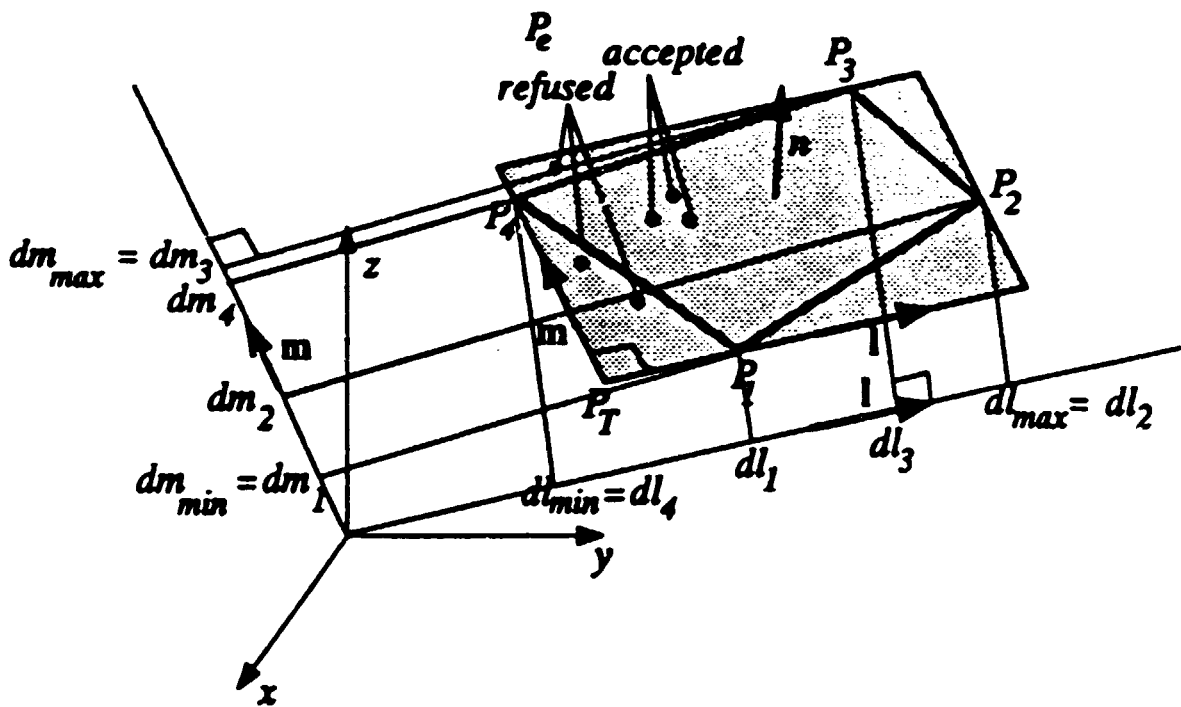
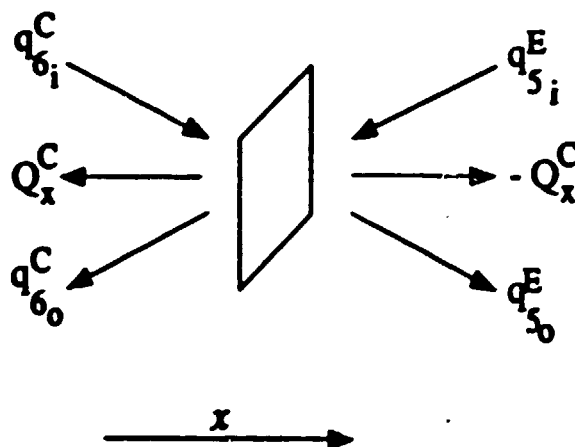
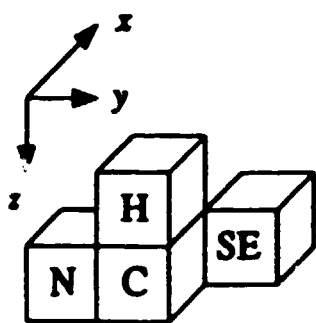


Figure 4 Emission from a wall zone with the help of a bounding rectangle

THE MONTE CARLO METHOD

THE IMAGINARY PLANES METHOD



$$q_{k_0} = \epsilon_k E_k + (1 - \epsilon_k) \left[\sum_{j=1}^6 f_{kj} q_{j_0} + \frac{E_g \overline{g^s k}}{A_k} \right]$$

$$q_{k_0} = \frac{Q_k}{A_k} + \frac{E_g \overline{g^s k}}{A_k} + \sum_{j=1}^6 f_{kj} q_{j_0}$$

$$Q_k = (q_{k_0} - q_{k_1}) A_k$$

$$S_i = \sum_{i=1}^m Q_i + \sum_{i=m+1}^6 q_i A_i \quad i = 1 \dots 6$$

IPM (continued)

$$[BM]\{Q\} = \{CM\}$$

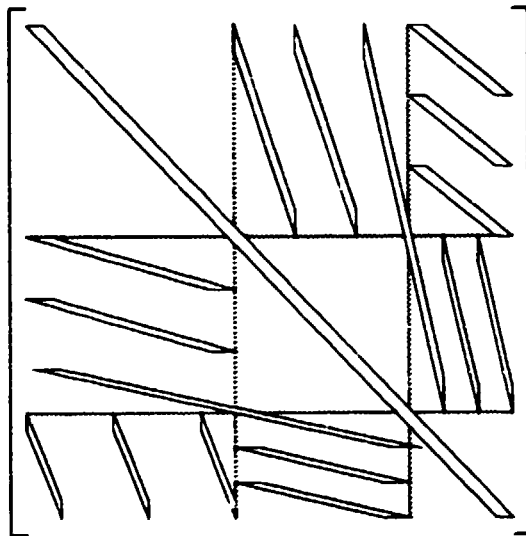
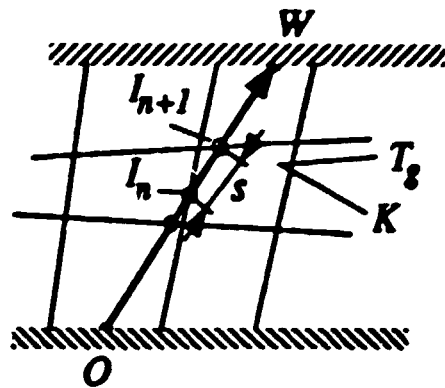


Figure 2. The storage pattern of matrix BM

$$q_k^C = (E_k^C - q_{k,n}^C) \epsilon_k^C / (1 - \epsilon_k^C)$$

THE DISCRETE TRANSFER METHOD



$$\frac{dI}{ds} = -KI + KI_b$$

$$I_{n+1} = I_n e^{-Ks} + (1 - e^{-Ks}) \frac{\sigma T_s^4}{\pi}$$

$$I_o = \frac{q_o}{\pi} = (1 - \epsilon) \frac{q_i}{\pi} + \frac{\epsilon \sigma T_s^4}{\pi}$$

$$q_{net} = q_o - q_i$$

$$q_i = \int_{2\pi} I \cos \beta \, d\Omega$$

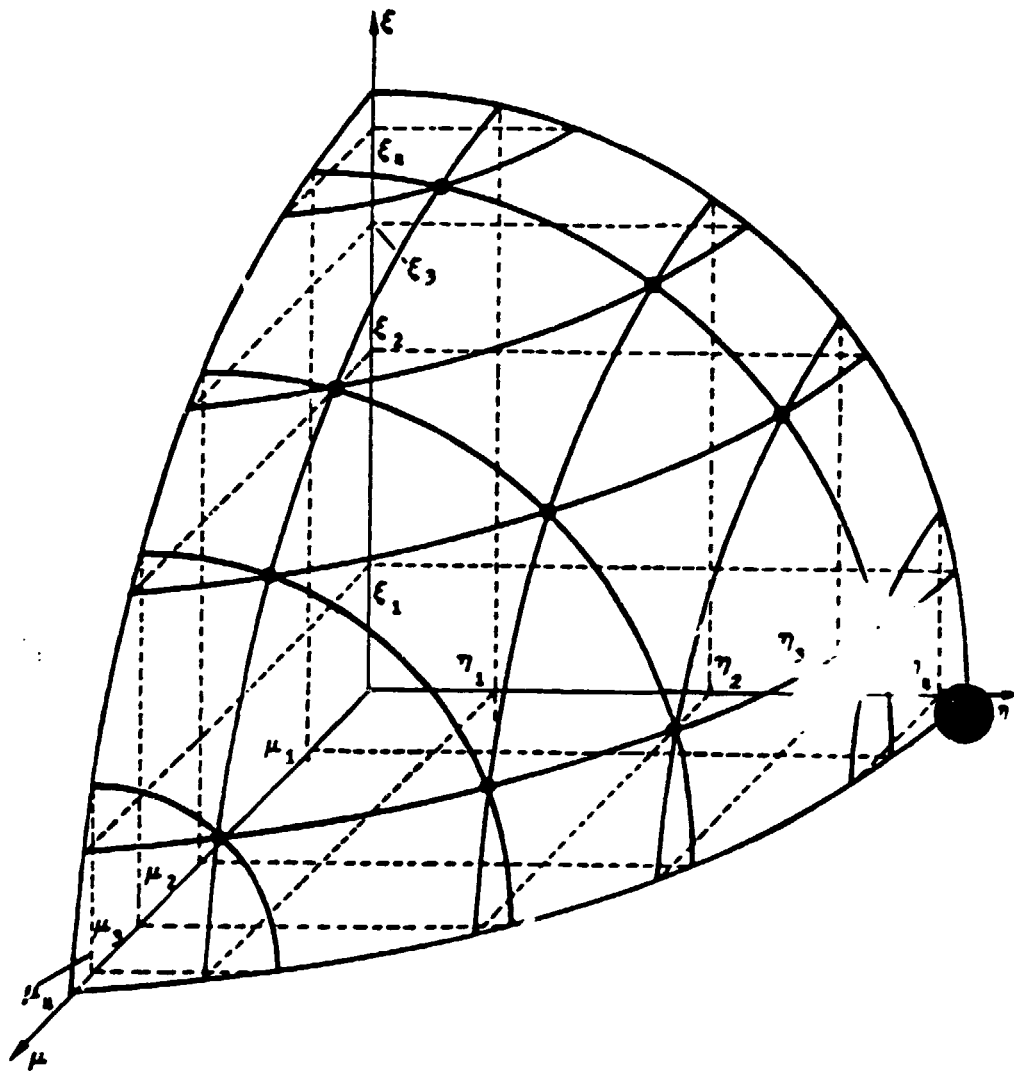
$$S_n = (I_{n+1} - I_n) dA \cos \beta \, d\Omega$$

THE DISCRETE ORDINATES METHOD

$$I_{face, leaving}(\vec{\Omega}) = \epsilon I_{b, face} + \frac{\rho}{\pi} \sum_{\vec{n} \cdot \vec{\Omega}_m < 0} w_m |\vec{n} \cdot \vec{\Omega}_m| I_{face, incident}(\vec{\Omega}_m) \quad \vec{n} \cdot \vec{\Omega} > 0$$

$$q_{face} = \pi I_{face, leaving}(\vec{\Omega}) - \sum_{\vec{n} \cdot \vec{\Omega}_m < 0} w_m |\vec{n} \cdot \vec{\Omega}_m| I_{face, incident}(\vec{\Omega}_m)$$

$$(\nabla \cdot \vec{q})_{CV} = 4\pi\kappa I_{b, CV} - \kappa \sum_m w_m I_{volume}(\vec{\Omega}_m)$$



$$\sum_{\xi_j > 0} w_j \xi_j^r = \frac{1}{2\pi} \int_0^{\pi/2} \int_0^{2\pi} \xi^r d\Omega = \frac{1}{r+1}$$

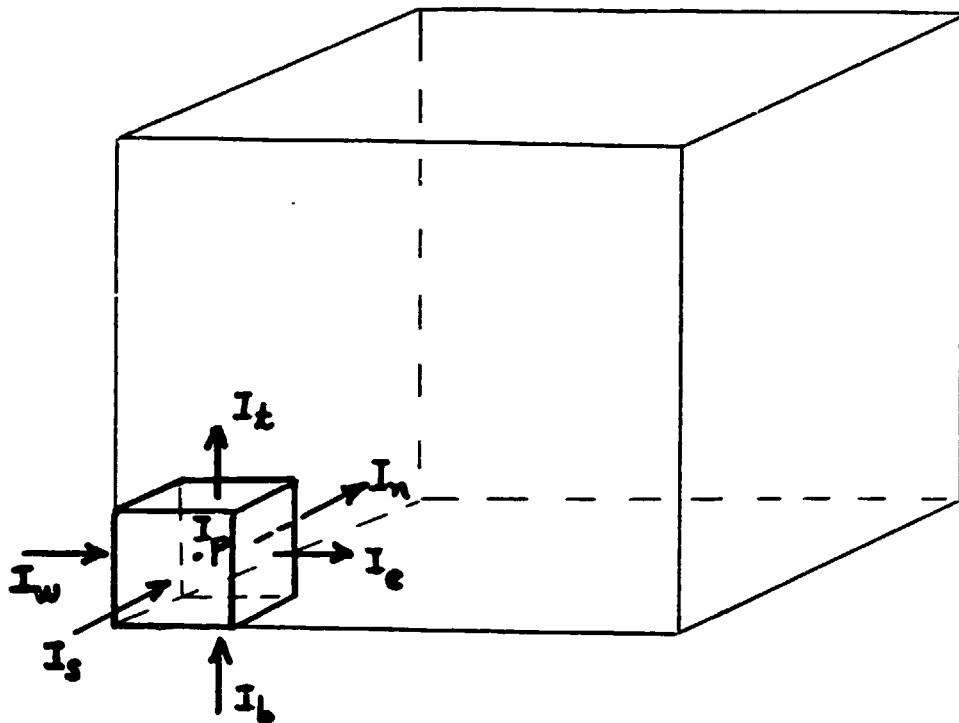
$$\nabla \cdot (\tilde{\Omega} I) = \kappa I_{b, gas} - \kappa I$$

$$\mu bc(I_e - I_w) + \eta ac(I_n - I_s) + \xi ab(I_t - I_b) = \kappa abc(I_{b, cv} - I_P)$$

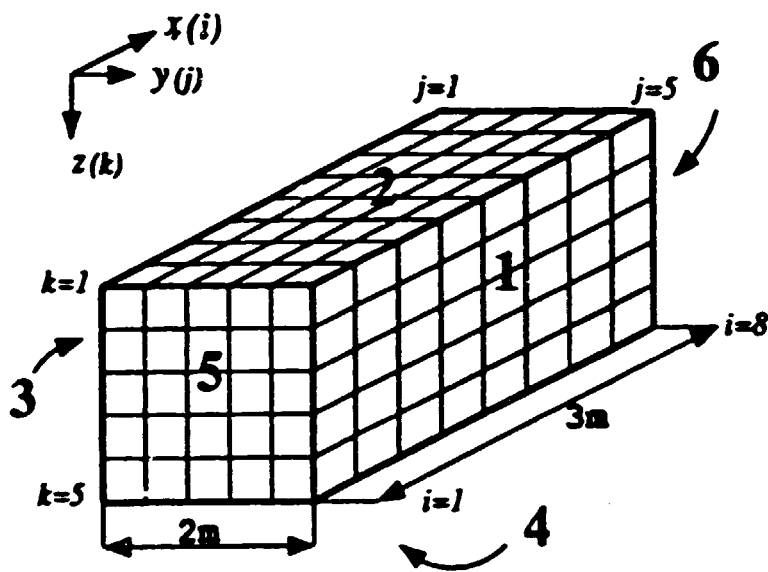
$$I_P = \begin{cases} \alpha I_e + (1 - \alpha) I_w \\ \alpha I_n + (1 - \alpha) I_s \\ \alpha I_t + (1 - \alpha) I_b \end{cases}$$

If $\alpha = 0.5$: central differentiation

$\alpha = 1.0$: upwind differentiation



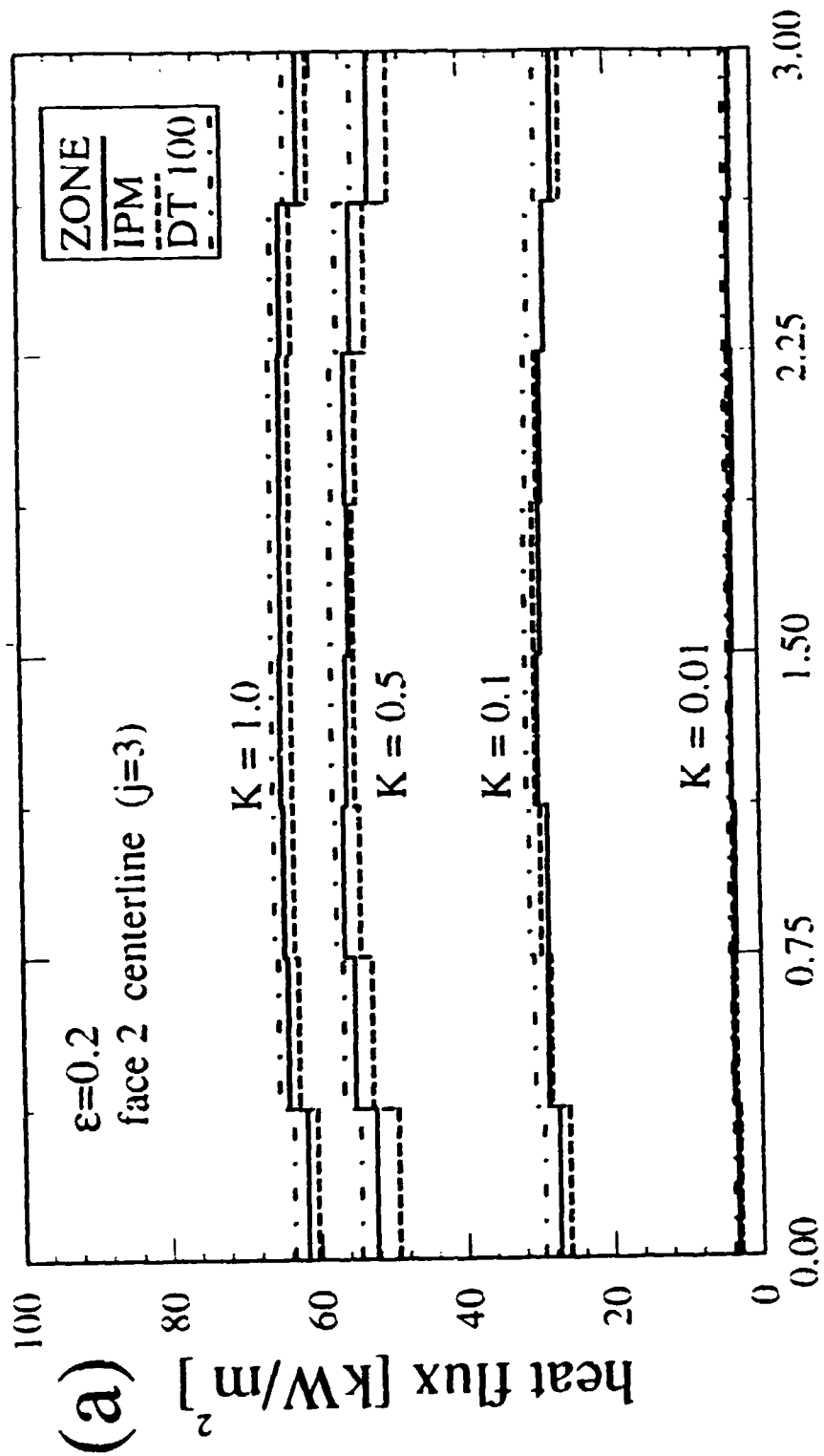
starting the differentiation



RECTANGULAR TEST ENCLOSURE

Table 1 Input data for the test in cartesian coordinates

Dimensions x, y, z	3m x 2m x 2m
Divisions	8 x 5 x 5
Temperatures (° C)	
faces 1, 3	300
faces 2, 4	500
faces 5, 6	400
gas	1300
Emissivities	
uniform on every face	0.2, 0.5, 0.8, 1.0 (variable)
Absorption coefficient	
uniform	0.01, 0.05, 0.1, 0.25, 0.5, 1.0, 2.0 m⁻¹ (variable)



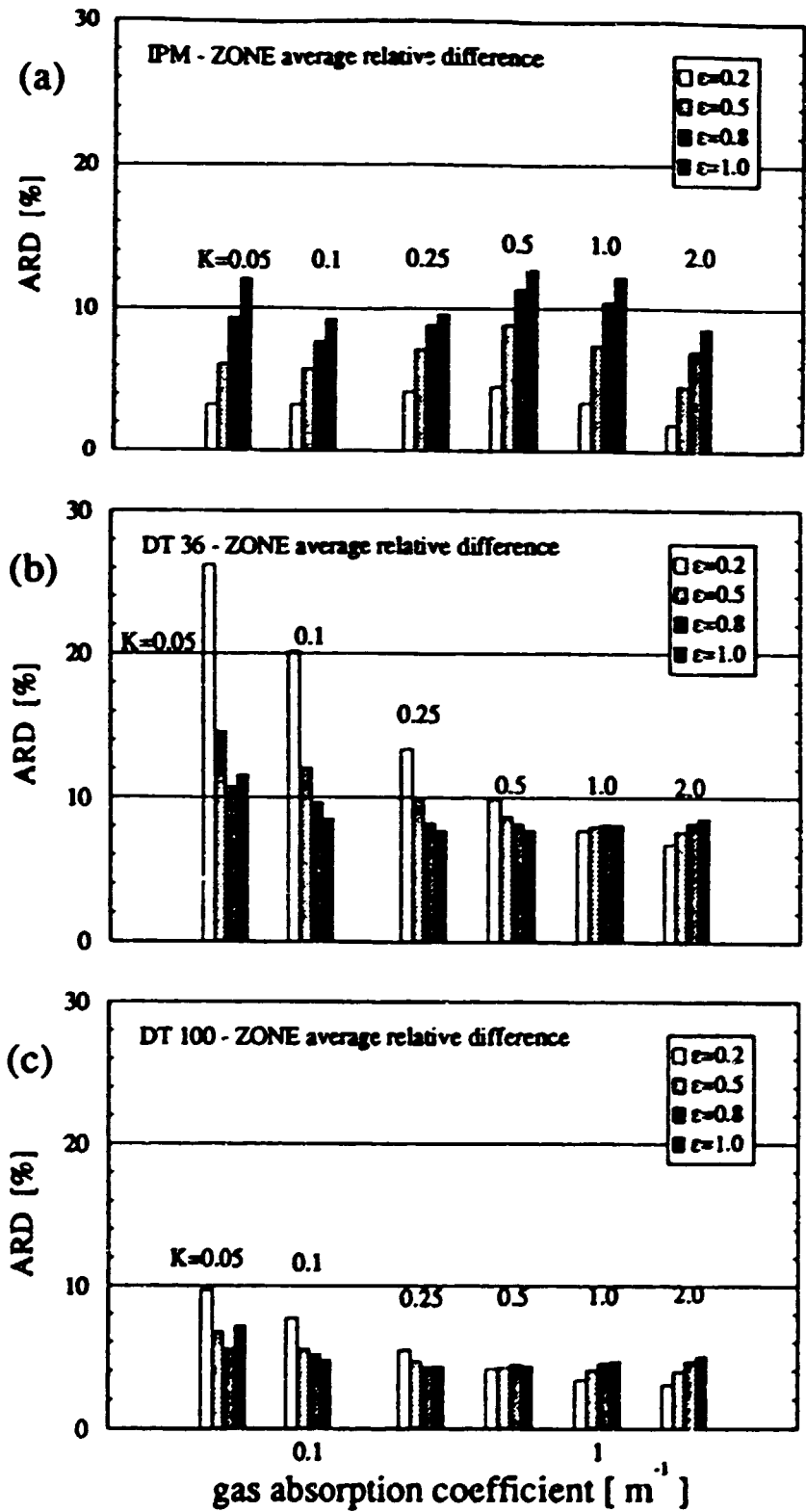


Figure 5 ARD variation with respect to gas absorption coefficient and surface emissivity; a. IPM, b. DT 36 solid angle divisions, c. DT 100 divisions.

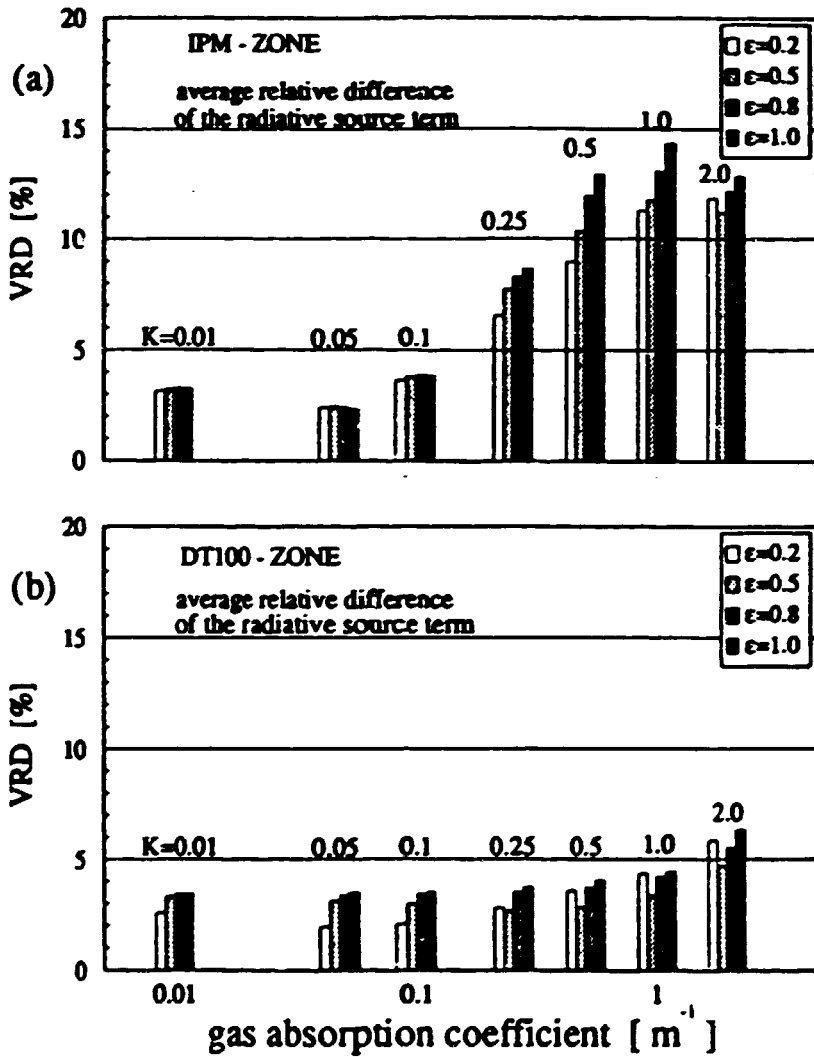
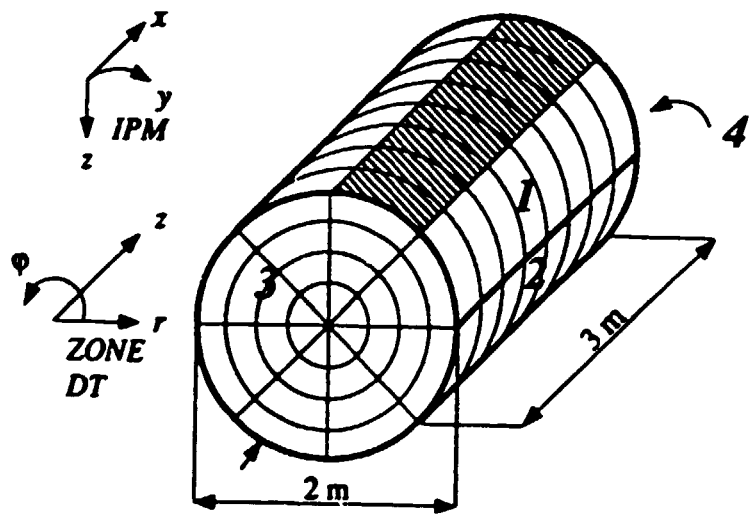


Figure 8 VRD variation with respect to gas absorption coefficient and surface emissivity; a. IPM, b. DT 100 divisions.



Cylindrical test enclosure

Table 4 Input data for the test in cylindrical coordinates

Dimensions	dia: 2 m, length: 3 m
Divisions	8 x 8 x 4 (x,y,z - z,φ,r)
Temperatures (° C)	
face 1 (upper hemicylinder)	600
face 2 (lower hemicylinder)	400
face 3	300
face 4	500
gas	1300
Emissivities	
uniform on every face	0.2, 0.5, 0.8, 1.0 (variable)
Absorption coefficient	
uniform	0.01, 0.05, 0.1, 0.25, 0.5, 1.0, 2.0 m ⁻¹ (variable)

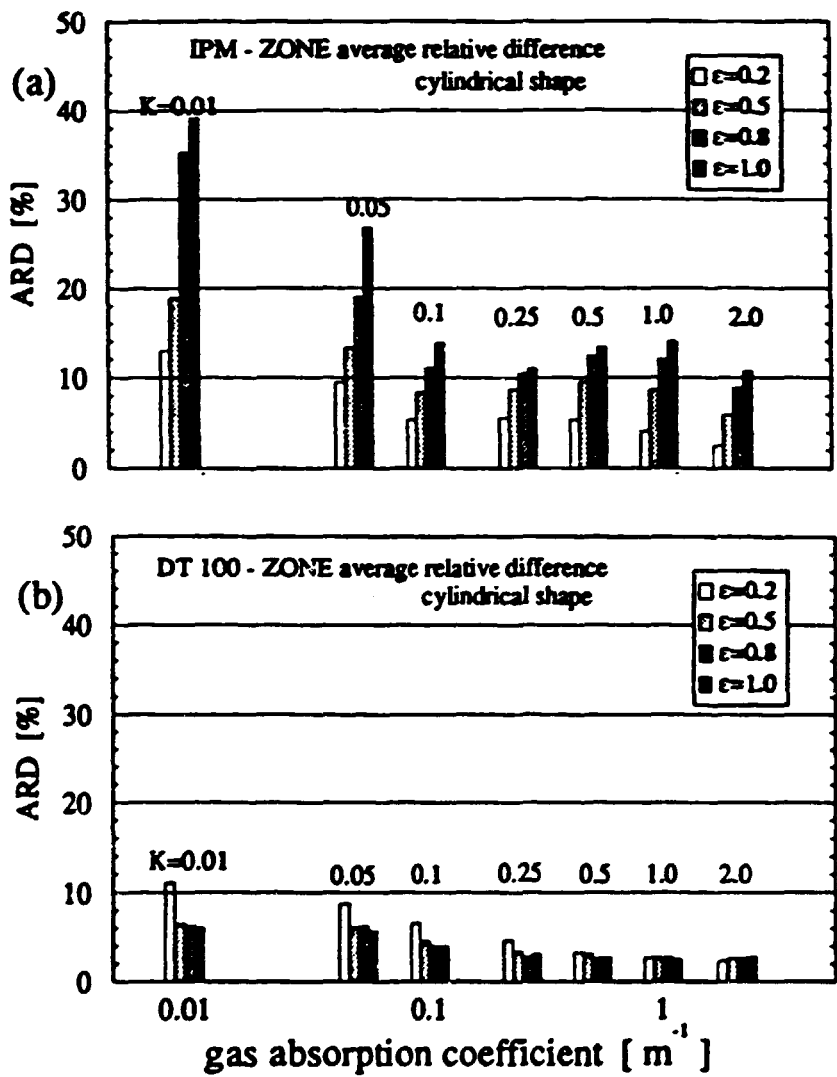


Figure 11 ARD variation with respect to gas absorption coefficient and surface emissivity (cylindrical case); a. IPM, b. DT 100 divisions.

Computation time of the three methods for some chosen values of ϵ and K (Computer: SGI 4D/340)

		CPU time [s]					
ϵ	K	zone	DT 36	DT 100	DT 400	DT 900	IPM
0.2	0.01	11780	187	565	1756	3725	40
	0.05	9415	165	513	1584	3535	
	0.1	7497	135	436	1336	2977	
	0.25	4835	98	308	996	2233	
	0.5	3234	67	214	747	1673	
	1.0	2110	52	148	582	1301	
	2.0	1327	37	124	415	929	
0.2	0.25	4853	98	308	996	2233	40
0.5		3315	60	205	665	1301	
0.8		2432	38	128	416	929	
1.0		2060	15	51	167	372	

Table 3 Summary of the comparison of IPM and DT (100 solid angle divisions) to ZONE with increased fineness of the grid

Divisions	Average relative diff [%]		Maximum relative diff [%]		Minimum relative diff [%]		Cpu time [s]		# of surf. zones
	IPM	DT	IPM	DT	IPM	DT	IPM	DT	
5 x 3 x 3	5.7	7.0	10.0	12.5	1.6	2.4	30	30	78
8 x 5 x 5	11.3	4.4	19.9	11.9	1.8	0.2	35	128	210
12 x 7 x 7	15.5	3.4	29.2	11.9	6.4	0.06	40	326	434
16 x 10 x 10	20.2	3.0	38.0	13.6	10.0	0.02	45	1024	840

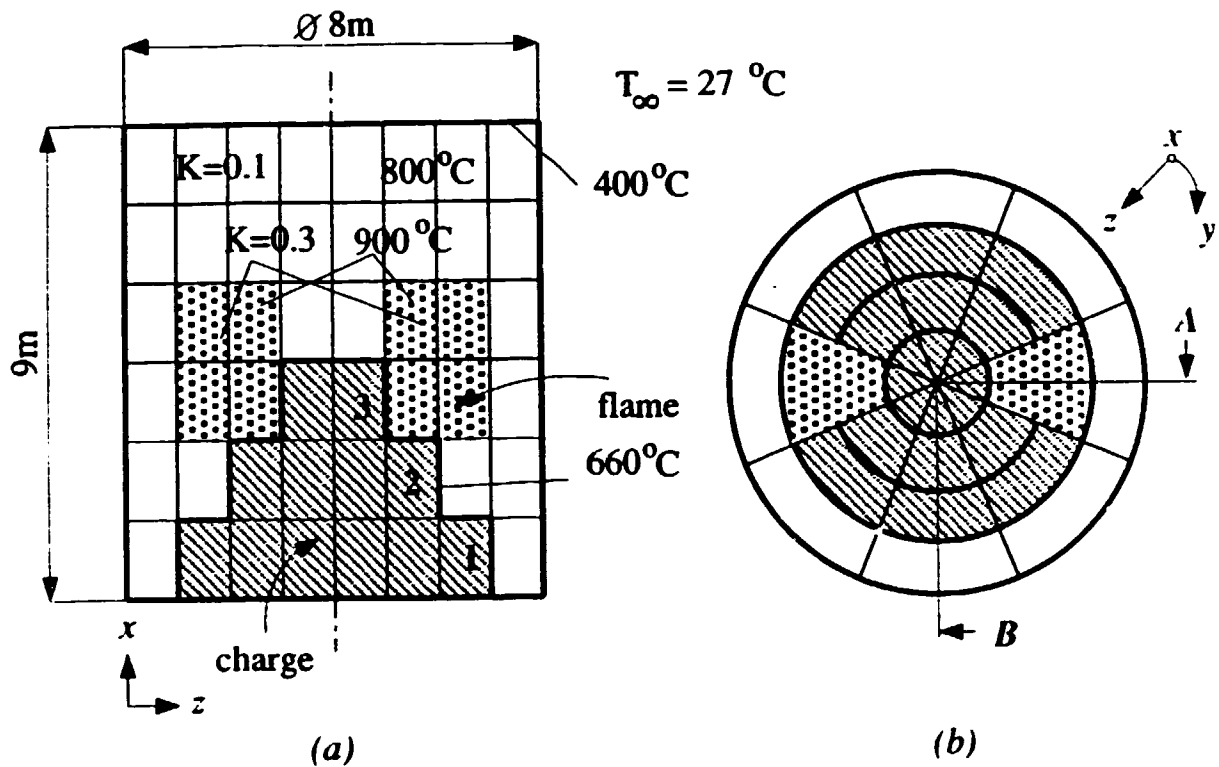
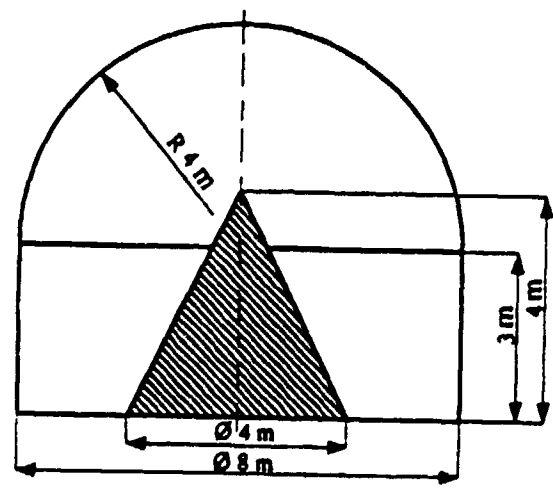
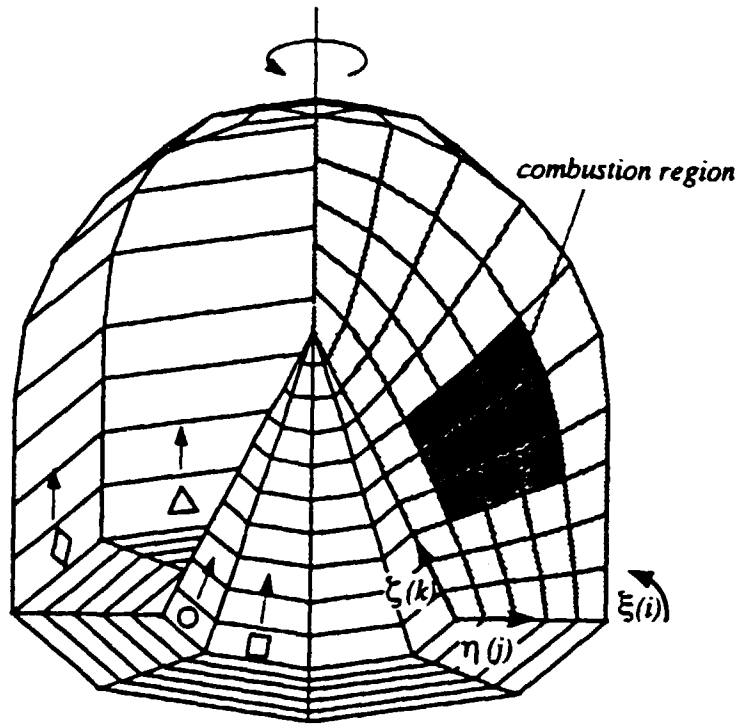


Figure 5. Description of the remelting furnace;
 (a) cross-section, (b) top view

Table 3. Results obtained with the IPM for the cylindrical furnace
(h and v refer to horizontal and vertical zone respectively)

Zone	Temperatures on the cylindrical wall [°C]			
	sector A		sector B	
	IPM	zone	IPM	zone
top	721	703	718	701
.	752	744	747	735
.	780	778	766	752
.	779	780	766	752
.	747	748	742	741
bottom	687	718	685	716

Zone	Heat fluxes on the charge [kW/m ²]			
	sector A		sector B	
	IPM	zone	IPM	zone
3h	15.5	10.9	14.2	8.8
3v	19.6	20.1	12.7	11.6
2h	19.7	19.2	12.9	10.8
2v	12.6	13.1	11.0	10.9
1h	12.9	12.5	11.2	10.6
1v	8.8	8.7	8.5	8.8



Input data for examples 1 and 2

Example 1		Example 2	
Number of divisions (ξ, η, ζ)			
8 x 5 x 10		8 x 15 x 10	
Temperature, °C			
bottom, cone	300	parallelepiped	300
cylinder, hemisphere	700	cylinders	500
gas	900	gas	1 000
flame zones	1 100		
Wall emissivities			
bottom, cone	0.6	parallelepiped	0.5
cylinder, hemisphere	0.8	cylinders	0.8
Gas absorption coefficients, m^{-1}			
gas	0.1	gas	0.1
flame zones	0.5		

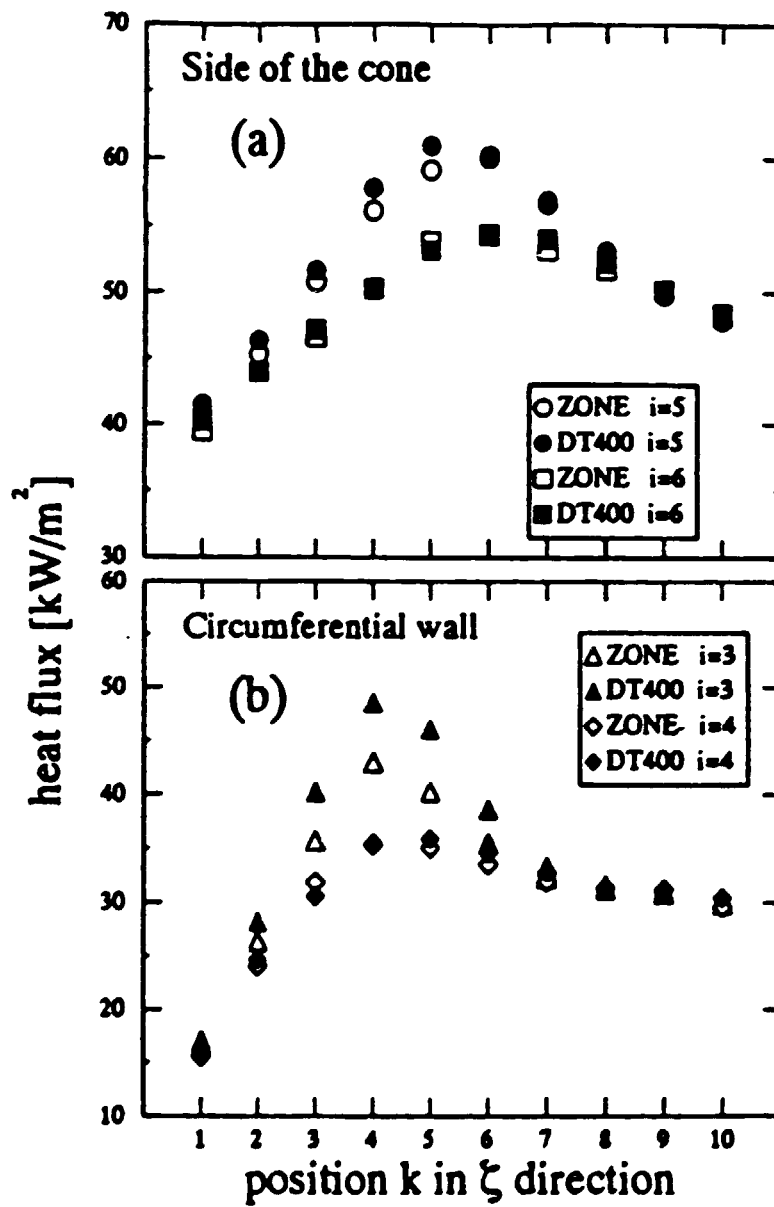


Figure 9 Calculated surface heat fluxes: (a) along the side of the cone; (b) along the outer shell.

Table 2 Comparison of the heat fluxes and the computation time, example/

Average relative difference	
fluxes on the surface zones (ARD)	2.5 %
volumetric sources in the gas zones (VRD)	9.8 %
Maximum relative difference (MRD)	
fluxes on the surface zones	16.0 %
volumetric sources in the gas zones	51.6 %
CPU time (HP9000-720)	
Zone method (6000 rays/surface or volume zone)	1563 s
DT method (400 div)	382 s

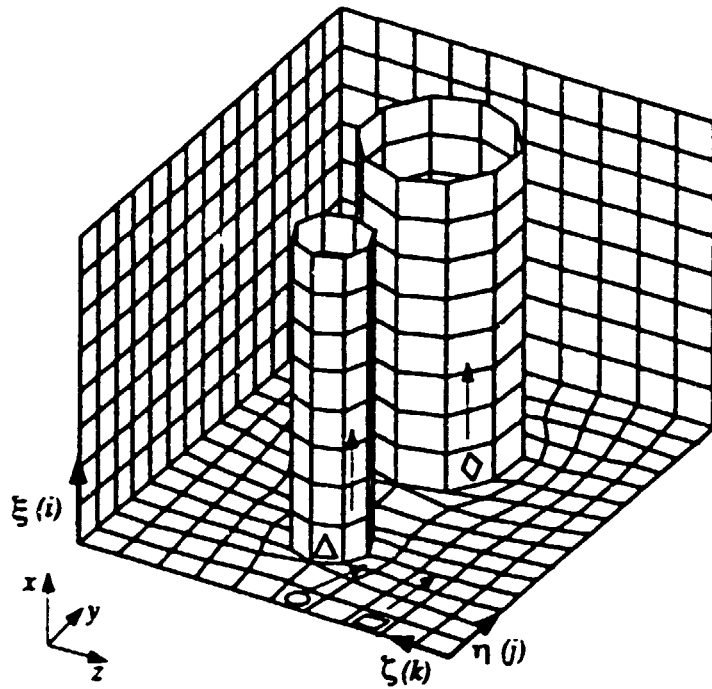


Figure 10 Details of the enclosure used in example 2.

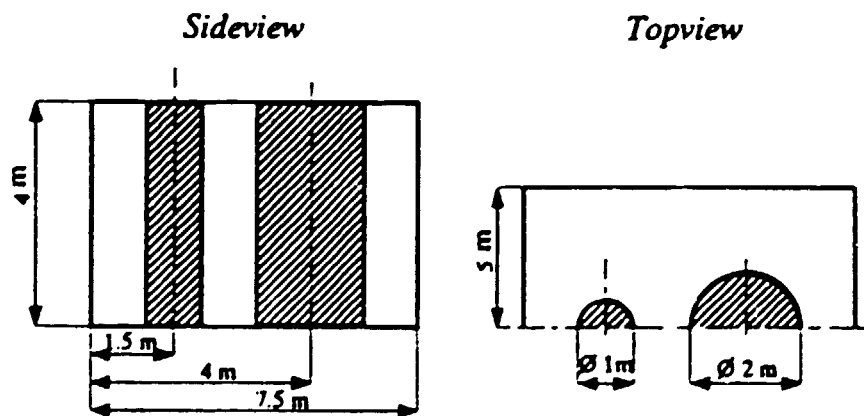


Figure 11 Geometrical data of the enclosure of example 2

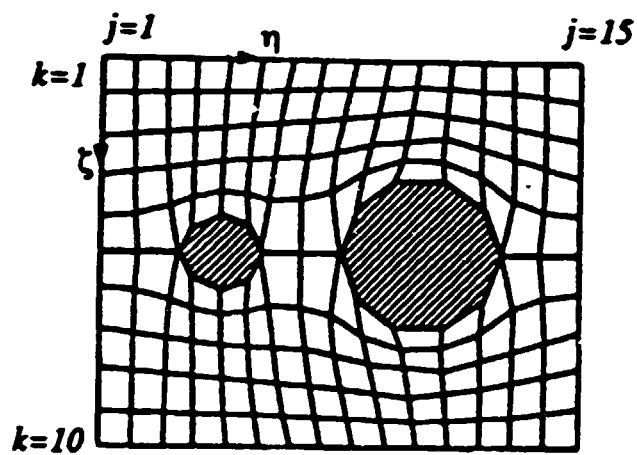


Figure 12 The 2D curvilinear grid of example 2

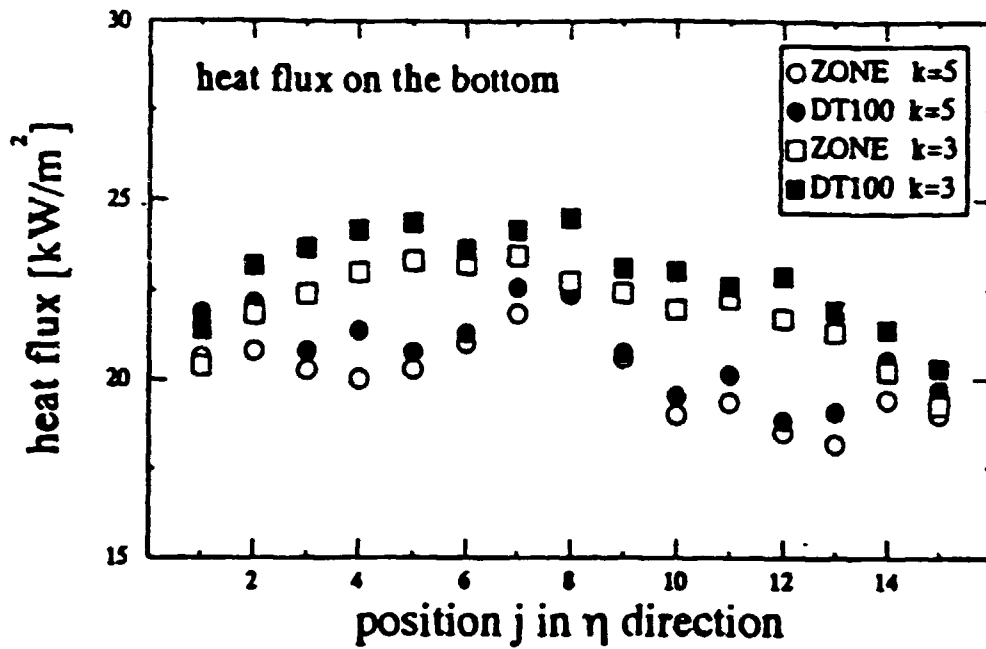


Figure 13 Calculated heat fluxes on the bottom plate of the parallelepiped

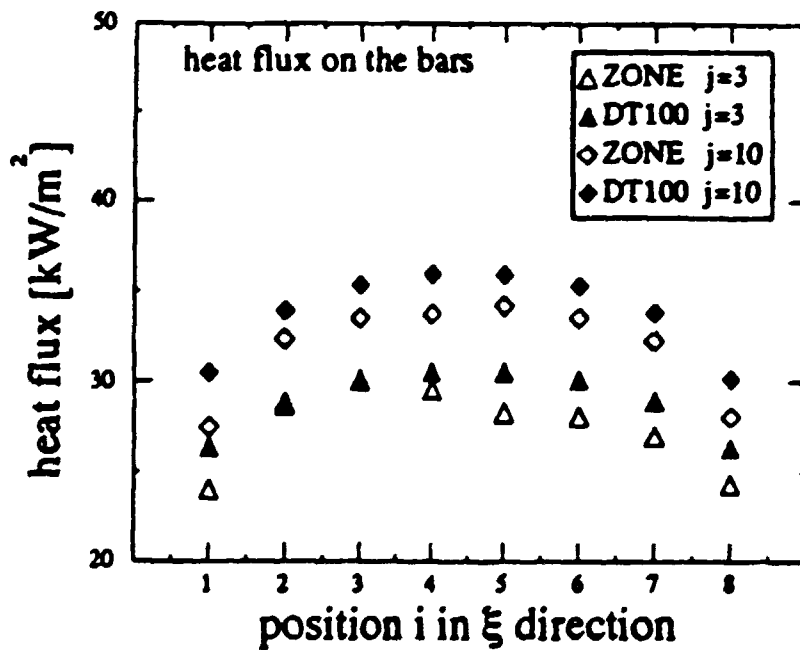


Figure 14 Calculated heat fluxes on the cylindrical bars

Table 4 Comparison of the heat fluxes and the computation time, example

Average relative difference

fluxes on the surface zones (ARD) 4.5 %

volumetric sources in the gas zones (VRD) 2.8 %

Maximum relative difference (MRD)

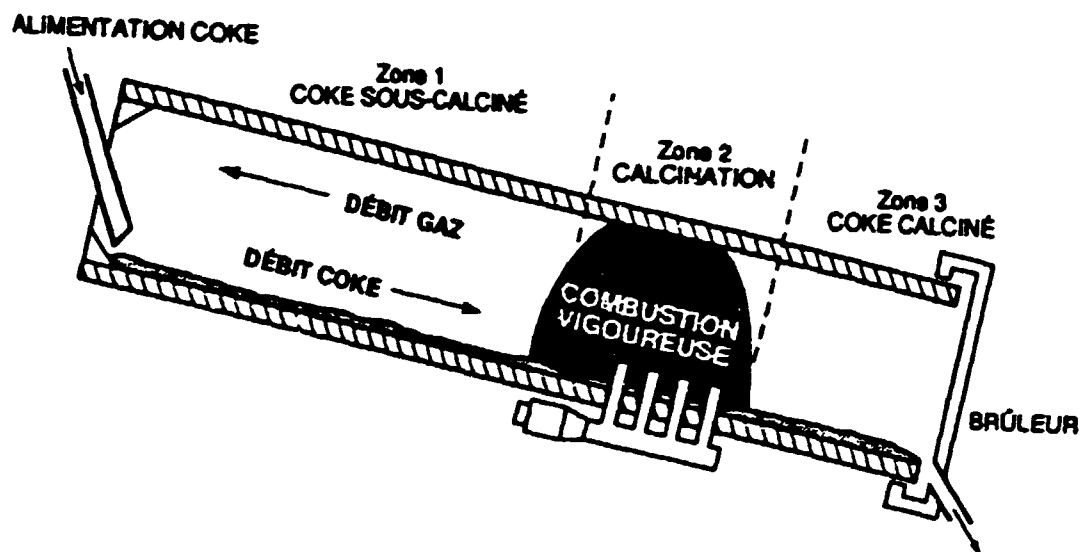
fluxes on the surface zones 14.7 %

volumetric sources in the gas zones 11.0 %

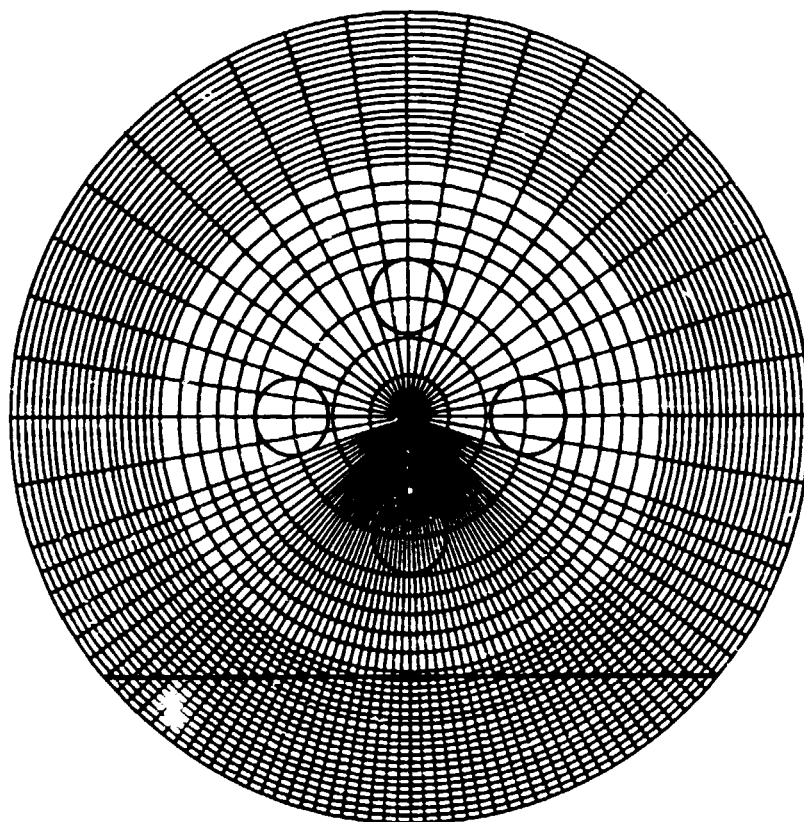
CPU time (HP9000-720)

Zone method (6000 rays/surface or volume zone) 9352 s

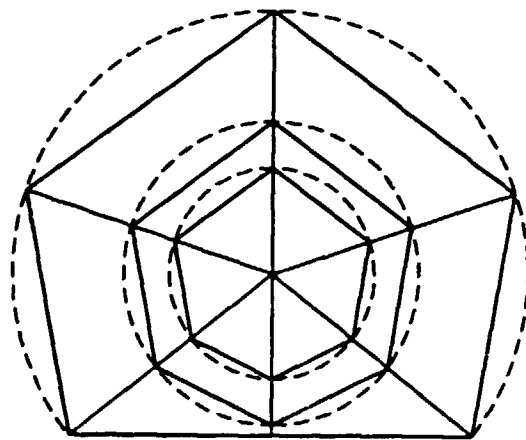
DT method (100 div) 785 s



**schematic view of the coke
calcination kiln**



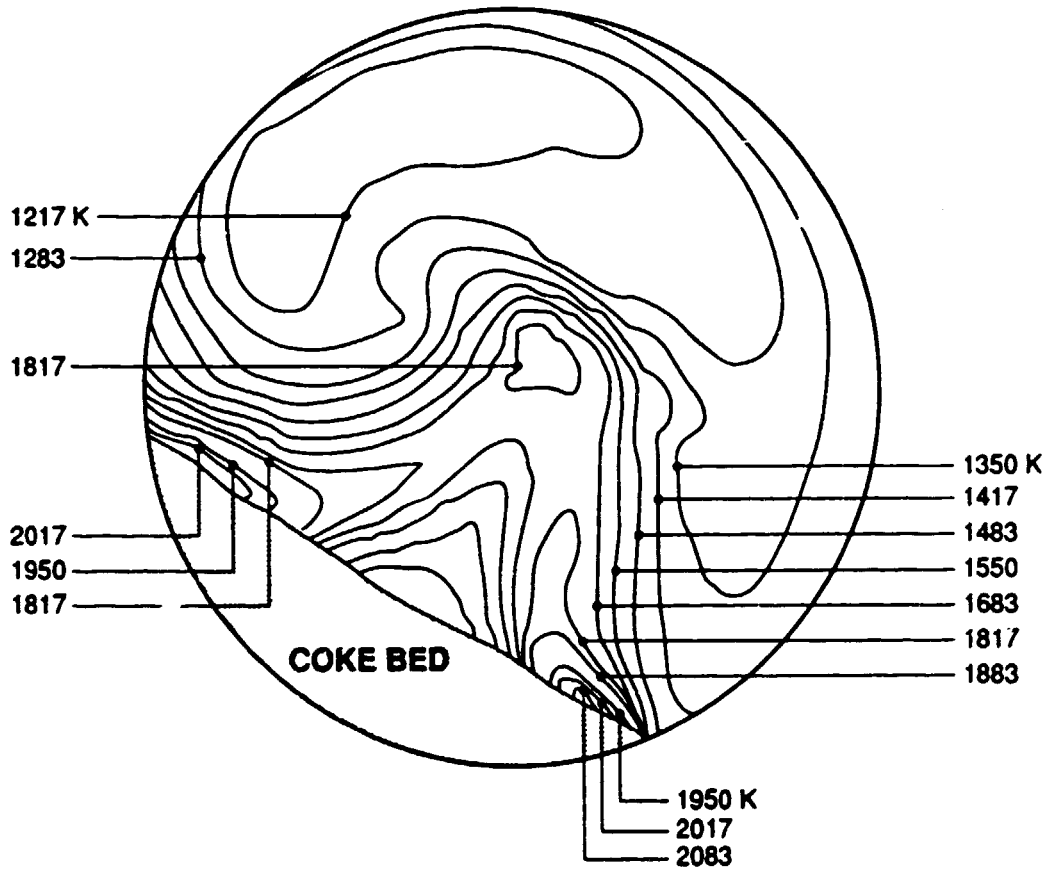
**Transversal discretization used
for solving the conservation equations**



**Transversal discretization used
for solving the radiative transfer (solid lines)**

$H_2 + \frac{1}{2} O_2 \rightarrow H_2O + \Delta h_{H_2}$
$C_{18}H_{12} + 21 O_2 \rightarrow 6H_2O + 18CO_2 + \Delta h_{C_{18}H_{12}}$
$CH_4 + 2 O_2 \rightarrow 2H_2O + CO_2 + \Delta h_{CH_4}$
$C + O_2 \rightarrow CO_2 + \Delta h_C$

$$R_x = -C_x \rho_{gas}^2 [x]^a [O_2]^b e^{-\frac{E}{RT}} \tau_s^{-1} ; \left[\frac{kg_x}{s m^3} \right]$$



PART 3

DESCRIPTION OF THE

MATHEMATICAL MODELS

AND

RESULTS

MELTER-HOLDER FURNACE

1-D ANALYTIC MODEL

1 - Introduction

- Important process: keeps Al liquid before casting
- Consumes 4.5 - 6 MJ/kg Al melted
- 20% efficiency

Questions:

- how increase efficiency and productivity ?
- what will be the effects of changes in
 - the sequence and duration of the operations
 - the size of the charge
 - stirring mode(continuous/discrete)
 - door management (closed/opened)

- 450 parameters
- physical phenomena involved:
 - metal: conduction, convection, phase change
 - chamber: radiation, convection, combustion, gas flow
 - roof, floor: conduction, radiation

2. Description of the furnace and its operation

2.1 The furnace

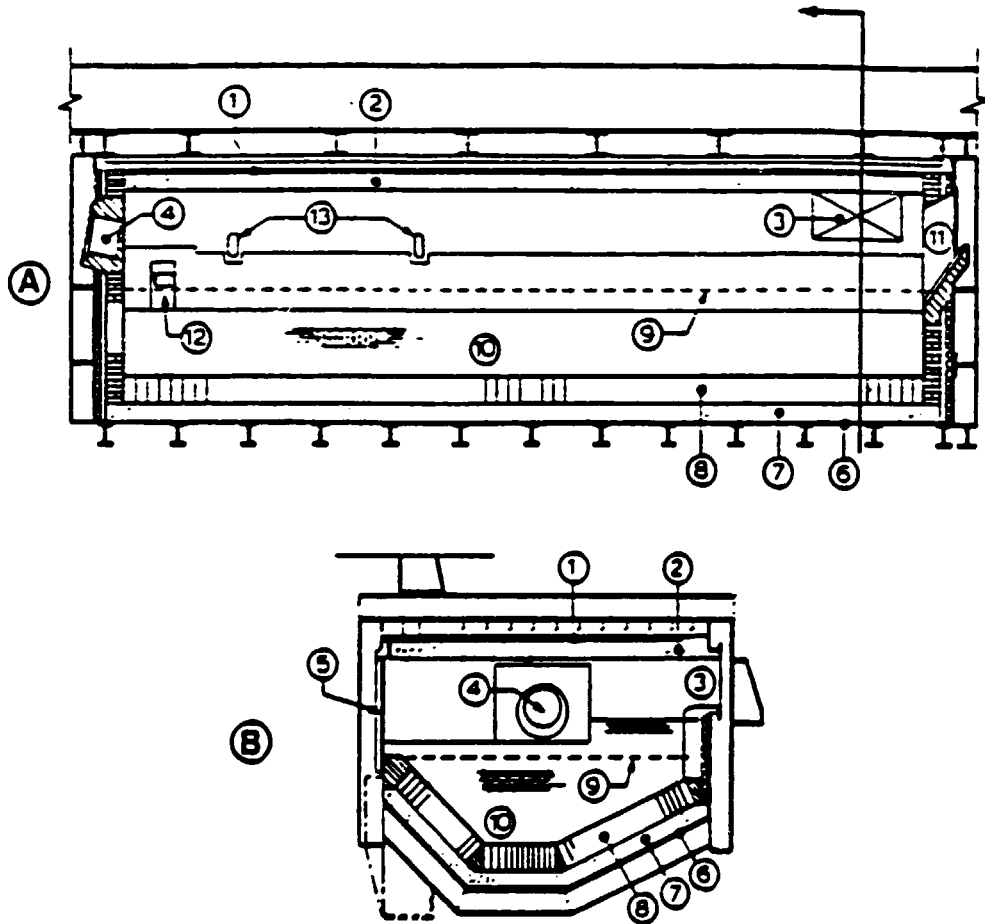


Figure 1— Cutaway views of the casting furnace.

A- Lengthwise B- Across

(1,2) roof (3) stack (4) burner (5) doors

(6,7,8) floor (9,10) metal (11) siphon

(12) casting spout (13) thermocouples.

2.2 The batch schedule

Table I. A Typical Schedule of a Batch

No.	Operation	Duration (s)	Burner on/off (Duration)	#Doors Open (Duration)
	loading the solid metal into the heel	1200	off	
1	heating the solid metal and heel	3200	on	
2	pause	400	off	
3	loading the liquid metal into furnace	1920	on (900) off (1020)	
4	heating the liquid and solid metals	3350	on	
5	pause	400	off	
6	first stirring	1270	off	1 (120)
7	pause	60	off	
8	heating	3500	on	
9	pause prior to alloying	550	off	
10	alloying	450	off	4 (450)
11	second stirring (the first 1200 seconds) simultaneously fluxing (2100 seconds)	2100	off	5 (2100)
12	skimming	1200	off	5 (1200)
13	pause prior to casting	300	off	

3. The model

- . dynamic
- . well-stirred

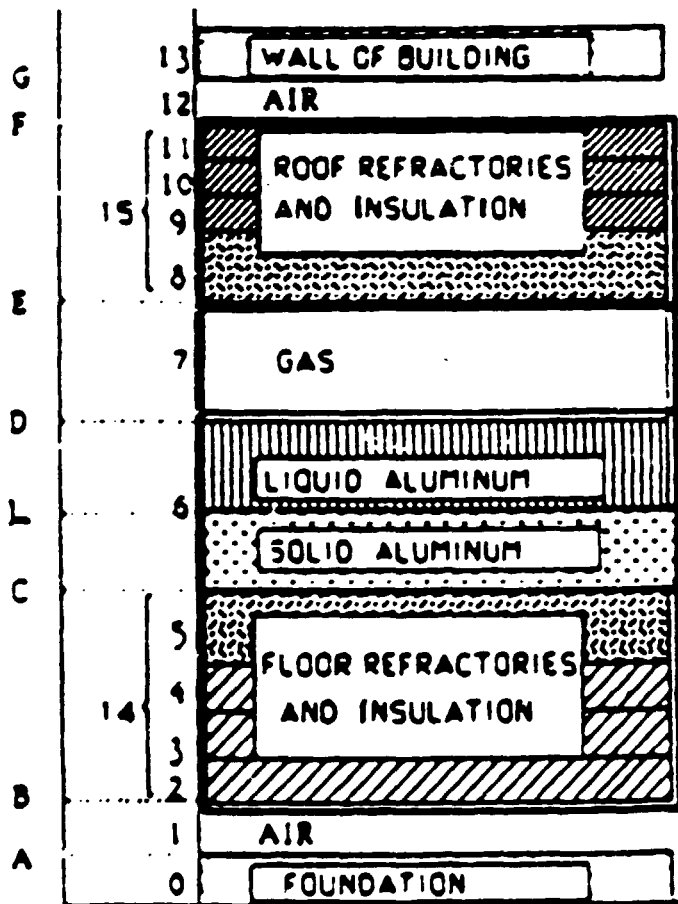


Fig. 2—Symbols used to identify the various components of the furnace and their interfaces.

Modeling the operations

- . QE : heat flow through roof

QEV : through roof proper

QEP : through open doors
(cold black surfaces)

- . stirring and fluxing:

$$\frac{d}{dt} \left(\frac{dT}{dy} \right) \text{ liq. metal} = f \text{ (volume flowrate of } N_2 \text{ or } Cl_2 \text{)}$$

- . skimming:

removal of a known mass of metal at the metal surface temperature

- . allowing:

addition of a known mass of metal at room temperature

- . roof and floor:

average thermal properties

4. The equations

4.1 The combustion chamber

$$V_7 c_{v7} \frac{dT_7}{dt} = Q_7 - (Q_D + Q_{EV} + Q_{EP}) \quad [1]$$

$$Q_7 = \sum_{i=1}^R \dot{n}_i \left(\bar{h}_f^\circ + \int_T^{\bar{T}_{Ri}} \bar{c}_{pi}(T) dT \right) - \sum_{j=1}^P \dot{n}_j \left(\bar{h}_f^\circ + \int_T^{\bar{T}_{Pj}} \bar{c}_{pj}(T) dT \right) \quad [2]$$

$$Q_D = A_D h_D (T_7 - T_D) + \sigma \left(\overrightarrow{GS_D} T_7^4 + \overrightarrow{S_{EV} S_D} T_{EV}^4 + \overrightarrow{S_{EP} S_D} T_{EP}^4 - \overleftarrow{GS_D} T_D^4 - \overleftarrow{S_{EV} S_D} T_D^4 - \overleftarrow{S_{EP} S_D} T_D^4 \right) \quad [3]$$

$$\frac{dU_7}{dt} = V_7 c_{v7} \frac{(T_7^\circ - T_7^{\circ-})}{\Delta t} = 0$$

T7 solved by Newton-Raphson at every time step (Eq. 1 is non linear)

$$T_{\gamma_R} = \left(1 - \frac{1}{d}\right) \eta_T (T_{FA} - T_E) + T_{\gamma_S} \quad [4]$$

$$\eta_T = \frac{(Q_D - Q_C) + (Q_E - Q_F)}{Q_T}$$

$$T_{\gamma_R} = \frac{1}{2} (\bar{T}_{FA} + T_{\gamma_S}) = \frac{1}{6} T_{FA} + \frac{1}{3} T_E + \frac{1}{2} T_{\gamma_S} \quad [6]$$

4.2 The metal

Enthalpy model

$$H(T) = \int_{T_f}^T \rho(T) c(T) dT \quad \text{for } T < T_f \quad [7a]$$

$$H(T) = \int_{T_f}^T \rho(T) c(T) dT + \rho L \quad \text{for } T > T_f \quad [7b]$$

$$\theta(T) = \int_{T_f}^T k(T) dt \quad \text{for all } T \quad [8]$$

$$\frac{\partial H}{\partial t} = \nabla^2 \theta \quad [9]$$

which, in 1-D, becomes:

$$\frac{\partial H}{\partial t} = \frac{\partial^2 \theta}{\partial x^2} \quad [10]$$

4.3 Floor, concrete and air

- 1D conduction equation

The 1-D conduction equation is to be solved for the floor:

$$\rho c \frac{\partial T}{\partial t} = k \frac{\partial^2 T}{\partial x^2} \quad [11]$$

Noting that $q = k \partial T / \partial x$ and $Q = Aq$, we have:

$$A \rho c \frac{\partial T}{\partial t} = \frac{\partial Q}{\partial x} \quad [12]$$

- air gap

$$M_1 c_{p1} \frac{\partial T_1}{\partial t} = Q_{B.C} - Q_{A.C} \quad [14]$$

- concrete foundation

The heat accumulated in the concrete foundation is

$$M_0 c_0 \frac{\partial T_A}{\partial t} = Q_A - Q_0 \quad [15]$$

$$Q_0 = \frac{k_0 A_0}{L_0} (T_A - T_0) \quad [16]$$

4.4 The roof

- . roof and walls
- . same strategy as for the floor

4.5 Resolution

- . finite differences with explicit integration
- . Newton-Raphson combined with Gauss-Jordan for the calculation of gas temperature T_7 and $T^{\circ}B$, $T^{\circ}F$.
- . all initial nodal temperatures specified (based on steady state at $t = 0$)

5. The results

Table IV. Data Input to the Model for Simulating the Batch Described in Table I

Mass of liquid metal heel	(kg)	15,000
Temperature of heel	(°C)	685
Mass of solid charge	(kg)	8,658
Temperature of solid	(°C)	22
Natural gas flowrate	(m ³ /h)	450
Excess air	(pct)	7
Mass of liquid metal introduced	(kg)	48,342
Temperature of liquid metal	(°C)	769
Nitrogen flowrate for stirring	(m ³ /min)	0.71
Temperature of nitrogen	(°C)	25
Chlorine flowrate for fluxing	(m ³ /min)	0.5
Temperature of chlorine	(°C)	25
Mass of alloying element added	(kg)	100
Mass of skim removed	(kg)	721

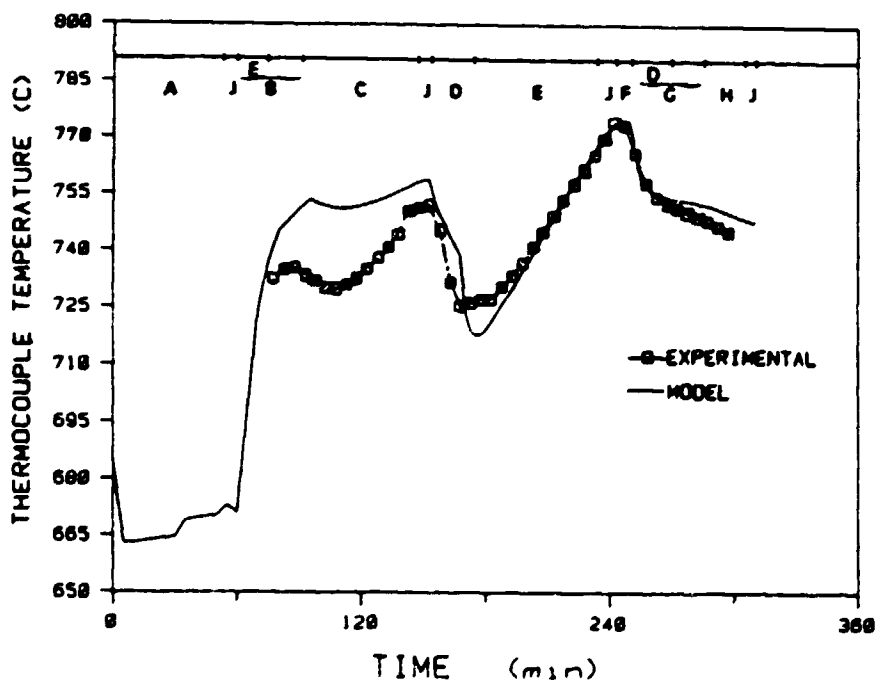


Fig. 3 — Metal temperatures, simulated and measured by thermocouple, at 30 cm below the melt surface. A: Preheating solid and heel, B: loading the liquid metal into furnace, C: heating the liquid and solid metals, D: stirring, E: heating, F: alloying, G: fluxing, H: skimming, and J: pause.

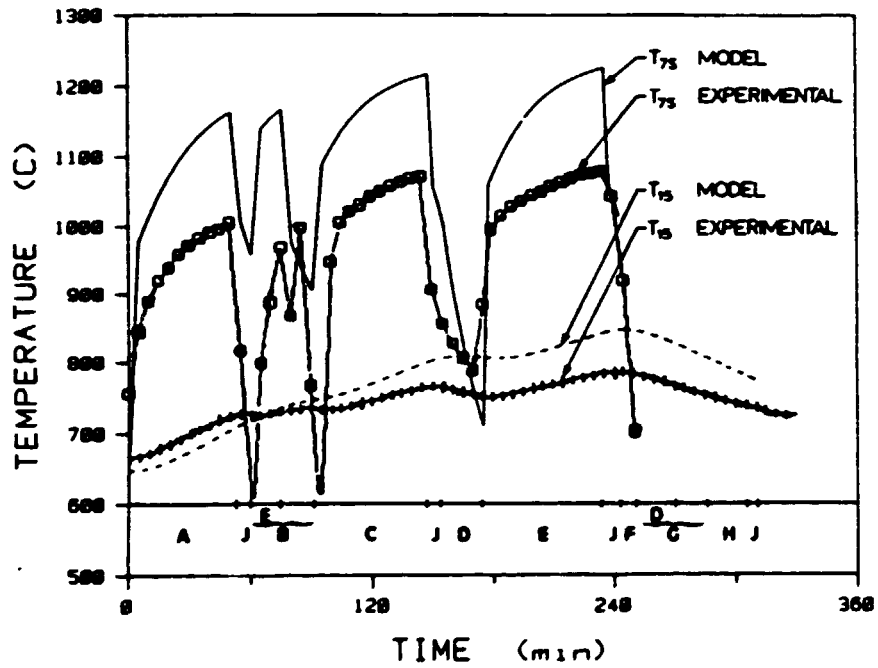


Fig. 4—Gas temperature at stack entrance T_{75} , and mid-thickness roof temperature T_{15} , both simulated and experimental.

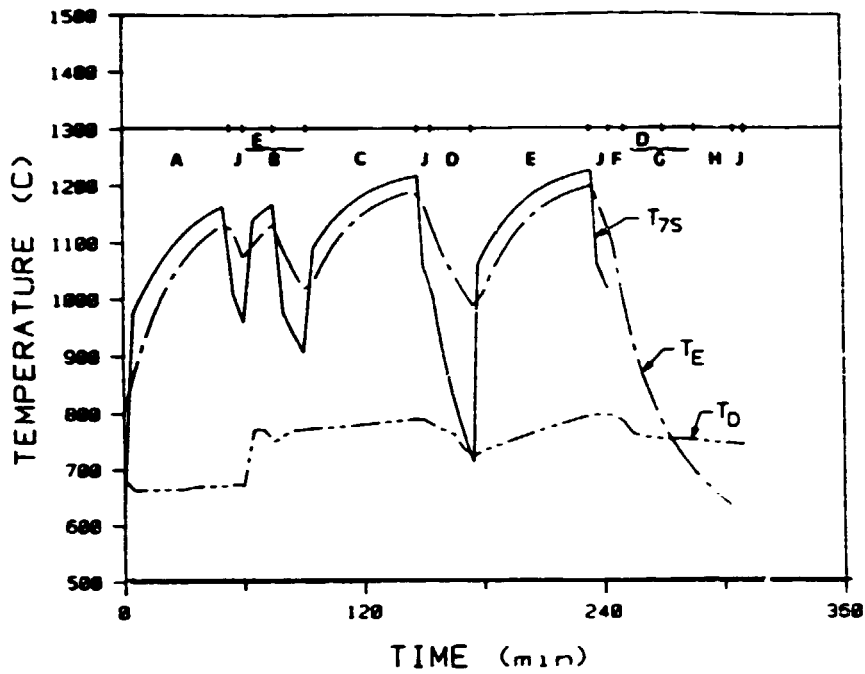


Fig. 5—metal surface temperature T_D , inner roof surface temperature T_E , and stack entrance gas temperature T_{75} , all simulated.

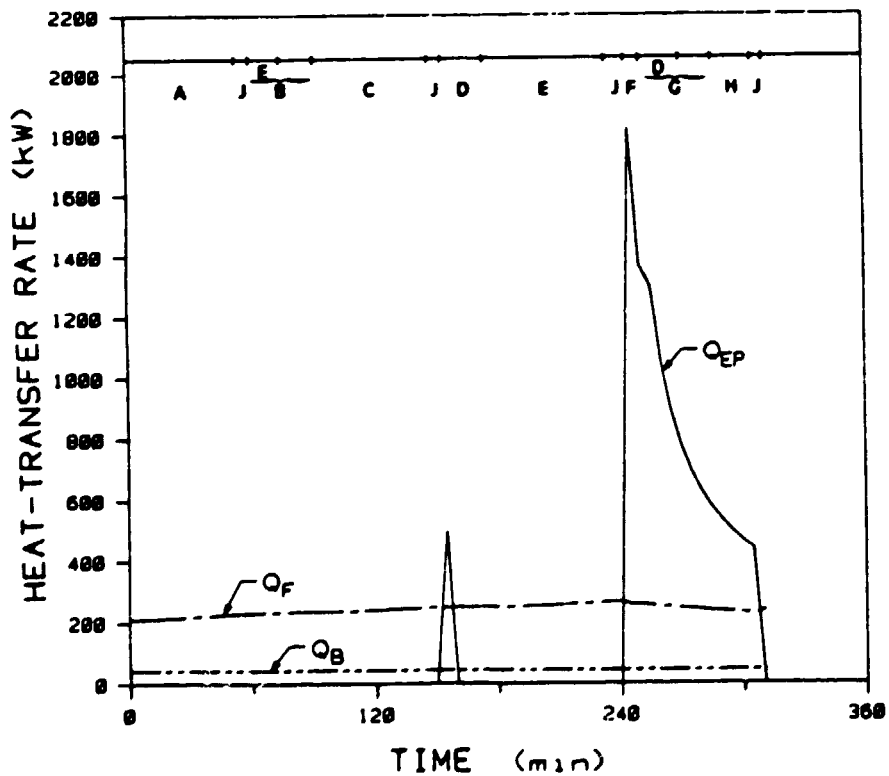


Fig. 6—Environmental heat losses via the roof (Q_F), the floor (Q_B), and the open doors (Q_{EP}), all simulated.

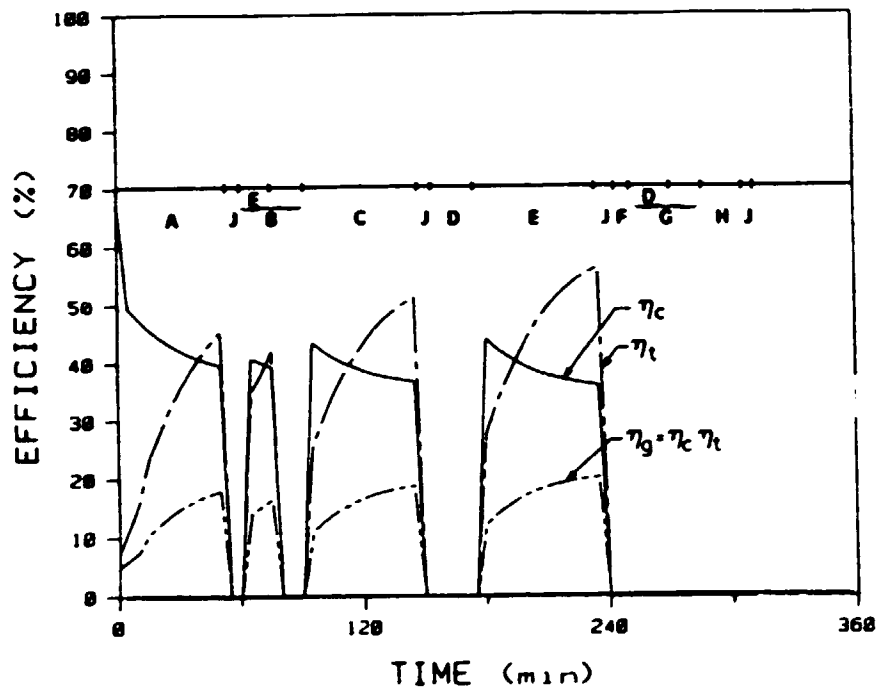


Fig. 7—Simulated values of thermal efficiency η_c , efficiency of heat transfer η_t , and global efficiency η_g .

$$\eta_c = \frac{Q_1}{Q_{\text{FUEL}}} \quad \eta_t = \frac{Q_D - Q_C}{Q_1} \quad \eta_g = \eta_c \eta_t$$

6. Other applications

6.1 The effect of continuous stirring of the melt

Table V. Effect of Continuous Stirring

	Conventional Batch	Continuous Stirring	Comparison
Melting rate (ton/hour)	4.18	5.40	gain 29 pct
Total batch time including 4-hour casting time (minutes)	554	536	gain 3.25 pct
Total energy consumed (GJ)	49.1	48.2	gain 1.9 pct

6.2 Closed - door operation

. technical challenge

Table VI. Effect of Closed-Door Operation

	Open-Door	Closed-Door	Comparison
Melting rate (ton/hour)	4.18	4.18	no change
Total batch time including 4-hour casting time (minutes)	554	537	gain 3 pct
Inner roof temperature (°C) (at batch end)	629	794	
Heat loss through doors (GJ)	3.16	0	
Total energy consumed (GJ)	49.1	44.5	gain 9.3 pct

6.3 Cost function evaluation

- cost function = $\frac{\text{specific consumption}}{\text{melting rate}}$

= $\frac{\text{m}^3 \text{ gas/ton sol. Al melted}}{\text{tons sol. Al melted/hours of heating}}$

- objective = $\frac{\downarrow}{\uparrow} \Rightarrow \downarrow$

= minimum value of the cost function

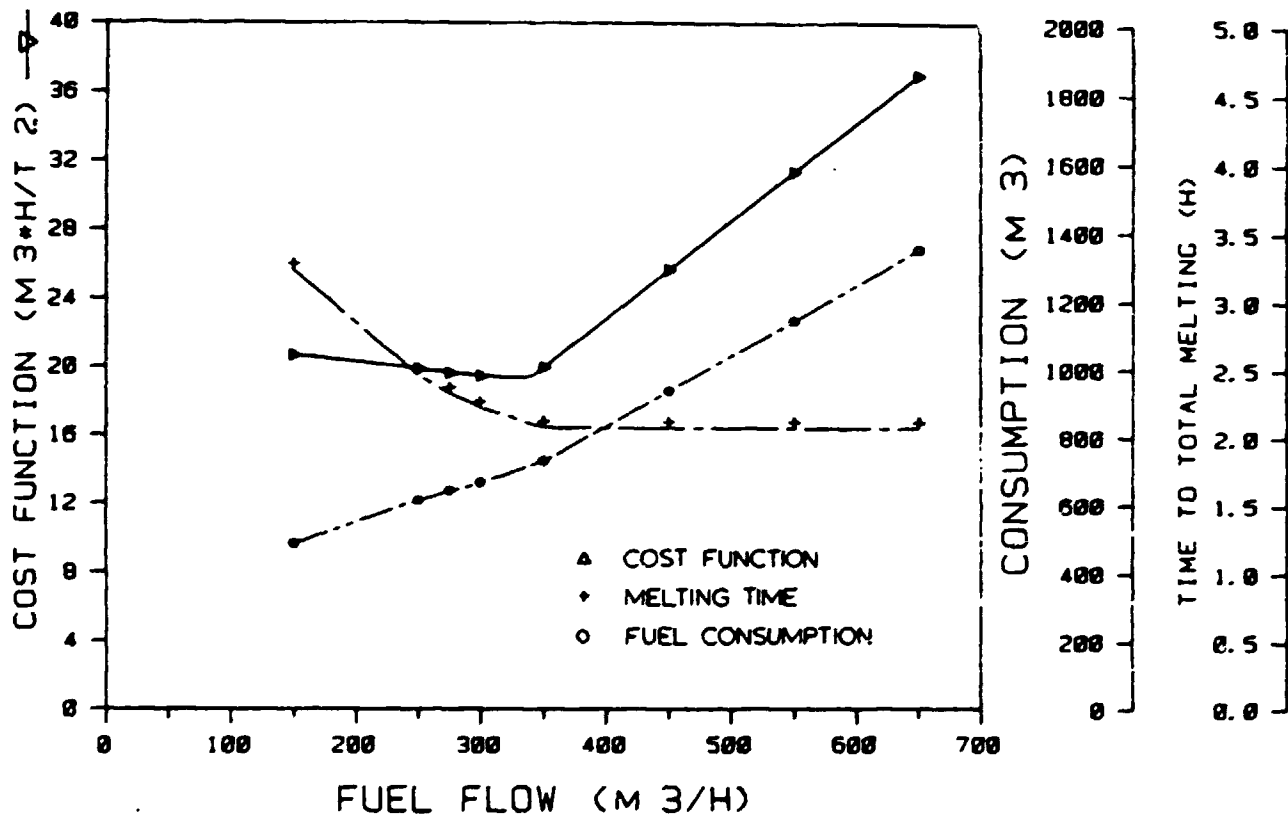


Fig. 8—Values of cost function for different fuel flowrates from 150 to 650 m³/h.

MELTER-HOLDER FURNACE

THE CONTROL MODEL

1- Introduction

- The challenge:

obtain a control model that is representative of the real process yet is simple enough for control and optimization purposes.

- The objective:

change the **analytic** model into a **control** model of the form

$$\dot{x} = Ax + Bu \text{ (linear or non-linear)}$$

- The methodology:

statistical approach using the data generated by the analytic model

2- Scope

Since the focus is laid on developing a model for fuel optimization, we are concentrating on a batch where only liquid metal is heated:

- loading of liquid metal
- **one hour heating period**
- stirring, fluxing, alloying, skimming

Only the one hour heating period is studied.

GRIPS/UQAC

INTERFACE COMPONENT

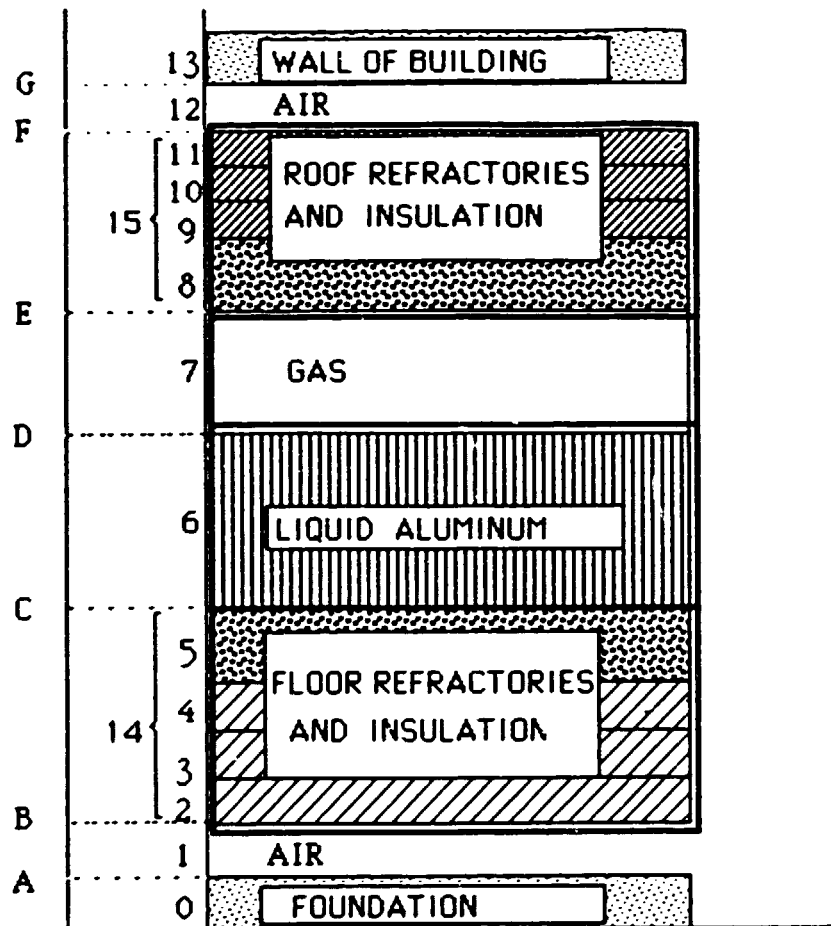


Figure 2— Symbols used to identify furnace components and their interfaces.

3. The analytic model and the need for simplification.

- Analytic model: 60 1D slices
- Control model: reduction dependent on the way the temperature and temperature gradients vary in the conducting medium.
- The simplified model must be **very accurate** in order to be applied for optimization studies (fuel optimization is likely to yield no more than a few % points in fuel consumption improvement).
- We choose a 10th order non-linear model:
 - roof: 6 subdivisions
 - model: 3 subdivisions
 - gas: 1 subdivision

4. The model

- . limits of the control volume:
 - from outer roof surface (F)
 - to inner floor surface (C)

- . All the equations must contain only the 10 state variables.

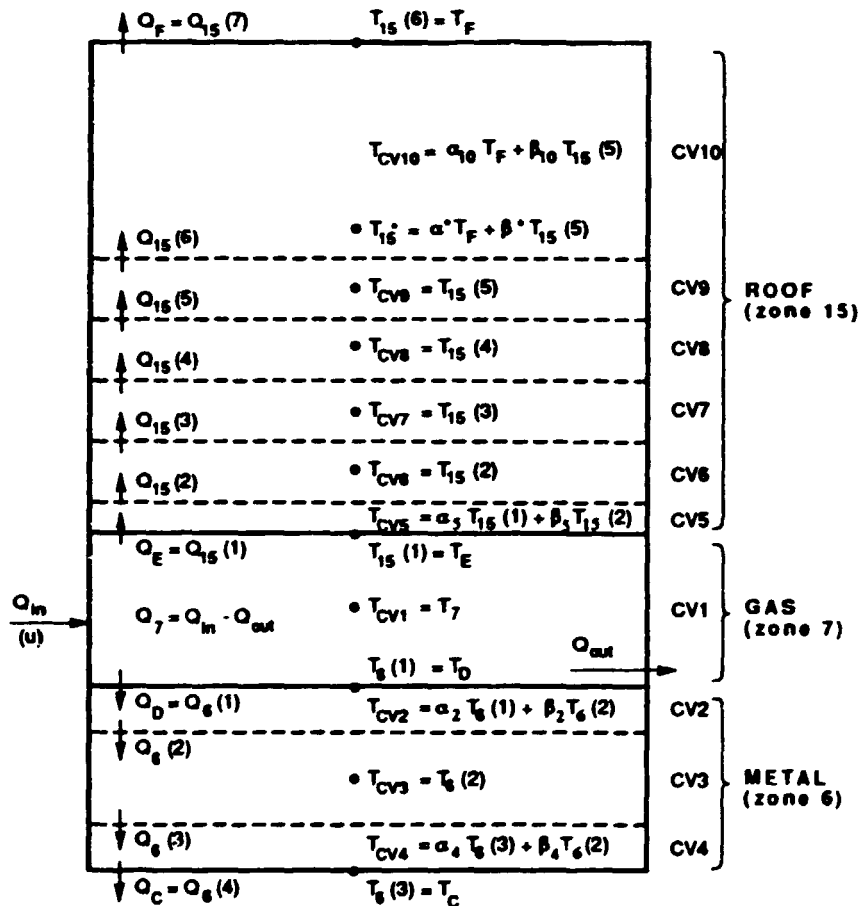


Figure 3— Discretization of the various furnace components into control volumes, showing the state variables (temperatures) and the heat flowrates.

4.1 Chamber (well stirred zone)

$$M_{CV1}C_7\dot{T}_7 = Q_7 - Q_D - Q_E$$

where the expressions of Q_7 and Q_D are:

$$Q_7 = \left(a_1 T_7^2 + a_2 T_7 + \frac{a_3}{T_7} + a_4 \right) u$$

$$Q_D = A_D h_D (T_7 - T_D) + \sigma \overrightarrow{GS_D} T_7^4 - \sigma \left(\overrightarrow{S_D G} + \overrightarrow{S_D S_E} \right) T_D^4 + \sigma \overrightarrow{S_E S_D} T_E^4$$

- Q_7, Q_D, Q_E (and Q_C, Q_F) are kept non-linear
- The directed exchange areas ($G_i \overrightarrow{S_j}, S_i \overrightarrow{S_j}$) are approximated by non linear functions of temperature.

$$\overrightarrow{GS_D} = c_1 T_7^3 + c_2 T_7^2 + c_3 T_7 + c_4$$

4.2 Metal (zone 6)

- Sliced in 3 zones (CV2 → CV4)
- oxide layer not considered
- justification for the number of zones:

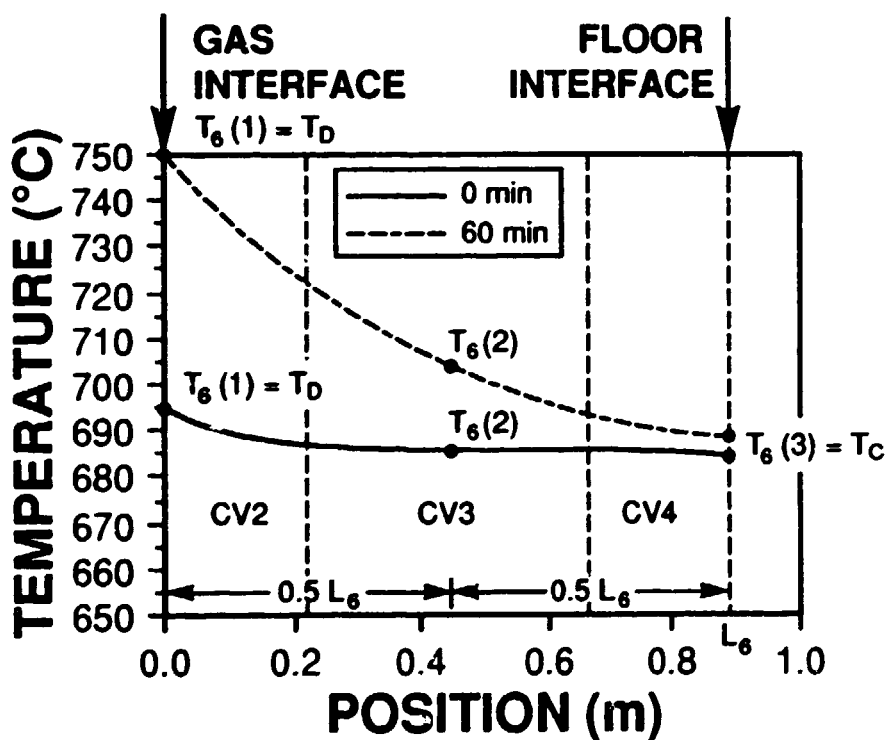


Figure 4— Metal temperature at start and end of heating period, showing the need for slicing the metal into 3 control volumes.

- equations:

$$M_{CV2}C_6\dot{T}_{CV2} = Q_6(1) - Q_6(2)$$

$$Q_6(1) = Q_D$$

$$Q_6(2) = \frac{k_D A_D}{0.5L_6} [T_6(1) - T_6(2)]$$

$$M_{CV3}C_6\dot{T}_{CV3} = Q_6(2) - Q_6(3)$$

$$Q_6(3) = \frac{k_D A_D}{0.5L_6} [T_6(2) - T_6(3)]$$

$$M_{CV4}C_6\dot{T}_{CV4} = Q_6(3) - Q_6(4)$$

$$Q_6(4) = Q_C = \frac{k_D A_D}{L_6/(N_6 - 1)} [T_6^{N_6-1} - T_6(3)]$$

4.3 Roof refractories (zone 15)

- Sliced in 6 zones (CV5 → CV10)
- Justification for the number of zone:

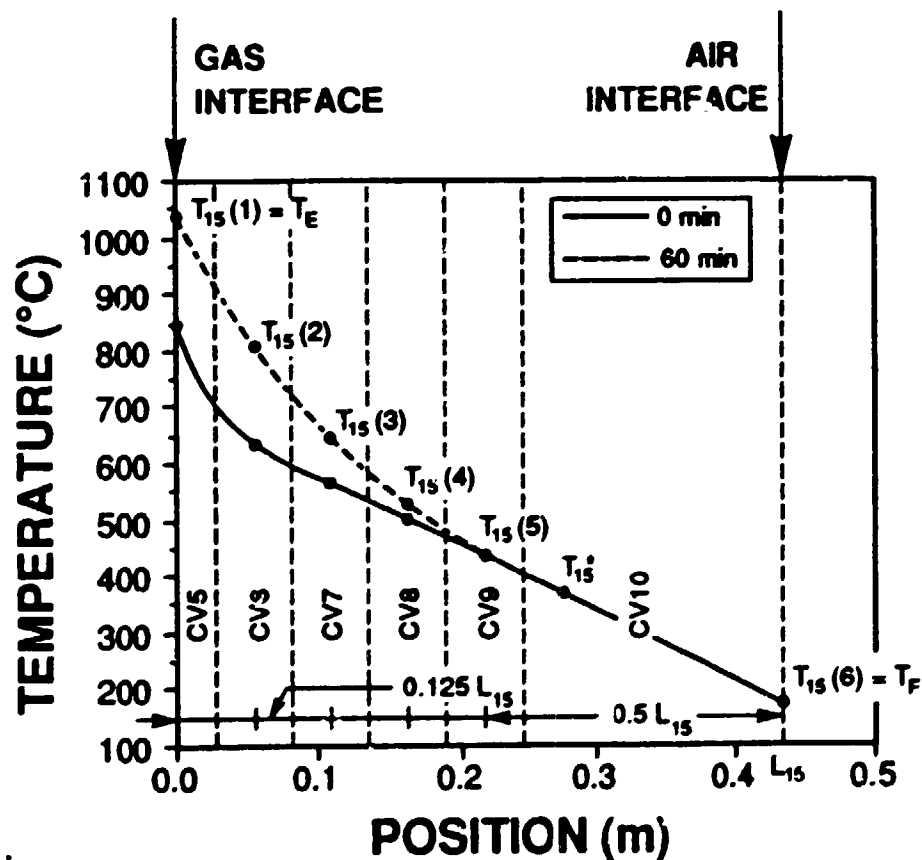


Figure 5— Refractories temperature at start and end of heating period, showing the need for slicing the refractories into 6 control volumes.

- equations:

for CV5 → CV8: same procedure as before
for the metal

for CV9:

$$M_{CV9}C_{15}\dot{T}_{CV9} = Q_{15}(5) - Q_{15}(6)$$

$$Q_{15}(6) = \frac{k_E A_E}{0.125 L_{15}} [T_{15}(5) - T_{15}^*].$$

$$T_{15}^* = \alpha^* T_{15}(6) + \beta^* T_{15}(7)$$

for CV10:

$$M_{CV10}C_{15}\dot{T}_{CV10} = Q_{15}(6) - Q_{15}(7)$$

$$Q_{15}(7) = Q_F = (1.1 \times 10^{-3} A_{F,M} + 1.65 \times 10^{-3} A_{F,V}) \\ \times (T_F - T_{12})^{4/3} + \sigma \epsilon_F A_F (T_F^4 - T_G^4)$$

$$T_6^{N_6-1} = c_{33}T_6(3) + c_{34}$$

$$T_{CV2} = \alpha_2T_6(1) + \beta_2T_6(2)$$

$$T_{CV3} = T_6(2)$$

$$T_{CV4} = \alpha_4T_6(2) + \beta_4T_6(3)$$

Where C_{33} , C_{34} , α_2 , α_4 , β_2 , β_4 are found by applying least-squares fits to the data obtained with the analytic model at 5 minute intervals.

4.4 Summary of model construction

- 10 first order **ODEs** (10 state variables)

$$T_7, T_6(1) \rightarrow T_6(3), T_{15}(1) \rightarrow T_{15}(6)$$

- complemented by non-linear expressions for:

$$Q_7, Q_C, Q_D, Q_E, Q_F$$

- the control variable is present in the expression for Q_7 .

Procedure for optimization:

- analytic model run for $50 < u < 500 \text{m}^3/\text{h}$
- control model then adjusted (by least-squares approximation) to the values obtained with the analytic model.

5. Results

- reported only for $u = 450 \text{ m}^3/\text{h}$

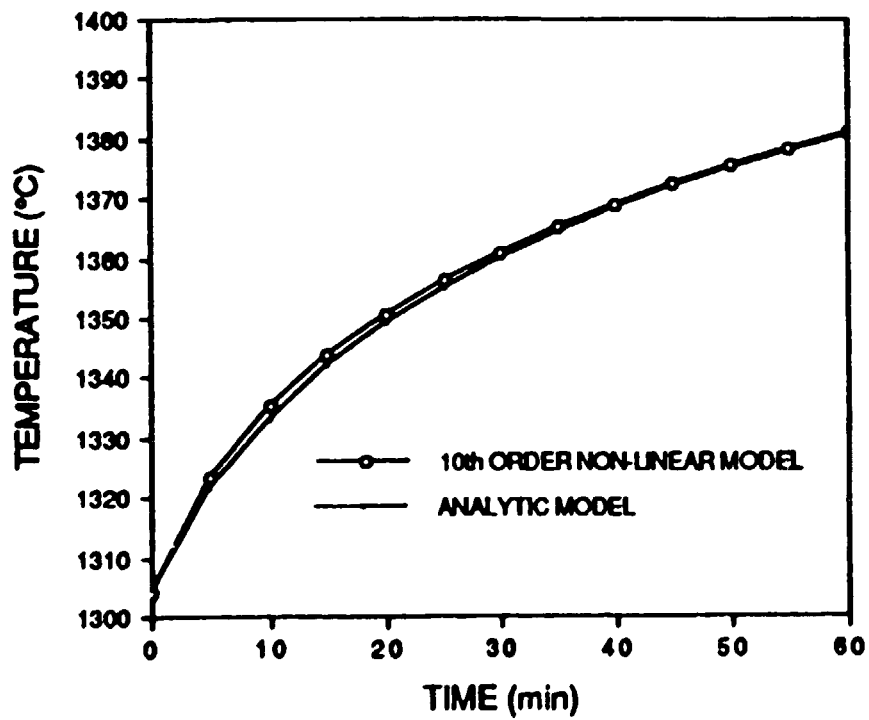


Fig. 6— Gas temperature obtained from analytic and simplified tenth-order nonlinear models.

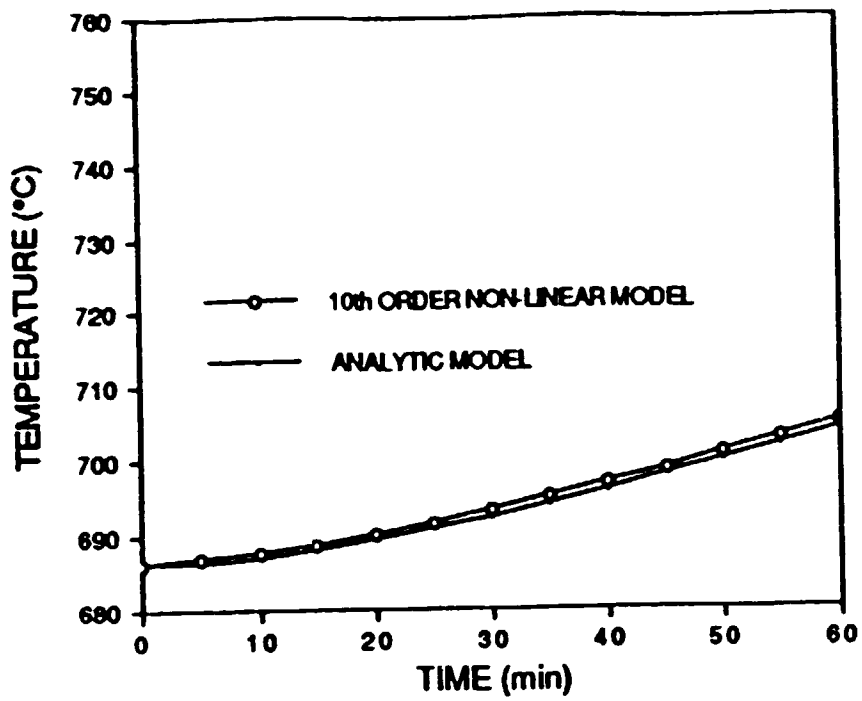


Fig. 8—Central-node metal temperature obtained from analytic and simplified tenth-order nonlinear models.

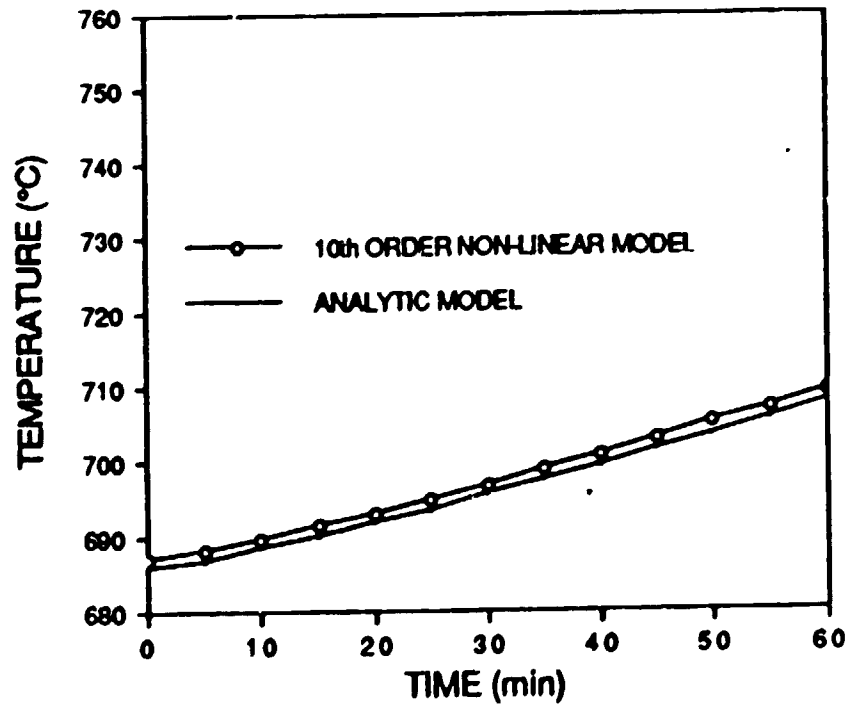


Fig. 9—Average metal temperature obtained from analytic and simplified tenth-order nonlinear models.

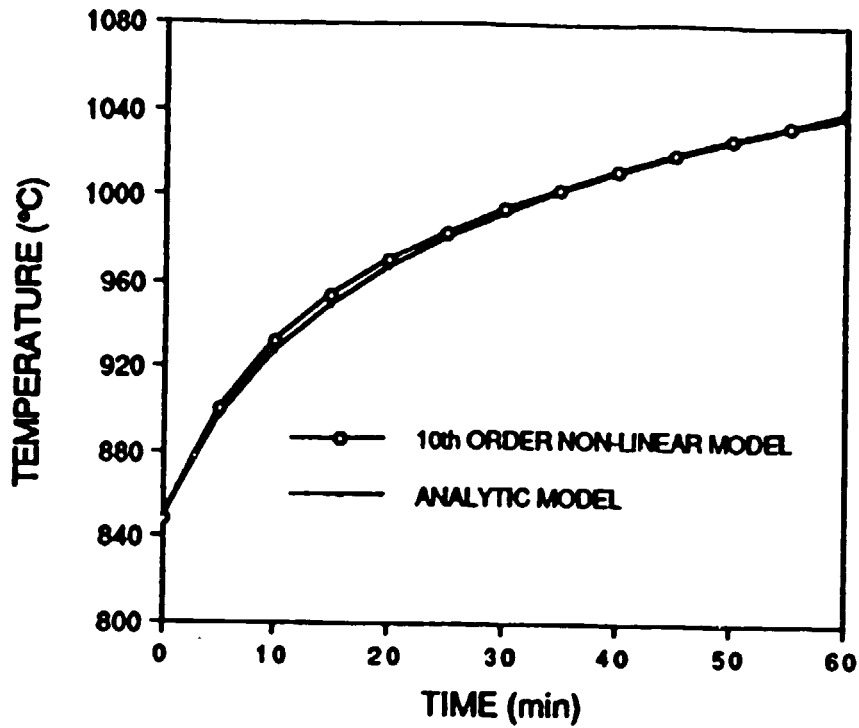


Fig. 10—Refractories inner-surface temperature obtained from analytic and simplified tenth-order nonlinear models.

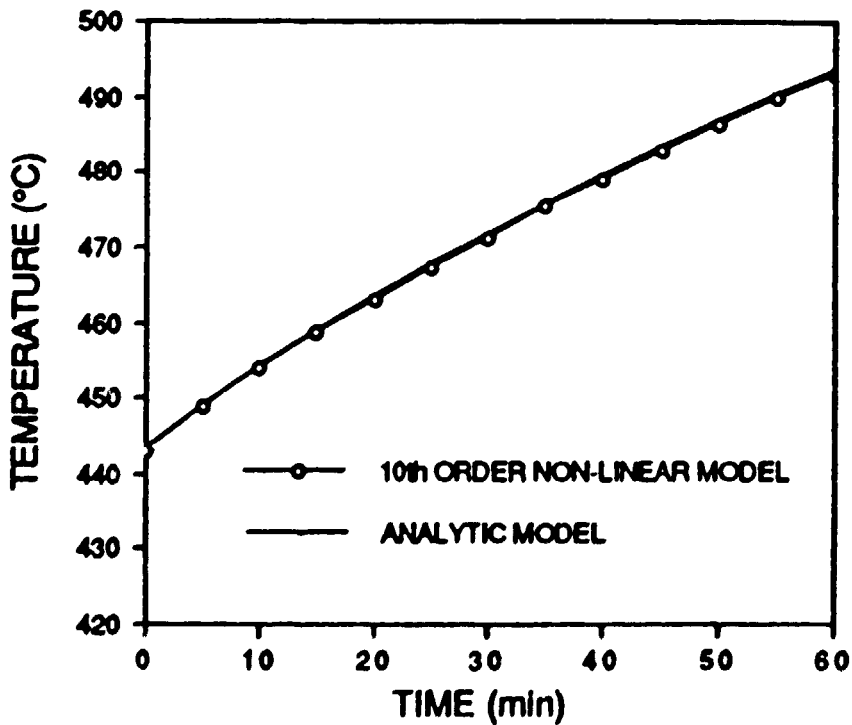


Fig. 11—Average refractories temperature obtained from analytic and simplified tenth-order nonlinear models.

SPECIFIC OPTIMAL CONTROL OF INDUSTRIAL THERMAL SYSTEMS

R. Ouellet, R.T. Bui, A. Meghlaoui

GRIPS

**Groupe de Recherche en Ingénierie des
Procédés et Systèmes**

**Université du Québec à Chicoutimi
Chicoutimi, Québec, Canada**

**8th International Conference on Numerical Methods in
Thermal Problems**

Swansea, 13th July, 1993

GENERAL OBJECTIVES

- Present a mathematical formulation for handling closed-loop non-linear control problems**
- Explain the application of the technique to minimize the fuel flowrate in an industrial furnace**

Reduced model

For the gas

$$\dot{T}_7 = (Q_7 - Q_D - Q_E)/(M_{CV1}C_7)$$

for the metal

$$\dot{T}_{CV2} = (Q_D - Q_6(2))/(M_{cv2}C_6)$$

$$\dot{T}_{CV3} = (Q_6(2) - Q_6(3))/(M_{cv3}C_6)$$

$$\dot{T}_{CV4} = (Q_6(3) - Q_C)/(M_{cv4}C_6)$$

for the refractories

$$\dot{T}_{CV5} = (Q_E - Q_{15}(2))/(M_{cv5}C_{15})$$

$$\dot{T}_{CV6} = (Q_{15}(2) - Q_{15}(3))/(M_{cv6}C_{15})$$

$$\dot{T}_{CV7} = (Q_{15}(3) - Q_{15}(4))/(M_{cv7}C_{15})$$

$$\dot{T}_{CV8} = (Q_{15}(4) - Q_{15}(5))/(M_{cv8}C_{15})$$

$$\dot{T}_{CV9} = (Q_{15}(5) - Q_{15}(6))/(M_{cv9}C_{15})$$

$$\dot{T}_{CV10} = (Q_{15}(6) - Q_F)/(M_{cv10}C_{15})$$

The CV_i ($i = 1, \dots, 10$) refer to the control volumes (zones) and the corresponding temperatures are approximated by

$$T_{CV2} = \alpha_2 T_6(1) + \beta_2 T_6(2)$$

$$T_{CV3} = T_6(2)$$

$$T_{CV4} = \alpha_4 T_6(2) + \beta_4 T_6(3)$$

$$T_{CV5} = \alpha_5 T_{15}(1) + \beta_5 T_{15}(2)$$

$$T_{CV6} = T_{15}(2)$$

$$T_{CV7} = T_{15}(3)$$

$$T_{CV8} = T_{15}(4)$$

$$T_{CV9} = T_{15}(5)$$

$$T_{CV10} = \alpha_{10} T_{15}(6) + \beta_{10} T_{15}(5).$$

FUEL-OPTIMAL CONTROL PROBLEM

Find minimum $u(t)$ to bring $y_3(t)$ from $y_3(0)$ to $y_3(t_f)$ where $y_3(t)$ is the central node liquid metal temperature. Final time t_f and final temperature $y_3(t_f)$ are prescribed.

2- Mathematical background

Cost function

$$J(\vec{u}) = \int_a^b \phi(\vec{y}(t), \vec{u}(t), t) dt$$

Equality constraint

$$\frac{d\vec{y}(t)}{dt} = \vec{f}(\vec{y}(t), \vec{u}(t), t)$$

Boundary conditions

$$\begin{aligned} \vec{M}(\vec{y}(a), a) &= \vec{0} \\ \vec{N}(\vec{y}(b), b) &= \vec{0} \end{aligned}$$

Inequality constraint

$$\vec{g}(\vec{u}(t), t) \geq \vec{0}$$

Closed-loop formulation

Control law

$$\vec{u}(t) = \vec{h}(\vec{x}(t), \vec{k})$$

New cost function

$$J^*(\vec{k}) = \int_a^b \phi^*(\vec{y}(t), \vec{k}, t) dt$$

New equality constraints

$$\frac{d\vec{y}(t)}{dt} = \vec{f}^*(\vec{y}(t), \vec{k}, t) \text{ with } \begin{cases} \vec{M}(\vec{y}(a), a) = \vec{0} \\ \vec{N}(\vec{y}(b), b) = \vec{0} \end{cases}$$

$$\frac{d\vec{k}}{dt} = \vec{0}$$

New inequality constraint

$$\vec{g}^*(\vec{y}(t), \vec{k}, t) \geq \vec{0}$$

Penalty method formulation

A new variable is introduced

$$\frac{dz(t)}{dt} = \left(g_1^* \left(\bar{y}(t), \bar{k}, t \right) \right)^2 G(g_1^*) + \left(g_2^* \left(\bar{y}(t), \bar{k}, t \right) \right)^2 G(g_2^*) + \dots + \left(g_m^* \left(\bar{y}(t), \bar{k}, t \right) \right)^2 G(g_m^*)$$

where g_i^* are the components of \vec{g}^* and $G(g_i^*)$ is a modified step function defined as follows:

$$G(g_i^*) = \begin{cases} 0 & \text{for } g_i^* \left(\bar{y}(t), \bar{k}, t \right) \geq 0 \\ s_i & \text{for } g_i^* \left(\bar{y}(t), \bar{k}, t \right) < 0 \end{cases} \quad \text{for } i = 1, \dots, m$$

where s_i are non-negative constants i.e. $s_i \geq 0$.

The new variable is added to the cost function

$$J_{\text{mod}}^*(\bar{k}) = \int_a^b \left(\phi \left(\bar{y}(t), \bar{k}, t \right) + \left(g_1^* \left(\bar{y}(t), \bar{k}, t \right) \right)^2 G(g_1^*) \right) dt + \dots + \int_a^b \left(g_m^* \left(\bar{y}(t), \bar{k}, t \right) \right)^2 G(g_m^*) dt.$$

The integrand is then extended to incorporate the Lagrangian multipliers :

$$\Phi(\bar{y}, \dot{\bar{y}}, \dot{\bar{z}}, \bar{k}, \dot{\bar{k}}, \bar{\lambda}, \bar{\eta}, t) = H(\bar{y}, \bar{k}, \bar{\lambda}, t) - \bar{\lambda}^T \dot{\bar{y}} - \bar{\eta}^T \dot{\bar{k}}$$

where the Hamiltonian H is defined as :

$$H(\bar{y}, \bar{k}, \bar{\lambda}, t) = o^*(\bar{y}, \bar{k}, t) + \bar{\lambda}^T \bar{f}^*(\bar{y}, \bar{k}, t) \\ + (g_1^*(\bar{y}, \bar{k}, t))^2 G(g_1^*) + \dots + (g_m^*(\bar{y}, \bar{k}, t))^2 G(g_m^*)$$

The optimality equations are obtained by applying the Euler-Lagrange equations :

$$\dot{\bar{\lambda}} = -\frac{\partial H}{\partial \bar{y}} \quad \text{with} \quad \begin{cases} \bar{\lambda}(a) = \left[\frac{\partial \bar{M}^T}{\partial \bar{y}} \right] \bar{\zeta} & \bar{M}(\bar{y}(a), a) = \bar{0} \\ \bar{\lambda}(b) = \left[\frac{\partial \bar{N}^T}{\partial \bar{y}} \right] \bar{\nu} & \bar{N}(\bar{y}(b), b) = \bar{0} \end{cases}$$

$$\dot{\bar{\eta}} = -\frac{\partial H}{\partial \bar{k}} \quad , \quad \bar{\eta}(b) - \bar{\eta}(a) = 0$$

Variable substitution

$$\dot{\bar{\omega}}(t) = -\frac{\partial H}{\partial \bar{k}} \quad , \quad \bar{\omega}(a) = \bar{\omega}(b) = \bar{0}$$

where $\bar{\omega}(t) = \bar{\eta}(t) - \bar{\eta}(a) = -\int_a^t \frac{\partial H}{\partial \bar{k}} dt$.

3– Application to the melter-holder furnace

Optimal problem

Cost function :

$$J = \frac{1}{2} \int_0^{t_f} u^2(t) dt$$

where

$$u(t) = k_p \Delta T_3(t) + k_i \int_0^t \Delta T_3(t) dt + k_d \frac{d\Delta T_3(t)}{dt}$$

with

$$\Delta T(t) = T_3(t_f) - T_3(t)$$

$$50 \leq u(t) \leq 500 \text{ m}^3/\text{h}$$

$$686^\circ\text{C} \rightarrow 705.1^\circ\text{C} \text{ in 1 hour}$$

4-Results

Table 1 Optimal and suboptimal results for the casting furnace, with and without constraint.

constraints	control law	constraints violation %	total fuel required (m ³)	optimal parameters			Cost function
				K _p (× 10 ⁻³)	K _i (× 10 ⁻⁷)	K _d	
with	optimal	0.	397.24	—	—	—	0.0489
	P	—	—	—	—	—	—
	PD	4.36	406.23	0.2974	—	0.3497	0.0495
	PI	3.56	410.75	0.3285	0.6165	—	0.0499
	PID	0.08	415.18	0.2944	0.4597	0.1502	0.0501
without	optimal	8.84	395.58	—	—	—	0.0489
	P	45.3	383.67	0.4724	—	—	0.0559
	PD	5.96	403.85	0.3073	—	0.3265	0.0494
	PI	7.34	406.02	0.3451	0.5365	—	0.0496
	PID	3.50	396.14	0.1644	-0.0212	-1.6143	0.0491

4-Results (continued)

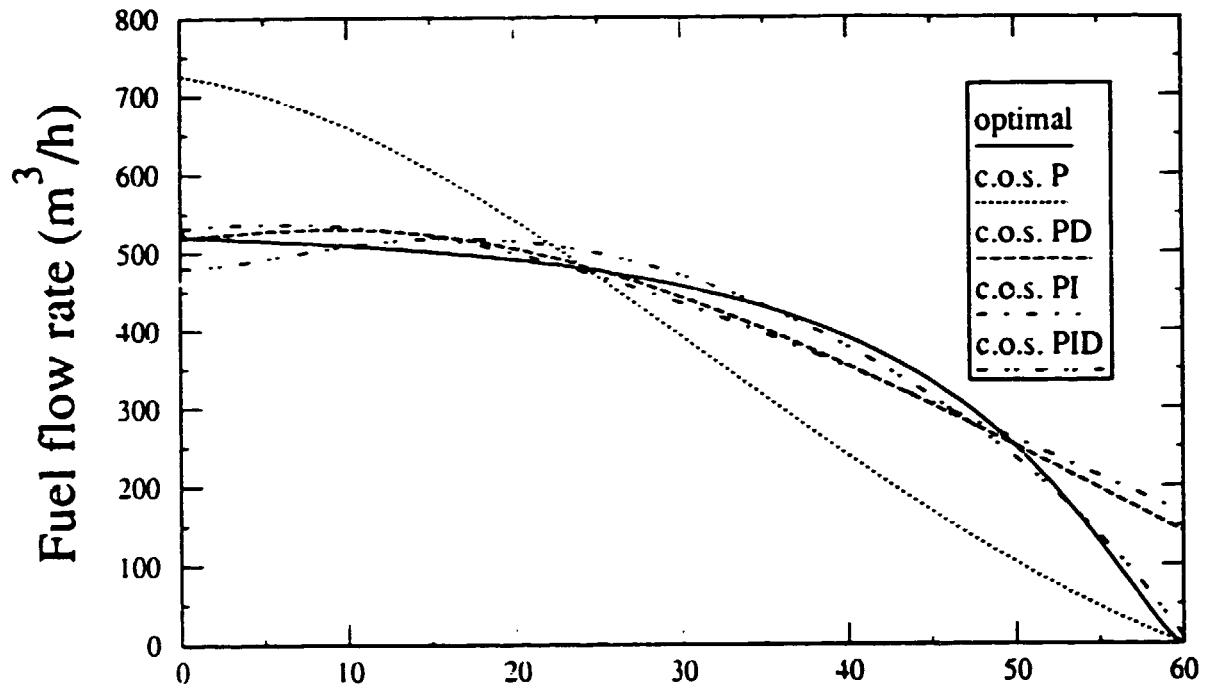


Figure 8 Optimal and suboptimal fuel flow rate without constraint on the control variable.

4-Results (continued)

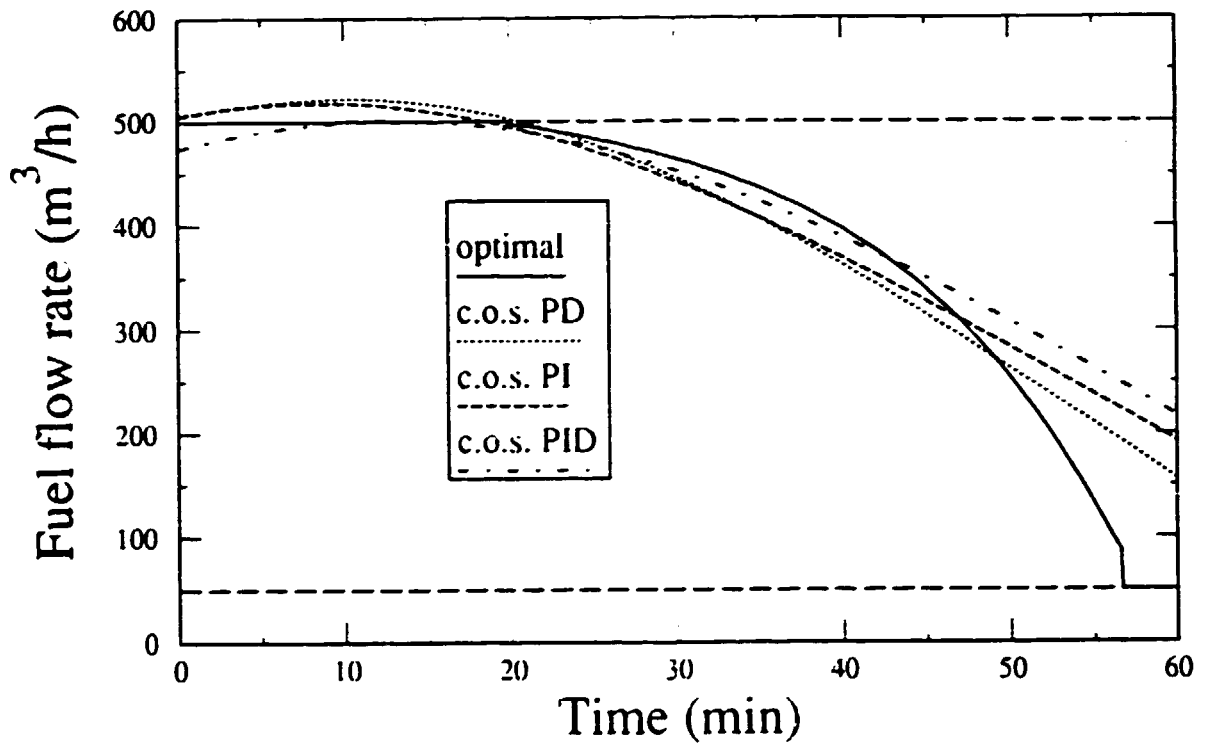


Figure 9 Optimal and suboptimal fuel flow rate with constraints on the control variable.

5. CONCLUSION

- There is a solution to the dilemma caused by the contradictory needs for a model with good representativity (high-ordered and sophisticated), and for a simpler model for control purpose.**
- The technique suggested in this paper enables the solution of open or closed-loop non-linear control problems for complex industrial processes.**
- It is necessary to optimize more than one control parameter to obtain a solution without violating the inequality constraint.**
- The method can be applied to other types of control systems (other than PID).**
- The solution procedure requires minimum labor.**

THE MELTER-HOLDER FURNACE

3-D MODEL

1 - Introduction

1 D : - Simulation of the changes in the experimental procedure

- Useful for optimization purposes

3 D : - Design purposes;

Changes in:

- Furnace geometry

- Position of the charge

- Level of liquid heel

- Chimney location

- **Need for a transient model**

(because of variations in the operating conditions and large time constant of the refractory walls).

- **Two parts in the model-** | -The chamber
| -The metal

Eventually linked together

- **One general code: PHOENICS**

OPERATION MODE OF A TYPICAL BATCH

Preheating the heel
(burner ON)

Charging the solid
(burner OFF)

Pouring the liquid metal
burner ON/10 crucibles)

Mixing with nitrogen lance
(burner ON)

Fluxing (burner ON)

Skimming (burner OFF)

Alloying (burner OFF)

Mixing with nitrogen lance
(burner ON)

Fluxing (burner ON)

Skimming (burner OFF)

Heating (burner ON)

Casting (burner OFF)

Scope of the 3D model
(about 320 minutes)

2. The combustion chamber

- Three main aspects:
 - Combustion kinetics of fuel
 - Motion of fluid
- Phoenics**
- Radiation : IPM coupled to **PHOENICS**

2.1 The general conservation equation

$$\frac{\partial}{\partial t} (\rho \phi) + \text{div} (\rho u \phi - \Gamma_{\phi} \text{grad } \phi) = S_{\phi}$$

where ϕ : general dependent variable

Γ_{ϕ} : turbulent exchange
coefficient of ϕ

S_{ϕ} : Source term (Combustion,
convection, radiation)

The integrated form is:

$$a_P \phi_P = a_N \phi_N + a_S \phi_S + a_E \phi_E + a_W \phi_W + a_H \phi_H + a_L \phi_L + a_P^o \phi_P^o + b$$

- o (superscript): Previous time step
- b: Discretized form of S_{ϕ}
- a: Relative to diffusion and convective flows through cell P

ϕ Stands for 8 variables:

Three components of velocity, two turbulence parameters, the gas enthalpy, the mixture fraction (f) and the mass fraction of unburned fuel (mfu)

Yields a set of 8 non-linear coupled equations for every cell; solved by PHOENICS (slabwise technique using a number of sweeps)

2.2 The radiation model (IPM)

$$\dot{Q}_{\text{comb}}^C + \sum_k [A_k^C \dot{q}_k^C - h^C A_k^C (T_k^C - T_g^C)] +$$

(real surfaces)

$$\sum_{i=1}^6 \dot{m}^i c_p^i (T_g^i - T_r) - \dot{m}^C c_p^C (T_g^C - T_r) +$$

$$(\dot{Q}_x^C - \dot{Q}_x^W) + (\dot{Q}_y^C - \dot{Q}_y^N) + (\dot{Q}_z^C - \dot{Q}_z^H) = 0$$

$$A_k^C \dot{q}_k^C + h^C A_k^C (T_k^C - T_g^C) + UA_k^C (T_k^C - T_a) = 0$$

- Equation (3) is a discretized form of the energy equation which can be solved by PHOENICS provided the code is fed with the appropriate source term (from IPM)

$$v^C s_h = (\dot{Q}_x^C - \dot{Q}_x^W) + (\dot{Q}_y^C - \dot{Q}_y^N) + (\dot{Q}_z^C - \dot{Q}_z^H) +$$

$$\sum_k [A_k^C q_k^C + h^C A_k^C (T_k^C - T_g^C)]$$

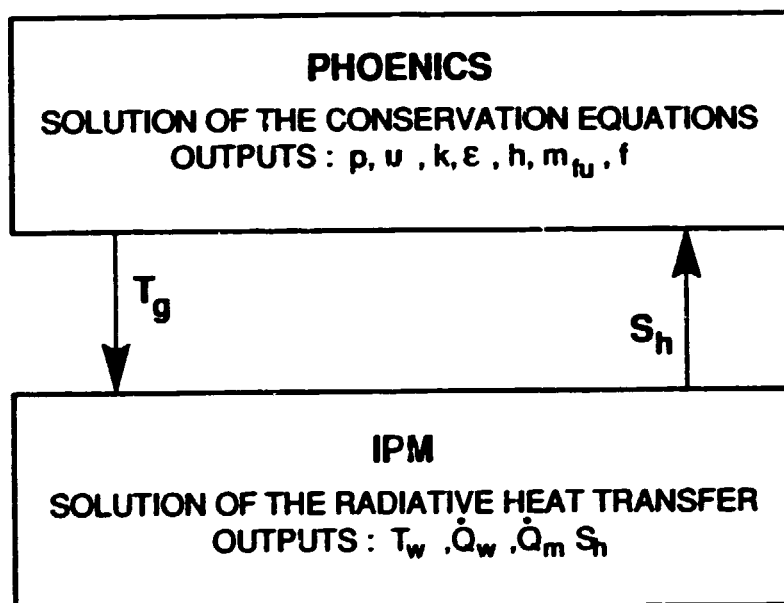
(real surfaces)

- Equation (4) is written for a steady state process; for a transient analysis the term $UA_k^C (T_k^C - T_a)$ is replaced by a numerical algorithm for the walls.

2.3 Coupling PHOENICS AND IPM

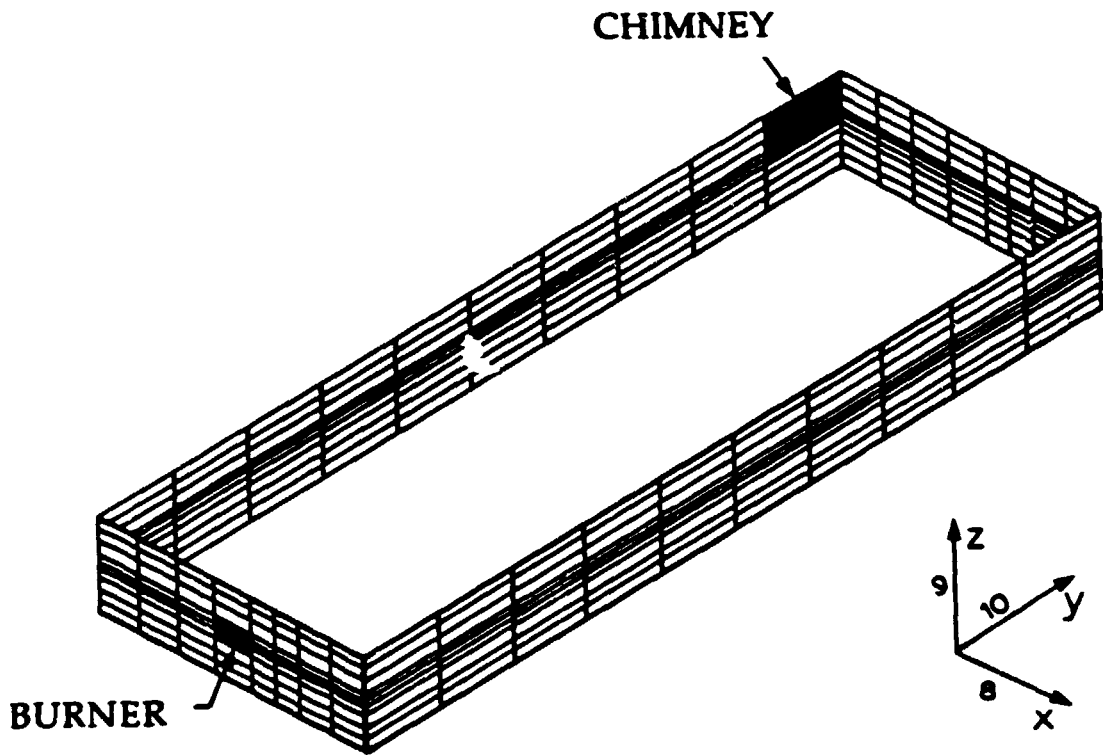
- Steady state regime.
 - Pressure, the 3 components of velocity and the 2 turbulence parameters (k, ε) are calculated on the basis of a STEADY STATE REGIME

Simplified steady state procedure

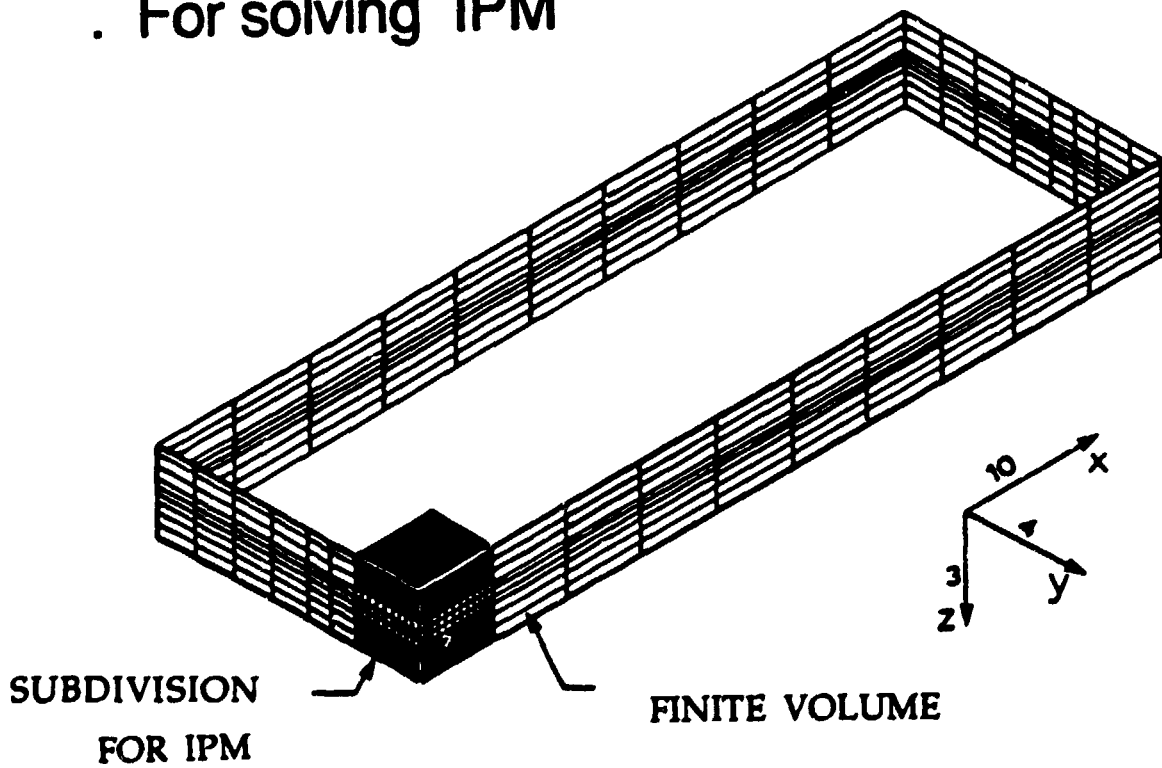


Grids used

- . For solving the conservation equations



- . For solving IPM



Interfacing the grids

- . Temperature values obtained by PHOENICS are averaged, and the results assigned to the corresponding IPM zone.
- . Heat fluxes and source terms obtained by IPM are uniformly distributed to all the corresponding PHOENICS cells.
- . Interaction once every 10 sweeps.

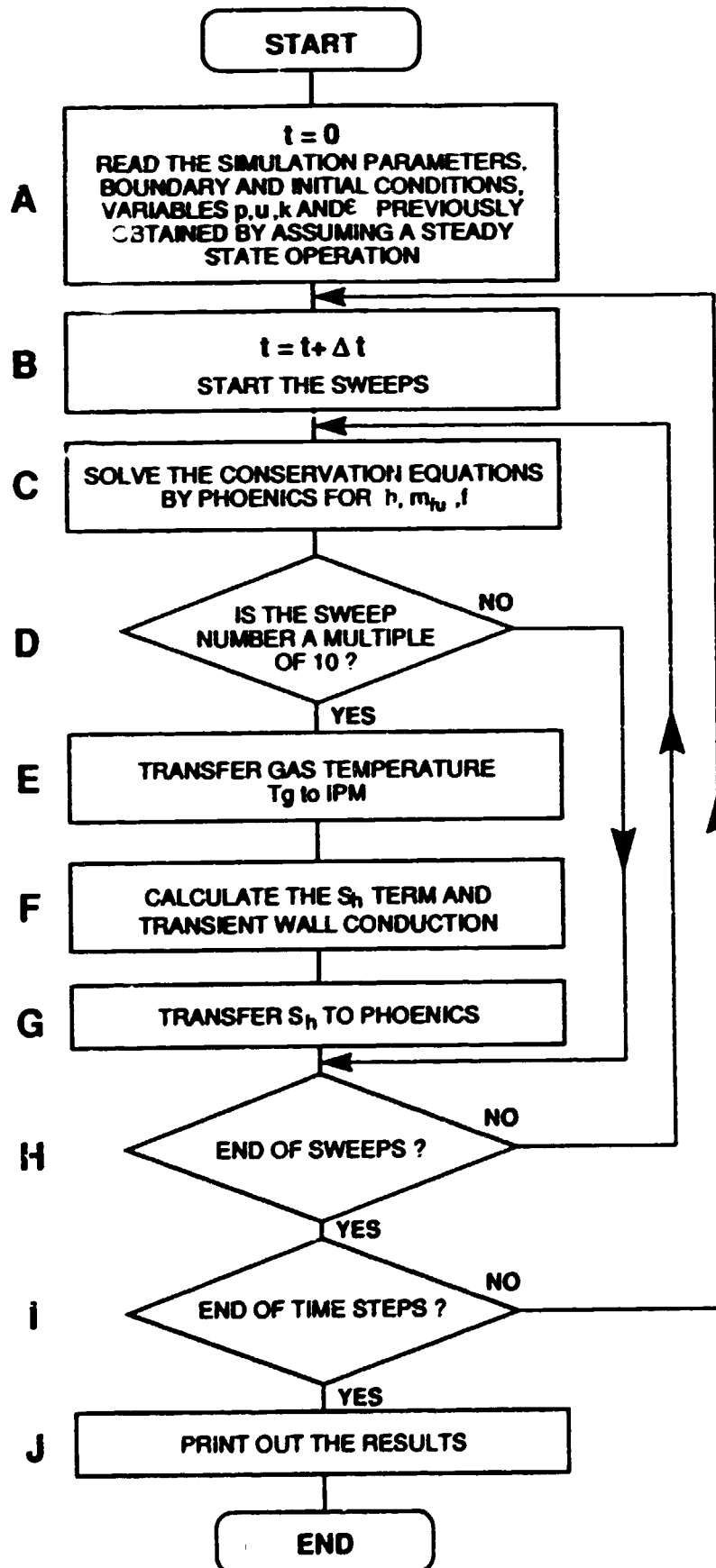
b) Transient regime

- **Effect of sequential operation and thermal inertia of refractories (not the metal in this case)**
- **The Stefan problem is not considered. A fixed temperature is assigned to the metal (for the moment)**
- **Ideally the above procedure is resumed at every time step**

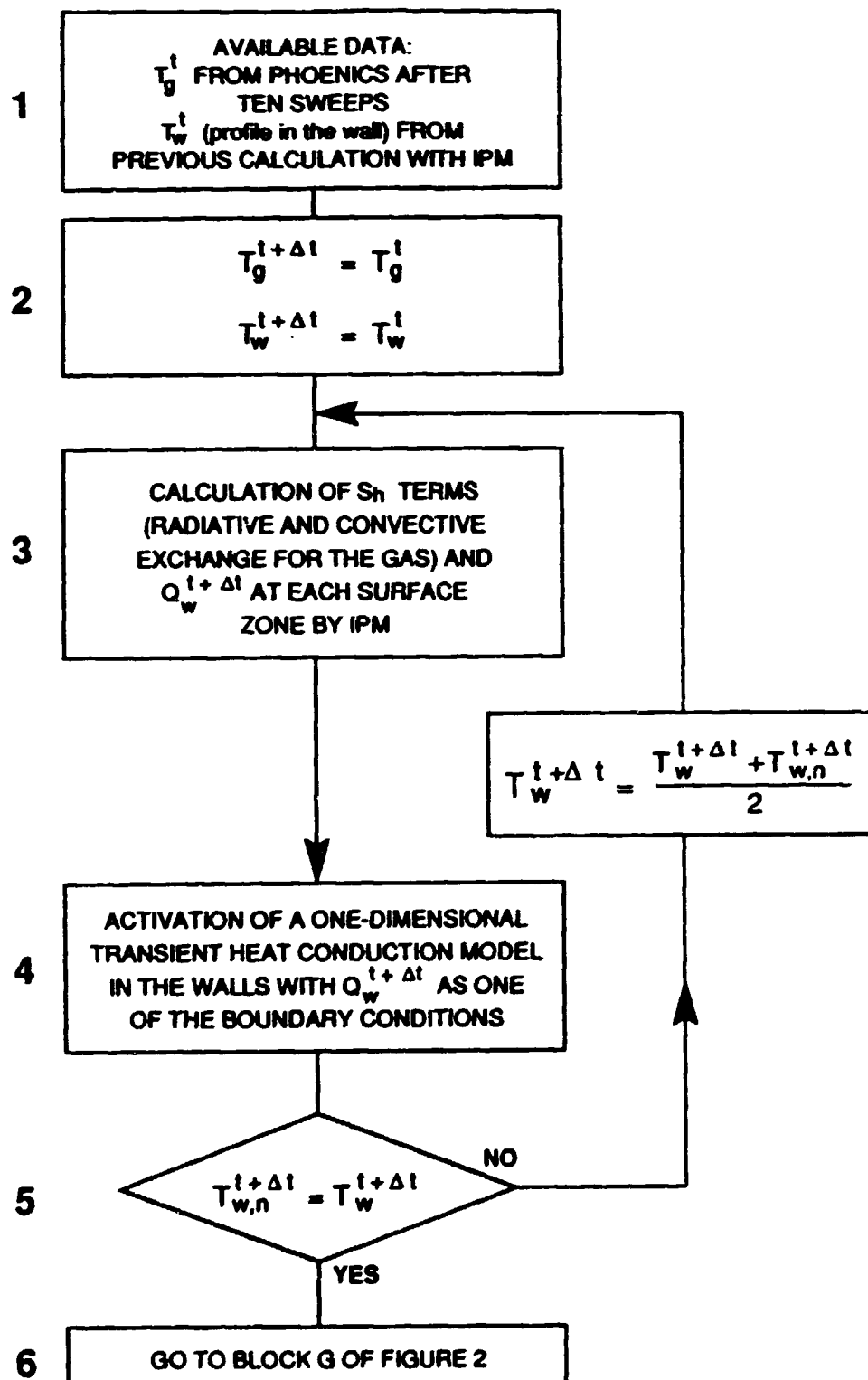
However:

- **the surface heat balance has to be changed (see above)**
 - **the CPU time should be kept minimal**
- **Six dependent variables (pressure, the 3 components of velocity, the 2 turbulence parameters) are calculated on the basis of a steady state regime and kept constant (semi-interactive procedure)**

Flowchart for the transient procedure



Description of Block F of Figure 2



2.4 The combustion model

- Eddy break-up model

$$R_{fu} = -C_o \rho \frac{\epsilon}{k} m_{fu}$$

where C_o : constant which has an influence on the flame length

R_{fu} : source term in the corresponding equation for the continuity of fuel. ... which, if multiplied by the heat of combustion, is part of the source term in the energy equation

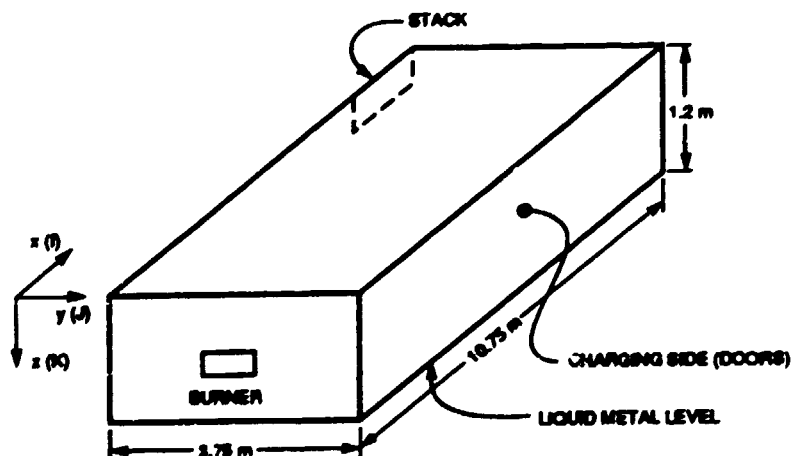
- The combustion is kinetically controlled: the mixture fraction (f) and the fraction of unburned fuel (m_{fu}) are followed by solving conservation equations

2.5 The semi-interactive procedure

- fully interactive:
calculation of 9 variables at each passage through block C (Fig.2)
- semi-interactive:
only h , f and m_{fu} are updated in block C
(p , u , v , w , k , ε — evaluated on the basis of a steady state regime)

2.6 Assessment of the semi-interactive procedure

a) Description of the test problem



Operating conditions and parameters

Fuel: type: natural gas; composition (% vol):
96.2 CH₄, 1.6 C₂H₆, 2.2 N₂; heating value
(MJ/m³ STP): 33.7; volumetric flowrate (m³/s
STP): 0.125; mass flowrate (kg/s): 0.091

Air: mass flowrate (kg/s): 1.55 (no excess air)

Combustion products: considered as a gray gas
with an absorption coefficient $K = 0.175 \text{ m}^{-1}$;
the thermodynamic properties are dependent
on temperature and obtained for a mixture
corresponding to that of a complete
stoichiometric combustion.

Emissivities: refractories: 0.6; charge (liquid
metal): 0.5

Heat transfer coefficients (W/m² K)

- overall (for steady state computations,
from inside surface to ambient air):
charging doors side: 1.30; opposite
lateral side: 0.86; roof: 1.37; burner and
opposite walls: 0.75
- convective: burner and opposite walls:
50.0; side walls: 25.0

Temperatures (K)

- ambient: 298; gas at burner entry: 333;
charge (bottom surface): 1033.
- initial: internal wall: 700; external
wall: 373 (with a linear profile between
the two); gas: 723.

Area of burner opening: 0.123 m²

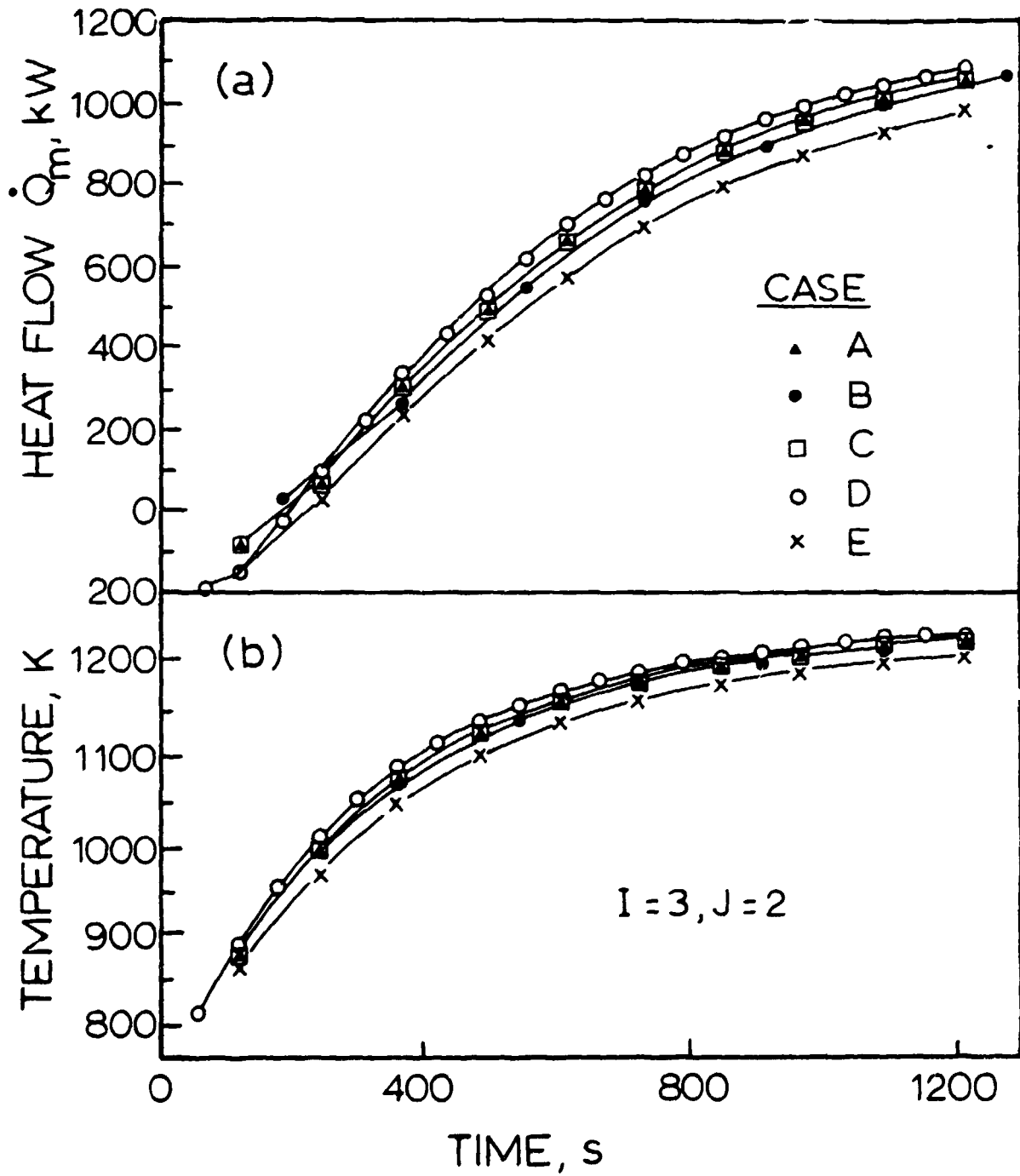
Grid sizes (x, y, z): IPM: 6x3x4; PHOENICS:
12x9x8

- firing at $t = 0$ with initial conditions given in the table
- heating for 1200 s.

Description of the cases studied

Table 2 Description of the cases studied.

Case	Procedure	Time step, s	Number of sweeps	Time ratio CPU/real time
A	Totally-interactive	120	250	21
B	"	180	250	16
C	"	120	100	10
D	"	60	250	44
E	Semi-interactive	120	100	4



3. The metal

3.1 Equations

Energy equation without convection in the melt:

$$\frac{\partial}{\partial t}(\rho T) - \nabla \cdot \left(\frac{k}{c} \nabla T \right) = S_T$$

where the latent heat is incorporated in the thermal properties

- $\rho c = \frac{dH}{dT}$ in each phase
- but at the interphase $\frac{dH}{dT} \rightarrow \infty$

this is solved by using a large value of ρc in the interval

$$T_f - \delta < T < T_f + \delta$$

Effective thermal properties method (ETP)

- specific heat:

$$\rho c_{eff} = \frac{\delta_{NS} \frac{\partial H}{\partial T} \Big|_{NS} + \delta_{EW} \frac{\partial H}{\partial T} \Big|_{EW} + \delta_{HL} \frac{\partial H}{\partial T} \Big|_{HL}}{\delta_{NS} + \delta_{EW} + \delta_{HL}}$$

$$\text{where } \delta = 1 \text{ if } \delta H > \rho L \\ = 0 \text{ otherwise}$$

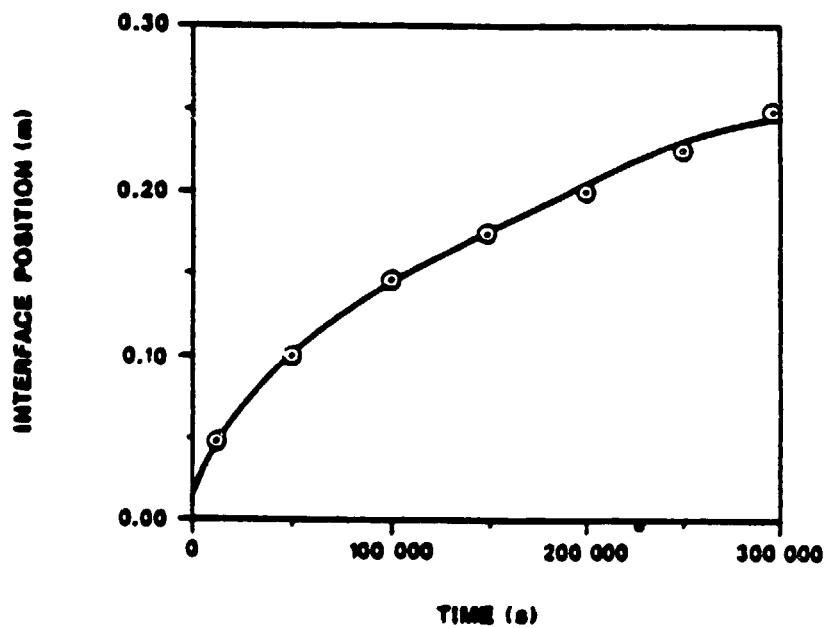
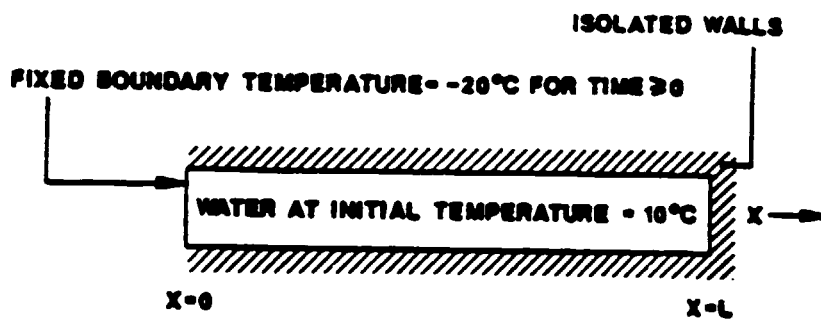
- thermal conductivity:

$$q_N = \int_{T_N}^{T_F} \frac{1}{k_N(T)} dT$$

$$\left. \frac{dw}{dT} \right|_{NS} = \frac{q_N - q_S}{T_N - T_S}$$

$$\frac{1}{k_{eff}} = \frac{\delta_{NS} \left. \frac{dw}{dT} \right|_{NS} + \delta_{EW} \left. \frac{dw}{dT} \right|_{EW} + \delta_{HL} \left. \frac{dw}{dT} \right|_{HL}}{\delta_{NS} + \delta_{EW} + \delta_{HL}}$$

3.2 Validation of ETP



3.3 Effect of natural and forced convection

- **Rigorous incorporation:**

solution of the complete energy and motion equations in the melt

- - CPU time too long
- convergence difficulty (due to high Ra)

- **Simplified method sought**

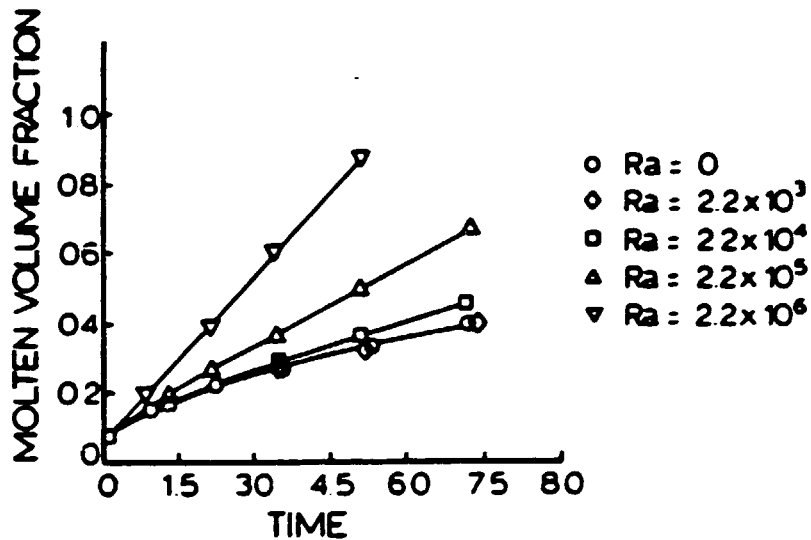
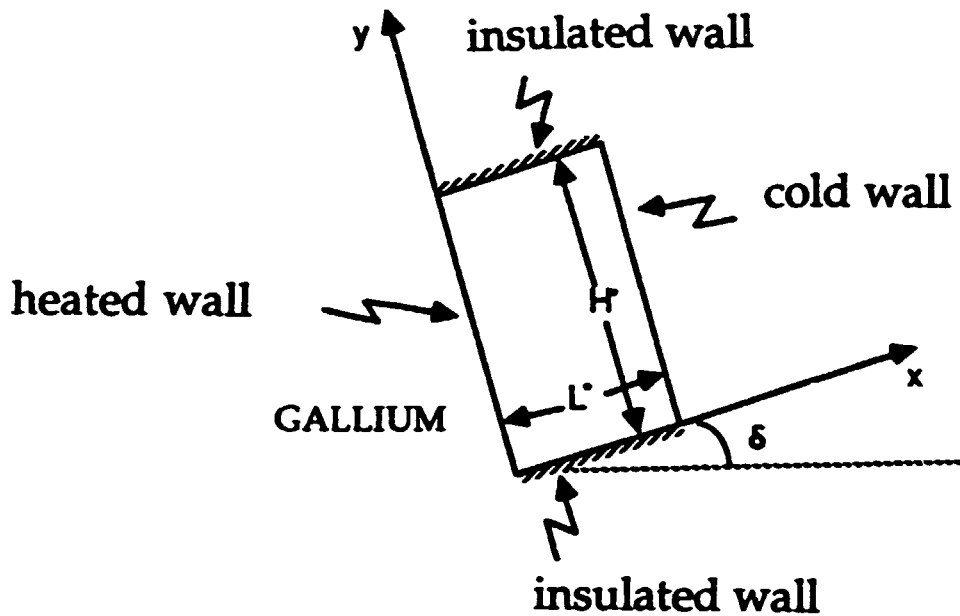
(in the context of a complex industrial problem)

- **Force convection dominates**

- arrival of crucibles (≥ 100 minutes)
- stirring and fluxing

- **Practical solution:**

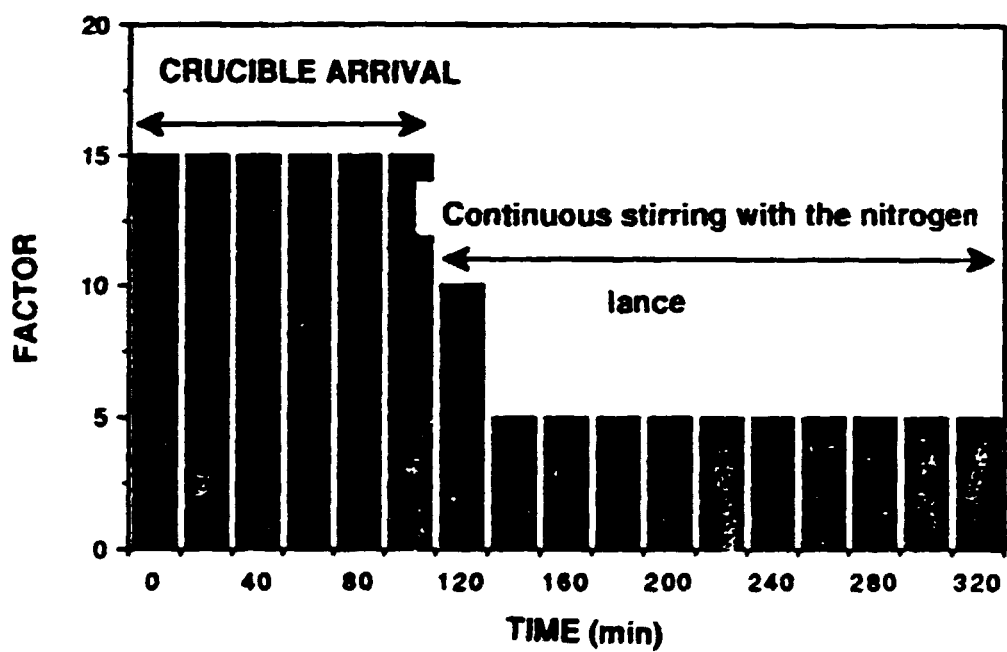
Consider only conduction in the melt, but use an augmented thermal conductivity for the liquid λ



- $k_{aug} = k_{real} \times C$

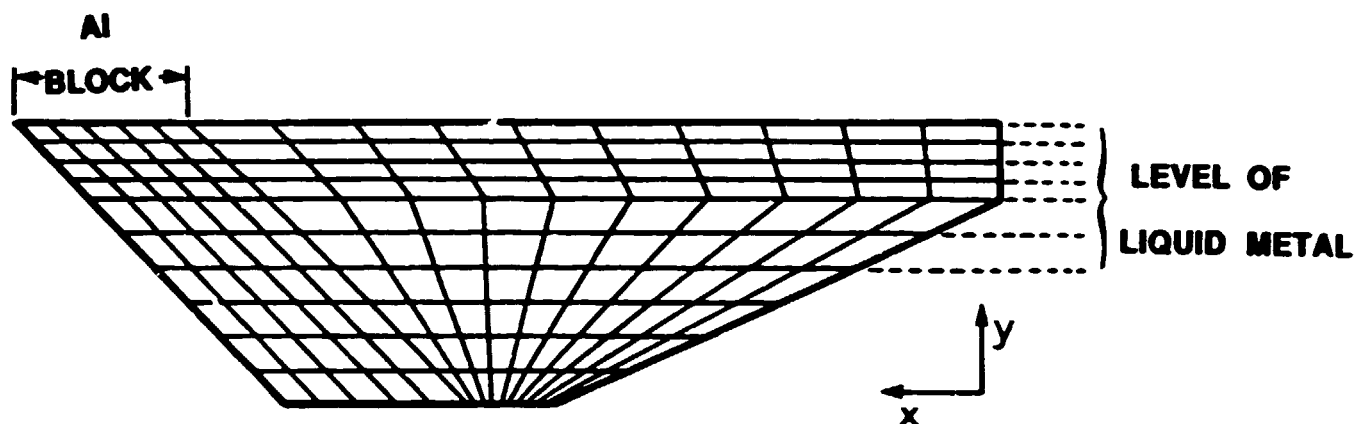
where C is obtained by calibration with the experimental melting rate

- disadvantage:
gives only global behaviour
- the concept is adapted to include also forced convection



AUGMENTED CONDUCTIVITY

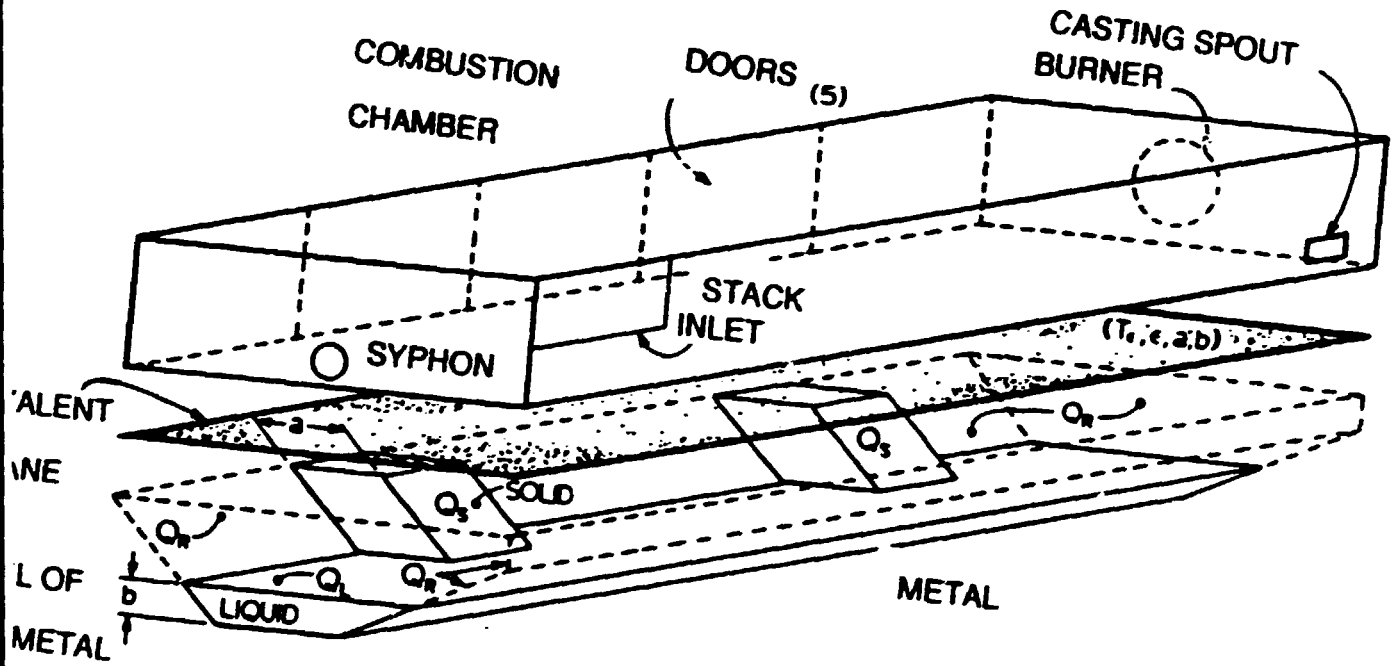
3.5 Grid used



- curvilinear grid
- horizontal subdivision dependent on the quantity of liquid added from the crucibles
- 3000 finite volumes (generated by Patran)
- pre and post-treatment procedures

4. Coupling combustion chamber and metal

- ensure continuous heat transfer between metal and gas
- allowance for changes in metal geometry with time
- utilization of an equivalent plane concept



4.1 Emissivity of the equivalent plane

- the metal control volume does not coincide with the equivalent plane

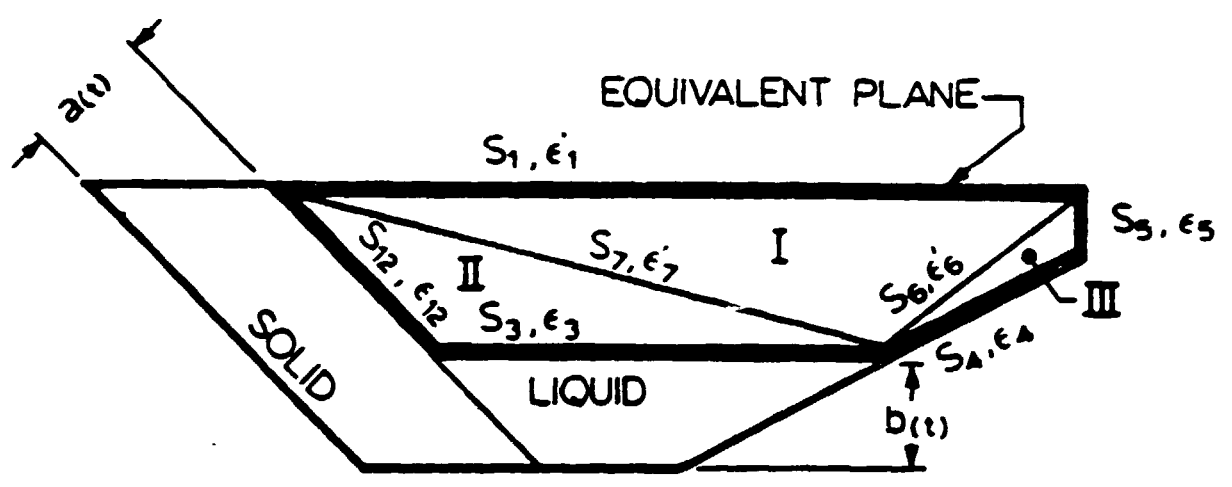


Figure 2- Principle for determining the effective emissivities

- the effective emissivity of plane 1 is obtained from a radiative balance in 2D (transversal plane through a solid block)
- stepwise manner:

$$\epsilon_7' = (\overline{S_2 S_7} + \overline{S_3 S_7}) / A_7$$

where $\overline{S_i S_j}$ = total exchange area between i and j, m²

A_7 = area of equivalent surface 7, m²

ϵ_7 = effective emissivity of surface 7

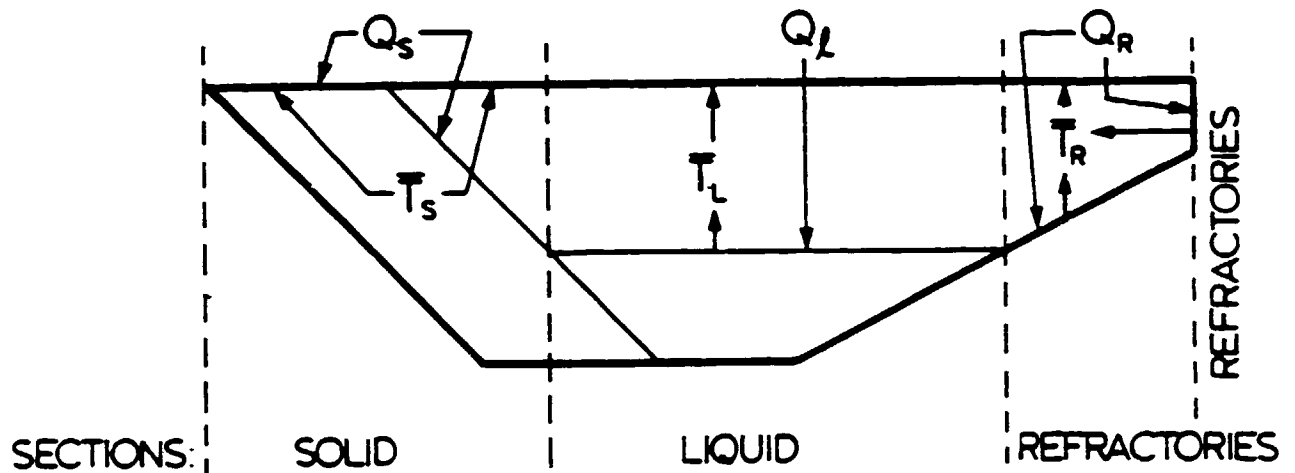
$$\epsilon_6' = (\overline{S_4 S_6} + \overline{S_5 S_6}) / A_6$$

$$\epsilon_1' = (\overline{S_1 S_6} + \overline{S_1 S_7}) / A_1$$

approximations:

- no exchange between solid blocks
- transparent gas
- not dependent on surface temperature

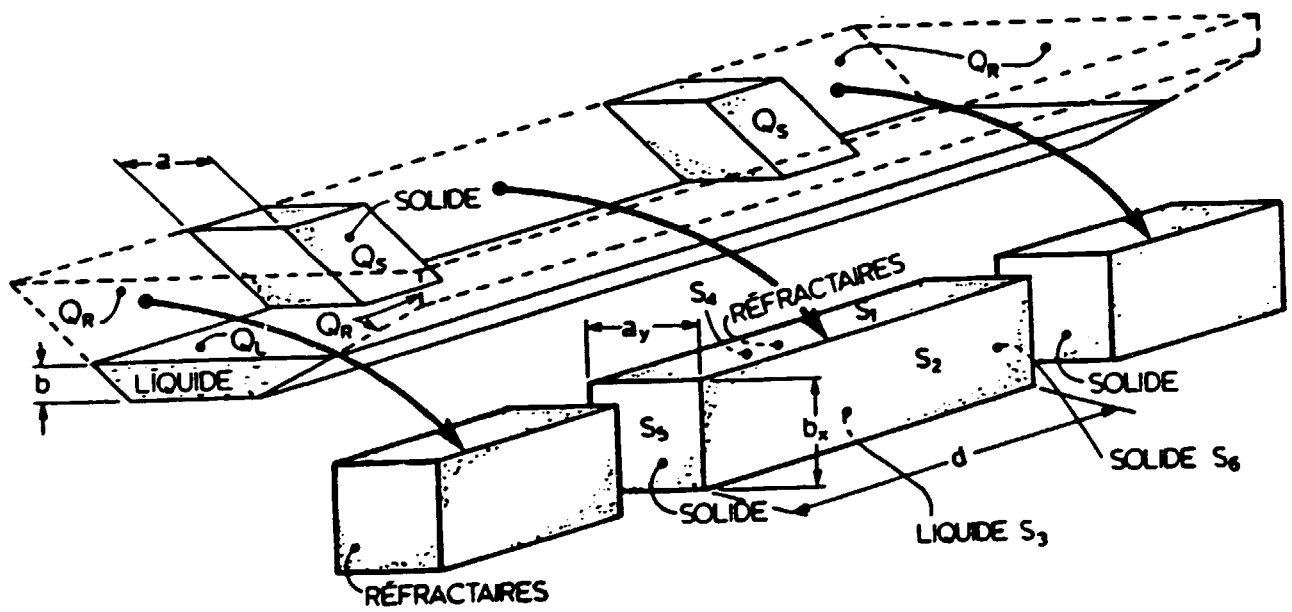
4.2 Temperature distribution at the equivalent plane



Convention used for assigning temperatures and heat flows

4.3 cross-sections falling between solid blocks

- 3D radiation exchange between blocks
- calculation of effective emissivity ϵ_{12} and incorporation into the 2D strategy



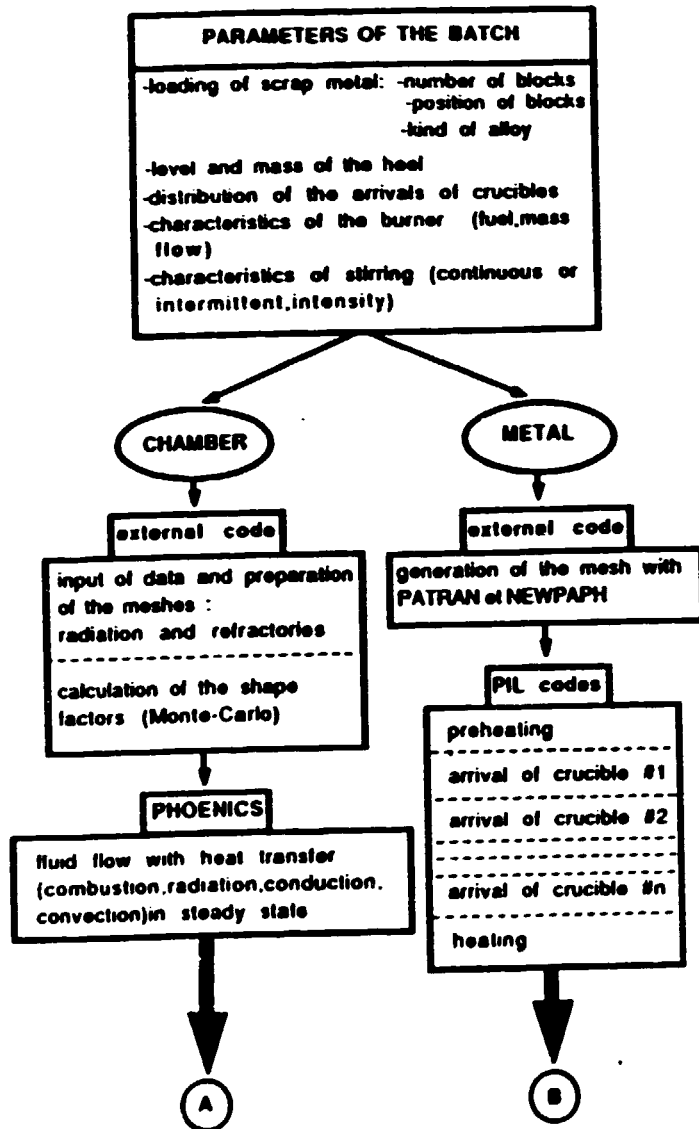


Figure 4a- Preparation of the data files

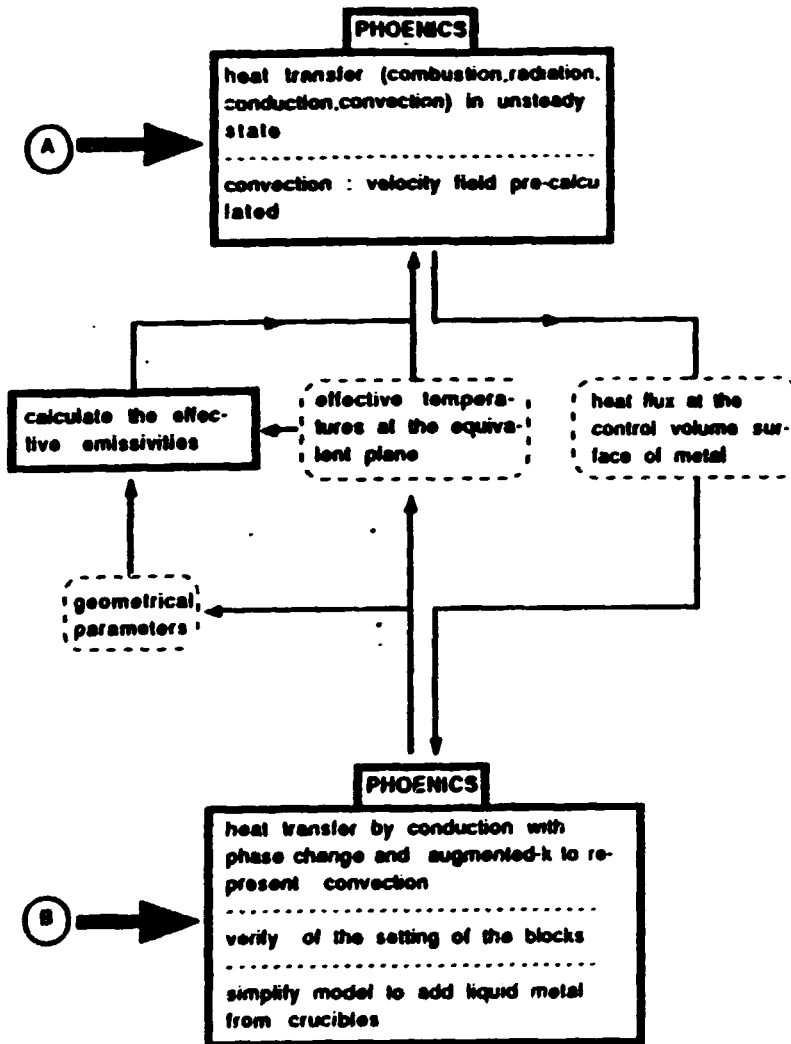


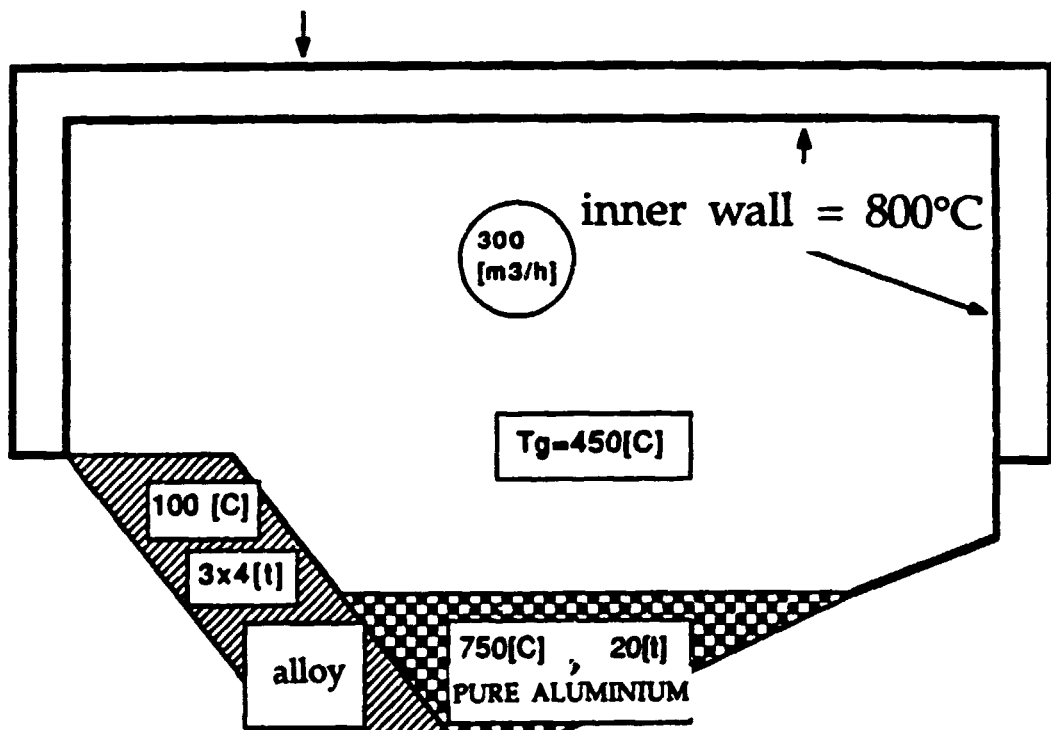
Figure 4b- The recurrent coupling process

6. Validation

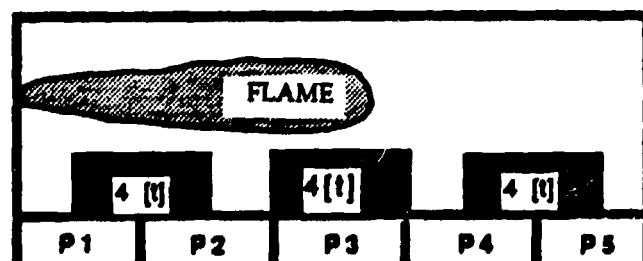
6.1 Description of the charge

INITIAL CONDITIONS

outer wall = 100°C



SOLID CHARGE

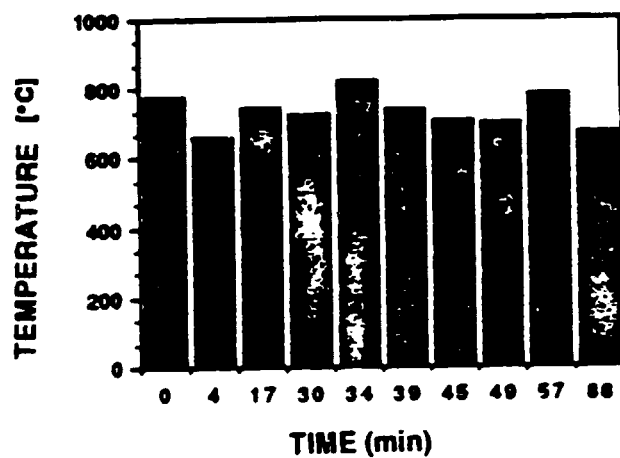


BLOC: 2.0 X 0.7 X 1.5 [M³]

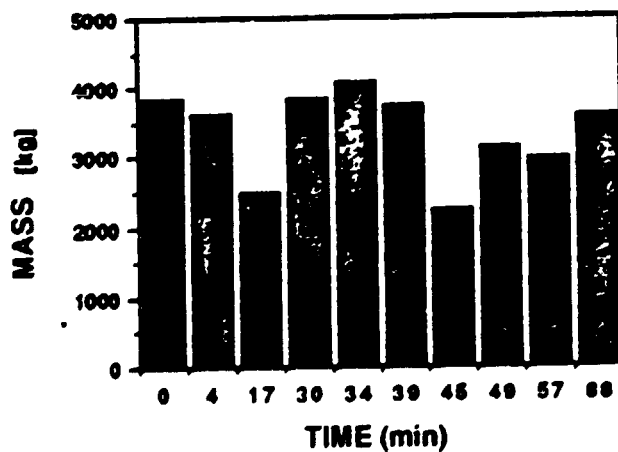


Addition of liquid Al

TEMPERATURE OF THE CRUCIBLES



MASS OF CRUCIBLES



6.2 Results (model)

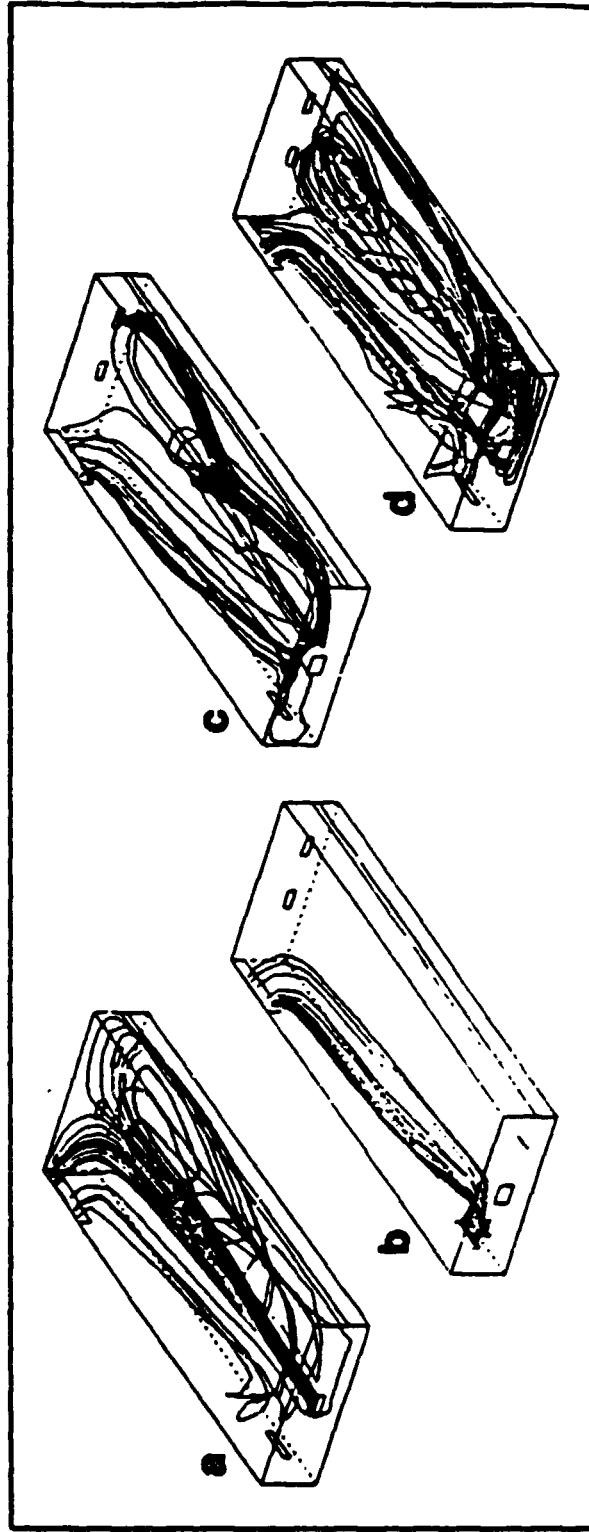
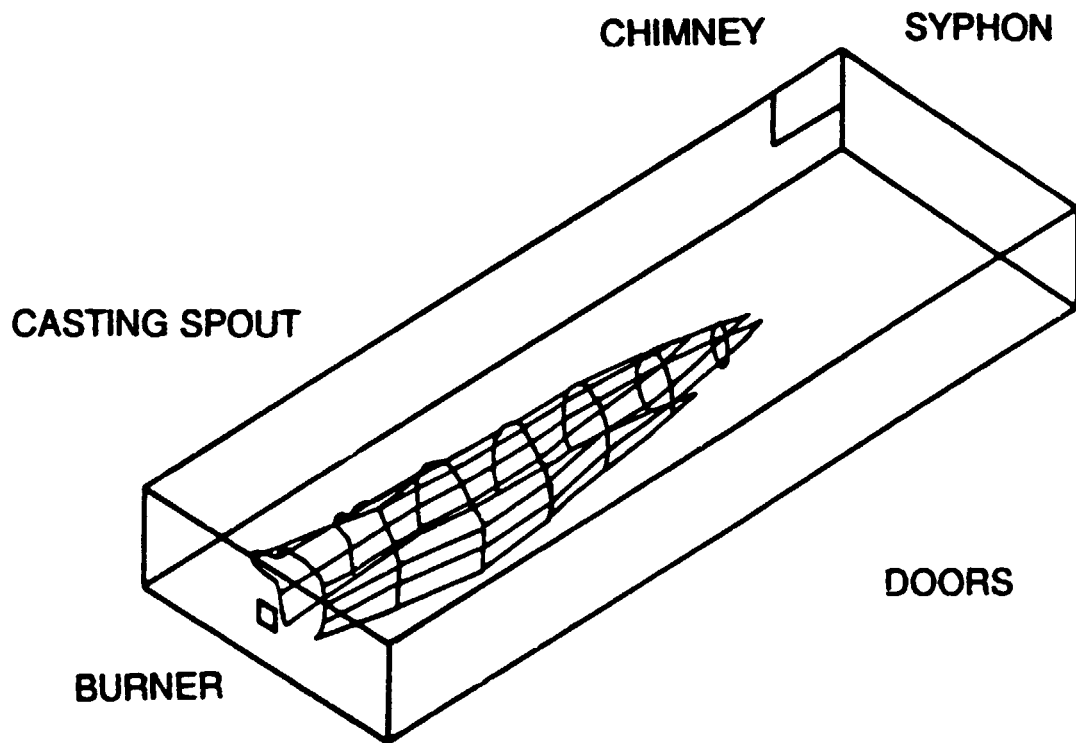
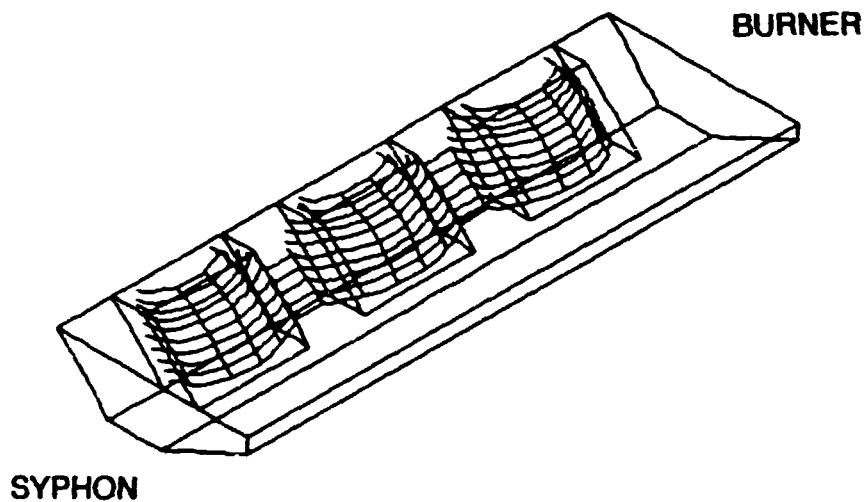


Figure 6. PHOENICS-ZONE output showing stream lines originating at the (a) burner, (b) spout, (c) siphon number 2 and (d) door gaps.

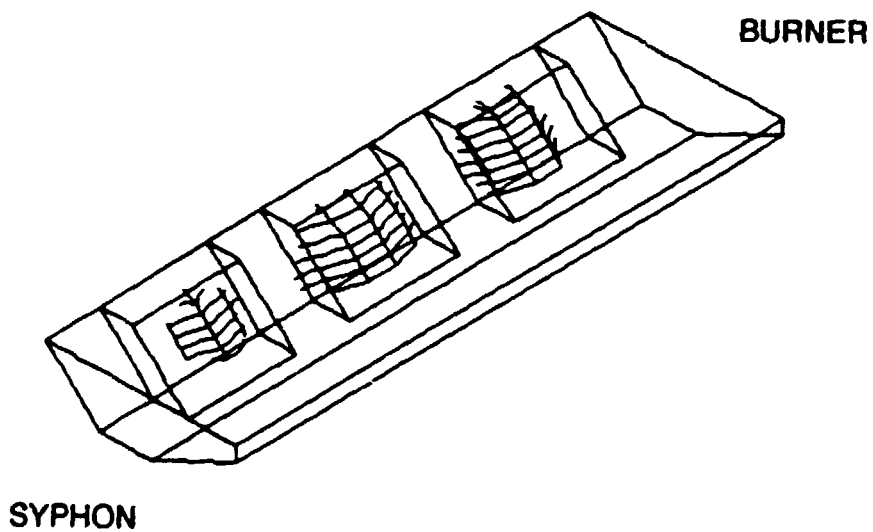


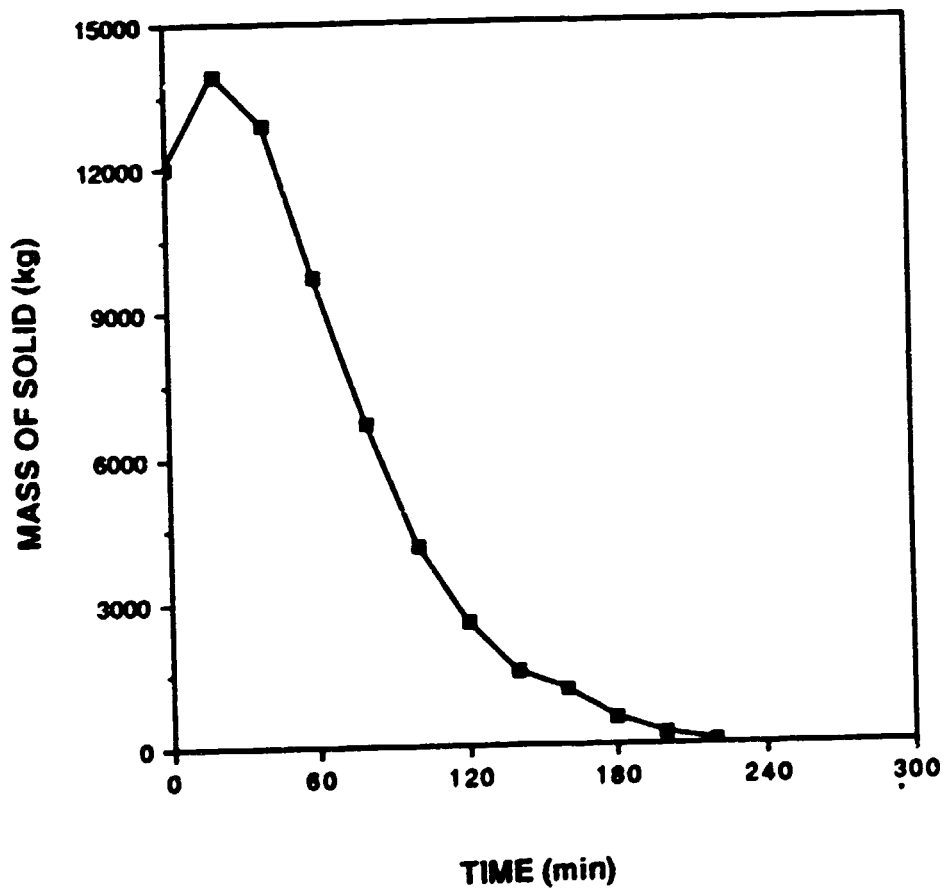
FLAME CONTOURS AS
REPRESENTED BY 0.01 RESIDUAL
FUEL ISOSURFACE

SOL-LIQ PHASE CHANGE BOUNDARY PROFILE AFTER
THE LAST ADDITION OF LIQUID ALUMINIUM (at 100 min)



SAME PROFILE AFTER 160 min

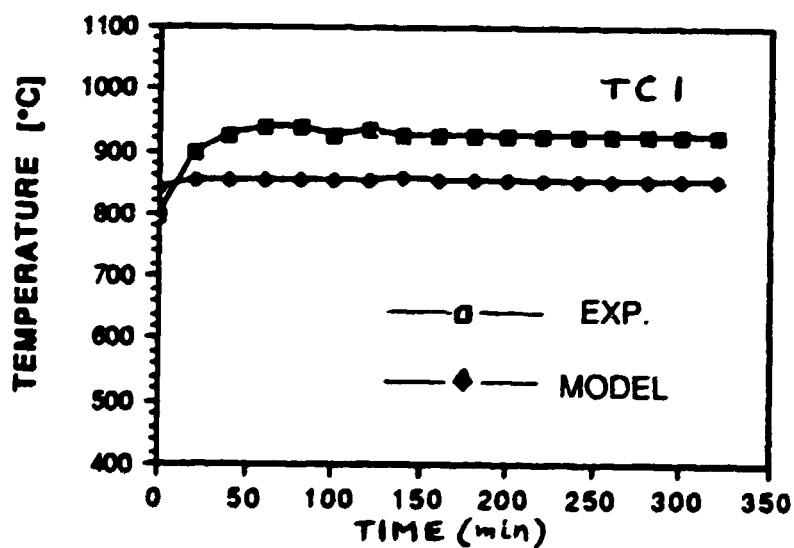
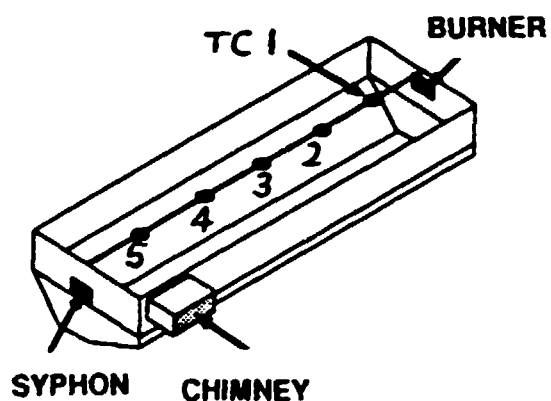


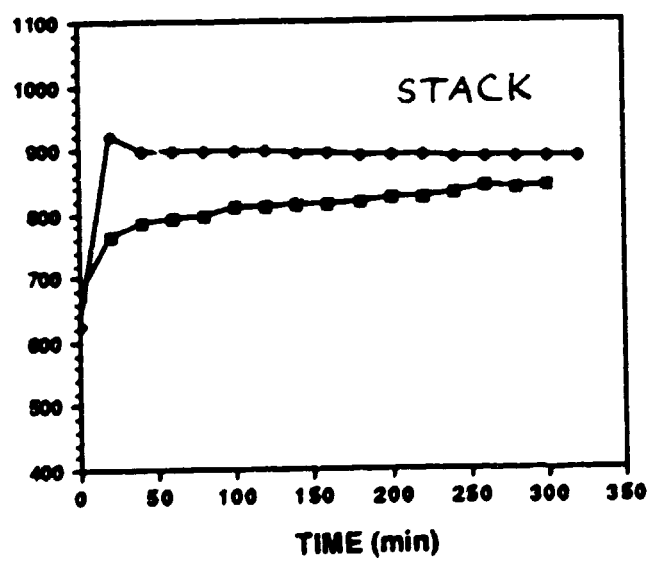
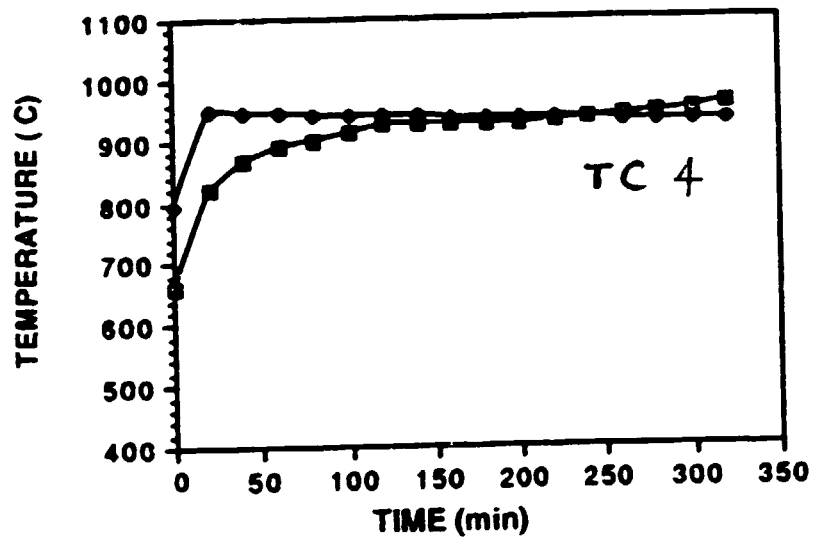
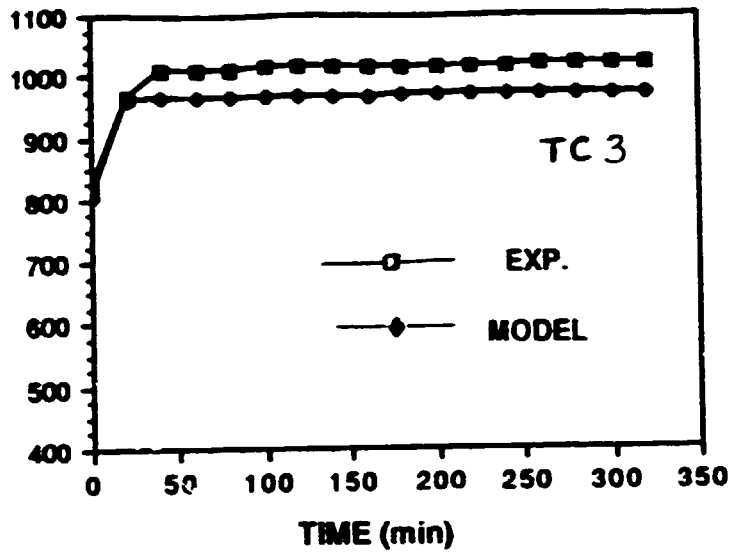


MASS VARIATION OF SOLID AL

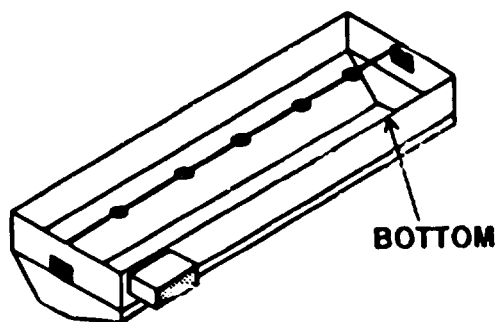
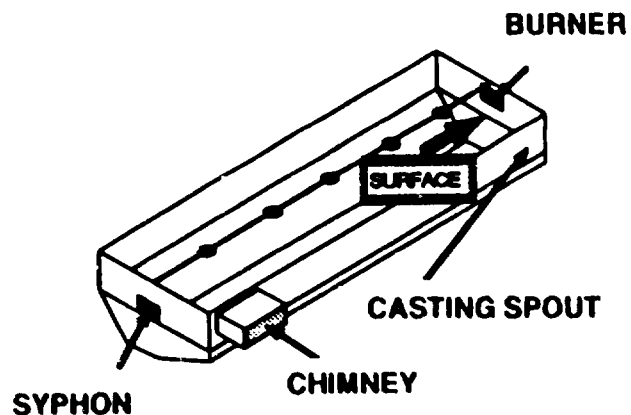
6.3 Results (comparisons with experimental data)

a) Combustion chamber

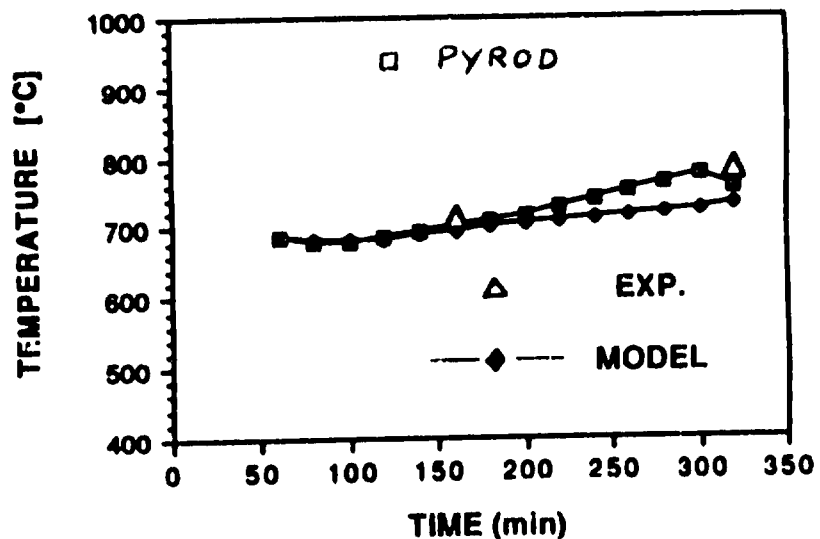




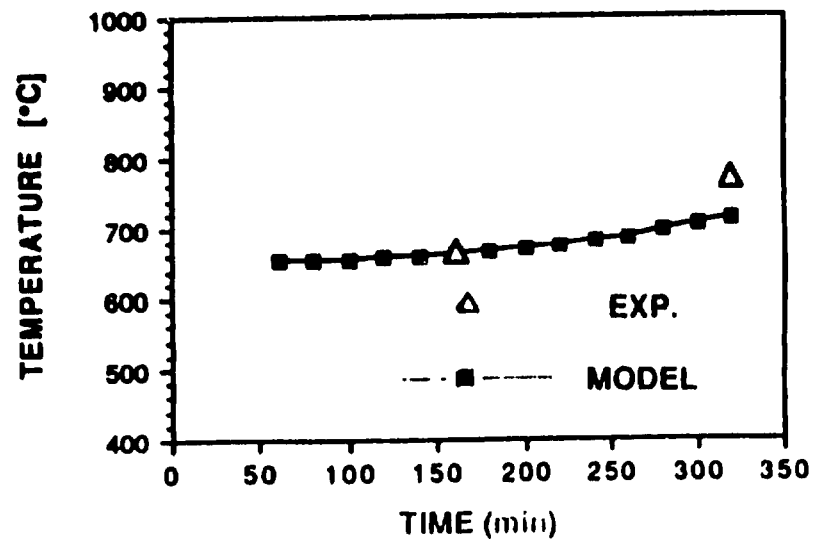
b) Metal



METAL TEMPERATURE AT THE SURFACE (NEAR THE CASTING SPOUT)



METAL TEMPERATURE AT THE BOTTOM



CONVECTIVE HEAT TRANSFER IN CIRCULAR REMELTING FURNACES

Laszlo I. Kiss
UQAC/GRIPS

THE MODEL

- **SCALING LAWS**

- ... geometric similarity
- ... ratio of convective and viscous momentum transfer (Reynolds number)
- ... buoyancy (plume)
- ... heat transfer modes (temperature level, surface properties)
- ... "feedback" by conduction within the pile & bath

↑↓

- ... boundary conditions

- **VISUALIZATION — TRANSPARENT WALLS**

MODELING THE SCRAP-PILE & BATH

- **SHAPE**

- **MATERIAL**

- cold study

- heat transfer experiments

- **COLD FLOW STUDY**

- ... visualization

- ... velocity field measurements

- **MEASUREMENT OF HEAT TRANSFER RATES**

- ... heat transfer coefficients

- ... surface temperature distribution

- **VISUALIZATION OF FLOW STRUCTURE**
- **METHODS**
 - ... fluorescent mini-tuft
 - ... “pop-corn”
 - ... smoke with laser-sheet illumination
- **BENEFITS**
 - ... understanding of flow behaviour
 - ... flow pattern, vortex formation
 - ... identification of highly turbulent, fluctuating zones
 - ... changes in local heat fluxes (near-surface velocities)
 - ... dead-zones, low heat-transfer domains
 - ... differences & interaction of burners
 - ... understanding mixing & gas exchange (residence time)

HEAT TRANSFER COEFFICIENT (*HTC*) MEASUREMENTS

- **METHODS**
- **LOCAL & AVERAGE VALUES**
- **BOUNDARY CONDITIONS**
- **PILE, FLAT-BATH, WALLS**
- **HOT-SPOT FORMATION**

METHODS TO MEASURE HTC-s

- STEADY-STATE METHODS

- ... *electrical heating*

- ... *fluid calorimetry*

- ... volume heating

- ... surface heating

- TRANSIENT METHODS

- ... whole-body (average)

- ... gauges/probes (local)

• LOCAL vs. AVERAGE VALUES

• BOUNDARY CONDITIONS

... *prescribed flux*

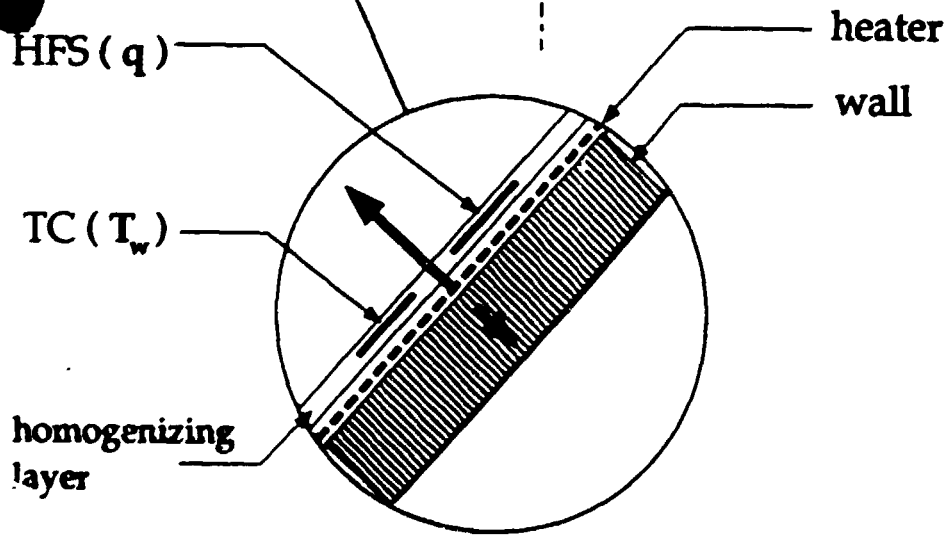
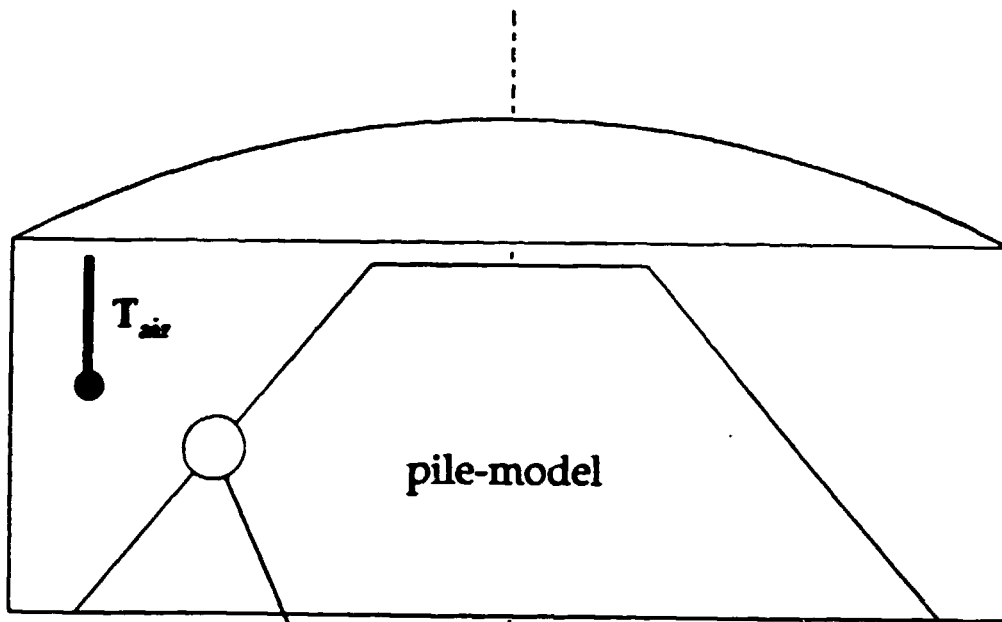
... *prescribed temperature*

HEATED SKIN (electrical)

- *guard heating*
- *direct measurement of local fluxes*
- **WHICH SURFACES?**
- **NUMBER OF SECTIONS?**
- **NUMBER OF MEASUREMENT POINTS?**

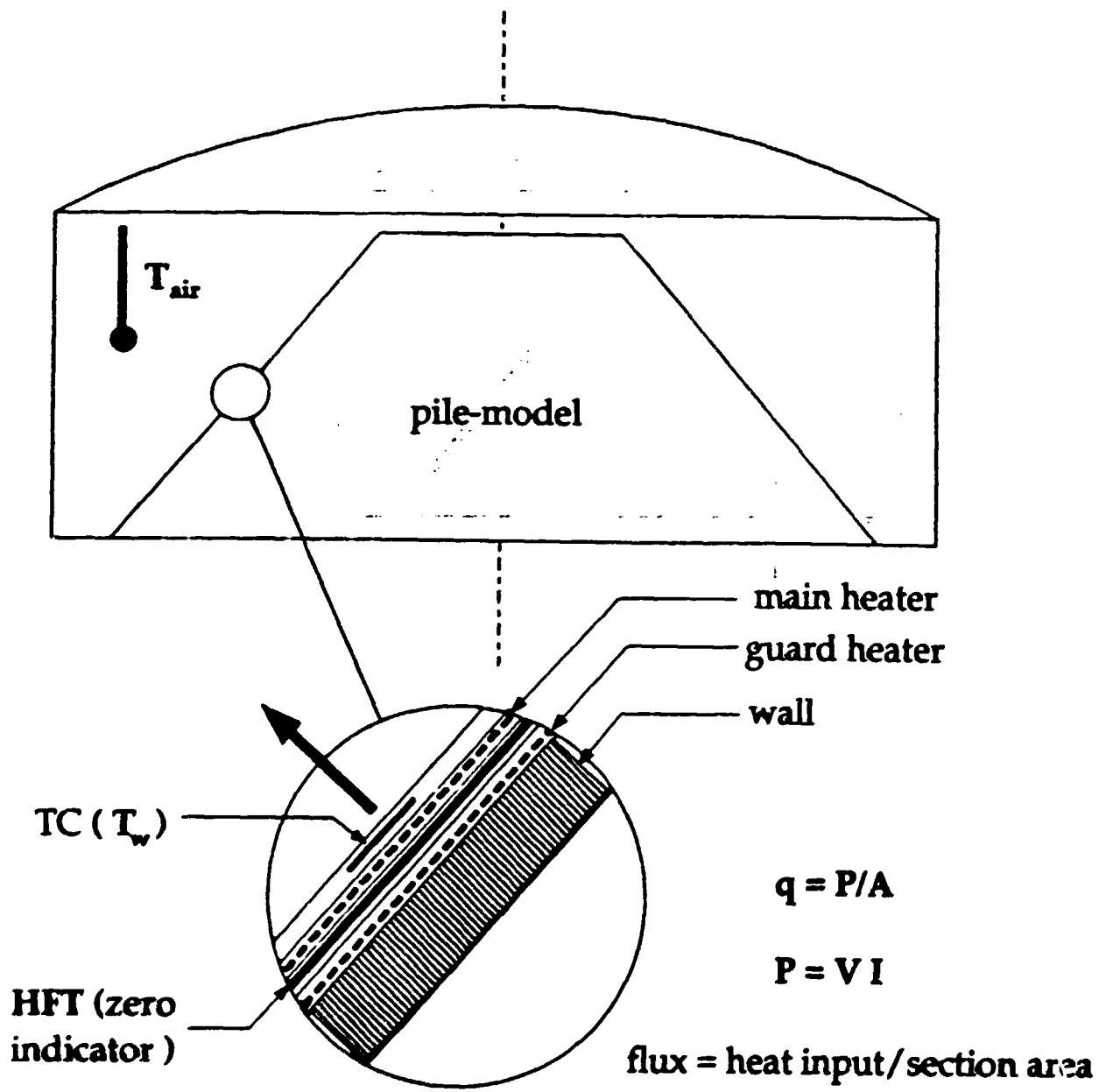
DIRECT MEASUREMENT OF FLUX

$$q = h (T_w - T_{air})$$



GUARD HEATER TECHNIQUE

$$q = h (T_w - T_a)$$



main heater
guard heater
wall

TC (T_w)

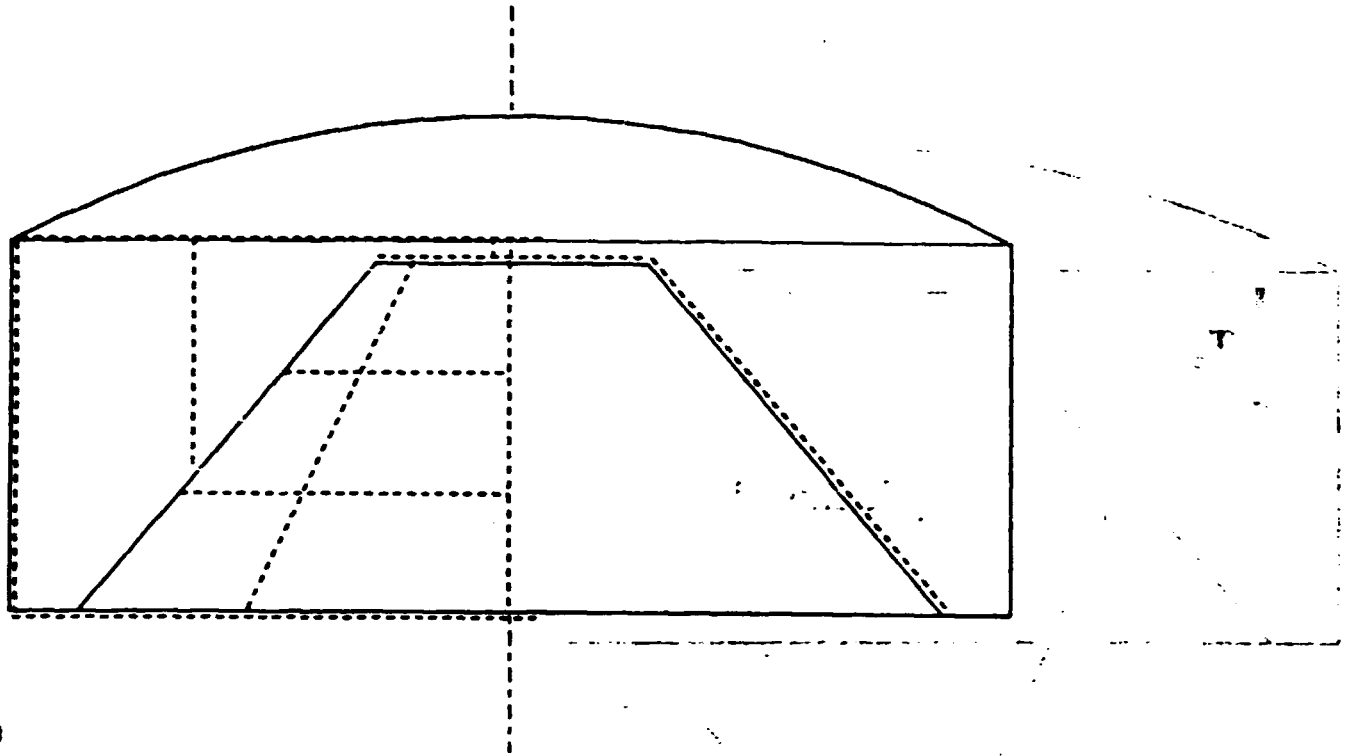
HFT (zero indicator)

$$q = P/A$$

$$P = VI$$

flux = heat input/section area

HEATED SECTIONS



0707 TH
(10/10/10)